Selection of RNA aptamers and their recognition of amyloid assemblies

Rachel Alexandra Mahood

Submitted in accordance with the requirements for the degree of Doctor of Philosophy

The University of Leeds

Astbury Centre for Structural Molecular Biology

September 2015

The candidate confirms that the submitted work is her own, except where work which has formed part of jointly-authored publications has been included. The contribution of the candidate and the other authors to this work has been explicitly indicated overleaf. The candidate confirms the appropriate credit has been given within the thesis where reference has been made to the work of others. This copy has been supplied on the understanding that it is copyright material and that no quotation from this thesis may be published without proper acknowledgement.

Acknowledgements

It is with great pleasure that I thank all the people who have helped me throughout my time in Leeds and who have made the completion of my PhD one of the most rewarding experiences of my life.

Firstly, to my supervisors, Prof. Sheena Radford and Prof. Peter Stockley. This work would have been impossible without your constant support, guidance and unwavering enthusiasm. I'm incredibly grateful for the time and hard work that has gone into all aspects of the project, and in preparing this thesis. Extra special thanks go to Sheena, for knowing exactly what to say during the toughest of times, and never allowing me to give up.

I'd also like to express my deepest gratitude to all members of the Radford and Stockley laboratories, past and present, who have provided endless advice and support during this project, but most importantly, kept me smiling. In particular, David Bunka, Claire Sarell and Simon White, who all understand the joys of amyloid and aptamers, and dedicated a huge amount of time to helping me with all aspects of the work. Thanks to Maya Pandya, Katie Stewart and Tiernan O'Malley for the help with the Aβ prep. Thanks also to Eric Dykeman, for his work on the bioinformatics, James Ault for the mass spectrometry and Matthew Jackson for all things α-syn (and the laughs along the way!).

I'd also like to thank our wonderful lab manager Nasir Khan. Nothing is ever too much to ask and I'm so grateful for your constant help and the endless supply of biscuits! The lab is a much more pleasant place to work because of you.

Huge thanks go to two of my favourite ladies, Lydia Young and Jan Saunders (co-founder of the stagnant puddle). It was such a pleasure, not only to collaborate with you two on the amazing work you did, but also to have you as such incredible friends. Jan, your help in the final few months (and throughout – I'll never forget the madness of our little corner!) was nothing short of amazing and I couldn't have done it without you. Special thanks also go to Claire, Sasha, Sophie and Helen; for all the sneaky Costa breaks and cocktails, and making the last four years so much fun. Extra special thanks go to my Leeds wifey, Nic, for being such a fantastic housemate for nearly 7 years! I have so many wonderful memories of our time in Leeds and will be very sad to leave.

Finally, I would like to thank all my lovely family, especially Mum and Dad; I certainly couldn't have done this without your love and encouragement. And Joe, thank you for being so patient and putting up with me – knowing I had you to come home to in the end kept me going, and I hope I've made you proud.

Abstract

Amyloidoses are a group of protein misfolding disorders which are characterised by the abnormal accumulation of highly ordered filamentous assemblies, known as amyloid fibrils. More than 50 human disease states are attributed to this phenomenon, many of which are neurodegenerative and pose an ever-increasing threat to our aging society. There is a clear need to dissect the processes behind such disorders, as well as to provide novel and much needed treatments and diagnostic reagents. This thesis was motivated by the recognition powers of RNA molecules, which can be discovered through the *in vitro* selection of RNA aptamers. RNA aptamers are a well-established class of research tools, imaging probes, diagnostic reagents and therapeutics, which are showing increasing promise in many fields, but are currently not exploited in the detection or treatment of amyloid disorders.

In this thesis, the recognition power of RNA aptamers was explored in targeting species associated with the most prevalent and deadly amyloid disorder, Alzheimer's disease. *In vitro* selection of RNA aptamers was performed against immobilised monomeric Aβ40, as well as two structurally distinct Aβ40 amyloid fibrils, formed *in vitro*. The anti-monomer aptamers were unable to recognise native, monomeric Aβ40 in solution but instead displayed enhanced affinity for the fibrillar forms. Using fluorescence polarisation, the anti-fibril aptamers have been shown able to cross-react with other fibril polymorphs, formed from both Aβ40 and the unrelated protein sequence, α-synuclein, indicating generic amyloid selectivity. Aptamers were, however, unable to recognise amyloid fibrils assembled from short amyloidogenic peptides. Amyloid recognition by aptamers was shown to be largely independent of the RNA sequence or structure. Further structural characterisation, including competition experiments with generic amyloid-binding molecules glycosaminoglycans, indicated that binding was most likely mediated through the phosphate backbone contacts with ordered repeats of positively charged regions of the amyloid assemblies.

Overall, the results demonstrate an inherent affinity for amyloid by RNA molecules, making it highly challenging to select aptamers able to distinguish between different cross-β assemblies. However, the seemingly universal amyloid-binding propensity demonstrated by RNA could allow development of generic amyloid detection tools, more effective than current methods. Furthermore, the work indicates the need to explore possible roles of RNA associations as a general amyloid toxicity mechanism.

Table of Contents

List of Figures

List of Tables

List of Abbreviations

Amino acids are abbreviated according to their standard three-letter or single-letter codes. Other abbreviations are as follows:

2A	Aβ40 fibril with 2-fold molecular symmetry
2'F	2'fluoro
2'OH	2'hydroxy
3Q	Aβ40 fibril with 3-fold molecular symmetry
A	Adenine
Å	Ångström
Aβ	Amyloid-beta
Aβ40	Amyloid-beta residues 1-40
Aβ42	Amyloid-beta residues 1-42
AD	Alzheimer's disease
AFM	Atomic force microscopy
AICD	Amyloid precursor protein intracellular domain
ALS	Amyotrophic lateral sclerosis
AMD	Age-related macular degeneration
APP	Amyloid precursor protein
APS	Ammonium persulphate
APSDs	Amylospheroids
α-syn	α-synuclein
ATP	Adenosine triphosphate
β_2m	β_2- microglobulin

BACE1	Beta- secretase 1
BBB	Blood brain barrier
bp	base pairs
BSE	Bovine Spongiform Encephalopathy
C	Cytosine
CCR5	Chemokine receptor type 5
CD4	Cluster of differentiation 4
cDNA	Complementary DNA
CJD	Creutzfeldt-Jakob disease
Cryo-EM	Cryo electron microscopy
CSF	Cerebrospinal fluid
CTFα	C-terminal fragment alpha
CTFβ	C-terminal fragment beta
CTP	Cytidine triphosphate
Da, kDa	Daltons, kilo daltons
DEPC	Diethylpyrocarbonate
DMEM	Dulbecco's modified eagle's medium
DMSO	Dimethyl sulfoxide
DNA	Deoxyribonucleic acid
DRA	Dialysis related amyloidosis
dsDNA	Double-stranded DNA
DTT	1,2-dithiothreitol
EB	Elution buffer
E. coli	*Escherichia coli*

EDTA	Ethylenediaminetetraacetic acid
EGCG	(-)-epigallocatechin 3-gallate
EGFR	Epidermal growth factor receptor
EM	Electron microscopy
EPR	Electron paramagnetic resonance
ER	Endoplasmic reticulum
ESI	Electrospray ionisation
EtBr	Ethidium bromide
EtOH	Ethanol
FCS	Fetal calf serum
FP	Fluorescence polarization
FRET	Förster resonance energy transfer
FTIR	Fourier transform infrared spectroscopy
G	Guanine
GAG	Glycosaminoglycan
GMP	Guanosine monophosphate
gp120	Envelope glycoprotein gp120
GTP	Guanosine triphosphate
h	hour
HCl	Hydrochloric acid
HER3	Human epidermal growth factor receptor 3
HFIP	Hexafluoro-2-propanol
hIAPP	Human islet amyloid polypeptide
HIV	Human immunodeficiency virus
HSR	Heat shock response

IAPP	Islet amyloid polypeptide
Im7	Colicin immunity protein 7
IPTG	Isopropyl β-D-1-thiogalactopyranoside
ITC	Isothermal titration calorimetry
K_d	Dissociation constant
K_{off}	Off-rate
K_{on}	On-rate
LB	Luria-Bertani
LBD	Lewy body dementia
LED	Light emitting diode
LMW	Low molecular wieght
LS	Light scattering
LTP	Long term potentitation
M	Molar
mA	Milliamp
MCI	Mild cognitive impairment
MD	Molecular dynamics
mg	Milligram
µg	Microgram
min	Minutes
mL	Millilitre
mol	Mole
MOPS	3-(N-morpholino)propanesulfonic acid
MRI	Magnetic resonance imaging

MS	Mass spectrometry
MST	Microscale thermophoresis
MTT	3-(4,5-dimethylthiazol-2-yl)-2,5- diphenyltetrazolium bromide
MWCO	Molecular weight cut off
NAC	Non-amyloid beta component
NBS	Non-binding surface
NGS	Next generation sequencing
NHS	*N*-Hydroxysuccinimide
NMDA	N-methyl-D-aspartate receptor
NMP (rNMP)	(Ribo) nucleoside monophosphate
NMR	Nuclear magnetic resonance
NTP (dNTP)	(Dioxy) nucleoside triphosphate
OD_{600}	Optial density at 600 nm
PAGE	Polyacrylamide gel electrophoresis
PBS	Phosphate buffered saline
PCR	Polymerase chain reaction
PD	Parkinson's disease
PEG	Polyethylene glycol
PET	Positron emission tomography
PICUP	Photo-induced cross-linking of unmodified proteins
PMSF	phenylmethanesulfonylfluoride
PolyP	Polyphosphate
Poly-Q	Polyglutamine
PrP	Prion protein

psi	Pounds per inch
RI	Refractive index
RNA	Ribonucleic acid
RNAi	RNA interference
RP-HPLC	Reverse phase HPLC
rpm	Rotations per minute
RT-PCR	Reverse transcription polymerase chain reaction
RU	Response units
RVGP	Rabies virus glycoprotein
s	Seconds
SAF	Scrape associated fibrils
sAPPα	Soluble amyloid precursor protein alpha
SDP	Sulphodichlorophenol
SDS	Sodium dodecyl sulphate
SEC	Size exclusion chromatography
SEC MALLS	Size exclusion chromatography multi-angle laser light scattering
SELEX	Systemic evolution of ligands by exponential enrichment
siRNA	Small interfering RNA
SOD1	Superoxide dismutase 1
SPR	Surface plasmon resonance
ssDNA	Single stranded DNA
ssNMR	Solid state nuclear magnetic resonance
T	Thymine
TBE	Tris/borate/EDTA

TEM	Transmission electron microscopy
TEMED	Tetramethylethylenediamine
ThT	Thioflavin T
TMR	Tetramethylrhodamine
TTR	Transthyretin
U	Uracil
UPR	Unfolded protein response
UTP	Uridine triphosphate
UV	Ultraviolet
VEGF	Vascular endothelial growth factor
v/v	Volume: volume ratio
WT	Wild-type
w/v	Weight: volume ratio
XNA	Xeno-nucleic acid
YIP	Yeast inorganic pyrophosphatase
λ	Wavelength

List of Amino Acid Abbreviations

A	Ala	alanine
C	Cys	cysteine
D	Asp	aspartate
E	Glu	glutamate
F	Phe	phenylalanine
G	Gly	glycine
H	His	histidine
I	Ile	isoleucine
K	Lys	lysine
L	Leu	leucine
M	Met	methionine
N	Asn	asparagine
P	Pro	proline
Q	Gln	glutamine
R	Arg	arginine
S	Ser	serine
T	Thr	threonine
V	Val	valine
W	Trp	tryptophan
Y	Tyr	tyrosine

1 Introduction

1.1 Amyloid disease: A modern epidemic

Protein aggregation, and specifically amyloid formation, has become a subject of intense research efforts in recent years, owing to the association of amyloid deposition with some of the most debilitating disorders to threaten human health in the modern world. Amyloid formation is defined by the conversion of normally soluble peptides and proteins into insoluble, highly-ordered, fibrillar aggregates, characterised by a distinctive cross-β type structure[1-4]. Despite a recent explosion of interest in the field, the phenomenon of amyloid formation, in fact, was discovered more than 150 years ago. Rudolph Virchow coined the term amyloid in 1854[5-7], based on the observation of abnormal, macroscopic structures in brain tissue. These structures stained blue upon application of iodine, indicative of the presence of starch. The term amyloid, therefore, was derived from the Latin "amylum" and Virchow evidently considered amyloid to be carbohydrate based. However, by 1859, Friedrich and Kekule first recognised that amyloid was proteinaceous[8] and attention shifted to the study of amyloid as a protein, and later, a class of proteins unrelated by amino acid sequence.

Through the years, advances in technology have revealed much about the amyloid structure. In 1922, Bennhold *et al*. [9] observed that the common, industrial dye, Congo red, was able to bind to amyloid deposits and later, polarisation light microscopy studies[10] revealed the enhancement of Congo red birefringence in the presence of amyloid, indicating the possibility of an ordered microscopic structure. This finding encouraged electron microscopy studies[11-14] where it was confirmed that all amyloid fibrils studied shared a similar, fibrillar ultrastructure. X-ray diffraction data[15, 16] demonstrated that the ordered structure of the fibrils was made up of a consistent, cross-β sheet architecture and this characteristic is now considered one of the defining criteria of amyloid.

Amyloid was long believed to be derived from a single substance, but it was not until the 1970s that the pioneering work of Benditt and Glenner first demonstrated the biochemical heterogeneity of amyloid[17-21]. Over the following decade, around 20 normally soluble proteins were found in amyloid deposits specifically associated with a range of disorders, now termed amyloidoses (or amyloid diseases). In some cases the deposition is localised

to a single organ (such as the brain in Alzheimer's disease or the pancreas in diabetes) or found in multiple organs or tissues, termed systemic amyloidoses.

Today, amyloidoses are known to be a biochemically and clinically heterogeneous group of disorders of protein folding. There are approximately 50 disorders[22] (discussed in Section 1.2.6), with diverse clinical pathologies, where the misfolding of normally soluble, functional protein leads to the conversion to an aggregated state and subsequent accumulation as amyloid deposits. The fact that many of these disorders are associated with aging (e.g. Alzheimer's disease), or with our increasingly sedentary lifestyles (e.g. Type II diabetes), means that amyloidoses account for some of the most common and debilitating medical conditions in the modern world[1, 3, 22]. Alzheimer's disease, probably the most well-known amyloid disorder, now represents the fifth most common cause of death in the UK overall and the leading cause for women[23]. It has recently been termed a "21st century plague"[24] as the current number of people living with the disorder is projected to triple in the next 40 years, with an estimated 80 million new cases worldwide[24, 25]. Research into amyloidosis, therefore, is required in tackling this wide range of increasingly prevalent disorders, which represent some of the greatest socio-economic challenges of our time[26-28].

1.2 Protein misfolding and aggregation

1.2.1 Principles of protein folding and misfolding

A native protein fold (the protein's specific, three-dimensional conformation) is often paramount to its function. Since the early 1960s, and Anfinsen's classic work on the renaturation of ribonuclease A[29], it has been known that all the information required for a protein to reach its native conformation is encoded within its primary sequence, and that the mechanism depends on a search for the structure with the lowest free energy and therefore highest thermodynamic stability. However, for a protein to sample all the possible conformations available, at random, in order for it to find its single functional fold, would be impossible on a biological timescale[30, 31]. This paradox was first considered by Levinthal[30, 32], who proposed that specific, kinetically controlled, protein folding pathways exist to reduce the number of conformations that need to be sampled to achieve the native fold. By rapid formation of local native-like structures with enhanced stability, fewer

species would be populated en route to the final energy minimum and folding would be achievable on a biologically appropriate timescale.

The process of reaching the native fold is often explained as the transition from the high-energy, unfolded state to the low-energy native conformation by traversing a "downhill" energy landscape[33]. The energy landscape describes the series of structural assemblies sampled en route to the native fold and is plotted as the free energy of the polypeptide chain, as a function of conformational space. An idealised energy landscape or "folding funnel" is shown in **Figure 1.1**, where the internal free energy decreases with the conformational entropy, until the minimum energy, native fold is achieved.

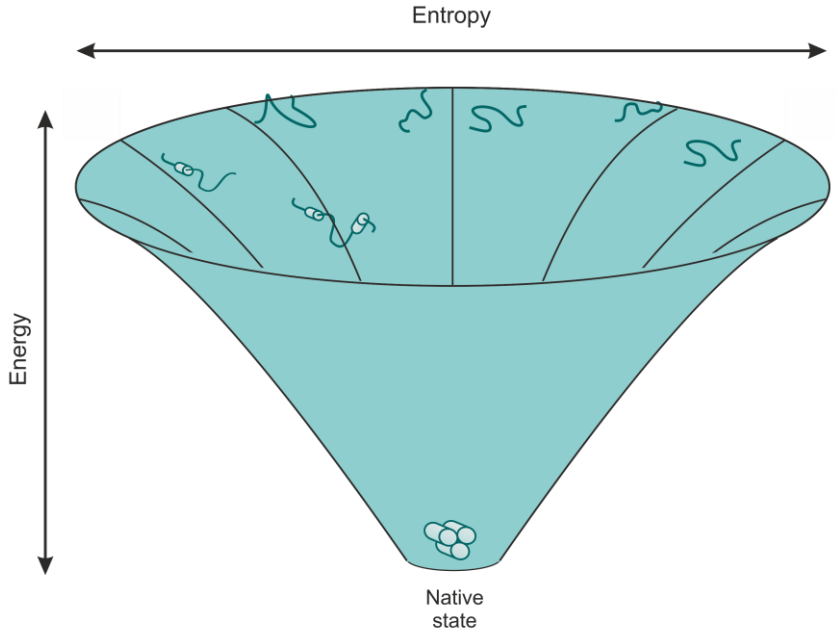

Figure 1.1 An idealised protein folding energy landscape. The funnel landscape represents the protein folding event as a stochastic search for the lowest energy native state, beginning as a disordered polypeptide chain, at the rim of the funnel, and progressing with increasing negative-free energy, to the native fold. The vertical axis represents internal free energy, whereas the horizontal axis indicates the conformational entropy. Figure redrawn and adapted from [34].

In reality, energy landscapes for the folding of most proteins are described as "rough" [35-37] (**Figure 1.2**), as the protein folds by populating several specific intermediate states, en route to the native conformation. These high-energy barriers and low-energy troughs are sampled before the correct folded and functional state is achieved. The species on the

energy landscape are in a state of flux[37] and many proteins will fluctuate around the minimal energy fold, forming some non-native contacts between residues. These species can represent functional or "on-pathway" conformations, however they are not the only structures available to the folding polypeptide. The event where a protein becomes trapped in an alternative, low-energy conformation is the basis of protein misfolding, where the formation of persistent, non-native interactions effect the protein's overall architecture and often its biological properties. Changes to the thermodynamic stability or the folding kinetics can increase the likelihood for a protein to adopt an unfavourable conformation. Various destabilising factors in the protein sequence, such as mutations, could contribute to this[3]. Changes in the cellular environment within which the newly synthesised polypeptide chain must fold, can also influence misfolding events, including pH, temperature, or changes in protein concentration, owing to overexpression or ineffective proteolysis[1, 3, 38, 39]. In these misfolded, partially folded or unfolded states, the hydrophobic core of the protein, usually buried in the native conformation, becomes exposed and prone to forming undesirable contacts with other molecules, and crucially, other misfolded proteins, leading to aggregation.

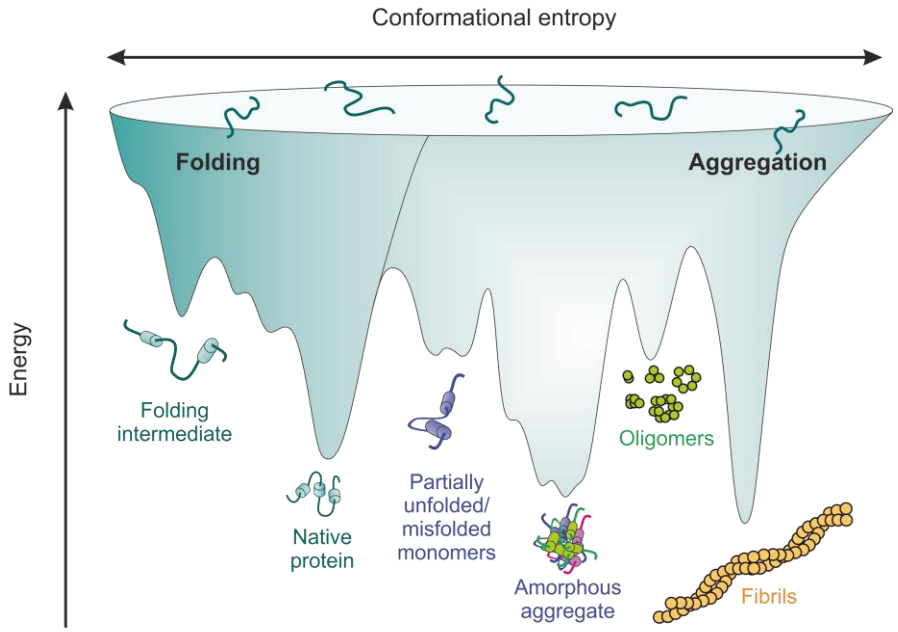

Figure 1.2 An energy landscape depicting protein folding and aggregation. The rough landscape illustrates the multitude of conformational states available to the polypeptide chain upon folding, and during misfolding and aggregation. Figure redrawn and adapted from [37].

Aggregated forms of proteins can be amorphous and consist of disordered assemblies of the same, or different, protein sequences. However, in several notable cases, aggregation can proceed to form ordered, self-associated species, known as amyloid fibrils[3, 4]. Interestingly, there is no clear similarity in the sequences, native structures or functions of the group of proteins known to form these highly ordered aggregates, yet they all adopt the same cross-β architecture[3]. Although the amyloid form is generally identified to be associated with disease, in recent years, a wide range of proteins that are not associated with any misfolding disorders have been shown to form characteristic fibrillar structures, indistinguishable from those formed in the disease states. This, along with the apparent lack of sequence homology, has led to the suggestion that, in principle, any polypeptide chain can adopt this amyloid structure[40-43].

1.2.2 Cellular response to aggregation

As protein misfolding can have such a profound effect on function, polypeptide sequences with an increased propensity to aggregate have been disfavoured throughout evolution (although some amyloid is functional[44, 45]). Conservation of proline and glycine residues (unlikely to form β-sheet rich structure, owing to conformational restraints and flexibility, respectively) as well as avoidance of extended stretches of hydrophobic residues, or sequences with alternating polar/non-polar residues, are all examples of strategies nature has adopted to reduce aggregation and maintain functional folding[46]. Proteins that must be natively-disordered for their function have also evolved to be generally less hydrophobic, with a higher net charge, reducing their inherent aggregation propensity[47]. However, polypeptides are clearly not entirely optimised and misfolding and aggregation can occur, often leading to devastating consequences.

Cells have developed a range of elaborate quality control mechanisms to deal with aberrant protein aggregation[48-51] (**Figure 1.3**). Molecular chaperones are conserved and ancient molecular machines that are required for correct folding and assembly of complexes, prevention of misfolding and aggregation, and in targeting a protein for degradation[52, 53]. The prevention of the accumulation of misfolded proteins is controlled firstly by the cell's heat shock response (HSR) or unfolded protein response (UPR)[54]. In response to a number of cellular stress signals, including but not limited to, temperature[55], expression of a range of chaperones is upregulated. These chaperone proteins then bind to exposed hydrophobic regions[56-58] in the misfolded monomers, and consequently, prevent further protein-protein

interactions[55]. A predominant family of chaperones are heat-shock proteins, which not only interrupt aberrant aggregation but are also often required for correct folding, under non-stress conditions. In cases where chaperones are unable to restore correct folding or function, large molecular machines known as chaperonins can be recruited, which isolate the misfolded entity within a central cavity, away from other cellular components, and promote refolding[56, 59, 60]. The UPR is another quality control system that controls the folding of eukaryotic proteins as they are co-translationally translocated in the endoplasmic reticulum (ER). The UPR prevents the export of misfolded or incorrectly post-translationally modified proteins, acting as a cellular "checkpoint". This too involves a number of ER chaperones, which may become saturated by an influx of misfolded species. This then leads to the activation of a network of intracellular signalling pathways (the UPR), upregulating proteins involved in folding, trafficking and degradation[61].

Many cell types have also developed strategies to sequester aggregates in specific cellular locations, reducing their effect on the rest of the cellular environment and possibly facilitating their removal[62-67]. In mammalian cells, inclusion bodies form in the ER (termed Russell bodies[68]) and the cytosol (aggresomes[68, 69]). Aggresomes can form and move to the nuclear envelope, via microtubule assisted transport, where chaperone expression is believed to be upregulated to combat the accumulation of misfolded species[68].

Degradation of aggregates is clearly the ultimate protective mechanism in the cell. In eukaryotes, aggregates are degraded by macroautophagy or the ubiquitin proteasome system[70]. In macroautophagy, whole aggregates are engulfed by a double-membrane, vesicular organelle, known as the autophagosome, which consequently travels through the cytosol to the lysosome. Upon fusing with the lysosome, the contents of the autophagosome can be degraded via acidic, lysosomal enzymes[71]. Alternatively, the ubiquitin proteasome system involves the recruitment of a multi-subunit proteolytic machine, the 26S proteasome. This complex specifically degrades proteins that are tagged for degradation by the covalent attachment of ubiquitin chains[72].

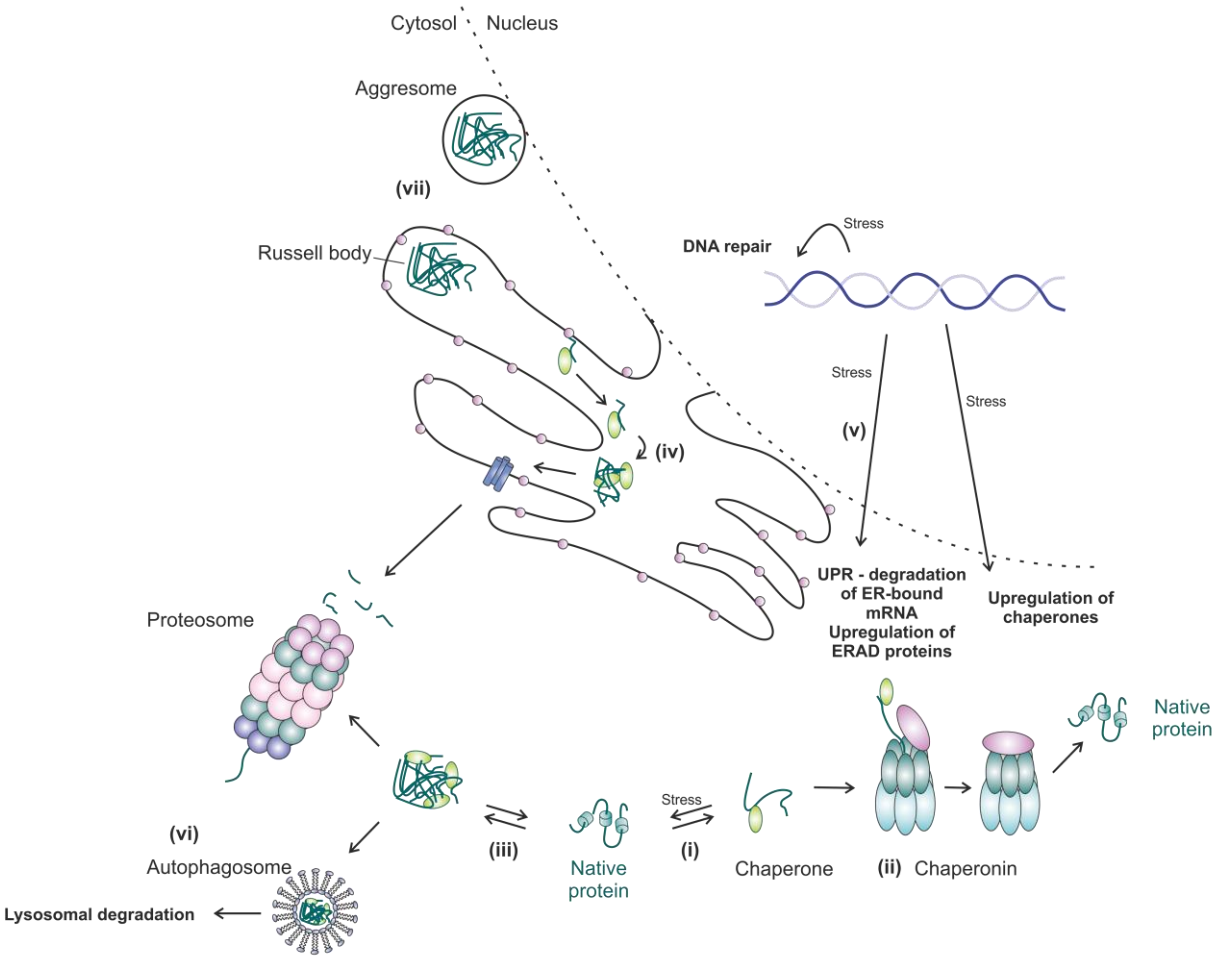

Figure 1.3 Controlling protein misfolding in the cell. Protein misfolding and aggregation activates a number of cellular quality control responses. Chaperones bind to the unfolding protein to prevent aggregation and promote correct folding **(i)**. If unsuccessful, the misfolded protein is transferred to the chaperonin where folding is promoted in a protected environment **(ii)**. If refolding is unsuccessful, or aggregation ensues, the protein is transferred to the proteasome for degradation **(iii)**. For secretory proteins, which are synthesised in the ER, misfolding is prevented by ER chaperones **(iv)**. If folding is unsuccessful, the protein is retro-translocated to the cytosol where it too is degraded by the proteasome. If the level of misfolding saturates the capabilities of the ER chaperones, the unfolded protein response (UPR) is activated **(v)**. Degradation of aggregates can also be dealt with via macroautophagy **(vi)**, where whole aggregates are engulfed by the autophagosome and targeted for degradation via the endocytic pathway. Specialised inclusions of aggregates can also form in the cytosol (aggresomes) and ER (Russell bodies) **(vii)**, sequestering the aggregates to reduce their effects on cellular processes and facilitating their removal.

1.2.3 Mechanism of amyloid formation

Amyloid formation is characterised by the aggregation of soluble proteins or peptides, into insoluble, fibre-like structures, via a number of oligomeric intermediate assemblies. The mechanism of fibril formation is known as nucleated-growth, where misfolded monomeric proteins first come together to form an ordered nucleus of a critical size that is necessary as a template for further deposition of monomers (**Figure 1.4**). The formation of the initial nucleus is thermodynamically unfavourable and occurs through rare, stochastic interactions[73]. This is the rate-limiting step of the aggregation mechanism, which leads to the initial lag phase in fibril formation kinetics. Addition of pre-formed fibril fragments, abolishes this initial lag phase and therefore supports the nucleated-growth model[74]. Once the initial, critical, elongation-competent nucleus is formed, addition of further monomers is thermodynamically favourable and proceeds rapidly to form the mature amyloid fibrils[75].

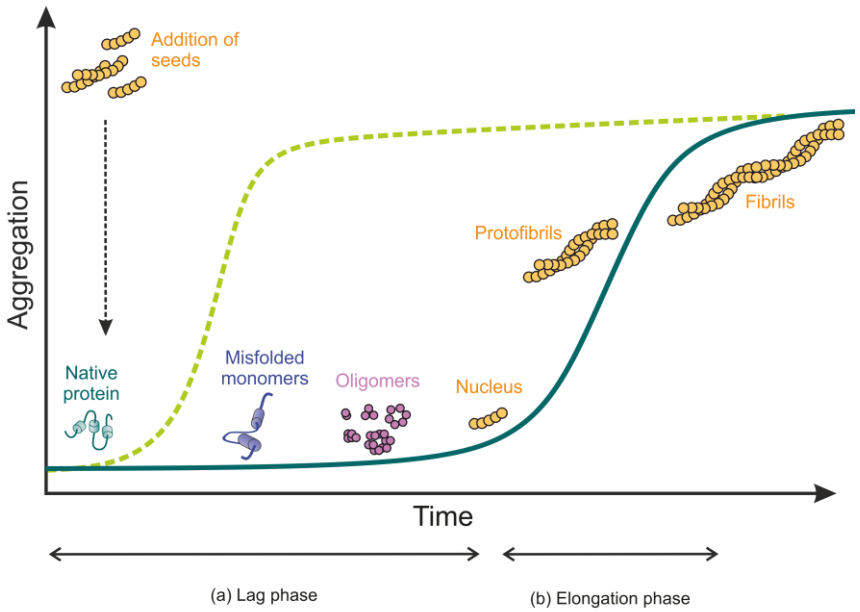

Figure 1.4 A schematic representation of the nucleated growth model of amyloid formation and the species populated en route to fibril formation. The formation of fibrils proceeds via two distinct phases; **(a)** the nucleation phase or "lag-phase" and **(b)** the elongation phase (solid line). The lag phase corresponds to a thermodynamically-disfavoured nucleation event, which is the rate limiting step that proceeds the rapid, thermodynamically-favourable elongation phase. The addition of "seeds", i.e. an elongation competent nucleus, to the beginning of the reaction, abolishes the rate limiting nucleation step and dramatically decreases the lag-time, templating fibril growth (dashed line). Redrawn and adapted from[76].

Although the primary nucleation step is required for the initiation of amyloid fibril growth it is not the only process that contributes to the creation of new filaments. Secondary processes exist where the creation of new fibrils is dependent on the existing aggregate population[75, 77] (**Figure 1.5**). Fibril fragmentation is one such example, where each fragmentation event increases the number of aggregation-competent ends and initiates new growth, leading to an exponential proliferation of fibrillar species[78-80]. Secondary nucleation is also possible, where the surface of existing filaments catalyses the formation of new aggregates, accelerating the rate of fibril formation via a positive feedback mechanism. These processes can contribute to both the observed lag phase and the subsequent fibril growth[77, 79]. Some recent *in vitro* studies of the aggregation of the 40 and 42 residue variants of the amyloid-β (Aβ) peptide revealed that, in both cases, rapid proliferation of aggregates is dominated by secondary nucleation[78, 81], where the formation of aggregates becomes exponential, due to the positive feedback mechanism upon the formation of fibrils. These additional aggregation mechanisms could be important in the progression of the disease, and the proliferation of toxic species between cells, and therefore indicates that therapeutic approaches may need to be considered to target fibril-catalysed secondary processes rather than (or in addition to) primary nucleation.

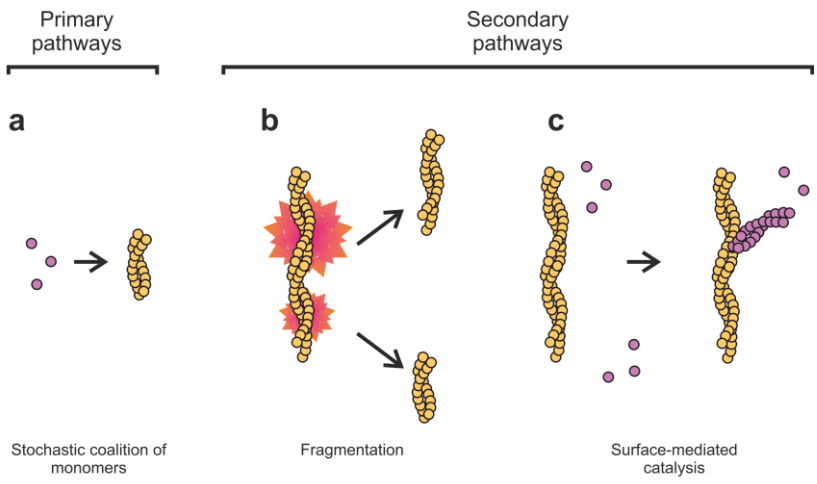

Figure 1.5 A schematic representation of the main primary and secondary processes that contribute to fibril formation. **(a)** Primary nucleation results in the formation of new aggregates from stochastic interactions of monomers. Secondary pathways depend on the pre-existence of aggregate and can enhance the fibrillation kinetics via a number of ways; fragmentation events **(b),** which produces new, elongation competent ends for further fibrillation and **(c)** surface-catalysed events, where new aggregate formation is dependent on the concentration of preformed fibril. Figure redrawn and adapted from [77].

1.2.4 Structure of amyloid fibrils

Amyloid fibrils formed from different protein sequences share remarkably similar structural features on the nanometer scale[3, 82]. Using imaging techniques such as transmission electron microscopy (TEM) or atomic force microscopy (AFM), amyloid fibrils appear as long, unbranched polymeric assemblies, often several microns in length[1, 3].

The core of the fibril is made up of an array of either parallel or anti-parallel β-strands, stacked perpendicular to the length of the fibril and held together in a highly ordered arrangement by backbone hydrogen bonds. This arrangement is known as cross-β and produces the characteristic X-ray fibre diffraction pattern observed for a large number of fibrils[15, 82, 83] (**Figure 1.6 a**). The pattern shows intense reflections at ~4.7 Å and 10 Å indicating the regular spacing of both the intra-sheet β-strand packing and the inter-sheet distances between two associating β-sheets, in the formation of the mature fibril (**Figure 1.6 b**). Fibrils usually consist of several protofilaments, which can associate in a number of ways (**Figure 1.6 c**), often by twisting together to form rope-like fibrils or through lateral associations to form ribbon-like structures that can be up to 30 nm in width[3, 82, 84-87].

Amyloid fibrils are also known to display universal dye binding properties. As well as exhibiting enhanced birefringence under polarised light upon Congo red binding[88], amyloid fibrils exhibit a conserved ability to bind aromatic dyes such a Thioflavin T (ThT), leading to enhanced fluorescent properties of such compounds[88-90]. This property, therefore, is often used to monitor fibril formation *in vitro* and further serves as an indication of the generic features shared by amyloid fibril structures.

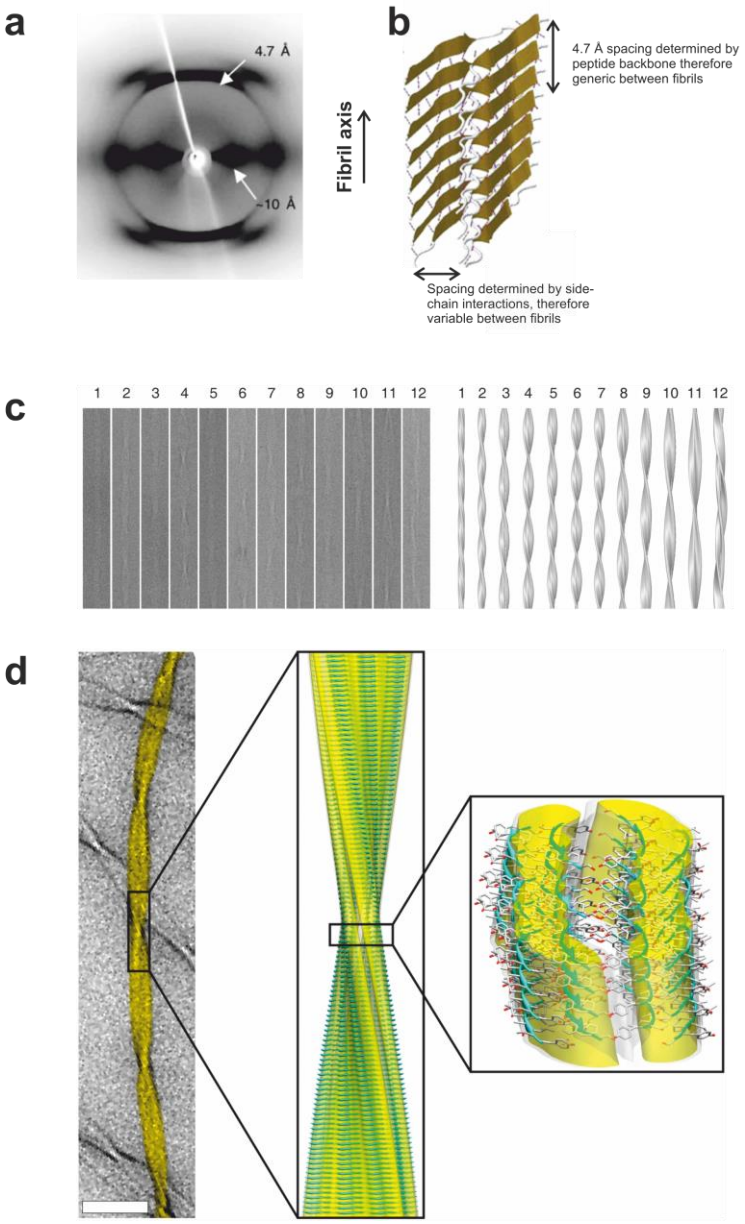

Figure 1.6 Structural characteristics of amyloid fibrils. **(a)** Amyloid fibrils display generic cross-β architecture. A typical X-ray diffraction pattern from fibrils formed from islet amyloid polypeptide (IAPP) is shown, with the characteristic reflections at 4.7Å and 10Å indicated[83]. **(b)** A cartoon representation of the cross-β structure inferred from the X-ray diffraction data. Spacing between β-strands is determined by the backbone hydrogen bonds and is consistently 4.7Å, whereas the spacing between β-sheets is more variable owing to side chain interactions. Taken from [1]. The direction of the fibril axis is indicated by a single headed arrow. **(c)** Cryo-EM reconstructions illustrating the variation in protofilament assembly leading to extensive structural polymorphism in amyloid fibrils[87]. **(d)** Example of a high-resolution fibril structure. The twisted morphology of the fibrils formed from the 11-residue fragment of transthyretin (TTR) as visualised by TEM (left). This technique, coupled with cryo-EM, allowed for reconstruction of the fibril (centre). Additional ssNMR data then allowed determination of the fibril structure at the atomic level (right) illustrating the hierarchical organisation of the amyloid fibril[91]. Images adapted from references where indicated.

Knowledge of the detailed molecular structures of amyloid fibrils is becoming increasingly available owing to recent developments in cryo electron microscopy (cryo-EM)[91, 92] and solid state NMR spectroscopy (ssNMR)[91, 93-95]. Recently, an atomic level structure of a fibril formed from the 11-residue variant of transthyretin (TTR) was demonstrated (**Figure 1.6 d**) revealing the intricate details of the packing interactions which facilitate in the formation of the hierarchical assembly of β-strands, into protofilaments, filaments and the mature fibril[91]. These techniques, therefore, have allowed confirmation of the general characteristics of the overall structure of the fibrils, which is indeed attributed to the hydrogen bonding pattern of the polypeptide core[1]. It also confirms the basis of structural variation seen between fibrils, which results from the manner by which side-chains are incorporated into the fibrillar architecture[3, 96], leading to polymorphism.

Structural polymorphism is not limited to fibrils formed from different protein precursors and seems instead to be an inherent feature of amyloid formation. Fibrils composed of the same precursor can exhibit entirely different packing arrangements within the fibril core. For example, fibrils formed from the 40-residue variant of Aβ (discussed in more detail in Section 1.3.4.3) have demonstrated the ability of a common precursor protein to form structures with entirely different organisations of the β-strands. For the most part Aβ40 fibrils form a parallel, in-register arrangement of β-strands, however, out of register and completely anti-parallel structures have been suggested in some cases[97-99]. Structural analysis of more than 30 amyloid forming peptides – fragments from full-length amyloidogenic proteins such as Aβ, tau, prion protein (PrP), insulin, α-synuclein among others[100], demonstrated that, although all fragments share the same cross-β spine, structural variations exist that expand the range of architectures available to a single protein species and could form the basis for different biological properties seen by different polymorphs. This same structural polymorphism is also seen for a number of larger amyloid forming sequences[97, 101-105] many of which are associated with disease states and therefore suggests a role for different morphologies in specific disease progressions. Distinct morphologies of fibrils, found present in the brains of Alzheimer's patients with entirely different clinical histories, indicates a role for polymorphism *in vivo,* that might correlate with variations in the disease[106].

In vitro studies also indicate that polymorphism can significantly alter the biological properties of amyloid assemblies[101-103, 107-114]. Two fibrillar polymorphs of α-synuclein (the amyloidogenic protein associated with Parkinson's disease) show entirely different abilities to propagate the formation of further aggregates, in the process commonly referred to as "seeding"[113]. This difference in ability to template further aggregation could have a

dramatic influence on the progression of the disease state. A current leading hypothesis in the field is that amyloid seeds can have prion-like infectivity[115, 116], where aggregates may initially form in only a small number of cells, before fragmentation and spreading to distinct regions of the brain. If the distinct structural morphology of a fibril determines the seeding ability, polymorphism would play a key role in the "aggressiveness" of a disease and possibly the variations in symptoms seen between patients[106]. Targeting distinct structural morphologies, therefore, may be critically important in treating amyloid disorders, as well as in identifying the key assemblies responsible for propagation and toxicity.

1.2.5 Other structures of the amyloidogenic pathway

Within the lag phase of amyloid fibril formation (**Figure 1.4**), a vast array of oligomeric, intermediate states can exist. These thermodynamically-stable intermediates may be formed both on- and off-pathway to mature fibrils, but detailed characterisation of the distinct oligomeric species formed has been a major challenge in the field, owing to their heterogeneous and transient nature. Insights into these structures, their formation and characteristics has been the focus of much research, as it is the general consensus that these oligomeric intermediates act as the main toxic entity in amyloid disorders, rather than the mature fibrils[54, 117-121].

Formation of soluble oligomers is common to all amyloid forming systems and it was proposed previously that conserved features of these intermediates may contribute to a generic pathogenic mechanism between amyloidoses[122, 123]. This hypothesis was supported by the finding that oligomers, characterised from a range of different amyloidogenic precursors, were found to display common features; being generally spherical, between 10-70 nm in diameter and crucially, recognisable by a conformational-specific antibody, A11[123]. These "A11-positive" oligomers are significantly more toxic to cells than fibrils of the same precursor[123]. Importantly, oligomeric aggregates formed from proteins not previously associated with any misfolding disorder, were also shown to be cytotoxic[122], furthering the idea that toxicity imparted by soluble, pre-fibrillar aggregates is an inherent property of protein aggregation.

Although the current consensus still implicates oligomers as more toxic entities than fibrils, it has become clear that the mechanisms underlying oligomer toxicity are more complicated than a single conserved feature. A vast number of structures have been discovered with

various degrees of toxicity, which can be broadly characterised based on their overall morphology[124]. The A11-positive oligomers represent one class of structures often termed pre-fibrillar, whereas the second major class, termed fibrillar, are expected to contain a higher degree of β-strand content and possess more structural similarity with the mature fibril. These oligomers are recognised by a second conformational-specific antibody, OC, which also recognises mature fibrils[125]. Owing to the lack of high resolution oligomer structures, these two antibodies serve as a convenient method of classifying intermediates, based on their underlying structural organisation, rather than size. Fibrillar oligomers (OC-positive) have been found ranging from dimers, up to >500 kDa in size[125], whereas A11-positive, pre-fibrillar oligomers range from approximately tetrameric to ~75 kDa[125]. This suggests that the two oligomer types are formed as part of two distinct pathways to aggregation (**Figure 1.7**), rather than the pre-fibrillar oligomers preceding the formation of the fibrillar oligomers. One pathway involves the direct formation of fibrillar oligomers (OC-positive) from monomers, which may represent seeds or nuclei that can directly elongate to form fibrils. The alternative pathway involves the formation of pre-fibrillar (A11-positive) oligomers which may need to undergo a conformational change to become a competent nuclei for monomer addition and fibril formation. With oligomeric assemblies able to readily interconvert[126], these simplified models may represent only two of an infinite number of possible pathways. Clearly more detailed insights into the various structures are required to allow further understanding of the mechanisms of amyloid formation and to elucidate any general toxic species.

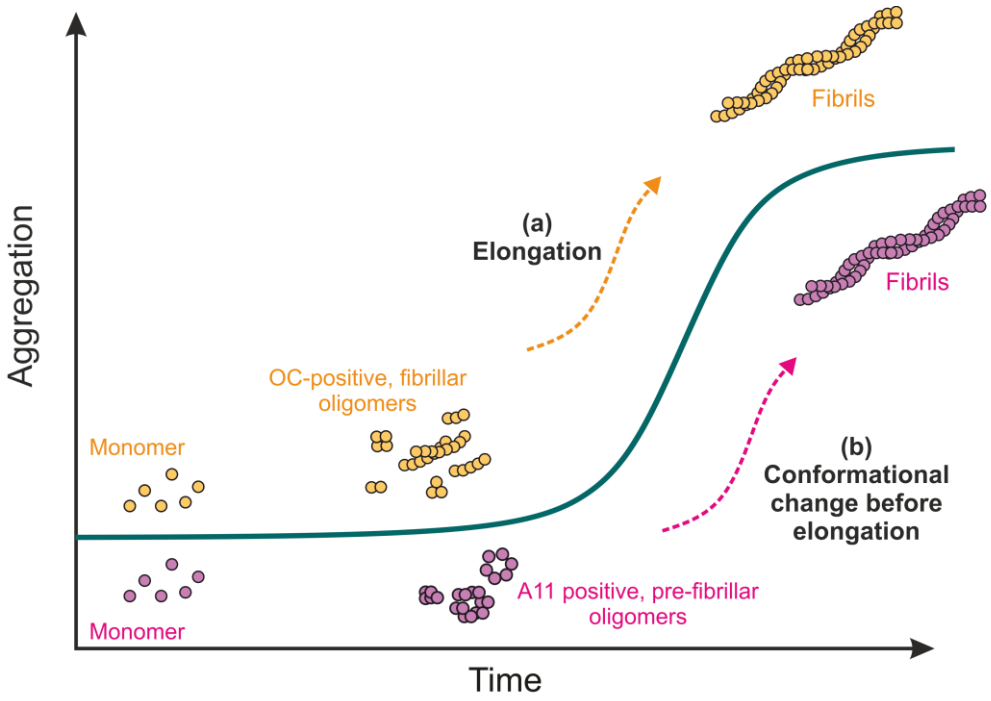

Figure 1.7 Schematic representation of two possible amyloid forming pathways. The existence of two distinct oligomer populations with differential reactivity to conformation-specific antibodies A11 and OC indicate two possible pathways to mature amyloid fibril formation; **(a)** where fibrillar oligomers (OC positive) elongate by simple monomer addition and **(b)** where pre-fibrillar, A11 oligomers undergo a conformational change before elongation. Figure redrawn and adapted from [124].

1.2.6 Amyloid formation and disease

A number of diseases result from the incorrect folding of proteins, one class of which involves ordered association that leads to the formation of amyloid deposits. Several of these amyloid diseases are neurodegenerative, where aggregates specifically accumulate in the brain and exert their toxic effects. These include the two most prominent forms of dementia, Alzheimer's disease and Parkinson's disease[127]. There are also several examples of non-neuropathic amyloidoses, which can specifically target a single organ (localised) or effect several areas of the body (systemic). Some of the main examples of amyloidoses are given in **Table 1.1**.

Disease	Precursor protein	Organ-specific/ Systemic (organ affected)	Extracellular amyloid deposits/ intracellular inclusions	Clinical features	Ref
Neurodegenerative					
Alzheimer's Disease	Amyloid-β (Aβ) peptide	Organ-specific (brain)	Extracellular	Progressive dementia	128
Alzheimer's Disease	Tau	Organ-specific (brain)	Intracellular	Progressive dementia	128
Parkinson's Disease	α-synuclein	Organ-specific (brain)	Intracellular	Movement disorder	129
Dementia with Lewy bodies	α-synuclein	Organ-specific (brain)	Intracellular	Dementia and motor problems	130
Transmissible spongiform encephalopathies	Prion protein	Organ-specific (brain)	Extracellular	Dementia, ataxia and psychiatric problems	131
Huntington's disease	Poly-Q expanded huntingtin	Organ-specific (brain)	Intracellular	Dementia and motor problems	132
Amyotrophic lateral sclerosis	Superoxide dismutase 1	Organ-specific (brain)	Intracellular	Movement disorder	133
Non-neuropathic					
Amyloid light-chain (AL) amyloidosis	Immunoglobulin light chain	Systemic	Extracellular	Renal failure	134
Dialysis related amyloidosis	B_2-microglobulin	Systemic (joints)	Extracellular	Renal failure and paraplegia	135
Lysozyme amyloidosis	Lysozyme	Systemic	Extracellular	Renal failure	136
Transthyretin amyloidosis	Transthyretin	Systemic	Extracellular	Peripheral neuropathy	137
Fibrinogen amyloidosis	Fibrinogen α-chain	Systemic	Extracellular	Renal failure	138
Type II Diabetes	Islet amyloid polypeptide (IAPP)	Organ-specific (pancreas - Islets of Langerhans)	Extracellular	Insulin deficiency and resistance, hyperglycaemia	139

Table 1.1 Examples of the major human disorders associated with amyloid deposition.

Exactly how aggregates exert their toxicity in different disease systems is not well understood but is thought most likely to occur through a gain of toxic function[3]. This is likely as a generic mechanism owing to the fact that non-disease related proteins can form amyloid structures that are inherently toxic[122]. There is currently no single consensus between amyloid disorders, in fact it is most likely that toxicity is mediated through a complex network of dysfunctions.

Several disorders are associated with extracellular aggregation (**Table 1.1**). These aggregates have been shown to activate signal transduction pathways (**Figure 1.8 i**), leading to apoptosis, and thus present a possible generic gain of function mechanism for disease-related amyloid deposits. For example, RAGE (receptor for advanced glycation end products) is a surface receptor which has been shown to interact with amyloid fibrils composed of several precursor proteins, including Aβ, IAPP and PrP[140, 141], leading to activation of cellular stress responses and immune responses.

Another possible strategy of amyloid-mediated toxicity is membrane disruption (**Figure 1.8 ii**). Amyloid-membrane interactions are well documented[142-148] and have been shown to lead to a perturbation of normal cellular activity, membrane damage and even complete rupture[147, 149-154]. This, too, is independent of precursor sequence and again could be a generic mechanism shared by several amyloidoses. Oligomers, formed from many amyloid precursors[54, 155-160] have been found to form pores in cellular membranes (**Figure 1.8 iii**), leading to problems with signal transduction, ion homeostasis and resulting in apoptosis or necrotic cell death. Unstructured monomers of IAPP and α-synuclein have also been shown to embed within the lipid bilayer[151, 161, 162] where amyloid formation proceeds and causes membrane disruption.

As discussed in Section 1.2.2, the cell has developed many strategies to deal with the accumulation of aggregates. Therefore, a possible universal toxicity mechanism could involve the sequestration of essential cellular components (**Figure 1.8 iv**), such as chaperones, leading to a competition for these components and a depletion of cellular resources. In one example, conducted in a yeast model of Huntington's disease, cytosolic huntingtin inclusions were found to sequester the molecular chaperone Sis1p, inhibiting the clearance of further, non-amyloid inclusions of unrelated proteins, which formed as a result of the disturbance of the protein quality control system. This chaperone competition mechanism could indeed apply to all amyloid disorders, especially in the case of age-related diseases where mechanisms of proteostasis are already in decline[163-165].

Because the native fold is usually essential for a protein to function (except in the case of intrinsically disordered proteins), most proteins will lose their ability to function upon misfolding and aggregation. Loss of function mechanisms could account, therefore, for the toxicity in some amyloidoses (**Figure 1.8 v**). This could be through aberrant interactions with any number of unrelated proteins, leading to a loss of function of the co-aggregate[166] (**Figure 1.8 vi**). Toxicity could also be attributed to the loss of biological function, specifically of the amyloidogenic protein in question. In Huntington's disease, the huntingtin protein is thought to play a protective role against apoptosis[167] and disturbance of this biological function may therefore lead to premature loss of neurons. In amyotrophic lateral sclerosis (ALS), the misfolded superoxide dismutase 1 (SOD1) is no longer able to turn over superoxide anions and therefore leads to a build-up of superoxide radicals[168]. For both of these diseases the mechanisms are still unclear[168, 169] and there are arguments contradicting the loss of function hypotheses in each case[167, 169]. In general, the toxic gain of function mechanism, possibly universal between the many amyloid disorders, is considered more likely.

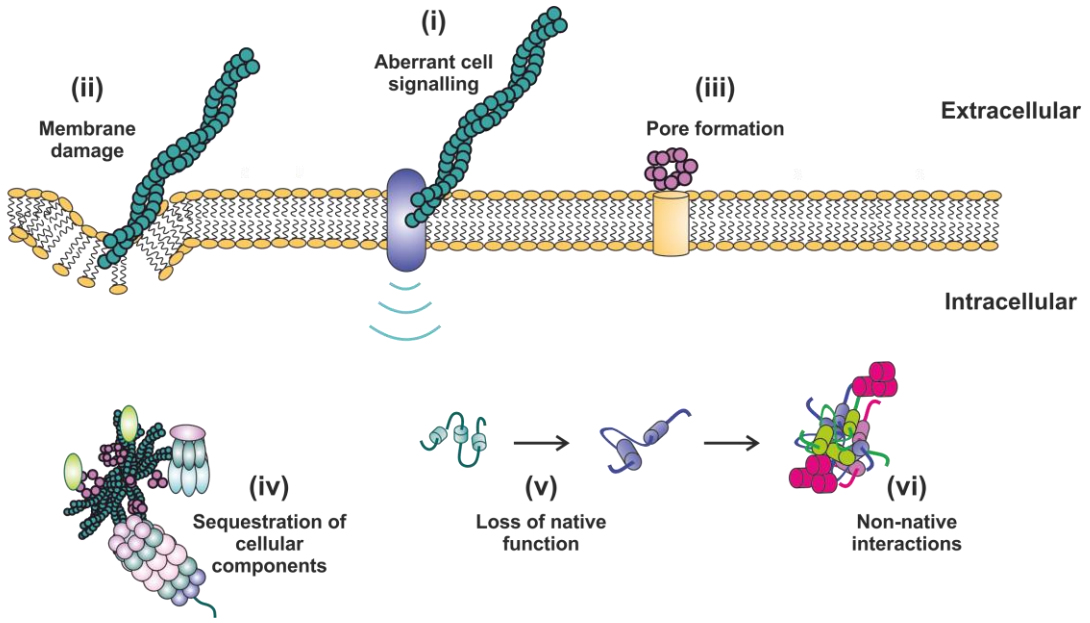

Figure 1.8 Mechanisms of amyloid toxicity. Many disorders are associated with extracellular aggregation which can exert toxicity via aberrant activation of cell signalling pathways **(i)** or membrane perturbation or rupture **(ii)**. Oligomeric aggregates formed on pathway to amyloid fibrils can exert cytotoxicity via pore formation **(iii)**. Possible toxic mechanisms of intracellular aggregates include sequestration of cellular components such as chaperones and other proteostasis machinery **(iv)**. Alternatively, aggregation could lead to a loss of native function of the amyloid precursor itself **(v)** or of other essential proteins, through non-native co-aggregation **(vi)**.

1.2.7 Therapeutic approaches to amyloid diseases

Owing to the many potential mechanisms underlying amyloid toxicity, the development of therapeutic strategies to intervene in these disorders is extremely challenging. A deeper understanding of the mechanisms involved is therefore the first major requirement to enable the development of suitable intervention strategies. Equally, the identity of the toxic species remains elusive, further hindering the search for effective therapies. Due to the complexity of the aggregation pathway, a number of plausible therapeutics are under review, as discussed below.

1.2.7.1 Inhibiting the production of the amyloid precursor

Perhaps the most obvious route to prevent aggregation is in reducing the level of the amyloid-competent protein in the cell. This strategy may not be feasible in cases where the amyloid precursor is required for function, but when the precursor is a by-product of abnormal processing of a larger, functional protein (as is the case for almost half of the known amyloid diseases[170]) it may prove effective. In the case of Alzheimer's disease (covered in detail in Section 1.3) the abnormal processing of the amyloid precursor protein (APP) leads to the formation of the aggregating peptide Aβ. Targeting the enzymes involved in this processing event, therefore, has been an attractive intervention strategy for many years. However, the challenge in this endeavour is modulating the abnormal process without disruption of the formation of functional fragments[171] or effecting the enzymes' ability to cleave alternative substrates[128, 172]. A phase III clinical trial of a γ-secretase inhibitor, Semagacestat, was aborted in 2010 due to worsening of cognitive impairment[173] expected to be a result of the inhibition of alternative cleavage events.

In diseases where the precursor is formed from the full-length protein, inhibition of expression with RNA interference (RNAi) may be plausible. Short, double stranded RNA molecules are introduced into cells to silence specific genes by targeting complementary mRNA for degradation[174-177]. RNA can be introduced with the use of viral vectors, where the vector can integrate into the neuronal genome and be expressed long-term. RNAi has shown promise in a number of amyloid disorders[177-180] but the delivery of such therapies across the blood brain barrier (BBB) is a challenge[181] and may only be feasible in disorders

that effect a small region of cells (such as Parkinson's) where vectors could be injected directly.

1.2.7.2 Stabilising the native protein

In the case of disorders where the precursor is a functional peptide or protein, stabilisation of the functional state may be a promising strategy. To date, only one commercially available treatment for an amyloid disorder exists, which works by stabilising the functional tetramers of transthyretin (TTR) in the neurodegenerative disorder, Familial amyloid neuropathy (FAP). In the disease state, the native tetramer dissociates, whereupon the partially unfolded monomers subsequently form amyloid aggregates[182, 183]. The Kelly group therefore developed a "pharmacological chaperone" Tafamidis; a small molecule which binds and kinetically stabilises the folded tetramer, preventing monomer dissociation, which is the rate-limiting step in TTR misfolding and aggregation (**Figure 1.9**)[184]. In the case of Tafamidis, its discovery was through the use of a structure-based design approach; a method which, unfortunately, is not applicable to the many natively disordered amyloid precursors, as they have no unique structure to target. However, further chemical chaperones have been found able to stabilise prion protein (PrP)[185] and Aβ[186] via alternative means.

1.2.7.3 Inhibition of the formation of toxic aggregates

Linked to the stabilisation of the native fold, inhibition of aggregation and, therefore, the prevention of the formation of toxic species, is an attractive therapeutic strategy for all amyloidoses. Development of ligands able to associate specifically with monomers and prevent aggregation, therefore, is an intense area of research.

Inhibition of fibril formation by the introduction of "β-sheet breakers" has been performed by various research groups. This strategy involves a peptide inhibitor which is able to associate through hydrogen bonding with the aggregate due to a complementary region, but is unable to promote further fibrillation. This could be through the presence of a bulky modification, such as the addition of a steroid at the N-terminus, which has been shown to effectively inhibit further addition of monomers in Aβ aggregation[187]. Alternatively,

substitution of key residues with prolines can reduce β-sheet formation[188, 189]. Similarly, the use of N-methyl modified peptides can be used to block fibril formation[190]. β-sheet breaking methods such as these have been found effective in inhibiting PrP, α-syn, IAPP and poly-Q aggregation *in vitro*[191-195].

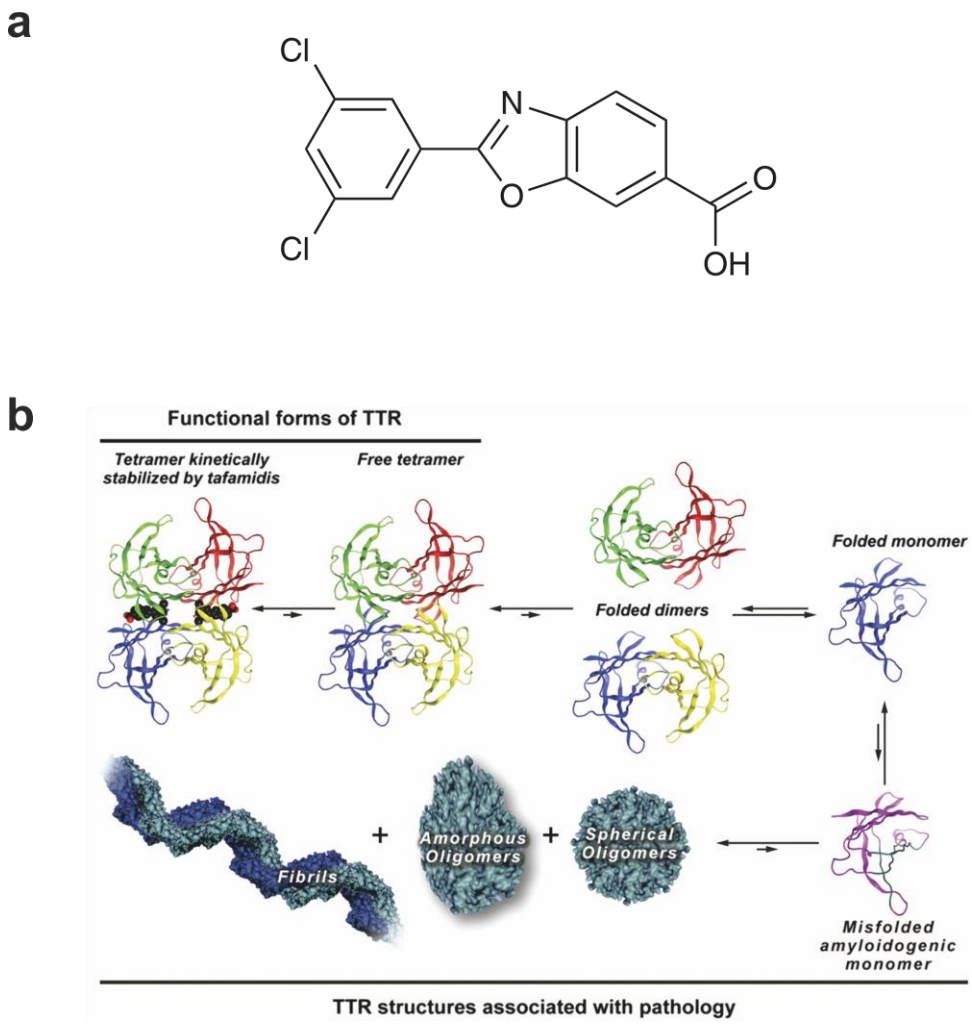

Figure 1.9 Tafamidis stabilises a functional tetramer of transthyretin (TTR) in treating Familial amyloid neuropathy (FAP). **(a)** The structure of Tafamidis. **(b)** The mechanism of action of Tafamidis. Tafamidis binds and stabilises the TTR tetramer (top left), dramatically reducing the dissociation to dimers and inhibiting the cascade to amyloid formation via the misfolded monomer (bottom right). Figure adapted from[196].

Therapeutic antibodies may have value in targeting amyloidoses, despite years of disappointing trials for some disorders (detailed for AD therapeutics in Section 1.3.5).

Antibodies are indeed able to inhibit aggregation[197, 198]. In fact, the A11 antibody, able to recognise an array of oligomeric structures from a variety of peptide precursors, is able to inhibit the toxic effects of the aggregates[123]. A major drawback of these molecules is that they are unable to cross the BBB and have been found to exert toxic side effects due to their immunogenic properties. Recently a small peptide "affibody" (an antibody mimetic which may have better BBB penetration owing to its smaller size[199]) was developed, which was able to bind Aβ with nanomolar affinity and subsequently prevent oligomerisation[200].

Small molecule inhibitors are another promising class of therapeutics in amyloid disorders, with advantages in their small size and therefore broad tissue penetration, lack of immune response and enhanced stability[201]. As all amyloid fibrils have long been known to bind to the dye molecules ThT and Congo red[88], it is unsurprising that an array of further aromatic compounds are able to bind amyloid. In many cases, the molecules are able to interfere with the aggregation process[202-209]. The aromatic rings found in many of these compounds are proposed to interfere with the π-stacking of aromatic residues, thought to be important in fibril formation[197, 210, 211]. Epigallocatechin 3-gallate (EGCG), one of the most well studied amyloid inhibitors, is able to prevent oligomerisation and to disaggregate preformed fibrils formed from Aβ, IAPP, TTR and Sup35, among others [202-208]. A number of small molecule amyloid inhibitors have proceeded to clinical trials[209, 212, 213] and could prove to be a viable approach in targeting these disorders.

Because the identity of the toxic species in unknown in the vast majority of amyloid disorders, targeting the earliest stages of aggregation might be the most promising strategy, as via this approach, all of the potential toxic entities will be prevented from forming. Only when more details of the toxic mechanisms associated with amyloid disease become clear, will the design of therapies targetting single structures from within the amyloid pathway become feasible. Recently, secondary nucleation processes (Section 1.2.3) have been found to be important in the propagation of aggregates[78, 81] and implicated in the formation of toxic species. Polymorphism of fibril structures (Section 1.2.4) has also been associated with different biological effects and may indicate additional routes to the prevention of the proliferation of toxic aggregates[106, 113]. The process of secondary nucleation adds to the complexity of the aggregation pathway and may mean that therapies targeted towards primary nucleation processes (the initial formation of oligomers from sporadic accumulation of monomers) alone, may be ineffective. Therapies targeting fibrillar assemblies, which stimulate these secondary processes may be required, therefore, for efficient inhibition of toxic aggregate formation.

1.2.7.4 Accelerating fibril formation

Mature amyloid fibrils are often considered the inert end-point of aggregation, as they have been found to be less cytotoxic than their oligomeric precursors[172]. This observation has led to the investigation of an alternative therapeutic approach, involving acceleration of aggregation towards the less toxic fibrils, therefore reducing the population of oligomers. Indeed, a peptide able to recognise Aβ and accelerate its aggregation was shown to reduce toxicity *in vivo*[214]. Although an interesting concept, there remains substantial evidence that fibrils exert toxic mechanisms of their own[149, 150, 215] and this should be considered when applying this approach in practice.

1.2.7.5 Stimulating aggregate degradation

As discussed in Section 1.2.2, a number of cellular mechanisms are in place to deal with misfolding and aggregation. Enhancing the regulatory processes of degradation systems may provide a further, universally applicable therapeutic strategy. Small molecules are currently being developed to enhance cellular chaperone levels and aid clearance of aggregates[216]. Drugs such as Geldanamycin can enhance chaperone levels[216, 217]. Augmentation of clearance mechanisms, through both autophagy and proteasome stimulation, could also be effective strategies, although increasing the turn-over of functional proteins could be a major side effect. Small molecules are under development which facilitate specific degradation of toxic misfolded proteins through the endocytic pathway[218].

A further possible strategy to encourage amyloid clearance is to inhibit stabilising interactions formed between aggregates and accessory molecules. Glycosaminoglycans (GAGs), apolipoproteins and serum amyloid P are a few of several accessory molecules that bind and stabilise fibrils[37, 170]. Disassembly and clearance of fibrils has been promoted through interference of the GAG-amyloid interaction[219], although disaggregation to more toxic oligomeric species could be an issue if these are not effectively cleared.

Owing to a lack of understanding of the toxic mechanisms of amyloid diseases, it has been difficult to design effective strategies for intervention, despite intense research and the numerous promising avenues mentioned above (and summarised in **Figure 1.10**).

Consequently, there is currently a lack of disease-modifying drugs and the available therapeutics act only to ameliorate symptoms[220]. The search for disease-modifying strategies must also be complemented with the development of effective, early-stage diagnostics, as evidence suggests the initial stages of aggregation occur decades before symptoms arise[221]. This suggests that administration of therapeutics when symptoms are already apparent may be futile, as extensive and irreversible damage may already be done.

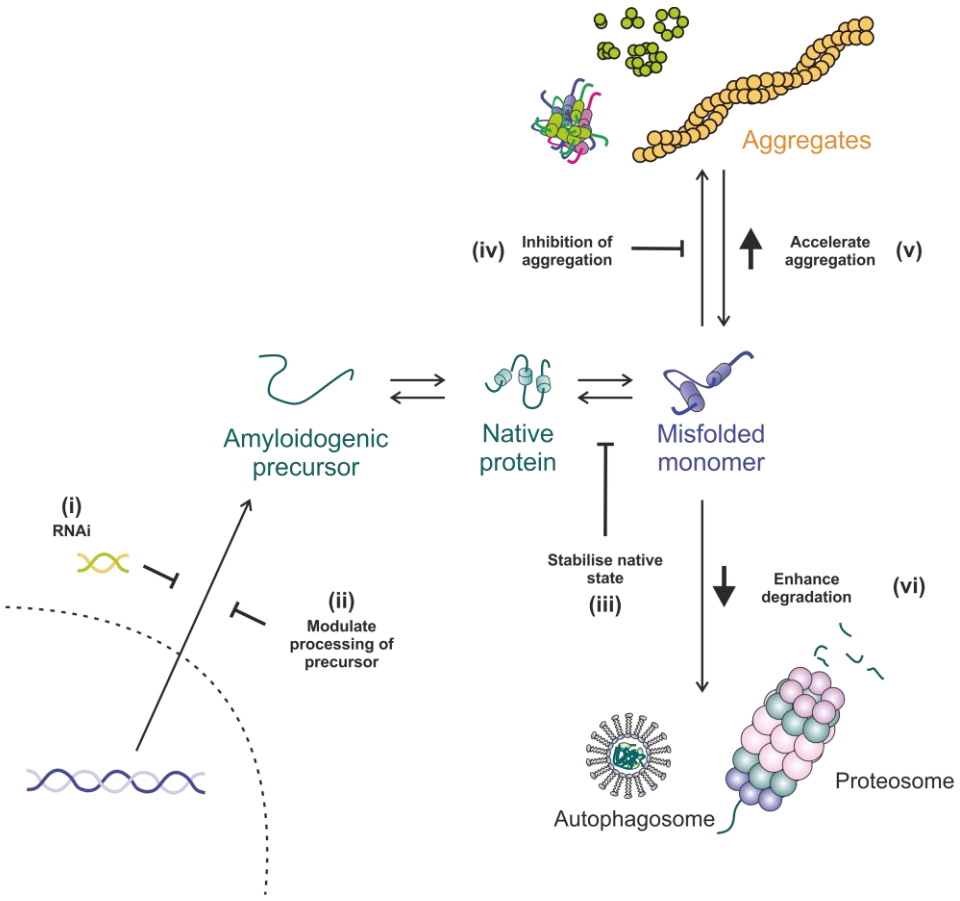

Figure 1.10 Major therapeutic strategies against protein aggregation. Prevention of the initial production of the amyloidogenic precursor peptide can be achieved by RNA interference **(i)** or through modulation of the processing events that give rise to such species **(ii)**. Stabilisation of the native functional state can be effective in preventing unfolding or misfolding **(iii)**. This can be achieved by upregulation of cellular chaperones or via treatment with stabilising small molecules/peptides. An attractive strategy is the inhibition of aggregation from misfolded monomers to potentially toxic oligomeric assemblies or fibrils, via β-sheet blockers, antibodies or small molecules **(iv)**. Conversely, promotion of aggregation to inert species **(v)**, with small molecules that accelerate elongation, can reduce toxicity. Protein aggregation can also be prevented by promoting degradation with the enhancement of proteostasis regulators **(vi)**.

1.3 Alzheimer's disease and Aβ

1.3.1 Alzheimer's disease

Alzheimer's disease (AD) is a debilitating, progressive and incurable neurodegenerative disorder, which is characterised by memory loss, severe cognitive impairment and eventually death[222]. The cognitive decline is accompanied by many behavioural and psychological symptoms, including hallucinations, delusions, apathy, anxiety and depression[223]. The symptoms of AD can differ in severity, yet invariably take a severe emotional toll on the patients and their caregivers. Current estimates indicate that, worldwide, more than 45 million people are suffering with AD[25], a figure that is increasing each year, owing to increased global life expectancy. The socio-economic burden associated with AD, therefore, is vast and the current worldwide cost in estimated to be in excess of $604 billion per annum[28]. These statistics emphasise an urgent need for advances in the effective prevention, treatment and diagnosis of this grave disorder.

As already mentioned (Section 1.2.6), Alzheimer's disease is an example of an organ-specific, neurodegenerative amyloid disorder and involves the aggregation of two major precursor proteins[224]: the amyloid β (Aβ) peptide (Section 1.3.2) which is found in extracellular deposits known as amyloid plaques[21] and tau, a microtubule-associated protein which forms intracellular, neurofibrillary tangles[225]. Together, these two amyloid assemblies are considered the pathological hallmarks of Alzheimer's disease[226] (**Figure 1.11**).

Tau is a neuronal, microtubule-associated protein, predominantly concentrated in axons[227]. It has several roles in stabilising microtubule structure[228], modulating microtubule-dependent transport of organelles and biomolecules[229] and is expected to play a role in apoptosis, through stabilisation of apoptotic factors upon phosphorylation[230]. However, hyperphosphorylation of tau has been implicated in the onset of AD, due to the enhanced aggregation propensity of the phosphorylated precursors, and its loss of function[228]. As work in this thesis targets the assemblies derived from the Aβ component of AD pathology, the remainder of this introductory section will focus on this peptide, although it should be noted that in the context of developing new therapies for this disorder, both tau and Aβ should be recognised as major molecular players[228].

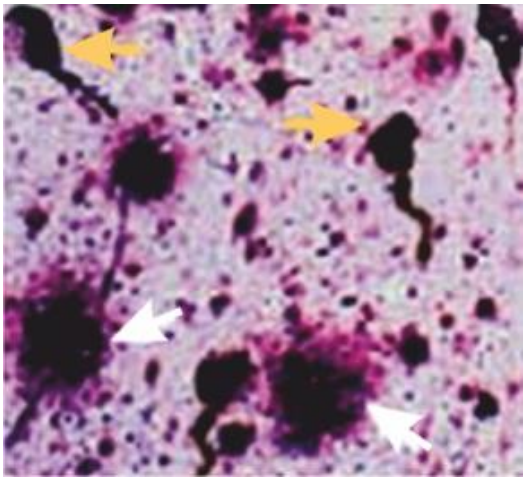

Figure 1.11 Extracellular amyloid plaques and intracellular neurofibrillary tangles are pathological hallmarks of AD. Post-mortem neuropathological analysis of AD brain. Extracellular amyloid deposits, composed primarily of Aβ, are indicated with white arrows. Cytoplasmic neurofibrillary tangles, composed of tau aggregates, are indicated by yellow arrows. Figure taken with permission from [168].

1.3.2 The Aβ peptide

Aβ is a 4.5 kDa peptide derived from the sequential enzymatic processing of the amyloid precursor protein (APP), via the action of β and γ secretases[231]. APP is a large membrane spanning protein, which has been found to be expressed across a range of cell types, yet its biological function remains largely unknown[232]. Within the central nervous system it is thought to be associated with cell adhesion, neuronal migration and synaptic transmission[233-235]. APP processing can proceed via two pathways, one of which is amyloidogenic, where Aβ is produced, and the other is non-amyloidogenic (**Figure 1.12**). The non-amyloidogenic route is the predominant pathway, where APP is initially cleaved by the α-secretase and subsequently the γ-secretase, resulting in the formation of fragments sAPPα, CTFα, AICD and p3. The cellular functions of these cleavage products are currently unclear[236]. The alternative, amyloidogenic route proceeds via an initial cleavage by the β-secretase (BACE1) enzyme, producing a shorter variant of the extracellular domain (sAPPβ). The longer transmembrane domain produced by this cleavage event is then further processed by the γ-secretase at various sites, producing Aβ peptides ranging in length between 39-43 residues. The two major forms (**Figure 1.13**) are produced by cleavage at positions 40 and 42. The resulting Aβ peptides are amphipathic, with a central

hydrophobic region known to be critical for amyloid formation[237-240]. The peptides also consist of a charged N-terminus and a hydrophobic C-terminal domain. The biological functions of the Aβ peptides remain unknown, although it has been proposed that Aβ40 could be involved in the modulation of synaptic transmission[241].

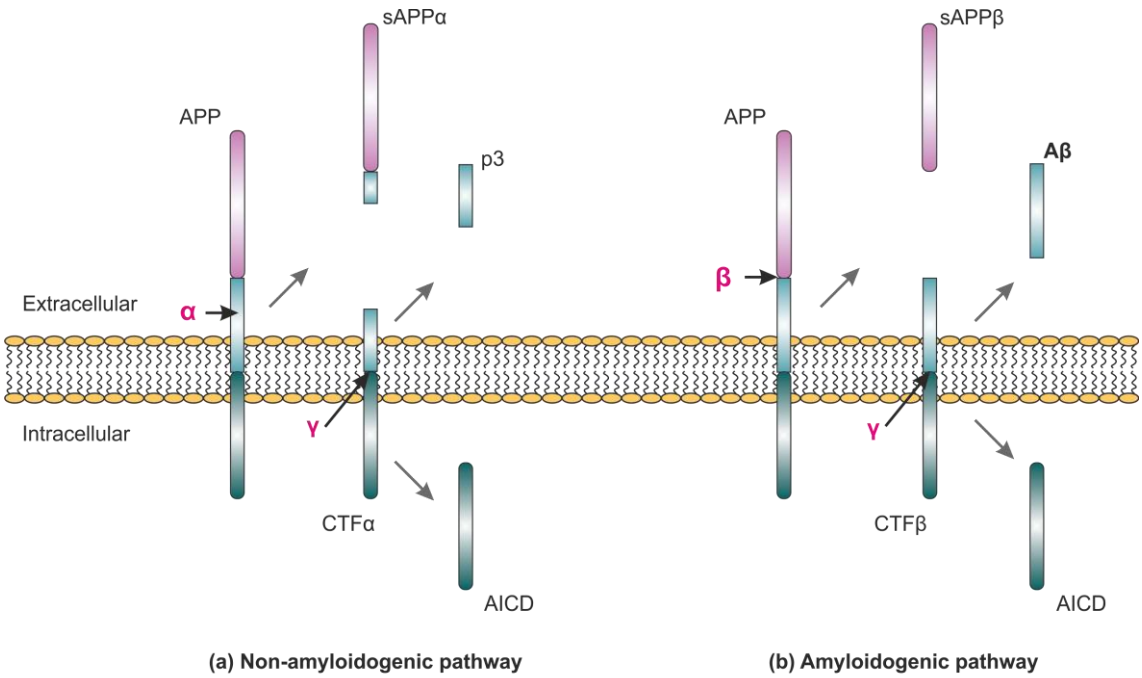

Figure 1.12 Pathways of APP processing. The majority of APP is processed via the non-amyloidogenic pathway **(a)**, with the action of α and γ secretases, producing non-amyloidogenic peptide fragments sAPPα, p3 and AICD. Alternatively, APP can be processed by cleavage with β and γ-secretases via the amyloidogenic pathway **(b)** producing the toxic Aβ peptide. Figure redrawn and adapted from [242].

Although Aβ40 is the predominant form of Aβ in the brain, cerebrospinal fluid and serum[243], Aβ42 is the subject of the most interest in AD pathology as it has higher aggregation propensity[244], owing to the additional hydrophobic residues Ile41 and Ala42. Aβ42 has been shown to be more toxic to neuronal cells[245-247]. The longer variant Aβ43, (with an additional Thr at position 43) is often overlooked, but has been reported to occur in equal abundance to its more well-known relatives, specifically within the dense plaque cores[248]. It has also been shown to be more amyloidogenic and neurotoxic than the 42 residue variant[249].

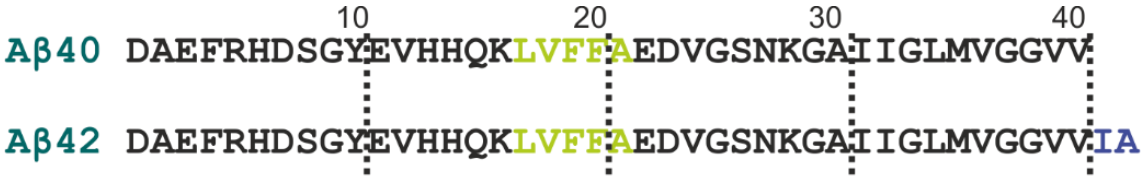

Figure 1.13 The amino acid sequences of Aβ40 and Aβ42. The additional hydrophobic residues Ile41 and Ala 42 are highlighted blue. The central hydrophobic region (residues 17-21) is highlighted green.

1.3.3 The amyloid cascade hypothesis

The amyloid cascade hypothesis has been central to AD research for more than 20 years and posits that the deposition of the Aβ peptide in the brain parenchyma is the critical event which ultimately leads to the onset of the disorder[250, 251]. Since the discovery of Aβ as the major component of AD plaques in the mid 1980s[21], substantial evidence has been presented to further support the role of Aβ in AD. The discovery that AD could be inherited in an autosomal dominant manner was a seminal event in AD research, as the mutation described[252] occurred within the gene encoding the Aβ precursor, APP. Further mutations have been found, subsequently, within genes that regulate the processing of APP, namely presenillin genes 1 and 2[253-255], which code for proteins involved in the regulation of the γ-secretase cleavage event, leading directly to Aβ production[256]. Duplication of chromosome 21 in individuals with Down's syndrome, which carries several genes involved in Aβ production, including APP itself, is thought to result in the early onset of AD in these patients, typically around age 40[257]. Further, mutations in genes that encode proteins thought to be responsible for efficient Aβ clearance[258-261] can reduce the age of disease onset. These mutations all ultimately increase Aβ production, or disrupt the balance between production and clearance, and therefore add further credence to the central amyloid hypothesis.

1.3.4 Neurotoxic assemblies of Aβ

As with all amyloid forming reactions, a vast number of intermediate structures can be populated en route to the final fibrillar aggregates that are deposited in senile plaques in

AD. The nature of the toxic assembly, that which causes the neuronal loss and synaptic dysfunction associated with AD, is the subject of much debate in the field[1, 24, 126].

The Aβ peptide itself exists as a natively unstructured monomeric entity, although some molecular dynamics (MD) simulations suggest that Aβ42 possesses a more constrained C-terminus than Aβ40, forming a β hairpin, which may be responsible for this variant's higher propensity to form amyloid[262]. Both major Aβ peptides (Aβ40 and Aβ42) are able to form an array of higher-order structures, enhanced through various stimuli, including most importantly, an increased concentration of the precursor peptide[263]. The amyloid forming pathways are apparently distinct between Aβ40 and Aβ42 since the dominant oligomeric species formed by Aβ42 are larger than those formed from the 40 residue peptide[264, 265].

1.3.4.1 Aβ oligomers

A wealth of evidence has been presented to support the hypothesis that it is the soluble, non-fibrillar oligomers that lead to synaptic toxicity in AD (reviewed in[266]) and provides a possible explanation for the apparent lack of correlation between amyloid plaque load and disease severity[267]. Within the lag phase of Aβ amyloid assembly, a large range of species from dimers[268], trimers[269] up to 56 kDa assemblies[270-272] have been reported and characterised. Pentamers (5mers), hexamers (6mers), low number oligomers (LNOs), globulomers (12mers), annular protofibrils, amylospheroids (APSDs) and Aβ40:42 mixed oligomers are further examples of the many species classified[123, 142, 273-278]. All of these species have displayed inhibition of long-term potentiation (LTP) in hippocampal brain slices; the primary experimental model for investigating learning and memory in vertebrates, thought to reflect the early cognition defects in patients with AD[279]. Of these examples, the majority have been shown to bind the A11 antibody and possess a predominantly spherical nature. However, the degree of β-sheet content and whether the assemblies exist on- or off-pathway to mature fibrils differs substantially[126, 280]. Further heterogeneity of Aβ oligomers is derived from the co-aggregation of the full-length peptides with multiple Aβ derived fragments[273, 281]. It is also especially complicated as Aβ oligomeric structures are readily able to interconvert and co-exist[126].

Based on a plethora of *in vitro* and *in vivo* experimental data, it is clear that oligomeric assemblies of Aβ impart neuronal toxicity and, most likely, play a role in the onset of disease. Several oligomeric assemblies have indeed been isolated directly from Alzheimer's brain

tissue[238, 277, 282, 283]. However, a lack of a consistent experimental description of the toxic entity, as well as the fact that the dynamic and transient nature of these intermediates has so far precluded their atomic level characterisation, has hindered the search for the generic features responsible for cell death and limits the suitability of the "toxic oligomer" as a drug target.

1.3.4.2 Aβ fibrils

Despite the reported lack of correlation between fibrillar plaque density and the severity of cognitive impairment[267, 284], at least one study supports the opposite conclusion[285]. The progression from a state of mild cognitive impairment (MCI) to AD has been found to correlate with the quantity of brain amyloid[286]. Similarly, although asymptomatic elderly have been shown to develop plaques, the quantity of the deposits are generally less than seen in AD patients[287].

Fibrils of Aβ40 have also been shown to be cytotoxic *in vitro*[97, 103, 215, 288]. A number of fibrillar oligomers, expected to share the cross-β architecture of mature fibrils, have also been identified and shown to induce cellular defects[215, 288, 289]. Aβ fibrils are able to cause oxidative damage[290] and initiate inflammation[291, 292]. Thus, fibrils remain as likely contributing agents in AD. Fibrillar assemblies of Aβ40 and Aβ42 have also been suggested as instrumental in the generation of potentially toxic oligomers through secondary nucleation mechanisms[77, 78, 293, 294] and depolymerisation[210] (Section 1.2.3).

With the recent advances in cryo-EM and ssNMR, several groups have endeavoured to solve the structure of the Aβ fibril[93, 103-106, 238, 295-299]. As with amyloid fibrils derived from other peptide precursors, a large degree of polymorphism is observed for fibrils formed of Aβ40 and Aβ42, however, the extent to which this is a consequence of differential *in vitro* conditions, rather than a true reflection of polymorphism in disease, remains unclear. Crucially, a recent study by Tycko *et al*. demonstrated the first experimentally derived structure of Aβ40 fibrils seeded directly from AD brain tissue[106]. They describe ssNMR data for fibrils derived from two AD patients presenting different clinical histories and remarkably found evidence that each patient possessed a single, predominant fibril structure that was morphologically distinct between the two brains. In addition, the unique morphology presented for each patient was consistent throughout several regions of that person's brain. This work, therefore, is the first indication that unique fibril morphologies

could be associated with distinct pathologies. It also provides compelling evidence for the prion-like infectivity mechanism of fibrils[116], where the proliferation throughout the brain is a direct consequence of fragmentation and spreading from a common, initial fibril structure. Based on these observations and those presented by others[107, 113] there is clearly merit in studying fibril polymorphism as a general phenomenon.

1.3.4.3 Structural models of the Aβ fibrils

Two *in vitro*-derived Aβ40 fibrils have been described by Tycko and colleagues that have been well defined structurally[93, 103-105]. These fibrils serve as a good model of fibril polymorphism, by indicating the substantial differences in amyloid structures that can result from the assembly of the same precursor peptide, under different aggregation conditions. One morphology is the 'striated ribbon' (2A –**Figure 1.14 a**), which was originally formed under agitating conditions[103] and exhibits a two-fold molecular symmetry as determined by ssNMR. Electron microscopy discerns no resolvable twist for the 2A morphology (constant width = 5.5 ± 0.5 nm) whereas the fibrils formed under quiescent conditions (3Q –**Figure 1.14 b**) display a periodic modulation in width (50-200 nm period, 12 ± 1 nm maximum width) consistent with a periodic twist. ssNMR indicates that the latter morphology consists of a three-fold molecular symmetry with a central cavity along the axis of the fibril. On the single peptide level, both 2A and 3Q fibrils exhibit an in-register, parallel cross-β conformation, with almost identical regions of β-strand, non-β-strand and disordered segments, yet with some key differences in quaternary contacts[104, 105], conformations within the non-β-strand segments (loops) and, of course, the overall symmetry. 2A fibrils contain a salt bridge between residues Asp23 and Lys28, which is absent in 3Q. 3Q instead displays a partial salt-bridge between Lys16 and Glu22. In both fibril types, the N-terminal residues 1-8 are structurally disordered, a feature consistent with other *in vitro* Aβ fibrils[95, 300]. Other key differences in quaternary contacts are highlighted in **Figure 1.14 c** and **d**. Interestingly, the two fibril morphologies exhibit significantly different toxicities in neuronal cell cultures, with the 3Q fibril being the more potent neurotoxin[103]. This raises the possibility that some fibril structures may be more pathogenic than others, which might lead to the discrepancies found in the correlation of disease symptoms and total amyloid deposition, mentioned previously.

Of the two brain-derived fibril morphologies (mentioned in Section 1.3.4.2) also identified by the Tycko group[106], only one was taken forward for full molecular structure determination. This fibril type was seeded from the brain of the patient presenting classic AD with possible, additional Lewy body dementia pathology. It displays the same in-register, parallel β-strand arrangement as most Aβ fibril models described to date[95, 104, 105, 301, 302], but does not have the same 2A or 3Q structure as formed *in vitro* (although it possesses three-fold symmetry - **Figure 1.14 e**). Also, unlike the *in vitro* models, strong NMR signals for the N-terminal residues indicate structural order in these regions. The general strand-bend-strand topology is retained, but involves larger non-β regions and an Asp23-Lys28 salt bridge.

Until recently, the related Aβ42 fibril structure has been poorly defined, despite extensive efforts[95, 303-307]. The first atomic model of a structurally homogenous Aβ42 fibril[299] indicates a distinct triple-parallel β-sheet arrangement (**Figure 1.14 f**), unlike the U-shaped, strand-bend-strand conformation conserved between almost every Aβ40 fibril modelled to date. This S-shaped motif is stabilised by a salt bridge between Lys28 and Ala42, indicating why such a structure may not be stable for Aβ40. Indeed, this Aβ42 fibril morphology was unable to template further fibril formation with Aβ40 monomers, suggesting that there may be unique pathways of misfolding and amyloid formation by Aβ40 and Aβ42. Such differences in the folding pathway of Aβ40 and Aβ42 are consistent with kinetic studies[308, 309] and some recent observations of distinct Aβ isoforms in the brains of AD mouse models[310].

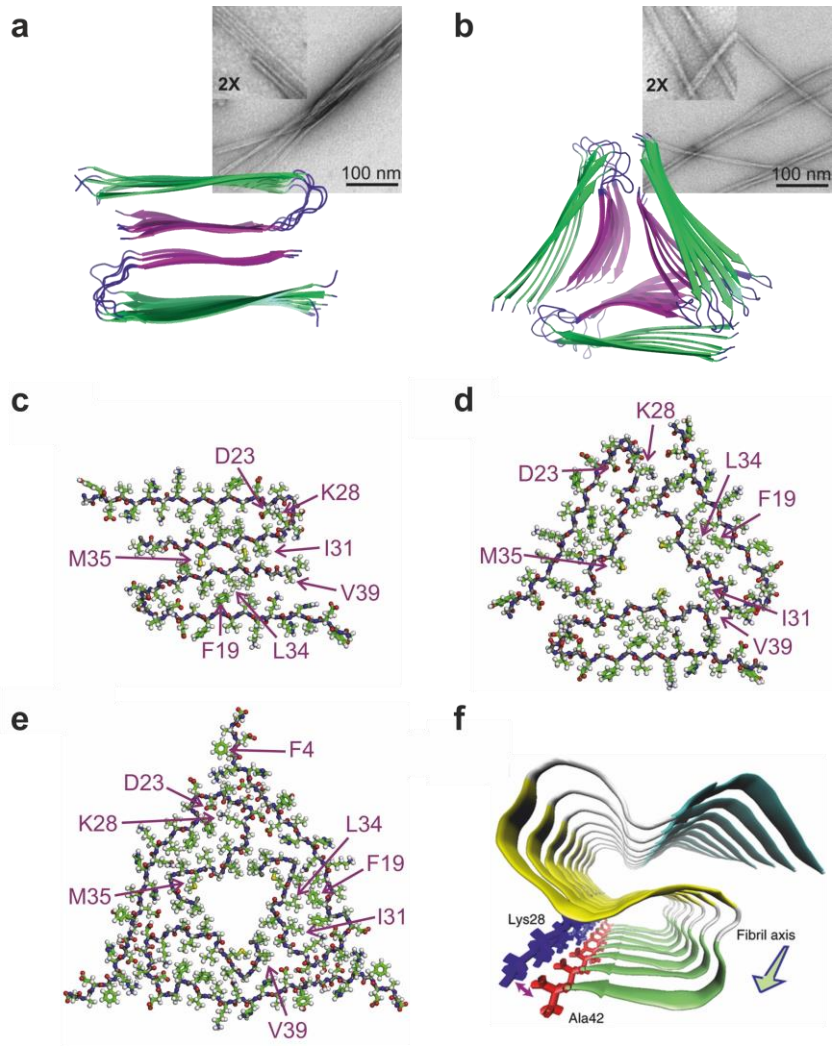

Figure 1.14 Structural models of Aβ fibrils. *In vitro* derived fibrils formed from Aβ40 under agitating (2A, **a**) or quiescent (3Q, **b**) conditions, have been structurally characterised using ssNMR by Tycko and colleagues[103-105] and display 2-fold and 3-fold molecular symmetries, respectively. Cartoon representations of the models are shown with the unstructured residues 1-8 omitted for clarity. Both fibrils are composed of a strand-turn-strand architecture and are shown with the N-terminal β-strand in green and the C-terminal β-strand in pink. Loop regions are represented in blue. The two fibrils present different overall morphologies as visualised by TEM. 2A fibrils present a striated ribbon structure, whereas 3Q fibrils demonstrate a periodic twist. TEM images are inset for each. Key quaternary contacts, that differ between the two fibrils are indicated for 2A **(c)** and 3Q **(d)**[106]. **(e)** The structural model of the *in vivo* derived Aβ40 fibril differs from the two *in vitro* models formed from the same precursor peptide[106]. **(f)** A cartoon representation of the recently elucidated Aβ42 fibril[299] with a unique triple, parallel β-sheet arrangement. The β-strand containing residues 12-18 are in cyan, 24-33 in yellow and 36-40 in green. Short coil or turn regions are in silver and disordered residues 1-10 are omitted. A unique salt bridge between Lys 28 (blue) and Ala42 (red) is indicated. All fibril models are viewed at the fibril cross section, with the axis of the fibril running into the page. Figures taken and adapted from references where indicated.

1.3.5 Current state of therapeutics and diagnostics in AD

Drugs currently approved for the treatment of AD do not prevent, halt or reverse the disease and only serve to ameliorate the symptoms[172]. These include inhibitors of acetylcholine esterase which increases the levels of the neurotransmitter acetylcholine, which is depleted in AD brains, leading to an impairment of normal cognition[311]. Antagonists of NMDA-type glutamate receptors are also used to prevent abnormal neuronal stimulation[312]. The impact of these drugs, however, is modest and transient. Development of new, disease-modifying therapeutics, thus, is essential in slowing the growing epidemic that is AD.

1.3.5.1 Reducing the production of Aβ

Several therapeutics have been trialled over the last two decades with the aim of decreasing the production or enhancing the clearance of Aβ. Drugs designed to inhibit β or γ-secretases have been ineffective so far, owing to difficulties in delivering such molecules across the BBB and a lack of specificity of the secretase substrates, resulting in cleavage of alternative substrates such as Notch and voltage-gated sodium channel subunits, both essential for normal cellular function[128]. The γ-secretase inhibitor Semagacestat (**Figure 1.15 a.i.**) failed phase III clinical trials due to worsening of disease symptoms[173]. A γ-secretase modulator, Tarenflurbil (**Figure 1.15 a.ii.**), which was designed to selectively lower Aβ42 production, in favour of the shorter and less toxic forms (Aβ37 and Aβ38)[313], was also ineffective in a phase III trial. This was ascribed to low potency and brain penetration[314]. Further studies into Notch-sparing γ-secretase inhibitors and more potent γ-secretase modulators are currently ongoing[314].

Inhibition of β-secretase (BACE1) is also under investigation. However, many compounds able to inhibit BACE1 have remained in the pre-clinical phase mainly owing to the same major problems encountered for inhibitors of γ-secretase. The active site of BACE1 is large and requires bulky inhibitors that are generally unable to penetrate the BBB. BACE1 also has other important physiological roles that need to be spared during inhibition. A phase I trial of β-secretase inhibitor CTS-21166 indeed demonstrated a reduction in plasma Aβ[315], but further clinical data into this candidate molecule is yet to become available.

Finally, in the same vein, the enhancement of α-secretase activity, the enzyme responsible for the non-amyloidogenic processing of APP (**Figure 1.12**) is another potential strategy in reducing Aβ reduction. Etazolate (**Figure 1.15 b**), a small molecule agonist for this enzyme, inhibits Aβ-induced neuronal death and demonstrated good tolerance and safety in a phase II study[316] but its clinical efficacy is yet to be confirmed.

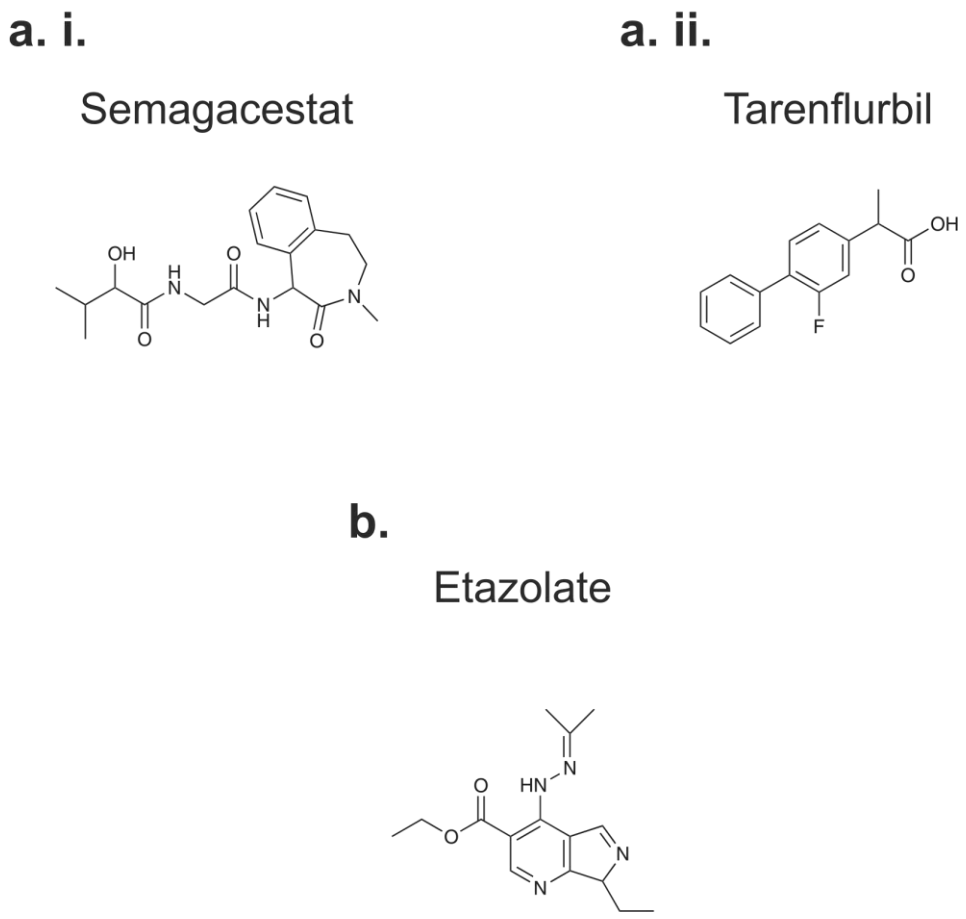

Figure 1.15 Small molecule modulators of the enzymatic processing of Aβ. Drugs designed to inhibit γ-secretase mediated production of Aβ **(a)** or enhance the alternative non-amyloidogenic processing of APP with agonists of the α-secretase **(b)** have shown various levels of success in clinical trials.

1.3.5.2 Maintaining the balance between production and clearance of Aβ

The increase in Aβ production associated with familial AD accounts for only ~5% of all instances, with AD occurring sporadically for the majority of patients[317]. This majority, therefore, do not have increased Aβ production resulting from mutations in the APP processing genes, but instead the balance of production and clearance of the aggregation precursor is somehow impaired. Strategies that target Aβ clearance mechanisms, therefore, may prove more effective in treating the majority of cases.

Many pharmaceutical companies have turned to immunotherapy to encourage amyloid clearance. Clearance of aggregates by both active (vaccination) and passive (monoclonal antibody) immunisation methods has been shown in animal models and is thought to occur by a variety of mechanisms, including direct disassembly of plaques, neutralisation of toxic oligomers, activation of phagocytosis and activation of specific-protein efflux processes[318]. Famously, the first active vaccination Phase II clinical trial with human Aβ42 (AN-1792) was initiated, after promising results in animal studies demonstrated a clear reduction in amyloid burden in mice[319-321] and no adverse effects during Phase I testing. Unfortunately, the trial was aborted in 2002 after an apparent activation of immune responses led to meningoencephalitis in a number of patients[322]. This study highlights the dangers of aberrant immune-response activation in antibody based therapies.

There are a number of Aβ-directed immunotherapies in clinical development that involve passive immunisation with antibodies directed against various forms of Aβ (reviewed in[323, 324]). These are all based on non-selective antibodies that are able to bind multiple Aβ species, ranging from monomer to mature fibrillar aggregates[323]. The fact that antibodies used are generally not specific for a single amyloid species could constitute a major drawback in the development of potent immunotherapies. If indeed the route to successful clearance was through specific targeting of oligomeric assemblies, for example, use of a non-selective Aβ antibody (that also binds monomers and fibrils) would most likely show low efficacy. This would be due to the extent of competition for antibody epitopes by the monomers and fibrils, which may not be the desired target but exist in higher concentrations in the AD brain[250, 325, 326]). This problem would also be further exacerbated by the low levels of antibodies that are able to penetrate the brain[327]. Nevertheless, passive immunisation trials have been conducted with moderate effects observed for a subset of patients. Bapineuzumab is a humanised, monoclonal antibody directed towards the N-

terminal domain (residues 1-5) of Aβ and recognises both soluble and aggregated Aβ in mice. It displayed no significant positive effects in a phase II trial and induced serious side effects in some participants. However, the antibody was able to produce significant benefits in a subset of patients who did not carry the apolipoprotein E ε4 allele (a genetic risk factor for late-onset sporadic AD) and therefore was approved for Phase III trials for the specific treatment of this patient group[318]. Solanezumab, a monoclonal antibody directed against the mid domain (residues 16-24) of Aβ, failed clinical trials in 2012, due to an apparent lack of potency. However, secondary analysis of the data indicated that the antibody may have been effective in slowing the cognitive decline in patients within the early stages of AD and therefore entered Phase III trials, the results of which are expected by late 2016[324]. If successful, solanezumab may represent the first disease-modifying drug for AD.

1.3.5.3 Preventing Aβ aggregation

One of the most attractive therapeutic strategies for all amyloid disorders, including AD, is the stabilisation of the native monomeric structure and prevention of aggregation (Sections 1.2.7.2 and 1.2.7.3). Despite extensive efforts in the development of small molecule and peptide-based aggregation inhibitors, and the promising results seen both *in vitro* and in animal models, only one Aβ aggregation inhibitor has reached Phase III clinical trials. Tramiprosate is an ionic small molecule which binds to soluble Aβ and maintains its random coil conformation, inhibiting aggregation and reducing plaque burden in mice models[328]. The compounds inhibitory effects are thought to be, in part, due to an interference of the ability of Aβ to bind glycosaminoglycans (GAGs), which promote fibrillation[329]. Results of the trial, however, were disappointing and were eventually discontinued, although recent data suggest that tramiprosate may promote the formation of tau inclusions[330] and highlight the importance of testing potential drugs on both AD pathologies.

Two further Aβ aggregation inhibitors under clinical review are Colostrinin[331], a mixture of proline-rich polypeptides (25% proline residues) isolated from ovine colostrum, that inhibit aggregation, and scyllo-inositol which stabilises non-toxic oligomers of Aβ40[332]. Both molecules produced beneficial effects in cellular and mouse models of AD, but demonstrated limited efficacy in Phase II trials[314, 331]. In addition, as metal ions such as Zn^{2+} and Cu^{2+} are known to be involved in Aβ amyloidosis[333, 334], metal ion chelators have shown inhibitory effects both *in vitro* and *in vivo*[335]. A number of metal protein attenuating

compounds, therefore, have been taken to clinical trials but are yet to show significant effects to confirm the validity of this approach[336, 337].

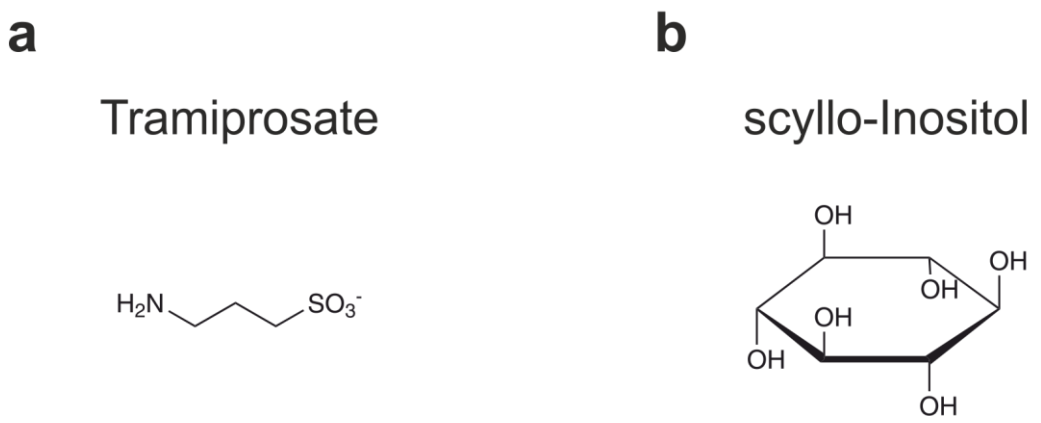

Figure 1.16 Examples of small molecules shown to inhibit Aβ aggregation in clinical trials. **(a)** Tramiprosate has been shown to bind and maintain Aβ in a random coil conformation. **(b)** Scyllo-Inositol stabilises a non-toxic oligomer of Aβ40. Both molecules inhibit aggregation and show beneficial effects in AD mouse models but demonstrated limited efficacy in human clinical trials.

1.3.5.4 Alternative strategies

A number of therapeutic approaches that are not directly linked to Aβ aggregation are also being investigated. These include modulators of tau phosphorylation, aggregation and degradation[227], anti-inflammatory drugs[338], anti-oxidants[339] and hormone therapies[340]. In addition, some strategies to target synaptic dysfunction[341-343] and autophagy[344] directly are also in development. However, so far no effective treatment has emerged from these efforts. Owing to the clear complexity of mechanisms contributing to AD pathology, it is likely that a combination of therapies will be required to effectively combat the disorder and, therefore, continued efforts into the development of new and innovative approaches is of paramount importance.

1.3.5.5 Diagnostics

Clinical diagnosis of AD is currently made using a combination of physical and neurological examinations, assessment of a patient's medical history, neuropsycological examination, neuroimaging and laboratory tests, with an accuracy of ~90%[345]. However, to date, definitive diagnosis can only be made post-mortem. The pathogenic process of AD is believed to begin decades before clinical onset of the disorder[171], with gradual neuronal loss in this prodromal phase. As proposed therapeutic strategies are likely to be most effective if administered before pathological changes spread throughout the brain, early diagnosis with reliable biomarkers is essential. In addition, more sensitive and specific imaging reagents might allow for earlier identification of people at risk of developing the disease and potentially distinguish between classic AD, mild cognitive impairment or other dementia types[346] and help tailor appropriate treatment options.

Currently, there are two principle AD amyloid biomarkers: amyloid positron emission tomography (PET) which measures the amount of Aβ aggregates in the brain parenchyma, and biochemical analysis of Aβ42 levels in the cerebrospinal fluid (CSF) (along with the detection of tau and phosphorylated tau[347]). The former requires the use of a ^{11}C-labelled modified derivative of Thioflavin T, known as Pittsburgh Compound B (PiB), which preferentially binds aggregated Aβ in dense plaques. It is, however, less sensitive to diffuse plaques and amorphous aggregates containing less β-sheet structure, as assessed in post-mortem studies[348-350]. This may suggest that the compound is insensitive to some prefibrillar deposits that may indicate an early disease pathology. Some additional ^{18}F-labelled amyloid ligands have also been developed[351-354] with similar amyloid retention as PiB. In AD, CSF levels of Aβ42 decrease to ~50% of the levels in aged-matched control individuals[355] due to aggregation of the peptide in the brain[356]. Together the inverse relationship between CSF Aβ42 and PiB binding leads to a relatively high diagnostic performance for AD[357]. One suggestion to further improve diagnostic accuracy is the measurement of the decrease in Aβ42:Aβ40 ratio as it is proposed to have a more marked reduction than Aβ42 alone[358]. Although the diagnostic value of these two methods is clear in established AD, current recommendations for diagnostic research criteria[359] put far greater emphasis on defining the pre-clinical states of AD and the development of sensitive biomarkers and imaging reagents that might allow the advancement of preventative therapies.

1.4 RNA aptamers

The discovery that RNA is not merely a carrier of genetic information, but a molecule capable of a vast number of biological applications, not only reinforces the idea of an RNA-based primordial world, but also indicates the great potential of RNA sequences as research tools, diagnostic reagents or therapeutics[360-364]. RNA has been shown to possess catalytic properties, in ribosomes and other ribozymes[365-368], and is also capable of forming complex three-dimensional structures, which mediate binding and molecular recognition. Aptamers are small nucleic acid ligands which adopt a functional secondary structure. The term was originally derived from the Latin 'aptus', meaning 'fitting', as these short, chemically synthesised oligonucleotides are able to fold into an array of structures that demonstrate specific target recognition, with dissociation constants often in the pico- to nanomolar range[361]. Owing to the breadth of possible structures available to oligonucleotides, it has been postulated that there is probably an RNA molecule with the ability to bind any biological target[369]. Their remarkable molecular recognition properties also mean that RNA aptamers are often directly compared with the ability of antibodies to recognise specific ligands. However, RNA aptamers demonstrate a number of advantages over antibodies, including simple chemical synthesis, reduced size, and limited immunogenicity[362]. Aptamers have already demonstrated their potential in a wide range of biological applications, from biotechnology to therapy[360, 361, 363], yet the commercial exploitation of such molecules has lagged behind other research areas (partly due to the issue of patents on aptamer technologies[370, 371]). Finally, more than two decades after their initial conception[369, 372, 373], aptamers are emerging as promising research tools.

1.4.1 Early development and SELEX

In the early 1990s, Szostak and Ellington pioneered the *in vitro* selection method that was first used to isolate specific binding aptamers for small organic dyes[369]. Two further groups[372, 373] also worked towards methods of synthesising large numbers of random sequence RNA, selecting out and amplifying those sequences with high affinity to a target of interest. The Joyce group used *in vitro* mutation, selection and amplification methods to isolate RNA oligonucleotides able to cleave DNA[372]. The Gold group used rounds of selection and amplification to identify sequences required for binding T4 DNA polymerase, and

subsequently coined the term SELEX; **S**ystemic **E**volution of **L**igands by **Ex**ponential Enrichment[373]. The process essentially works as a paradigm of Darwinian evolution (**Figure 1.17**). *In vitro* selection experiments can be carried out with double stranded DNA (dsDNA), single stranded DNA (ssDNA) or RNA, as well as synthetic nucleic-acid-like polymers (termed xeno-nucleic acids, XNA)[374]. In the remainder of this thesis, the term aptamer will refer to selected RNA molecules, unless otherwise stated.

The SELEX procedure has remained largely unaltered since its conception, but various improvements and optimisation over the years means that the process is now highly efficient and extensively automated[375, 376]. The procedure begins with the generation of a random nucleic acid pool, which can be readily amplified (and transcribed in the case of RNA) and be able to form an array of diverse structures. Therefore, the first requirement is the design of a degenerate DNA library, containing a random region to generate structural diversity, and two fixed flanking regions to allow primer-based amplification (**Figure 1.17 a**). The 5' region must also encompass a T7 RNA polymerase promoter sequence to allow *in vitro* transcription in the case of RNA aptamer selection. A key consideration is the length of the random region. The sequence space available within a nucleic acid library is 4^N (where N is the length of the random region). In a typical *in vitro* selection experiment, the maximum number of molecules that can be handled is $\sim 10^{15}$ [(ref 377)]. Therefore a library with a random region of only 24 nucleotides is required to achieve this. However, in order to promote the RNA molecule's folding into functional conformations, the random region may need to be longer than this and libraries are typically 30-60 nucleotides in length[377]. This presents a problem in that only a fraction of the potential sequence space is available in these experiments, however this is circumvented to some extent by the lack of proof reading functionality in the enzymes used for PCR amplification, transcription and reverse-transcription (RT-PCR), that means sequences not initially represented in the naïve pool may arise via mutation in the later rounds[377].

Once the initial pool is designed and synthesised, it is incubated with the target entity and sequences which bind are isolated and amplified. Partitioning of the bound species can be conducted in a variety of ways, with use of nitrocellulose filters, separation on various support matrices (such as magnetic beads or agarose/silica resins) or via column chromatography[360]. High affinity aptamers have also been isolated using Surface plasmon resonance (SPR) to isolate sequences with the slowest off-rates[378, 379], and capillary electrophoresis has also been used[380]. Bound species are then eluted and amplified to give an enriched pool of molecules for further iterations of the protocol. Typical numbers of SELEX rounds are between 10 and 20[(ref 360)] although high-affinity sequences have been

shown to be isolated from a single round of *in vitro* selection[381, 382]. The resultant enriched pool is then sequenced to allow identification of conserved motifs that exhibit high affinity interactions with the target.

1.4.2 Modifications and technical innovations

Major technical improvements in selection technologies have emerged since the earliest aptamers were developed, including significant reduction in the time taken for high affinity species to be isolated. The Ellington group were first to automate the SELEX process[376, 383] such that it is now possible to isolate high affinity aptamers in a matter of days, when previously it could take several months[383].

Polynucleotides are susceptible to degradation via nucleases, and to a lesser extent, chemical or physical factors[384]. Therefore, a key area of improvement in aptamer technologies has involved enhancement of aptamer biostability, with a series of chemical modifications designed to stabilise the molecules and extend their lifetime *in vivo* (**Figure 1.18**). Although highly dependent on sequence and structure, it is generally the case that RNA is degraded in seconds, and DNA within minutes, via blood-borne nucleases[384]. Substitutions made at the 2′-position of pyrimidines are effective at reducing degradation rates[385, 386] and therefore introduction of 2'-fluoro (2'F), 2'-amino and 2'-O-methyl pyrimidines is a method commonly used to increase the stability of aptamers[384, 387-395]. The use of 4' thio pyrimidines has also been reported[396], as well as a number of modifications to the C5 position of pyrimidines[397-402]. Another stabilising modification frequently used in selections is the substitution of the internucleotide phosphodiester linkage with a phosphorothioate[403-405]. Since these chemical substitutions might alter the structure compared with wild-type aptamers, selections are performed with libraries synthesised from modified nucleotides, a method that was made possible through the advent of mutant polymerases that allow the incorporation of these bulkier substrates during enzymatic steps[406, 407]. A further, elegant approach to generate nuclease-resistant aptamers is through the use of L-ribose based nucleotides, to generate biostable “spiegelmers”[408]. As nucleases are faithfully stereospecific[409], they confer effective resistance. However, because RNA polymerases will not function with enantiomers of the natural D-ribose, the protocol requires selection against an enantiomeric target molecule. Synthetic preparation of a speiglemer to match the selected aptamer is then able to bind the original, wild-type target

of interest and display identical properties[408]. The major limitation with this approach is that it is only applicable to smaller targets.

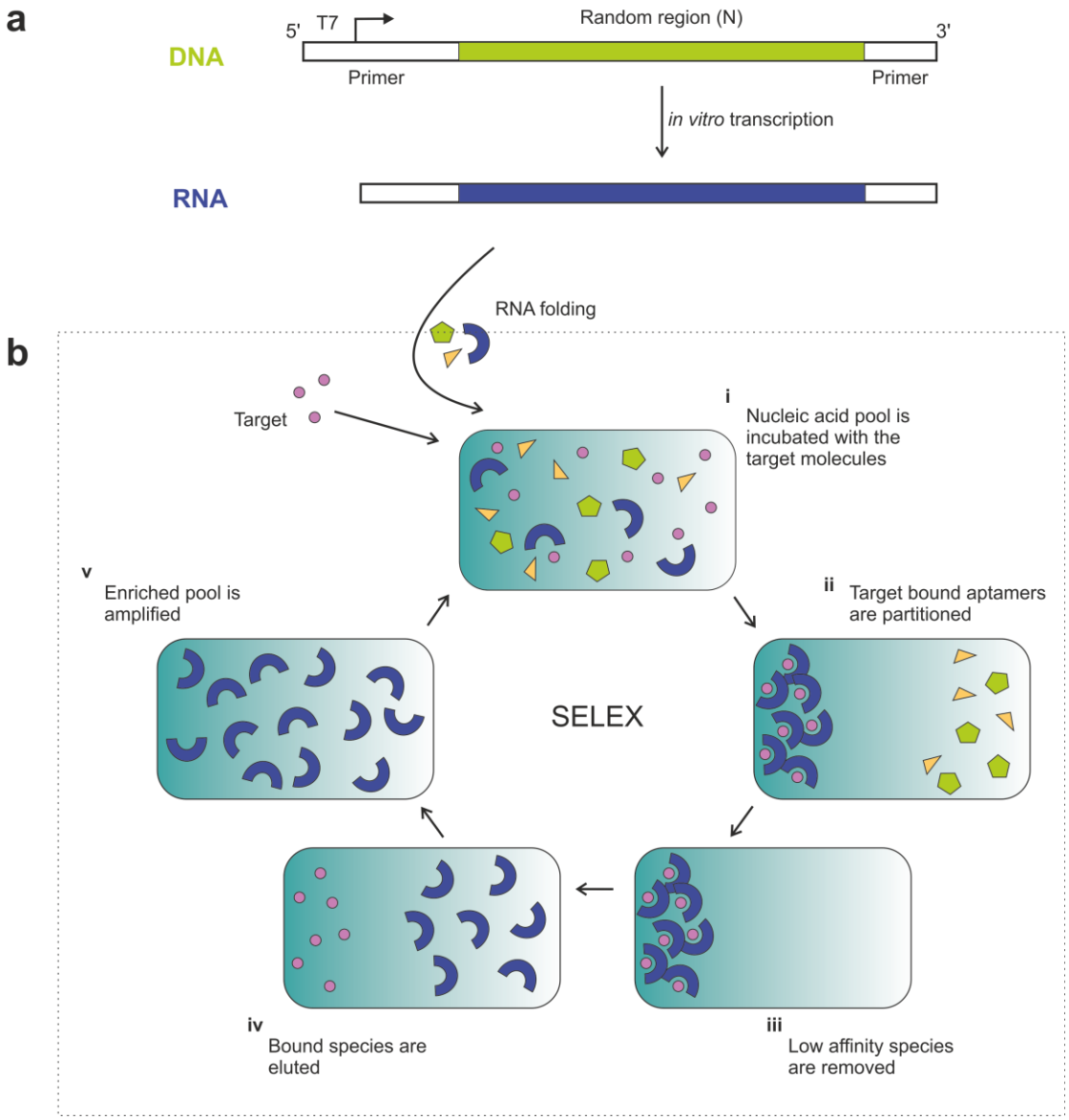

Figure 1.17 Schematic overview of the SELEX protocol. **(a)** A degenerate nucleic acid library is designed with a central random stretch of nucleotides, flanked by two constant primer regions for PCR amplification. The 5' primer region contains a T7 RNA polymerase promoter sequence to allow *in vitro* transcription of the degenerate pool in the case of RNA aptamer selection. **(b)** Basic outline of a single SELEX round. The naïve nucleic acid pool is incubated with the target molecule **(i)** which are then partitioned **(ii)** to remove lower affinity species **(iii)**. Bound species are then eluted **(iv)** and amplified **(v)** for further iterations of the protocol. Typically 10-20 rounds are performed before sequencing of the enriched library and aptamer characterisation. Figure redrawn and adapted from[360].

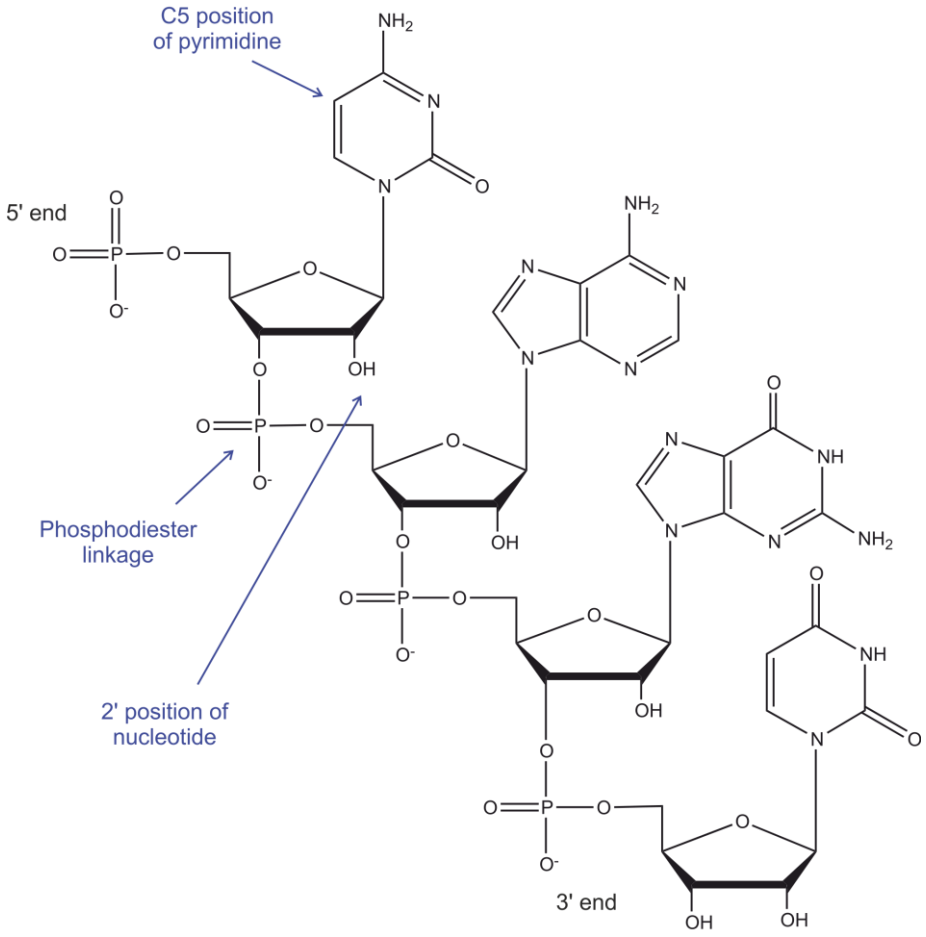

Figure 1.18 Aptamer modificiations. Structure of an RNA oligonucleotide with the sites of common modifications used to increase nuclease resistence, indicated.

Bioavailability is another key problem that has required optimisation, in order to establish aptamer technologies as suitable as *in vivo* diagnostic or therapeutic tools. The susceptibility of small polynucleotides towards rapid renal clearance can be avoided with chemical modifications to increase their size, including the attachment of polyethylene-glycol (PEG)[393, 410-413], cholesterol[414], biotin-streptavidin[415] or lipoproteins[416], all of which have been demonstrated. Unconjugated aptamers have been shown to clear from the mouse circulatory system within 5-10 minutes, whereas PEG-aptamer conjugates have shown circulatory retention up to 24 h[387].

Innovations in the SELEX protocol have also enabled improvements in aptamer specificities and isolation of aptamers with specific properties, thereby expanding the repertoire of

aptamer functions. Toggle-SELEX introduces related targets through alternating cycles, to broaden the range of specificities between species[417, 418]. Photo-SELEX has been shown to improve binding affinities by UV-induced crosslinking of light sensitive nucleotides[419] and tailored-SELEX can be implemented to create shorter aptamer sequences using ligation and cleavage of primers, before and after amplification. The latter methodology is advantageous, as shorter aptamers are more amenable to chemical synthesis and therefore more applicable in various downstream applications, owing to the reduced cost of production[420]. Using traditional SELEX methodology, aptamers are typically >80 nucleotides long[377] and require further processing to be suitable for large-scale production. This is usually achieved by identification of the minimal sequence required for recognition, post-selection, and validation that the aptamer "fragment" retains its function. Recently, selections have been carried out using living cells, termed cell-SELEX[421]. This method involves selection of aptamers against cell surface biomarkers, avoiding the need for purification of targets or even prior knowledge into the identity of the biomarker. Counter selection with control cells that do not express the target biomarker allows specific ligands to become enriched.

1.4.3 Applications of aptamer technologies

1.4.3.1 Therapeutics

Aptamers possess many features that make them suitable candidates for use in the clinic. They are able to form tight and specific interactions with theoretically any target, therefore they are likely to work via antagonistic mechanisms, through interactions with cellular proteins and subsequent disruption of native protein-protein interactions or other functions. Indeed, many aptamers selected to bind specific proteins have been shown to inhibit their function[422-427]. For an aptamer to be an effective antagonist, high specificity and affinity are required to maintain a prolonged interaction, as well as a long half-life in the relevant biological compartment. The variety of potential modifications mentioned in Section 1.4.2**,** are in place to fulfil these criteria and produce aptamers with great therapeutic potential. Aptamers have also been found to display agonist-like activity. For example, aptamers selected against the human epidermal growth factor receptor 3 (HER3),

a type I receptor tyrosine kinase, were shown to promote oligomerisation of the receptors, leading to inhibition of phosphorylation[428].

1.4.3.1.1 Aptamer delivery

Therapeutic targets can be divided into two classes; intracellular and extracellular. Aptamers directed against extracellular targets could be simply administered intravenously or subcutaneously, with pharmacokinetic data suggesting that RNA delivered via these routes is readily distributed to target cells[429]. Although aptamer degradation and clearance is inevitable, repeat administration could be feasible until treatment is complete. Targeting of oligonucleotides to specific cell types has been shown via a number of methods including modification with cholesterol to mediate association with low-density lipoproteins and delivery to the liver[414]. Tagging aptamers directly with lipoproteins, specific to other cell types, is another attractive strategy[430].

If the aptamer target is intracellular, delivery across the membrane is a further consideration and potential challenge. The negative charge of oligonucleotides means that they do not readily cross the anionic cell membranes[431]. However, a number of options are available, including liposome vesicle transport and the use of viral vectors[427, 432, 433]. Indeed, aptamers themselves have been used to facilitate delivery of siRNA for RNA interference, through conjugation of aptamer sequences specific for certain cell-surface receptors[431, 434, 435]. Viral vector systems can also be utilised in delivering sequences to be endogenously produced within the cell of interest, termed "intramers"[432]. The technique works by transfection of cells with a retroviral vector that encodes the aptamer sequence, leading to long-term expression of the aptamer *in situ*.

1.4.3.1.2 Aptamers vs. antibodies

Aptamers can be thought of much in the same way as monoclonal antibodies; owing to the similarities in affinity and specificities achievable by aptamers and antibodies, the two recognition molecules are often directly compared[361]. Antibodies are undoubtedly one of the most useful reagents in both therapeutics and research, with four of the top ten biopharmaceuticals being monoclonal antibodies, worth more than $24 billion in US sales

alone[436]. They do, however, have several limitations, where aptamers could provide a safer and more convenient alternative[361]. Firstly, unlike the traditional methods of antibody production, no organisms are required for the simple, *in vitro* selection of oligonucleotide aptamers. Once a single, functional aptamer sequence has been isolated and optimised for clinical use, aptamers can be produced chemically in a readily scalable process. On the other hand, antibodies are produced biologically in a process that is more difficult to scale-up without adverse effects to the products' characteristics and where viral or bacterial contamination can effect product quality[361].

One of the major advantages of nucleic acid technologies, over antibodies as therapeutics, is that RNA elicits no immunogenic response, which has been shown to limit the suitability of immunotherapy in some instances, through the emergence of unwanted side effects, such as inflammation[437]. There has been no evidence of antibodies being generated in response to synthetic nucleotides[362], nor problems arising from an innate immune response, that has previously been associated with recognition of viral RNAs[438, 439]. Any possibility of these issues occurring is eliminated in aptamer therapy via modifications to 2' nucleotides, which have been shown to abolish any Toll-like Receptor responses[440].

Aptamers are generally much smaller than antibodies (**Figure 1.19**), which is advantageous due to their increased availability to biological compartments and efficiency of entry[384]. It also means that aptamers are often able to target molecules that might be otherwise inaccessible to antibodies, owing to steric hindrance[364]. An example of this was seen when researchers attempted to target the interaction between HIV-1 viral coat protein gp120 and the host cell receptor CD4 and its associated co-receptor CCR5, which are hijacked during viral entry[441, 442]. The CCR5 binding site on gp120 was shown to be inaccessible to antibodies, due to occlusion by an adjacent hypervariable region[441]. However, an RNA aptamer specific for the co-receptor binding region was able to access the obscured epitope and neutralise infectivity[442, 443]. This further indicates that aptamers could demonstrate a wider range of functionalities than antibodies. In addition, some methods of antibody development are limited in the ability to use negative selection pressure, which is simple to incorporate during *in vitro* selection of aptamers. This could mean that aptamers have the potential to be more selective than antibodies. They can also be used in instances where a target is unavailable to antibodies, owing to problems with expression in a functional, recombinant form, such as cell-surface receptors. Development of aptamer technologies, to extend or improve the work of antibodies, therefore, is an exciting prospect that may advance areas of research where antibodies have previously failed.

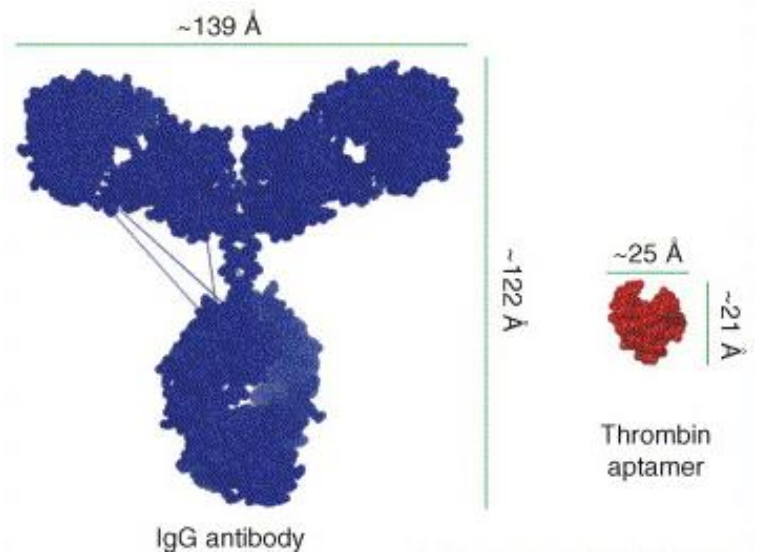

Figure 1.19 A comparison of aptamer and antibody size. Space filling models depicting the estimated sizes of an antibody (human IgG) compared to a 17 residue anti-thrombin DNA aptamer[397]. Figure taken with permission from [364].

1.4.3.1.3 Aptamers in the clinic

In 2004 the first RNA aptamer-based drug was approved for use by the Food and Drug administration (FDA), to treat age-related macular degeneration (AMD), the major cause of blindness and visual impairment in the elderly[444]. Pegaptanib, known commercially as Macugen™, is an RNA oligonucleotide which works to inhibit binding of VEGF165 to its receptor and therefore antagonises its pro-angiogenic effects. This RNA aptamer was initially selected from a 2'F pyrimidine library with a 30 nucleotide random region (N30)[410] (78 nucleotide total length) and truncated to 27 nucleotides to decrease synthesis costs (**Figure 1.20**). The 2'-ribo purines were replaced with 2'-O-methyl modified purine to increase nuclease resistance, a 3' terminal cap (3'-3'-linked deoxythymidine) to reduce 3'-exonuclease-mediated degradation and a 5' linked 40 kDa PEG moiety, which increases the inhibition of VEGF function in mouse models, probably through prolonged tissue residence and plasma half-life[410]. Pegaptinib is administered once every 6 weeks and works to ameliorate the loss of vision that results from aberrant angiogenesis in AMD[445].

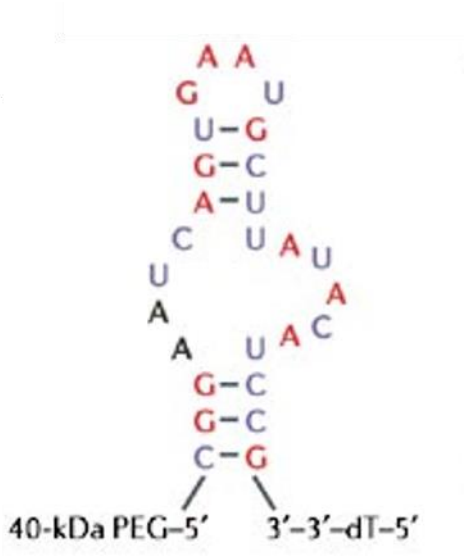

Figure 1.20 Sequence and predicted secondary structure of Pegaptinib. 2'-O-methyl modified purines are highlighted red and 2'F modified pyrimidines are highlighted blue. Unmodified ribonucleotides are shown in black. The position of the 5' 40 kDa PEG moiety and the 3' terminal cap are indicated. Figure taken from [393].

Currently, several other aptamer based therapeutics are in the process of clinical evaluation, targeting proteins involved in disorders including several cancers, type II diabetes and pathologies associated with blood clotting dysfunction and stroke (reviewed in [361, 446, 447] **Table 1.2**). Aptamer technologies are also becoming a popular methodology in anti-viral intervention and, although an anti-viral aptamer has yet to be approved for clinical trials, it is an active area of research (reviewed in [448]). The host-viral interface is an increasingly popular aptamer target as nucleic acid-protein interactions are critical to viral replication. Therefore, the plethora of protein targets which already possess nucleic acid binding properties (for example, the presence of basic residues), are likely to be suitable targets for nucleic acid ligands. Consequently, aptamers have been selected to target a number of viral proteins involved in several stages of the viral replication cycle, including viral entry[443, 449] and replication[450, 451]. Overall, although aptamer therapies are in their infancy in comparison to immunotherapeutic approaches, their versatile and adaptable technologies suggest aptamers have great potential to become attractive tools in the clinic.

Aptamer name (Company)	Condition targeted	Current status
Pegaptanib/ Macugen™ (Pfizer/Eyetech)	Age-related macular degeneration (AMD)	Approved in the US and EU
E10030 (Ophthotech)	Age-related macular degeneration (AMD)	Awaiting Phase III
ARC1905 (Ophthotech)	Age-related macular degeneration (AMD)	Phase I
RB006 (Regardo Biosciences)	Coronary artery disease	Awaiting Phase III
ARC1779 (Archimex)	Von Willebrand's disease	Awaiting Phase III
NU172 (Nuvelo/ARCA Biopharma)	Coronary artery disease	Phase II
ARC19499 (Archimex)	Haemophilia	Phase I/II (status uncertain)
AS1411 (Antisoma)	Renal cell carcinoma/non-small cell lung cancer	Awaiting Phase III
NOX-A12 (Noxxon Pharma)	Tumour	Phase II
NOX-E36 (Noxxon Pharma)	Type II diabetes	Phase IIa

Table 1.2 Current status of aptamers undergoing clinical trials. Table reproduced and adapted from [447].

1.4.3.2 Diagnostics and biosensors

The versatility of nucleic acid aptamer technologies has meant that aptamers are beginning to play increasingly important roles in a range of diagnostic applications, from disease diagnosis via imaging, detection of diseased cells in tissues and serum and in the discovery of novel biomarkers[452-454]. Aptamers have also been shown to function as sensors in environmental and food analyses, and even in the detection of biological terrorism threat agents[455].

The high affinity and specificity achievable with aptamers make them ideal diagnostic reagents. The simple chemistries involved in conjugating dyes or functional groups to allow detection is also an advantageous feature of aptamers. For example, fluorescently-labelled nucleotides could be incorporated for confocal microscopy or 2-photon imaging, Cy5-tagged nucleotides for near infrared imaging, as well as ^{18}F or ^{19}F labelling for PET and MRI approaches, respectively. Importantly, aptamers are also rapidly cleared from the bloodstream, leading to sensitive detection with high target to background ratios[452]. As mentioned for therapeutic applications, modifications be can optimised for better biodistribution and clearance.

Development of aptamers as imaging reagents has been especially successful in cancer research[456-460] but other disease processes have also been studied[461-463]. Imaging tumours via selective delivery of radionucleotides has been demonstrated[464], which is particularly useful, as residual radioactive aptamers are rapidly cleared and excreted, avoiding toxicity to normal tissues that has been shown to result from the slow clearance of radioactive antibodies[464]. Aptamers conjugated to contrast reagents for magnetic resonance imaging (MRI) have also been developed for specific tumour detection[459] as well as activatable fluorescent aptamers[465] and quantum dot conjugates[460]. Fluorescence-based imaging reagents are especially versatile, as ligand-induced conformational changes can be exploited to induce fluorescence resonance energy transfer (FRET), differential fluorescent dye binding or quenching[360]. A recent report of an activatable aptamer imaging probe that targets a membrane protein on the surface of human leukemic cells[465] is especially innovative in that the optical signal is quenched in the unbound state, but upon ligand binding, a conformational rearrangement in the aptamer dissociates the quencher from the fluorophore. With the development of automated high-throughput isolation of aptamers and the relative simplicity in chemical modifications that allow sensitive detection, large scale diagnostic arrays should be feasible with these reagents[466].

In addition to a role as imaging reagents, aptamers could also be used to aid clinical diagnosis, through both detection of known biomarkers and discovery of new ones[452]. Aptamers have already become a useful tool in detecting diseased cells in tissue sections and even in trace amounts in the bloodstream. For example, an RNA aptamer that targets the cell-surface epidermal growth factor receptor (EGFR), which is upregulated in a number of cancers[467], has been used to quantitate the number of diseased cells in the serum by capture on a surface[468]. Coupling fluorescently labelled aptamers with flow cytometry has also been used to detect a variety of cancer cells from mixed cells in media[469, 470] and with some optimisation could be extended to detection in *ex vivo* samples. The success so far achieved in imaging and biomarker detection by aptamers for cancer targets is encouraging, but is yet to be extended to many other disease processes. However, the clear advantages of aptamer technologies over antibodies and other traditional diagnostic reagents, should mean that aptamers could become valuable tools for clinicians in a wide range of applications.

1.4.3.3 Research tools

In addition to therapeutic and diagnostic applications, aptamers can be used as analytical tools and laboratory reagents in a number of biochemical or cell-based assays, much like antibodies. Their key advantages over antibodies could again lead to greater, more specific detection abilities, with broader applications[360]. By utilising aptamers that disrupt protein interactions, it would be possible to dissect and characterise cellular pathways. The exquisite recognition capabilities of aptamers could also be used to probe specific protein structures, involved in various disease processes.

Another obvious use for these highly specific and high affinity molecules as a laboratory reagent is as an affinity purification medium. Several examples of the use of aptamers in a laboratory setting already exist[471-474], one notable example being the use of an anti-selectin aptamer to purify a selectin-receptor protein directly from Chinese hamster ovary cells[471]. This methodology is said to achieve 15,000 fold purification in a single step. Aptamers, therefore, could provide major advantages in these applications, owing to the high level of discrimination demonstrated between closely related species. Indeed, an aptamer purification method was employed to isolate D-arginine-vasopressin from its L-enantiomer, which was shown not to associate to the aptamer-derivatised medium[472]. Also, tag-cleavage steps are not required for these single step methods leading to potentially greater product recovery[360].

In summary, aptamer technologies have already demonstrated enormous potential in a variety of applications. Although these tools are gaining momentum in some research fields, namely cancer research and virology, they have been slow to emerge in other areas. With recent technological innovations, including rapid and stringent selection strategies, the future for aptamer research is bright, and these promising reagents should finally begin to take their place in the clinical and research arenas.

1.4.4 Examples of RNA aptamers in amyloid disorders

1.4.4.1 Anti-prion aptamers

Prion protein (PrP) is the causative agent in a range of protein aggregation disorders, such as Creutzfeldt-Jakob Disease (CJD) in humans, Bovine Spongiform Encephalopathy (BSE) in cattle and Scrapie in sheep[475]. The conversion of the normal cellular prion protein (PrP^{C}), a predominantly α-helical isoform, to an abnormal β-sheet rich amyloidogenic variant (PrP^{Sc}), is thought to lead to the pathogenesis of these disorders. Selections against various assemblies of PrP represent some of the most successful cases of anti-amyloid aptamers. In one example, Rhie *et al*.[476] demonstrated selection of 2'F-pyrimidine-modified RNA aptamers (116 nucleotides total length, with an N60 randomised region) against purified, scrapie associated fibrils (SAF) isolated from hamster brain; a preparation therefore containing a range of PrP conformations associated with infectivity. The lead aptamer, SAF-93 (**Figure 1.21 a.i.**), was shown to bind to SAF with high affinity (dissociation constant (k_d) = 23.4 ± 1.2 nM) and cross-reacted with a related, β-sheet rich oligomeric assembly, indicating recognition of a consistent epitope conserved between the amyloid forms. In contrast, the relative affinity of the RNA for the α-helical form (PrP^{C}) was much reduced (10-fold higher K_d). This finding was explained through the identification of two distinct RNA binding sites between the PrP isoforms. These included a non-specific RNA binding site in the unstructured N-terminus, which also encompassed a "hinge-region" (residues 90-110) which is occluded in the α-form. The aptamer was also shown to inhibit the accumulation of the proteinase K resistant β-sheet rich assemblies (PrP^{res}). Later work by the group[477] built on these original findings by determining the minimum structural elements required to maintain aptamer recognition and specificity to the β-rich variants (**Figure 1.21 a.ii.**); identifying regions that were amenable to modification, without loss of function, and thereby facilitating the design of modified aptamers, more amenable to a range of downstream applications. Together, the work highlights the many potential uses for aptamers in amyloid systems, from their ability to avidly and specifically bind a range of amyloid assemblies, their inhibitory potential and their utility in probing conformational differences between amyloid structures.

Other examples of anti-prion aptamers mainly target the helical isoform[391, 478, 479]. In one such example[391] 2'F-amino-pyrimidine-modified aptamers were raised, from an N40 library, against a short fragment of full-length PrP (residues 90-141) which is thought to be

involved in the conversion from PrP^{C} to PrP^{Sc} [191, 480, 481]. Binding studies of the isolated sequence, aptamer DP7 (**Figure 1.21 b**), indicated an ability to bind to full-length recombinant PrP and inhibit PrP^{Sc} formation in a prion-infected cell line.

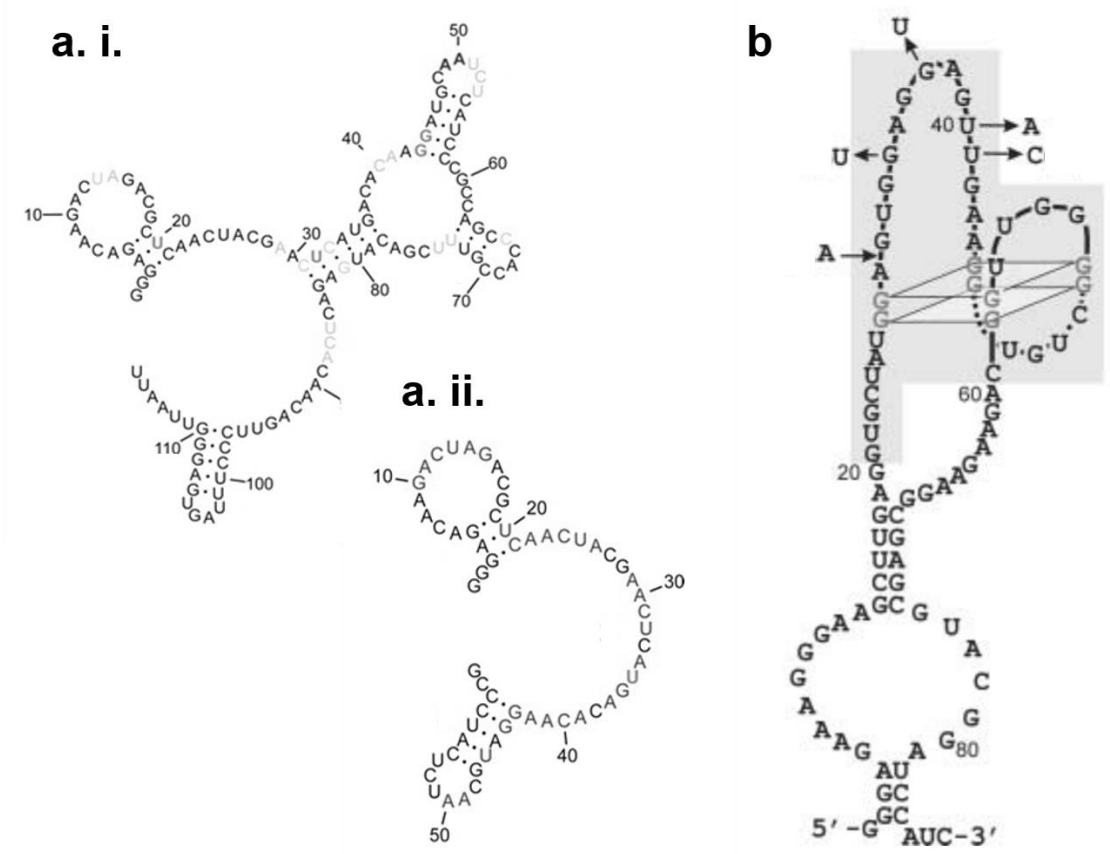

Figure 1.21 Examples of anti-prion (PrP) aptamers. **(a)** Predicted secondary structures of aptamer SAF-93 determined with the Mfold structure prediction algorithm, constrained with information from structure-sensitive nuclease digestion. **(a. ii)** Predicted secondary structure of the 60-residue truncation product from SAF-93, named SAF-$93_{(1\text{-}60)}$. Figures adapted from Sayer *et al*.[477]. **(b)** The proposed secondary structure of aptamer DP7. Figure adapted from[391].

1.4.4.2 β_2-microglobulin aptamers

β_2-microglobulin (β_2m) is the amyloidogenic protein associated with Dialysis-related amyloidosis (DRA), a disorder in which aberrant aggregation of this folded monomer leads to the accumulation of fibrillar deposits in the joints of patients undergoing long-term haemodialysis[482]. Bunka *et al*.[483] demonstrated RNA aptamers able to recognise a range of β_2m fibrils of distinct structural morphologies (long-straight (LS), worm-like (WL) and rod-like (RL) **Figure 1.22 a**), as well as the monomeric precursor, indicating the conservation of a structural epitope between the assemblies. The aptamers, which were raised from an N60 randomised RNA library with no modifications (predicted secondary structure of WL-2, an anti-WL fibril aptamer shown in **Figure 1.22 b**), were also shown to cross-react with fibrils from other amyloidogenic precursors, including *ex vivo* assemblies of β_2m and lysozyme, isolated from patients with the respective amyloidoses. The work supports the idea that amyloid species formed from a number of unrelated peptide precursors share common structural features, which can be targeted by aptamer ligands, and that raising aptamers to synthetic amyloid formed *in vitro*, can be directly relevant to the isolation of aptamers against *in vivo*, disease-associated fibrils.

More recently, an RNA aptamer raised against monomeric β_2m was shown to be able to discriminate this target protein from its N-terminally truncated variant ΔN6[484]. As well as displaying remarkable discriminatory power in this system, the aptamer B6min (2'F modified 44-nucleotides (**Figure 1.22 c**), truncated from the 110 full length variant, which was selected from within an N30 library) was able to disrupt the kinetics of co-polymerisation of the two proteins. Co-polymerisation is a feature common to many other amyloid forming peptides[309, 485-488], which adds significantly to the complexity of amyloid systems, producing further fibril polymorphs, with diverse architectures, stabilities and biological properties[309, 485, 489]. Aptamers like the one described here, may therefore help in discriminating distinct amyloid species from a pool of closely-related molecules, decipher the underlying mechanisms of aggregation and inform the design of novel therapies and diagnostics.

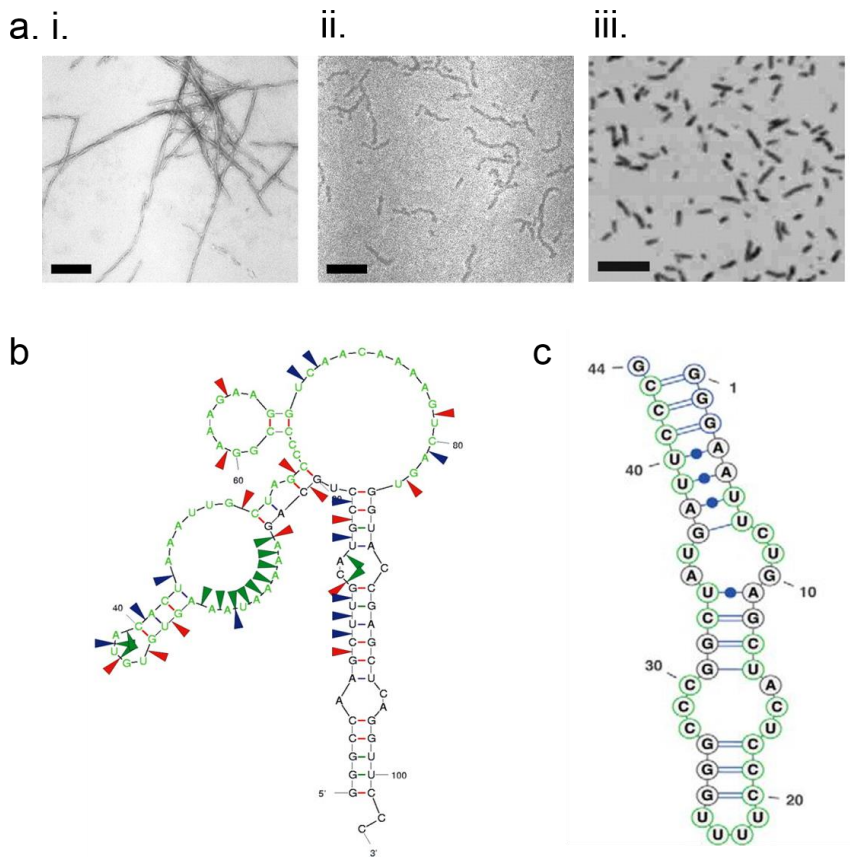

Figure 1.22 Examples of anti-β_2m aptamers. **(a)** Distinct morphologies of β_2m fibrils imaged by negative-stain EM in the case of (i) Long-straight (LS) fibrils and (ii) Worm-like fibrils (WL). Rod-like fibrils (iii) were imaged by AFM. Each scale bar represents 200 nm. **(b)** The predicted secondary structure of aptamer WL-2. Nucleotides corresponding to the random region are highlighted green. Coloured arrows indicate sequence-specific enzymatic cleavage sites used to validate the predicted structure. Cleavage by RNase T1 (G-specific, red), RNase A (U and C specific, blue), S1 (single-strand specific, green) are indicated. **(c)** Secondary structure predicted for B6min. 2'F pyrimidines are circled in green. Figures adapted from [483] and [490].

1.4.4.3 Aβ aptamers

Several examples of aptamers raised against different Aβ assemblies exist in the literature and provide indication that targeting this natively-unstructured peptide, as well as its various higher-order assemblies, is a distinct possibility. The earliest example of an anti-Aβ RNA aptamer was isolated by Ylera *et al.*[491]. Here, aptamers were selected from an N70, unmodified RNA library, against monomeric Aβ40, immobilised on a Sepharose support

resin. Nanomolar affinity of the selected RNA aptamers was reported for the immobilised monomer, however the authors were unable to demonstrate binding of the aptamer to the monomeric peptide in solution. Instead, the aptamers were shown to bind fibrils, allowing the group to speculate that problems with the aggregation propensity of Aβ meant that aptamers had preferentially targeted aggregates formed during the immobilisation process. The work highlights the difficulty in aptamer selection against these highly aggregation-prone monomeric species. However, more than a decade after this initial publication, the lead aptamer sequence from the selection, β55 (**Figure 1.23 a.i.**), was taken forward in the development of an optical imaging reagent to detect amyloid plaques[492]. By use of both biotin-modified and fluorescently-tagged RNA sequences Farrar *et al*. were able to visualise amyloid plaques in *ex vivo* human AD brain sections (**Figure 1.23 a.ii.**), and *in vivo*, in transgenic AD mice models. The *in vivo* 2-photon imaging methodology also allowed visualisation of a diffuse "halo" of positive staining on the periphery of the plaques (**Figure 1.23 a.iii.**), indicative of reactivity towards oligomeric species that often surround the dense core of the aggregate. Dot blot analysis confirmed that the aptamer sequence did indeed bind both fibrillar and oligomeric Aβ.

A further example of aptamers selected against Aβ assemblies reported the potential for RNA to interfere with amyloidosis[493]. Takahashi and colleagues expanded on previous work in the field by selecting unmodified RNA aptamers from an N40 naïve library, against an "oligomeric model" of Aβ40, assembled on the surface of gold nanoparticles. Despite the author's report of relatively moderate binding affinities for the target assemblies (K_d ~ 10 μM) two aptamers (N2 and E2 **Figure 1.23 b**) were able to redirect the assembly mechanism, by inhibiting the formation of typical fibrils. Instead aptamer co-incubation resulted in the formation of oligomers, protofibrils and amorphous aggregate, as assessed by TEM.

Finally, another study where oligomeric assemblies of Aβ40 were specifically targeted was performed by Rahimi *et al*.[494], where they selected RNA aptamers against a covalently-stabilised Aβ40 trimer. Aptamers in this study were again unmodified, and from an N49 RNA library, and were reported to contain a high G-content, however no sequences were given. The authors found that upon characterisation of individual selected aptamer sequences, the RNA displayed no affinity for the trimeric or other low-molecular weight (LMW) species and instead associated most tightly with the fibrils. The lead sequences (KM33 and KM41) were also shown to associate with a panel of further fibrils from numerous precursors, including Aβ42, lysozyme, PrP(106-126), IAPP, calcitonin and

insulin. This work again indicates a conserved structural motif common between many amyloid assemblies.

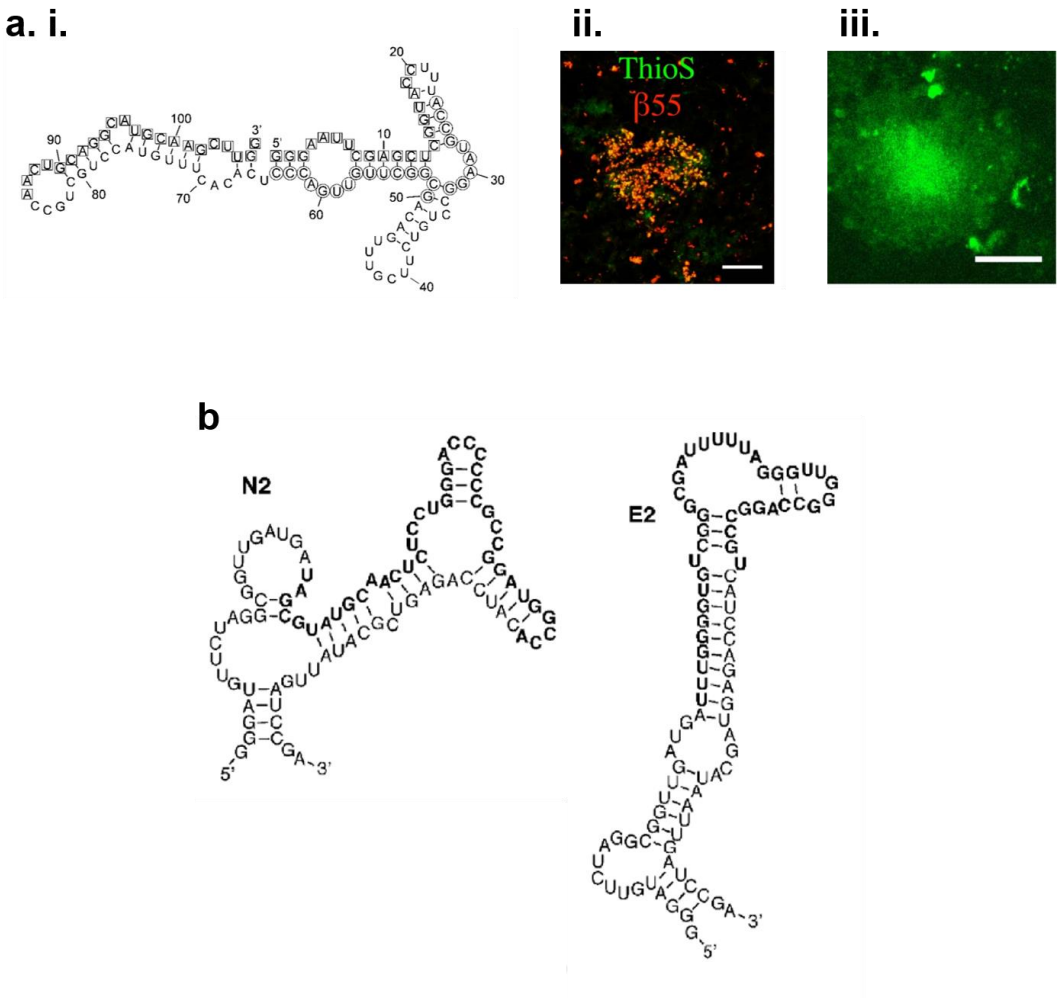

Figure 1.23 Examples of anti-Aβ40 aptamers. **(a. i.)** The predicted secondary structure of β55. The nucleotides corresponding to the primer regions are boxed. Regions conserved between this aptamer sequence and other related sequences from motif analysis of the selected pool are circled. **(ii)** Confocal imaging of a human AD brain section stained with biotinylated-β55 red and showing co-localisation with amyloid-specific dye Thio-S (green). Scale bar: 50 μm. **(iii)** In vivo 2-photon microscopy plaque images from an AD mouse brain, 1 h after topical application of fluorescein-labelled β55. Scale bar: 20 μm. **(b)** Predicted secondary structures of N2 and E2 aptamers with randomised regions in bold. Images are adapted from [491-493].

1.4.4.4 Other anti-amyloid aptamers

In addition to the RNA aptamers selected against the above amyloid assemblies, there are some examples of DNA aptamers raised as analytical tools against α-syn[495, 496] (associated with Parkinson's disease) and the Sup35 yeast prion[497]. In the case of α-syn, aptamers were raised which selectively bound oligomeric α-syn assemblies over the natively-unstructured monomer[495] despite selection against a supposedly monomeric solution. A later study by the same group[496] isolated further DNA aptamers this time against soluble oligomers of α-syn, which also displayed cross-reactivity with prefibrillar assemblies of Aβ40. Similarly, DNA aptamers raised against Sup35 fibrils[497] were able to bind to various other aggregated states, including the SDS-insoluble Sup35 aggregates isolated directly from yeast cells and two further amyloid aggregates formed from murine PrP(90-231) and a 103Q poly-Q expanded variant of huntingtin.

Overall, although there are relatively few examples of anti-amyloid aptamers represented in the literature, the studies published indicate that aptamers could indeed play an important role in dissecting these mysterious disease systems, sensitively detecting and characterising the distinct structures involved, and potentially interfering with pathogenesis.

1.5 Aims of this thesis

Alzheimer's disease (AD) represents one of the greatest health challenges of our generation. There is an urgent need for novel therapies, diagnostics and further insights into the processes underlying this disorder, and other amyloid diseases alike. The aim of this study, therefore, was to harness the power of RNA aptamer technologies in these endeavours. The focus of the work was to isolate RNA sequences, through the SELEX approach, specific for a number of assemblies of the Aβ40 peptide. A small cohort of individual aptamer sequences, isolated from each of the selection pools would be assessed for their target binding affinity, and specificity, before lead sequences would be chosen for further characterisation. Only after confirmation of the aptamers' avidity and specificity for their own target assemblies, could the project proceed to address the secondary aim; development of the aptamers as either novel therapies, diagnostic reagents or use them to probe disease processes and expand our knowledge of the mechanisms underlying amyloidosis.

The work presented in Chapter 3 outlines the *in vitro* selection of RNA aptamers against both monomeric Aβ40 and the two well-characterised and structurally distinct fibrillar assemblies from Tycko *et al*.[103-105] 2A and 3Q (Section 1.3.4.3). The resultant enriched pools were sequenced with next generation methodology, isolating $\sim 10^6$ possible binding sequences for each of the structures. A thorough bioinformatic analysis of the sequencing data was then undertaken in order to isolate lead aptamer sequences from the vast quantity of possible binders. Chapter 4 documents the characterisation of anti-monomer aptamers, with emphasis on the challenges in optimising suitable techniques to study binding to this small, aggregation prone peptide, in its monomeric form. Chapter 5 covers the characterisation of the anti-fibril aptamers and the extent of their specificity for their cognate fibril morphologies. Upon the discovery that RNA aptamers display generic cross-β selectivity, the focus shifts to probing the structural elements responsible for the lack of binding specificity, in the context of both amyloid structure, RNA sequence and comparison to another generic amyloid-binding polyanion, heparin. Finally, despite a lack of discrimination between amyloid assemblies, some practical uses for aptamers as imaging reagents or inhibitors are described.

2 Materials and methods

2.1 Materials

2.1.1 Technical equipment

Equipment	Manufacturer
Centrifuges	
Avanti J-26 XP Centrifuge	Beckman Coulter, Brea, CA, USA
GenFuge 24D Centrifuge	Progen Scientific, London, UK
MiniSpin plus F-45-12-11	Eppendorf, Hauppauge, NY, USA
Incubators, mixers & shakers	
Gallenkamp Economy Incubator Size 1	Sanyo, Watford, UK
ORBISAFE Orbital Incubator	Sanyo, Watford, UK
Stuart Magnetic Stirrer SB161	CamLab, Cambridge, UK
Stuart Orbital Incubator S150	Bibby Scientific, Stone, UK
Stuart Vortex Mixer SA8	Bibby Scientific, Stone, UK
Gel electrophoresis equipment	
Vari-Gel midi system	CamLab, Madingley, UK
Slab Gel Electrophoresis Chamber AE-6200	ATTO, Tokyo, Japan
Standard Power Pack P25	Biometra, Goettingen, Germany
OmniPAGE Maxi system	Geneflow, Staffordshire, UK
Protein purification equipment	
ÄKTAprime plus	GE healthcare, Little Chalfont, UK
Superdex™ 75 GL 10/300 gel filtration column	GE healthcare, Little Chalfont, UK
Superdex™ Peptide 10/300 GL gel filtration column	GE healthcare, Little Chalfont, UK
HiLoad Superdex™ 75 26/60 gel filtration column	GE healthcare, Little Chalfont, UK
Fluorometer	
Photon Technology International fluorometer	Ford, West Sussex, UK
Spectrophotometer	
UltroSpec 2100 pro UV/Visible Spectrophotometer	GE healthcare, Little Chalfont, UK
UV-1800 UV/Vis Spectrophotometer	Shimadzu, Kyoto, Japan
Nanodrop 2000 UV/Vis Spectrophotometer	Thermo Scientific, Surrey, UK

Microplate readers

FLUOstar OMEGA plate reader	BMG Labtech, Aylesbury, Bucks, UK
NEPHELOstar Galaxy laser-based nephelometer	BMG Labtech, Aylesbury, Bucks, UK
CLARIOstar plate reader	BMG Labtech, Aylesbury, Bucks, UK
EnVision 2013 Multilabel plate reader	Perkin Elmer, Waltham, MA, USA

Microscopes

JEOL JEM-*1400* Transmission Electron Microscope	JEOL Ltd., Tokyo, Japan
Zeiss LSM 700 Confocal microscope	Zeiss, Oberkochen, Germany

Mass spectrometer

Synapt high definition mass spectrometry (HDMS) quadrupole-time-of-flight mass spectrometer (Micromass UK Ltd., Waters Corpn., Manchester, UK), equipped with a Triversa automated nano-electrospray ionisation (ESI) interface (Advion Biosciences, Ithaca, USA)

Other equipment

Biacore 3000 Surface Plasmon Resonance	GE healthcare, Little Chalfont, UK
Monolith NT.115 Microscale Thermophoresis	NanoTemper, Munich, Germany
Soniprep 150 Ultrasonic Disintegrator	MSE, London, UK
Corning Costar 3881 96-well plate	Corning Life Sci, The Netherlands
Corning 3575 384-well plate	Corning Life Sci, The Netherlands
Grant JB1 Unstirred Waterbath	Grant Instruments, Shepreth, UK
InGenius Gel Documentation System	Syngene, Cambridge, UK
Jenway 3020 Bench pH Meter	Bibby Scientific, Stone, UK
Series 2100 Media Autoclave	Prestige Medical, Minworth, UK
SnakeSkin Pleated Dialysis Tubing; 3,500 MWCO	Thermo Scientific, Surrey, UK
Techne Dri-Block Heater DB-2A	Bibby Scientific, Stone, UK
Heto PowerDry PL3000 Freeze drier	Thermo Scientific, Surrey, UK

2.1.2 Chemicals

A	
Acrylamide, 30% (w/v): 0.8% (w/v) bisacrylamide	Severn Biotech, Kidderminster, UK
Acetonitrile	Fisher Scientific, Loughborough, UK
Agar	Melford Laboratories, Suffolk, UK
Ampicillin	Formedium, Norfolk, UK
Ammonium acetate	Sigma Life Sciences, St. Louis, USA
Ammonium bicarbonate	Sigma Life Sciences, St. Louis, USA
Ammonium persulphate, APS	Sigma Life Sciences, St. Louis, USA
Ammonium sulphate	Thermo Scientific, Surrey, UK
B	
Benzamidine	Sigma Life Sciences, St. Louis, USA
Bromophenol blue	Sigma Life Sciences, St. Louis, USA
C	
Calcium chloride	Melford Laboratories, Suffolk, UK
Carbenicillin	Formedium, Norfolk, UK
Chloramphenicol	Sigma Life Sciences, St. Louis, USA
Chloroform:isoamyl alcohol	Sigma Life Sciences, St. Louis, USA
Congo red	Sigma Life Sciences, St. Louis, USA
D	
DEPC-treated H_2O	Severn Biotech, Kidderminster, UK
Dimethyl sulphoxide, DMSO	Sigma Life Sciences, St. Louis, USA
1,2-Dithiothreitol, DTT	Formedium, Norfolk, UK
DNase I (bovine)	Sigma Life Sciences, St. Louis, USA
E	
Ethanol	Fisher Scientific, Loughborough, UK
Ethidium bromide (EtBr)	Sigma Life Sciences, St. Louis, USA
Ethylenediaminetetraacetic acid, EDTA	Sigma Life Sciences, St. Louis, USA
G	
Glutamax	Invitrogen, Paisley, UK
Glycerol	Fisher Scientific, Loughborough, UK
Glycogen	Thermo Scientific, Surrey, UK
Guanidinium HCl	Fisher Scientific, Loughborough, UK
H	
Hellmanex	Sigma Life Sciences, St. Louis, USA
Heparin (LMW)	Iduron, Manchester, UK
1,1,1,3,3,3 Hexafluoro-2-propanol (HFIP)	Sigma Life Sciences, St. Louis, USA
Hyaluronic acid dp8	Iduron, Manchester, UK
Hydrochloric acid, HCl	Fisher Scientific, Loughborough, UK
I	
Isopropyl β-D-1-thiogalactopyranoside, IPTG	Melford Laboratories, Suffolk, UK

L	
LB broth, granulated	Melford Laboratories, Suffolk, UK
Lysozyme	Sigma Life Sciences, St. Louis, USA
M	
Magnesium acetate	BDH Laboratory Supplies, Poole, UK
Magnesium chloride, $MgCl_2$	Sigma Life Sciences, St. Louis, USA
Manganese chloride tetrahydrate	Sigma Life Sciences, St. Louis, USA
3-(N-morpholino)propanesulphonic acid (MOPS)	Sigma Life Sciences, St. Louis, USA
N	
Niad-4	ChemShuttle, China
P	
Phenol:$CHCl_3$ (5:1, pH 4.5)	Ambion, UK
Phenylmethanesulfonyl fluoride (PMSF)	Fisher Scientific, Loughborough, UK
Phosphate buffered saline (PBS)	Thermo Scientific, Surrey, UK
R	
RNAse inhibitor (murine)	New England Biolabs, Herts, UK
S	
Sodium azide, NaN_3	Sigma Life Sciences, St. Louis, USA
Sodium borate, $Na_2B_4O_7$	Sigma Life Sciences, St. Louis, USA
Sodium chloride, NaCl	Fisher Scientific, Loughborough, UK
Sodium dodecyl sulphate, SDS	Sigma Life Sciences, St. Louis, USA
Sodium hydroxide, NaOH	Fisher Scientific, Loughborough, UK
Sodium phosphate dibasic, Na_2HPO_4	Sigma Life Sciences, St. Louis, USA
Sodium phosphate monobasic, NaH_2PO_4	Sigma Life Sciences, St. Louis, USA
Sodium sulphate, Na_2SO_4	Sigma Life Sciences, St. Louis, USA
Spermidine	Sigma Life Sciences, St. Louis, USA
T	
Tetramethylethylenediamine (TEMED)	Sigma Life Sciences, St. Louis, USA
Thioflavin T	Sigma Life Sciences, St. Louis, USA
Trifluoroacetic acid	Fisher Scientific, Loughborough, UK
Tris-(hydroxymethyl)-aminomethane (Tris)	Melford Laboratories, Suffolk, UK
Trypsin EDTA	Sigma Life Sciences, St. Louis, USA
Tween-20	National Diagnostics, Atlanta, USA
U	
Uranyl acetate	Sigma Life Sciences, St. Louis, USA
Urea	MP Biomedicals, UK
Y	
Yeast inorganic pyrophosphatase	Sigma Life Sciences, St. Louis, USA

2.1.3 Antibiotics, markers and dyes

Antibiotic	Solvent	Stock solution (mg/mL)	Working concentration (µg/mL)	Sterilisation
Ampicillin	Purite 18 MΩ H_2O	100	100	Filter sterilised through 0.2 µm filter
Carbenicillin	Purite 18 MΩ H_2O	100	100	
Chloramphenicol	100% (v/v) ethanol	25	25	

Table 2.1 Antibiotics used in this study.

Marker	Manufacturer
Mark 12™ Protein Standard	Invitrogen, Paisley, UK
Precision Plus Protein™ Dual Xtra Standards	Bio-Rad, Hemel Hempstead, UK
10 bp DNA ladder	Invitrogen, Paisley, UK

Table 2.2 DNA and protein markers used in this study.

Dye	Manufacturer
GelPilot DNA Loading dye, 5 x	QIAGEN, Crawley, UK
Gel loading buffer II (Denaturing PAGE)	Ambion, Paisley, UK
Instant Blue Stain	Expedeon Protein Solutions, UK
Ethidium Bromide (0.1 µg/mL) in Tris borate EDTA (TBE)	Severn Biotech Ltd, UK

Table 2.3 Dyes used in this study.

2.1.4 Kits

Kit	Manufacturer
QIAquick PCR purification kit	QIAGEN, Crawley, UK
Wizard ® Plus SV Minipreps DNA purification system	Promega, Southampton, UK
RNA Clean and Concentrator™-5	Zymo Research, Irvine, CA, USA
Illustra Microspin G-25 columns	GE healthcare, Little Chalfont, UK
PD10 desalting columns	GE healthcare, Little Chalfont, UK
Illustra NAP5 columns	GE healthcare, Little Chalfont, UK
KAPA2G Robust PCR kit	Kapa Biosystems, London, UK
HiScribe™ T7 High Yield RNA synthesis kit	New England Biolabs, Herts, UK
Transcriptor Reverse Transcription kit	Roche, West Sussex, UK

Table 2.4 Kits used in this study.

2.1.5 Media and buffers

Media	Components
Luria-Bertani (LB) Media	10 g Bacto-tryptone 5 g Yeast extract 10 g NaCl Made up to 1 L in Purite 10 MΩ H_2O autoclaved 20 min at 121 °C, 15 psi

Table 2.5 Media used in this study.

Solid medium was prepared by addition of 1.5% (w/v) agar (Melford Laboratories, UK) prior to autoclaving. Antibiotics were added to media once cooled to < 50 °C.

Buffer	Components
2 x SDS reducing loading buffer	50 mM Tris- HCl, pH 6.8 100 mM DTT 2% (w/v) SDS 0.1 % (w/v) bromophenol blue 10% (v/v) glycerol
SDS PAGE cathode buffer	200 mM Tris-HCl, pH 8.25 200 mM Tricine 0.2% (w/v) SDS
SDS PAGE anode buffer	400 mM Tris-HCl, pH 8.8
Tris-borate-EDTA (TBE) buffer	890 mM Tris, pH 8.3 20 mM EDTA 890 mM Boric acid Made from 10 x TBE powder (Applichem, Germany)
Transcription buffer (10 x)	400 mM Tris acetate, pH 8.0 150 mM Magnesium acetate 0.5 mM Manganese chloride tetrahydrate 138 mM Spermidine
MOPS selection buffer	80 mM MOPS 96 mM NaCl, pH 7.5
Fibril formation buffer (Aβ40/Aβ16-22)	25 mM sodium phosphate, 0.01% (w/v) NaN_3, pH 7.5
Fibril formation buffer (α-synuclein)	20 mM Tris-HCl 100 mM NaCl 0.01% (w/v) NaN_3, pH 7.5

Table 2.6 Buffers used in this study.

2.2 Molecular biology methods

2.2.1 Bacterial strains

***E. coli* XL1–Blue** (Stratagene, Cambridge, UK)

endA1 gyrA96(nal^R) thi-1 recA1 relA1 lac glnV44 F'[::Tn10 proAB$^+$ lacI^q Δ(lacZ)M15] hsdR17(r_{K^-} m_{K^+})

***E. coli* DH5α** (Invitrogen, Paisley, UK)

F$^-$ endA1 glnV44 thi-1 recA1 relA1 gyrA96 deoR nupG Φ80d*lacZ*ΔM15 Δ(*lacZYA-argF*)U169, hsdR17(r_{K^-} m_{K^+}), λ–

***E. coli* BL21 (DE3) pLysS** (Stratagene, Cambridge, UK)

F$^-$ ompT gal dcm lon hsdS_B(r_{B^-} m_{B^-}) λ(DE3) pLysS(cm^R)

***E. coli* BL21 (DE3)** (Stratagene, Cambridge, UK)

F$^-$ ompT gal dcm lon hsdS_B(r_{B^-} m_{B^-}) λ(DE3 [lacI lacUV5-T7 gene 1 ind1 sam7 nin5])

2.2.2 Preparation of competent *E. coli* cells

A 10 mL culture of the desired *E. coli* strain was grown overnight in LB media, at 37 °C. This culture was used to inoculate (1:20) a 100 mL LB culture, which was grown at 37 °C, 200 rpm, until the OD_{600} reached 0.4 - 0.45. Cells were centrifuged in a pre-chilled rotor at 1,400 x *g*, 4 °C for 10 min and the pellet resuspended in 10 mL of sterile, pre-chilled 100 mM $CaCl_2$. This was incubated on ice for 10 min and centrifuged for a further 10 min at 1,400 x *g* at 4 °C. The pellet was then resuspended in 2 mL of 100 mM $CaCl_2$, 30% (v/v) glycerol and divided into 100 µL fractions and frozen on dry ice. Competent cells were stored at -80 °C.

2.2.3 Transformation and cultivation of *E. coli* cells

Plasmid DNA (50 – 200 ng) was added to 50 µL thawed, competent cells and incubated on ice for 30 min, with occasional, gentle agitation. The cells were then heat shocked for 45 s at 42 °C and incubated on ice for a further 10 min before the addition of 500 µL sterile LB (without antibiotic). The mixture was incubated at 37 °C with 200 rpm agitation for 2 h, to allow the cells to express appropriate resistance genes, before 20 - 200 µL was spread on LB agar plates, containing antibiotic resistance. Plates were incubated overnight at 37 °C.

2.2.4 Preparation of plasmids

10 mL LB cultures containing the appropriate antibiotic resistance, were inoculated from single bacterial colonies picked from transformation plates, and grown overnight (37 °C, 200 rpm agitation). Cells were pelleted at 4000 x *g* and plasmid DNA was extracted using Wizard® Plus SV miniprep DNA purification kit, according to the manufacturer's instructions. DNA was eluted in sterile, nuclease-free H_2O, and stored at -20 °C for subsequent transformation reactions. The concentration of plasmid DNA was determined by absorbance measurement at 260 nm (A260), where A260 = 1 was assumed to be equivalent to 50 µg/mL dsDNA[498]. DNA was sequenced by Beckman Coulter Genomics sequencing service using universal T7 promoter primers.

2.2.5 Plasmids

Plasmids encoding WT Aβ40 (pETSac, **Appendix 7.1.1**) were kindly provided by Dr. Sara Linse (Lund University, Sweden) and Prof. Dominic Walsh (Harvard Institute of Medicine, USA).

pET23a plasmid encoding α-synuclein were provided by Prof. Jean Baum (Department of Chemistry and Chemical Biology, Rutgers University, NJ, USA).

The plasmid encoding K16A Aβ40 was created from the above Aβ40 plasmid by site-directed mutagenesis, which was carried out by Dr. Katie Stewart (School of Molecular and Cellular Biology, University of Leeds).

2.3 Protein expression and purification methods

2.3.1 Expression and purification of Aβ40

2.3.1.1 Expression of recombinant Aβ40

Buffer	Composition
10 x Buffer A	100 mM Tris-HCl 10 mM EDTA pH 8.5
1 x Buffer A	1:10 dilution of 10 x Buffer A in H_2O
Inclusion body denaturant	8 M Urea in 1 x Buffer A

Table 2.7 Buffers used in Aβ40 purification.

BL21 (DE3) pLysS cells were transformed with plasmid encoding Aβ40 as described (Section 2.2.3). A single colony was picked to inoculate 100 mL overnight starter cultures (37 °C, 200 rpm). 10 mL of overnight culture was used to inoculate 10 x 500 mL sterile LB cultures, prepared in 2 L baffled, conical flasks. Ampicillin (100 µg/mL) was added to each flask before incubation at 37 °C, with 200 rpm agitation, until an optical density (OD_{600}) of 0.5 was reached. Protein expression was induced with the addition of filter-sterilised isopropyl β-D-1-thiogalactopyranoside (IPTG) at a final concentration of 0.5 mM. Cultures were then further incubated until OD_{600} reached a plateau and cells reached steady state (approx. 3.5 h, typical $OD_{600} \sim 1.2$). Cells were harvested by centrifugation at 6000 x *g* (4 °C for 15 min) and pellets were pooled and resolubilised in 25 mL H_2O, before storage at -20 °C. Optimisation of this protein expression protocol is described in Section 3.3.

2.3.1.2 Isolation and lysis of inclusion bodies containing Aβ40

2.5 mL of 10 x Buffer A (4 °C) was added to the 25 mL cell suspension from Section 2.3.1.1 to establish a 1 x Buffer A solution. DNase (~0.5 mg), phenylmethanesulfonyl fluoride (PMSF, 1 mM) and benzamidine (2 mM) were added to the suspension and stirred at 4 °C for 1 h. The solubilised pellets were passed through a blunt-end syringe needle (Terumo Global Pharmaceutical Solutions, NJ, USA) to further homogenise, before sonication for 30 s (9.5 mm probe, 10 μm amplitude). The homogenate was centrifuged at 30,000 x *g*, 15 min at 4 °C, and supernatant removed. The pelleted inclusion bodies were resolubilised in 1 x Buffer A and the sonication – centrifugation process repeated once more. The pellet was resolubilised in inclusion body denaturant (**Table 2.7**) and agitated using a magnetic stirrer, for up to 1 h. The suspension was then sonicated and centrifuged a third time (as before) and the supernatant, now containing solubilised Aβ40, was collected and diluted 1 in 4 in 1 x Buffer A for anion exchange purification.

2.3.1.3 Anion exchange purification

Anion exchange purification of Aβ40 was performed in batch format to avoid problems associated with Aβ aggregation during column chromatography[499]. All buffers used in this stage of the purification were pre-cooled to 4 °C. 35 mL of Q-Sepharose Fast Flow resin (GE Healthcare) was equilibrated with 1 x Buffer A, before addition of the crude urea lysate (urea concentration ~2 M after dilution) and incubation at 4 °C, with gentle rocking, for 30 min. Batch purification was set up in a 250 mL Büchner funnel, with Whatman 1 filter paper, fitted to a vacuum glass bottle and vacuum pump. The resin was washed twice with 50 mL pre-chilled 1 x Buffer A, containing 0 then 25 mM NaCl, before peptide elution with 5 x 50 mL washes of 1 x Buffer A containing 125 mM NaCl. Finally, high-salt (1 x Buffer A plus 250 mM NaCl) and high-salt plus urea (1 x Buffer A plus 250 mM NaCl, 8 M urea) fractions were applied to the resin to remove any remaining protein species. Each eluate was stored at 4 °C to avoid aggregation before dialysis. 3,500 MWCO dialysis tubing was prepared according to manufacturer's instructions. Aβ40-containing fractions were dialysed against 50 mM ammonium bicarbonate, with a total 4 x 5 L changes over 24 h. Fractions were then lyophilised to concentrate the semi-purified peptide.

2.3.1.4 Size exclusion chromatography (SEC)

Lyophilised Aβ40, purified partially by anion exchange chromatography, was resolubilised in 10 mL of 50 mM Tris-HCL, pH 8.5, containing 7 M guanidinium-HCl. The solution was loaded onto a HiLoad™ 26/60 Superdex 75 prep grade gel filtration column (GE Healthcare), connected to an ÄKTA prime LC system, in 5 mL batches. The column was pre-equilibrated in 50 mM ammonium bicarbonate, which was also the mobile phase in which the protein was eluted. The ÄKTA programme used is outlined in **Table 2.8**. Aβ40 was eluted in a single peak at approximately 180 mL. All SEC was performed at 4 °C. Typical yields from this Aβ40 preparation was 4 mg/L culture.

Breakpoint (mL)	Flow rate (mL/min)	Fraction size (mL)	Injection valve position
0	2	0	Load
4	2	0	Inject
20	2	0	Load
50	2	4	Load
360	2	0	Load
362	End		

Table 2.8 ÄKTA programme for size exclusion chromatography of Aβ40.

2.3.1.5 Sodium dodecyl sulphate polyacrylamide gel electrophoresis (SDS-PAGE)

A Tris-Tricine buffered SDS-PAGE system was used to monitor protein expression and purification as it was deemed most suitable for resolving smaller peptides such as Aβ (Aβ40 = 4458 Da). The two-layered gel system was constructed from two glass plates, separated by a 1.5 mm spacer, according to manufacturer's instructions. Components for the resolving and stacking portions of the gel are outlined in **Table 2.9.**

APS and TEMED were added to the other components immediately before pouring. The resolving gel was quickly poured to fill the first 4/5th of the gel plates. 200 µL of H_2O was carefully dispensed on to the top of the gel to create a straight edge. This resolving gel fraction was allowed to set completely (minimum 1 h) before the water was poured off. APS and TEMED were then added to the stacking gel solution, which was then poured and a comb inserted to create sample loading wells. The assembled gels were allowed to set for a further 1 h before electrophoresis.

Samples were diluted with 2 x SDS reducing loading buffer (**Table 2.6**) and boiled for 5 min, before centrifugation for 10 min at 16,000 x *g*.

Component	Volume for resolving gel (mL)	Volume for stacking gel (mL)
30% (w/v) acrylamide:0.8% (w/v) bis acrylamide	7.50	0.83
3M Tris-HCl, 0.3% (w/v) SDS, pH 8.45	5.00	1.55
H_2O	0.44	3.72
Glycerol	2.00	-
10% (w/v) ammonium persulphate (APS)	0.10	0.20
Tetramethylethylenediamine (TEMED)	0.01	0.01

Table 2.9 Components of a Tris-tricine buffered SDS-PAGE gel. Volumes stated to cast two 8 x 10 cm mini-gels, with a 1.5 mm spacer.

For analysis of whole cell lysates, 1 mL samples were centrifuged at 16,000 x *g* for 15 min and the supernatants removed. 100 µL of loading buffer was added directly to the pellet, boiled and centrifuged as described above. 15 µL was loaded onto the gel.

SDS PAGE was carried out with cathode buffer (**Table 2.6**) in the inner reservoir of the gel tank and anode buffer (**Table 2.6**) in the outer reservoir. Gels were run with an initial constant current of 30 mA, until the samples had entered the resolving gel, at which point

the current was raised to 60 mA. Gels were run for approximately 1.5 h, until the dye front reached the end of the gel.

Gels were stained (**Table 2.3**) for 15 min, before de-staining in H_2O for a minimum of 1 h and imaging with an InGenius Gel documentation system (Syngene, Cambridge, UK).

2.3.2 Expression and purification of α-synuclein

Wild-type α-synuclein (α-syn) was expressed in BL21 DE3 *E. coli* cells from a pET23a vector (**Appendix 7.1.2**). 10 x 1 L sterile LB fractions were inoculated with 10 mL from an overnight 100 mL starter culture (Section 2.3.1.1), in the presence of 100 µg/mL carbenicillin. Cells were incubated at 37 °C for 4 h, prior to induction with 0.5 mM IPTG at an approximate OD_{600} = 0.6. Protein was expressed for 5 h post-induction, before harvesting by centrifugation (6000 x *g*, 15 min, 4 °C).

Pellets were resuspended in 25 mM Tris-HCl, pH 8.0 lysis buffer, containing 100 µg/mL lysozyme, 50 µg/mL PMSF and 20 µg/mL DNase. The pellet was then homogenised and disrupted by french press (30,000 psi), before heating to 80 °C in a water bath for 10 min. The homogenate was then centrifugated (30,000 x *g*, 4 °C, 30 min) and the protein, isolated in the soluble fraction, was precipitated with 50% (w/v) ammonium sulphate at 4 °C, 30 min. The suspension was centrifuged at 30,000 x *g* and the pellet resuspended and precipitated again in 50% (w/v) ammonium sulphate, 4 °C, 30 min. After a further centrifugation (30,000 x *g*, 4 °C, 30 min) the pellet was resuspended in 20 mM Tris-HCl, pH 8.0 for anion exchange.

The partially purified α-syn was loaded onto a 500 mL Q-Sepharose anion exchange column with a 20 mM Tris- HCl, pH 8.0 mobile phase. Protein was eluted with a linear gradient of 500 mM NaCl and monitored by absorbance at 280 nm. Fractions containing α-syn were analysed by SDS-PAGE, dialysed against 50 mM ammonium bicarbonate and lyophilised.

Semi-purified protein from anion exchange purification was resuspended in 20 mM sodium phosphate, pH 7.5, and loaded onto a HiLoad™ 26/60 Superdex 75 prep grade gel filtration column. The protein was eluted from the column with 20 mM sodium phosphate, pH 7.5 at a flow rate of 2 mL/min and the major peak collected and dialysed against 50 mM ammonium bicarbonate and lyophilised. Purified protein was stored at – 20 °C. A typical yield from this preparation was 45 mg/L culture.

2.3.3 Quantification and validation of purified protein

Purified peptides were quantified by absorbance at 280 nm (A280). Concentration (c) was calculated with the Beer-Lambert equation (**Equation 2.1**). Extinction coefficients at 280 nm (ε_{280}) were calculated from the peptide sequence in ProtParam[500] and are given in **Table 2.10**. Path length (l) is 1 cm.

$$A280 = \varepsilon_{280} cl \qquad \textit{Equation 2.1}$$

The identity of recombinantly expressed protein was assessed by electrospray ionisation mass spectrometry (ESI-MS) analysis. Any ESI-MS analyses in this thesis were performed by Dr. James Ault, MS Facility, School of Molecular and Cellular Biology, University of Leeds.

2.3.4 Acquisition of other peptides

Aβ16-22 was prepared by automated solid-phase peptide synthesis and kindly provided by Dr. George Preston and Prof. Andrew Wilson (School of Chemistry, University of Leeds). Ccβ-p was synthesised and provided by Dr. Kevin Tipping (School of Molecular and Cellular Biology, University of Leeds).

K16A Aβ40 was expressed and purified according to the WT Aβ40 protocol (Section 2.3.1)

S129C α-synuclein labelled with a TMR-maleimide fluorescent label (Invitrogen) was made by Dr. Matthew Jackson (School of Molecular and Cellular Biology, University of Leeds), expressed and purified according to the WT α-synuclein protocol (Section 2.3.2) and labelled according to manufacturer's instructions (Invitrogen).

Recombinantly expressed L3F Im7 was made and purified by Dr. Alice Bartlett (School of Molecular and Cellular Biology, University of Leeds). Recombinantly expressed β_2m was made and purified by Dr. Claire Sarell (School of Molecular and Cellular Biology, University of Leeds).

Sequences of all major proteins used in this thesis, and their properties, are given in **Table 2.10.**

Peptide	Sequence	Production method	Molecular Weight (Da)	Extinction coefficient ($\varepsilon 280/M^{-1} cm^{-1}$)
Aβ40	MDAEFRHDSGYEVHHQKLVF FAEDVGSNKGAIIGLMVGGVV	Recombinantly expressed	4458	1490
Aβ16-22	Ac-KLVFFAE-NH_2	Synthetic	853	-
Ccβ-p	Ac-SIRELEARIRELEARIG-NH_2	Synthetic	2011	-
α-synuclein	MDVFMKGLSKAKEGVVAAAE KTKQGVAEAAGKTKEGVLYVG SKTKEGVVHGVATVAEKTKEQ VTNVGGAVVTGVTAVAQKTVE GAGSIAAATGFVKKDQLGKNE EGAPQEGILEDMPVDPDNEAY EMPSEEGYQDYEPEA	Recombinantly expressed	14460	5960
L3F Im7	MEHHHHHHEFKNSISDYTEAE FVQLLKEIEKENVAATDDVLD VLLEHFVKITEHPDGTDLIYYP SDNRDDSPEGIVKEIKEWRAA NGKPGFKQG	Recombinantly expressed	10881	9970
β_2m	MIQRTPKIQVYSRHPAENGKS NFLNCYVSGFHPSDIEVDLLKN GERIEKVEHSDLSFSKDWSFYL LYYTEFTPTEKDEYACRVNHV TLSQPKIVKWDRDM	Recombinantly expressed	11862	20065

Table 2.10 Amino acid sequences and properties for the proteins used in this thesis. Recombinant peptides contain an additional N-terminal Methionine. Chemically synthesised peptides are both N-terminally acetylated and C-terminally amidated.

2.4 Fibril formation and characterisation

2.4.1 Seeded Aβ40 fibril formation

Original Aβ40 seed stocks of both 2A and 3Q fibril morphologies were kindly provided by Dr. Robert Tycko (NIH, Bethesda, USA).

Aβ40 seeds were diluted to 5% (v/v) in sterile-filtered fibril formation buffer (**Table 2.6**) and sonicated (5 s ON/ 45 s OFF, x 3), with a Soniprep 150 microprobe sonicator (amplitude 10 μm) on ice. Lyophilised Aβ40 peptide was dissolved at 0.9 mg/mL in the seed-containing buffer and briefly vortexed, before quiescent growth at room temperature for a minimum of 18 h. To produce daughter seeds for further reactions, fibrils prepared as above were

grown for 18 h and sonicated for 5 s (microprobe, 10 μm amplitude). After 7 days of elongation, an additional sonication cycle (5 s ON/ 45 s OFF, x 3), was undertaken to fragment fibrils into new seeds.

2.4.2 *De novo* Aβ40 fibril formation

To create fibrils from primary nucleation of monomers, without distinct seeded morphologies, Aβ40 peptide was dissolved at 0.9 mg/mL in fibril forming buffer (**Table 2.6**) and aliquotted into 100 μL fractions, in separate wells of a Corning NBS 96 well microplate (Corning Life Sci, The Netherlands) and sealed with transparent, gas permeable plastic film (Breathe Easy, Sigma Aldrich). The fibrils were formed at 37 °C with 600 rpm orbital agitation, using a NEPHELOstar Galaxy laser-based Microplate nephelometer (BMG LABTECH, Germany) as an incubator, for 18 h. Fibril formation was monitored by nephelometry.

2.4.3 Seeded α-synuclein fibril formation

Fibrils formed as seed stocks were made by incubation of 300 μM α-synuclein, in 20 mM Tris-HCl, 100 mM NaCl, 0.01% (w/v) NaN_3 , pH 7.5 buffer, in 500 μL final volumes in 1.5 mL Eppendorf tubes. Samples were agitated constantly at 600 rpm on a Thriller thermoshaker incubator (Peqlab). After 1 week of elongation, fibrils were transferred to 2 mL glass vials (Chromacol) and fragmented mechanically via a custom built precision stirrer, at 1000 rpm, for 48 h. This fragmentation yielded seeds which were used to elongate further fibril reactions.

Seeded reactions were set up with the addition of 10% (v/v) pre-formed seed at a final protein concentration of 200 μM, in 20 mM Tris-HCl, 100 mM NaCl, 0.01% (w/v) NaN_3, pH 7.5 buffer. Mixtures were made up in 1.5 mL Eppendorf tubes and fibril elongation carried out at ambient temperature with intermittent shaking (5 s 600 rpm, 10 min stationary) on the thriller shaker, to reduce fibril settling. Fibrils were allowed to form for a minimum of 4 days, after which total fibril yield was >95%. Fibrils containing 10% monomer equivalent TMR-labelled S129C α-syn for live-cell imaging studies were made in the same manner as wild-type seeded fibrils, at a final protein concentration of 300 μM.

Fibrils were fragmented at 1000 rpm with the precision stirrer, for 24 h, before experiments.

2.4.4 Aβ16-22 fibril formation

Aβ16-22 fibril reactions were set up by dilution of a 20 mM peptide stock in 100% (v/v) DMSO to 400 μM final concentration in 25 mM sodium phosphate, pH 7.0. The mixture was vortexed briefly to ensure homogeneity and incubated at room temperature for a minimum of 15 days, without agitation.

2.4.5 Ccβ-p fibril formation

A 10 mM peptide stock in 100% (v/v) DMSO was diluted to 200 μM final concentration in phosphate buffered saline (PBS) and incubated at 37 °C, without agitation, for a minimum of 18 h.

2.4.6 Transmission electron microscopy

Fibril formation was verified and morphology observed by negative stain transmission electron microscopy. 3 μL of sample was loaded onto a carbon coated copper specimen grid (Agar Scientific Ltd, UK) and left for 30 s, before blotting against filter paper. 2 x 10 μL drops of H_2O were loaded to briefly wash the grid, before blotting again and staining with 10 μL 2% (w/v) uranyl acetate, for 30 s. The grid was then finally blotted and allowed to dry completely. Images were captured with a Jeol JEM 1400 Transmission Electron Microscope, 120 kV.

2.4.7 Fibril yield determination by SDS-PAGE

40 µL fibril samples were centrifuged at 16,000 x *g* for 20 min, to separate the insoluble fibril pellet from any remaining soluble peptide. Supernatants were removed and added to an equal volume of 2 x SDS reducing loading buffer (**Table 2.6**). Pellets were resolubilised in 40 µL of 25 mM sodium phosphate, pH 7.5, and also diluted in loading buffer. 20 µL of each sample were analysed by SDS PAGE (Section 2.3.1.5) along with 20 µL of whole fibril sample (pre-centrifugation) as a reference.

2.4.8 Fibril yield determination by calibrated high performance liquid chromatography (HPLC)

Fibril yield for smaller peptide fragments (ccβ-p/Aβ16-22) was estimated with HPLC analysis of the remaining soluble fraction after centrifugation of fibril samples. A calibration curve was constructed from 5 µL injections of reference solutions (200, 100 and 50 µM of monomeric peptide stock in 100% DMSO) onto a C18 reverse phase column (Phenomenex – HPLC performed by Mr Martin Huscroft, School of Chemistry, University of Leeds). Separation was monitored with UV absorbance at 210 nm and peak area of each calibrant was plotted as a function of concentration. 200 µL fibril samples were separated into soluble and insoluble fractions via centrifugation at 16,000 x *g* for 20 min. The top 100 µL of supernatant was removed and frozen over solid CO_2 and lyophilised. Peptide material was then resuspended in 100 µL 100% HFIP, sonicated for 10 s (Soniprep 150, micro probe, 10 µm amplitude) and incubated at room temperature for 1 h. The sample was then centrifuged briefly at 16,000 x *g* to remove insoluble buffer salts. The top 25 µL was removed and diluted into 75 µL DMSO for injection. Peak area from 5 µL injections was measured at 210 nm and concentration determined from the calibration. The value calculated was then corrected for 8-fold dilution during sample preparation. Fibril yield was estimated from the concentration of soluble material using **Equation 2.2**.

$$Yield\ (\%) = \frac{mol_{total} - mol_{soluble}}{mol_{total}} \times 100 \qquad \textit{Equation 2.2}$$

2.5 Target preparation for *in vitro* selection

2.5.1 Biotin labelling of Aβ40 assemblies

EZ Link™ NHS-LC-LC Biotinylation Reagent (Pierce, Thermo Scientific) was dissolved in 25 mM sodium phosphate buffer, pH 7.5, to a concentration of 1 mg/mL, immediately before use. The peptide species to be labelled (Aβ40 monomer or fibrils) was dissolved into 25 mM sodium phosphate buffer, pH 7.5, and made up to the appropriate protein concentration depending on the molar ratio to biotinylation reagent required. Reactions were allowed to proceed for various timescales to obtain the desired level of labelling (discussed in Section 3.4.2). Reactions were then quenched with 1/10th volume 1 M Tris -HCl, pH 8.0, before buffer exchange to remove free biotin. For ESI-MS analysis to determine labelling levels, dialysis with 2,000 MWCO devices (Slide-A-Lyzer™ MINI, Thermo) was conducted against H_2O or 100 mM ammonium acetate. Biotinylated fibrils were pelleted at 4,000 x *g*, for 20 min at room temperature, and the buffer removed. This was repeated three times to achieve sufficient buffer salt removal for MS. The fibrils were then redissolved in the same volume of 1,1,1,3,3,3 hexafluoro-2-isopropanol (HFIP) and incubated at 37 °C overnight, with 200 rpm agitation, to allow complete depolymerisation. HFIP was dried off with a gentle stream of N_2 gas, leaving dried sample to be redissolved in 100 mM ammonium acetate, pH 7.5, suitable for analysis by ESI-MS. Biotinylated samples for aptamer selection were buffer exchanged post labelling into MOPS selection buffer (**Table 2.6**) via dialysis (monomer) or centrifugation (fibrils).

2.5.2 Immobilisation of peptide species to streptavidin-coated microspheres

300 µL streptavidin-coated microspheres (10 mg/mL Dynabeads™, Dynal Biotech) were washed three times by magnetic partitioning for 2 min, removal of all buffer and exchange into the same volume of MOPS selection buffer (**Table 2.6**), before incubation with biotin-modified targets. The concentration required to saturate beads was based on the peptide binding capacity (400 pmol/mg) given in the product manual. Total protein concentration added was at a 20 x excess to this value, to allow complete saturation. Beads were incubated

at room temperature with gentle agitation for 18 h. Beads were then washed a further three times. The efficiency of bead binding was assessed by absorbance measurement at 280 nm, of the peptide solution, before and after magnetic partitioning.

2.6 RNA methods

2.6.1 Polymerase chain reaction (PCR)

PCR reactions were set up to amplify the initial DNA libraries/individual aptamer clone templates to be transcribed. The technique uses a thermostable DNA polymerase to amplify a DNA sequence, with the addition of dNTPs and oligonucleotide primer ends. Reactions were set up in 50 µL total reaction volumes and component quantities are outlined in **Table 2.11**.

Component	Volume (µL)	Final concentration
5 x KAPA Buffer	10	1 x
5 x KAPA Enhancer 1	10	1 x
KAPA dNTP mix (10 mM)	1	0.2 mM each
Template DNA (1 µM)	1	20 nM
Primer 1 (100 µM)	0.25	0.5 µM
Primer 2 (100 µM)	0.25	0.5 µM
KAPA Robust G2 Polymerase (5 U/µL - KAPA Bioscience)	0.25	1.25 U
H_2O	27.75	-

Table 2.11 Components of a typical 50 µL PCR reaction using a KAPA2G Robust PCR kit (Kapa Biosystems).

The PCR programme used is outlined in **Table 2.12**.

Step	Temperature (°C)	Time (min)
Initial denaturation	95	2
Denaturation	95	0.5
Annealing	60	0.5
Elongation	72	0.5
Repeat denaturation, annealing and elongation (x 10)		
Final elongation	72	2

Table 2.12 Temperature cycle for a typical PCR reaction.

PCR products were purified by Qiagen PCR purification kit (according to manufacturer's instructions) and DNA eluted in nuclease-free H_2O. In cases where more concentrated PCR products were required for high-yield transcriptions, several PCR reactions were pooled and concentrated via this PCR purification method. PCR products were analysed by native PAGE (Section 2.6.2) and stored at -20 °C.

2.6.2 Native polyacrylamide gel electrophoresis (Native PAGE)

Native PAGE (rather than typical agarose gel electrophoresis) was used to analyse DNA, to allow resolution of shorter sequences. Samples were diluted in a 5 x GelPilot DNA loading dye (**Table 2.3**). Gels were cast in 20 x 20 cm glass plates with a 1 mm spacer. Gel components are given in **Table 2.13**. Gels were run at 300 V, for 1.5 h in a 1 x TBE running buffer. Gels were stained in 0.1 μg/mL ethidium bromide (EtBr) in TBE and imaged with an InGenius Gel documentation system (Syngene, Cambridge, UK).

Component	Volume (mL)
30% (w/v) 29:1 acrylamide:bisacrylamide	11.5
5 x TBE	7
H_2O	16
10% (w/v) APS	0.35
TEMED	0.035

Table 2.13 Components of a 10% acrylamide native PAGE gel. Volumes allow casting of a single 20 x 20 cm gel with 1 mm spacers.

2.6.3 *In vitro* transcription of 2'F RNA aptamers

In vitro transcription reactions were set up in 50 µL final volumes. Components are given in **Table 2.14**. The reaction mixture was incubated at 37 °C for 6 h in a PCR thermocycler. Y639F/ H784A T7 RNA polymerase was recombinantly expressed and purified by Dr. David Bunka (School of Molecular and Cellular Biology, University of Leeds). Mutant polymerase was required in transcription of non-canonical 2'F RNA. The Y639F mutation eliminates inflexibility of the hydrogen bonding potential of the 2'F substituent of the substrate NTP, thereby tolerating 2'F modifications. H784A enhances modified NTP incorporation further, by providing more space in the active site, reducing occlusion of the minor groove side of the 3'-rNMP:template base pair, therefore relaxing the barrier to efficient extension of transcripts during addition of non-canonical NMPs at the 3'-end[406].

Component	Volume (µL)	Final concentration
10 x transcription buffer (**Table 2.6**)	5	1 x
1 M DTT	2	40 mM
100 mM NTP mix (1:1:1:1 ATP:2′F CTP:GTP:2′F UTP)	2.5	5 mM each
dsDNA template (from 50 µL PCR (Section 2.6.1) – typical conc. 500 ng/µL)	5	50 ng/µL
Yeast Inorganic Pyrophosphatase (YIP) (1 U/µL)	0.5	0.5 U
Y639F/H784A T7 RNA polymerase (3.7 µM stock)	5	370 nM
DEPC-treated H_2O	30	-

Table 2.14 Components of a typical *in vitro* transcription reaction.

2.6.4 *In vitro* transcription of 2′OH RNA aptamers

Transcription of 2′OH RNA does not require mutant T7 RNA polymerase and, therefore, HiScribe™ T7 High Yield RNA Synthesis kit (NEB) was used, according to the manufacturer's protocol. Volumes were scaled up for 50 µL reactions.

2.6.5 Transcription with modified nucleotides

2.6.5.1 Alexa488 labelling of RNA by incorporation of modified UTP

Incorporation of modified nucleotides requires alteration to the transcription mixes outlined in **Table 2.14**. To prepare 2′F Alexa UTP labelled RNA, the nucleotide mix was supplemented with 1/80th concentration of ChromaTide® Alexa Fluor® 488-5-UTP (Molecular Probes – altered nucleotide mix given in **Table 2.15**) to give final RNA products

with 1 fluorescent UTP per molecule, on average. To calculate average UTP incorporation, absorbance at 260 nm was corrected for the dyes contribution using **Equation 2.3** and the correction factor for Alexa488 UTP at 260 nm = 0.3 (obtained from the manufacturer's protocol). The absorbance maximum of Alexa488 is 493 nm. Base: dye ratio was calculated using **Equation 2.4** where ε_{dye} = 62,000 M^{-1} cm^{-1} and ε_{base} = 8,250 M^{-1} cm^{-1}. This value was divided by the number of nucleotides in the sequence to give the average number of dye molecules/RNA molecule.

$$TrueAbs_{260} = \left(Abs_{260} - (Abs_{493} \times 0.3)\right) \qquad \textit{Equation 2.3}$$

$$base{:}\,dye = \left(TrueAbs_{260} \times \varepsilon_{dye}\right)/(Abs_{493} \times \varepsilon_{base}) \qquad \textit{Equation 2.4}$$

Components for transcription reactions are given in **Table 2.16**.

Component	Volume (mL)	Final molar concentration (mM)
ATP	5	10
2′F CTP	5	10
GTP	5	10
2′F UTP	6.25	9.875
ChromaTide® Alexa Fluor® 488-5-UTP	4.94	0.125
DEPC-treated H_2O	23.81	-

Table 2.15 Components of NTP mix for the enzymatic incorporation of Alexa488 dUTP.

Component	Volume (µL)	Final concentrations
10 x transcription buffer (**Table 2.6**)	5	1 x
1 M DTT	2	40 mM
NTP mix (**Table 2.15**)	12.5	4 x dilution mix from **Table 2.15**
dsDNA template (from 5 x 50 µL PCR pooled and concentrated (Section 2.6.1) – typical conc. 2.5 µg/µL)	10	500 ng/µL
Yeast Inorganic Pyrophosphatase (YIP) (1 U/µL)	0.5	0.5 U
Y639F/H784A T7 RNA polymerase (3.7 µM stock)	10	740 nM
DEPC-treated H_2O	10	-

Table 2.16 Components of a typical 50 µL transcription reaction used in incorporation of Alexa488 dUTP.

2.6.5.2 5′ Biotin labelling of RNA

To prepare 5′ biotin labelled transcripts, the NTP mix was altered according to **Table 2.17**, with 5′ biotin GMP. Transcription reactions were set up according to the standard protocol (Section 2.6.3).

Component	Volume (mL)	Final molar concentration (mM)
ATP	12.5	25
2′F CTP	12.5	25
GTP	3.13	6.25
2′F UTP	12.5	25
5′ Biotin GMP	9.38	18.75

Table 2.17 Components of NTP mix for the enzymatic incorporation of 5′ biotin GMP.

2.6.6 Alexa488 labelling of RNA via 5′ amino modification

5’ amino modified RNA was fluorescently labelled via an amine-reactive sulfodichlorophenol ester. 3 µL of Alexa Fluor® 488 5-SDP Ester (10 mM, Invitrogen) was added to 6 µL of 200 µM 5' amino modified RNA in DEPC-treated H_2O, with 1 µL 1 M sodium borate, pH 8.3. The reaction mixture was incubated at room temperature for 4 h, with gentle agitation on a roller. 10 µL of Gel Loading Buffer II (Ambion) was added to the mixture and the labelled RNA was gel purified, as described (Section 2.6.8.2).

2.6.7 Denaturing polyacrylamide gel electrophoresis (Denaturing PAGE)

RNA products were analysed (and in some cases purified (**Table 2.18**, Section 2.6.8.2) by denaturing PAGE.

Gels were constructed from 20 x 20 mm plates with a 1 mm spacer. The gels were made up of 10% (w/v) 19:1 acrylamide:bisacrylamide, in 1 x TBE buffer and 8 M urea (Ultrapure Sequagel® urea gel, National Diagnostics – manufacturer’s protocol for a 10% gel) and pre-run at 15 W for 2 h before sample loading. Samples were prepared with the addition of Gel Buffer II (Ambion) containing 95% deionised formamide, 0.025% (w/v) SDS, 18 mM EDTA, bromophenol blue and xylene cyanol, and boiled for 5 min. Gels were then run at 15 W for 1.5 h and stained with 0.1 µg/mL EtBr in TBE buffer.

2.6.8 RNA purification methods

Transcripts were subject to DNase treatment by the addition of 1 µL of TURBO™ DNase (Life Technologies) and incubation at 37 °C for 15 min.

RNA was purified via different protocols depending on the level of purity required for the subsequent application. The purification methods used are outlined in **Table 2.18**.

Purification method		Application	Method
RNA Clean resin (Agencourt RNAClean XP, Beckman Coulter)		Robotic selections	According to manufacturer's instructions
Phenol chloroform extraction/ethanol precipitation (Section 2.6.8.1) followed by…	Illustra microspin G-25 column (GE Healthcare)	Basic desalting	According to manufacturer's instructions
	RNA Clean and Concentrate™-5 column (Zymo)	2'OH, > 17 nt	According to manufacturer's instructions
	Gel extraction	2'F, Alexa488 labelled, high yield	(Section 2.6.8.2)

Table 2.18 Summary of purification methods utilised in producing aptamers for various applications during this study.

2.6.8.1 Phenol chloroform extraction and ethanol precipitation of RNA

Acidified phenol (pH 4.5) was used to partition RNA from protein and DNA contaminants. DNase treated RNA was added to 2 x volume of acid phenol:$CHCl_3$ (5:1, pH 4.5, Ambion), vortexed for 30 s and centrifuged at 16,000 x *g* for 30 s, to partition the organic and aqueous phases. The top aqueous layer, containing RNA, was carefully aspirated and added to 2 x volume of chloroform:isoamyl alcohol (24:1), before the mixing and centrifuging process was repeated.

RNA was then precipitated by the addition of 1/5th volume of 10 M ammonium acetate, 1/100th volume 20 mg/mL glycogen (Thermo Scientific, UK) and 2 x volume of ice cold ethanol. Samples were frozen at -20 °C for a minimum of 18 h. Precipitates were centrifuged for 2 h at 16,000 x *g*, 4 °C, and washed twice with the addition of 500 µL 70 % ethanol and 20 min centrifugation at 16,000 *x g*, 4 °C. Pellets were dried for 10 min at 40 °C in a rotary evaporator and resolubilised in DEPC-treated H_2O for storage at -20 °C, before further purification.

2.6.8.2 Extraction and purification of RNA from denaturing PAGE

To purify RNA products from denaturing gel extracts, gels were constructed according to the protocol outlined in Section 2.6.7, with 1.5 mm spacers and larger sample combs for loading larger sample volumes. Gel components were scaled up to 50 mL.

Samples (post ethanol precipitation) were solubilised in 10-20 µL of Gel Buffer II (Ambion) and boiled for 10 min. Samples were loaded onto gels and run as normal. Once separation was complete, gels were stained in freshly prepared EtBr (0.1 µg/mL) made up in nuclease free TBE/H_2O, for 10 min and de-stained briefly in water. Bands were excised and gel fragments suspended in 50 µL 10 mM Tris-HCl, pH 8.5 (Buffer EB, Qiagen). Samples were frozen overnight at -80 °C. Gel fragments were then subject to repeat cycles of 2 h agitation on a roller at room temperature, removal of buffer containing RNA and a fresh 50 µL of EB applied. This was repeated three times until a final volume of 150 µL was pooled, precipitated as described (Section 2.6.8.1), resolubilised in DEPC-treated H_2O, and stored at -20 °C.

2.6.9 Reverse transcription PCR (RT-PCR)

Conversion of RNA products to their dsDNA precursors was conducted via reverse transcription, followed by PCR. The typical reaction mixture is given in **Table 2.19**. Samples were incubated at 52 °C for 1.5 h, followed by the addition of PCR mix (**Table 2.11**, scaled up to 80 µL final volumes). PCR was performed according to the same thermocycling programme described in Section 2.6.1, **Table 2.12**.

Component	Volume (µL)	Final concentrations
RNA sample	35	-
5 x Buffer (Transcriptor)	10	1 x
dNTP mix (10 mM)	2	400 nM
Primer 2 (100 µM)	1	2 µM
DEPC-treated H_2O	1	-
Transcriptor Reverse Transcriptase (20 U/µL, Roche)	1	20 U

Table 2.19 Components of a typical 50 µL RT-PCR reaction using a Transcriptor Reverse Transcription kit (Roche).

2.7 SELEX methods

2.7.1 RNA library preparation

RNA libraries were transcribed from naïve DNA library templates designed by Dr. David Bunka and synthesised commercially (Thermo Hybaid). Sequences and associated primers are shown in **Figure 2.1.**

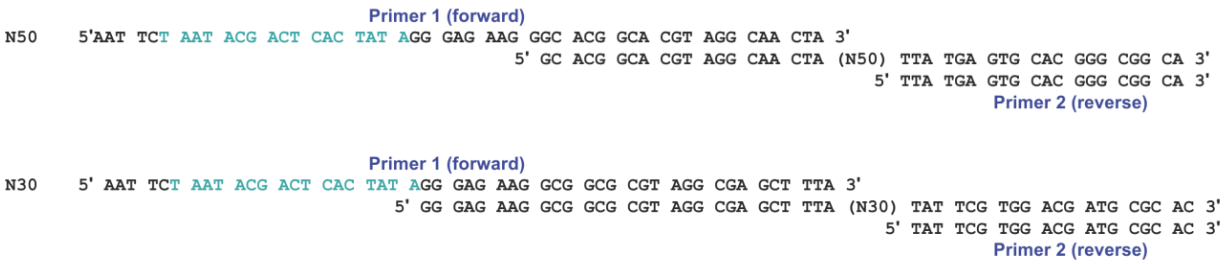

Figure 2.1 Schematic representation of the N50 and N30 naïve DNA templates used in this study. Sequences in blue correspond to the T7 promoter sequence in Primer 1 (forward) in both libraries.

2.7.2 SELEX protocol

The basic SELEX protocol is described here. Modifications to this standard protocol were made to include solution capture rounds and competition elution rounds, which are described (Sections 2.7.4 and 2.7.5).

The naïve 2'F pyrimidine modified RNA library was transcribed as previously described (Section 2.6.3) and DNase treated with the addition of 4 µL DNase and 6 µL 10 x DNase Buffer (Promega). RNA was purified by RNAClean XP resin (Agencourt) according to the manufacturer's protocol. All steps were performed in MOPS selection buffer (**Table 2.6**) unless otherwise stated. 50 µL of purified RNA was added to 50 µL 2 x MOPS selection buffer and incubated with 20 µL pre-washed biotin-saturated streptavidin-coated microspheres for 15 min at room temperature, with gentle agitation on a roller. The beads were partitioned via a magnetic separation rack (2 min) and the unbound fraction was removed and incubated with 20 µL target beads. Beads were partitioned again (2 min) and the unbound fraction was removed. Beads were washed by sequential additions of 125 µL of MOPS selection buffer to partitioned beads (10 x 1 min). Beads were then resuspended in 35 µL DEPC-treated H_2O and transferred to 200 µL PCR tubes where 40 µL of mineral oil was dispensed on top of the mixture to avoid evaporation. The sample was then heated to 95 °C for 5 min in a PCR thermocycler. RNA was reverse transcribed by addition of RT mixture (Section 2.6.9) and PCR amplified for the next round. DNA products were analysed by native PAGE (Section 2.6.2) to monitor selection.

2.7.3 Automated selection rounds

Automated selection rounds were undertaken using a Biomek 2000 laboratory automated work station (Beckman Coulter). Selections were carried out in 96-well PCR plates (Thermo Fisher Scientific). Automated programmes were written by Dr. David Bunka and Dr. Simon White.

2.7.4 Target capture selection rounds

Capture selection rounds were utilised to promote binding specificity for the non-immobilised, and therefore native target conformation. 50 µL of the RNA pool was incubated with 50 µL of the 20 µM biotin-labelled target peptide species (which had not been pre-immobilised), for 15 min at 25 °C. Calculation of the concentration of target species required was based on peptide binding capacity (400 pmol/mg). The mixture was then added to 0.5 mg of pre-washed, un-conjugated streptavidin microspheres and incubated for 30 min, rolling at room temperature, to capture complexes from solution. Beads were then magnetically separated, washed three times with 1 mL of selection buffer, before elution as described in the basic SELEX protocol (Section 2.7.2).

2.7.5 Competition elution selection rounds

Following standard immobilised target incubation and washing steps, described in the basic protocol (Section 2.7.2), aptamers with greater affinity for native, non-immobilised species were competed from their bead bound state with solution target challenges. 35 µL of the un-modified target peptide species was incubated with the beads for 10 min (25 °C, rolling). Beads were partitioned (2 min) and the buffer (containing competitor peptide species and associated RNA) was removed. This step was repeated with a higher concentration of competitor, to challenge further aptamer species from the immobilised target (concentrations of competition solutions are given in Sections 3.5.1 and 3.5.2). After removal of this second competition, 35 µL of DEPC-treated H_2O was added to the beads and heat elution of the remaining aptamers was conducted according to the standard procedure.

2.7.6 Stringency parameters throughout selection

Various experimental conditions were altered in later rounds of the SELEX protocol to increase stringency of selection. These include alterations to incubation times, temperatures, target concentrations and numbers of washes. Alterations are summarised for each type of selection round in **Table 2.20**.

Selection round	Incubation step	Incubation conditions	Target bead volume (µL)	Wash conditions
Robotic rounds 1-5		15 min 25 °C	20	125 µL 1 min 25 °C x 10
Robotic rounds 6-10		5 min 37 °C	10	125 µL 1 min 25 °C x 13
Competition	Target binding	15 min 25 °C	20	125 µL 1 min 25 °C x 10
	Solution target binding	10 min 25 °C		
Target capture	RNA:fibril incubation	15 min 25 °C	50	1 mL 1 min 25 °C x 3
	Bead incubation	30 min 25 °C		

Table 2.20 Conditions used during different selection rounds to alter selection stringency.

2.7.7 Bioinformatic analysis of next generation sequencing (NGS) data

Scripts for aptamer sorting and base-composition evaluation were written by Dr. Eric Dykeman (Department of Mathematics, University of York, UK) in Perl programming language. The data obtained from NGS contains both the forward and reverse sequence reads. These two files were amalgamated into a single data file containing all raw sequences. The aptamer sorting script initially searches for user-defined primer sequences, in both the forward and reverse direction, with a tolerance threshold where 12 correct nucleotides constitutes a "hit". The script then generates the complementary sequence of any hits in the reverse direction and combines identical pairs as a single read in the forward direction. The script then searches for sequences with the correct random region length (user-defined stringency set at ± 15 nucleotides for N50 aptamers, ± 10 for N30). These filtered sequences were then sorted into exact matches, which were quantified and ranked in order of frequency of occurrence.

The output of the above analysis was then used in the base-composition evaluation. The script searches for, and quantifies, the number of times each nucleotide is represented within the randomised-region and calculates this as a percentage of total nucleotides.

2.8 *In vitro* techniques

2.8.1 Size exclusion chromatography multi-angle laser light scattering (SEC-MALLS)

Size exclusion chromatography was performed on an ÄKTA micro system coupled to a Wyatt Dawn TREOS multiangle laser light scattering detector. MALLS data were analysed using Wyatt Astra software (version 6.0). SEC separation was carried out with a Superdex™ Peptide 10/300 GL column (GE Healthcare) with filtered and degassed MOPS selection buffer (**Table 2.6**) and run at a flow rate of 0.3 mL/min, at room temperature. Lyophilised Aβ40 was dissolved in the same buffer, to a concentration of 1 mg/mL. 50 µL was injected at time points 0 and 3 h. The 3 h sample was incubated at 4 °C prior to injection.

2.8.2 Surface plasmon resonance

An SA sensor chip (GE Healthcare) containing a dextran matrix and pre-derivatised with streptavidin, was docked into the Biacore 3000 instrument (GE Healthcare), which was primed with MOPS selection buffer (**Table 2.6**) containing 0.005% (v/v) Tween20. Biotinylated peptide was injected at a flow rate of 10 µL/min until an appropriate response was achieved (typically 25 RU for Aβ40 – appropriate RU of immobilisation for peptides of specific MW were calculated with Biacore application support (Available online: https://www.biacore.com/lifesciences/Application_Support)). Flow cell 1 was left blank to serve as a baseline. Further flow cells were either derivatised with control peptides or larger doses of target ligand. Purified RNA to be tested was dialysed against the running buffer prior to analysis. The dialysate was filtered and used directly as the running buffer during the experiments, to reduce refractive index changes upon injection. All assays were conducted at a flow rate of 10 µL/min. Samples were injected for 300 s at 10 µL/min. Surfaces were regenerated with buffer containing 50 mM NaCl or 0.05% (w/v) SDS for subsequent sample injections. Data were processed with BIAevaluation software (GE Healthcare).

2.8.3 Pull-down assays

Aβ40-saturated streptavidin beads were diluted serially into MOPS selection buffer (**Table 2.6**) to create a gradient of peptide concentrations. Aptamer was added at each dilution point to the same final concentration (500 nM in gel-based pull-down assays, 30 nM in fluorescent pull-down assays). The complex was incubated at room temperature for 15 min to allow association. Beads were separated from solution on a magnetic rack for 2 min and unbound RNA was aspirated off. In pull-down assays where unbound fluorescent RNA was measured, the unbound fraction was loaded into glass capillaries (Nanotemper, standard-treated) and the fluorescence intensity measured with excitation at 470 nm and emission at 520nm, using the Monolith™ NT .115 Microscale thermophoresis (MST) instrument, set up to read fluorescence intensity only. In gel-based pull-down assays, unbound RNA was removed and beads were washed three times with buffer (1 min separation on magnet, 125 µL washes, consistent with standard SELEX conditions - Section 2.7.2). Elution of bound RNA was conducted by the addition of 35 µL DEPC-treated H_2O, to each sample, and heating to 95 °C for 5 min. RT-PCR mixtures (Section 2.6.9) were then added directly to the samples to amplify all bound RNA. Bound RNA fractions at each protein concentration were analysed by native PAGE (Section 2.6.2) and stained with 0.1 µg/mL EtBr in TBE (**Table 2.6**) for 5 min, before 5 min de-staining in H_2O. Images were taken using an InGenius gel documentation system (Syngene) and densitometry of the resultant bands was measured with Genetools software.

Data were fitted, using OriginPro 8.6, to a modified Hill function (**Equation 2.5**) which takes into account signal change upon binding. *START* is where the curve begins, *END* is where the curve ends (either higher or lower than *START*), x is concentration of titrant, K_d is the dissociation constant and *n* is the Hill coefficient.

$$y = START + (END - START)\frac{x^n}{{K_d}^n + x^n} \qquad \textbf{Equation 2.5}$$

2.8.4 Microscale thermophoresis (MST)

A stock solution of Alexa488 labelled aptamer was heated in a PCR thermocycler to 98 °C for 5 min before cooling by 0.1 °C/s until a final temperature of 25 °C was reached, to thermally anneal the RNA. This stock RNA was then added, at 250 nM final concentration, to aliquots of unlabelled Aβ40 peptide at concentrations ranging from 12 nM to 100 μM. Mixtures were incubated at room temperature for 15 min. The RNA: protein mixtures were loaded into individual standard treated capillaries (Nanotemper) and analysed with the Monolith™ NT.115 MST instrument. Excitation was 470 nm, emission 520 nm. MST power was 40%, LED power 95%. Data were processed with NanoTemper Analysis software.

2.8.5 Fluorescence polarisation

A Biomek 2000 laboratory automation work station (Beckman Coulter) was utilised to set up fluorescence polarisation (FP) assays in a 384-well plate format. Pre-formed fibrils were diluted serially (a 2/3 regime) into MOPS selection buffer (**Table 2.6**), in triplicate, before addition of Alexa488 labelled aptamer, at a final concentration of 10 nM. The total volume in each well was 40 μL. Polarisation was measured using a Perkin Elmer EnVision 2103 MultiLabel plate reader (excitation 480 nm, emission 535 nm). Polarisation was calculated from parallel (I_{II}) and perpendicular ($I_{\perp}$) intensity at 535 nm using **Equation 2.6**. The G factor is an instrument factor set to 1. For competition polarisation experiments, titrations of competitor ligands were used to dissociate fluorescent aptamers from their complex with fibrils. Aliquots of the fibril: aptamer complex, at concentrations sufficient to produce 65% of the FP response in the direct binding experiments, were set up in individual tubes. Competitor ligand at varied concentrations (produced through serial dilution into buffer) was added to each aliquot of the complex and incubated at room temperature for 30 min. Aliquots were transferred to 384-well plates for detection as described above. Assays were set up in triplicate. Data were plotted as average ± SEM (n = 3) and were fitted to the Hill function outlined in Section 2.8.3, **Equation 2.5**.

$$Polarisation = \frac{I_{II} - (G \times I_{\perp})}{I_{II} + (G \times I_{\perp})} \qquad \textit{Equation 2.6}$$

2.8.6 Niad 4 fluorometry

50 µL samples containing 10 µM Aβ40 and 10 µM Niad 4 in 25 mM sodium phosphate buffer, pH 7.5 plus a final concentration of 1% (v/v) DMSO, were prepared in low volume, NBS low binding 96-well microplates (Corning) and sealed with hydrophobic, transparent plastic film (Breathe-easy®, Sigma). Plates were incubated at 25 °C in a CLARIOstar plate reader for 60 h with intermittent agitation (5 s shaking at 600 rpm, 5 min intervals). Fluorescence intensity was monitored over time with excitation at 490 nm and emission measured at 615 nm. When fibril formation was monitored in the presence of aptamer, RNA was added at a final concentration of 10 µM with RNase inhibitor (murine, New England Biolabs) at a 1 in 40 dilution, in line with manufacturer's recommendations.

2.8.7 Ionic strength calculation

Ionic strength for the glycosaminoglycans used in this study was estimated by taking the number of charges on a single disaccharide unit and multiplying by the average number of disaccharides in the full-length polymer. For example, LMW heparin has an average MW of 4,600 Da, which equates to ~8 repeat units of the disaccharide (**Figure 5.27 a**). Therefore, the net charge of LMW heparin is taken as -32 and ionic strength (I) calculated according to **Equation 2.7**, where C_i is the molar concentration of ions and Z_i is the total charge.

$$I = \frac{1}{2}\sum (C_i)\,(Z_i)^2 \qquad \textit{Equation 2.7}$$

2.9 *In vivo* techniques

All cell culture and imaging work was carried out with full supervision by Dr. Matthew Jackson (School of Molecular and Cellular Biology, University of Leeds). MTT and ATP assays were carried out by Dr. Jackson.

2.9.1 Cell culture

SH-SY5Y cells were cultured in Dulbeccos Modified Eagles Medium (DMEM) (Sigma) containing phenol red (Sigma), 10% (v/v) foetal calf serum (Biosera), 1% (v/v) Glutamax (Invitrogen), 100 IU/mL penicillin and 100 µg/ml streptomycin, in 75 cm^3 flasks (Corning). Cells were incubated at 37 °C, 5% CO_2 and passaged when they reached 60 - 80% confluence, using a 1% (v/v) trypsin EDTA solution (Sigma).

2.9.2 MTT/ATP cell viability assays

Cells were plated out at 15,000 cells / well in 96-well microplates in 200 µL DMEM medium. Following 24 h incubation, samples were dosed (with fibrils/aptamer/control samples) and incubated for a further 24 h at 37 °C, 5% CO_2. 1% (w/v) NaN_3 was used as a positive control for cell death. In the case of MTT assays, 10 µL of a 10 mg/mL solution of MTT (Sigma), in PBS, was added per well and samples were incubated for a further 1.5 h. The medium was then removed and resulting formazan crystals resuspended in DMSO (Sigma). The amount of MTT reduction was quantified by absorbance at 570 nm with subtraction at 650 nm to correct for cellular debris. Cellular ATP levels were measured using a luminescent ATPlite assay kit (Perkin Elmer) in accordance with manufacturer's instructions. Luminescence was measured using a BMG Labtech Plate Reader.

2.9.3 Confocal imaging

Cells were plated out at 300,000 cells per mL in imaging dishes (WPI-Europe FD35-100). Following 24 h incubation, samples were dosed with Alexa488 labelled aptamers (Section 2.6.5.1) and 10% (monomer equivalent) TMR-labelled fibrils and incubated for a further 24 h at 37 °C, 5% CO_2. Lysotracker deep red or Cell Mask deep red (both Life Technologies) were used at 100 nM and 0.5 µg/mL, respectively. Cells were washed three times with 1 mL phenol red-free media, prior to imaging on a Zeiss LSM 700 Confocal Microscope with a 63 x objective.

3 Selection of RNA aptamers against assemblies of Aβ40

3.1 Objectives

The primary aim of the work described in this thesis was to exploit the exquisite molecular recognition power of RNA aptamers in amyloid-forming systems; specifically in the selection of aptamers able to recognise different species during the aggregation of the amyloid-β peptide, Aβ40. This chapter outlines the rationale behind choosing specific Aβ40 assemblies as selection targets, the purification of recombinantly expressed Aβ40 peptide and the preparation of the target assemblies. Furthermore, the *in vitro* selection of RNA aptamers against Aβ40 fibrils and their precursor monomeric peptide is described.

3.2 Aβ40 monomer and fibrils as targets for aptamer selection

As discussed in Section 1.2.6, the development of agents able to detect and/or treat amyloid disorders presents a significant problem in both academic and pharmaceutical research[1, 3]. Structural information into the process of amyloid aggregation is limited and therefore development of new ligands, by structure-based design, is especially challenging in these systems. For this reason, an *in vitro* selection approach was proposed, to develop nucleic acid based ligands as potential new tools in the context of Aβ40 aggregation. The aims were to a) aid fundamental studies into the molecular mechanisms underlying the aggregation process, b) provide potential new diagnostic reagents and c) develop new intervention strategies into Aβ40 assembly into amyloid. The first major question, therefore, was which of the many species involved in this highly complex system are the most appropriate selection targets to enable us to meet these objectives.

3.2.1 Aβ40 monomer

The natively unstructured monomeric peptide is the starting point of Aβ40 aggregation. Via currently poorly defined mechanisms, this unfolded monomer assembles spontaneously into oligomeric species, which may be cytotoxic and are believed to cause the cell death associated with neurodegeneration and AD[126] (covered in detail in Section 1.3.4). While the identity of the toxic species is hotly debated, species ranging from dimers[268], through to larger oligomers[270, 271, 501] and finally fibrils[97, 103, 215, 502] themselves have been implicated. It is logical, therefore, that the monomeric peptide should be one target in our selections, as this could lead to several possible avenues of intervention. It may be possible to trap the peptide in this seemingly inert monomeric state, preventing its aggregation to higher order and potentially more toxic species, or even to target the peptide for degradation, before aberrant accumulation ensues.

Monomeric Aβ40 is also an attractive selection target from a diagnostic point of view, especially as it is the most abundant form of Aβ in the brain, cerebrospinal fluid (CSF) and the serum[243]. Aβ42 levels in the CSF is an already well-established biomarker in AD, along with the detection of tau and phosphorylated tau[347]. However, it is the general consensus that all three of these biomarkers are required for accurate diagnosis (with confidence >90%[345]) and a single definitive marker has yet to be developed[359]. Analysis of the Aβ42:40 ratio is one common suggestion for improved AD diagnosis[358, 503]. The superior recognition power achievable by aptamer technologies could help in providing these much needed new tools.

3.2.2 Aβ40 fibrils of distinct morphology

Although fibrils are often overlooked as the major toxic entity in amyloid disorders[1, 124, 126], there remains substantial evidence that these end-point structures are interesting in the context of disease. Toxicity has been attributed to fibrils and plaques in several recent studies[147, 502, 504] and they are also implicated in producing further toxic species through secondary processes. These include secondary nucleation mechanisms, leading to the accumulation of new toxic oligomers via surface mediated catalysis[77, 78] or fragmentation, and "molecular shedding" of toxic species from pre-formed fibrillar aggregates[505]. Aptamers raised against fibrillar assembles, therefore, could be useful in several of these

instances, by specific blockage of secondary nucleation sites or by capping the ends of fibrils to prevent production of further toxic structures.

Structural polymorphism is another important attribute of Aβ fibril formation. As discussed in Section 1.3.4.2, many distinct structures have been proposed for both Aβ40 and Aβ42 fibrils[104, 105, 299]. It has also been suggested that differences in fibril structure could correlate with differences in pathology[106]. Therefore, development of recognition molecules, able to distinguish between fibril structures derived from a single precursor peptide, would be invaluable in advancing AD diagnostics.

The 2A and 3Q structures of Aβ40 fibrils[103, 105] (reviewed in Section 1.3.4.3) are ideal targets for RNA aptamer selection for a number of reasons. Firstly, there is structural information available for each of these morphologies, which will greatly aid the study of fibril recognition by aptamers. Further, evidence suggests that by producing new fibrils via seeded elongation, the individual morphologies are maintained, providing homogenous fibril samples for selection[103-105]. Raising aptamers against these two fibril morphologies, both composed from Aβ40, will demonstrate the power of RNA aptamers as a recognition molecule and, if successful, will provide the first instance of ligands able to distinguish between different cross-β containing structures of the same protein sequence.

3.3 Expression and purification of recombinant Aβ40

The following expression and purification of Aβ40 was adapted and optimised based on the published methodology outlined by Linse and colleagues[499]. All optimisation was aided by helpful discussions with Dr. Tiernan O'Malley (Brigham and Women's Hospital, Harvard Medical School, MA, USA).

3.3.1 Protein expression trials

The plasmid containing the gene encoding Aβ40 (PetSac-Aβ40, **Appendix 7.1.1**) was transformed into competent BL21 (DE3) pLysS *E. coli* cells and grown on selective agar plates overnight (Section 2.2.3). Aβ40 produced for this work contains an additional N-terminal methionine to facilitate recombinant expression and it is this 41-residue product

that will be referred to as Aβ40, unless otherwise stated. Single colonies were used to inoculate overnight starter cultures (100 mL, LB media), which in turn were used to inoculate 12 x 1 L cultures of LB with antibiotic selection (Section 2.3.1.1) for large-scale protein expression. Cells were cultured at 37 °C, 200 rpm until an optical density at 600 nm (OD_{600}) = 0.5 was reached and protein expression was then induced with the addition of 0.5 mM IPTG. Cells were then grown overnight (16 h) at 25 °C, 200 rpm, before collection by centrifugation. SDS-PAGE analysis was used to monitor protein expression from induced and un-induced samples (**Figure 3.1 a**).

Protein expression levels were initially low and varied substantially between flasks. Therefore, trials were conducted to optimise expression. Several parameters were tested including most importantly, flask type, culture volume, and the duration and temperature of growth post-induction of protein expression with IPTG. The trials revealed that optimum expression was achieved when 500 mL cultures in 2 L baffled, conical flasks were utilised, most probably because of the increased aeration volume[506] (**Figure 3.1 b**). Another important factor in increasing expression was culturing the cells at 37 °C post-induction for 3-4 hours. By monitoring optical density throughout this phase, cell growth was shown to plateau and extending growth beyond 4 hours led to a decrease in expression. These conditions were used, therefore, for the expression of Aβ40 throughout this thesis.

3.3.2 Purification of Aβ40

The purification method also initially followed that described by Linse *et al.*[499]. After successful, high level expression, cells were disrupted in Tris-HCl and subjected to several rounds of sonication and centrifugation, to isolate and wash the inclusion bodies containing Aβ40. Inclusion bodies were then solubilised with buffer containing 8 M urea (Section 2.3.1.2) before 1 in 4 dilution to reduce urea concentration and facilitate binding to Q Sepharose resin for the next stage of purification. This inclusion body isolation was also optimised from that described[499]. By reducing the number of sonication/centrifugation rounds, significant product losses were avoided, without compromising on the purity achieved at this stage. **Figure 3.2 a** shows the three supernatants S1, S2 and S3, isolated from three successive rounds of sonication followed by centrifugation. The majority of

contaminants are removed in S1 and, by reducing the number of subsequent centrifugation steps, less Aβ40 was lost while sufficient purity was maintained.

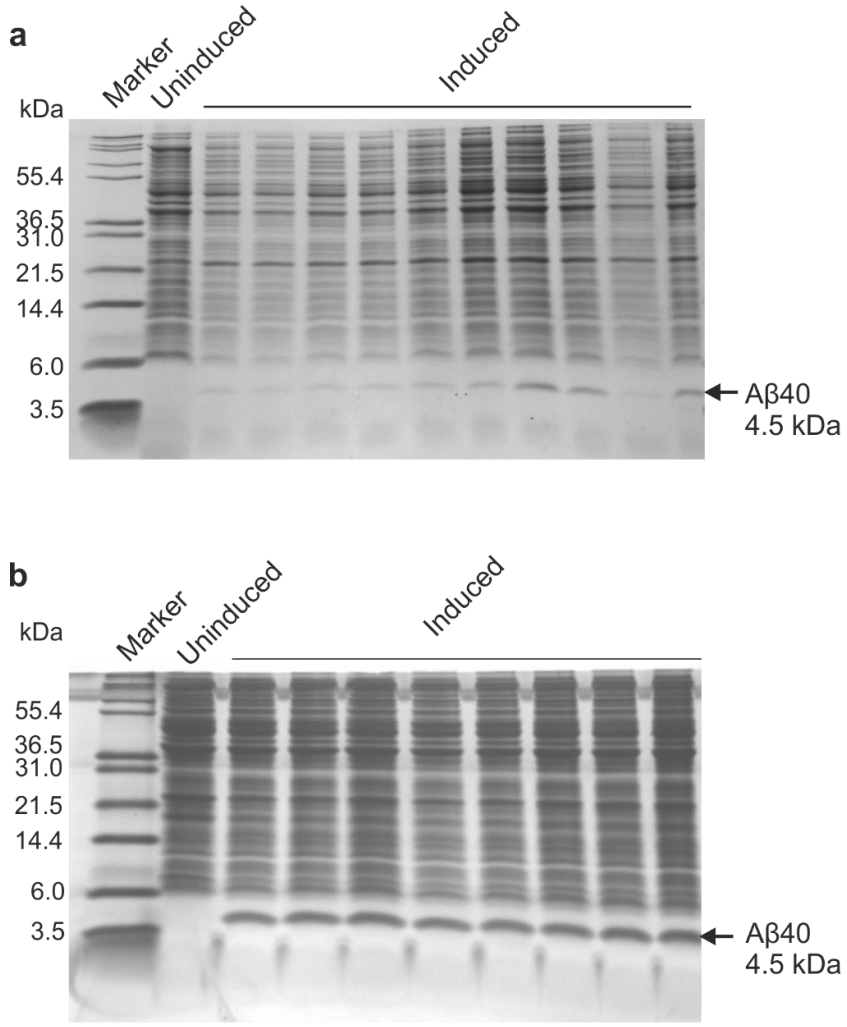

Figure 3.1 Optimisation of Aβ40 expression and purification. **(a)** Reduced and varied expression observed when 1 L *E. coli* cultures were grown in standard conical flasks at 25 °C, overnight. **(b)** Typical over-expression levels yielded under optimised conditions, (500 mL cultures, 2 L baffled flasks, cultured for 3.5 h post induction with IPTG). 1 mL whole cell samples (taken from individual replicate flasks), before (Uninduced) and after (Induced) induction were pelleted and boiled in 2 x loading buffer prior to analysis. (Section 2.3.1.5) The sizes of molecular weight markers are given in kDa.

Aβ40 was then further purified by ion exchange chromatography in a batch format. Column chromatography was previously shown to be unsuitable at this stage[499], as much lower

yields of monomeric peptide were obtained. The batch method presumably avoids aberrant aggregation on the ion exchange column, as a result of high local concentration of the semi-purified product. Protein was eluted from the resin by firstly washing with Tris-HCl buffer, pH 8.5, containing 0 M and then 25 mM NaCl before step-wise elution with 5 x 50 mL 125 mM NaCl fractions. All fractions were analysed by SDS-PAGE (**Figure 3.2 b**). Those confirmed to contain Aβ40 were pooled prior to further purification.

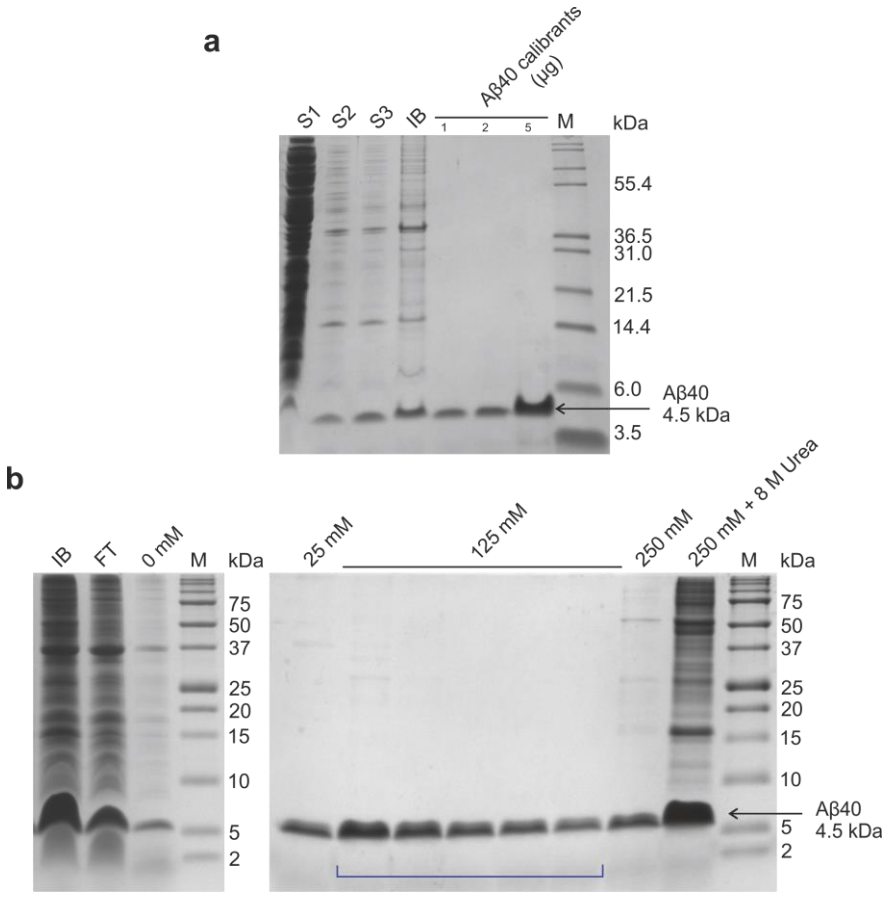

Figure 3.2 Anion exchange purification of Aβ40. **(a)** SDS PAGE analysis of the inclusion body isolation stages of the purification protocol. S1, S2 and S3 denote supernatants from three sequential centrifugation steps. IB indicates the final inclusion-body-containing fraction. Three pure Aβ40 calibrants (containing 1, 2 and 5 μg Aβ40) were loaded to allow estimation of peptide yield at each stage. **(b)** SDS PAGE of fractions collected during batch anion exchange purification. IB indicates the inclusion body fraction isolated before binding to Q-Sepharose resin. FT denotes the flow-through. Concentrations of NaCl in the salt-containing fractions are indicated. Fractions pooled and taken forward for further purification are indicated with the blue bracket. Size in kDa of the protein markers are indicated.

The purification protocol described by Linse *et al*.[499] recommends that, following ion exchange chromatography, Aβ40 should be further purified by molecular mass fractionation, using centrifugal filtration devices, claiming that pure product is obtained from this simple two-step method. However, the results in **Figure 3.3 a.i.** shown that the protein is not sufficiently pure following filtration. Further purification via Reverse Phase High Performance Liquid Chromatography (RP-HPLC) was attempted, whereby the concentrated filtrate (final volume 10 mL) was passed through a semi-preparative C18 column and eluted with an increasing gradient of acetonitrile (**Figure 3.3 a.ii.**). A major peak was observed at 40% acetonitrile, corresponding to the Aβ40.

Mass spectrometric analysis of the purified fraction indicated the presence of a 2179 Da contaminant, corresponding in mass to a C-terminal degradation product (**Figure 3.3 a.iii.**). Although this fragment existed in low levels (typically ~10% of total peptide yield), this degradation was consistently observed between preparations. Further optimisation was conducted in an attempt to remove this contaminant. It was also observed that the typical yields of Aβ40, as a consequence of the additional HPLC purification step, were reduced substantially from those reported by Linse *et al*.[499]. The yield was typically <0.5 mg of pure Aβ40 per L of culture, compared with the reported 10-20 mg/L[499]. The RP-HPLC method was switched, therefore, in favour of size exclusion chromatography (SEC). After the anion exchange purification, the peptide-containing fractions were dialysed against 50 mM ammonium bicarbonate and lyophilised. The dried peptide was redissolved in Tris-HCl buffer, pH 8.5, containing 7 M guanidinium HCl, to a final volume of 10 mL, and loaded onto a Superdex™ 75 GL 10/300 gel filtration column. The peptide was eluted in 50 mM ammonium bicarbonate and monitored by absorbance at 280 nm (**Figure 3.3 b.i.**). SEC was performed at 4 °C to further reduce the likelihood of degradation of purified product. Fractions containing Aβ40 were identified by SDS PAGE analysis, pooled and lyophilised, and protein identity was confirmed by mass spectrometry (**Figure 3.3 b.ii**.).

This optimised purification method (outlined in detail in Section 2.3.1) was utilised hereafter, in producing all Aβ40 peptide species for experiments in this thesis. Typical peptide yields via this methodology are >4 mg pure Aβ40 per L culture.

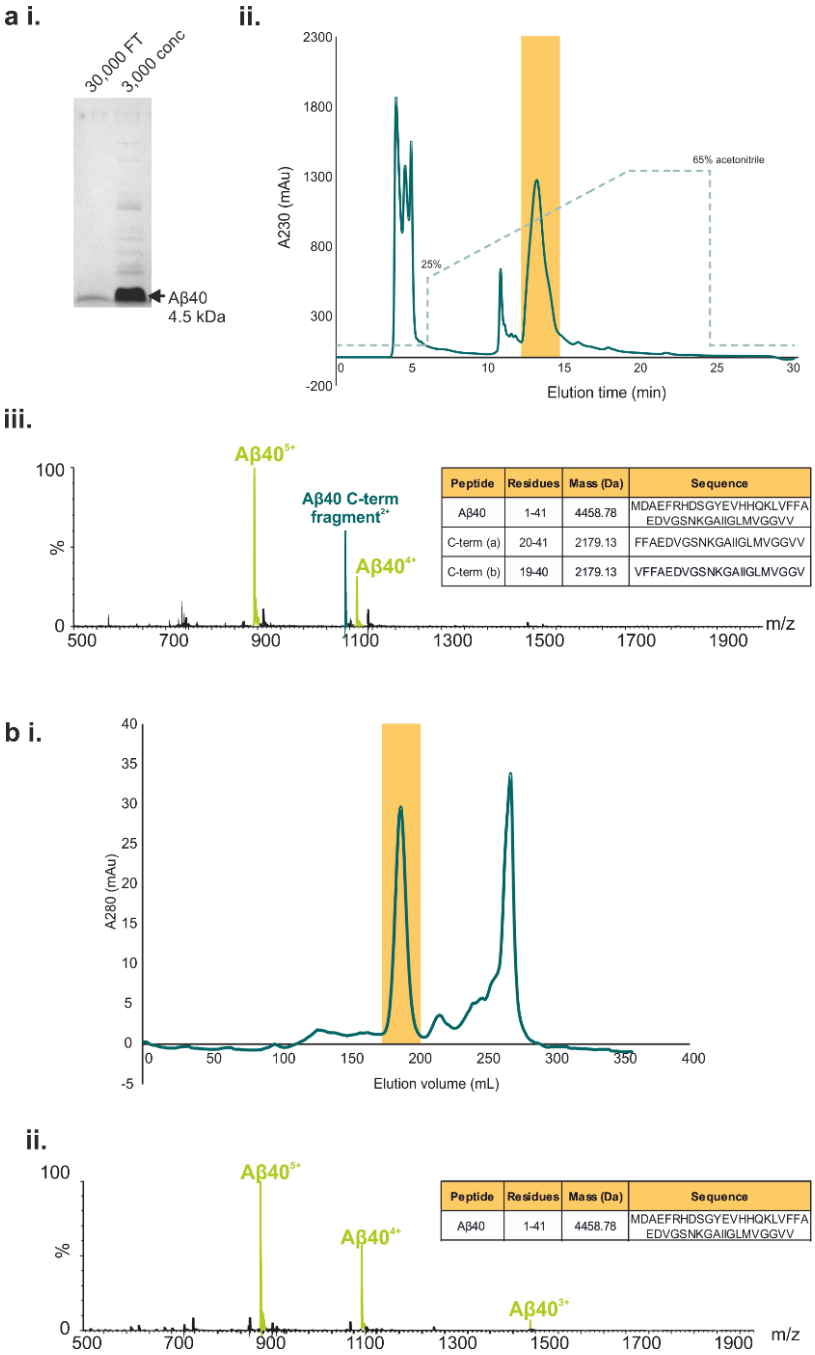

Figure 3.3 Optimisation of Aβ40 purification. **(a)** The initial protocol used for the purification of Aβ40. **(i)** SDS PAGE analysis of the fractions isolated from centrifugal filtration. 30,000 FT indicates the flow through isolated after 30,000 MWCO filtration. 3,000 conc indicates the fraction concentrated by 3,000 MWCO filtration. **(ii)** RP-HPLC purification of the concentrated fraction (peak containing predominantly Aβ40 highlighted in yellow) using a 25-65% gradient of acetonitrile. Elution was monitored by absorbance at 230 nm. **(iii)** ESI-MS analysis of the peptide products isolated from the major peak in **a**. **ii.** indicates a persistent degradation product of 2179 Da, determined as a C-terminal fragment of Aβ40. Sequences and masses of the two possible fragments, compared to full length Aβ40 with additional N-terminal Met – table inset. **(b)** A typical SEC elution profile of Aβ40 monitored at 280 nm. The peak corresponding to Aβ40 is highlighted yellow. **(b. ii)** ESI-MS analysis of purified Aβ40, post-SEC chromatography.

3.4 Preparation of Aβ40 targets for aptamer selection

3.4.1 Preparation of Aβ40 fibril morphologies "2A" and "3Q' via seeding

Fibrils were formed via elongation from pre-formed seeds of Aβ40 in either 2A or 3Q morphology, kindly provided by Dr. Rob Tycko (National Institutes of Health, MD, USA). Seeded fibril formation reactions were set up with 5% (w/v) seed and 0.9 mg/mL monomeric Aβ40, in 25 mM sodium phosphate buffer, pH 7.5. Fibrils were grown for 18 h under quiescent conditions and, consistent with the Tycko *et al*. seeding protocol ([103] and personal communication), samples were sonicated at this stage to promote an additional "self-seeding" event (Section 2.4.1). This step reportedly leads to increased incorporation of any residual monomer by formation of new elongation-competent ends. Fibrils were then grown for a further 5 days, quiescently, and the resulting fibril morphologies assessed by negative stain transmission electron microscopy (TEM – Section 2.4.6). The micrographs confirmed the formation of long, un-branched amyloid fibrils, however a large proportion of the fibrils formed accumulated into large "clumps" or "plaques" (**Figure 3.4 a**) which is a common observation for amyloid fibrils[75]. It was decided that it would be advantageous to find suitable conditions where this lateral association was reduced, in order to expose as many potential aptamer binding sites as possible along the length of the fibril. Seeding reactions, therefore, were monitored by TEM, at various time points during growth (**Figure 3.4 a**), to determine the appropriate incubation time when fibrils were fully elongated, yet still diffuse and hence suitable for immobilisation for aptamer selection. The results suggested that after 18 h of elongation and without the additional sonication step, fibrils were sufficiently elongated but more sparsely distributed, suggesting less inter-fibril association at this time point. By centrifugation of the fibrils and separation of the pellet and soluble fraction, it was possible to assess fibril yield via SDS PAGE analysis (**Figure 3.4 b**). The results show that after 18 h growth, all of the Aβ40 peptide was incorporated into fibrils. Therefore, 18 h was determined as optimal for the preparation of fibrils as selection targets.

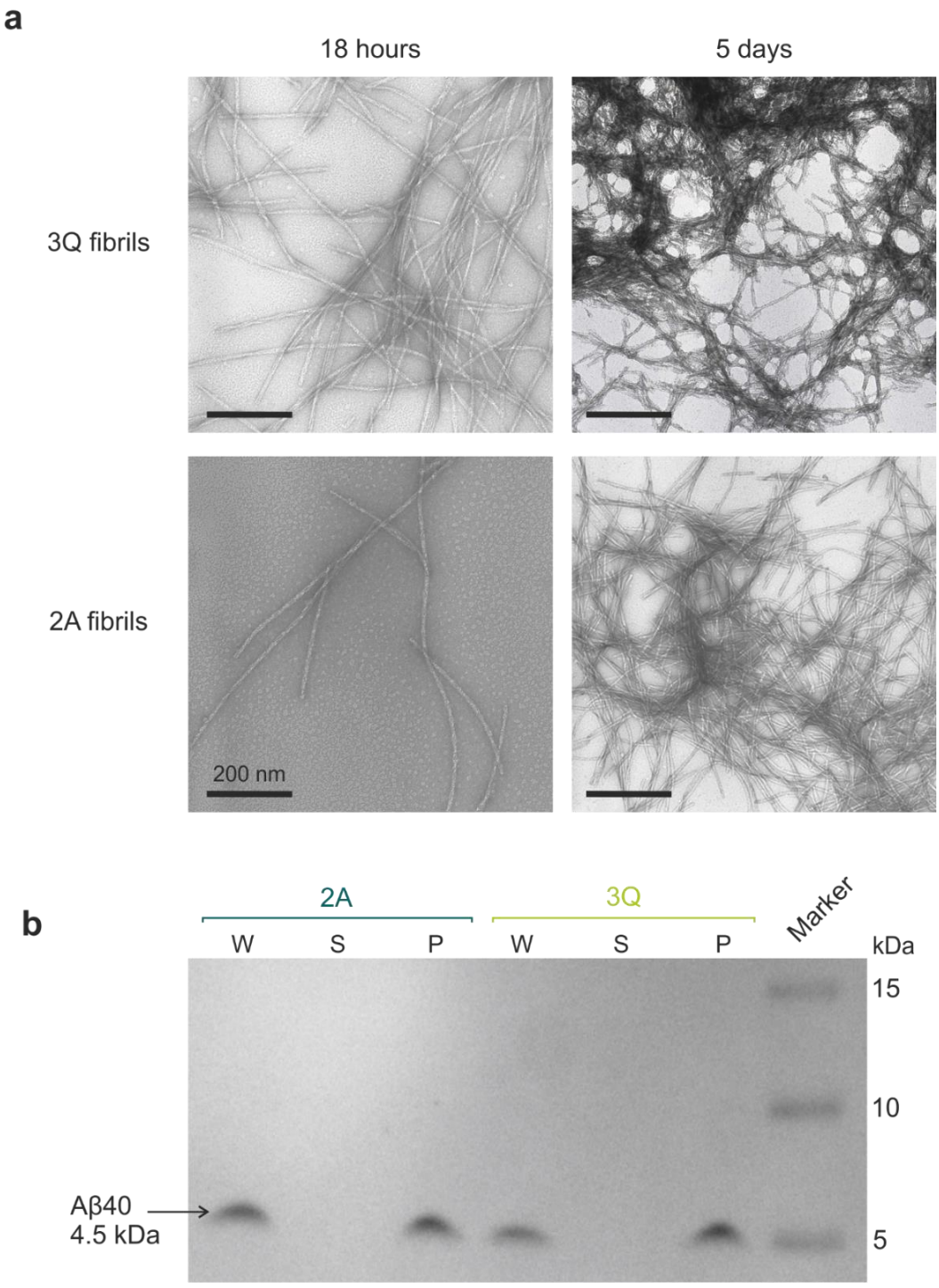

Figure 3.4 Seeded formation of 3Q and 2A fibrils of Aβ40. **(a)** TEMs of 3Q and 2A fibrils, after 18 h and 5 day incubation. Scale bar = 200 nm. **(b)** Yields of 2A and 3Q fibrils formed after incubation for 18 h were determined by SDS PAGE of soluble (S) and pelleted (P) fractions and compared with the whole protein content of the sample pre-separation by centrifugation (W). Molecular weight markers are indicated in kDa.

3.4.2 Biotin labelling of selection targets for immobilisation

In order to allow partitioning of bound and unbound RNA species during the SELEX protocol (outlined in Section 1.4.1), it was decided that immobilisation by biotin modification and conjugation of the Aβ40 protein species to streptavidin-coated magnetic microspheres would be employed. Biotin labelling was carried out with EZ Link™ NHS LC LC biotin (Section 2.5.1), which is an NHS-ester activated biotinylation reagent for labelling primary amines (typically lysine residues or the amino-termini of proteins and peptides). The extent of modification can be fine-tuned by alteration of reaction times, pH, temperature and concentrations of reagents. Therefore, trials were conducted to optimise labelling conditions for each target assembly.

3.4.2.1 Biotin labelling trials: Labelling fibrils

Fibril targets were biotin-labelled post fibril formation as it was uncertain whether the unique, single morphologies (2A and 3Q) would be maintained if biotin-modified monomers were incorporated during the seeded elongation reaction. It was important, therefore, to optimise the biotin labelling of pre-formed fibrils, such that only a small proportion of the monomers within the fibril are labelled (less than 10%). The goal was to ensure that the majority of the fibril was un-modified and therefore free of the microsphere surface.

Biotin labelling trials were set up whereby the stoichiometry of biotin reagent to fibril concentration (based on monomer-equivalent) and reaction times were tested. The degree of biotinylation achieved under each condition was assessed by recovering the fibril as a pellet by centrifugation, followed by depolymerisation in 100% (v/v) HFIP overnight (Section 2.5.1) and mass spectrometric analysis.

Table 3.1 outlines the conditions explored. The results revealed that 2A and 3Q fibrils, although composed of the same monomeric subunits, react with the biotinylation reagent to different extents, presumably due to differences in the availability and/or reactivity of primary amines in the two fibril types. This is unsurprising owing to their differing morphologies (**Figure 3.5 a** and **b**). K28 is salt bridged in 2A fibrils, yet only partially salt bridged in the 3Q fibril morphology[103]. It was found that 2A fibrils required a 2.6 molar

excess of biotin reagent (**Figure 3.5 c.i**.) over a 5 min reaction, to achieve a similar level of labelling to 3Q fibrils produced by 4-fold less reagent (1:0.65, **Figure 3.5 c.iii.**), over 30 s.

Fibril	Stoichiometry (Molar monomer equivalent fibril concentration : biotin)	Reaction duration (min)	% mono-biotinylated
2A	1 : 2.6	30	20
	1 : 2.6	10	20
	1 : 2.6	5	< 10 (**Figure 3.5 c.i.**)
3Q	1 : 2.6	30	50
	1 : 2.6	10	50
	1 : 2.6	5	50 (**Figure 3.5 c.ii.**)
	1: 0.65	1	10
	1 : 0.65	0.5	< 10 (**Figure 3.5 c.iii.**)

Table 3.1 Conditions trialled in biotin labelling of 2A and 3Q fibrils. See Section 2.5.1 for details of the protocol used.

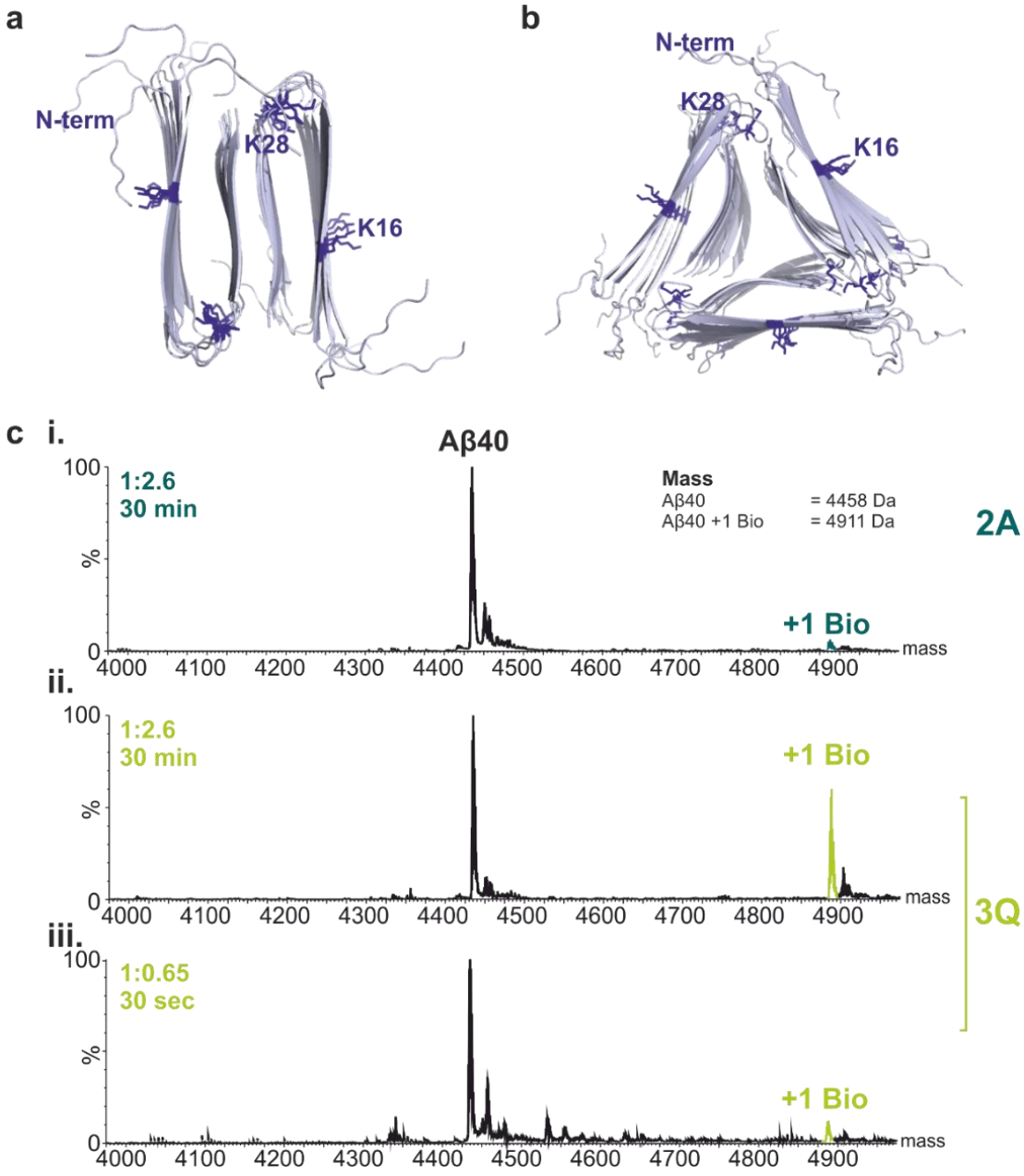

Figure 3.5 Labelling of 2A and 3Q fibrils with NHS-ester activated biotin. Structural models of 2A **(a)** and 3Q **(b)** fibrils with positions of the reactive lysine residues K16 and K28 (blue sticks) and N-terminus indicated. Models comprise six layers of hydrogen-bonded peptides, stacked with the fibril axis running perpendicular to the plane of the page and were produced from coordinate pdb files 2LMN and 2LMP, respectively. The first eight residues have been modelled, without NMR restraints, to illustrate the presence of an unstructured N-terminal region. **(c)** Maximum entropy ESI mass spectra depicting the resultant extent of labelling under different biotinylation reaction conditions for 2A (**c.i**, teal) and 3Q (**c.ii** and **c.iii**, green) fibrils. Levels of biotin labelling at a single position are shown at 1:2.6 molar ratio of fibril (monomer equivalent) to biotin reagent, with a 30 min reaction time (**c.i** and **c.ii**) and 1:0.65 molar ratio for 30 s **(c.iii)**. Expected masses are 4458 Da and 4911 Da for un-modified and singly biotinylated Aβ40, respectively.

To determine whether there was a difference in the relative positions of the biotin labels between the two fibril types, tandem mass spectrometry (MS/MS) with electron transfer dissociation (ETD) was performed by Dr. James Ault (Mass Spectrometry Facility, School of Molecular and Cellular Biology, University of Leeds). ETD fragments peptide ions by electron transfer from a radical anion, producing c and z peptide fragments[507]. This allows assignment of fragments containing modifications, in this case biotin, by fragmentation of the full-length Aβ40 and can therefore be used to determine the position of the modification. Accordingly, samples of both the 2A and 3Q fibrils, biotinylated to approximately 10% under the optimised conditions for each, were buffer exchanged and depolymerised as described (Section 3.4.2.1) for normal mass spectrometric analysis. The samples were then resolubilised in 50% acetonitrile, 0.1% formic acid and analysed by MS/MS ETD. The fragmentation spectra for each fibril morphology (**Appendix 7.2**) indicate that biotinylation occurs predominantly at the N-terminus and at residue K16 (K17 in this recombinantly-expressed Aβ40 with the additional N-terminal methionine) in both fibril types. Far fewer fragments corresponding to K28 labelling are seen, suggesting less labelling at this position. This is consistent with the K28 residue being more buried in the loop region of the fibril structure (**Figure 3.5**). As there is no significant difference in the fragmentation spectra from the two fibril samples, it suggests that the enhanced biotin reactivity seen by 3Q fibrils is more likely due to the extra K16 residue per unit length of this assembly; a consequence of the 3-fold molecular symmetry.

To prepare biotinylated fibrils for immobilisation, free biotin was removed from the mixture via buffer exchange, by gentle centrifugation and washing of the fibrils (Section 2.5.1). Fibrils were exchanged into MOPS selection buffer (80 mM MOPS, 96 mM NaCl, pH 7.5) and immobilised for selection as described in Section 2.5.2. Bead loading was verified with absorbance measurements at 280 nm of the peptide solution before and after magnetic partitioning (data not shown).

3.4.2.2 Biotin labelling trials: Labelling monomeric Aβ40

By contrast with biotinylation of Aβ40 in 2A and 3Q fibrils, where the percent modification was carefully controlled to be <10% of the monomers present, the level of Aβ40 monomer biotinylation was optimised to give a maximum of one biotin per peptide, whilst minimising labelling of two or more primary amines. This was to ensure that Aβ40 monomers were immobilised to the streptavidin beads at a single site, while leaving a number of positively

charged residues free, which could be critical in providing binding epitopes for the RNA aptamers.

Table 3.2 provides details of the conditions tested to achieve the most appropriate biotinylation levels in labelling Aβ40 monomer. Samples were dialysed against 100 mM ammonium acetate, pH 7.5 and the extent of labelling was assessed by ESI-MS. The results showed that a three-fold molar excess of biotin reagent and a 15 min reaction time was necessary to yield 40% biotinylation at a single position (**Figure 3.6**). Increasing the proportion of biotinylation reagent increased the amount of di, tri and tetra-modifications (data not shown).

Stoichiometry (Molar concentration : biotin)	Reaction duration (min)	Biotinylation level
1 : 1	15	20% mono-biotinylated
1 : 10	15 30	Very high levels of doubly or triply labelled
1 : 20	15 30	
1 : 2.5	15	30% mono-biotinylated
1 : 3	15	40% mono-biotinylated (**Figure 3.6**)
1 : 4	15	50% mono-biotinylated (levels of additional labelling starting to increase)

Table 3.2 Conditions trialled in biotin labelling of Aβ40 monomer. See Section 2.5.1 for the protocol used.

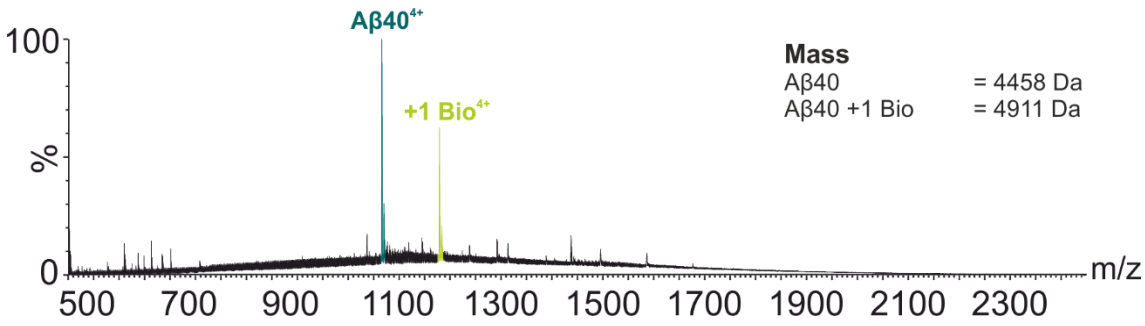

Figure 3.6 Biotin labelling of Aβ40 monomer. ESI-MS analysis indicating biotin (+1 Bio) modification at a single site. Both unmodified Aβ40 and the single biotin labelled form are shown in the 4+ charge state only. Expected masses are 4458 Da and 4911 Da for un-modified and singly biotinylated Aβ40, respectively.

Once Aβ40 monomer was labelled under these optimised conditions, the reaction mixture was quenched with the addition of 1M Tris-HCl, pH 8.0 and the sample dialysed against 80 mM MOPS, 96 mM NaCl, pH 7.5 (MOPS selection buffer) at 4 °C for 2 h, using 2000 MWCO Slide-A-Lyzer™ MINI dialysis devices (Section 2.5.1), to remove free biotin and exchange the sample into buffer for selection of RNA aptamers.

3.4.3 Aβ40 remains monomeric over immobilisation timescale

Given the known, rapid aggregation propensity of Aβ40[81, 491, 499], it was imperative to analyse whether aggregation of the peptide could commence within the biotinylation and subsequent purification time course (<3 h) and, therefore, whether the species immobilised, and subsequently selected against, was indeed monomeric Aβ40. SEC traces at time points 0 and 3 h, post-dissolution of lyophilised peptide into selection buffer, indicated the presence of a dominant species, eluting at a volume consistent with monomeric Aβ40 (**Figure 3.7 a**). However, SEC alone could not provide accurate sizing of the Aβ40 species, owing to the fact that the elution profile of the unstructured Aβ peptide cannot be compared with the behaviour of standard, globular calibrants. Therefore, SEC combined with multi-angle laser light scattering (SEC MALLS) was utilised to assess the nature of the Aβ40 species eluting from the column, as this technique allows absolute measurement of molecular weight (MW) by coupling mass separation with light scattering (LS) (**Figure 3.7 b**) (Section 2.8.1).

a

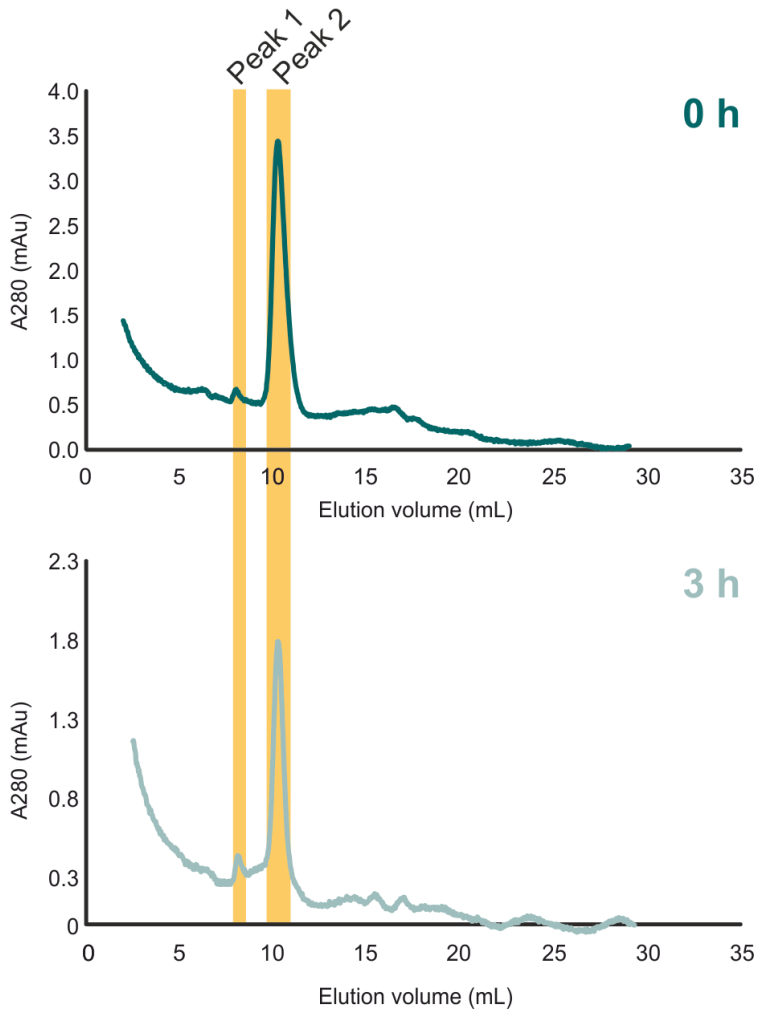

b

Injection time (h)	Peak 1 Mw (Da)	Peak 2 Mw (Da)
0	-	6.735×10^3
3	9.672×10^4	4.514×10^3

Figure 3.7 Aβ40 remains predominantly monomeric over the immobilisation timescale. **(a)** SEC analysis (Section 2.8.1) of Aβ40 at time points 0 and 3 h post re-solubilisation in MOPS selection buffer. The 3 h sample was incubated at 4 °C before injection. **(b)** Absolute molecular weights calculated from LS data (using Wyatt Astra software, version 6.0), corresponding to the two major peaks in the SEC separation. Peak 1 and Peak 2 are highlighted in yellow and indicated on the chromatograms.

At t = 0 h, the major peak eluting from the SEC column had an absolute molecular weight of 6.735×10^3 (± 1.9%) Da, indicating a possible monomer-dimer equilibrium at this time point

(mass of monomeric Aβ40 = 4.458 x 10^3 Da). After 3 h of incubation at 4 °C (mirroring the conditions during the buffer exchange of biotinylated monomer for immobilisation) the major peak, eluting at approximately the same volume, had a suggested molecular weight of 4.514 x 10^3 (± 2.3 %) Da, corresponding almost exactly to the expected mass of Aβ40 monomer. The decrease in mass over the 3 h incubation is probably due to equilibration of the sample after re-solubilisation, rather than disaggregation of dimers. A second peak, with a smaller elution volume, indicating the presence of some larger aggregates, was observed in low levels at both time points. LS data could not be used to assign an absolute MW for this peak at t = 0, however, as this species became more highly populated at t = 3 h, a mass of 9.672 x 10^4 (± 3.0%) Da was calculated. This is evidence for the formation of some larger aggregates (possibly ~ 20mers) over the 3 h time course. However, the vast majority of Aβ40 remains monomeric under these conditions. Therefore, the biotinylation and buffer exchange protocol devised was deemed suitable in obtaining predominantly monomeric peptide for immobilisation. It was then assumed that after immobilisation on the surface of the beads, self-association of the monomeric Aβ40 would no longer be able to occur.

3.5 Selection of RNA aptamers

Selection of RNA aptamers firstly required synthesis of a combinatorial oligonucleotide library, made up of a central, randomised region, flanked by two regions with fixed sequences (**Figure 3.8 a**). These fixed primer regions are necessary for amplification of the library, during the selection process, via RT-PCR. The ssDNA library (N50 –sequence given in Section 2.7.1) was designed by Dr. David Bunka (University of Leeds) and synthesised commercially. Although initially thought to be comprised of a completely random library, where all 4 nucleotide bases are represented equally within the randomised region, some bias in the base-composition exists for this pool and is discussed later (Section 3.7). A random region of 50 nucleotides was chosen as it creates the potential for a highly diverse starting library (4^{50} individual sequences). As detailed in Section 1.4.1, the actual sequence space available is more limited in practice, owing to the total number of molecules in a typical RNA pool (10^{15}), and consequently only a fraction of the library's potential sequence coverage will be encompassed within the pool. Nevertheless, an N50 library was deemed appropriate, as this longer central region allows for the potential formation of more diverse secondary structural elements. To obtain an RNA library from this DNA template, a T7 bacteriophage RNA polymerase promoter sequence was incorporated into the 5' primer

extension. The ssDNA was then amplified by PCR (Section 2.6.1) to produce the dsDNA template required for *in vitro* transcription.

Modified oligonucleotide libraries are often used in SELEX as they provide aptamers with inherent resistance to nuclease-mediated degradation[384] (Section 1.4.2). Accordingly, a 2'F modified pyrimidine library (**Figure 3.8 b**) was used in these selections and to allow efficient incorporation of these chemically substituted nucleotides, a Y639F/H784A mutant of T7 RNA polymerase was utilised. This mutant polymerase works by a) eliminating the inflexibility of the hydrogen bonding potential and therefore substrate recognition compared to the wild-type polymerase and b) providing more space in the active site and therefore relaxing the barrier to extension of transcripts with non-canonical nucleotides[406, 508, 509] (Section 2.6.3).

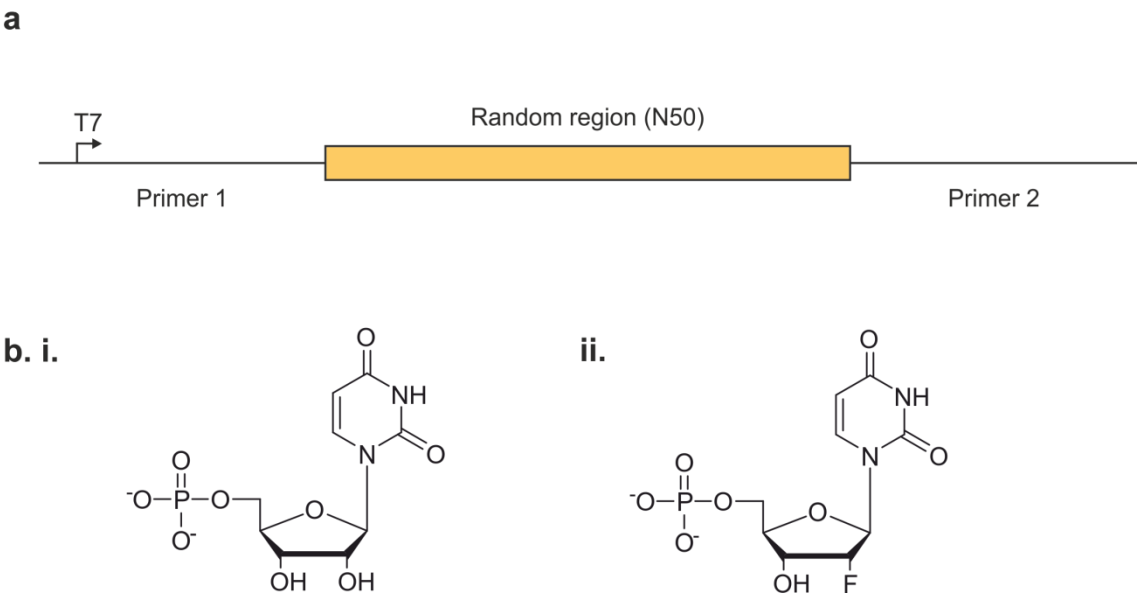

Figure 3.8 Design of a 2'F pyrimidine modified oligonucleotide library for RNA aptamer selection. **(a)** Schematic of the ssDNA template used in creating the randomised N50 RNA library. Full sequences for both the DNA template and primer oligonucleotides are given in Section 2.7.1. **(b)** Comparative chemical structures of 2'OH **(b.i)** and 2'F modified **(b.ii)** nucleotides used in the 2'F pyrimidine library. Uridine is shown as an example.

3.5.1 Selection of RNA aptamers against Aβ40 monomers

Selections against Aβ40 monomer were carried out by Dr. David Bunka as part of my initial training into the use of the liquid handling robot and general RNA techniques.

A 50 µL *in vitro* transcription reaction, containing a 2'F pyrimidine, 2'OH purine dNTP mix (Section 2.6.3) was set up to create the starting naïve RNA pool (~10^{15} sequences), which was DNase treated and purified (Section 2.6.8). 50 µL of RNA was then mixed with 50 µL 2 x MOPS selection buffer before incubation with 20 µL of biotin linker-saturated streptavidin beads. This step was included during every SELEX round, as a negative selection, to ensure that RNA aptamers with affinity towards the biotin linker and/or the streptavidin beads themselves were removed at each stage. The beads were then partitioned by magnetic separation and the unbound fraction removed and added to 20 µL of Aβ40 saturated beads (35 ng Aβ40 immobilised) for positive selection. The magnetic beads were partitioned, the unbound fraction removed and the beads, with associated aptamers, were washed ten times with 125 µL of selection buffer. 35 µL of nuclease-free H_2O was added to the washed beads and the bound RNA was eluted by heating the mixture to 95 °C. The mixture was then cooled, before the addition of reverse transcription mix (Section 2.6.9) to produce cDNA products, which were PCR amplified for the next round.

After this initial manual selection round, the process was automated by use of a liquid handling robot (Section 2.7.3), whereby four iterations of the above protocol were performed. RT-PCR products from each round were then analysed by native PAGE (Section 2.6.2) to confirm the isolation of aptamers of the correct size (121 bp) (**Figure 3.9 a.i.**). A second manual selection was then performed (R6) before a further four rounds of automated selection (R7-10), which followed the same basic selection process as described above. Some modifications, to increase stringency, were made to these later SELEX rounds. Target incubation was altered from 15 min at 25 °C to 5 min at 37 °C. This was to drive the selection of aptamers with faster on rates (K_{on}), as opposed to during the early selection rounds, where stringency was deliberately low to avoid the loss of lowly populated binders. The volume of target beads (and therefore the concentration of target peptide) was halved to increase the competition between aptamer sequences for the available epitopes. The number of wash steps was also increased, thereby selecting against aptamers with higher off rates (K_{off}) and again promoting selection of aptamers with enhanced affinity. The increased stringency in these latter selection rounds results in the bands corresponding to

isolated aptamers becoming progressively less intense, as the stringency drives the selection towards fewer, more specific aptamers (**Figure 3.9 a.ii.**).

Six solution-competition rounds (R11-16) were included at the later stages of this anti-Aβ40 monomer selection protocol, to promote recognition of native conformations that had not been immobilised or modified. In these selection rounds, after standard binding and wash steps, beads were challenged with various concentrations of un-modified target peptide, in solution, to compete bound aptamers from the immobilised targets. 35 µL of 25 µM Aβ40, in MOPS selection buffer, was incubated with the target bound RNA for 10 min at 25 °C. This fraction was removed and the process repeated with a 50 µM Aβ40 challenge. The remaining RNA associated with the immobilised Aβ40 was then heat eluted, as described for the standard protocol (Section 2.7.2). All three eluate fractions were then reverse transcribed and PCR amplified before analysis by native PAGE. In rounds 11-15, the DNA isolated from the 50 µM Aβ40 competition eluate was taken forward in each case, as this was expected to contain aptamers with the highest affinity for solution targets. In the final competition round (R16 - **Figure 3.9 b**), the 50 µM Aβ40 eluate (after 20 PCR cycles) was PCR purified and taken forward for next generation sequencing.

Figure 3.9 c outlines the overall SELEX procedure for the selection of anti-monomer aptamers. Detailed experimental procedures for each type of selection round, including all stringency conditions adopted at each stage, are given in Section 2.7.

3.5.2 Selection of anti-fibril aptamers

The following RNA aptamer selections against the two morphologically distinct Aβ40 fibrils, were carried out personally, with supervision from both Dr. David Bunka and Dr. Simon White (School of Molecular and Cellular Biology, University of Leeds).

RNA aptamer selection against the 2A fibril morphology was undertaken with the same N50 library used in the anti-Aβ40 monomer selections. Anti-3Q fibril aptamers were selected from a different N30 degenerate pool (Section 2.7.1), to avoid problems with cross-contamination between the N50 and N30 libraries. Both DNA template libraries were designed by Dr. Bunka and synthesised commercially in the same manner as described previously (Section 3.5.1), before amplification and transcription to give the initial starting RNA library for SELEX.

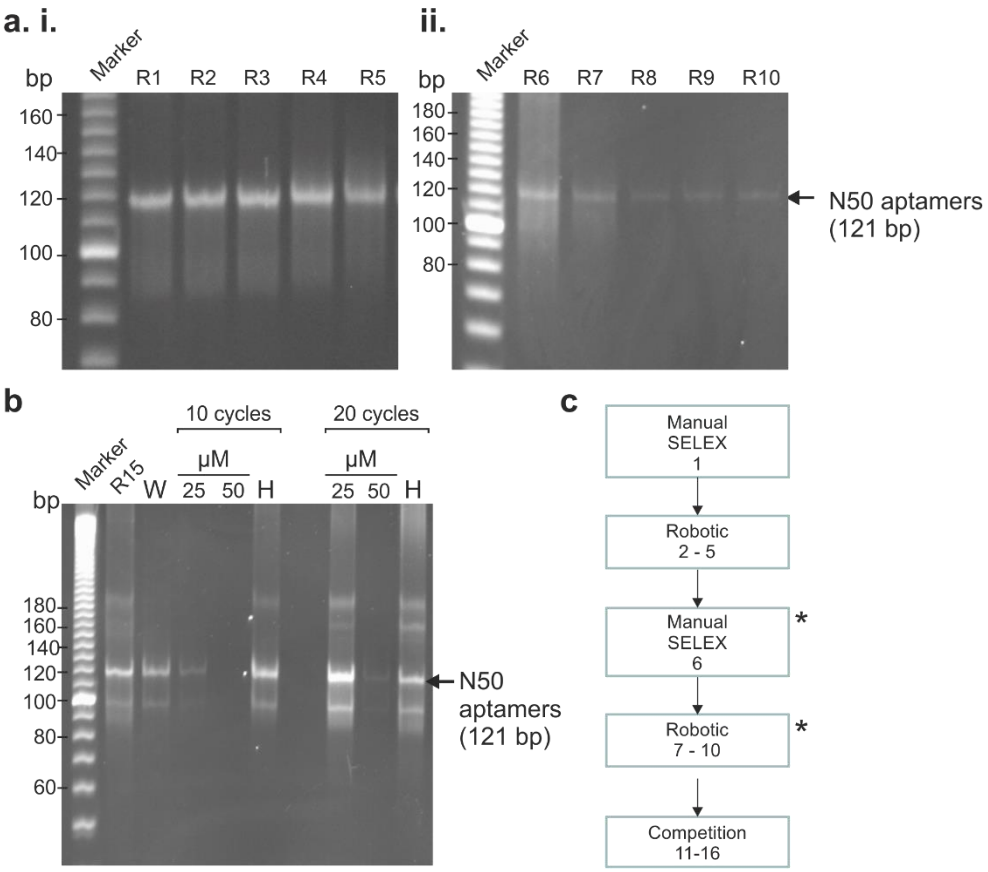

Figure 3.9 Anti-Aβ40 monomer aptamer selection. **(a)** Native PAGE analysis of DNA products at the end of each selection round (R1-5 **(i)**, R6-R10**(ii)**) after RT-PCR (10 cycles). **(b)** The final competition round (R16) for anti-monomer SELEX. The pool amplified from the previous round (R15) and the first wash fraction (W) are shown. Solution challenges, with 25 μM Aβ40 (25), 50 μM Aβ40 (50) and the heat elution (H) sampled after both 10 and 20 PCR cycles are indicated. Here, and throughout unless otherwise stated, the sizes of molecular weight markers (10 bp DNA ladder, Invitrogen) are given in base-pairs. Data courtesy of Dr. David Bunka. **(c)** Flow chart outlining the full SELEX protocol for anti-monomer selection. * denotes rounds where stringency parameters were increased (See Section 2.7 for detailed protocols).

The general procedure for anti-fibril aptamer selection (**Figure 3.10 a**) was similar to the strategy used for selection of Aβ40 monomer aptamers. The key difference was in the inclusion of an initial pull-down capture round, where the RNA pool was first incubated with biotin modified fibrils, free in solution. After incubation, streptavidin beads were added to capture the biotin-fibrils and any bound RNA. Accordingly, 50 μL of the RNA aptamer pool was added to 50 μL of a 20 μM biotin-labelled fibril solution and incubated for 15 minutes with gentle agitation. The mixture was then added to 0.5 mg of washed, un-conjugated

streptavidin beads and incubated for a further 30 min. This strategy allowed for the entire complex to be pulled out of solution, to aid in the isolation of aptamers against native fibril epitopes. The beads were then separated by magnetic partitioning, washed three times with 1 mL MOPS selection buffer and the bound RNA eluted and RT-PCR amplified as described (Section 2.7.4). The resultant RNA pool was then taken forward for subsequent automated and competition selection rounds (**Figure 3.10 a**). Detailed selection procedures for all variations on the standard protocol are given in Section 2.7.

As in the case of the anti-monomer selection, the final round for each of the fibril selections included competition elution with free, unmodified fibril targets in solution (**Figure 3.10 b**). In these instances, challenges were 10 and 20 μM fibril (monomer equivalent concentration). In both cases, the 20 μM eluate was PCR purified and sequenced.

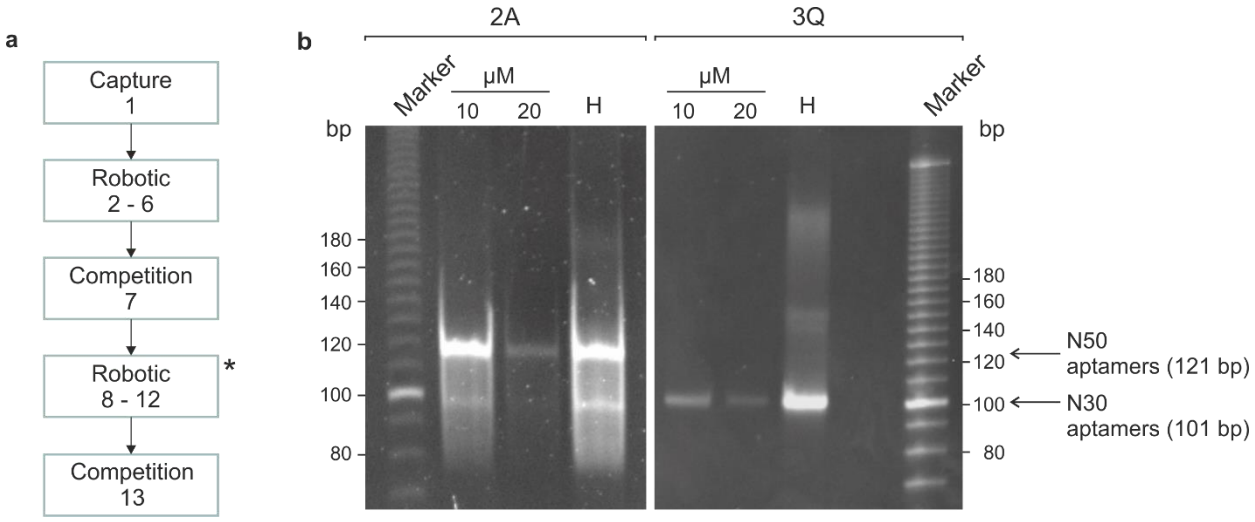

Figure 3.10 Anti-fibril aptamer selection. **(a)** Flow chart outlining the SELEX protocol for the anti-fibril aptamer selection. * denotes rounds where stringency parameters were increased. **(b)** The final competition elution rounds for each anti-fibril selection analysed by native PAGE. DNA products isolated from the solution challenges with 10 μM (10) and 20 μM (20) fibrils (monomer equivalent concentration), as well as the heat eluted fraction (H), are indicated.

3.6 Next generation sequencing of enriched pools

The conventional approach of cloning, colony-picking and Sanger sequencing of a small number of colonies (typically 10-100[ref 377]) has shown success in RNA aptamer selections by finding the most frequently occurring sequences, enriched through SELEX. However, by use of next generation sequencing (NGS) it is possible to sequence up to 10^7 different sequences from a SELEX pool and therefore analyse sequence frequencies at much higher resolution. This technique was employed here, in the analysis of the enriched pools isolated from the three anti-Aβ40 selections. The DNA pools acquired from the final RT-PCR step of the selections were PCR purified (Section 2.6.1) and sent for NGS analysis. Preparation of the DNA libraries and sequencing via an Ilumina MiSeq platform was carried out by Dr. Sally Fairweather (Leeds Institute of Molecular Medicine, St. James Hospital, Leeds).

The general concept of NGS is similar to the Sanger approach, where a DNA polymerase catalyses the incorporation of fluorescently-labelled dNTPs into a DNA strand, during sequential cycles of DNA synthesis[510]. The nucleotides are identified by fluorophore excitation, at the point of incorporation, during each successive cycle. Using a reversible-terminator based method, addition of a single base, as it is incorporated, can be detected. An overview of the NGS library preparation and sequencing chemistry is given in **Figure 3.11**. Briefly, the library is prepared by ligation of adapter oligonucleotides at both the 5' and 3' end of the input DNA sequences, which are then PCR amplified and purified. DNA sequences are then captured on a flow-cell via complementary base-pairing to a lawn of surface-bound oligonucleotides, corresponding to the adapters. This allows bridge amplification to produce dense clusters of clones. After cluster generation is complete, sequencing can be initiated by the addition of the four reversible, terminator bound, fluorescently labelled dNTPs, sequencing primers and DNA polymerase. Fluorescence upon incorporation of a base is recorded for each individual clone cluster, followed by a chemical de-blocking step to remove the fluorophore and the 3'-terminal blocking group, for the next sequencing cycle. This way, hundreds of thousands of sequence clusters can be read simultaneously, in a parallel process, leading to vast sequence coverage of the enriched aptamer pools.

NGS analysis of the three anti-Aβ40 aptamer selections yielded 660,000 sequence reads for the anti-monomer pool, and 41 million and 7.5 million for anti-2A and anti-3Q fibril selection pools, respectively. The next challenge, therefore, was to devise a strategy to

handle such volumes of sequencing data and to select only a few lead aptamers for further work and characterisation.

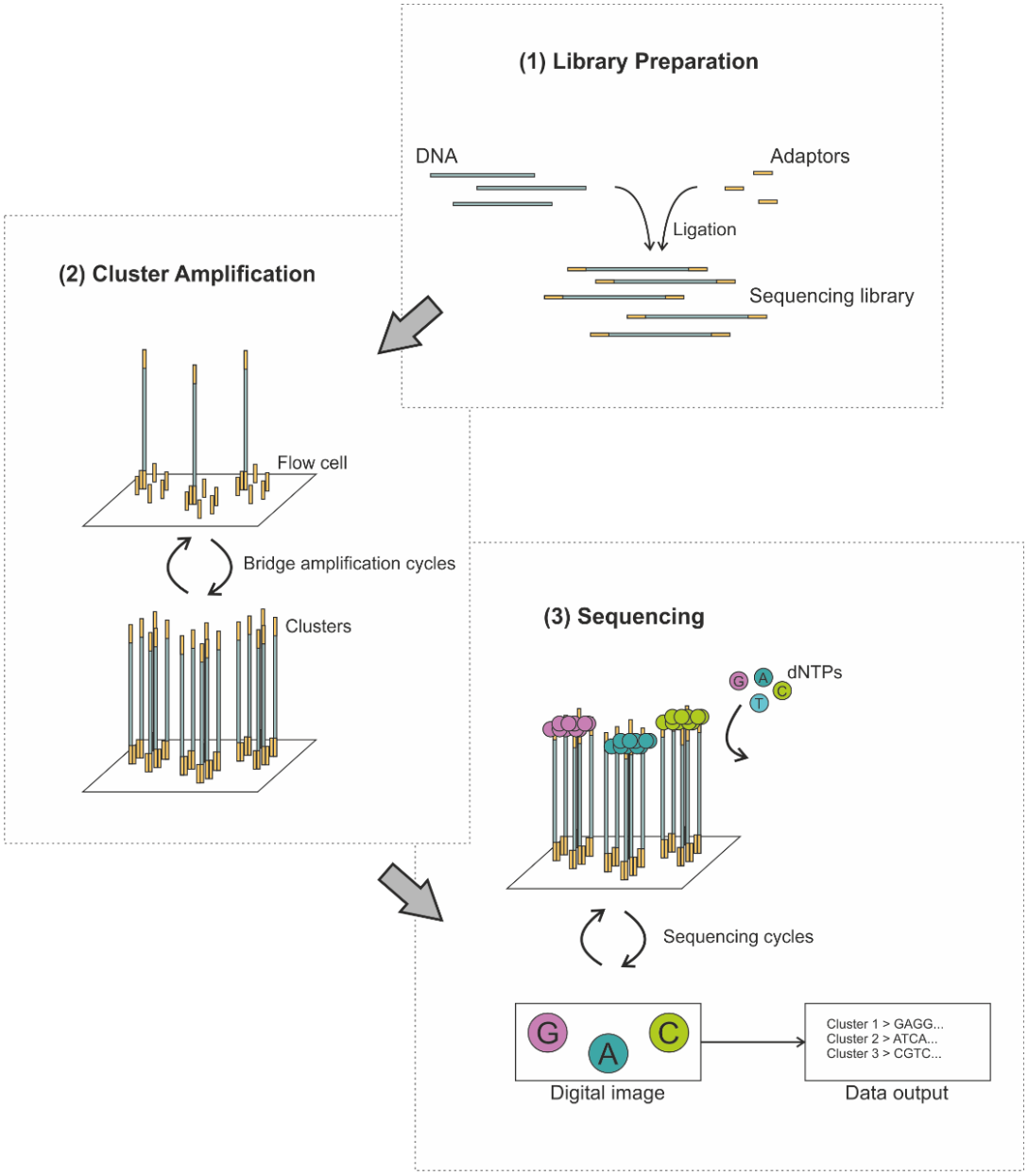

Figure 3.11 Overview of the next generation sequencing (NGS) process. **(1)** The NGS library is prepared by ligating specialised oligonucleotide adaptors to both the 3' and 5' ends of the DNA. **(2)** The library is loaded into a flow cell where the DNA strands hybridise to the surface via specific base-pairing to surface-bound oligonucleotides, complimentary to the adaptors. The bound strand is then amplified into a clonal cluster through bridge amplification. **(3)** Sequencing reagents (including fluorescently-labelled, reversibly-terminated dNTPs) are added and the first base is incorporated. The emission of the newly-incorporated fluorescent base is recorded for each cluster before removal of the fluorophore and 3' blocking group for the next cycle. Imaging of each fluorescent base, as it is incorporated into the complementary strand, allows the sequence of the clone in each cluster to be built. Figure redrawn and adapted from [511].

3.7 Analysis of next generation sequencing data

In collaboration with Dr. Eric Dykeman (Department of Mathematics, University of York, UK), a bioinformatics-based approach was utilised to identify aptamers for further characterisation. The basis of the strategy was to identify the unique aptamers from within the total sequence reads and rank them in order of occurrence. Then, a closer analysis of the most populous unique aptamers, through sequence alignment, would allow clustering of related sequences into motif "families" and identification of the extent of minor variation between sequences. Representative aptamers could then be chosen from each cluster for downstream characterisation.

An aptamer sorting script (written by Dr. Dykeman) was applied to identify and rank the aptamers in order of the most frequently occurring single sequence. The script firstly identifies the correct 5' and 3' primer regions (specified for each pool) and filters out sequences that are not of the correct random region length (details of script stringency parameters given in Section 2.7.7). Once filtered, 395,874 such matches were determined from the anti-Aβ40 monomer pool, with 994,679 (2A) and 1,593,643 (3Q) sequences from the two anti-fibril pools. The script then counts and ranks the identical sequences in order of their occurrence. The frequency distributions of the top 500 most populous unique sequences, for each of the three selection pools, are given in **Figure 3.12** - **Figure 3.14**. Part **b** of each of these figures shows a zoomed region of the frequency plots to visualise and compare the selected data with the number of occurrences of identical sequences derived from NGS analysis of the respective naïve pools. The data suggest that SELEX has been successful in all cases, as individual sequences are clearly enriched above the baseline number of individual sequences populated in the un-selected pool. In addition, there is a highly populated lead sequence in each case (aptamer 1) and a rapid decrease in population of further sequences. This is consistent with the principle that the higher affinity binders should be preferentially amplified during iterative SELEX rounds. Ranking unique aptamers in order of decreasing occurrence in the sequenced pools also provides a convenient naming system, whereby aptamer names correspond to their position in the ranking, e.g. 3Q1: the most abundant sequence from the 3Q selection, 3Q2: the second most abundant, etc..

From an initial look at the sequences represented within each of the enriched pools, it was immediately apparent that there were differences in the relative representation of the four nucleotide bases. Sequences of the randomised regions of the enriched anti-Aβ40 monomer and anti-2A fibril selection pools were purine-rich, whereas the anti-3Q fibril aptamers

generally contained poly-U repeats. These differences in base-composition could be an indication that aptamers have been selected that are specific for different epitopes between these related targets. Therefore, to probe this further, analysis of the base-composition of the filtered sequences was carried out and compared to the base-composition of the naïve starting libraries, as a shift in the relative representation of each nucleotide base may, firstly, further indicate the successful selection of sequences and, secondly, imply specificity for distinct target epitopes. This was done with a second aptamer analysis script (written by Dr. Dykeman- Section 2.7.7), which scans the randomised region of the filtered sequences identified from the selected pool and quantifies the number of times each nucleotide base is represented. The same analysis was conducted on the naïve pools, for comparison. The data is given in part **c** of **Figure 3.12, Figure 3.13** and **Figure 3.14** for the anti-Aβ40 monomer, anti-2A and anti-3Q fibril selections, respectively. There is clearly evidence for biases in the relative base-composition between each pool, with anti-Aβ40 monomer and anti-2A fibril aptamers containing a GA bias (71.5% and 69.6% GA content, respectively) and the anti-3Q fibril aptamers showing a much higher representation of uracil (45.4%). However, these base biases are seemingly carried through from the starting libraries, which also show the same base preferences (**Figure 3.12** - **Figure 3.14,** purple bars). Some changes in the distribution of represented bases could possibly have resulted as a consequence of selection. For example, the U-bias in the anti-3Q aptamer pool becomes more prominent (from 35.5% in the starting pool to 45.4% post-SELEX), but this is difficult to interpret. Nevertheless, the selections were clearly undertaken with naïve pools that contained considerable bias, therefore the desired full diversity of a random pool was not sampled during SELEX. Despite this finding, certain sequences were clearly enriched during the selection and it is from these highly populated sequences that representative aptamers were chosen for further characterisation.

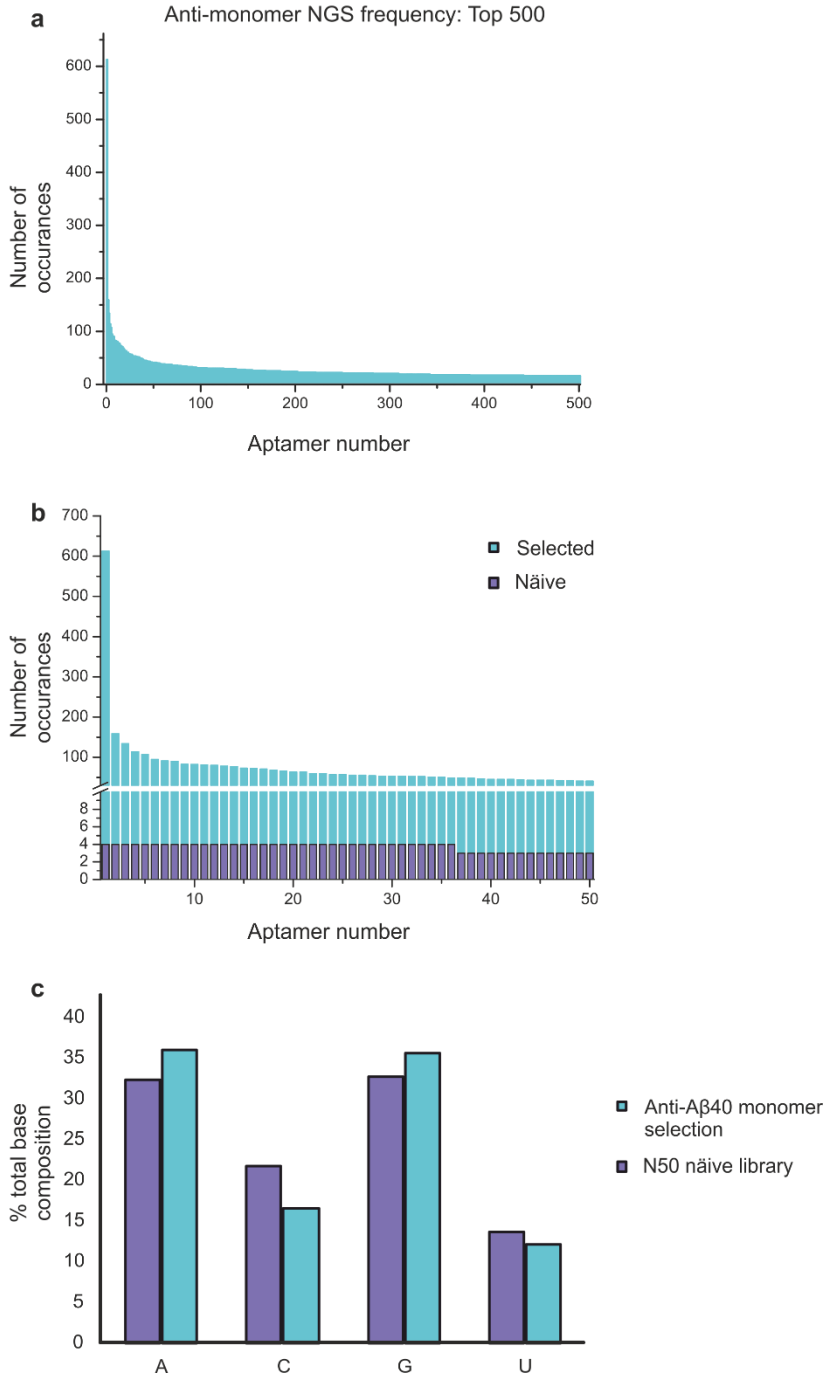

Figure 3.12 Bioinformatic analysis of the top 500 most frequently occuring, unique aptamer sequences from the anti-Aβ40 monomer selection. **(a)** Frequency plot illustrating the occurance of each of the top 500 sequences isolated from the filtered NGS data from the anti-Aβ40 monomer selection pool. **(b)** A closer look at the number of occurances of the top 50 sequences from the anti-Aβ40 monomer pool, compared to the number of occurances of unique single sequences within the starting library (purple histogram overlaid). **(c)** The relative distribution of the four nucleotide bases in the enriched, filtered pool (blue bars) compared to the starting library (purple bars).

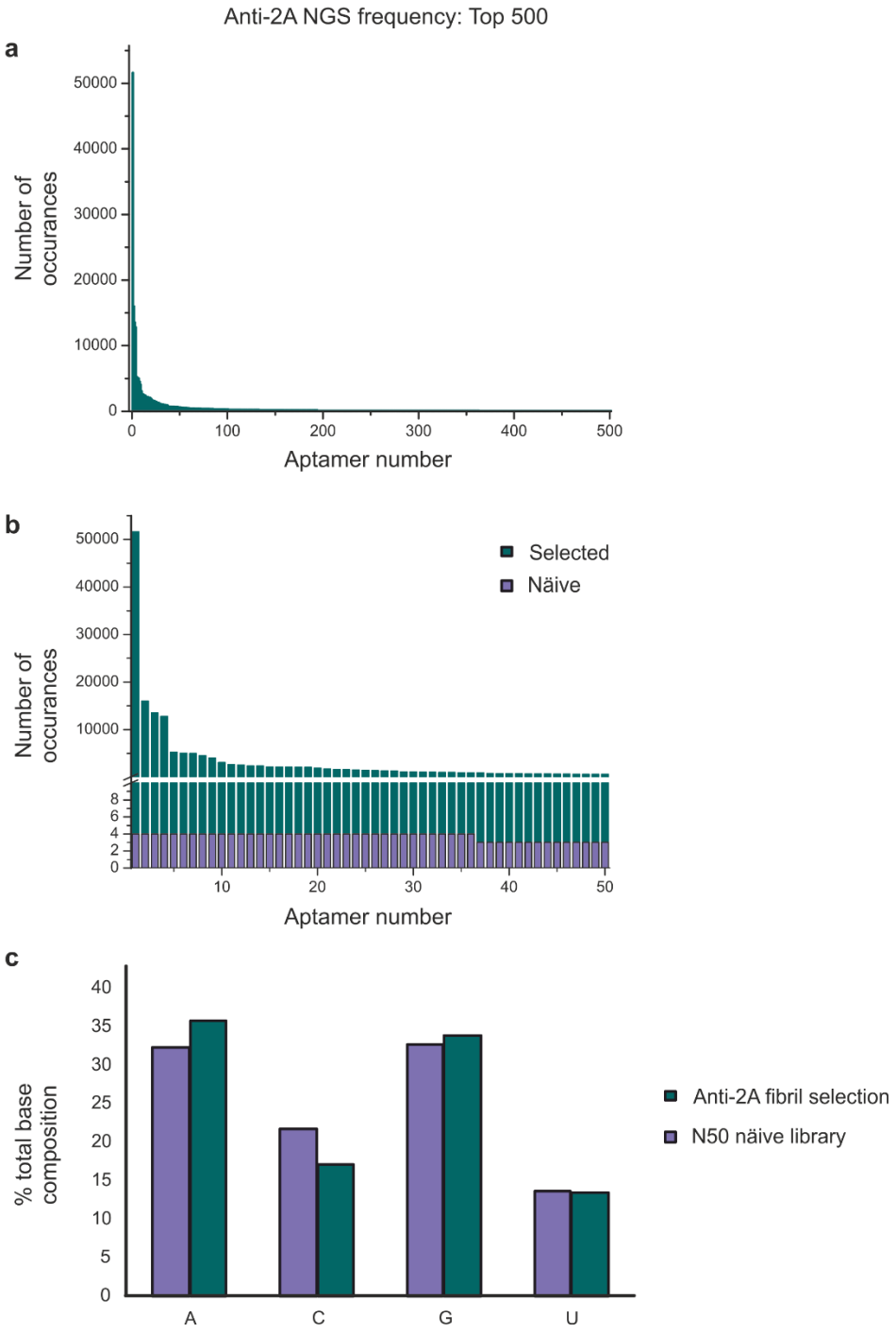

Figure 3.13 Bioinformatic analysis of the top 500 most frequently occuring, unique aptamer sequences from the anti-2A fibril selection. **(a)** Frequency plot illustrating the occurance of each of the top 500 sequences isolated from the filtered NGS data from the anti-2A fibril selection pool. **(b)** A closer look at the number of occurances of the top 50 sequences from the anti-2A fibril pool, compared to the number of occurances of unique single sequences within the starting library (purple histogram overlaid). **(c)** The relative distribution of the four nucleotide bases in the enriched, filtered pool (teal bars) compared to the starting library (purple bars).

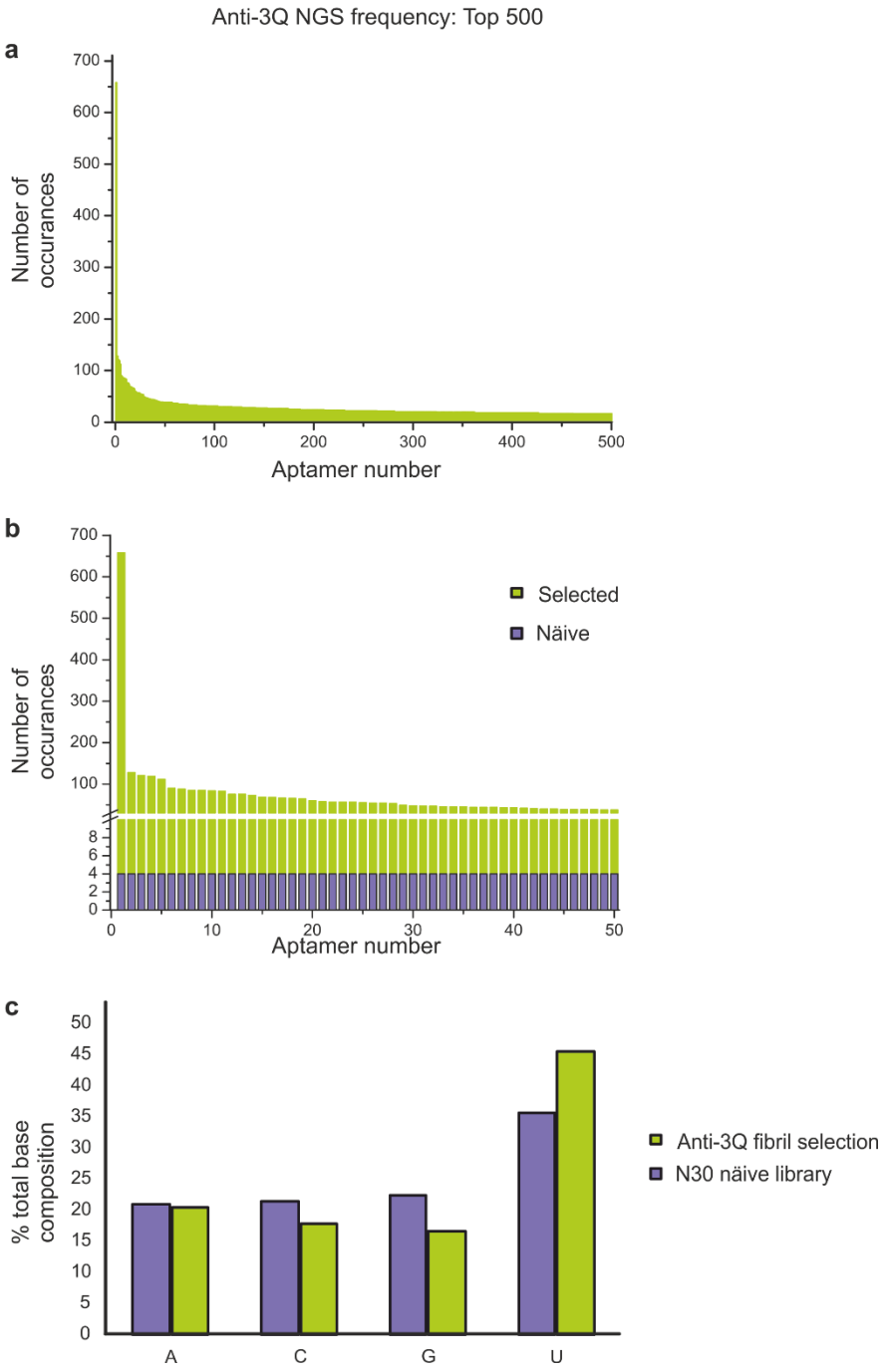

Figure 3.14 Bioinformatic analysis of the top 500 most frequently occuring, unique aptamer sequences from the anti-3Q fibril selection. **(a)** Frequency plot illustrating the occurance of each of the top 500 sequences isolated from the filtered NGS data from the anti-3Q fibril selection pool. **(b)** A closer look at the number of occurances of the top 50 sequences from the anti-3Q fibril pool, compared to the number of occurances of unique single sequences within the starting library (purple histogram overlaid). **(c)** The relative distribution of the four nucleotide bases in the enriched, filtered pool (green bars) compared to the starting library (purple bars).

The most abundant sequences for each selection pool were analysed for sequence similarity using the multiple alignment software Genebee[512]. Since Genebee is not designed to process more than 500 clones, it was the 500 topmost enriched sequences that were selected for analysis. In each case, the total number of aptamers that are represented within the top 500 sequences is only a fraction of the total sequences filtered from the sorting script (3.5% for anti-Aβ40 monomer, 24% anti-2A fibrils and 0.9% anti-3Q fibrils). There is clearly a significant number of sequences that cannot be analysed via this methodology, however as these sequences are significantly less populated, they are therefore likely to be of less interest. The sequences excluded from the Genebee analysis corresponds to those that are represented less than 16 times each in the case of both the 3Q and monomer selections, compared to the topmost aptamer's representation of 658 and 613 times, respectively. In the case of 2A fibril aptamers, whose sequencing yielded significantly larger amounts of data, the topmost occurring aptamer occurred 51,626 times and the top 500 unique sequences represent all aptamers that occurred more than 57 times each. **Table 3.3** summarises the analysis of selected aptamers for each pool.

Selection	Raw sequence reads	Filtered aptamers	Total sequences in top 500	Total sequences in top 500: % of filtered
Aβ40 monomer	0.7 million	395,874	13,914	3.5
2A fibril	41 million	994,679	240,945	24
3Q fibril	7.5 million	1,593,643	13,810	0.9

Table 3.3 Summary of the bioinformatics analysis of the three Aβ40 selections. Raw sequence reads corresponds to the unfiltered, raw data from NGS. Filtered aptamers are the sequences with correct SELEX primers and random region length, identified from the raw sequence reads.

Genebee analysis of the top 500 most commonly occurring sequences resulted in the identification of conserved motifs for each selection pool. Motifs identified through Genebee are ranked in order of their degree of similarity, with a score designated to a given motif known as the power of alignment. The power score is an estimation of the degree of similarity and takes into account the length of identical regions within the motifs, as well as "thickness" or number of sequences within the motif[513]. The ten motif families with the highest power score are given as the output of the Genebee analysis. An example of the

strongest local alignment, taken from the anti-2A fibril selection, is given in **Figure 3.15** and entire datasets, which include the ten strongest families within the top 500 sequences for each selection pool, can be found in **Appendix 7.3**.

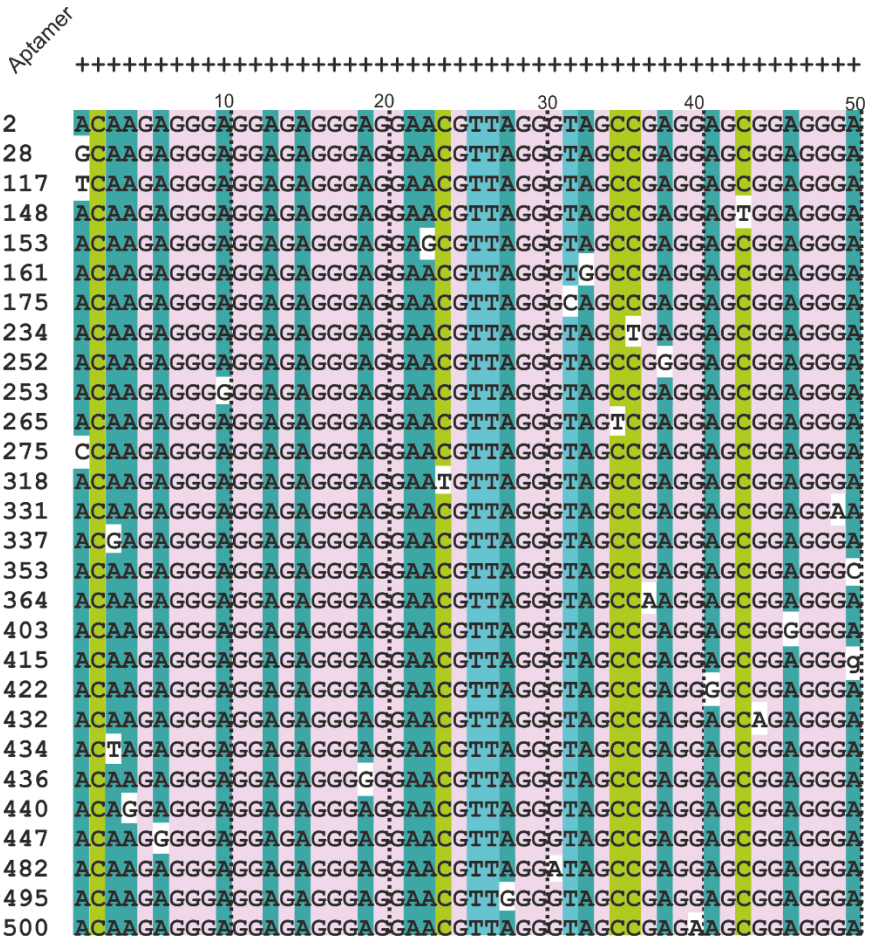

Figure 3.15 Genebee sequence alignment of the top 500 most commonly occuring sequences yields sequence motifs or "families". An example of the strongest motif family identified from Genebee multiple alignment analysis of the top 500 sequences from the anti-2A fibril selection pool. Aptamer number indicates the position of the sequence in the occurrence ranking. + indicates strong identity at that position. Bases are colour coded according to the following: G (pink), A (teal), C (green), T (blue). DNA sequences corresponding to the RNA aptamers are shown.

The most abundant aptamer sequences for each pool (the top 5) are generally represented within the ten alignment motifs with the highest power scores. The further sequences within the motifs often differ by only a single nucleotide (see **Figure 3.15** for one such example, **Appendix 7.3** for full datasets). This indicates that the most populous aptamers

are likely to be "ancestors" of related sequences and therefore the sequences lower in abundance and excluded from the genebee analysis (below top 500) may well be derivatives of the highly populated sequences that have been analysed. Although Illumina MiSeq has one of the lowest reported error rates of all the NGS platforms (<0.4% [514]), this substitution and read error will contribute to the number of imperfect sequences and suggests it is indeed valid to take the most populous aptamers forward.

The ten sequence families isolated for each of the three selection pools were then used to find representative sequences to take forward for characterisation. Mfold secondary structure prediction was used to examine structural motifs from within the aligned families. Within each motif, a random selection of the sequences were chosen and analysed for their predicted secondary structure. As expected, for the most part, sequences within a given family shared common secondary structure and therefore only one representative sequence was taken forward. However, in some cases, where the alignment power was generally weaker, more structural diversity was predicted within a family, and therefore more than one representative sequence, each with a distinct structural element, were considered. **Figure 3.16** shows an example of two motifs from the anti-3Q fibril aptamer pool where the secondary structure predication indicate diverse or common structures within a given motif.

Although mentioned above that the most populous sequences are usually represented within the ten families derived through Genebee sequence alignment, there are a few cases where these abundant sequences are not represented. This is particularly true for the anti-Aβ40 monomer selections, where the motifs are not as well populated with related sequences as the two anti-fibril pools (**Appendix 7.3**). To ensure these highly populated sequences were not neglected from our sampling strategy, the five most populous aptamers were also analysed for secondary structure. If the putative fold was distinct from those chosen from the alignment motifs, these too were considered for further analysis.

Between 5 and 8 aptamer sequences (**Figure 3.17 a**) were chosen from each selection pool, based on this bioinformatic sampling (summarised in **Figure 3.17 b**). The Mfold secondary structure predictions represent the major conserved motifs within each pool and are given in **Figure 3.18 - Figure 3.20**. Chosen structures generally contain discrete secondary structure in the random region which consists of a mixture of extended and interrupted stem-loop structures. In most cases, these are supported by separate structural elements formed by the primer regions, however, sometimes the primer region is directly involved in forming the base-paired elements of the central region. Aptamers with these discrete

structural elements were chosen, as these regions may represent the functional structure or binding epitope of the aptamers. As shorter aptamers are more easily synthesised and more versatile in most downstream applications, it was desirable to isolate aptamers that could be easily truncated to their minimal functional binding sequences, once the binding properties of the full-length aptamer have been properly characterised.

Owing to the high proportion of repetitive guanosine residues in the anti-Aβ40 monomer and anti-2A fibril aptamers (presumably a result of their selection from the GA biased selection libraries), it was hypothesised that these sequences would likely form G-quadruplex structures. A G-quadruplex (also known as G-quartet or G-tetraplex) is a common structural motif that can be formed from both DNA and RNA. A G-quadruplex consists of G-rich sequences forming various four-stranded structures, where the guanine bases associate in a square-planar arrangement through Hoogsteen hydrogen bonding[515]. The structure is further stabilised by monovalent cations that occupy the central cavity between the strands. Using a quadruplex forming G-rich sequences prediction algorithm (QGRS)[516], the ability to form G-quadruplex structures was predicted for all five anti-2A fibril aptamers chosen from the next generation sampling, and all but one of the anti-Aβ40 monomer aptamer sequences (M1 was the only sequence predicted not to form a G-quadruplex). The anti-3Q aptamers generally do not contain repetitive G residues, except in the case of 3Q1 which, interestingly, does not display the same U-rich bias as shown for the majority of aptamers selected in the anti-3Q fibril selection. This sequence instead displays a bias towards GA nucleotides (76.6%) and is the only anti-3Q fibril aptamer from the cohort that is predicted to form a G-quadruplex structure.

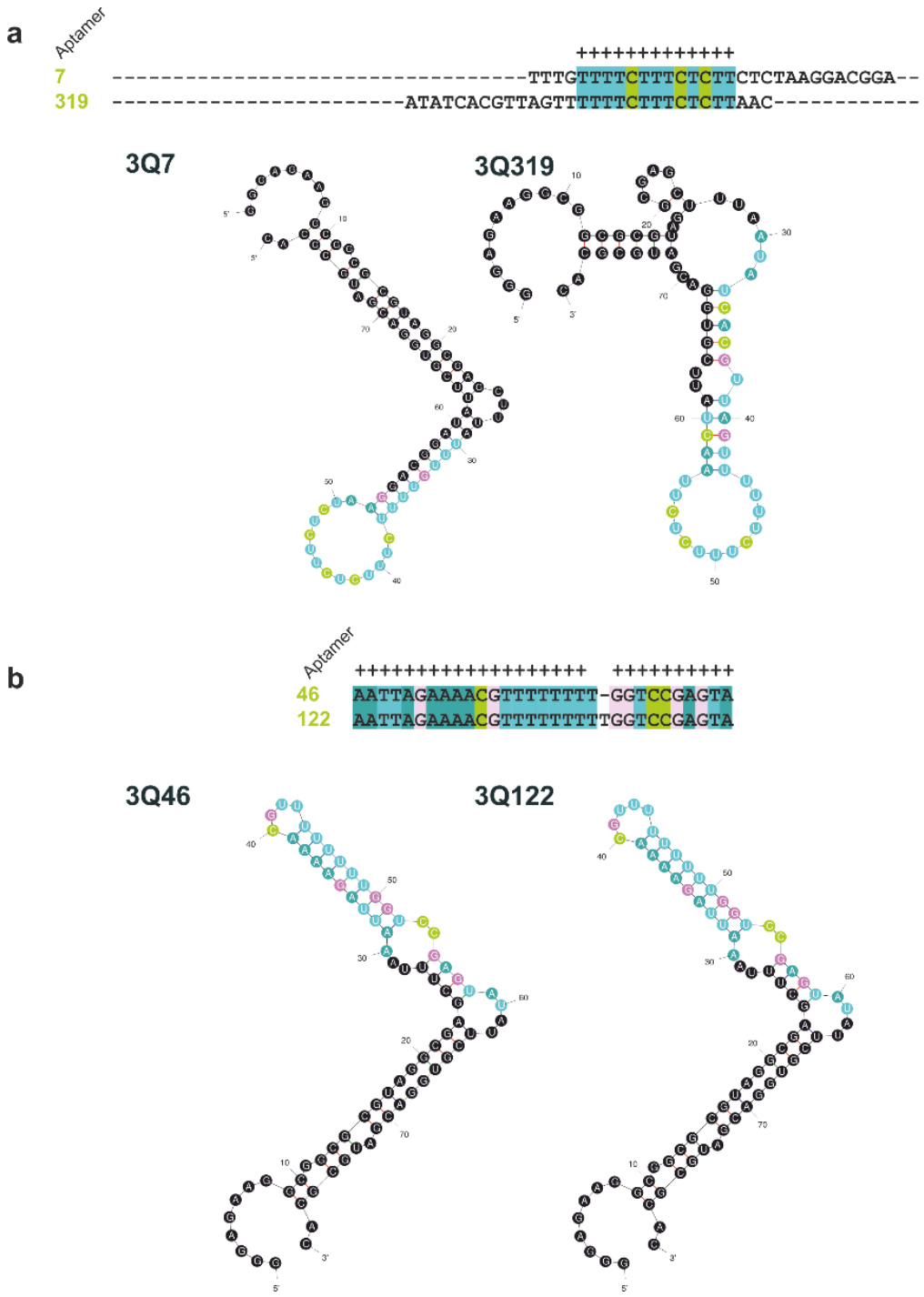

Figure 3.16 Mfold secondary structure prediction analysis of aptamer motifs. Examples of motifs, derived from the Genebee sequence alignments, where more than one distinct structure was populated **(a)** and, conversely, where structures represented were near identical **(b)**. Only the two sequences from the motifs for which secondary structure analysis was performed are shown for clarity. Full alignment data are given in **Appendix 7.3**. Bases corresponding to the random region of the aptamer are represented with coloured circles and the 5′ and 3′ primer regions in black circles. Bases are colour coded according to the same scheme in **Figure 3.15**.

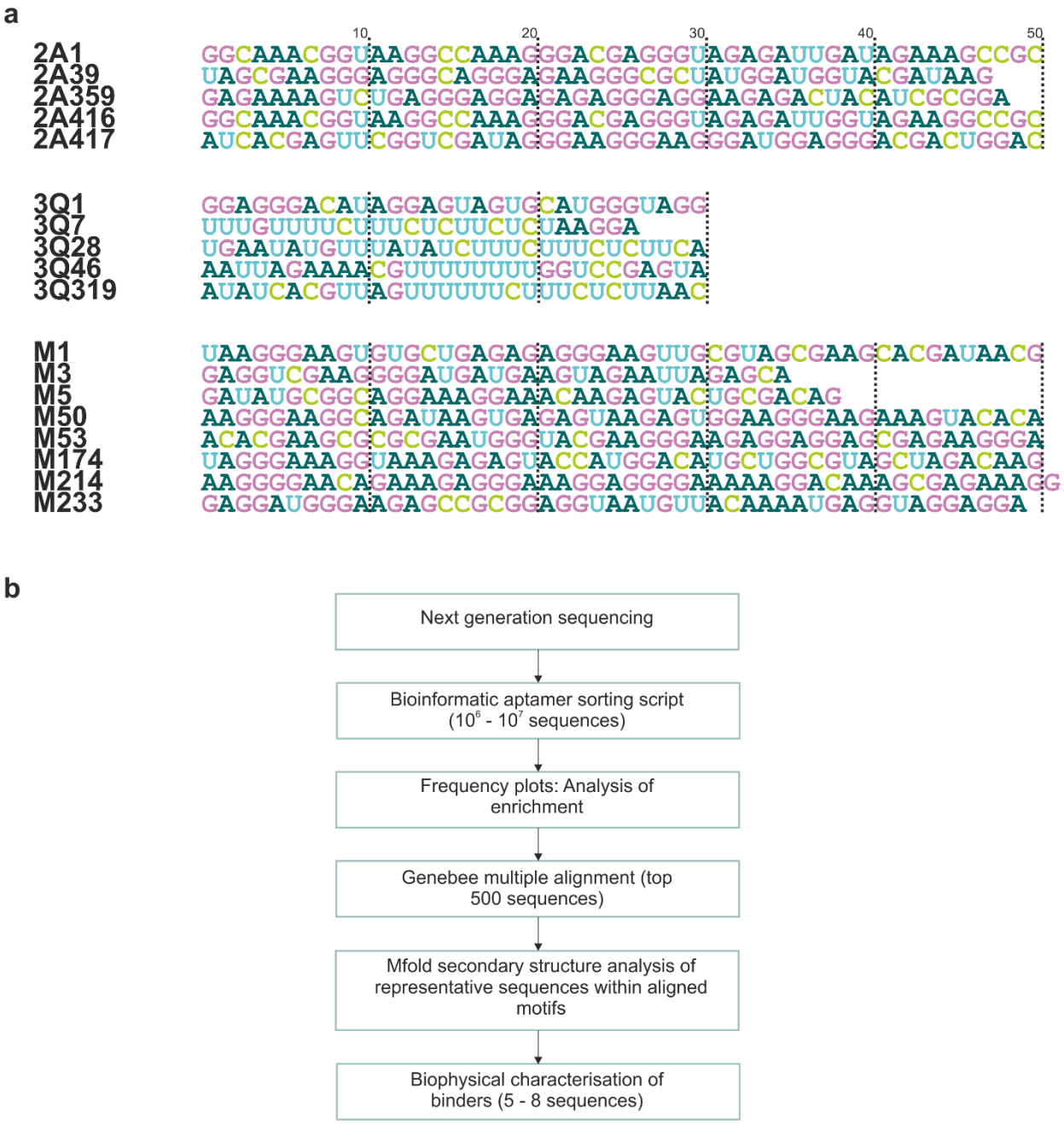

Figure 3.17 Isolation of hit aptamers from bioinformatic sampling. **(a)** Sequences of the lead aptamers chosen from each selection pool. **(b)** Flow chart outlining the bioinformatics based strategy employed to process ~10^7 sequences per selection and isolate lead sequences.

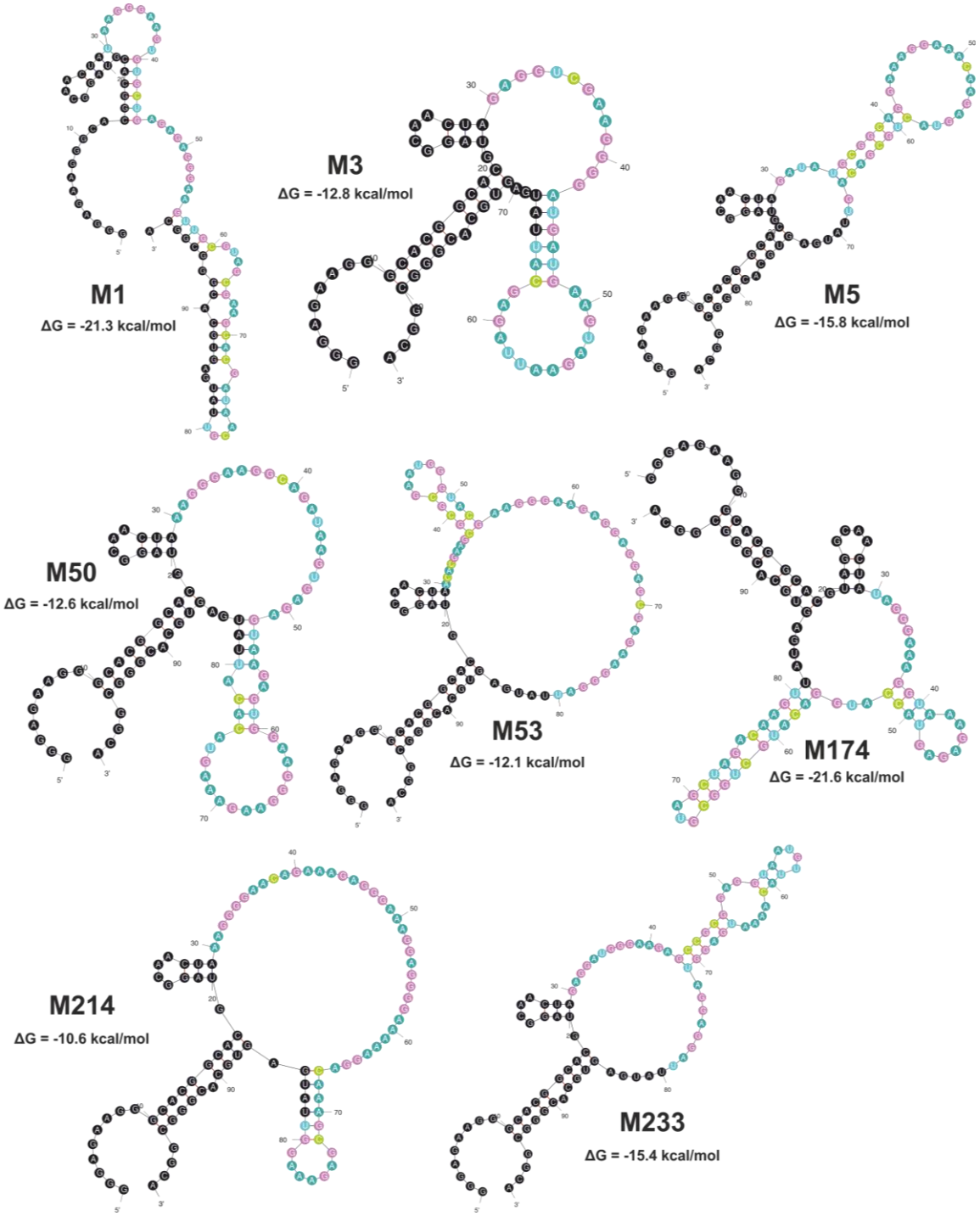

Figure 3.18 Structures of the lead aptamers from the anti-Aβ40 monomer selection. Mfold predicted secondary structures for the eight lead aptamers chosen from the anti-Aβ40 monomer selection pool. The predicted lowest free energy fold is given for each sequence. Bases are colour coded according to the same scheme in **Figure 3.15**.

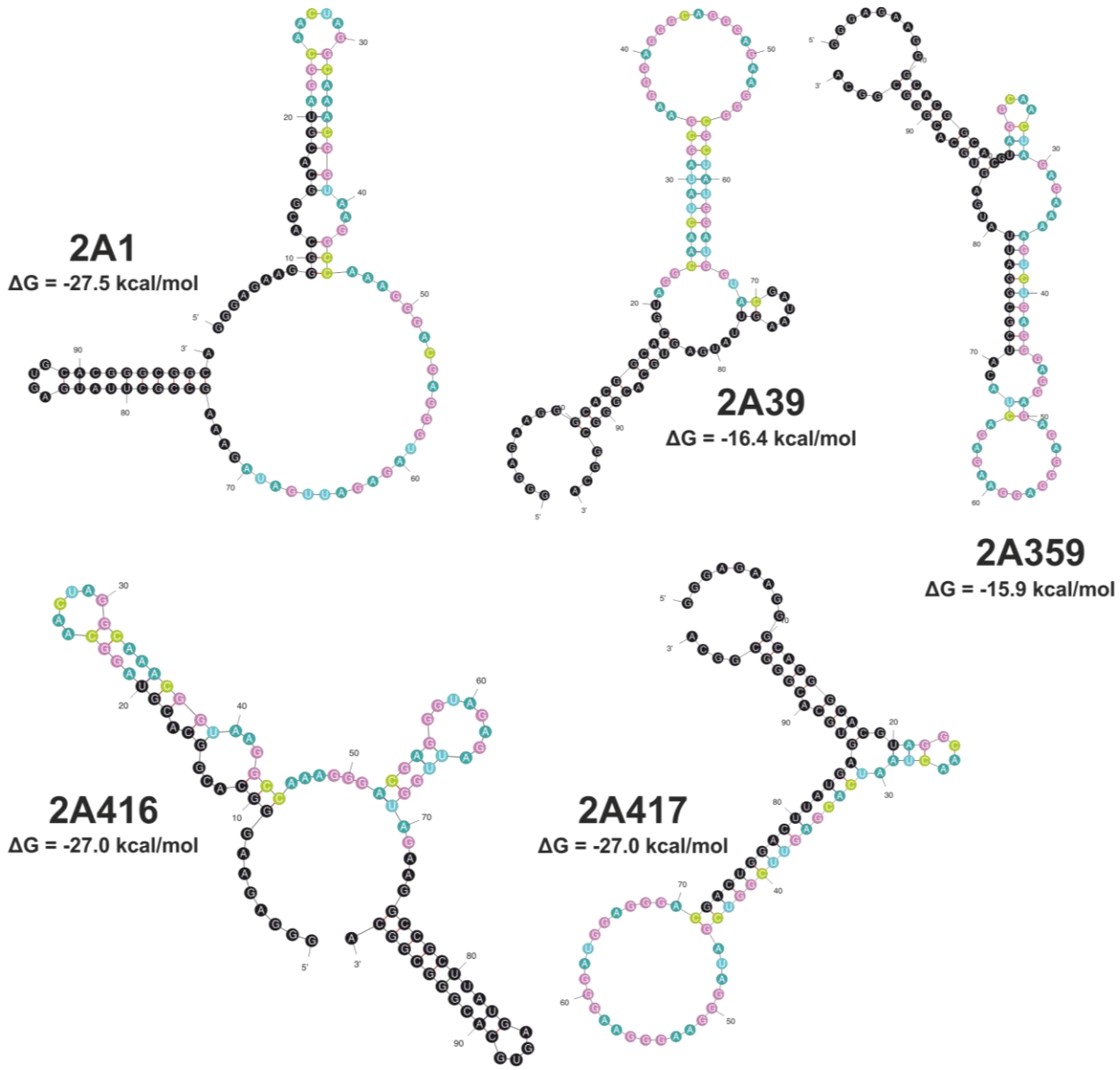

Figure 3.19 Structures of the lead aptamers from the anti-2A fibril selection. Mfold predicted secondary structures for the five lead aptamers chosen from the anti-2A fibril selection pool. The predicted lowest free energy fold is given for each sequence. Bases are colour coded according to the same scheme in **Figure 3.15**.

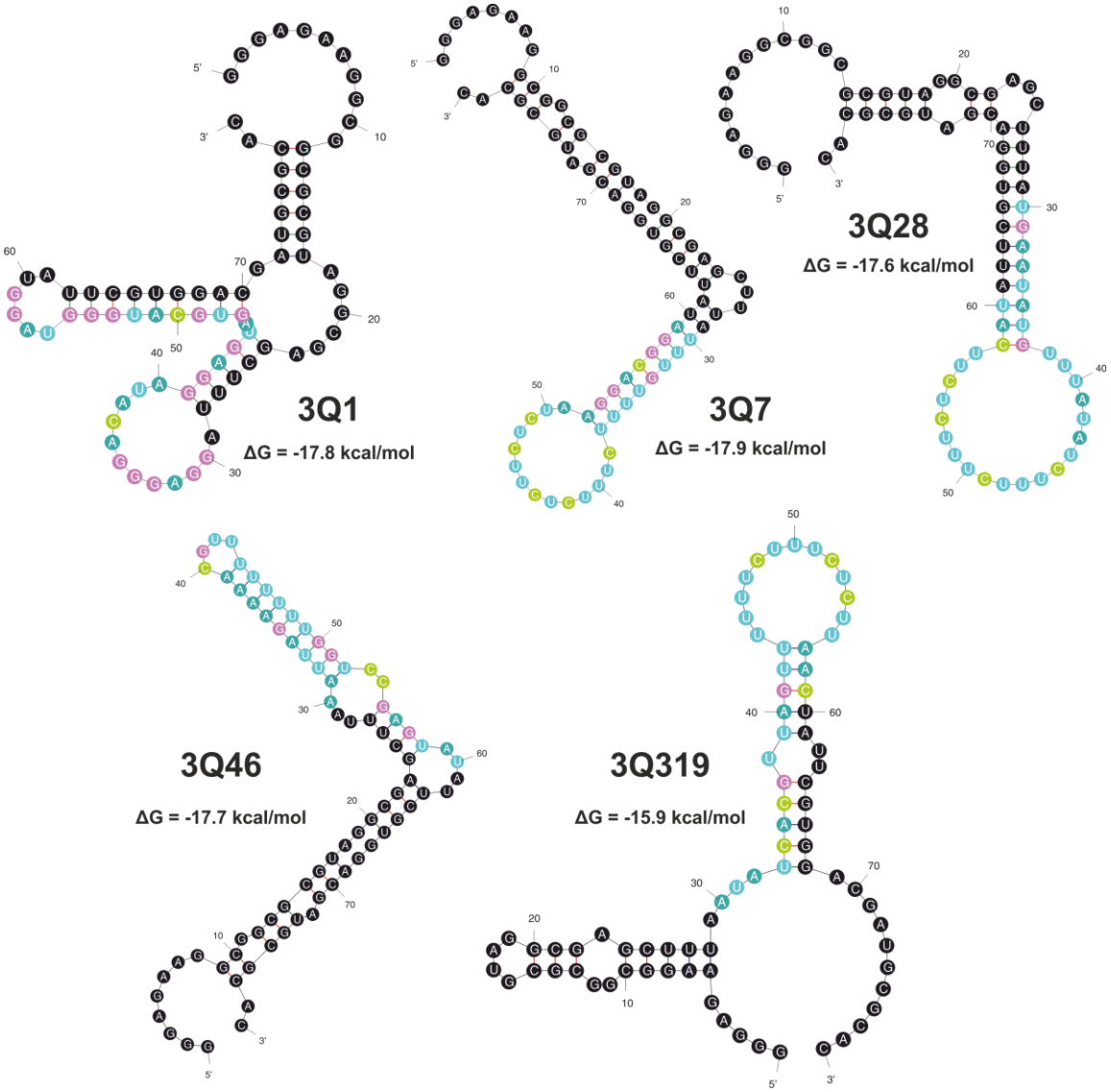

Figure 3.20 Structures of the lead aptamers from the anti-3Q fibril selection. Mfold predicted secondary structures for the five lead aptamers chosen from the anti-3Q fibril selection pool. The predicted lowest free energy fold is given for each sequence. Bases are colour coded according to the same scheme in **Figure 3.15**.

3.8 Discussion

One of the major requirements in tackling amyloid disorders is the development of new diagnostic and therapeutic intervention strategies. A central challenge in this endeavour is the development of ligands that recognise and interact specifically with species involved in amyloidosis; a problem that is exacerbated by the lack of structural knowledge of the assemblies involved. In the case of Aβ40, the monomeric precursor is intrinsically disordered and, therefore, not amenable to conventional structure based ligand design. Only a few examples of rationally designed ligands for Aβ monomer exist. These are generally peptides designed around fragments of the Aβ peptide itself (often the aggregation prone residues 16-21) which bind and block further aggregation[517, 518], in some cases by incorporating β-sheet blocking residues such a prolines[188] or through the incorporation of bulky chemical groups, such as cholesterol[187] . The vast majority of existing anti-Aβ40 monomer ligands have instead been derived via directed evolution type approaches. Peptide-based affimers have been selected via phage display from randomised protein libraries and revealed nM affinity to monomeric Aβ40[519]. A plethora of small molecule binders to Aβ monomers have also been isolated through various screening protocols[202, 520-526], however specificity is often a major caveat. Many anti-Aβ antibodies have been isolated and demonstrate binding to specific portions of the peptide sequence, in many cases, leading to the prevention of oligomer and fibril formation[527-529]. Although antibodies are indispensable research tools and have shown significant promise as therapeutic agents in AD animal studies, they have not yet shown success in human clinical trials, in targeting AD[530] (discussed in detail in Chapter 1, Section 1.3.5). RNA aptamer selection, therefore, was considered an exciting alternative technology to develop Aβ40-monomer-specific reagents.

In the case of amyloid fibrils, structural information is more accessible and therefore there is more scope for the design of recognition molecules. Again, there are many examples of antibodies developed to recognise fibrillar assemblies of Aβ[125, 531], as well as numerous small molecule ligands[524, 525, 532, 533]. These molecules, although useful as research tools, often are not specific to a single amyloid morphology and serve as generic amyloid detectors. To date, no ligand has been developed able to distinguish between different cross-β fibril structures of the same sequence. The aim here, therefore, was to generate ligands with superior recognition powers, through nucleic acid aptamer based technologies.

Aptamers, although well established in other research areas[360, 364, 446, 448, 452, 534], have been slow to emerge in the amyloid field. Of the few examples of Aβ targeted aptamers that exist[491, 493, 494], most have encountered issues with poor selectivity for their intended targets (monomeric or LMW oligomers) and, despite being selected against Aβ40 monomers, have shown enhanced affinity for the aggregated form. It was hoped that with our improved selection methodology, combined with NGS, aptamers with affinity for the monomeric Aβ40 peptide might be selected, for the first time. Firstly, the immobilisation method used involved biotin conjugation with a 30.5 Å alkyl chain spacer arm, to eliminate possible steric hindrance by the label. Such modification has been shown not to interfere with amyloid assembly[483, 535], suggesting preservation of the native structure. Target preparation conditions were also carefully controlled to maintain the peptide in a monomeric state, as much as possible, before selection. During the selection protocol itself, six of the selection rounds comprised of competition elutions, driving the affinity towards un-modified, monomeric Aβ40.

There has so far been little interest in Aβ fibrils as targets for RNA aptamers, most probably owing to the fact that oligomeric structures are often considered the main species of interest in amyloid toxicity[123, 126, 142, 266, 267]. However, anti-Aβ fibril aptamers do exist in the literature, in most cases as a by-product of unsuccessful selections against monomeric or oligomeric assemblies[491, 494]. These aptamers show considerable cross-reactivity with fibrils derived from other amyloidogenic peptides, including fibrils of Aβ42, lysozyme, IAPP, Prion106-126, calcitonin and insulin[494], reinforcing the view that amyloid fibrils share common structural features. To avoid this problem in the selections described here, and hence to find aptamers with enhanced recognition properties, the inclusion of counter selections against alternative fibril morphologies were considered to drive specificity. This would entail incubation of the RNA pool with an alternative fibril type and only the low affinity, unbound fraction would be taken forward for selection against the target morphology. However, previous experience with amyloid selections in our laboratory showed that the inclusion of these counter selection rounds could lead to the removal of the vast majority of RNA from the pool[490]. This observation firstly affirms that there is considerable overlap in the epitopes between different amyloid assemblies, but also suggests that it is indeed difficult to raise aptamers against such similar polymorphs. Therefore, counter selections with fibrils of the alternative morphology were omitted from the protocol and it was decided that the two anti-fibril selections would be conducted independently and the product RNA sequences would be screened for cross-reactivity post-selection. These experiments are described in Chapter 5.

One of the major advantages of the protocol developed here was the availability of next generation sequencing (NGS) to aid in the development of effective aptamers. Until recent years, and in all anti-Aβ aptamers reported to date[491, 493, 494], aptamer sequences were isolated from enriched selection pools using traditional cloning and sequencing methods. This method, although generally successful in accessing the most frequently occurring clones, only allows for the analysis of relatively few sequences (10-100 [ref 377]) compared with NGS technologies (10^7 sequences). It is possible, therefore, that in previous selection attempts, the highest affinity aptamers were not sampled from the selection mixtures, owing to the fact that only a small proportion of the selected sequences could be scrutinised using conventional methods.

The anti-Aβ40 monomer and anti-2A and 3Q fibril selections described in this chapter were successful in isolating aptamer pools, where specific sequences were enriched and highly populated. Conserved sequence and structural motifs were identified from the 500 most abundant sequences, allowing for isolation of lead aptamers for further characterisation. By comparison of the sequences chosen from each selection pool, differences in the overall base compositions are apparent (**Figure 3.17**). Anti-2A fibril aptamers are purine rich, whereas anti-3Q aptamers generally contain poly-U repeats. Although this was found to be a consequence of selection from naïve libraries containing considerable bias, enrichment of specific sequences within this pool was still apparent and aptamers were therefore chosen from these highly populated sequences. Interestingly, 3Q1, the most highly populated aptamer from the anti-3Q fibril selection, does not contain the same U-rich motif as the other aptamers from the corresponding pool. 3Q1 displays instead a more diverse base composition, with a bias towards purines (76.6% GA content). The fact that this aptamer sequence (and others possibly derived from it, within its corresponding aligned motif (**Appendix 7.3**)) has been selected despite the prominent uracil bias, is further encouragement that this selection has been successful. With the use of NGS analysis, it has recently become clear that base distribution bias is a common feature of synthetic SELEX libraries. Companies are now focusing on the synthesis of superior combinatorial libraries, where the bias is eliminated, leading to better quality starting libraries for selection[536]. Although neither this knowledge nor technology was available at the beginning of this project, it is worth noting that the diversity of the starting pool, used here, will have been compromised to some extent. Similarly, we must also be aware that there may be certain biases in other stages of the selection process (PCR, transcription) and the NGS itself, which might contribute to the optimal binding sequences being underrepresented. For example, PCR amplification is known to be biased towards GC-neutral sequences[537]. Despite these

limitations, which are a problem for all nucleic acid aptamer selection strategies, aptamer sequences have been selected and preferentially amplified and only the biophysical characterisation of their specificity and affinity towards their cognate targets will confirm the success of the SELEX experiments, and their potential in various downstream applications. Characterisation of the anti-Aβ40 monomer and anti-fibril aptamers are described in the following two chapters.

4 Characterisation of RNA aptamers against Aβ40 monomer

4.1 Objectives

In Chapter 3, the selection of RNA aptamers against three distinct Aβ40 assemblies was described; two fibrils with unique structural morphologies (2A and 3Q) and the intrinsically disordered monomeric peptide. This chapter describes the characterisation of the aptamer sequences chosen from the anti-monomer selection.

Aptamers were selected against monomeric Aβ40 peptide immobilised via biotin linkage to streptavidin microspheres. As the SELEX protocol included several rounds of competition elution, it was expected that individual aptamers would display enhanced affinity for the peptide monomer in solution, over its immobilised counterpart. In this chapter, development of assays to assess aptamer binding to Aβ40 monomer is discussed.

4.2 Development of assays to monitor aptamer binding to monomeric Aβ40 in solution

By use of the bioinformatic sampling, described in Chapter 3 (Section 3.7), the 0.7 million potential binding aptamers, isolated from NGS, were reduced to eight lead sequences (**Figure 3.18**). The next objective was to characterise the binding properties of these eight aptamers, in order to rank the sequences for binding affinity. By isolating aptamers with the highest affinity for the native monomeric Aβ40 target, and demonstrating specificity in binding this peptide, it would then be possible to focus the study on one, or a few, "hit" aptamers. This would enable detailed structural characterisation and, hopefully, lead on to development of RNA molecules as inhibitory or discriminatory compounds.

The first challenge was the design of appropriate *in vitro* assays to determine binding by the individual aptamers to Aβ40. Owing to the aggregation propensity of Aβ40, one requirement of the binding assays was that they were able to be conducted over short timescales and at relatively low concentrations. Also, for the purpose of screening several

aptamers, the RNA itself could only be synthesised on a relatively small scale (3 μg from a typical 50 μL *in vitro* transcription reaction- Section 2.6.3). Therefore, the binding assays tested also required the use of as little material as possible. Techniques often used to study protein: nucleic acid interactions in solution, such as isothermal titration calorimetry (ITC)[538] and nuclear magnetic resonance (NMR)[539] were ruled out at this initial screening stage, as large quantities and relatively high concentrations of RNA would be required. Because the main aim of the anti-monomer selections was to isolate aptamers able to recognise monomeric peptide, assays involving modification to the peptide structure, such as addition of fluorescent tags, were also not desirable.

4.2.1 Microscale thermophoresis

Microscale thermophoresis (MST) is a powerful method for analysis and quantification of biomolecular interactions, which works by measuring the behaviour of biomolecules in microscopic temperature gradients. During an MST experiment (**Figure 4.1**) a localised temperature gradient is induced by an infrared laser, focused onto the sample in low volume glass capillaries. Fluorescently labelled molecules, which are initially evenly distributed and diffusing freely in solution, experience a thermophoretic force in the temperature gradient. The movement of the fluorescent molecule can be monitored by the change in fluorescence intensity at a fixed point within the capillary. When the laser is switched off, the molecules diffuse back to establish a homogenous mixture once more. The motion of the molecule within the temperature gradient is sensitive to changes in hydration shell, size or charge, any of which can be affected upon ligand binding. By monitoring thermophoresis of the fluorescent molecule at a range of non-fluorescent ligand concentrations, changes in thermophoretic properties upon binding can be observed. Binding constants can therefore be elucidated via this method[540-543].

MST was considered an appropriate assay to quantitate the binding by the aptamer sequences to Aβ40 monomer, as experiments can be conducted on extremely small sample volumes (< 4 μL) and at low concentrations (pM-nM)[540]. The method has previously been applied to a range of studies, from monitoring small molecule interactions[544, 545] to protein: protein[546-548] and protein: nucleic acid[549-551] interactions, and even in monitoring large protein complex formation[552, 553]. The technique can accurately deduce dissociation constants in less than 10 min per sample and access a vast range of affinities (from pM to mM)[540]. MST was especially desirable as solution measurements could be made, without

need for immobilisation of one of the binding partners. However, fluorescent labelling was required and it was decided that optimisation of an aptamer labelling protocol would first be undertaken.

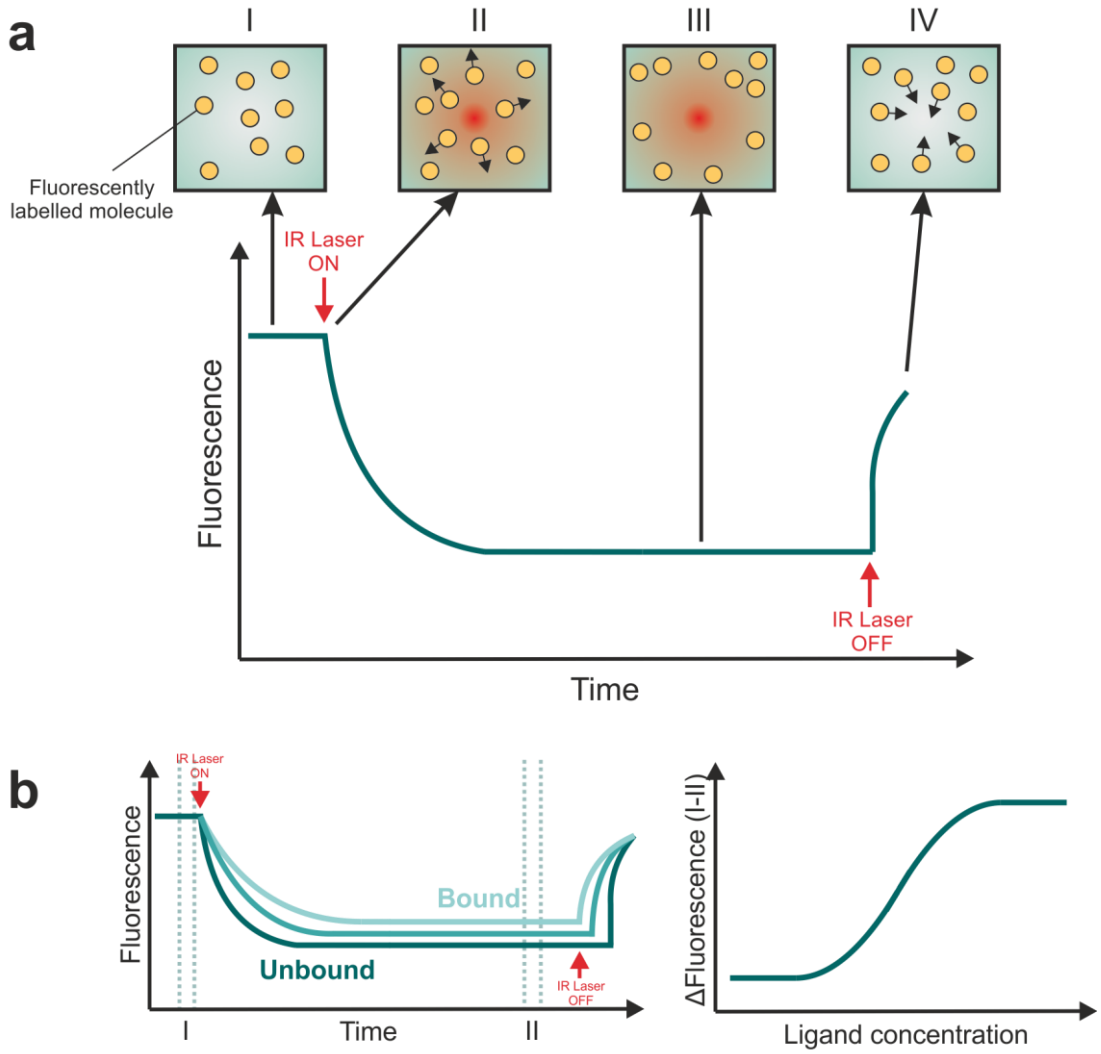

Figure 4.1 Principles of microscale thermophoresis (MST) analysis of molecular interactions. MST measures the movement of fluorescent molecules in a temperature gradient. **(a)** Molecules which are diffusing free in solution **(I)** are irradiated with an infrared laser (represented by red spot) producing a microscopic temperature gradient. The fluorescent molecule will move within this gradient **(II)** and can be monitored over time as the fluorescence intensity changes from a fixed point **(III)**. When the laser is switched off, molecules return to re-establish an equilibrium **(IV)**. **(b)** Differences in thermophoresis of the molecule at different ligand concentrations is monitored and changes in the fluorescence before the laser is switched on **(I)** and after thermophoresis **(II)** are plotted as a function of ligand concentration to quantify binding. Adapted from [540].

4.2.1.1 Optimisation of fluorescent labelling of RNA

In order to produce individual aptamer sequences for binding assays, DNA templates for each of the eight aptamers were commercially synthesised (Eurofins Genomics, Ebersberg, Germany). Each sequence was flanked by the same primer sequences from the N50 library (Section 2.7.1) to allow PCR amplification. These were then amplified with the same primer oligonucleotides used for the initial libraries, which introduce the T7 promoter sequence into the dsDNA product, for *in vitro* transcription. Y639F/H784A T7 RNA polymerase was again used to allow the incorporation of the 2'F modified pyrimidines.

The synthesis of fluorescently labelled RNA can be achieved through the addition of fluorescently labelled nucleotides, directly into the transcription mixture, leading to incorporation of the fluorophore at random sites within the sequence. Using this method, the fluorescent nucleotides can be added at variable concentrations to limit labelling levels. A protocol already established in the Stockley laboratory by Dr. David Bunka, was used to produce fluorescently labelled aptamers via the incorporation of ChromaTide® AlexaFluor® 488-5-dUTP (**Figure 4.2**). The NTP mix was altered to include a 1/80th dilution of this modified UTP and added to the transcription reaction (components given in Section 2.6.5.1). This protocol produces aptamers with approximately one fluorescent dye per RNA molecule, on average, which can be calculated from UV-Vis absorbance measurements at 260 nm and the absorbance maxima of the dye, 493 nm. However, optimisation of both the standard transcription reaction (Section 2.6.3) and purification of the resultant aptamers was required to improve both yield and purity of the RNA produced.

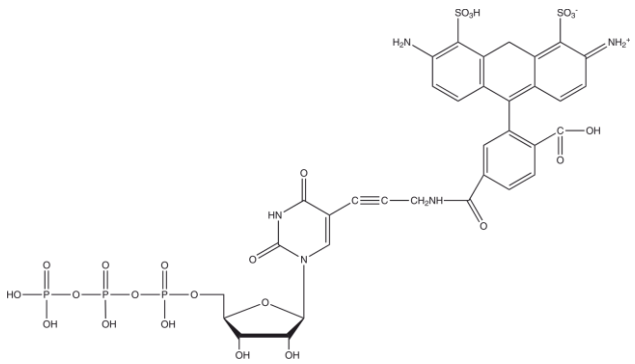

Figure 4.2 Chemical structure of ChromaTide® Alexa Fluor® 488-5-dUTP used to fluorescently label aptamers for binding studies.

To improve the amount of total RNA produced during *in vitro* transcription, trials were conducted into the optimum polymerase and DNA template concentrations required. Increasing the final Y639F/H784A T7 RNA polymerase concentration to 740 nM (2 x that required in standard transcription, Section 2.6.3) and increasing the DNA template concentration, by pooling and concentrating five PCR reactions (Section 2.6.1 - final DNA template concentration of ~ 500 ng/μL), improved the amount of 2'F modified, Alexa488 labelled RNA produced (**Figure 4.3 a**), as assessed by denaturing PAGE.

The next stage to be optimised was the purification of the fluorescent transcripts. The general protocol for RNA purification involves DNase treatment and acidified phenol chloroform extraction of the RNA (Section 2.6.8.1), followed by ethanol precipitation. This was then usually followed by a rapid, column purification step (Illustra microspin G-25, GE Healthcare) to remove free nucleotide and other small contaminants. However, it became clear that in the case of the fluorescently-labelled aptamers, this standard desalting method was not sufficient to remove all free-nucleotides (**Figure 4.4**). The final yield of aptamer was also dependent on several stages of this purification, including the ethanol precipitation and free-nucleotide removal steps, and these too required some optimisation.

Addition of the carrier, or co-precipitate, glycogen, was firstly shown to make a significant difference in the yield of RNA during the precipitation stage, again estimated from denaturing PAGE (**Figure 4.3 b**). On the other hand, trials into the use of different salts or alcohols (conditions trialled outlined **Figure 4.3 b**, table inset) during the precipitation, demonstrated no major effect on the yield of recovered RNA (**Figure 4.3 b**). The addition of 1/5th volume 10 M ammonium acetate, 1/100th volume 20 mg/mL glycogen and 2 x volume ethanol was shown to achieve marginally higher recovery than the other conditions trialled (**Figure 4.3 b**) and, therefore, was implemented in all subsequent aptamer purifications.

In the case of the removal of free-nucleotide, several commercially available columns were tested, including various size exclusion columns and silica-gel based RNA clean-up systems, as well as gel extraction from denaturing PAGE gels (Section 2.6.8.2) (results summarised in **Table 4.1**). All nucleotide removal methods had a significant impact on total RNA recovery (estimated to be less than 10% recovered, based on PAGE analysis **Figure 4.4**). However, extraction of RNA by gel extraction was found to be a more effective method as, although the technique has a similar impact on total RNA recovery, free-nucleotide removal was 100% (**Figure 4.4**). Total yield of RNA via this methodology remained variable, with yields of ~1 μM in 50 μL being typical. This was sufficient for most applications, but when

higher yields of fluorescent aptamer were required, the production was scaled up, by pooling several transcription reactions before the phenol chloroform extraction stage.

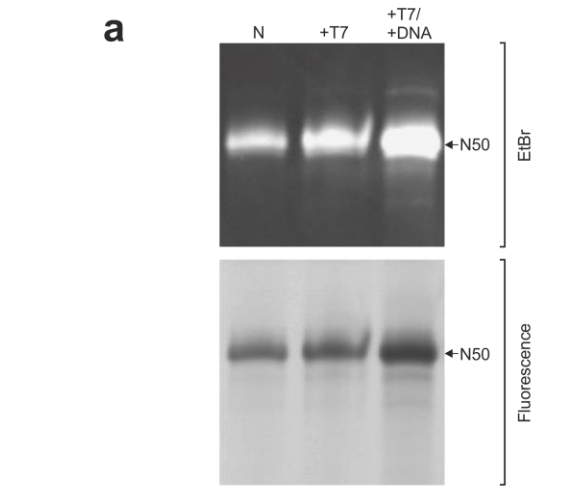

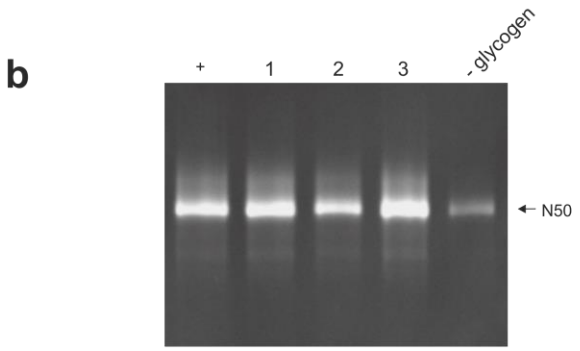

Condition	Salt	Co-precipitate	Alcohol
1	1/10th vol. 4 M sodium chloride	1/100th vol. 20 mg/mL glycogen	2 x vol. ethanol
2	1/10th vol. 3 M sodium acetate, pH 5.2	1/100th vol. 20 mg/mL glycogen	1.1 x vol. isopropanol
3	1/5th vol. 10 M ammonium acetate	1/100th vol. 20 mg/mL glycogen	2 x vol. ethanol

Figure 4.3 Optimisation of the transcription conditions and ethanol precipitation of 2'F Alexa488 labelled aptamers. **(a)** Denaturing PAGE analysis comparing levels of RNA transcription under "normal" transcription conditions (N - used for transcription of non-fluorescent 2'F aptamers (Section 2.6.3)), with increased polymerase concentration (+T7) and with increased polymerase and DNA template concentration (+T7/+DNA). **(b)** Denaturing PAGE analysis showing levels of RNA yielded under different ethanol precipitation conditions, compared with a sample before precipitation (+) (conditions 1, 2 and 3 are outlined in the accompanying table). – glycogen indicates an RNA sample treated as condition 3, without glycogen.

Technique	Separation technology	Score	Conclusion
Illustra G-25 microspin column	SEC	*	Poor removal of nucleotides and very poor yield of total RNA in both cases. Slightly better yield of RNA when larger volume, gravity flow NAP5 columns used over G-25.
Illustra NAP5 column	SEC	**	
RNeasy mini column	Silica-based	*	Nucleotide removal good but yield of total RNA extremely poor. Both methods work well for unlabelled RNA. RNeasy columns only work for aptamers > 100 nucleotides.
Clean & Concentrator™-5 column	Silica-based	**	
Gel extraction	PAGE	***	Generally poor yield of total RNA but nucleotide removal is 100%. Method can be easily scaled up to increase yield.

Table 4.1 Methods tested to optimise free-nucleotide removal in the purification of Alexa488 labelled aptamers. Conditions are scored from the most (three stars) to the least (one star) favourable.

A typical absorbance spectrum of purified 2'F Alexa488 labelled aptamer (aptamer M1 – 99 nucleotides) is shown in **Figure 4.5**, where average dye incorporation is calculated (Section 2.6.5.1, **Equations 2.3** and **2.4**) by the absorbance measurements at 260 nm and the absorbance maximum of the fluorophore at 493 nm. In this example, average Alexa incorporation is 1.48 Alexa molecules/RNA. Dye incorporation was found to vary between preparations (1.0 - 1.5 dye/RNA on average). A260/280 ratios greater than 2.0 (indicating pure RNA[554]) were typically achieved via this optimised methodology (in this example A260/280 = 2.1). The overall yield of RNA in this example is 4.3 µM in 50 µL.

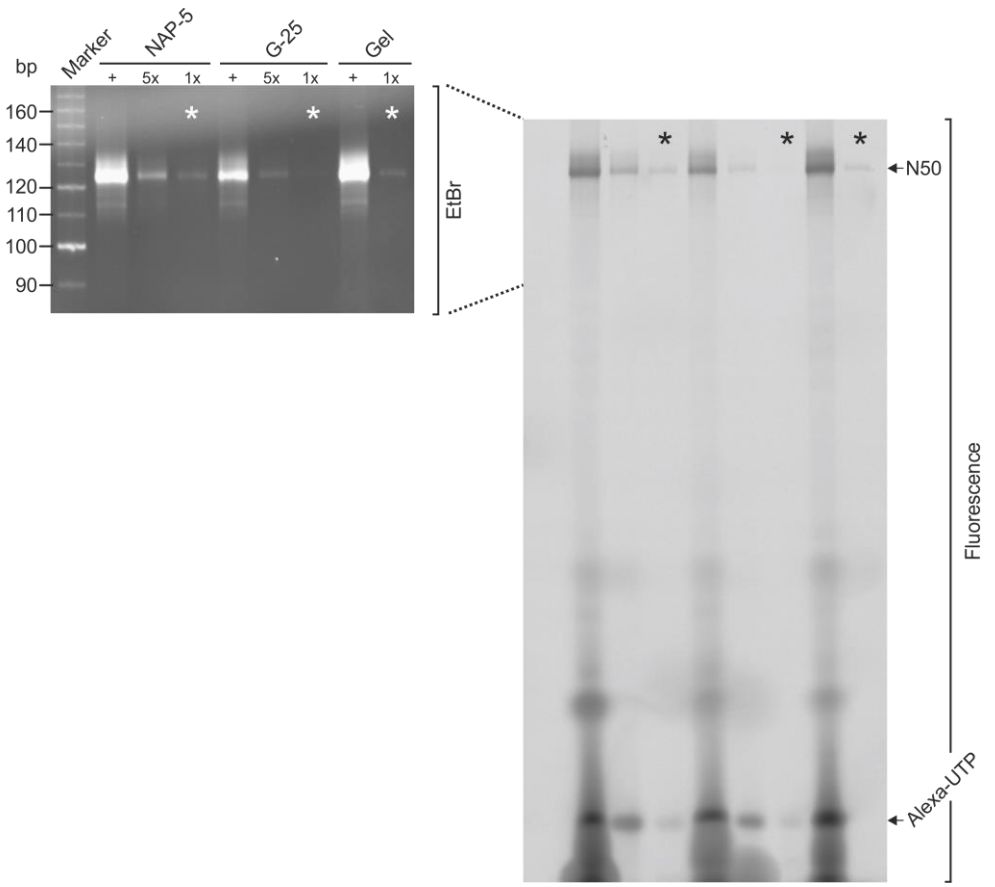

Figure 4.4 Comparison of techniques to remove contamination with free-nucleotides. Denaturing PAGE analysis comparing yield and removal of free-nucleotides by different purification methods. The amount of nucleotide remaining can be seen at the bottom of the right hand gel image (denoted Alexa-UTP). Purification by NAP-5 column, G-25 column and gel extraction are indicated. Different volumes of sample were loaded to aid comparison (indicated 5 x and 1 x) and only 1 x lanes (further marked *) can be directly compared for yield. Products from each purification method are compared with a sample before purification (+). The same gel is shown analysed by both ethidium bromide staining and fluorescence scanning with a Fujifilm 5100 fluorescence image analyser (indicated).

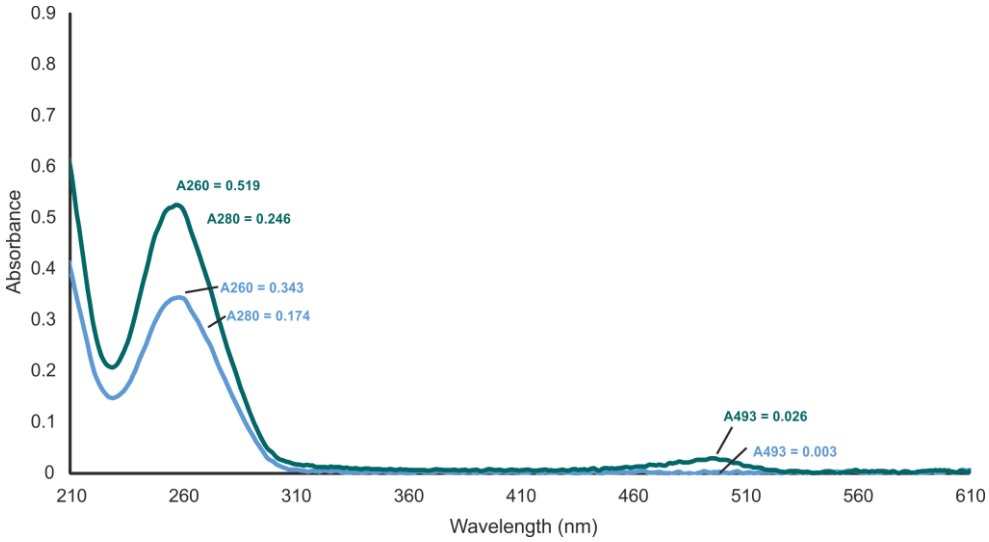

Figure 4.5 Verification of Alexa488 UTP incorporation in a typical labelled aptamer sample. A typical UV-Vis absorbance scan of a 2'F Alexa488 labelled aptamer is shown (teal). 260/280 ratio is 2.1, indicating pure RNA. Average dye incorporation is calculated by Equations 2.3 and 2.4 (Section 2.6.5.1), which in this case equates to 1.48 Alexa dye molecules/RNA molecule. Comparison to an unlabelled RNA sample of similar concentration (2.8 μM) is shown in the blue spectrum.

4.2.1.2 Analysis of aptamer binding to Aβ40 monomer by MST

MST experiments to assess the binding by the aptamer sequences to Aβ40 monomer were conducted in the same MOPS buffer used during selection. A final concentration of 250 nM 2'F Alexa488 aptamer was incubated with aliquots of freshly resolubilised Aβ40 peptide, at peptide concentrations ranging from 12 nM to 100 μM. Solutions were incubated for 15 min at room temperature, before 4 μL of each titration point was loaded, via capillary diffusion, into individual glass capillaries and analysed (Section 2.8.4). Four aptamers, M1, M50, M53 and M214 (a selection of the eight planned to be screened) were tested via this method (**Figure 4.6**), in order to set up suitable assay parameters. The data obtained suggested that for all four aptamers, there was no impact on their thermophoretic properties upon addition of increasing concentration of monomeric Aβ40 peptide, suggesting there was no interaction. Thermal denaturation and re-annealing of the aptamer stocks, to promote correct folding of the aptamers, before incubation with the peptide ligand, was shown to have no effect (shown for aptamers M50, M53 and M214, **Figure 4.6**) and hence no

interactions between the selected aptamers and monomeric Aβ40 were observed by this method.

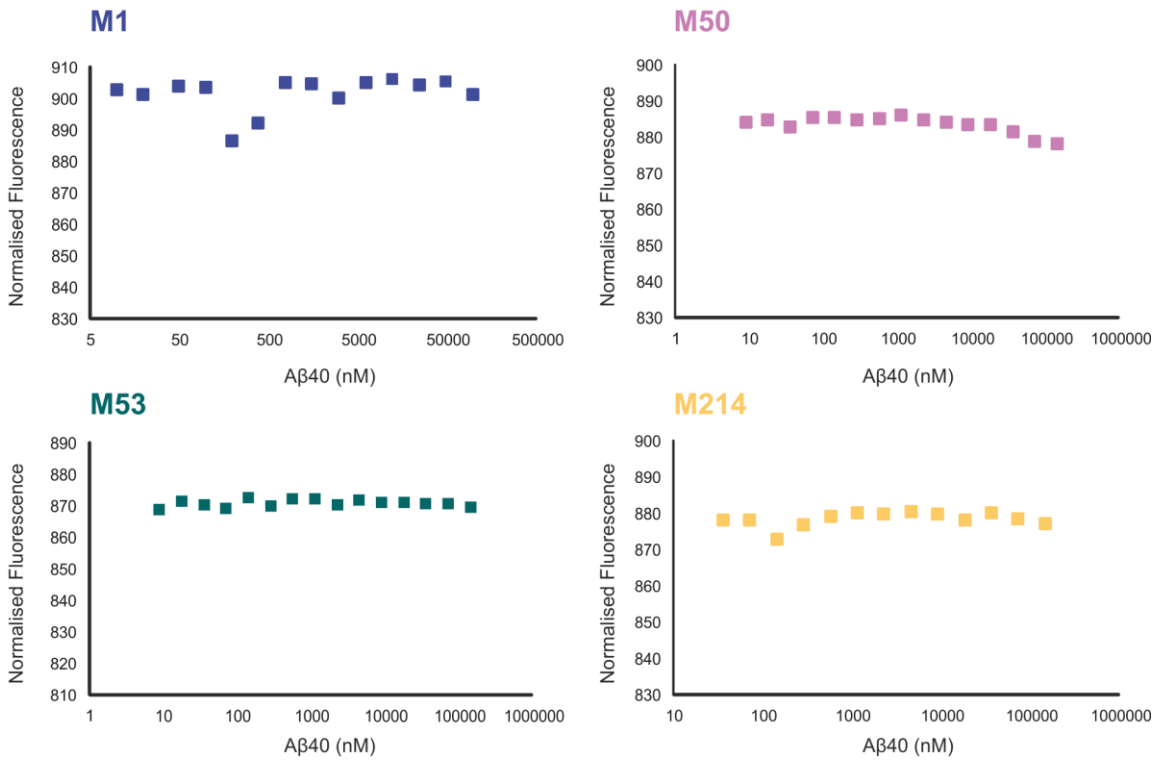

Figure 4.6 MST shows no interaction between anti-Aβ40 monomer aptamers and Aβ40 in solution. 2'F Alexa488 labelled aptamers were assayed against a titration of Aβ40 monomer by MST. Data for aptamers M1 (blue), M50 (pink), M53 (green) and M214 (yellow) are indicated.

4.2.2 Development of further solution binding studies

Since the MST data suggested that the selected aptamers do not bind monomeric Aβ40 in solution, further assays were conducted to detect binding. One approach considered was monitoring the change in intrinsic fluorescence of Aβ40 upon aptamer interaction. Intrinsic fluorescence of proteins is derived from the aromatic amino acids tryptophan, tyrosine and, to a lesser extent, phenylalanine, and can be sensitive to structural changes that may occur upon binding[555]. Aβ40 has no tryptophan residues and only one tyrosine at position 10, meaning the peptide is weakly fluorescent and therefore may be insensitive to binding.

Nevertheless, tyrosine quenching experiments have been used previously to quantitate Aβ40 interactions[556, 557]. When incubated with the unlabelled aptamer M1, no fluorescence change was observed upon aptamer titration (results not shown). It was unclear whether the lack of signal change was due to a lack of aptamer binding to Aβ40 monomer or whether an interaction could be taking place which did not alter the fluorescence of Aβ40's single tyrosine residue. Similarly, incubation of Aβ40 with Alexa488 labelled aptamer did not result in any detectable fluorescence intensity change (**Figure 4.7 a** and **b**). These assays support the conclusion that aptamers do not bind Aβ40 monomers significantly.

Next, fluorescence polarisation (which is discussed in more detail in Section 5.2.1) was used to monitor binding of Aβ40 and aptamer M1. In this assay, the degree of polarisation of light emitted by a fluorophore is sensitive to the change in mass as a consequence of a binding event[558]. Again, it was uncertain whether the small mass change induced upon Aβ40 (MW = 4458 Da) binding to the RNA aptamers (MW ~30 kDa) would induce a significant change in polarisation, however the technique has been employed previously in studying this peptide binding to fluorescently labelled RNA[493]. The titration of Aβ40 monomer against a fixed concentration (10 nM) of the Alexa488 fluorescently-labelled aptamer M1 (**Figure 4.7 c**) resulted in no change in fluorescence polarisation of the RNA. This data also supports the conclusion that there is no detectable interaction between the aptamer and the monomeric Aβ40 peptide in solution.

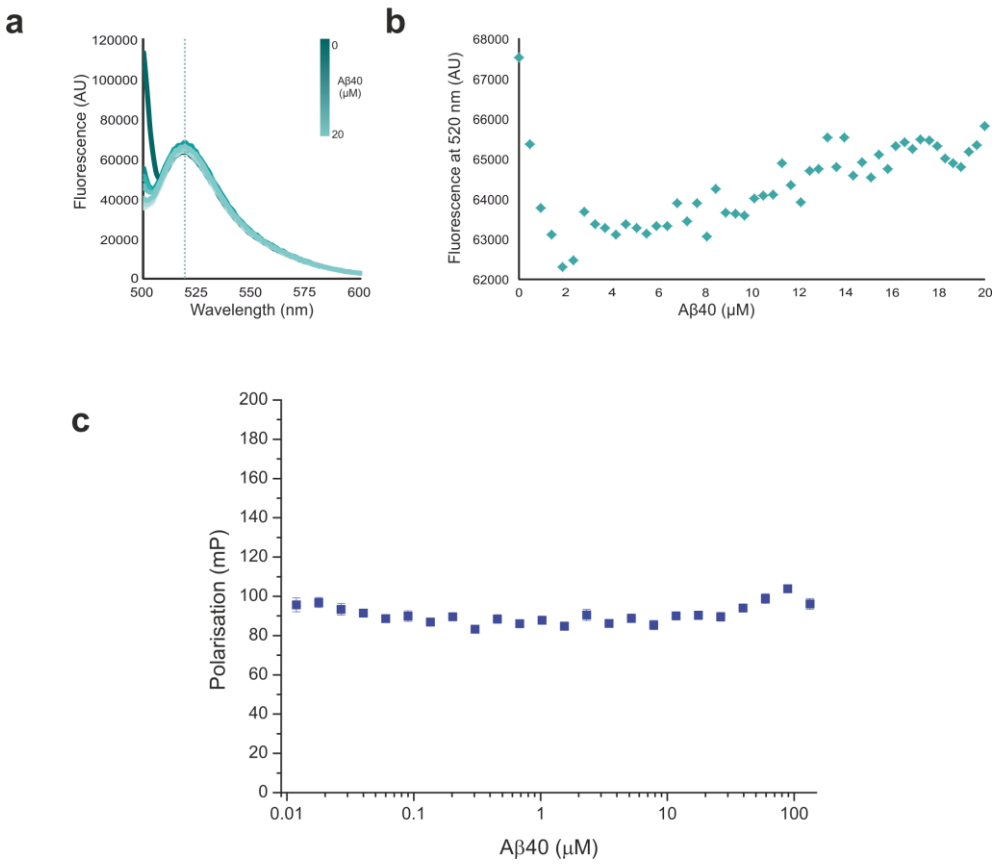

Figure 4.7 Solution assays demonstrating no detectable interaction between Aβ40 monomer and aptamer M1. **(a)** Fluorescence emission spectra of Alexa488 labelled aptamer M1 upon titration with Aβ40 monomer. **(b)** Intensity at 520 nm from the series of emission scans in (**a**, dotted line) was plotted as a function of Aβ40 concentration. No quenching of the Alexa488 dye is observed. **(c)** Fluorescence polarisation of Alexa488 labelled aptamer M1 upon titration with Aβ40 monomer.

4.3 Investigation of aptamer binding to immobilised Aβ40

Despite the inclusion of six rounds of solution competition elution during the SELEX procedure (Section 3.5.1), introduced to promote binding to native peptide, the aptamers were not able to recognise Aβ40 monomer by any of the techniques discussed above. It was therefore decided that the aptamers affinity for the immobilised peptide would be investigated, to confirm whether surface immobilisation was required to present the Aβ40 conformation that was recognised and selected against.

4.3.1 Surface plasmon resonance (SPR)

Surface plasmon resonance is a technique that monitors real-time biomolecular interactions. The technique (**Figure 4.8**) monitors the formation of complexes on a surface and displays a signal proportional to the extent of this interaction[559, 560]. The test ligand is directly conjugated to a gold-coated surface and the potential binding partner, or analyte, is injected as a continuous flow over the surface. Light is focused onto the gold surface where it is reflected. At a specific angle of incidence the phenomenon of SPR occurs, where some of the reflected light is absorbed, with energy transferring to electrons in the gold layer, producing surface plasmons. This results in decreased intensity of light detected at this resonance angle. The angle at which SPR occurs is dependent, and highly sensitive to, the changes in refractive index at the surface. These changes in refractive index are induced through mass changes on the surface and, therefore, can be used to monitor association and dissociation of biomolecules. Once a test analyte is injected and the interaction monitored, the surface is regenerated, removing the analyte and resulting in a new ligand-saturated surface for the next sample to be tested.

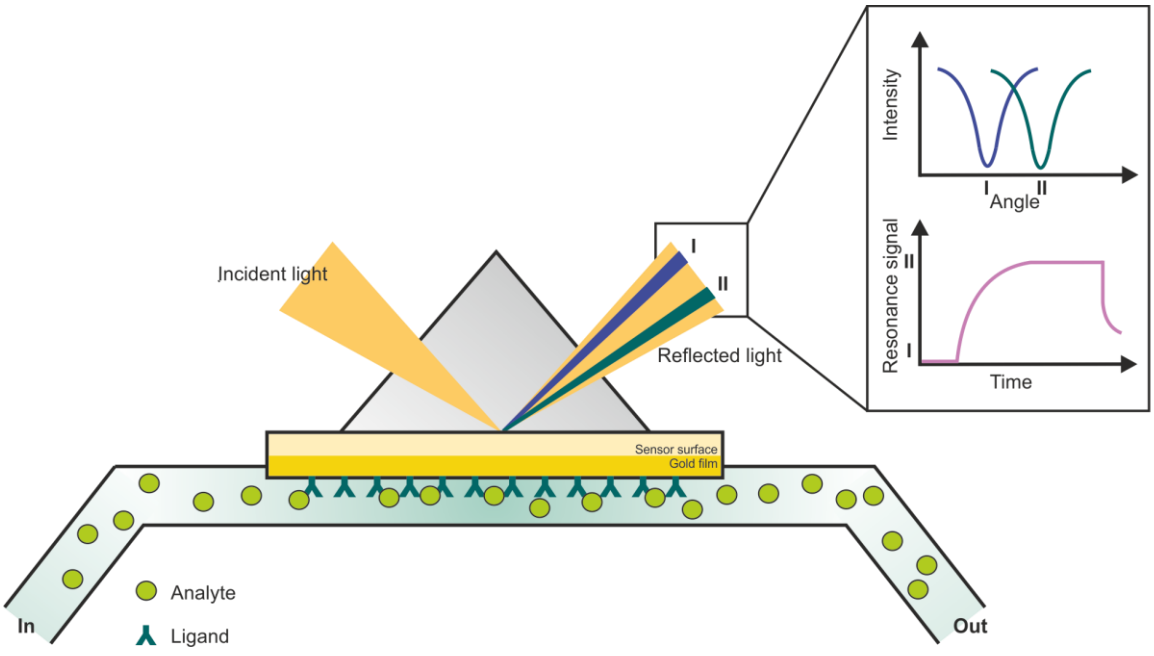

Figure 4.8 Principles of surface plasmon resonance (SPR). SPR monitors the change in refractive index (RI) when biomolecules interact on a gold-coated surface. The angle of incidence at which plasmons are produced is dependent on the RI and detected as a decrease in intensity, which is monitored over the time course of an interaction. Adapted from [559].

SPR was thought to be a useful alternative method to screen the aptamers against the immobilised monomeric Aβ40 target. By use of an SA sensor chip (GE Healthcare), pre-derivatised with streptavidin, the same biotin immobilisation strategy optimised for aptamer selection (Section 3.4.2) could be used to immobilise the peptide for analysis by SPR. By immobilisation through sequential injection of a dilute solution of biotin-modified Aβ40, aggregation could also be avoided. Aβ40, therefore, was biotin labelled, as previously described, and immobilised onto the SPR sensor chip (Section 2.8.2). The theoretical, optimal level of peptide to be deposited on the flow cell for effective SPR can be calculated (Section 2.8.2) and is often maintained at the lowest level possible to give an acceptable response, in order to reduce limitations of ligand binding rates through mass transport of the analyte[561]. Therefore, in accordance with these recommendations, only 25 response units (RU) of Aβ40 monomer were deposited on the sample flow cell. Another flow cell with 500 RU Aβ40 was prepared to ensure a sufficient response would be seen. To account for any background response, a reference flow cell was left blank as a control. Similarly, a control protein, β_2-microglobulin (β_2m) (kindly provided by Dr. Claire Sarell, University of Leeds) was immobilised on the final available flow cell, as an additional reference, and to allow assessment of binding specificity.

The 2'F aptamers M1 and M50 were transcribed *in vitro* and purified, before dialysis into the SPR running buffer, which was again the same MOPS buffer used in the aptamer selections, with the addition of 0.005% (v/v) Tween 20. The dialysate directly taken from the aptamer dialysis was used as the running buffer in the experiment to minimise any refractive index changes on the surface, as a result of buffer injection only. 10 µL of 1 µM aptamer RNA was injected over the flow cells and the association and dissociation monitored, before regeneration of the surface (with 0.5 M NaCl) for the next aptamer injection (Section 2.8.2). The results of these experiments did not provide any evidence of specific association of the aptamers with the immobilised Aβ40 monomers. A typical response from injection of aptamer M1 is shown in **Figure 4.9**, where the response seen in all four flow cells, including the controls, was similar. The response is also very low (<30 RU) and therefore presumably reflects a small RI change on the surface as a result of the analyte injection. After background correction, therefore, no binding response was observed for either of the aptamers with monomeric Aβ40 on the sensor surface.

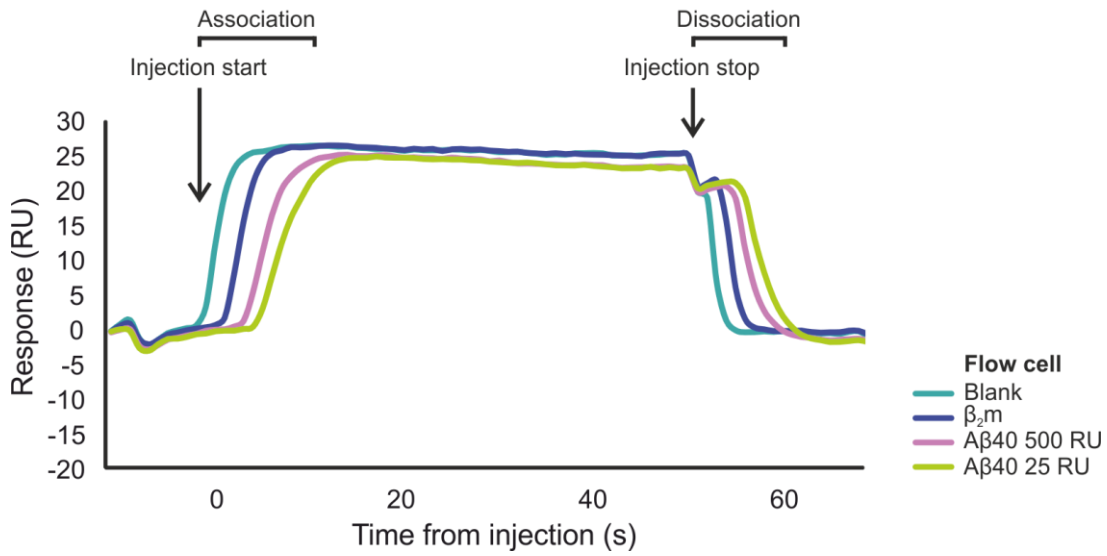

Figure 4.9 SPR analysis of the aptamer M1 association with immobilised monomeric Aβ40. Aptamer M1 demonstrates no specific interaction with Aβ40 monomers immobilised onto a streptavidin chip surface. The relative response from all four flow cells are colour coded as indicated.

Various changes were made to the experimental conditions, in an attempt to optimise the assay. Running buffers containing higher concentrations of surfactant (up to 0.05% (v/v) Tween 20) were trialled to reduce any non-specific interactions with the control flow cells, which may have been masking any association seen with Aβ40. Injections of higher concentrations of aptamer (aptamer M1 assayed up to 5 μM, results not shown) were also explored, to enhance any signals upon binding. Despite these attempts, no aptamer association was observed with Aβ40 monomers, under any of these conditions, using SPR.

Although the Aβ40 monomer was immobilised to the SPR chip using the same biotin modification used during selection, the surface of the SA chip differs to the bead surface, as the streptavidin tetramers are conjugated to carboxymethlyated dextran. It is possible, therefore, that this difference in immobilisation surface could be altering the conformation of the target peptide and, therefore, the aptamer binding epitopes available. In order to test the affinity towards the actual selection target, binding assays, where Aβ40 was immobilised to the streptavidin-coated microspheres used in selection, were developed, as described in the following section.

4.3.2 Aptamer pulldown assays

In order to quantify binding of the selected RNA aptamers to the bead-immobilised form of Aβ40, a pulldown assay was developed. Streptavidin-coated microspheres, identical to those used in the aptamer selection, were saturated with Aβ40, as described (Section 2.5.2). Sequential dilutions of these Aβ40 beads were then set up to create a gradient of protein concentrations ranging from 80 nM to 1.6 μM. Each aptamer was added to each dilution of beads at a final RNA concentration of 500 nM. After incubation for 15 min and removal of the unbound RNA by magnetic separation, the beads were washed 10 times with selection buffer, consistent with the SELEX conditions (Section 2.7.2). Any remaining bound RNA at each peptide concentration was then heat eluted and reverse-transcribed by the addition of a master solution of RT mix (Section 2.6.9) directly to the boiled-bead aliquots. Resultant DNA was then amplified for analysis by native PAGE. Levels of associated RNA at each Aβ40 peptide concentration were determined through the measurement of band densitometry, from gels stained with ethidium bromide (EtBr). Raw densitometry values were then plotted as a function of peptide concentration, to determine binding constants for each aptamer.

Preliminary experiments with aptamer M1 showed promising results in that there was a clear association of this aptamer with the immobilised peptide (**Figure 4.10 a**). The dissociation constant for this single experiment could be calculated as 125 nM, using a Hill fit of the data (Section 2.8.3, **Equation 2.5**). However, upon extension of this gel densitometry approach to a 96-well format, where all aptamer sequences were tested in triplicate, it became clear that this method was not reproducible. An example showing three further replicates of aptamer M1 binding to Aβ40-loaded beads (**Figure 4.10 b**) demonstrates an apparent dissociation constant of 3.9 ± 58 nM. The error in this case is considerable and indicates the difficulty in accurate determination of affinity via this method. Error in this assay is most probably derived from inaccuracy in densitometry. Because analysis by native PAGE requires detection with EtBr staining after the gel has run (as opposed to addition of EtBr in the gel mixture, pre-casting) staining can be non-uniform across the gel, leading to error in the densitometry readings.

The pulldown experiment indicates that there is an association of the aptamers and Aβ40 when immobilised to a bead. Quantitative comparison of the binding of the eight aptamers via this method was, however, not feasible owing to the lack of reproducibility.

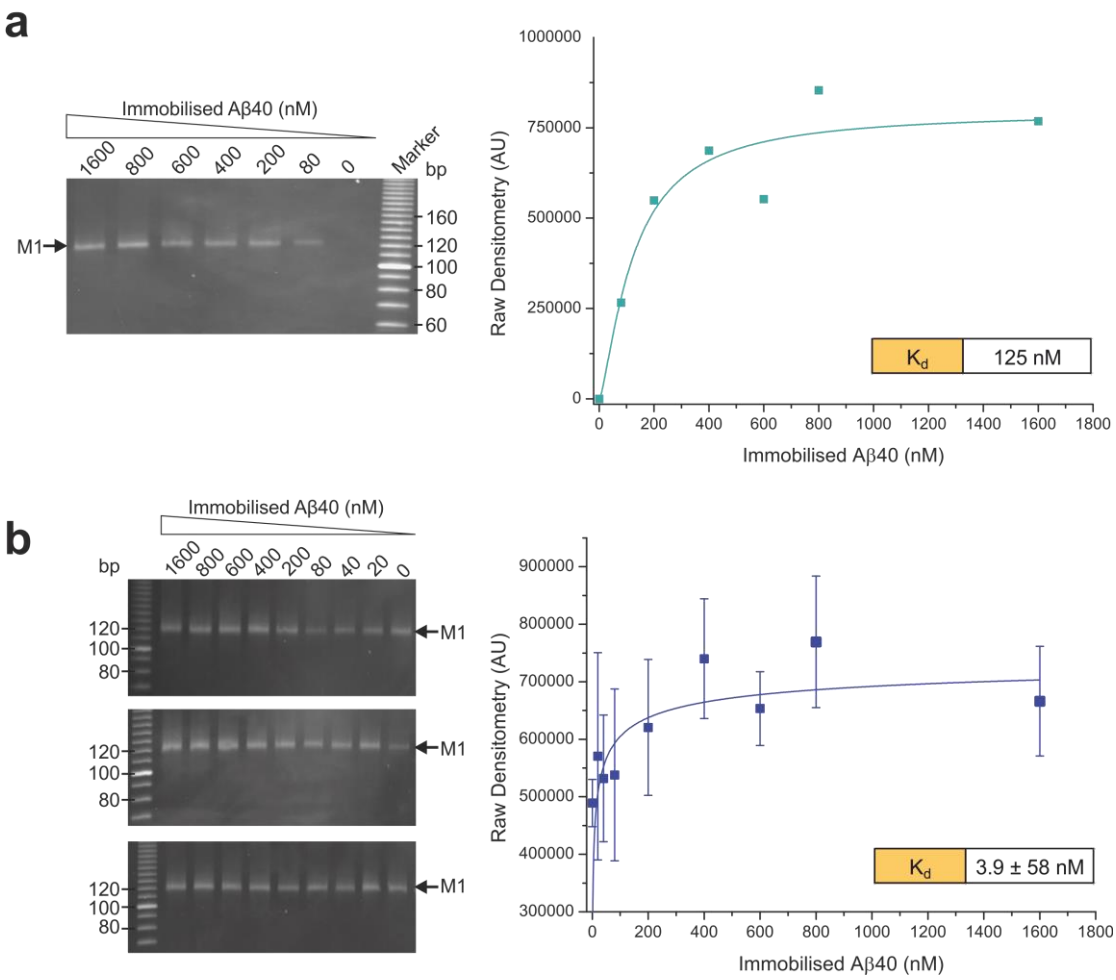

Figure 4.10 Preliminary pulldown experiments indicate aptamer M1 association with immobilised Aβ40 peptide. **(a)** Native PAGE analysis of RT-PCR products from RNA associated with Aβ40 saturated beads at a range of peptide concentrations. Densitometry values are plotted as a function of immobilised Aβ40 concentration (teal) and a dissociation constant of 125 nM (inset) can be determined. **(b)** Three replicate gels of aptamer pulldown over a larger concentration range demonstrate the irreproducibility in this assay, reflected as the large errors in the densitometry plot (blue). The data is fitted to a Hill equation (**Equation 2.5**), weighted by the error, to guide the eye, and the putative dissociation constant determined (inset).

To circumvent the problem of irreproducibility associated with indirect detection using RT-PCR followed by gel staining and densitometry, other methods for direct detection of the RNA were investigated. Alexa488 labelling of the RNA was deemed an appropriate reporter, as the preparation of fluorescent RNA transcripts was previously optimised for experiments using MST (Section 4.2.1.1) and sensitive detection could be achieved. Therefore, an assay was designed in which the concentration of RNA was measured by fluorescence intensity of

the unbound fraction, after bead partitioning. Aβ40 saturated beads were again sequentially diluted to create the peptide concentration gradient. In this case, beads were first concentrated to 10 mg/mL (through partitioning and resolubilising the beads in 1/10th volume of buffer) to enable higher peptide concentrations to be assayed (up to 20 μM). Fluorescently labelled aptamer was added at a final concentration of 30 nM to each dilution of beads and incubated for 15 min. Beads were partitioned on a magnetic rack and the unbound fractions were transferred to fresh tubes before the fluorescence intensity of each was measured (Section 2.8.3). Analysis of the eight anti-Aβ40 monomer aptamers against the Aβ40 saturated beads demonstrated a clear association, with an average binding constant of ~ 1.8 ± 0.2 μM (**Figure 4.11**).

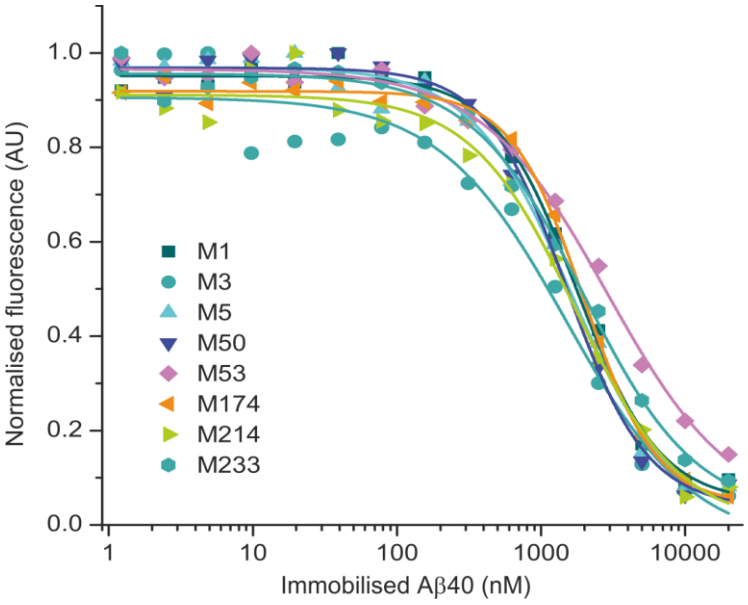

Aptamer	K_d (μM)
M1	1.8 ± 0.14
M3	1.5 ± 0.52
M5	1.6 ± 0.19
M50	1.5 ± 0.12
M53	2.8 ± 0.48
M174	2.0 ± 0.15
M214	1.7 ± 0.30
M233	2.0 ± 0.27

Figure 4.11 Aptamers associate with streptavidin-bead immobilised Aβ40 with micromolar affinity. Fluorescence intensity of the unbound RNA fraction at a range of immobilised peptide concentrations are indicated for each of the eight aptamer sequences. Dissociation constants derived from a Hill function (**Equation 2.5**) are given (inset). Fluorescence was normalised to the intensity of free RNA when incubated with no target.

Each of the eight aptamers tested were shown to bind to bead immobilised Aβ40 monomers with similar affinity (**Figure 4.11**, inset table). This was perhaps surprising as the sequences do not originate from the same consensus motif generated during the sequence alignments and are predicted to display different structures (**Figure 3.18**). They were also

represented with very different relative frequencies in the selected pools (613 times for M1, compared with only 22 times for M233), which should suggest they have different affinities to the target and hence were amplified to different extents throughout the selection. However, the aptamers are all GA rich and this similar base composition within their key structural elements could be the major requirement in their target recognition.

Further pulldown assays were performed, with each of the eight aptamers, to different batches of Aβ40 saturated beads, to determine the reproducibility of the assay. A representative example is given in **Figure 4.12 a,** where aptamer M50 is assayed against three separate preparations of Aβ40-loaded beads. The results revealed that the experiment is not highly reproducible, in that M50 shows binding constants ranging from 270 ± 11.9 nM to 12.4 ± 3.4 μM to the different bead batches. This variability implies that the aptamer-binding epitope on Aβ40 may be displayed differently when immobilised in different bead batches. However, despite these apparently large inconsistencies, the association is specific to Aβ40. This was demonstrated by assaying the aptamers in this same pulldown format against biotin-saturated control beads and beads conjugated to a control protein, Im7 (**Figure 4.12 b**). Im7 is an 87-residue immunity protein[562], with a similar pI to Aβ40 (4.98 compared with 5.30 for Aβ40) but has a predominantly alpha-helical structure and, therefore, was used as a control for non-specific interactions. Over an equivalent concentration range, the majority of RNA is recovered in the unbound fraction. This indicates that there is no association to the biotin linker and that the aptamers are specific to bead immobilised Aβ40 epitopes.

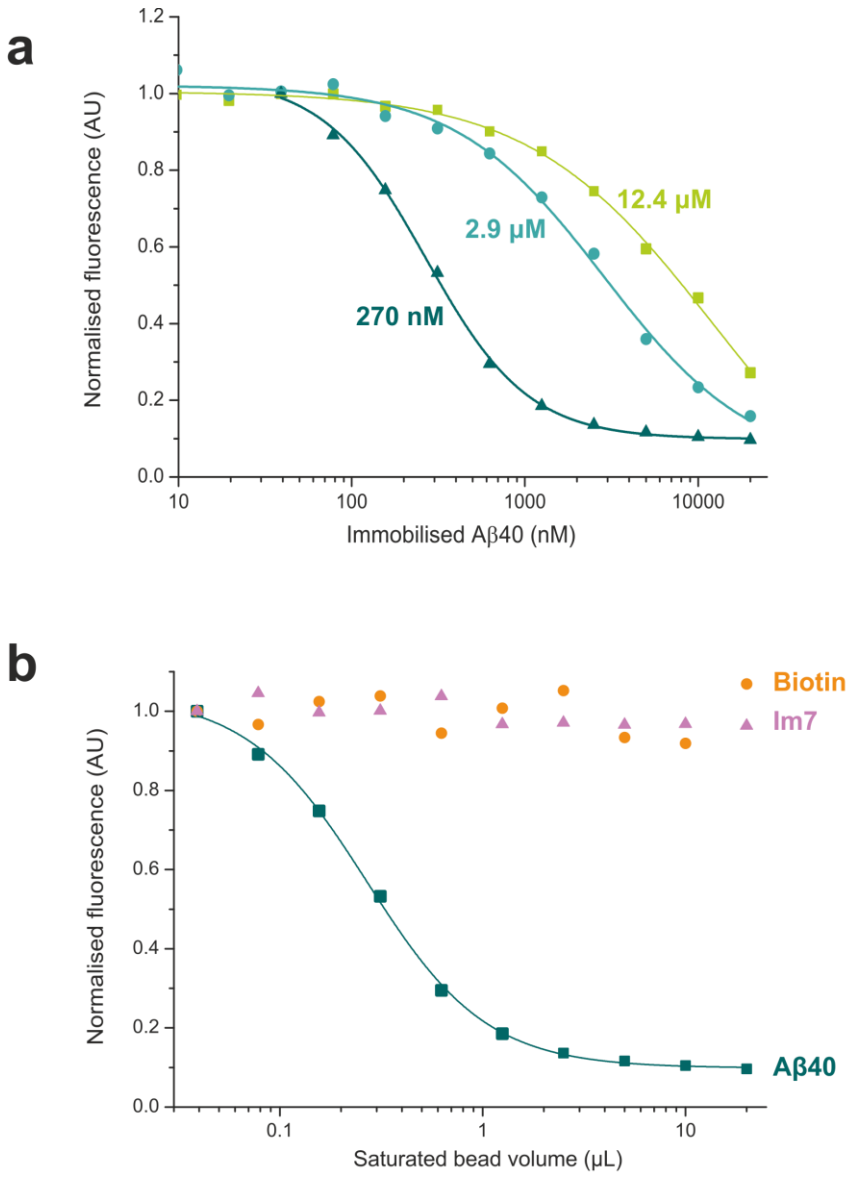

Figure 4.12 Analysis of the reproducibility and specificity of aptamer binding to immobilised Aβ40. **(a)** Fluorescence pulldown assay demonstrating the variability in apparent binding affinities between three separate batches of Aβ40-saturated streptavidin beads and Alexa488 labelled aptamer M50. The association of aptamer M50 to the three different batches are represented in teal, blue and green. **(b)** Fluorescence pulldown assay demonstrating the specificity of binding of aptamer M50 to immobilised Aβ40. Aptamers display association to Aβ40 (teal) that is not observed over an equivalent titration of beads saturated with biotin (orange) or Im7 (pink). Fluorescence is normalised to the intensity of RNA when incubated with no target.

4.4 Discussion

Selection of RNA aptamers against the monomeric Aβ40 target was carried out with the main aim of finding recognition molecules for this intrinsically disordered peptide. This could in turn pave the way for the development of new inhibitors or diagnostic reagents. Chapter 3 describes the selection of RNA aptamers against Aβ40 monomer, isolating an RNA pool enriched with sequences which fell into discrete structural motifs. This enrichment in frequency of single sequences, over that seen in the naïve pool, demonstrates that aptamers have been selected preferentially and, therefore, should display affinity and selectivity for the target peptide.

Although the first ten rounds of selection were against a monomeric model of Aβ40 (Aβ40 immobilised by biotin modification and conjugated to streptavidin via a 30 Å spacer arm), the final six rounds of selection involved competitive elution of aptamers with Aβ40 monomer, free in solution. It was expected, therefore, that the aptamers chosen from the enriched pool would display affinity for the free monomer and the aim of the work described in this chapter was to confirm this.

4.4.1 Quantitation of RNA aptamer binding to Aβ40 monomer

A major challenge of the work described in this chapter was finding appropriate binding assays to study interactions of the RNA molecules with monomeric Aβ40, without need for immobilisation of the peptide. Assay development was hindered by two major factors: firstly the limitations in synthesis of large quantities of 2'F modified RNA and secondly, the properties of Aβ40.

Many of the conventional biophysical methods used to study protein: nucleic acid interactions in solution (without significant modification or immobilisation), such as ITC[538] and NMR[539] were not possible for analysis of the selected RNA aptamers, at this initial screening stage. This is due to the requirement of large quantities of concentrated sample for these techniques. ITC, a gold-standard assay for determination of binding constants in solution[563], requires no modification to either binding partner or immobilisation and, therefore, is a true label-free method. Biomolecular interactions are measured directly through the heat evolved upon association and parameters such as the dissociation constant

(K_d) and stoichiometry of a given interaction can be determined directly[538]. However, the major drawback of ITC, that which made it unsuitable in the investigation described herein, is the large sample consumption required to generate a sufficiently strong heat signal, typically 0.5 - 1.5 mL of 10^{-5} M solutions[564]. Another technique used to study solution interactions is NMR which, through titration experiments, can provide information about binding constants[565, 566], specificity of binding[567], as well as detailed information into the structure and epitopes of the interacting molecules[568]. Again, these experiments require concentrated (typically ~ 100 μM in ~300 μL[569]), isotopically labelled and homogenous samples[565] which would be difficult to provide in the case of an aptamer-Aβ40 interaction (at least for the 121 nucleotide length aptamers used in this chapter). If lead aptamer sequences were discovered through other binding assays, and minimal, functional RNA structures determined, shorter RNA molecules could be chemically synthesised on larger scales, making either of these methods feasible.

Mass spectrometry was also considered as an option to study the association of the aptamers and Aβ40 monomer, as measurements of dissociation constants have been demonstrated using this technique[570-573]. Soft ionisation methods such as electrospray ionisation (ESI) allow non-covalent interactions to be maintained in the gas-phase[574] and binding parameters elucidated this way have previously shown good agreement to solution-derived K_ds[575, 576]. However, the technique requires optimisation of instrumental conditions and extensive sample clean-up to be viable. Samples would need to be exchanged into MS compatible buffers, and all traces of non-volatile salts removed, to produce spectra of sufficient quality to extract binding coefficients. Owing to the relatively low yields of 2'F RNA produced by *in vitro* transcription and the poor recovery via most desalting methods (**Figure 4.3**, **Table 4.1**) this route of analysis was not pursued.

In order to study the association with monomeric Aβ40 peptide, it was important to avoid modifications to the protein that may interfere with the binding epitope. Therefore addition of external fluorophores to the peptide, necessary for experiments such as fluorescence polarisation (FP) was ruled out. Use of a peptide's intrinsic fluorescent properties can be exploited to monitor binding events, if the association induces structural changes that impinge upon the environment of the aromatic residues[555]. As mentioned in Section 4.2.2, intrinsic fluorescence quenching experiments were attempted and indicated no detectable association of Aβ40 monomer with aptamer M1. However, it was unclear whether the fluorescence of Aβ40 was too low to detect binding or whether an interaction was occurring at a position distal to the single tyrosine residue.

As options for suitable assays were clearly limited, it was decided that fluorescent labelling of the aptamers would provide the best alternative. There was still the problem of external fluorophores interfering with binding, but this would be less so when labelling the RNA over the peptide, for two reasons. Firstly, the labelling strategy utilised involved random incorporation of the fluorescent UTP at several sites within the structure. This means that the resultant RNA will contain a random distribution of molecules, with labels at various positions. Therefore, if the label is obscuring the epitope in one area of the molecule, then the heterogeneous RNA mix will contain aptamers where the label is elsewhere and should not interfere with binding. Secondly, the aptamers are larger than Aβ40, with more possible labelling sites, again allowing production of a more heterogeneous mixture when labelled. Unfortunately, when fluorescence polarisation (FP) studies were carried out, no change in polarisation was observed upon titration with Aβ40, again indicating a lack of association with the labelled aptamer. The only drawback to labelling the RNA in a FP experiment, is that the assay is dependent on mass change upon binding, which means the more sensitive titrant should be the larger of the two species[558]. In this case, as Aβ40 was the unlabelled ligand, the changes in polarisation of light emitted from the larger labelled aptamer may be minimal, rendering the assay insensitive.

Microscale thermophoresis is a relatively new technology to measure biomolecular interactions and was also considered as a method to quantitate binding of aptamers to Aβ40 monomers in solution. The major advantages of MST is the small sample volumes (< 4 μL) and low concentrations of labelled aptamer required (nM), as well as the dynamic range of dissociation constants accessible (pM to mM)[541]. Unlike the previously mentioned fluorescence-based assays, this technique should provide more conclusive insights into the binding event, as it is not dependent on a single property of the binding molecule, such as mass or intrinsic fluorescence. Although the exact theory is debated[577, 578], the behaviour of molecules in a thermal gradient is thought to be sensitive to size, charge and hydration shell. Because at least one of these properties should be perturbed in a given interaction, MST is considered a flexible and sensitive technique[540, 543]. Indeed, MST has previously been used to monitor interactions between peptides of similar size to Aβ40[547, 548, 579], as well as small molecules[544, 545]. In fact, it is stated that there is virtually no limitation on size or molecular weight for this technique[541]. Despite the advantages of the method, no binding was observed between the aptamers and Aβ40 in solution.

4.4.2 Insights from surface binding studies

When it became clear that aptamer binding to Aβ40 in solution could not be detected, the hypothesis that surface presentation of the monomer might be required for binding was explored. Indeed, binding of all eight aptamers was observed for Aβ40-saturated streptavidin beads in the fluorescent aptamer pulldown assay (**Figure 4.11**). Moreover, the binding was specific to Aβ40 (**Figure 4.12**). However, the assay was not reproducible between bead preparations; in fact the different batches exhibited a profound effect on apparent binding ability of the RNA (K_ds differ by 2 orders of magnitude in the case of aptamer M50 **Figure 4.12 b**). Discrepancies in total immobilised peptide concentration should not be a contributing factor, as the beads are prepared via incubation with a large excess of modified Aβ40 (20-fold, Section 2.5.2). This means that complete saturation of available streptavidin binding sites should be achieved each time. Another explanation could be that different conformations or assemblies of Aβ40 exist and become trapped on the surface of the beads, and that this heterogeneous mixture of conformations cannot be faithfully reproduced between each preparation. If aptamers are only able to recognise a single conformation, and this is represented to different extents between bead batches, then the effective concentration of this conformer would differ each time. Therefore, the apparent binding affinity would also change, depending on the proportion of the epitope presented in that batch.

If the conformation recognised by the aptamers was not the monomer but instead a small proportion of aggregate, this same effect would be expected. These data therefore call into question the species against which aptamers were originally selected. It was assumed that aggregation would not occur after immobilisation and great care was taken to avoid aggregation before biotin modification and conjugation to beads (Section 3.4.3). If however a small proportion of aggregate did persist before immobilisation, it is possible that this was selected against. The local concentration of peptide created near the surface, upon immobilisation, could have accelerated the aggregation, leading to the deposition of some higher order species. It is not inconceivable that aptamers may preferentially bind to an ordered, structured aggregate over the disordered monomer, even if the aggregated species existed in relatively low abundance.

The data also suggest that the solution elution rounds of selection, included to promote binding to soluble monomer, may have failed to produce such aptamers. The hypothesis that aptamers may have been selected against small amounts of higher order assemblies on

the bead surface, could explain the lack of solution binding observed. If the selected RNA sequences have a preference for the structured aggregate, the elution with monomeric peptide could be isolating the aptamers with the poorest affinity for the aggregate, which are readily dissociated when challenged with a competitor. Albeit, these RNA sequences will have had enough affinity to avoid dissociation during wash steps, however non-specific associations with the monomer could have liberated some lower-affinity bound RNA from the bead targets. Alternatively, a small amount of aggregate may have existed in the Aβ40 monomer solutions used as competitive targets during these competition selection rounds and, again, been preferentially bound by the aptamers, resulting in dissociation from the bead-bound state.

4.4.3 A precedent for higher order aggregate binding by anti-Aβ40 aptamers

Among the few other anti-Aβ40 monomer aptamers described in the literature, recognition of higher-order amyloid assemblies, despite selection against purified low-molecular weight (LMW) targets, is a common theme. Ylera *et al*.[491] demonstrated the selection of RNA aptamers against an N-terminally cysteine modified variant of Aβ40. The thiol moiety was used to covalently couple the peptide to a thiopropyl-activated Sepharose column for selection. These authors endeavoured to maintain the monomeric state of the peptide by performing the coupling reaction in 60% (v/v) HFIP, a commonly used agent to monomerise amyloid structures[580, 581]. After eight rounds of SELEX, aptamers were isolated with conserved sequence motifs, indicative of successful selection. However, upon investigation of a single sequence (β55), it became apparent that the aptamer had no affinity for monomeric Aβ40. Analytical affinity chromatography demonstrated an apparent K_d of 29 nM against the immobilised target, yet the authors were unable to demonstrate monomer affinity by counter elution with free peptide, nor via a mobility shift assay. Instead, the aptamer's affinity for amyloid fibrils was demonstrated via electron microscopy. The authors concluded that the lack of specific interaction with monomer was most probably due to aggregation of the Aβ40 on the Sepharose column, and hence aptamers were selected against an aggregated form. This is in spite of monomerising treatment with HFIP. It should be noted, however, that most protocols require 100% (v/v) solutions of HFIP to promote complete fibril depolymerisation[581]; in fact stable oligomers of Aβ40 have been shown to form in solutions containing lower concentrations of this fluorinated alcohol[582].

Aggregation of target peptide in the environment of the same affinity column employed in their SELEX, has also been demonstrated previously in the selection of aptamers against another disordered peptide, substance P[583].

The problem of isolating a single purified Aβ40 conformation for selection is further demonstrated in a study by Rahimi *et al.*[494]. Here, the authors attempted to select aptamers against a covalently-stabilised trimer of Aβ40, generated using photo-induced cross-linking of unmodified proteins (PICUP)[584] and purification via PAGE[585]. When characterising sequences isolated from the enriched pools, it was found that none of the aptamers bound to the trimeric target in solution, or LMW (predominantly monomeric) Aβ40. Again, aptamers were instead found to bind to fibrillar assemblies. These limited examples, along with the work described in this chapter, suggest that the immobilisation strategies required in selection protocols are a source of aberrant aggregation and, therefore, it is difficult to be sure which species is being selected for.

Aptamers generated by Takahashi and colleagues[493] are the only example of aptamers reported to display measurable affinity to monomeric Aβ40. Aptamers were selected against Aβ40 conjugated to colloidal gold nanoparticles and two sequences were obtained and characterised. These aptamers demonstrated affinity for immobilised Aβ40 via a pulldown assay (no K_ds reported) as well as recognition of Aβ40 in solution, with binding constants in the order of 10^{-5} M. However, the fluorescence anisotropy method used to elucidate these dissociation constants show a change in anisotropy of 0.008 units (equivalent to ~ 8 mP units in the FP analysis of the aptamers shown in **Figure 4.7**). Although the authors comment on this small change as a result of the small mass of Aβ40, this level of signal would lie within the noise of this experiment and therefore binding parameters extracted from this data are doubtful.

The gold nanoparticle conjugation method of immobilisation utilised in the work described by Takahashi *et al.*[493] was originally developed as a molecular mimic of spherical oligomers in the generation of the oligomer-specific antibody A11[586]. By coupling Aβ40 to the colloidal gold in this manner, the resultant gold-peptide conjugates displayed remarkably similar properties to naturally occurring Aβ40 oligomers[587]. Using this molecular mimic as the antigen, the antibody produced was found to be specific for oligomeric structures and showed no reactivity with soluble Aβ or fibrillar assemblies. It is possible, therefore, that the arrangement of Aβ40 monomers on the surface of nanoparticles, such as in the case of the streptavidin beads used in this study, could be mimicking higher order assemblies and, therefore, aptamers may reflect a preference for these structures.

Data presented in this chapter suggest that although there was a clear enrichment of specific sequences from SELEX, individual aptamers were not able to recognise the monomeric target in solution. The aim of isolating specific recognition molecules towards this intrinsically disordered peptide, therefore, has not been achieved, most probably owing to problems with the immobilisation strategy required for selection. Affinity for the immobilised target was confirmed, however reproducibility in the binding ability of the aptamers highlights the issues in selecting against heterogeneous samples of Aβ40. It was decided that the project would now be focused on aptamer recognition of fibrillar and higher-order assemblies of Aβ. Chapter 5 focuses on aptamers derived from the two anti-fibril selections and their reactivity and specificity. Recognition of fibrillar assemblies by the anti-monomer aptamers, discussed in this chapter, is also investigated, to test the hypothesis that these aptamers might have affinity for aggregated forms of Aβ40.

5 Characterisation of RNA aptamers against amyloid fibrils of distinct morphology

5.1 Objectives

As discussed in Chapter 3, selections were carried out against two distinct structural morphologies of Aβ40 fibrils, 2A and 3Q. Analysis of the resultant sequences demonstrated an enrichment of sequences, from which five lead aptamers were chosen for each target fibril, based on consensus sequence motifs and predicted secondary structure.

The aim of this chapter was to assess the specificity of these aptamers for their target fibril morphology and their ability to recognise amyloid fibrils derived from other amyloidogenic peptides. This is important as no other ligand has yet been developed able to recognise a single amyloid morphology and would be invaluable as a research tool and diagnostic reagent, especially in light of the recent implication of fibril polymorphism in the etiology of different disease pathologies[106].

5.2 Assessment of aptamer binding to cognate fibril targets

The first objective was to confirm that single aptamer sequences had affinity for the fibril targets against which they were selected. Five aptamers were chosen from each pool (**Figure 3.17**) based on their different structural elements (**Figure 3.19** and **Figure 3.20**). Anti-2A aptamers were selected from an N50 library and demonstrated a purine-rich base composition, whereas the N30 derived anti-3Q aptamers generally contained poly-U repeats within the stems and loops of their randomised regions. The only exception was 3Q1, the most populous aptamer sequence from the 3Q selection (represented 658 times) which demonstrates a GA rich sequence, more consistent with the anti-2A aptamers. Although it is difficult to predict RNA binding specificity based on sequence alone (especially since the aptamers were seemingly selected from biased starting libraries, discussed in Section 3.7), these observations might suggest that aptamers from the two pools should demonstrate selectivity for unique epitopes between the fibril structures. On

the other hand, 3Q1 might be expected to demonstrate recognition for a conserved structure between these two Aβ40-derived fibrils.

5.2.1 Fluorescence polarisation (FP)

Fluorescence polarisation (FP), mentioned briefly in Section 4.2.2, was the main technique employed in the assessment and quantitation of binding by the anti-fibril RNA aptamers.

FP (**Figure 5.1**) is based on the measurement of the degree of polarisation of light emitted from a fluorescent molecule, which is inversely proportional to the rate of molecular rotation. When a fluorescently labelled molecule is excited by polarised light, the resultant emission will be largely depolarised owing to the rapid reorientation of the fluorophore during the lifetime of the excited state. However, if this labelled ligand is bound by a larger molecule, the rotational speed of the complex will be reduced and thus the emitted light will remain significantly polarised. This property of FP means it can be used to measure binding events (as long as there is a significant decrease in the rotation correlation time), as the observed polarisation will be proportional to the fraction of bound ligand[555, 558].

FP was used in Section 4.2.2, to monitor monomer binding by fluorescently labelled anti-Aβ40 monomer aptamers. It was unclear whether the small molecular weight change upon Aβ40 binding (4458 Da) would produce a change in FP sufficient for detection or whether the peptide would not associate with the aptamers tested. In the case of fibril binding, the high molecular weight of the polymeric fibrillar complex (estimated > 30 MDa based on the mass-per-length of 3Q fibrils[103] and an estimated average fibril length of 1 μm) should be sufficient to induce a substantial change in polarisation and was therefore considered an ideal assay to determine whether the aptamers selected against fibrils bind to their targets. FP is also amenable to semi-high throughput analysis, requiring low nM amounts of fluorescent aptamer and < 30 μL sample volumes, when performed in a multi-well plate format. Assays were set up in 384-well plates and fibril titrations were delivered by robotic dispensing (Section 2.8.5).

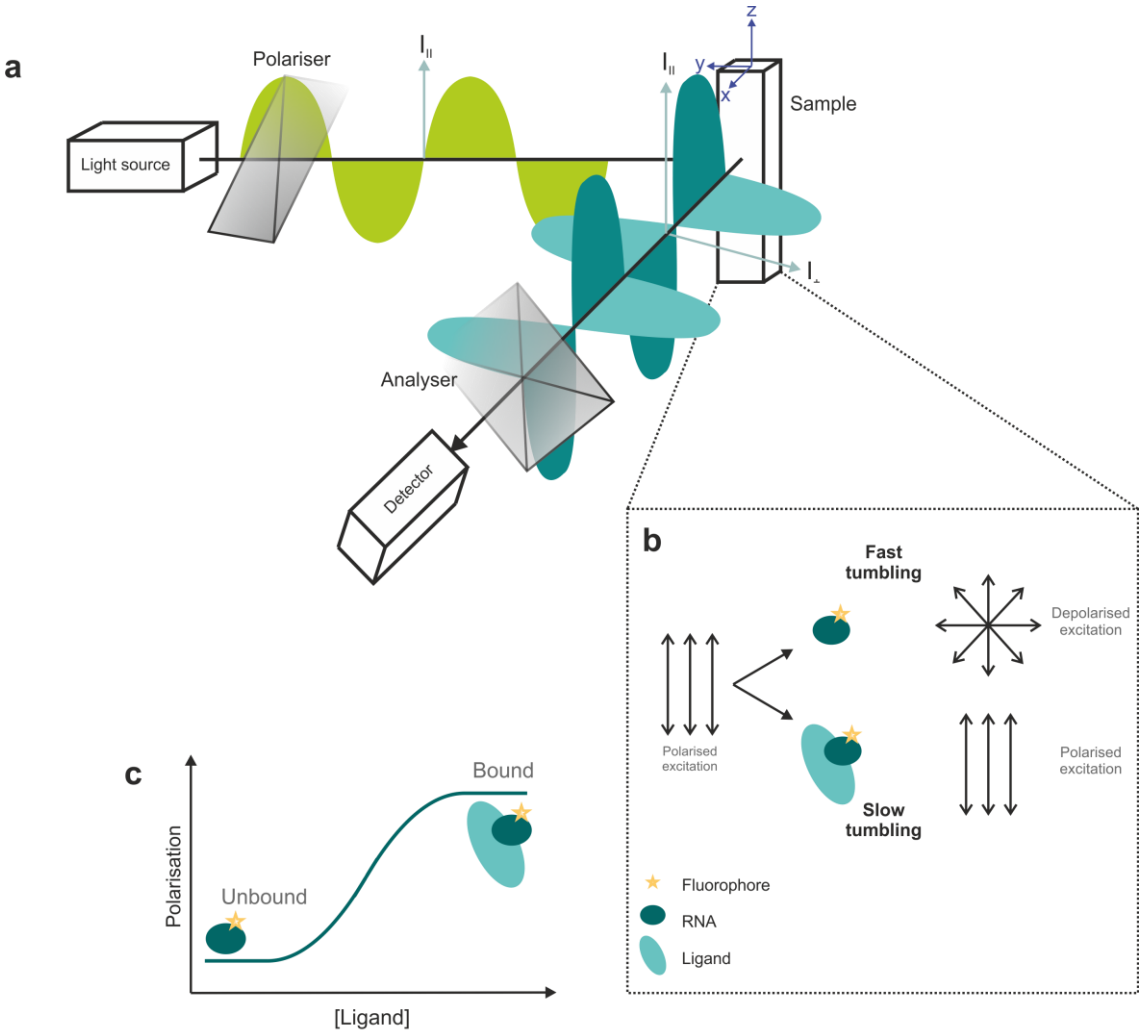

Figure 5.1 Principles of fluorescence polarisation (FP). **(a)** Schematic representation of a fluorescence polarisation experiment. Fluorophores in the sample are excited by polarised light, emitting light that is depolarised to a degree dependent on the rate of molecular tumbling, **(b)**. The intensity of polarised light in both the z (I_{II}) and the y ($I_{\perp}$) axis is measured as a function of ligand concentration **(c)** to quantitate the interaction. Adapted from[588].

5.2.2 Aptamers bind to their cognate fibril targets in solution

The five aptamer sequences isolated from each selection (**Figure 3.17**) were produced by *in vitro* transcription from individual DNA templates and were fluorescently labelled via the enzymatic incorporation of Alexa488 dUTP, according to the protocol optimised in Section 4.2.1.1. 200 μM stocks of 2A or 3Q fibrils were made via seeding reactions for 18 h (Section 2.4.1) as described for the production of fibrils as selection targets. As before, the presence of long straight amyloid fibrils was confirmed by EM (**Figure 5.2 a** and **Figure 5.3 a**) and 100% incorporation of monomer into the fibrillar aggregate was confirmed by SDS PAGE analysis of soluble and insoluble peptide fractions after centrifugation (example data shown for both fibril types in **Figure 3.4**). These stocks were then titrated serially against a fixed concentration (10 nM) of fluorescent aptamer, in 384-well plates, by use of a liquid handling robot (Section 2.8.5). Concentrations of fibril were calculated as monomer equivalent, based on the concentration of starting peptide material in the fibril formation reactions. Titrations for each aptamer sequence were set up in triplicate to demonstrate the reproducibility of the results.

In the case of every aptamer sequence assayed, titration against its own fibril target resulted in an increase in polarisation, consistent with binding (**Figure 5.2 b** and **Figure 5.3 b**). The degree of reproducibility between replicates was variable, owing to the inherent heterogeneity of the fibril samples. Although a single structural morphology can be reproduced faithfully through seeded elongation[105], the average length distribution of fibrils will vary between samples. This would lead to a variable number of available epitopes and could contribute to the variability observed. Nevertheless, upon averaging three replicates for each aptamer sequence and plotting on the same axis for comparison (**Figure 5.4 a** and **b**), apparent dissociation constants in the high nM to low μM range were elucidated by fitting to a modified Hill function (**Equation 2.5**). The sigmoidal response observed suggests that binding is specific and the Hill coefficients (n) of 1 ± 0.25, found for each aptamer, indicate non-cooperative binding to a single site (inset tables in **Figure 5.4 a** and **b**).

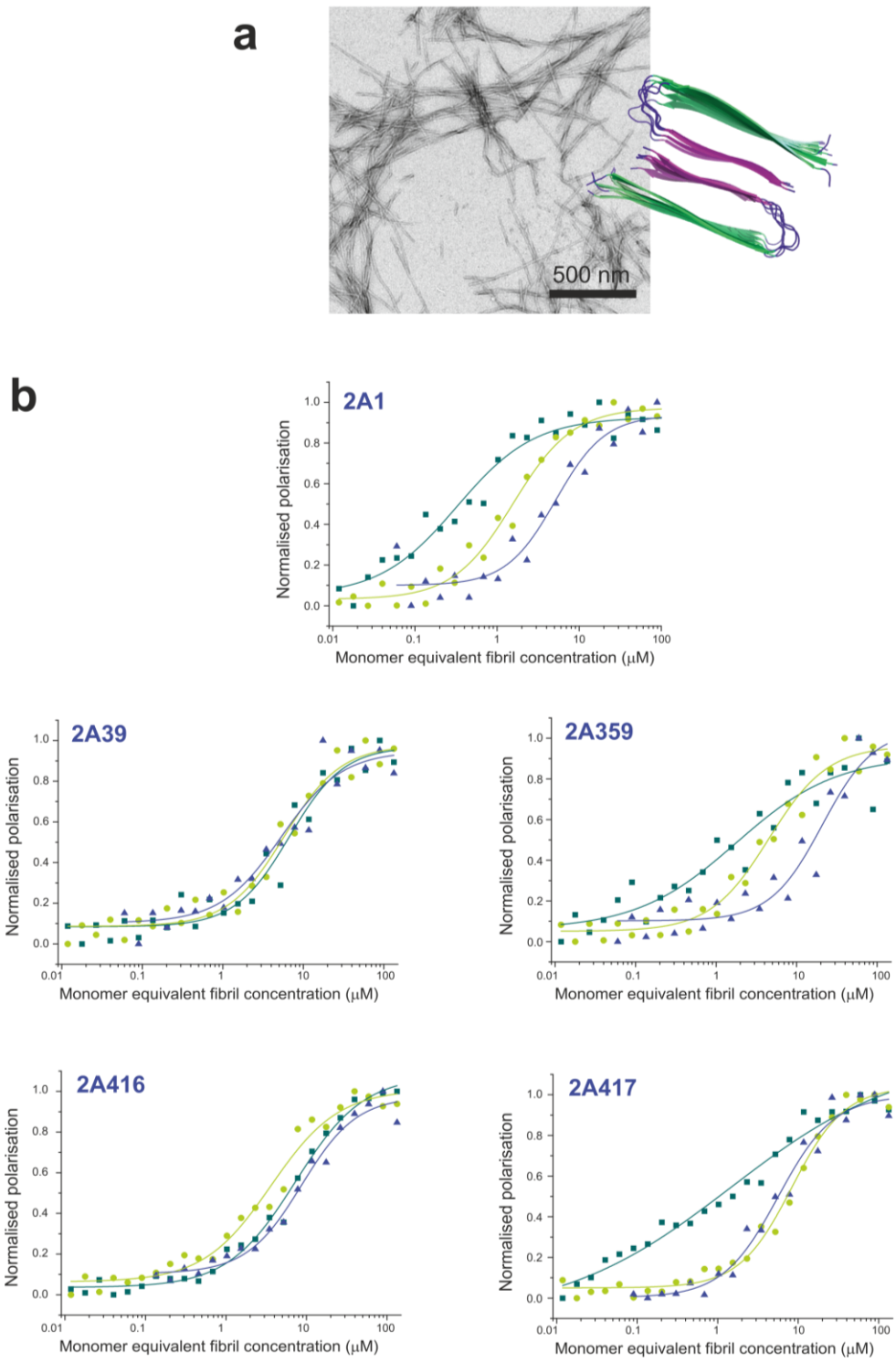

Figure 5.2 Analysis of 2A fibril binding by anti-2A aptamers. **(a)** Negative stain EM of 2A fibrils. A cartoon representation of the 2A fibril is inset (pdb file 2LMN) with unstructured residues 1-8 omitted for clarity. **(b)** Normalised FP responses for each aptamer sequence as a function of monomer equivalent fibril concentration. Experiments were carried out in MOPS selection buffer, pH 7.5 at 25 °C. Three replicates for each aptamer are shown. The identity of each aptamer is labelled in each plot.

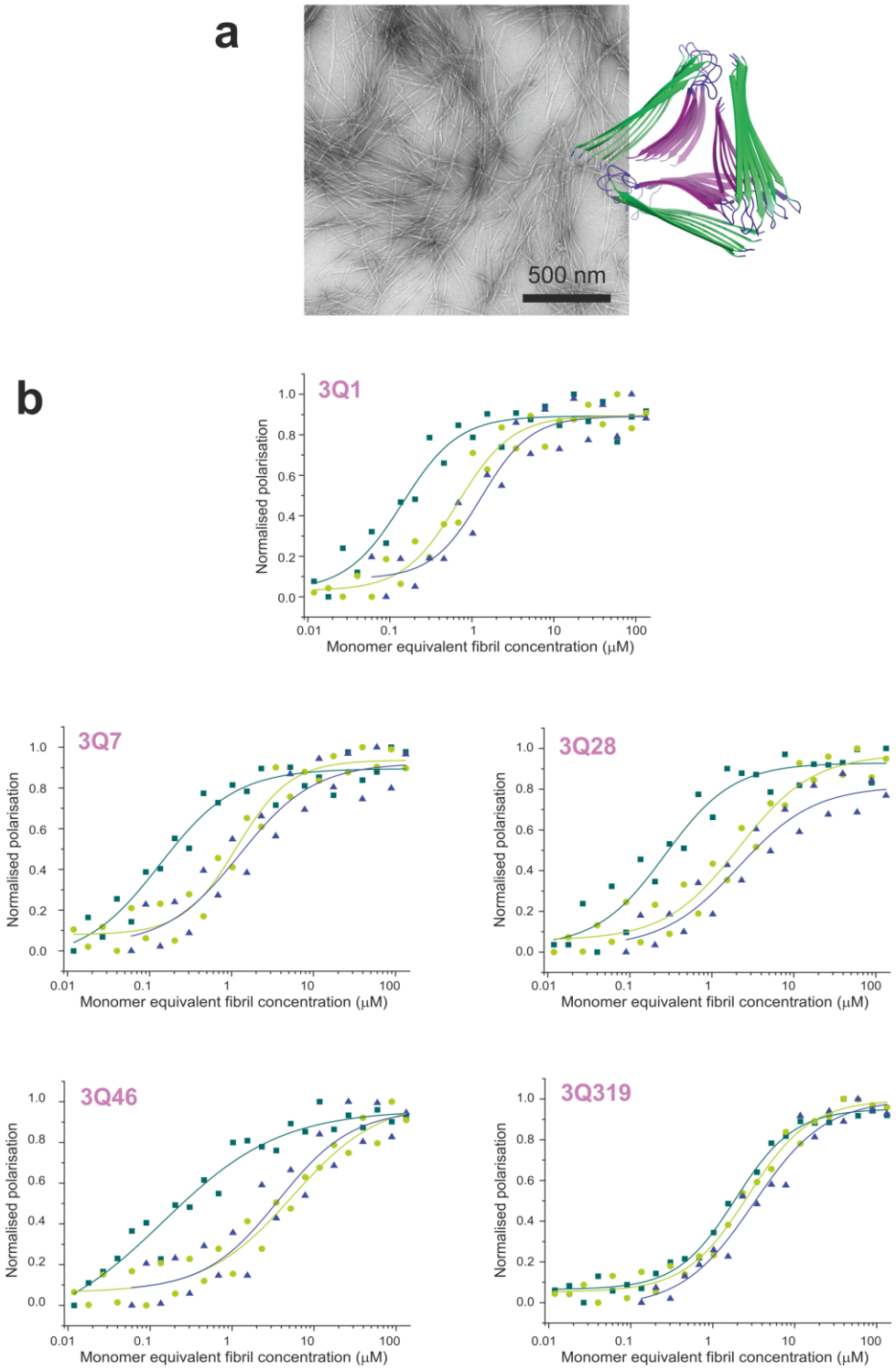

Figure 5.3 Analysis of 3Q fibril binding by anti-3Q aptamers. **(a)** Negative stain EM of 3Q fibrils. A cartoon representation of the 3Q fibril is inset (pdb file 2LMP) with unstructured residues 1-8 omitted for clarity. **(b)** Normalised FP responses for each aptamer sequence as a function of monomer equivalent fibril concentration. Experiments were carried out in MOPS selection buffer, pH 7.5 at 25 °C. Three replicates for each aptamer are shown. The identity of each aptamer is labelled in each plot.

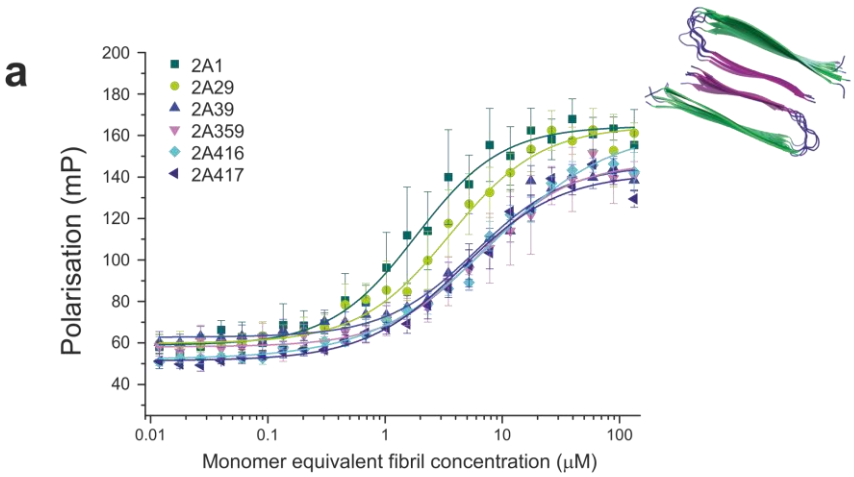

Aptamer	k_d (μM)	n
2A1	1.84 ± 0.26	1.19 ± 0.14
2A29	3.57 ± 0.40	1.12 ± 0.10
2A39	5.95 ± 0.68	1.12 ± 0.12
2A359	6.35 ± 0.94	1.11 ± 0.12
2A416	8.10 ± 1.63	0.84 ± 0.07
2A417	4.58 ± 0.77	1.05 ± 0.12

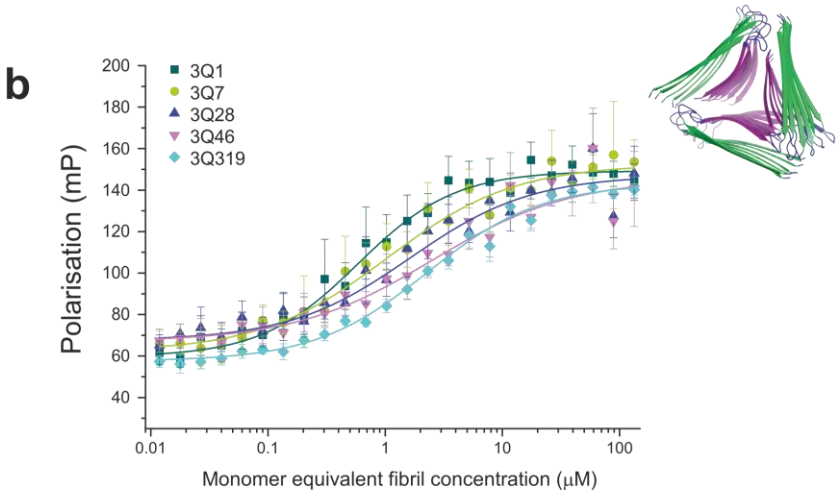

Aptamer	k_d (μM)	n
3Q1	0.58 ± 0.07	1.05 ± 0.11
3Q7	1.04 ± 0.18	0.80 ± 0.11
3Q28	1.64 ± 0.40	0.84 ± 0.15
3Q46	2.52 ± 0.85	0.74 ± 0.16
3Q319	2.29 ± 0.20	0.90 ± 0.07

Figure 5.4 Individual aptamers are able to bind to their cognate fibril target. FP analysis from **Figure 5.2 b (a)** and **Figure 5.3 b (b)** showing individual aptamers binding to their cognate fibril targets, 2A and 3Q, respectively. Cartoon representations of each fibril structure are also given (inset - pdb files 2LMN and 2LMP, respectively). An average of three replicates for each anti-fibril aptamer are shown. The dissociation constants (K_d) and n values (n) for each interaction are given in the corresponding tables.

Dissociation constants for 2A aptamers against 2A fibrils demonstrated weaker binding, in general, than 3Q aptamers for 3Q fibrils (1.8 – 8.1 μM and 0.6 - 2.3 μM, respectively). The FP analysis also enabled the five aptamers from each selection to be ranked in order of binding affinity. Although aptamers demonstrate similar affinity for their cognate fibril targets, the dissociation constants generally correlate with the order of the aptamer's frequency from the selected pool, further evidence that the highest affinity sequence from the pool was preferentially amplified in the SELEX procedure. This correlation is particularly clear for the anti-3Q aptamers. In the case of the anti-2A aptamers, 2A1 demonstrated the highest affinity value of 1.8 ± 0.26 μM, whereas the aptamers 2A39, 2A359, 2A416 and 2A417 displayed similar binding curves, with K_d values in the 5 - 8 μM range. A titration against aptamer 2A29, a sequence not chosen for the initial screen, was added to determine whether it would display a dissociation constant intermediate of that seen between the tightest binder 2A1 and the remaining four sequences, which was indeed the case (**Figure 5.4 a**). Plotting the dissociation constants determined from the FP analysis, as a function of aptamer frequency from the NGS of each of the selected pools, further illustrates the correlation (**Figure 5.5**).

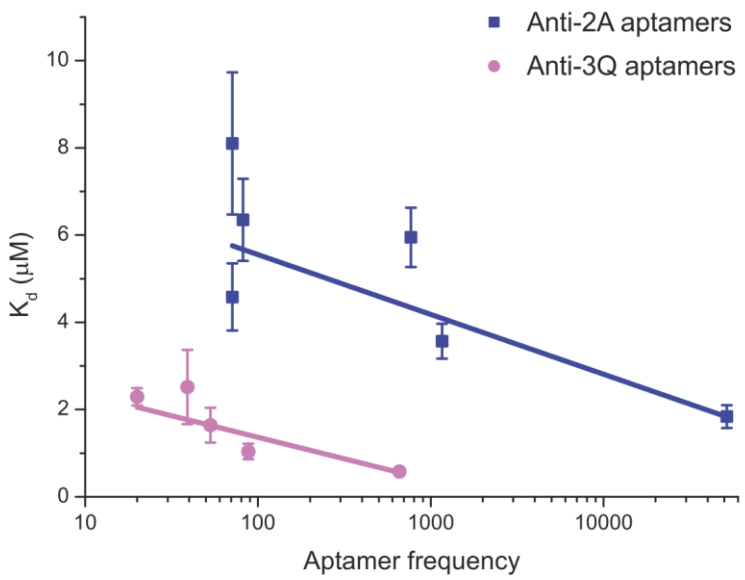

Figure 5.5 Dissociation constants for aptamers binding to their cognate fibril targets correlates with the aptamers' frequency from the selected pools. Graphical representation of the correlation between aptamer frequency from the selected pools and the K_d for their cognate target association, determined from the FP experiments (**Figure 5.4**).

To ensure that the binding observed by these aptamers was not an artefact of fluorescent labelling, a competition experiment was designed in which displacement of the fluorescently-labelled aptamer upon titration with its unlabelled counterpart was measured. If the fluorescently labelled aptamer is displaced fully by the unlabelled competitor, the FP response should fall from the more polarised bound state to the depolarised state, as seen for the labelled ligand free in solution. To examine this hypothesis, 2'F modified aptamer 2A1, without the fluorescent label, was titrated against the fluorescent 2A1 aptamer:2A fibril complex, which was fixed at a concentration equivalent to 65% bound (26 μM fibril: 10 nM aptamer), calculated from the direct binding experiment in **Figure 5.4**. The identical aptamer, but lacking Alexa488, was able to displace the labelled RNA indicating that the binding is not driven by the presence of the fluorophore (**Figure 5.6**). The dissociation constant of the unlabelled RNA, was estimated from this experiment as 310 nM, substantially tighter binding than that seen in the direct binding assay. This suggests that the presence of the fluorescent label (one Alexa488 per aptamer sequence – Section 4.2.1.1) reduces the binding affinity and therefore leads to an underestimation of the dissociation constant. The competition FP experiment may thus give a more accurate representation of affinity. Unfortunately, the concentration of unlabelled competitor RNA required for this single experiment (> 10 μM aptamer) is much greater than the concentration of labelled aptamer needed in the direct binding set up (< 10 nM) and therefore was not feasible in the assessment of several aptamers, with the number of replicates required to ensure reproducibility.

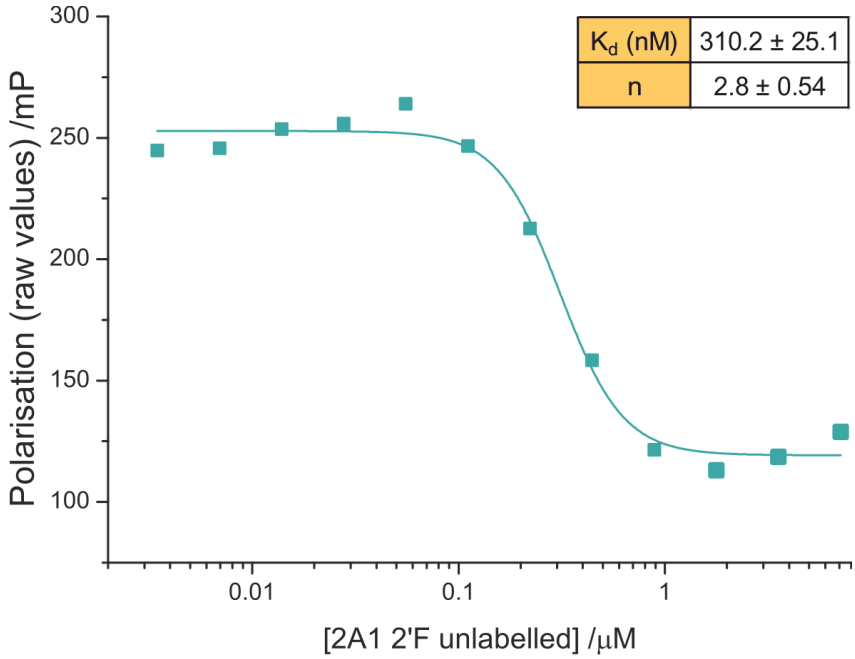

Figure 5.6 Aptamer binding is not facilitated through the fluorescent modification in FP**.** A titration of unlabelled 2'F aptamer 2A1 was added (up to 8 μM) to a mixture of 2A fibrils (26 μM) and Alexa488-labelled aptamer (10 nM), leading to a displacement of the labelled-aptamer, as monitored by FP. The experiment was conducted in MOPS selection buffer, pH 7.5, at room temperature.

A similar experiment was set up to determine whether the 2'F modification, present in all aptamers throughout the selection, altered the binding affinity of the aptamers tested. 2'OH aptamers 2A1, 2A417, 3Q1 and 3Q319 (lacking Alexa488 dUTP labelling) were made from an unmodified-dNTP containing transcription mix (Section 2.6.4) and titrated against their equivalent Alexa488-labelled 2'F counterparts in complex with their cognate fibrils (aptamers 2A1 and 2A417 in complex with 2A fibrils, aptamers 3Q1 and 3Q319 in complex with 3Q fibrils). Again, 2'OH aptamers were able to dissociate the bound 2'F RNA and dissociation constants were determined for three out of the four aptamers assayed (3Q319 did not reach a plateau over the concentration range studied and data could not be fitted). K_ds differed from those found for the 2'F Alexa488 labelled aptamers, with both 2A1 and 2A417 showing tighter binding when not 2'F modified and 3Q1 showing weaker binding in the 2'OH form. The results suggest that the modification with 2'F pyrimidines influences the aptamer recognition motifs but, nonetheless, binding is observed for all aptamers in both their 2'OH and 2'F forms.

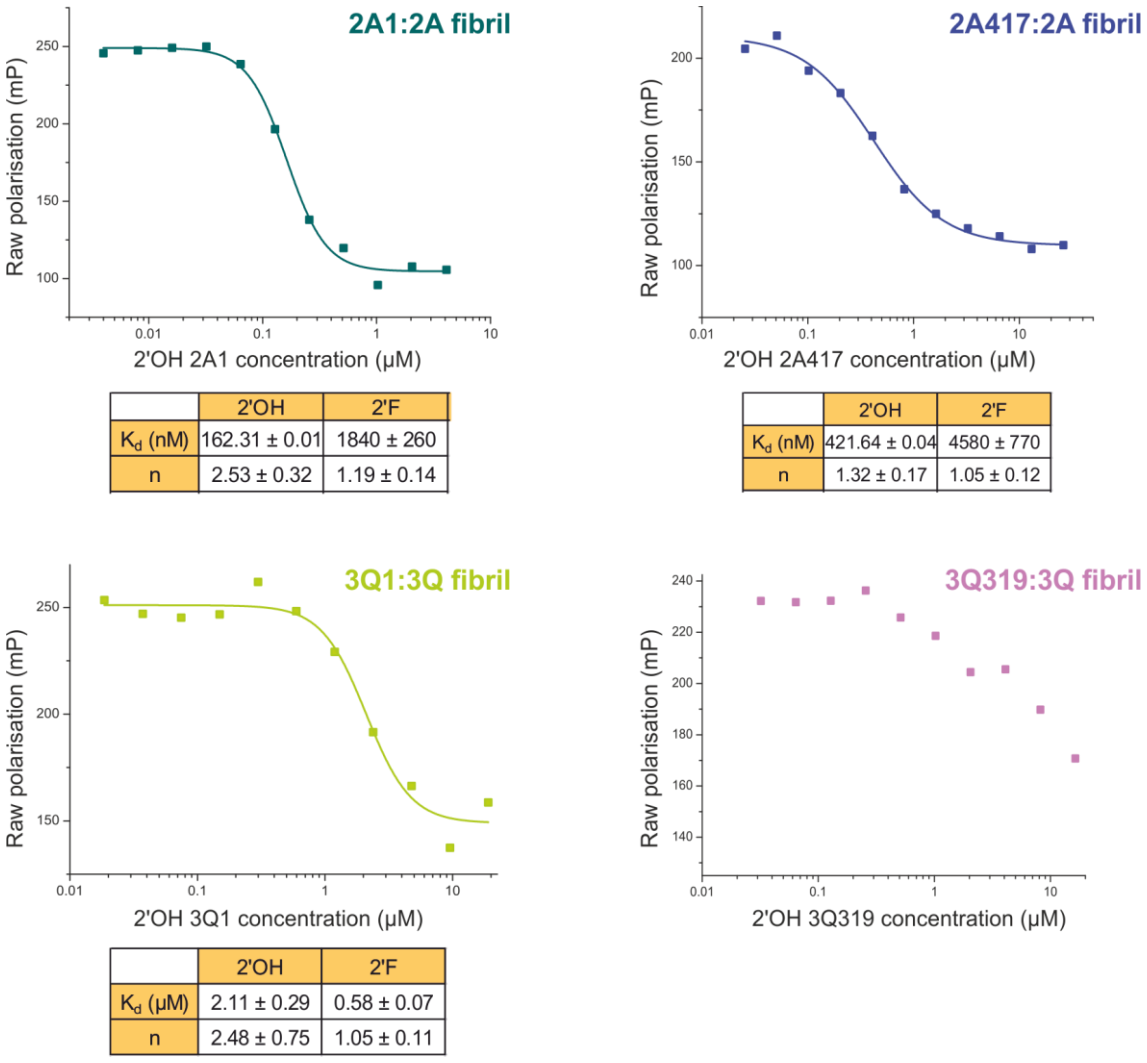

	2'OH	2'F
K_d (nM)	162.31 ± 0.01	1840 ± 260
n	2.53 ± 0.32	1.19 ± 0.14

	2'OH	2'F
K_d (nM)	421.64 ± 0.04	4580 ± 770
n	1.32 ± 0.17	1.05 ± 0.12

	2'OH	2'F
K_d (μM)	2.11 ± 0.29	0.58 ± 0.07
n	2.48 ± 0.75	1.05 ± 0.11

Figure 5.7 2'OH aptamers are able to bind to the fibril targets. Competitive FP experiments for aptamers 2A1 (teal), 2A417 (blue), 3Q1 (green) and 3Q319 (pink) against their 2'F Alexa488 aptamer counterparts in complex with their cognate fibrils. Data are shown for a single experiment for each aptamer. Dissociation constants determined from a Hill fit (methods) are indicated in the accompanying tables for aptamers 2A1, 2A417 and 3Q1, and compared to the K_d and n values determined for 2'F modified aptamers in the direct FP experiments shown in **Figure 5.4**.

5.3 Cross-reactivity with alternative Aβ40 fibril morphologies

To determine whether the aptamers selected are able to recognise fibrils of the alternative morphology, the direct FP binding experiment was repeated, but the non-cognate fibril type was titrated against the fluorescently-labelled aptamers from the other selection pool (3Q fibrils were titrated against anti-2A selected aptamers and *vice versa*). In each case, two aptamers were assayed (2A1 and 2A417 against 3Q fibrils and 3Q1 and 3Q319 against 2A fibrils - **Figure 5.8**). The results showed that all aptamers cross-react with the alternative fibril morphology.

Dissociation constants observed for all eight aptamer-fibril combinations tested lie within the same range as those seen for their cognate targets (high nM to low μM). However, due to the different batches of fibrils used in the analyses, the precise K_d values for individual aptamers differ from those previously seen. From this it became clear that K_d values of different fibril batches could not be used to accurately compare the ability of the aptamers to bind the different fibril targets. Only a direct comparison of the aptamers, on the same single batch of fibrils, can give insight into the relative affinity to an individual fibril type. Therefore, comparison of the binding of four aptamers 2A1, 2A417, 3Q1 and 3Q319 against a single batch of 2A fibrils was carried out (**Figure 5.8 a**). The results of this experiment demonstrated that the anti-2A aptamers indeed possess higher affinity to 2A fibrils than the non-cognate anti-3Q1 aptamers (inset table in **Figure 5.8 a**). Contrastingly, when the same four aptamers were tested against a single batch of 3Q fibrils, no significant discrimination was seen. All four aptamers bound with approximately the same affinity (~ 1 μM **Figure 5.8 b**), with non-cognate aptamer 2A1 demonstrating marginally tighter binding over the four sequences tested. These data demonstrate that although the aptamer sequences have different sequence and structure, anti-2A and anti-3Q aptamers bind both fibril morphologies with similar affinity, displaying some discrimination in the case of the 2A fibrils and not for 3Q. This suggests that the aptamers recognise epitopes conserved between the two fibril types.

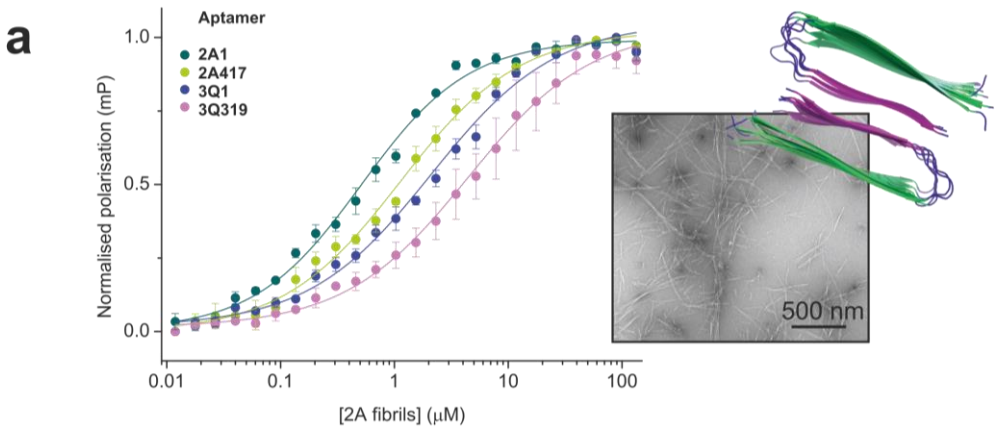

Aptamer	k_d (μM)	n
2A1	0.51 ± 0.04	0.92 ± 0.07
2A417	1.13 ± 0.08	0.83 ± 0.05
3Q1	2.11 ± 0.22	0.80 ± 0.07
3Q319	4.44 ± 0.42	0.80 ±0.06

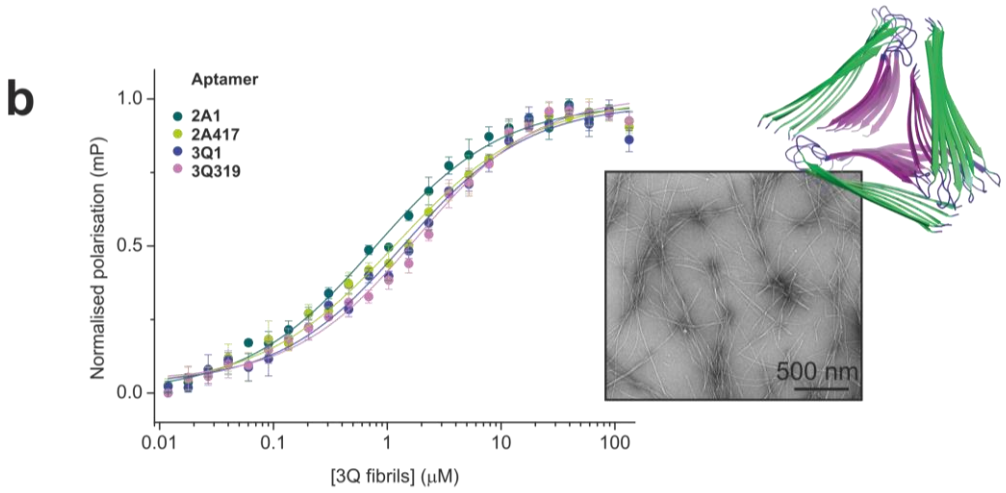

Aptamer	k_d (μM)	n
2A1	0.77 ± 0.07	0.77 ± 0.06
2A417	1.21 ± 0.14	0.72 ± 0.07
3Q1	1.41 ± 0.20	0.80 ± 0.10
3Q319	1.81 ± 0.22	0.81 ± 0.08

Figure 5.8 Aptamers are able to recognise fibrils of different structural morphology. FP analysis of aptamers 2A1 (teal), 2A417 (green), 3Q1 (blue) and 3Q319 (pink) against 2A **(a)** or 3Q **(b)** fibrils. Three replicates were averaged for each aptamer-fibril association. Negative stain electron micrographs of the fibril sample used in each experiment are inset along with the cartoon representation of the fibril morphology in each case (pdb files 2LMN and 2LMP for 2A and 3Q fibrils, respectively). Dissociation constants for each interaction are given in the respective tables, obtained by fitting the data to the Hill equation (**Equation 2.5**). All FP experiments were conducted in MOPS selection buffer, pH 7.5, at room temperature.

To analyse whether the aptamers cross-react with other Aβ40 fibril morphologies, fibrils were formed via *de novo* growth (without the addition of pre-formed seeds) and assayed against the same four aptamer sequences as above. *De novo* derived fibrils contain an array of different morphologies[103, 589] and, therefore, serve as a stringent assessment of whether the aptamers display recognition to epitopes found within all Aβ40 fibrils or features unique to the seeded fibrils studied so far.

Fibrils were formed by incubation of 200 μM monomeric Aβ40, overnight, with agitation at 600 rpm in a NEPHALOstar plus plate reader, in the same buffer used in the seeded fibril reactions (Section 2.4.2). Fibril formation was monitored by nephalometry (**Figure 5.9 a**) and fibrils were shown to be fully elongated within 6 hours. After 18 h elongation, the yield of fibrils was calculated to allow accurate estimation of monomer equivalent fibril concentration for the FP titrations. This was assessed in the same manner as for the seeded fibrils (by SDS PAGE analysis of the soluble and pelletable fractions after separation by centrifugation – Section 2.4.7). This analysis confirmed that 100% of the monomeric peptide had been incorporated into the fibrils in 18 h (**Figure 5.9 b**). Assessment of fibril morphology by electron microscopy confirmed the presence of long, unbranched and sometimes twisted fibrils (**Figure 5.9 c**).

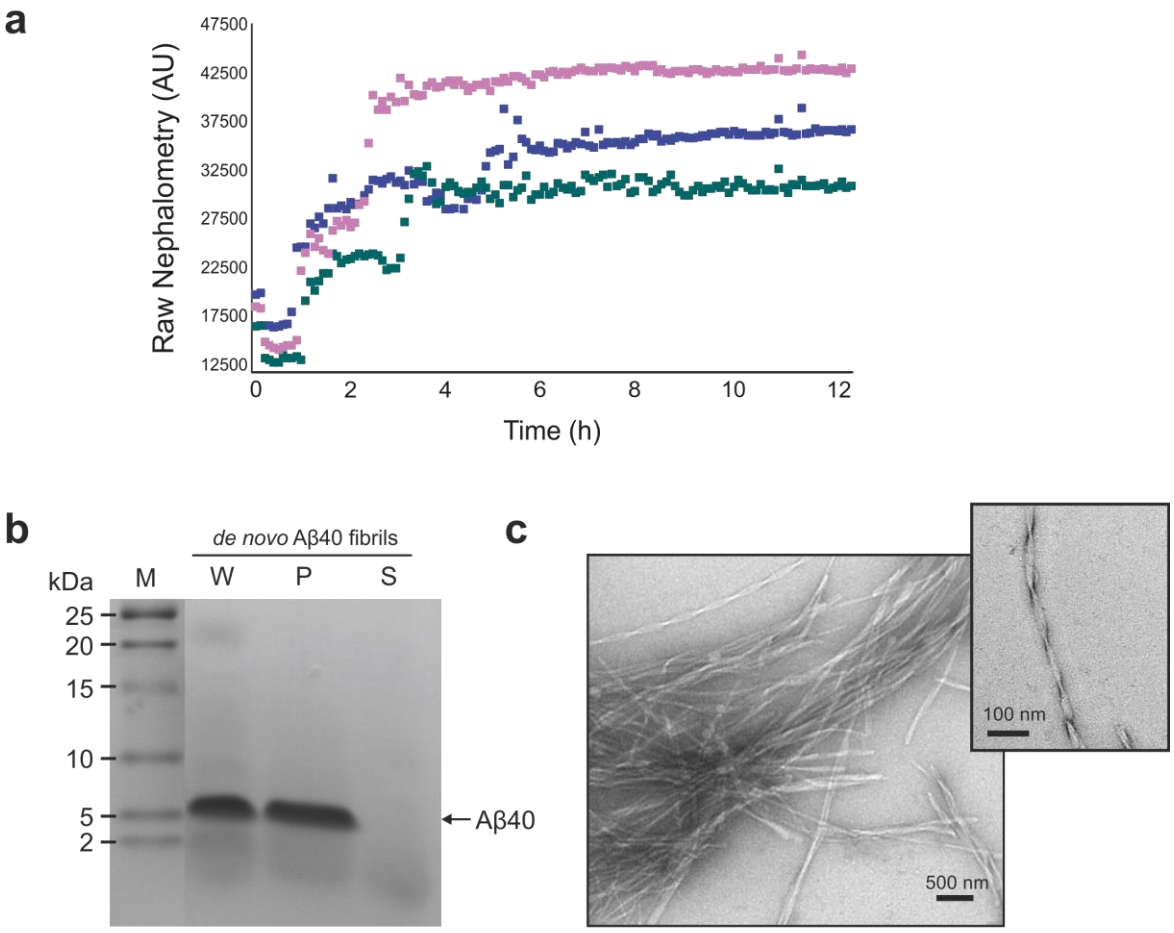

Figure 5.9 Formation and characterisation of *de novo* Aβ40 fibrils. **(a)** Nephelometry of fibrils formed from 200 μM monomeric Aβ40 in 25 mM sodium phosphate buffer, pH 7.5, with 600 rpm agitation, shown over the first 12 h. Data from three representative wells are shown. **(b)** SDS PAGE analysis of fibril yield after 18 h elongation, comparing soluble (S) and pelleted (P) fractions to a whole protein sample from the fibril mix, pre-separation (W). Molecular weight markers are indicated in kDa. **(c)** Negative stain electron micrographs of *de novo* Aβ40 fibrils after 18 h elongation.

Analysis by FP demonstrated that all four of the aptamers assayed associate with the *de novo* fibrils of Aβ40 of mixed morphology (**Figure 5.10 a**). The dissociation constants (1.3 – 1.8 μM) indicate similar binding affinity to that demonstrated against their target fibril assemblies. As seen with 3Q fibrils, the different aptamer sequences demonstrate no significant differences in their ability to bind these Aβ40 fibrils.

One discernible difference in the binding demonstrated against this fibril morphology was the difference in Hill coefficient (n), which is indicative of the cooperativity of binding[590]. The slope of the binding curves observed against *de novo* Aβ40 fibrils is clearly steeper (shown more clearly in **Figure 5.10 b** for aptamer 2A1). The average n value for the four aptamers tested against the *de novo* fibrils is 1.6 ± 0.12. An n value > 1 suggests that there are two or more binding sites and that there is positive cooperativity, where the binding of one substrate facilitates the binding of another. Cooperativity is difficult to interpret in the case of fibrillar targets, as the binding response is monitored as a function of monomer equivalent concentration and not fibril molarity. Nevertheless, the differences between the curves presented for each of the four aptamers tested against *de novo* fibrils, compared with the seeded structures, suggests there may be differences in the binding modes, even though the apparent affinity is similar.

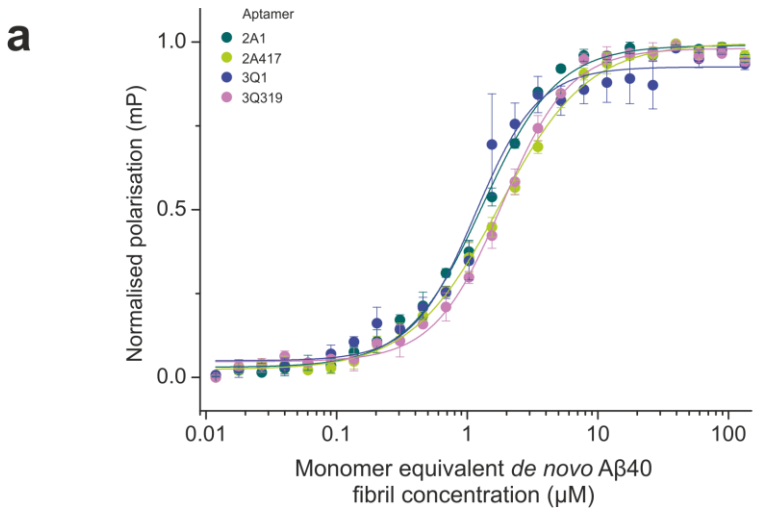

Aptamer	k_d (μM)	n
2A1	1.30 ± 0.06	1.51 ± 0.09
2A417	1.76 ± 0.07	1.28 ± 0.06
3Q1	1.15 ± 0.09	1.80 ± 0.23
3Q319	1.84 ± 0.07	1.67 ± 0.09

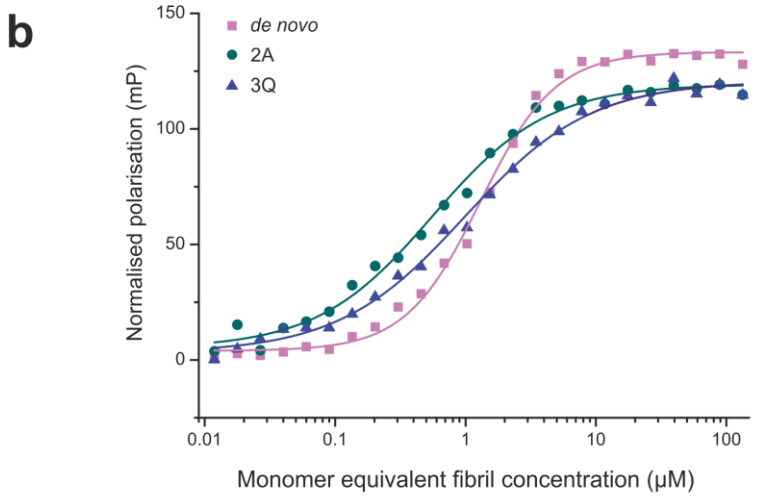

Figure 5.10 Aptamers are able to cross-react with unseeded (*de novo*) Aβ40 fibrils. **(a)** FP analysis demonstrating similar binding responses by aptamers 2A1 (teal), 2A417 (green), 3Q1 (blue) and 3Q319 (pink) to *de novo* derived Aβ40 fibrils. Three replicates were averaged for each association. Dissociation constants (K_d) and n values are indicated for each interaction in the corresponding table. **(b)** A single replicate of aptamer 2A1 binding to 2A fibrils (teal circle), 3Q fibrils (blue triangle) and *de novo* fibrils (pink circle) are overlaid to compare differences in apparent binding cooperativity.

5.4 Analysis of aptamer cross-reactivity with fibrils from other amyloidogenic proteins

To determine whether the aptamers 2A1, 2A417, 3Q1 and 3Q319 are able to cross-react with fibrils derived from other precursor peptides, binding studies were conducted against a selection of unrelated fibrils with varying structural features, including Parkinson's disease associated α-synuclein (α-syn), an amyloidogenic fragment of full-length Aβ (Aβ16-22) and the synthetic amyloid ccβ-p.

5.4.1 α-synuclein

α-synuclein (α-syn) is a 140 amino acid protein (**Figure 5.11 a**) from a family of peptides found to be abundant in the brain. Synucleins (including α, β and γ-synuclein) share 55-62% sequence identity and are all comprised of a similar three-domain organisation (**Figure 5.11 b**). The amino terminal domains are made up of a series of 11-residue repeats, with the consensus sequence KTKEGV separated by inter-repeat regions of 5-8 amino acids[591]. In α-syn, this region is able to form α-helical structure upon interaction with membranes[592-594]. The central domain of α-syn is predominantly hydrophobic and is known as the non-amyloid-β component (NAC) domain, named so as it was originally discovered through its co-purification with Aβ from amyloid plaques from AD patients[595]. This region is thought to be essential in the formation of amyloid fibrils from α-syn[596]. The acidic C-terminal domain of α, β and γ-synuclein is comprised of mostly negatively charged residues and remains largely unfolded, even in the lipid-bound form[591]. Synucleins are found concentrated in the nerve terminals and close to synaptic vesicles[597-599] and, although their cellular function is poorly understood, it has been suggested that they are involved in the trafficking of synaptic vesicles[600-602] and regulation of neurotransmitter release[603-605].

Despite the conserved sequence identity and domain organisation between the three synucleins, α-syn is the only fibril-forming peptide of the family[606] and the only synuclein associated with the filamentous inclusions known as Lewy bodies[607, 608], the main neuropathic feature of Parkinson's disease. Lewy bodies are round, cytoplasmic inclusions made predominantly of fibrillar aggregates of α-syn, but also containing other proteins such as ubiquitin[609] and the molecular chaperone αB-crystallin[610].

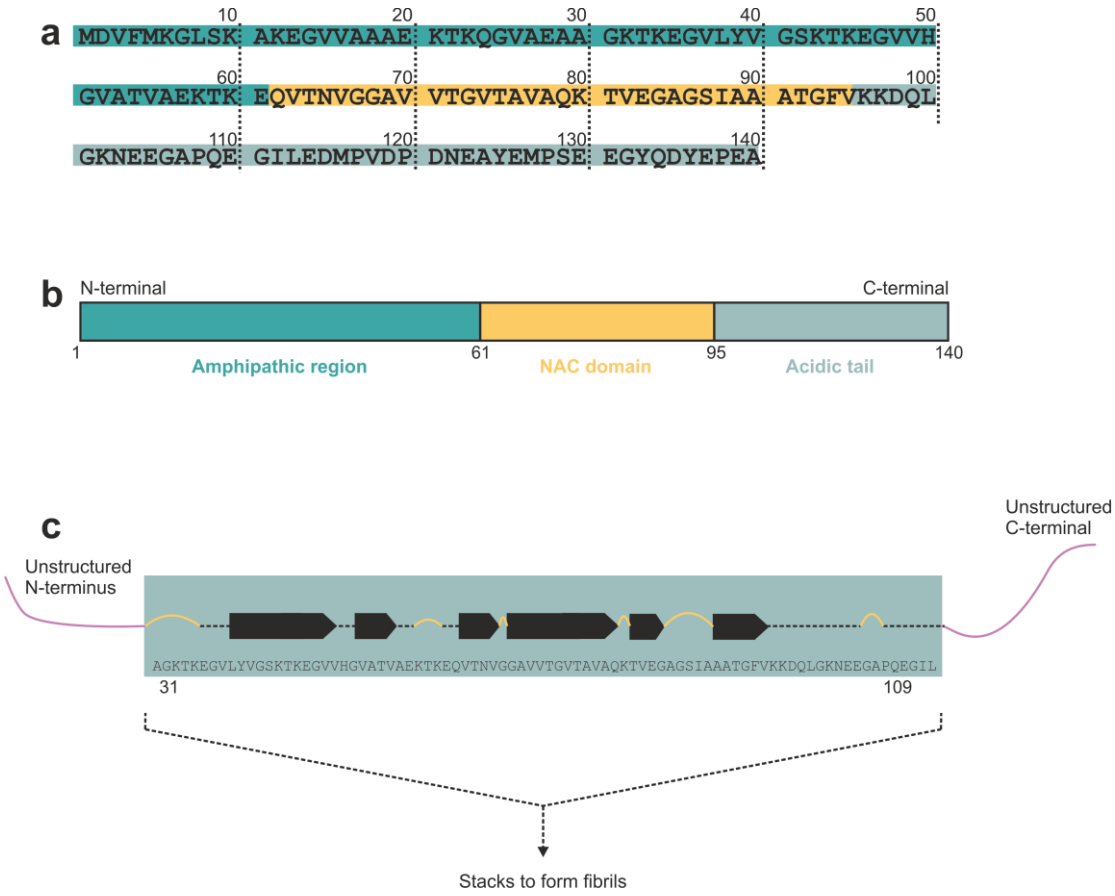

Figure 5.11 Sequence and structure of α-syn fibrils. **(a)** The amino acid sequence of α-synuclein. The amphipathic N-terminal region (which consists of a series of imperfect 11-residue repeats containing the consensus sequence KTKEGV), the NAC region, and the C-terminal acidic tail are highlighted in different colours to correspond to the domain organisation outlined in **(b)**. **(c)** The proposed secondary structural elements in the core region (residues 31 - 109) of α-syn fibrils based on ssNMR measurements by Comellas *et al.*[611]. Black arrows indicate β-strands, curved yellow lines correspond to turn or loop regions, and dashed lines indicate areas where no experimental data was available. The unstructured N- and C- terminal regions are represented as pink solid lines.

Monomeric α-syn is natively unstructured[612, 613] and assembles from a random-coil conformation, via a range of intermediate species, into typical β-sheet rich, amyloid fibrils[606]. As with Aβ amyloidosis, the oligomeric structures are most often linked to neurotoxicity[614] and a range of spherical[615, 616], annular[617, 618] and chain-like[619] structures have been implicated. Fibrils are often considered to be the inert end-point of aggregation, although there is evidence to suggest a toxic mechanism for these higher order species[107, 147].

There is currently no definitive structure known for α-syn fibrils, but several studies have shown them to be composed of several protofilaments, in which the β-sheets are organised perpendicular to the fibril axis[606], parallel and in-register[620, 621]. Limited proteolysis, EPR and ssNMR studies have shown that residues 31 - 109 of the protein are folded in a repeated β-sheet motif that forms the core of the protofibril[620-626] and the N- and C-terminal regions remain flexible and disordered (**Figure 5.11 c**). Hydrogen/deuterium exchange NMR experiments by Vilar *et al*. reported five distinct protected regions in this core leading to their model of a protofilament composed of five layered β-sandwich[623]. However, a more recent study[611], with more comprehensive assignment of secondary structure within this core region, was proposed indicating that this region is formed by six distinct strands; two repeats of a long β-strand followed by two shorter β-strands. The consensus, however, is that the β-sheet rich core region stacks to form the protofilament structure and the C- and N-terminal regions remain disordered on the surface. These protofilaments are then thought to assemble into mature fibrils of at least two distinct structural isoforms[623, 624], the most well characterised of these being the ribbon and fibrillar morphologies where protofilaments lie parallel to each other (ribbon) or twist around each other (fibrillar)[107].

Given the wealth of structural information[606, 620, 621, 623, 624] and the prevelence of PD[127], α-syn fibrils were selected as a second model amyloid in order to determine the extent of aptamer cross-reactivity with fibrils formed from unrelated, larger protein sequences.

5.4.2 Aptamers display cross-reactivity with α-synuclein fibrils

Wild-type α-syn was expressed from a pET23a plasmid containing a synthetic gene encoding its sequence (**Appendix 7.1.2**) and purified by anion exchange chromatography, followed by size exclusion separation (**Figure 5.12 a**). Full details of the expression and purification protocols are given in (Section 2.3.2). The purity of the resultant protein was verified by mass spectrometric analysis (**Figure 5.12 b**) and the preparation protocol was found to yield 45 mg pure protein/L culture. This protein was then used to form fibrils for the aptamer binding analysis.

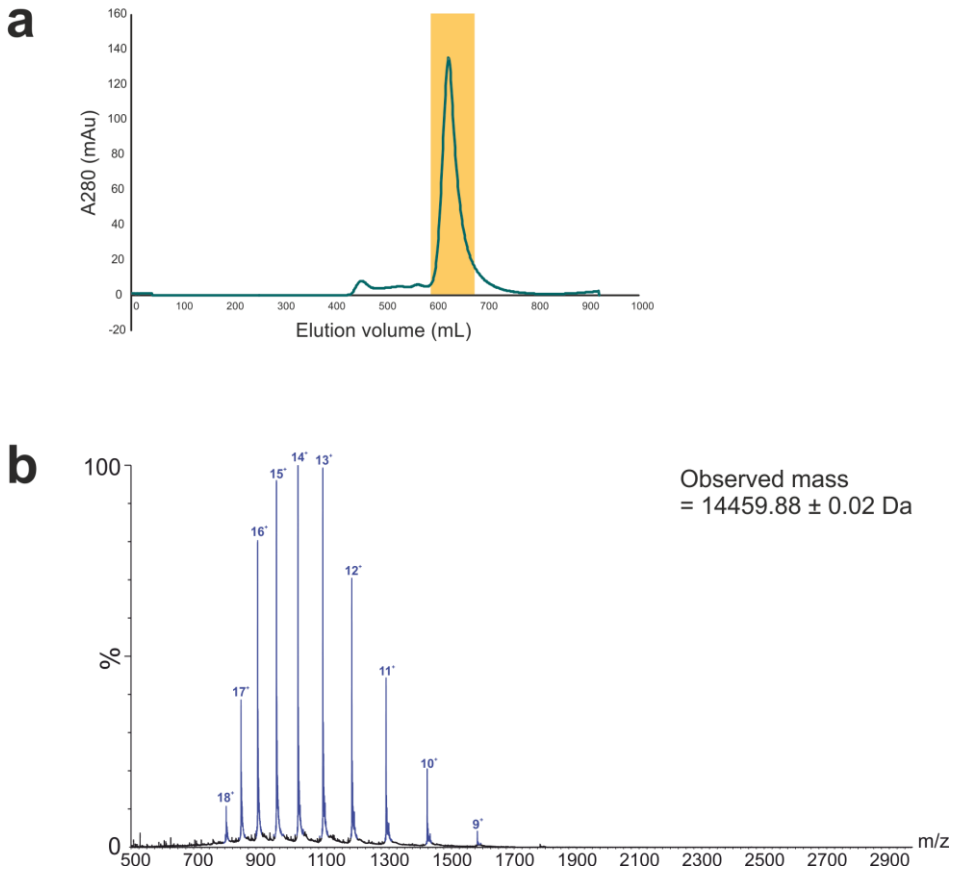

Figure 5.12 Purification of recombinantly expressed α-syn. **(a)** A typical α-syn elution profile from the final SEC stage of the purification (detailed in Section 2.3.2). Pure α-syn elutes as the dominant species (highlighted yellow). **(b)** ESI-MS analysis of purified α-syn. The observed mass of 14459.88 Da is indicated in the spectrum, (expected mass 14460.1 kDa).

In order to create fibril samples, a seeding protocol was employed rather than formation via *de novo* assembly, as work previously conducted in the group by Dr. Matthew Jackson and Dr. Theo Karamanos found that seeded samples demonstrate much higher efficiency of monomer incorporation (unpublished results). The seed stocks were first made by incubation of α-syn at 300 μM final protein concentration, in 20 mM Tris-HCl, 100 mM NaCl, 0.01% (w/v) NaN_3, pH 7.5, with constant 600 rpm shaking on a thriller thermoshaker (Section 2.4.3). After 7 days of elongation, the resultant fibrils were fragmented with 1000 rpm stirring on a home-built precision stirrer (Section 2.4.3), for 48 h. The seeds were then used to elongate further fibril samples. 10% (v/v) seed stock was added to 200 μM monomeric peptide, in the same buffer, and incubated for a minimum of 4 days, this time with only intermittent shaking (5 s at 600 rpm, at 5 min intervals), introduced to reduce fibril settling during formation (Section 2.4.3). The incorporation of monomer after 4 days of elongation was assessed by SDS-PAGE analysis (**Figure 5.13 a**). The results showed that > 95% of the peptide is incorporated into the insoluble fibrillar pellet. α-syn has self-proteolytic properties[627] which is evident here from the existence of some fragment bands seen in the SDS-PAGE gel. The presence of some proteolytic fragments was unavoidable in all fibril formation reactions, but as the vast majority of the peptide in the fibrils remains full-length, the fibril samples made by this protocol were considered of sufficient quality to conduct the aptamer binding investigations. Negative stain TEM of the fibril samples confirmed the presence of long, unbranched amyloid fibrils (**Figure 5.13 b**), mostly presenting a straight morphology consistent with the model of protofibrils laterally associating[107]. α-syn fibrils are inherently polymorphic and the presence of a twisted protofibril morphology was also evident in some micrographs (**Figure 5.13 b,** inset).

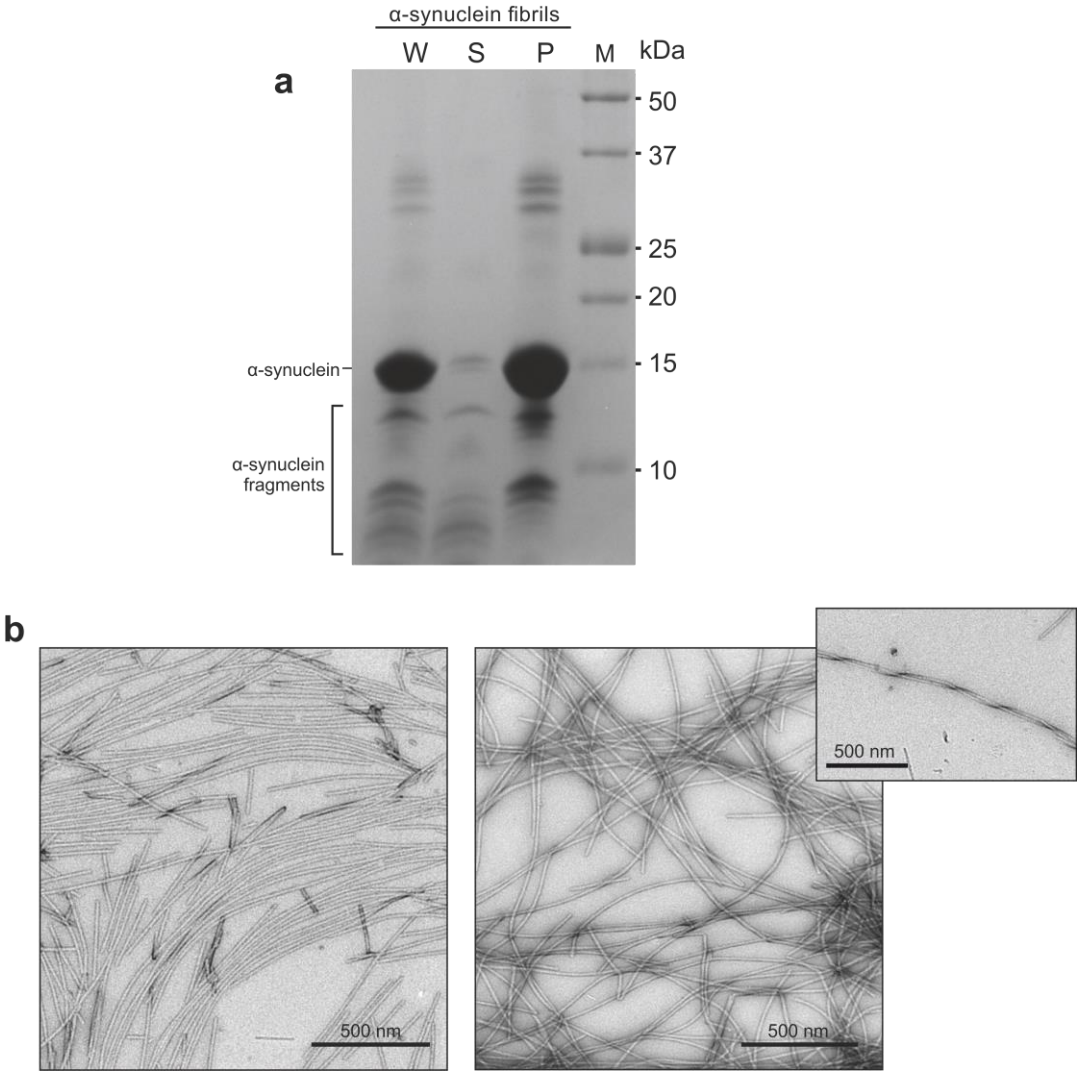

Figure 5.13 Formation and characterisation of α-syn fibrils. **(a)** SDS PAGE analysis of fibril yield, comparing soluble (S) and pelleted (P) fractions to a whole protein sample from the fibril mix, pre-separation (W). Molecular weight markers are indicated in kDa. **(b)** Negative stain electron micrographs of α-syn fibrils presenting a dominant "straight" morphology with some instances of twisted morphologies present (inset).

Fluorescence polarisation was again utilised to assess whether the α-syn fibrils are recognised by the four aptamers 2A1, 2A417, 3Q1 and 3Q319 (**Figure 5.14**). An increase in polarisation as a function of fibril concentration was again observed, indicative of the aptamers binding to this unrelated fibril type. Dissociation constants for the interactions range from 2.7 – 21 μM a lower affinity than for the cognate Aβ40 fibrils, for which K_ds ranged from 0.58 – 8.1 μM, in the direct-binding polarisation experiments (Section 5.2.2). Aptamer recognition of fibrils, therefore, is not simply dependent on the precursor protein

sequence, but the affinity of the interaction may be effected to some extent by it. Of the four aptamers tested, differences were observed in their relative ability to bind α-syn fibrils, with the same order of affinity shown against the Aβ40 fibril morphology 2A being observed (2A1 is the tightest binder, followed by 2A417, 3Q1 then 3Q319). The cooperativity of binding is also similar to that seen in the aptamer-2A fibril interactions (n = ~1), except for 3Q1, however this fit could be skewed due to larger errors in the pre-transition (unbound) data points of this binding curve. It is clear from these data that aptamers are able to bind generic features of amyloid that are conserved between assemblies, even when derived from entirely different precursor peptides.

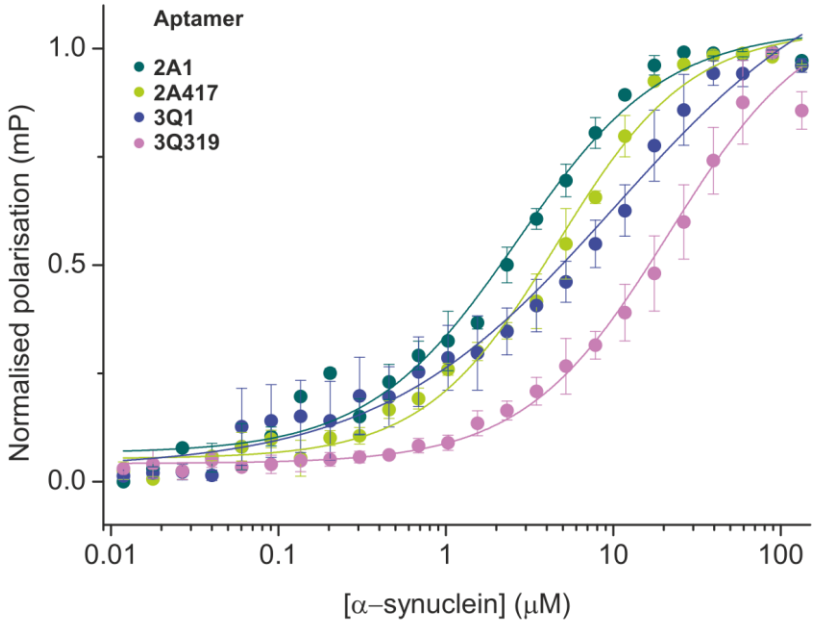

Aptamer	k_d (μM)	n
2A1	2.66 ± 0.33	1.00 ± 0.11
2A417	4.61 ± 0.45	1.10 ± 0.10
3Q1	10.2 ± 3.72	0.62 ± 0.10
3Q319	21.4 ± 4.33	1.01 ± 0.12

Figure 5.14 Aptamers are able to recognise fibrils from the unrelated amyloid protein α-syn. FP analysis demonstrating α-syn fibril binding by aptamers 2A1 (teal), 2A417 (green), 3Q1 (blue) and 3Q319 (pink). Three replicates were averaged for each association. Dissociation constants (K_d) and n values are indicated for each interaction in the corresponding table.

5.4.3 Aβ16-22

To examine the nature of the conserved aptamer binding epitope, the simple cross-β architecture synonymous with amyloid fibrils was considered a likely candidate. Typical cross-β structure is formed when individual β-sheets are organised perpendicular to the axis of the fibril and are spaced 4.7 Å apart[82] (**Figure 1.6**). This gives rise to a characteristic X-ray diffraction pattern, with meridional and equatorial bands at 4.7 Å and ~ 10 Å, respectively, which are observed for all amyloid fibrils[15, 82]. To determine whether this simple feature of amyloid is the main epitope for aptamer binding, a fibril which contains a simple cross-β architecture was chosen. Aβ16-22 (KLVFFAE - **Figure 5.15**) is a self-assembling fragment of full-length Aβ which spans the central hydrophobic region of the peptide and, along with many other Aβ fragments[100, 628-632], has been shown to form amyloid fibrils *in vitro*[633-636]. This peptide has been identified as forming the cross-β spine of full-length fibrils[95, 104, 628] and, therefore, was chosen as the model amyloid structure to examine aptamer selectivity for the cross-β motif.

Fibrils of Aβ16-22 were first described and modelled in atomic detail by Balbach *et al*.[633]. Using X-ray diffraction, Fourier transform infrared spectroscopy (FTIR) and ssNMR, the authors determined that the fibril structure of Aβ16-22 is comprised of anti-parallel, in-register β-sheets (**Figure 5.15**). The proposed in-register alignment leads to a β-sheet arrangement in which the side chains present in such a way as to produce two distinct faces of the β-strand; Leu17, Phe19 and Ala21 forming the hydrophobic face and Lys16, Val18, Phe20 and Glu22 displaying on the opposing, hydrophilic side (**Figure 5.15**). The precise structure in terms of β-sheet stacking is unknown for these fibrils, although several molecular dynamic (MD) simulations suggest that 2, 3, 4[637] or even 5[634] anti-parallel β-sheets can associate to form the mature fibril. Unlike the amyloid fibrils studied in this thesis so far, Aβ16-22 fibrils have no dynamic unstructured regions decorating the surface of the fibril and, therefore, should provide insight into whether the cross-β spine itself is involved in the aptamer recognition motif.

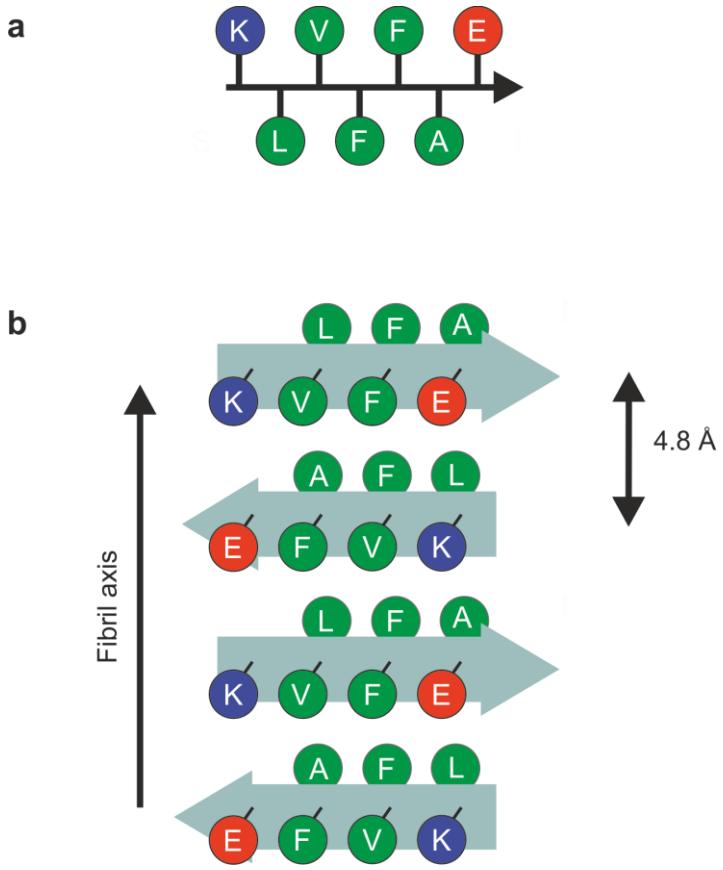

Figure 5.15 Sequence and structure of Aβ16-22. **(a)** The amino acid sequence of the Aβ16-22 peptide represented as a β-strand conformation as seen along the β-sheet plane, where amino acid side chains are represented as spheres. **(b)** Schematic representation depicting the anti-parallel, in-register β-sheet structure formed by Aβ16-22 peptides. Residues are coloured according to their properties: positively charged (blue), negatively charged (red), hydrophobic (green).

Fibrils of Aβ16-22 were formed from synthetic peptide, synthesised and purified by Dr. George Preston (School of Chemistry, University of Leeds). Fibril reactions were set up at final peptide concentrations of 400 μM, in 25 mM sodium phosphate buffer, pH 7.5, and incubated, without shaking, at room temperature for 15 days (Section 2.4.4). After 15 days of elongation, the presence of fibrillar structures was confirmed by negative stain EM. The results showed fibrils with a high degree of polymorphism (**Figure 5.16 a**). It was necessary to assess fibril yield and, therefore, to estimate monomer equivalent fibril concentration in the binding experiments, however, SDS-PAGE analysis of the pelletable material was not feasible because of the size of the peptide. Aβ16-22 also lacks aromatic residues and hence it is not visible by UV spectroscopy at 280 nm. Therefore, the monomer

remaining in the soluble fraction after separation by centrifugation was measured by a calibrated HPLC approach, in which peptide content was monitored by absorbance at 210 nm (Section 2.4.8). **Figure 5.16 b** shows the HPLC calibration by injection of 50, 100 and 200 µM samples of monomeric Aβ16-22. Injection of an equal volume of the soluble fraction taken from a pelleted fibril sample (after 15 days incubation) showed that 72% of the peptide was incorporated into fibrils. This fibril yield is consistent with the efficiency of fibril formation documented previously for this peptide[638].

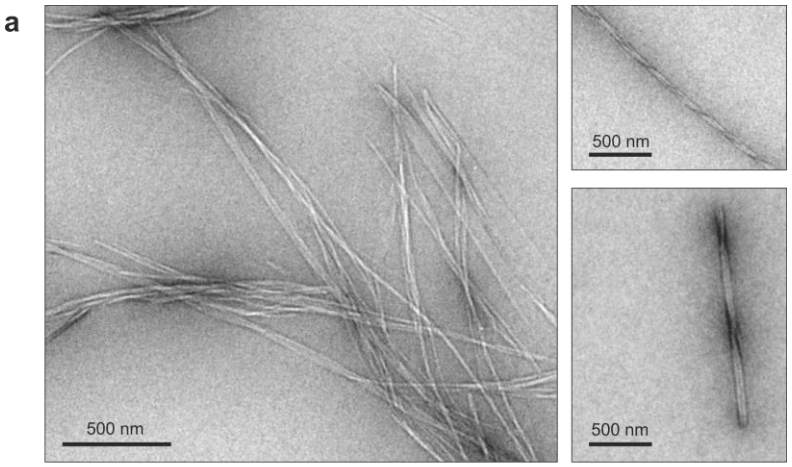

b. i.

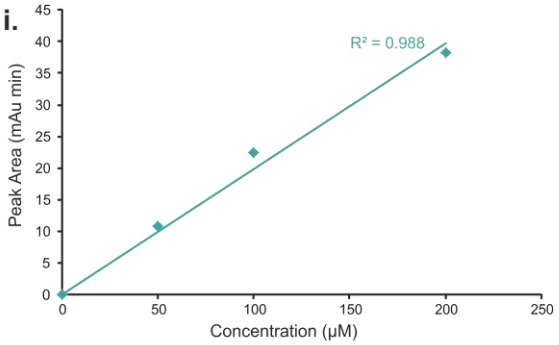

b. ii.

Peak Area (mAu min) soluble fraction	Concentration (µM)	Concentration (µM) corrected for dilution	Yield (%)
2.76	13.87	110.93	72.27

Figure 5.16 Formation and characterisation of Aβ16-22 fibrils. **(a)** Negative stain EM of Aβ16-22 fibrils displaying several distinct morphologies. **(b. i.)** HPLC calibration used to estimate fibril yield. **(b. ii.)** Peak area was calculated from an injection of the equivalent volume of the soluble fraction after fibril sample separation, calculated from the standard curve and expressed as a percentage of total peptide before fibril formation (400 µM).

To assess binding of Aβ16-22 fibrils to aptamers 2A1, 2A417, 3Q1 and 3Q319 and to allow comparison of binding over the same fibril concentrations assayed for the previous fibril types, the monomer equivalent concentration of fibril titrated was corrected for this 72% yield. FP analysis over this concentration range showed that the four aptamers tested were unable to recognise these fibrils (**Figure 5.17**). This was compared with a single control assay of 3Q1 binding to 3Q fibrils conducted on the same day as a positive control. These data suggest that the cross-β backbone structure present in the Aβ16-22 fibrils is not sufficient for aptamer binding. The amyloid binding ability of aptamers 2A1, 2A417, 3Q1 and 3Q319, therefore, presumably does not result from their common cross-β fold.

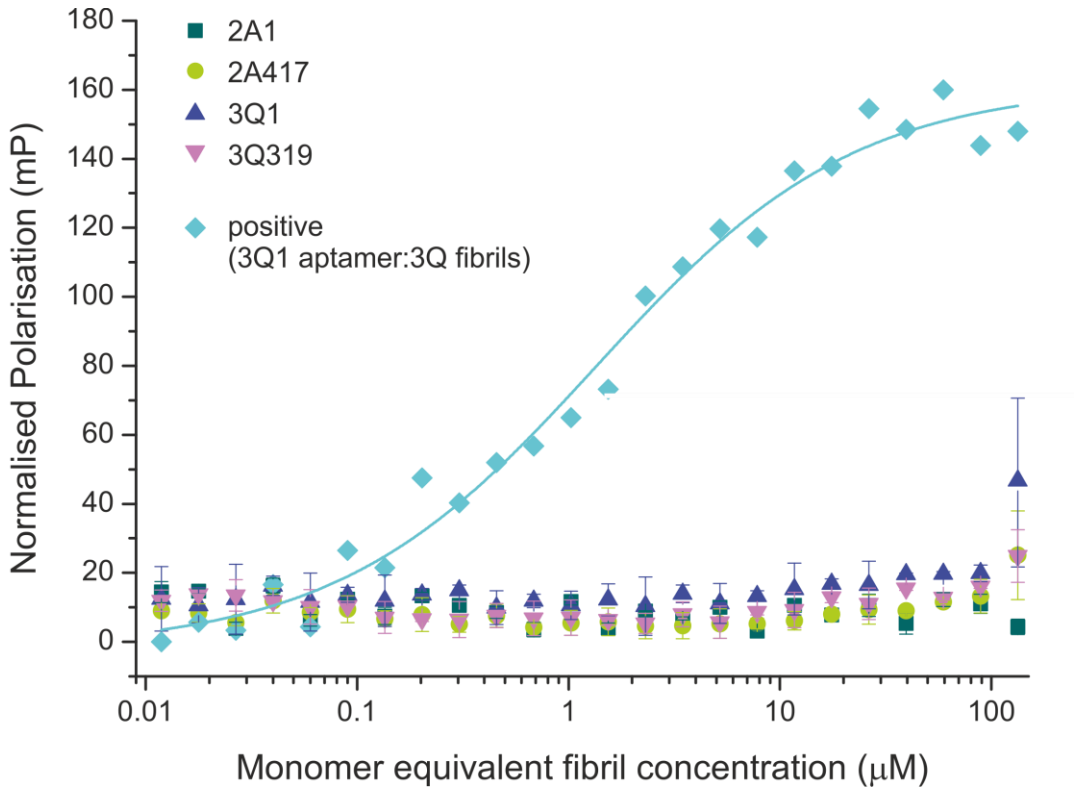

Figure 5.17 Aptamers are unable to bind Aβ16-22 fibrils. FP analysis demonstrating the inability of aptamers 2A1 (teal), 2A417 (green), 3Q1 (blue) and 3Q319 (pink) to bind Aβ16-22 fibrils. Three replicates were averaged for each association. The data are compared with a single replicate of positive control aptamer 3Q1 binding to 3Q fibrils, conducted on the same day (pale blue), fitted to the Hill equation (K_d = 1.34 ± 0.24 μM, n = 0.71 ± 0.10).

5.4.4 ccβ-p

ccβ-p (**Figure 5.18 a**), is a 17-residue, synthetic, amyloid-forming peptide. It was originally designed by Kammerer and colleagues[639] as a model peptide for studying the molecular interactions required for amyloid formation. ccβ-p forms a native coiled-coil structure at ambient temperatures that rapidly converts to amyloid fibrils at elevated temperatures. These fibrils possess the typical cross-β architecture, as confirmed by CD, TEM, characteristic Congo-red green birefringence and X-ray diffraction data[639]. FTIR also indicates that the β-strands forming the core of the fibrils are anti-parallel and ssNMR distance measurements indicates an out-of-register alignment where Ala7 is hydrogen bonded to Leu14 on the adjacent strand. The structural model proposed for ccβ-p (**Figure 5.18 b** and **c**) and the related ccβ-Met[640] is a laminated cross-β structure made up of a minimum of three β-sheets, where each strand is fully extended. The inter- and intra-sheet packing is composed of the maximum number of hydrophobic contacts and this results in the out-of-register, anti-parallel arrangement, consistent with experimental data[639].

This model fibril was chosen as a further control for aptamer cross-reactivity as it is again predicted to form a simple cross-β structure without the flexible termini present in the predicted Aβ40 and α-syn fibril structures. Ccβ-p fibrils also present a number of positively charged residues on the surface (**Figure 5.18**), as opposed to the fibrils formed from Aβ16-22 which possess only a single lysine residue (K16) at the edge of the β-strand (**Figure 5.15**). The ccβ-p model peptide fibril, therefore, would provide insight into whether the presence of positively charged residues on the surface of the cross-β structure is necessary and sufficient for amyloid binding by the anti-Aβ40 aptamers.

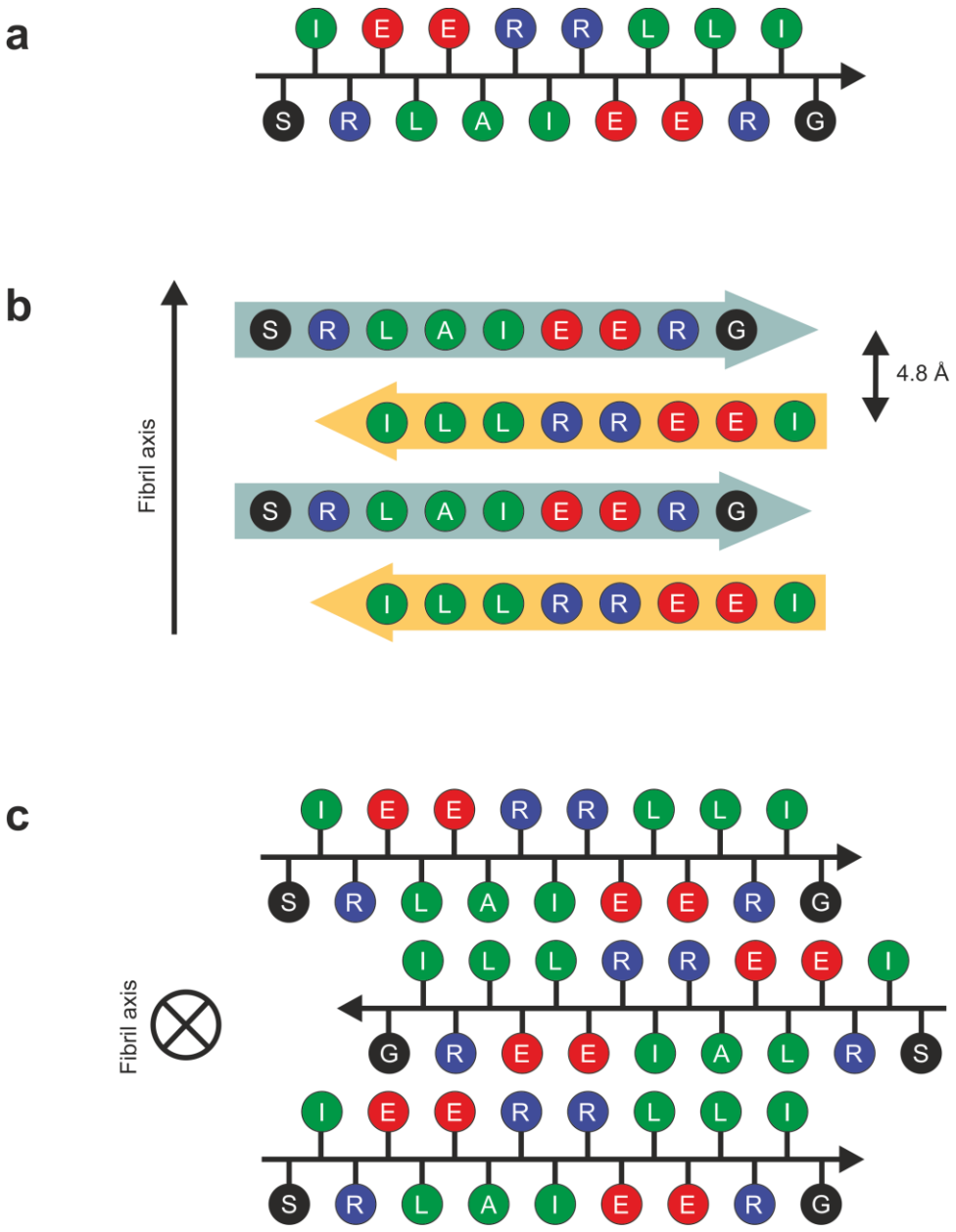

Figure 5.18 Sequence and structure of ccβ-p. **(a)** The amino acid sequence of the ccβ-p peptide represented as a β-strand conformation, as seen along the β-sheet plane, where amino acid side chains are represented as spheres. **(b)** A schematic representation of four β-strands viewed perpendicular to the fibril axis, depicting the anti-parallel and out-of-register conformation proposed. The grey and yellow arrows discriminate between the two faces of the β-strand. **(c)** View of the proposed model for the fibril cross-section. Residues are coloured according to their properties: positively charged (blue), negatively charged (red), hydrophobic (green), polar or glycine (black). Adapted from[639].

Ccβ-p was synthesised and kindly provided by Dr. Kevin Tipping (School of Molecular and Cellular Biology, University of Leeds). Fibrils were formed from monomeric ccβ-p by incubation at 37 °C, without agitation, for 18 h, yielding fibrils with 100% monomer incorporation, as assessed by calibrated HPLC analysis (**Figure 5.19 a**). Negative stain EM was again used to confirm that the aggregates formed were indeed fibrillar (**Figure 5.19 b**).

a

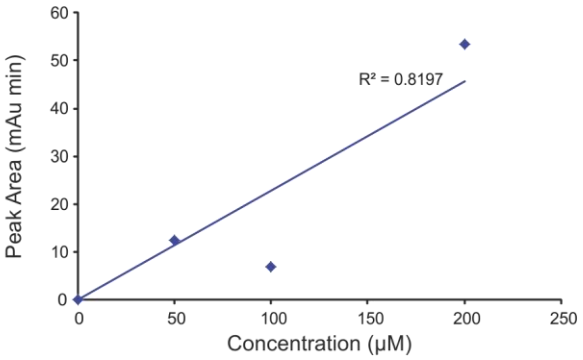

Peak Area (mAu min) soluble fraction	Concentration (μM)	Concentration (μM) corrected for dilution	Yield (%)
0.00	0.00	0.00	100.00

b

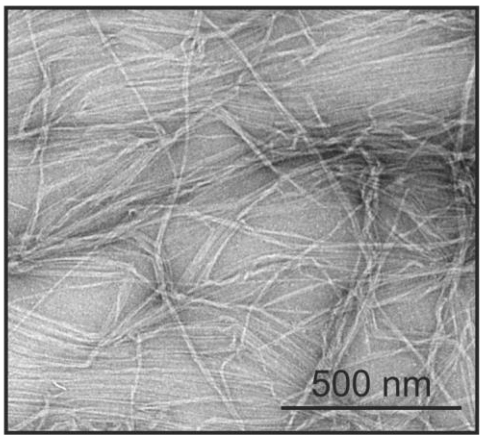

Figure 5.19 Formation and characterisation of ccβ-p fibrils. **(a)** HPLC calibration used to estimate fibril yield. Peak area was calculated from an injection of the equivalent volume of the soluble fraction, after fibril sample separation, calculated from the standard curve and expressed as a percentage of total peptide before fibril formation (200 μM). **(b)** Negative stain electron micrograph of ccβ-p fibrils.

Figure 5.20 shows the FP analysis of aptamers 2A1 and 3Q1 against synthetic ccβ-p amyloid fibrils and, as seen for the peptide fragment fibril Aβ16-22, demonstrates that the two aptamer sequences are unable to recognise this fibril morphology. The results were again compared with a single replicate of the positive control aptamer 3Q1 binding to 3Q fibrils, performed on the same day. These data further support the hypothesis that aptamers have some discrimination between amyloid assemblies and that recognition cannot be simply due to the presence of positively charged residues on the fibril structures, or a cross-β fold.

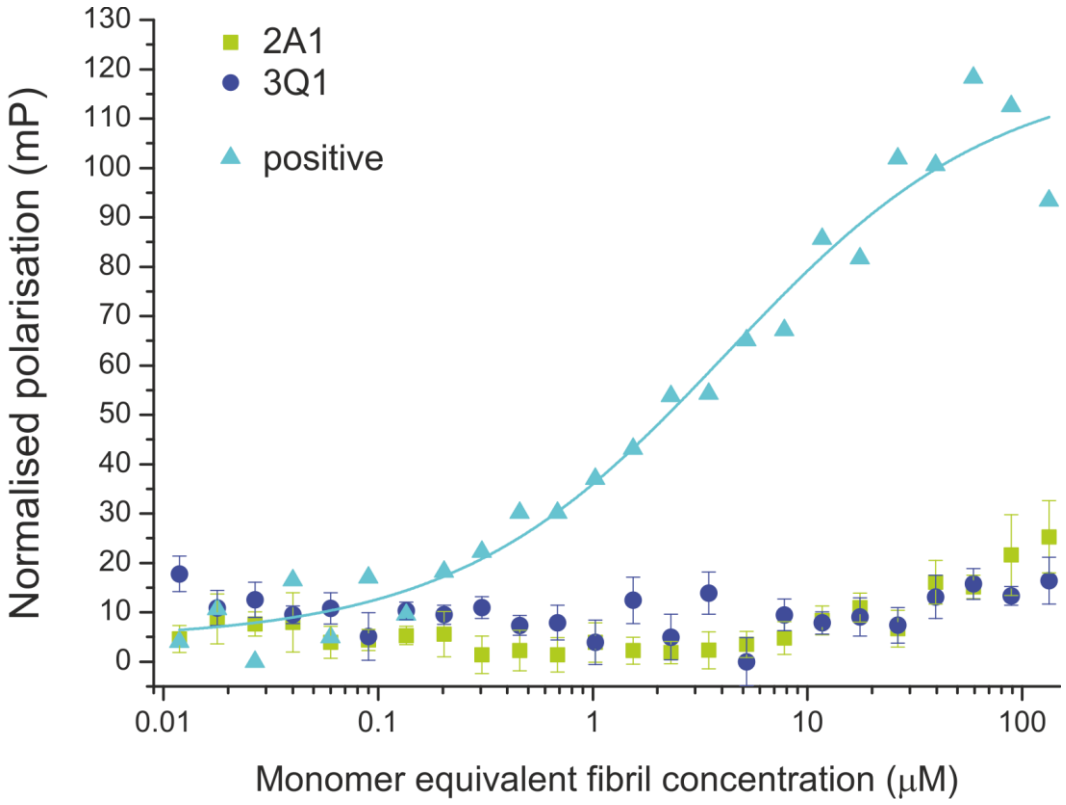

Figure 5.20 Aptamers are unable to bind to ccβ-p fibrils. FP analysis demonstrating an inability for aptamers 2A1 (green) and 3Q1 (blue) to bind ccβ-p fibrils. Three replicates were averaged for each association. Data are compared to a single replicate of positive control aptamer 3Q1 binding to 3Q fibrils, conducted on the same day (pale blue), fitted to a Hill equation (K_d = 4.15 ± 1.30, n = 0.69 ± 0.14).

5.5 Examining the influence of aptamer sequence and structure on amyloid binding specificity

5.5.1 Primary RNA sequence

The cross-reactivity studies presented so far have shown that the aptamer sequences selected against defined structures of Aβ40 fibrils are able to bind fibrils of different morphology, from the same Aβ40 peptide precursor and the unrelated protein sequence of α-syn, but not amyloid fibrils formed from shorter peptide sequences (Aβ16-22 and ccβ-p). To understand the nature of the selectivity for generic amyloid epitopes, investigation into common features of the RNA aptamers themselves was next undertaken.

The differences in base composition and lack of conserved motifs between aptamer sequences isolated from the two pools (**Figure 3.17**) initially suggested that the aptamers would possess specificity for their selection targets. This was based on the assumption that RNA sequences would dictate the secondary structural elements that confer binding specificity. The data presented thus far suggests that binding specificity is not strongly dependent on RNA sequence, as aptamers with little sequence similarity bind the various fibrils with similar affinity. The small differences in affinity seen between some aptamer sequences may indicate that primary sequence has a role in modulating the binding, but presumably is not the dominant process driving the recognition.

To test this further, a series of aptamers with unrelated primary sequences were tested for their ability to recognise the various amyloid fibrils. β55 (**Figure 5.21 a**) is an aptamer sequence characterised by Ylera *et al.*[491] that was originally selected against monomeric Aβ40 yet, according to their publication, shows enhanced affinity for Aβ40 fibrillar assemblies. β55 shares no sequence similarity with the aptamers selected against monomer or fibrillar Aβ40 in this study and, therefore, was used as a further test of how the primary sequence of RNA may determine or modulate binding specificity.

β55, fluorescently-labelled with Alexa488 dUTP as described in Section 4.2.1.1, was transcribed (Section 2.6.5.1) and FP analysis against 2A and 3Q fibrils was conducted (**Figure 5.21 b**). The data indicate similar binding affinity of β55 for both fibril types (2.47 ± 0.33 μM for 2A and 1.69 ± 0.12 μM for 3Q) which is also similar to that determined for the anti-2A and anti-3Q aptamers (0.6 - 8.1 μM).

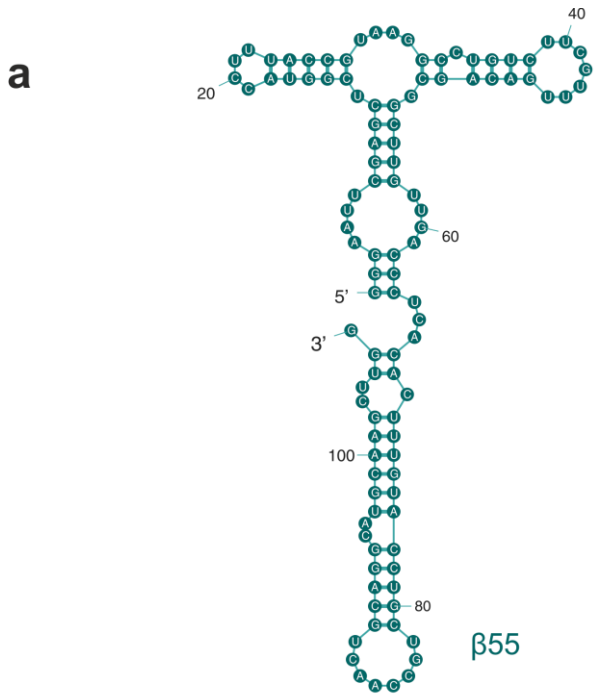

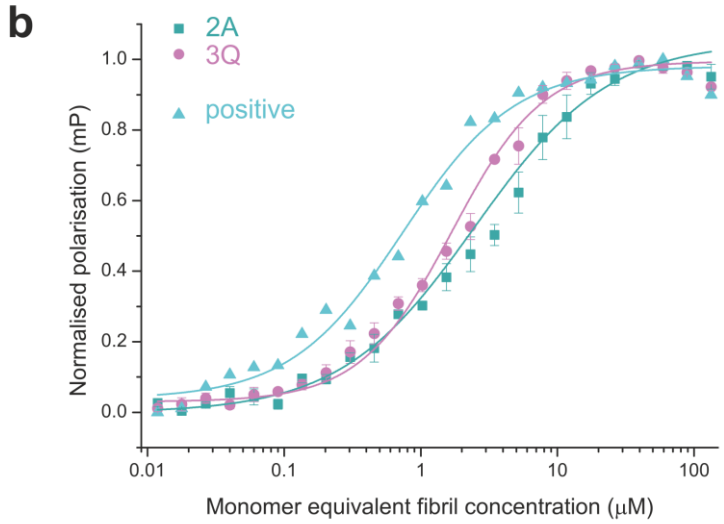

Aptamer	Fibril	k_d (μM)	n
β55	2A	2.47 ± 0.33	0.89 ± 0.08
β55	3Q	1.69 ± 0.12	1.30 ± 0.12
3Q1	3Q	0.74 ± 0.07	1.06 ± 0.11

Figure 5.21 The control anti-Aβ40 monomer aptamer β55 binds to 2A and 3Q fibrils with similar affinity. **(a)** The sequence and predicted secondary structure of aptamer β55. **(b)** FP analysis demonstrating binding of β55 to 2A (teal) and 3Q (pink) fibrils. Data were compared with a single replicate of control aptamer 3Q1 binding 3Q fibrils, conducted on the same day (positive – blue triangles). The dissociation constant (K_d) and n values are given in the corresponding table, obtained by fitting a Hill plot (**Equation 2.5** – solid line).

Similarly, the aptamer sequence M1, selected against monomeric Aβ40 in this study, was also tested for its ability to bind Aβ40 fibrils. As discussed in Chapter 4, aptamers from the anti-monomer selection were characterised and found unable to recognise monomeric Aβ40 peptide, unless immobilised on a bead surface. It was predicted that the aptamers may have been selected against an aggregated Aβ40 species, trapped during the immobilisation process, and this was tested here. Indeed, using FP analysis, M1 was shown to bind 2A, 3Q and *de novo* Aβ40 fibrils (**Figure 5.22**), confirming the notion that the anti-monomer aptamers are able to recognise higher-order species, but also providing further evidence that the aptamer recognition is not entirely dependent on RNA sequence. M1 shares no substantial extended sequence motifs in common with the 3Q aptamers and is only similar to the 2A aptamers in the GA bias (alignment data in **Appendix 7.4**), which was a consequence of their selections from the same naïve library. Nevertheless, binding affinities of M1 to each Aβ40 fibril morphology (1.56 – 3.5 μM given in table in **Figure 5.22**) was comparable to that of aptamers selected against these fibrillar targets (0.6 - 8.1 μM).

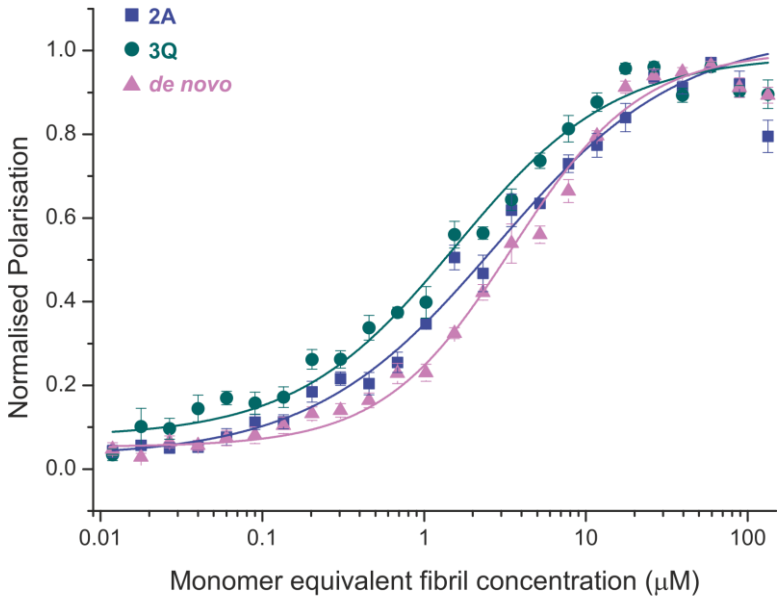

Fibril	k_d (μM)	n
2A	2.81 ± 0.36	0.76 ± 0.07
3Q	1.56 ± 0.23	0.88 ± 0.12
de novo	3.50 ± 0.33	1.09 ± 0.09

Figure 5.22 Anti-monomer aptamer M1 binds to Aβ40 fibrils. FP analysis demonstrating binding of M1 to 2A (blue), 3Q (teal) and *de novo* (pink) Aβ40 fibrils. Three replicates were averaged for each association. The K_d and n values are given in the corresponding table, calculated from a Hill plot of the data (**Equation 2.5**).

Next, RNA aptamer sequences selected by others against a series of unrelated, non-amyloid targets were tested for their ability to recognise amyloid fibrils. Sequences isolated from selections (conducted by Dr. David Bunka, Dr. Simon White and Dr. Nicola Derbyshire, respectively - all University of Leeds) against viral proteins (dengue virus E protein, aptamer DV1, and rabies virus glycoprotein, aptamer RVGP1), as well as an aminoglycoside aptamer[418] (NGGA1) were chosen for this analysis (**Figure 5.23**). Aptamer DV1 was selected from a 2'OH N50 library, whereas aptamers NGGA1 and RVGP1 were selected from 2'F N30 and N50 libraries, respectively, and, therefore, these control sequences are of similar size to the anti-Aβ40 aptamers. Sequence alignment with Genebee[513] confirmed that there are no obvious conserved extended sequence motifs between these sequences and any of the aptamers selected against the three Aβ40 targets (**Appendix 7.4**).

The three control aptamers were transcribed in the presence of Alexa488 dUTP from a 2'F pyrimidine NTP mix, as described (Section 2.6.5.1), for FP analysis. Aptamer DV1 was shown to bind with similar affinity (K_d = 0.67 – 1.99 μM) as the anti-2A and anti-3Q aptamers when assayed against both 2A and 3Q fibrils (**Figure 5.24 a**). The aptamers NGGA1 and RVGP1, were also able to bind to 2A/3Q fibrils. They each display similar affinity for 3Q fibrils as demonstrated by the anti-fibril aptamers (K_ds = 2.5 and 2.1 μM for NGGA1 and RVGP1, respectively) and lower apparent affinity for 2A fibrils (data could not be fitted over the concentration range assayed - **Figure 5.24 b**). NGGA1 and RVGP1 were also assayed against Aβ16-22 fibrils and show no association with this fibril type. Taken together, these data confirm that the primary sequence of the RNA aptamers is not the dominant process driving recognition. Moreover, the results suggest that RNA sequences may possess a generic ability to bind to fibril structures (at least of longer protein sequences).

a

DV1
5'- GGGCACGGCACGUAGGCAACUACUUCGUGGCUCACGCGUGAGUCUCUAUUACUAACCAU
AAAGACCGGAGAUUAUGAGUGCACGGGCGGCA -3'

NGGA1
5'- GGGAGAAGGCGGCGCGUAGGCGAGCUUUAUAGGACGCCCACUGGCCAGUAACGUCCGCC
UAUUCGUGGACGAUGCGCAC -3'

RVGP1
5'- GGGCACGGCACGUAGGCAACUAAAUUAUAUAACGGAUUUAAUACGAGCACCUCUCUUCC
UUAUUUCGGUUAUGAGUGCACGGGCGGC -3'

b

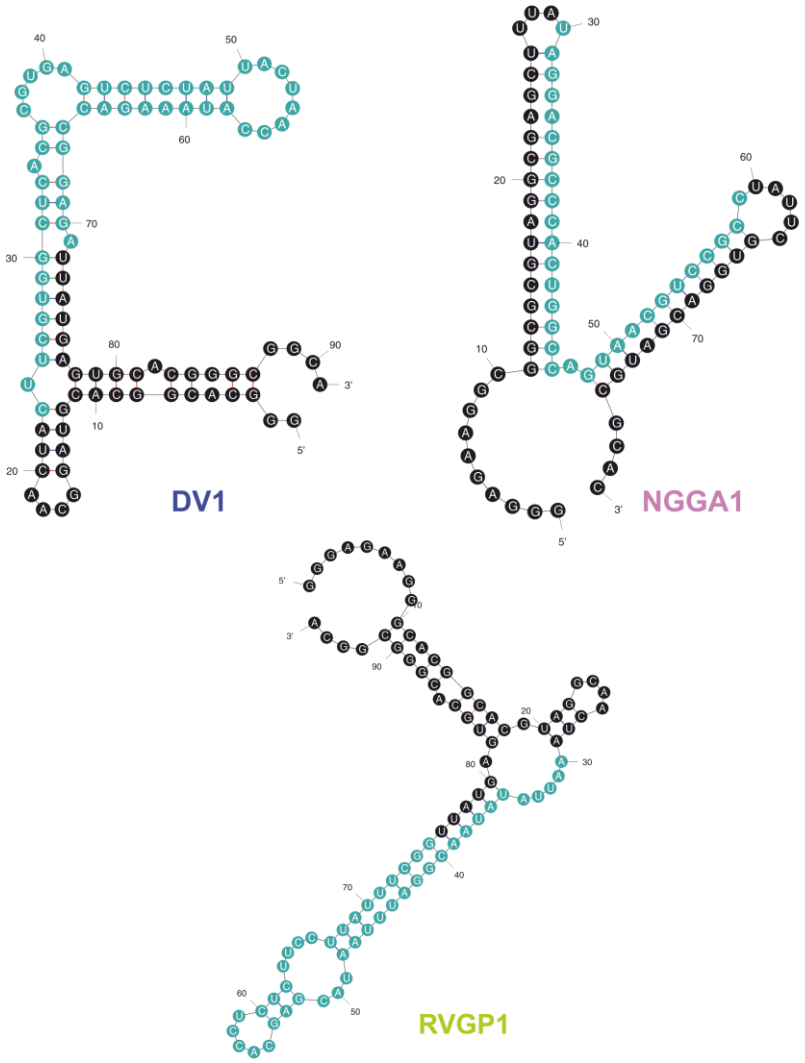

Figure 5.23 Control aptamer sequences. **(a)** RNA sequences of the three aptamers DV1, NGGA1[418] and RVGP1. **(b)** Mfold predicted secondary structure of the control aptamers. Randomised regions are highlighted in teal.

a

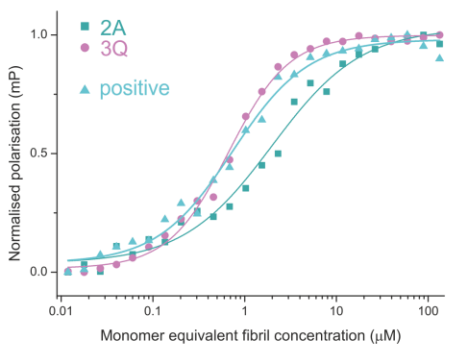

DV1

Aptamer	Fibril	k_d (μM)	n
DV1	2A	1.99 ± 0.25	0.90 ± 0.10
DV1	3Q	0.67 ± 0.03	1.32 ± 0.08
3Q1	3Q	0.73 ± 0.07	1.06 ± 0.11

b. i.

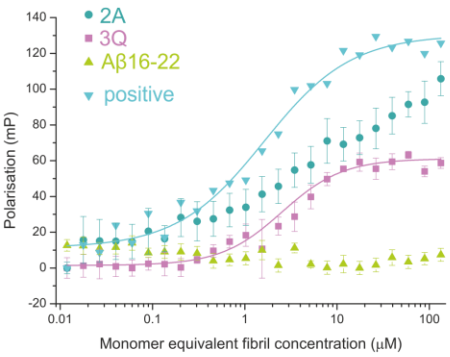

NGGA1

Aptamer	Fibril	k_d (μM)	n
NGGA1	2A	-	-
NGGA1	3Q	2.52 ± 0.36	1.31 ± 0.16
NGGA1	Aβ16-22	-	-
3Q1	3Q	1.61 ± 0.25	0.92 ± 0.14

b. ii.

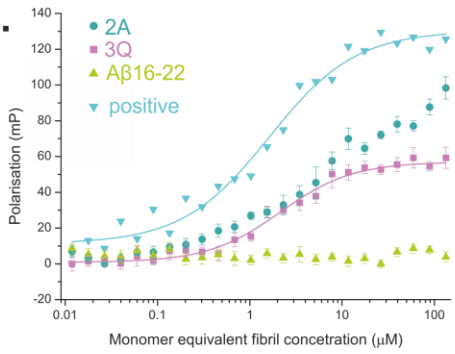

RVGP1

Aptamer	Fibril	k_d (μM)	n
RVGP1	2A	-	-
RVGP1	3Q	2.10 ± 0.19	1.10 ± 0.12
RVGP1	Aβ16-22	-	-
3Q1	3Q	1.61 ± 0.25	0.92 ± 0.14

Figure 5.24 Aptamer recognition of amyloid assemblies is not dependent on primary RNA sequence. **(a)** Aptamer DV1 binds to 2A (teal) and 3Q (pink) fibrils with similar affinity to positive control aptamer 3Q1 against 3Q fibrils (blue triangle). **(b)** FP analysis of aptamers NGGA1 **(i)** and RVGP1 **(ii)** against 2A fibrils (teal), 3Q fibrils (pink) and Aβ16-22 fibrils (green). Three replicates were averaged for each association and compared with a single replicate of positive control 3Q1 binding to 3Q fibrils (blue triangle). Data were fitted to a Hill equation (**Equation 2.5**), except in the case of NGGA1 and RVGP1 binding to 2A (**b. i.** and **b.ii**) where data did not reach a plateau over the tested concentration range and could not be fitted, and in binding to Aβ16-22 where there is no association. K_d and n values for each association are given in the accompanying table.

5.5.2 The effect of secondary structure of the RNA aptamer on fibril recognition

The aptamer sequences, studied in this thesis so far, display different secondary structural motifs. Extent of base pairing and the positions and sizes of loop and bulge regions (discussed in Chapter 3 for all the lead anti-Aβ40 aptamers – Section 3.7) within the predicted structures vary, and there is no clear conserved structural element that could explain the similar binding properties of the different aptamers against the amyloid targets. To investigate the role of the secondary structure of RNA in amyloid binding, a 118 nucleotide, unstructured RNA R118 (designed by Dr. Alexander Borodavka, University of Leeds) was analysed for amyloid fibril binding by FP. This sequence is comprised of 92% C and U repeats and predicted by Mfold analysis to form little stable secondary structure (**Figure 5.25**). The RNA molecule was synthesised commercially, from wild-type 2'OH NTPs and modified with a 5'-amino group. This was used for Alexa488 labelling with an Alexa Fluor® 488 5-sulfodichlorophenol ester (Section 2.6.6), which was also carried out by Dr. Borodavka.

Interestingly, the results of the FP analysis showed that the RNA sequence R118 was able to bind to all three of the Aβ40 fibril types (2A, 3Q and *de novo*) with comparable affinity to each other (1.4 – 4.6 μM) and to that of the cognate RNA aptamers 2A1, 2A417, 3Q1 and 3Q319. R118 also displays the same difference in cooperativity previously observed for aptamers binding 3Q/2A fibrils *versus de novo* Aβ40 fibrils (Table inset in **Figure 5.26**). Again, R118 did not bind Aβ16-22 fibrils, mirroring the behaviour of all other aptamers analysed. These results clearly indicate that RNA possesses generic amyloid binding ability that is not dependent on its primary sequence or secondary structure. The amyloid epitope recognised by the RNA is currently unclear, but is not the simple cross-β spine of the fibrils as demonstrated by the lack of association, of all aptamers studied, to Aβ16-22 assemblies.

a

R118

5'- AGACCUAUUCUCUUUUUCUCUCCUUUUCCCCCCUGUUGCUUUAUUUUCCUUCUUUGCCU
UUUUCUCUCUUUUUUUUUCUUUUUUCCCUUUCUGCUUUCCUCCCCUAUUCUCCCCUCUU -3'

b

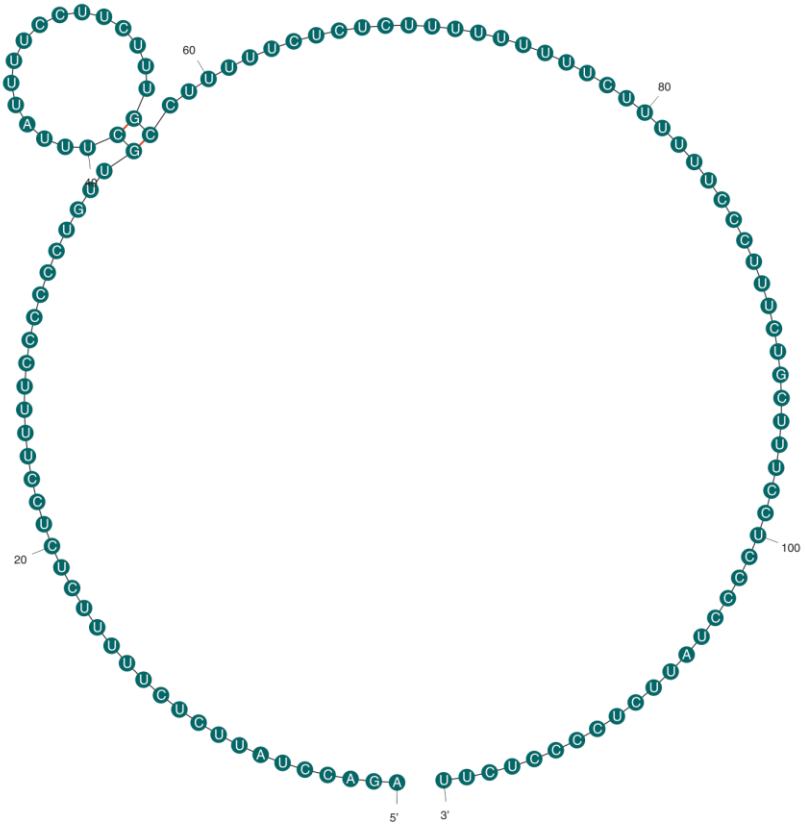

Figure 5.25 Sequence and structure of R118 aptamer. **(a)** RNA sequence of unstructured RNA molecule R118. **(b)** The Mfold predicted secondary structure for the RNA sequence, R118.

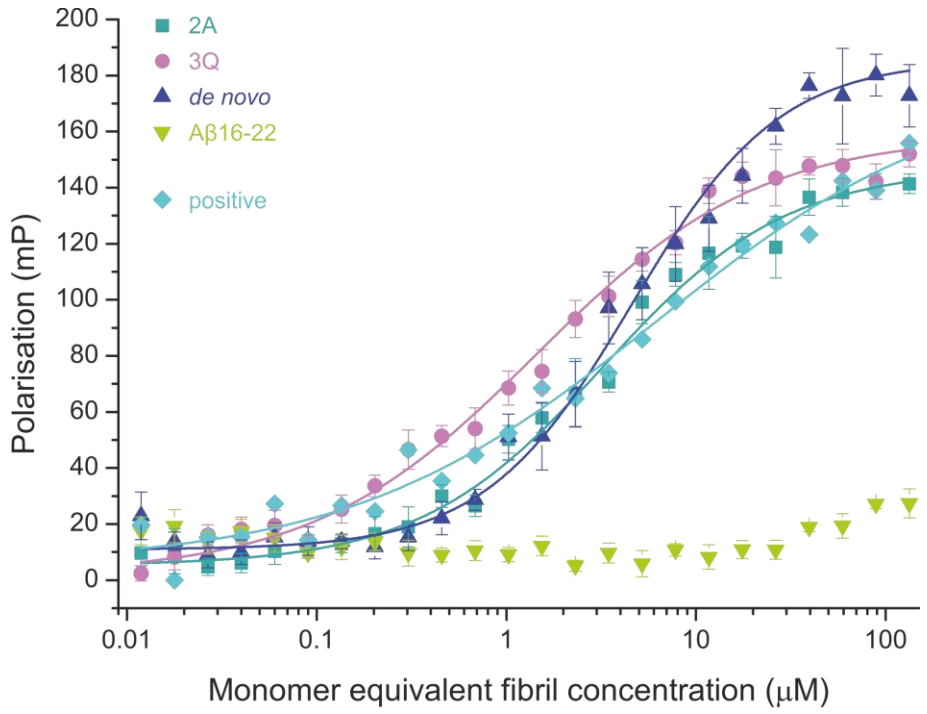

Aptamer	Fibril	k_d (μM)	n
R118	2A	3.24 ± 0.32	0.90 ± 0.08
R118	3Q	1.44 ± 0.18	0.74 ± 0.07
R118	de novo	4.58 ± 0.55	1.12 ± 0.09
R118	Aβ16-22	n/a	n/a
3Q1	3Q	6.10 ± 2.42	0.54 ± 0.10

Figure 5.26 Unstructured RNA molecule, R118, can associate with amyloid fibrils. FP analysis demonstrates binding of R118 to 2A (teal), 3Q (pink) and *de novo* Aβ40 fibrils (blue), as well as a lack of recognition of Aβ16-22 fibrils (green). Data are compared with a positive control aptamer 3Q1 association with 3Q fibrils (pale blue diamonds). Dissociation constants and n values are given for each interaction, derived from a Hill fit of the data (**Equation 2.5**).

5.5.3 Analysing the effects of polyanions on fibril recognition

Glycosaminoglycans are highly negatively charged linear polysaccharides made up of repeat disaccharide units of an amino sugar (N-acetylated or N-sulphated hexosamine) and either a uronic acid or galactose (**Figure 5.27 a**)[641]. There are two types of GAGs: non-sulphated, such as hyaluronic acid, and sulphated GAGs that include heparin, heparan sulphate and chondroitin sulphate, amongst others[642].

GAGs have been found to be associated with amyloid assemblies isolated from AD brains[643-645] and many, if not all, extracellular amyloid plaques[646]. Indeed, many *in vitro* studies have shown GAGs to play important roles in accelerating fibril formation[329, 647-650], stabilising fibril structures[651, 652] and altering the resultant fibril morphology[653]. Heparin is the most highly sulphated GAG and has been the focus of most studies into GAG associations with amyloid[646]. Heparin has been shown to accelerate the rate of fibril formation by several amyloid proteins, including tau[654, 655], α-syn[656], human islet amyloid polypeptide (hIAPP)[657], β_2m[658, 659] as well as Aβ[648-650]. It is thought that heparin is particularly influential in amyloid formation because of its high sulphate content. This sulphate moiety has been shown to be critical in the Aβ-GAG interaction[649, 660, 661], supporting the idea that electrostatics are important in the association of GAGs with amyloid fibrils. Precisely how Aβ fibrils and GAGs interact is currently unknown, although residues 13-16 (HHQK) are predicted to be involved, consistent with the nature of non-amyloid GAG binding proteins, where clusters of basic residues are important[642, 662]. Interestingly, work by Madine *et al.*[663] demonstrated differential heparin binding ability by the two Aβ40 morphologies used as selection targets in this work, 2A and 3Q. LMW heparin (average MW = 4.6 kDa) was shown to associate much more weakly with 2A fibrils than 3Q. ssNMR of the 3Q-LMW heparin interaction indicated that the chemical shift of residues in the unstructured N-terminus and apices of the triangular morphology were most perturbed by heparin, indicating these areas as potential binding sites (discussed in detail later, Section 5.8, **Figure 5.35**). Very few chemical shifts were seen for the 2A-heparin interaction leading to the conclusion that the heparin interaction is weak in this case.

A competition FP experiment was set up to determine whether the fluorescently-labelled aptamers could be dissociated from their fibril-bound state, by titration with an increasing concentration of LMW heparin (**Figure 5.27 a**), to deduce whether the two polyanions share similar binding properties and epitopes. The results showed that the four aptamers 2A1, 2A417, 3Q1 and 3Q319 were each competed from their fibril-bound state (with both 2A and 3Q fibrils) by LMW heparin (**Figure 5.27 b** and **c**). Heparin was shown to readily dissociate the aptamers from 3Q fibrils, producing a sigmoidal response with a steep transition, indicative of a specific competition for the aptamer binding site. Surprisingly, given that heparin has been previously shown to associate only very weakly with 2A fibrils[663], the same dissociation profile, induced by titration with LMW heparin, was demonstrated for aptamers from this fibril type, indicating that heparin must be competing for the aptamer epitope in the same way as seen against 3Q fibrils. The dissociation constants for heparin binding to the fibrils was determined as ~2-4 μM by these

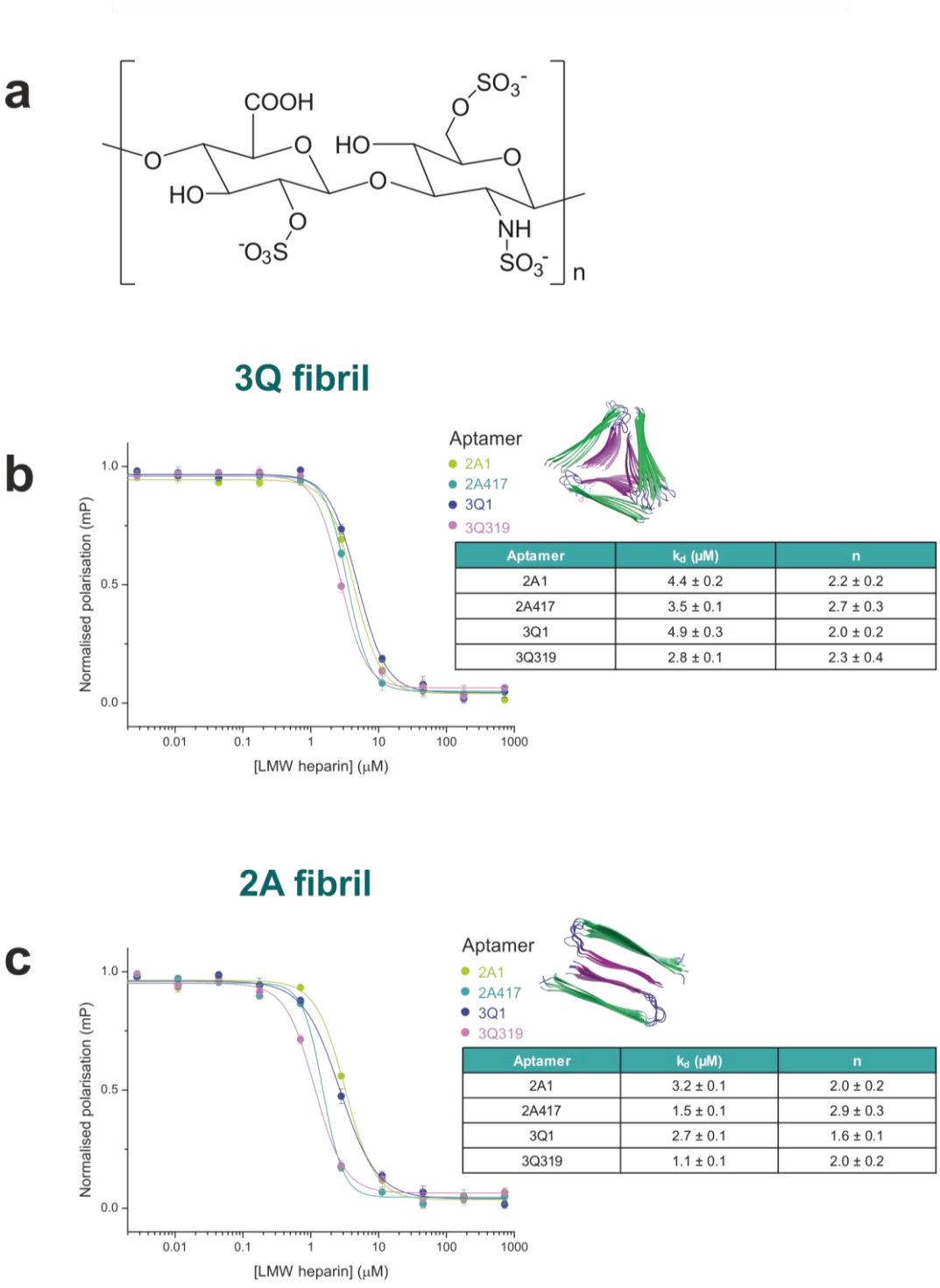

Aptamer	k_d (μM)	n
2A1	4.4 ± 0.2	2.2 ± 0.2
2A417	3.5 ± 0.1	2.7 ± 0.3
3Q1	4.9 ± 0.3	2.0 ± 0.2
3Q319	2.8 ± 0.1	2.3 ± 0.4

Aptamer	k_d (μM)	n
2A1	3.2 ± 0.1	2.0 ± 0.2
2A417	1.5 ± 0.1	2.9 ± 0.3
3Q1	2.7 ± 0.1	1.6 ± 0.1
3Q319	1.1 ± 0.1	2.0 ± 0.2

Figure 5.27 LMW heparin competes for the aptamer binding site. **(a)** Structure of a single disaccharide unit of heparin. **(b)** Competition fluorescence polarisation showing dissociation of aptamer 2A1 (green), 2A417 (teal), 3Q1 (blue) and 3Q319 (pink) from 3Q fibrils, as a function of LMW heparin concentration. **(c)** As **(b)** but for 2A fibrils. Three replicates were averaged for each competition and the data fitted to a Hill equation (**Equation 2.5**). K_d and n values are given for all competitions in the accompanying tables.

competition assays, tighter than that previously estimated for LMW heparin and 3Q fibrils (34 μM)[663], and the average n value of 2.3 indicates some cooperativity. The possibility that the heparin was competing for aptamer binding by an association with the RNA itself was unlikely as the FP signal returns to the value of free labelled RNA (raw data shown in **Figure 5.28 a**). This possibility was further ruled out using a gel-shift assay, where RNA pre-incubated with LMW heparin ran in line with free RNA samples, suggesting no interaction (**Figure 5.28 b**).

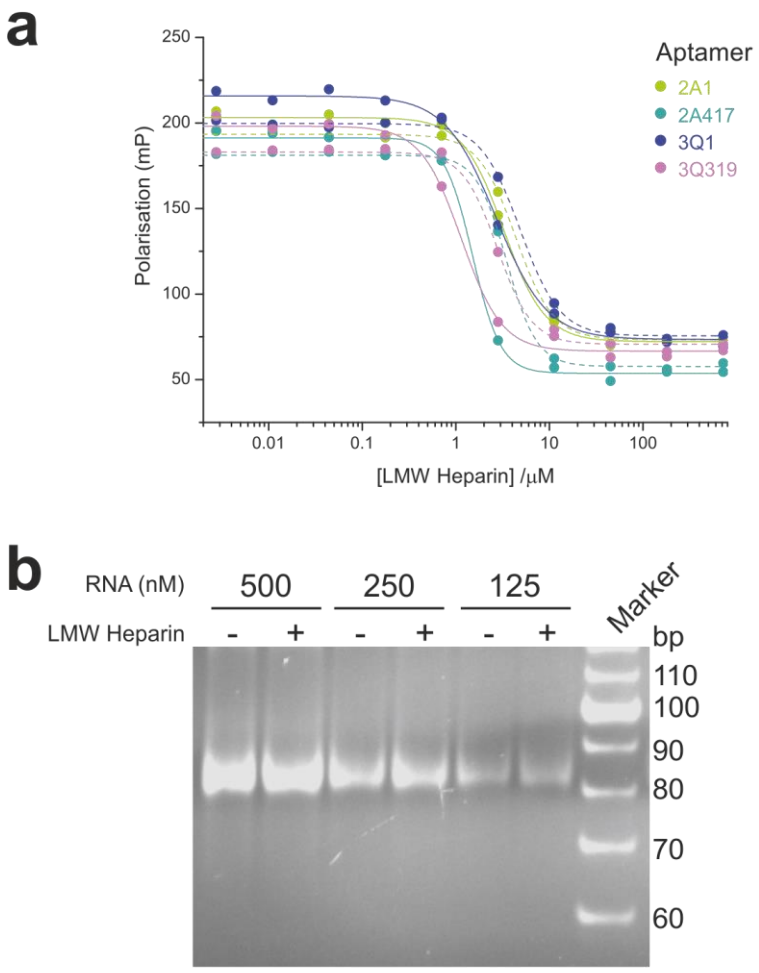

Figure 5.28 RNA dissociation by heparin is due to competition for fibril epitopes. **(a)** Raw data from **Figure 5.27** demonstrating the FP signal plateau after dissociation which is consistent with free fluorescent RNA in solution. Aptamer dissociation from 2A fibrils (solid lines) and 3Q fibrils (dotted lines) are shown for each aptamer. Aptamer colour codes are the same as **Figure 5.27** and fitted to a Hill equation in the same way. **(b)** Gel-shift assay at three RNA concentrations (500, 250 and 125 nM – as indicated). Samples plus or minus 50 μM LMW heparin are shown for each RNA concentration.

As interactions of heparin with amyloid fibrils are thought to be electrostatically driven[649, 660], electrostatics may also be important in the interactions of RNA. It was postulated that if aptamer binding was simply due to electrostatic contacts with fibrils, titration of monovalent salt of the equivalent ionic strength as LMW heparin would also perturb the binding in the same manner. The ionic strength of LMW heparin was estimated (Section 2.8.7) based on the average of eight disaccharide units in LMW heparin and four negative charges per disaccharide unit. This calculation indicated that 5 mM NaCl has an equivalent ionic strength as 10 μM LMW heparin. However, titration of 50 mM NaCl was unable to dissociate the aptamer 2A1 from its complex with 2A fibrils (**Figure 5.29 a**). Indeed, the aptamer was only shown to dissociate at salt concentrations exceeding 600 mM, with a much shallower dissociation profile, consistent with non-specific competition. These data suggest, therefore, that the interaction of LMW heparin and RNA with amyloid fibrils cannot be entirely due to simple electrostatic interactions. Rather, the spacing and multivalancy of the negative charges of these polyanionic chains must play a role in recognition. To test this further, titration of the equivalent concentration of the non-sulphated GAG, hyaluronic acid, (HA- **Figure 5.29 b**) against both the 2A1 aptamer-2A fibril and the 3Q1 aptamer-3Q fibril complexes (**Figure 5.29 c. i.**) was carried out, as this is the only GAG that completely lacks sulphate groups[641]. It was employed as a control GAG in these titration experiments to determine whether the periodic arrangement of the negative charges in heparin were responsible for the displacement of the aptamers. Interestingly, HA was not able to dissociate the aptamers, providing further evidence that it is the spacing of the negatively charged sulphates that gives rise to the affinity of LMW heparin to amyloid. A further control experiment with an increasing concentration of Na_2SO_4 was conducted to ensure the competition was not a consequence of the sulphate moiety and thus owing to the structural arrangement on the polymer. Accordingly, 2.5 M Na_2SO_4 was unable to displace the aptamers (**Figure 5.29 c. ii.**). This result also suggests that ionic strength alone cannot account for the aptamer displacement seen by high concentrations of NaCl (the Na_2SO_4 solution with much higher overall ionic strength was unable to cause dissociation) and the interaction, therefore, may be anion specific, but further work is required to confirm this.

Taken together the data presented indicate that a generic amyloid binding model exists for both RNA aptamers and LMW heparin that, in the case of the RNA, could be driven by the negatively charged phosphodiester backbone, analogous to the periodic, negatively charged sulphate-driven interaction demonstrated for LMW heparin. If this were the case, it would explain why primary sequence and secondary structure of the RNA apparently have little effect on the fibril binding ability of RNA.

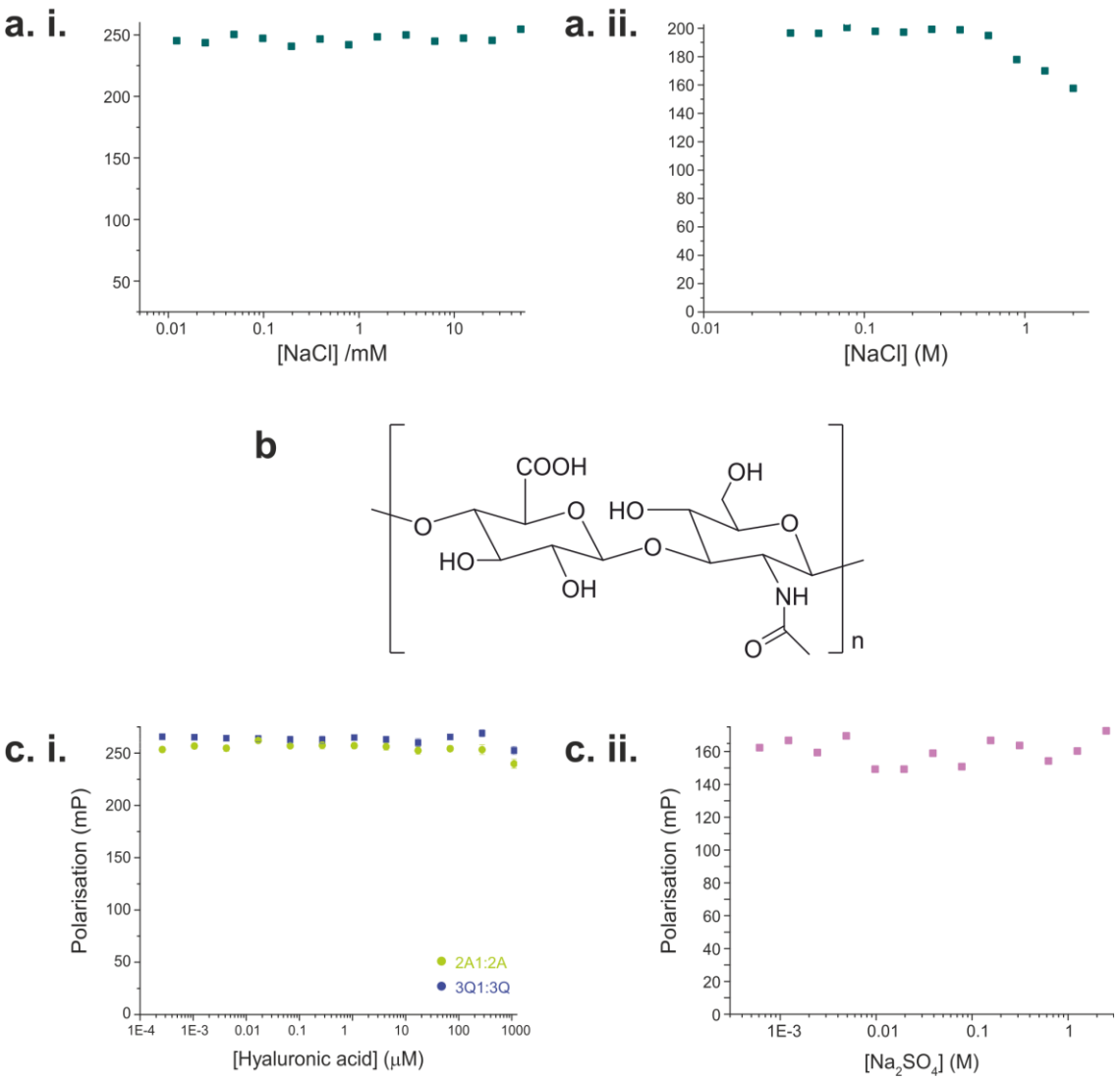

Figure 5.29 Spacing of the sulphate moieties in GAGs are required for aptamer dissociation from amyloid fibrils. **(a)** Competition FP showing aptamer 2A1 is not displaced from the complex with 2A fibrils by 50 mM NaCl **(i)** and only begins to dissociate at concentrations exceeding 0.6 M **(ii).** **(b)** Structure of a single disaccharide unit of hyaluronic acid (HA). **(c. i.)** Competition FP of aptamer 2A1 and 2A fibrils (green) and 3Q1 and 3Q fibrils (blue) upon titration of with HA. **(c. ii)** Competition FP of the aptamer 2A1:2A fibril complex (pink) with Na_2SO_4.

5.6 Assessing aptamer sensitivity for amyloid with *in vitro* cell imaging

Given the amyloid binding propensity so far demonstrated by the anti-Aβ40 aptamers selected in this thesis, it was next investigated whether the anti-Aβ40 fibril aptamers are able to detect amyloid in cell culture models, with the potential for further development as optical imaging tools.

Previous work in the Radford laboratory[664-668] has shown that fibrils formed from β_2m, α-syn and other disease-associated amyloid fibrils, interact with, and disrupt, lipid membranes. The fibril-membrane association can be visualised via confocal microscopy, by co-localisation of fluorescently-labelled amyloid fibrils and membrane-specific fluorescent dyes. This approach has previously been used to monitor both the plasma membrane association by amyloid fibrils and the internalisation of fibril fragments via the endocytic pathway, both of which occur in a fibril length dependent manner[664]. It is thought that this internalisation of amyloid fibrils by cells leads to perturbation of the endolysosomal pathway, altering the trafficking of lysosomal membrane proteins and disrupting protein degradation processes[666]. This is supported by the observation that the incubation of fragmented fibrils with human cells has been shown to lead to a decrease in the cellular reduction of the tetrazolium dye 3-(4,5-dimethylthiazol-2-yl)-2,5-diphenyltetrazolium bromide (MTT)[666], a substrate commonly used to measure cell viability[669], that is indicative of lysosomal function. However, the MTT reduction induced by amyloid fibrils has recently been shown not to correlate with cell viability, as determined through cellular ATP assays[669]. It is therefore suggested that amyloid fibrils impart an effect on intracellular trafficking pathways, which does not result in cell death, yet may play a role in amyloid diseases.

Here, the SH-SY5Y cells (a human neuroblastoma cell-line, commonly used to study neuronal function[670]) were incubated with a mixture of fluorescently-labelled α-syn fibrils and Alexa488 aptamers, in order to assess a) whether the aptamer-fibril complex could be visualised using live-cell confocal microscopy and b) whether the incubation of aptamers alters the ability of the amyloid fibrils to associate with membranes and cause cellular defects. TMR-labelled S129C α-syn monomers (kindly provided by Dr. Matthew Jackson, University of Leeds) were mixed 1 in 10 with wild-type α-syn monomers and used to form fibrils at a final protein concentration of 300 μM, in 20 mM Tris-HCl, 100 mM NaCl buffer,

pH 7.5 (Section 2.4.3). The fibrils were fragmented using a home-built precision stirrer (Section 2.4.3) for 24 h, to give a final average length of 300 - 400 nm, measured using AFM (kindly performed by Dr. Matthew Jackson) using methods as described[664]. Labelled fibril samples were then incubated for 2 h, at a final monomer-equivalent protein concentration of 80 μM, with 500 nM Alexa488 labelled aptamer 3Q319. The mixture was then added to SH-SY5Y cells at a final protein concentration of 1 μM (6.25 nM aptamer concentration) and incubated overnight (18 h – Section 2.9.3). The localisation of the amyloid-fibrils and aptamers was then visualised using live-cell confocal microscopy (all cell culture and imaging work was conducted with Dr. Jackson, Section 2.9).

Cells incubated with labelled α-syn fibrils alone demonstrate both an association with the plasma membrane and internalisation to lysosomes, which can be seen by the co-localisation of the TMR-labelled fibrils with membrane specific dyes CellMask and Lysotracker, respectively (**Figure 5.30** and **Figure 5.31,** α-syn fibrils alone panel). Samples where fibrils were pre-incubated with Alexa488 aptamers demonstrate complete co-localisation on the plasma membrane surface and, in some instances, within the lysosomes (**Figure 5.30** and **Figure 5.31**, aptamer + α-syn fibrils). Importantly, fluorescent aptamer could not be detected in the background (**Figure 5.30** and **Figure 5.31**, aptamer alone) and was detected only when associated with the fibrils.

In order to assess whether pre-incubation with aptamer alters the fibril internalisation process, and the resultant perturbation of lysosomal function, MTT and ATP assays were conducted (by Dr. Jackson, Section 2.9.2). The results indicate that aptamer incubation had no effect on the MTT reduction induced by the α-syn fibrils (**Figure 5.32 a**). The aptamer also imparted no further effect on cell viability, as assessed by cellular ATP levels (**Figure 5.32 b**). Together, these data and the confocal imaging indicate that fluorescently-labelled anti-fibril aptamer 3Q319, and presumably other aptamer sequences that have been shown to bind to fibrils to similar extents *in vitro* (although not tested here), could indeed be developed as sensitive amyloid detection reagents in cell assays. The amyloid-aptamer complex was visualised at a low final RNA concentration (6.25 nM used in this instance) and demonstrated no background interactions with other cell components.

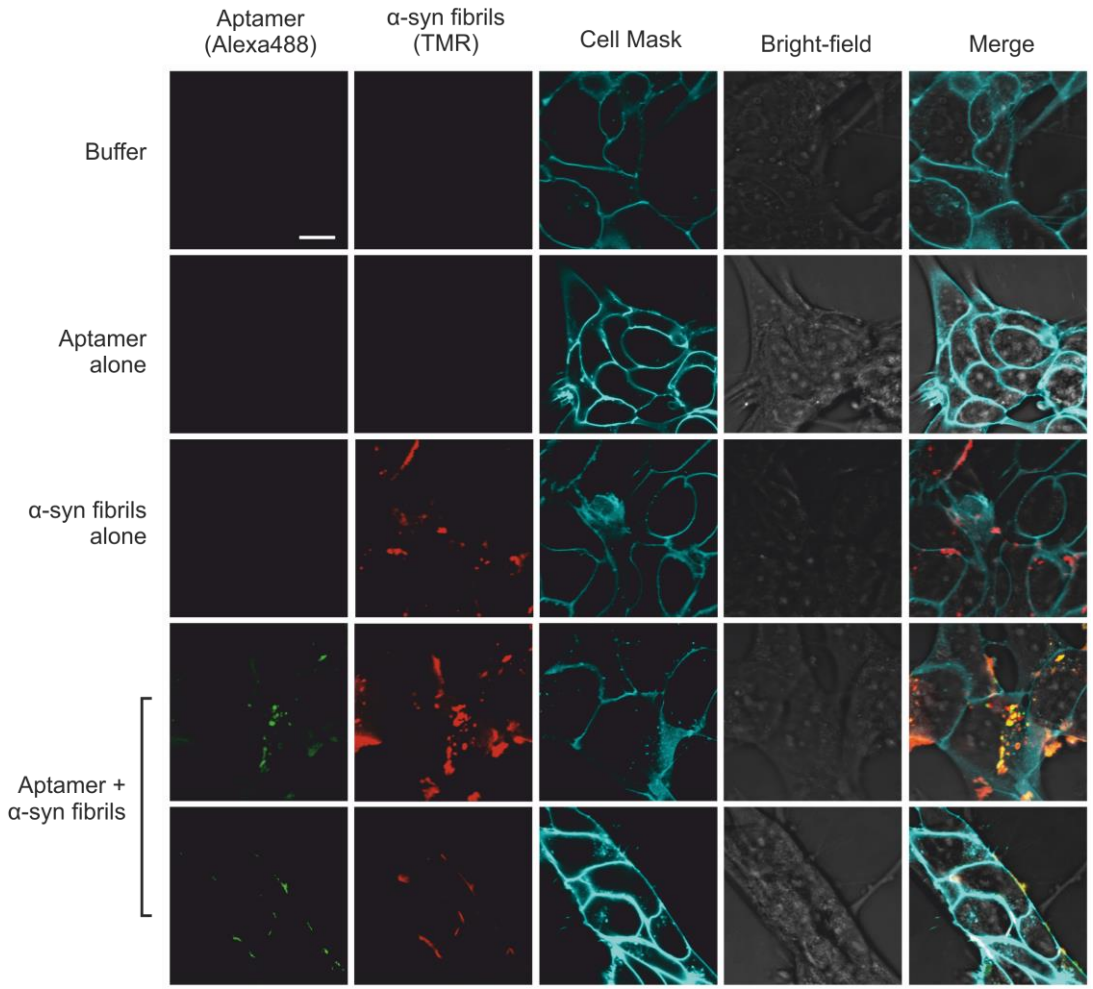

Figure 5.30 Alexa488 labelled aptamer 3Q319 demonstrates co-localisation with TMR-labelled α-syn fibrils and association with the plasma membrane. SH-SY5Y cells were incubated overnight with 1 μM (monomer equivalent) fragmented, TMR-labelled α-syn fibrils, which had been previously incubated (2 h) with Alexa488 aptamer 3Q319. Cells were also stained with the plasma membrane specific dye CellMask and cell associated fluorescence was visualised by live-cell confocal microscopy. TMR, Alexa488, CellMask and phase-contrast (bright-field) images are shown individually and merged. In the merged image, yellow indicates co-localisation of aptamer (Alexa488) and α-syn fibrils (TMR), white indicates co-localisation of aptamer, fibril and the CellMask dye. Scale bar = 10 μM. Experiments performed with Dr. Matthew Jackson.

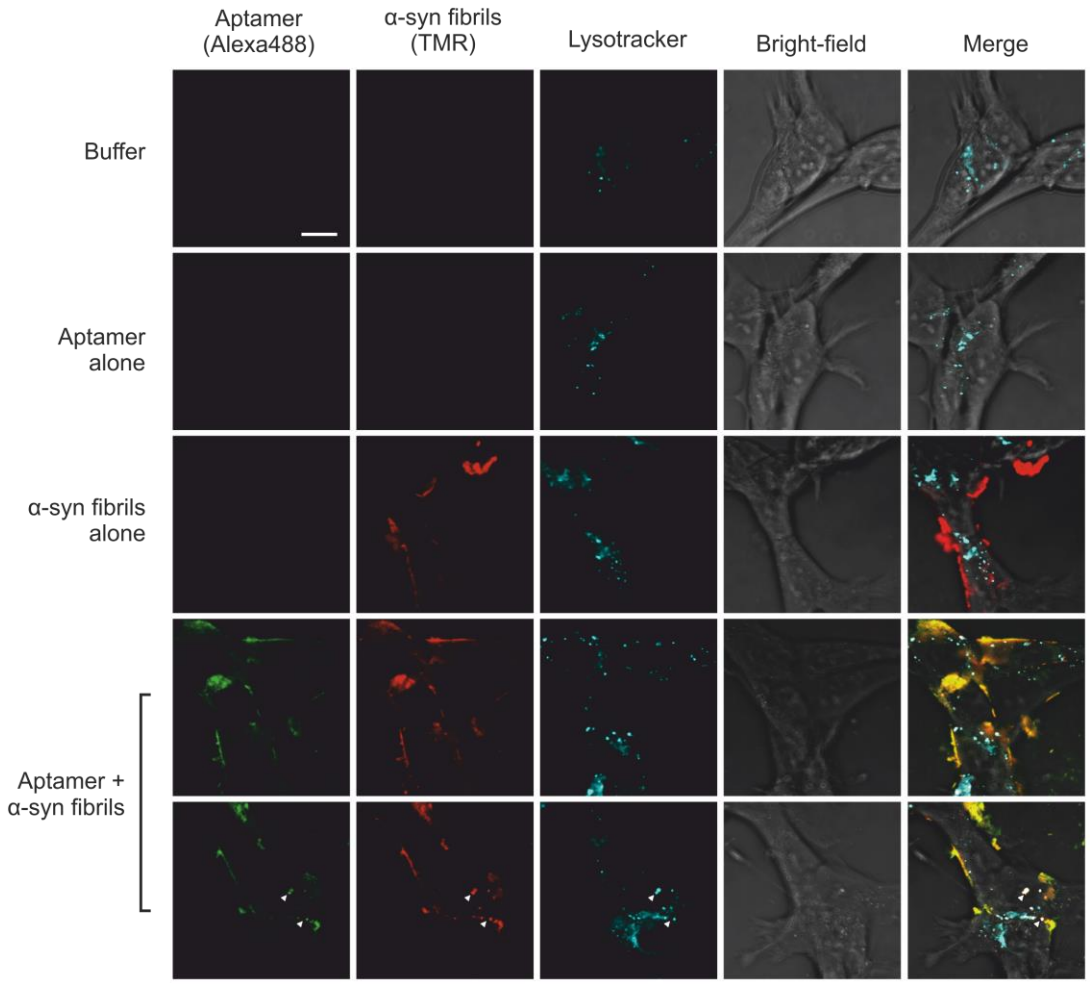

Figure 5.31 Alexa488 labelled aptamer 3Q319 demonstrates co-localisation with TMR-labelled α-syn fibrils and association with the lysosomes. SH-SY5Y cells were incubated overnight with 1 μM (monomer equivalent) fragmented, TMR-labelled α-syn fibrils, which had been previously incubated (2 h) with Alexa488 aptamer 3Q319. Cells were also stained with the lysosome-specific dye Lysotracker and cell associated fluorescence was visualised by live-cell confocal microscopy. TMR, Alexa488, Lysotracker and phase-contrast (bright-field) images are shown individually and merged. In the merged image, yellow indicates co-localisation of aptamer (Alexa488) and α-syn fibrils (TMR). Areas where co-localisation of aptamer, fibril and the Lysotracker dye can be seen are further indicated with white arrows. Scale bar = 10 μM. Experiments performed with Dr. Matthew Jackson.

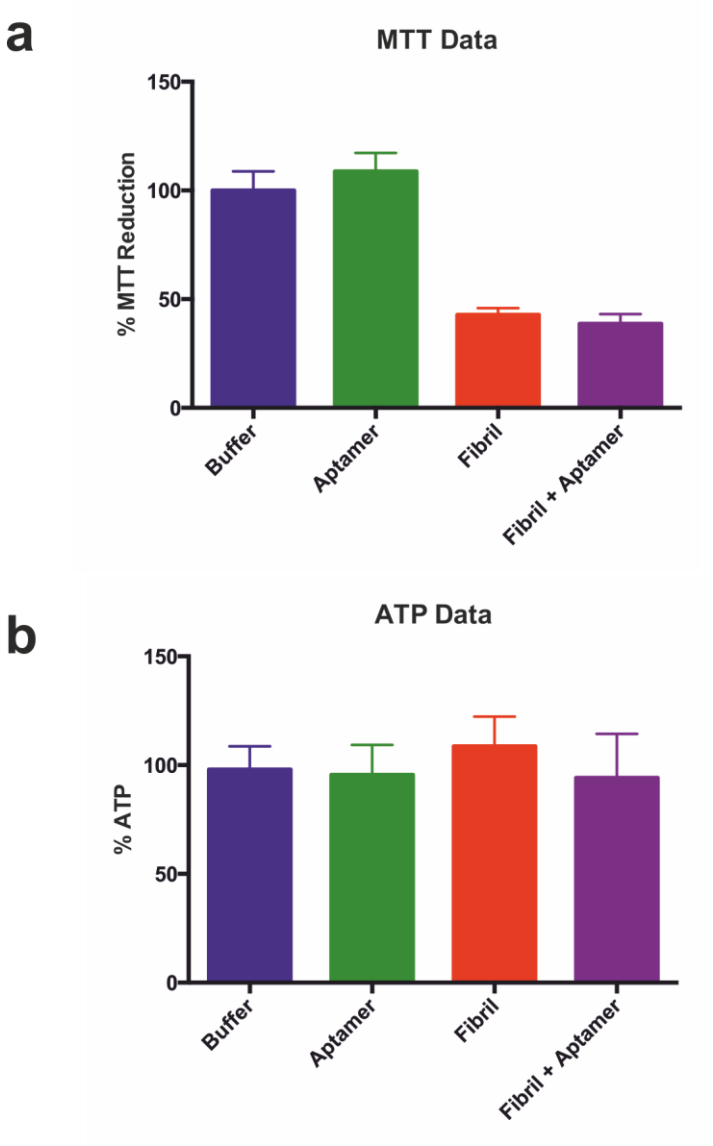

Figure 5.32 Aptamer 3Q319 has no effect on fibril induced cell defects. SH-SY5Y cells were incubated for 24 h in the presence of 6.25 nM Alexa488 3Q319 aptamer (Aptamer - green), 1 μM TMR-labelled, fragmented α-syn fibrils (Fibril - red) or pre-incubated samples of aptamer and fibrils, mixed at the same final concentration (Fibril + Aptamer – purple). The reduction of MTT **(a)** or reduction of cellular ATP levels **(b)** were assayed. The percentage of MTT reduction and the ATP concentration relative to control cells treated with fibril formation buffer (Buffer – blue) are given. Data courtesy of Dr. Matthew Jackson.

5.7 Evaluation of the effect of aptamer binding on fibril formation

It is commonly known that polyanionic molecules, such as GAGs[649, 650, 654, 656, 657, 659], can influence the aggregation pathways of amyloidogenic proteins and, in some cases, are necessary to initiate such reactions[654, 671, 672]. Therefore, the effect of the RNA aptamer sequences selected in this thesis, on the formation of amyloid by Aβ40, was assessed.

Aptamers 2A1, 3Q1 and M1 (the most frequently occuring aptamer sequences isolated from the anti-2A fibril, anti-3Q fibril and anti-Aβ40 monomer selections, respectively) were transcribed *in vitro* from 2'OH dNTPs and purified (Section 2.6.4). Aptamers were then mixed at a 1:1 molar ratio with monomeric Aβ40 (final concentrations 10 μM) in 25 mM sodium phosphate buffer, pH 7.5, in the presence of 10 μM Niad 4; an amyloid specific dye that exhibits increased fluorescence upon amyloid binding and, therefore, can be used to monitor amyloid fibrillation kinetics[673]. Assays also included the presence of an RNase inhibitor, owing to the use of nuclease-susceptible 2'OH aptamers (Section 2.8.6). Assays were set up in triplicate. The morphology of resultant aggregates was also assessed using TEM analysis.

The results of these experiments (**Figure 5.33**) showed that, under these experimental conditions and in the absence of aptamer, Aβ40 forms amyloid fibrils with an average lag time of 23.7 ± 1.4 h. The fibrils display a typical long, straight morphology by negative stain TEM (**Figure 5.33** – positive). Incubation with anti-fibril aptamers 2A1 and 3Q1 results in a similar overall increase in Niad 4 fluorescence, consistent with fibril formation, with no significant effect on the average lag times (22.2 ± 2.2 h and 18.5 ± 0.5 h, respectively - **Figure 5.33 d**). Amyloid fibrils of typical long straight morphology were observed by TEM analysis, however, a large population of amorphous aggregate (that was not observed in Aβ40 alone control samples) was seen in all samples where 2A1 or 3Q1 aptamers were present. Interestingly, in the case of the anti-Aβ40 monomer aptamer M1, two of the three replicates showed no increase in Niad 4 fluorescence over 60 h and only amorphous aggregate by TEM, indicating possible inhibition of fibril formation by this aptamer. The TEM analysis of the single replicate that did display increased Niad 4 fluorescence, with a comparable lag-time to the positive control samples (25.2 h compared with 23.7 h - **Figure 5.33 d**), again contained a large proportion of amorphous aggregate. Based on these data, it is possible that incubation of the anti-Aβ40 aptamers may have an effect on fibril formation by Aβ40,

especially in the resultant morphology of aggregates. However, further work at excess aptamer concentrations may be necessary to confirm the inhibitory effect seen by aptamer M1.

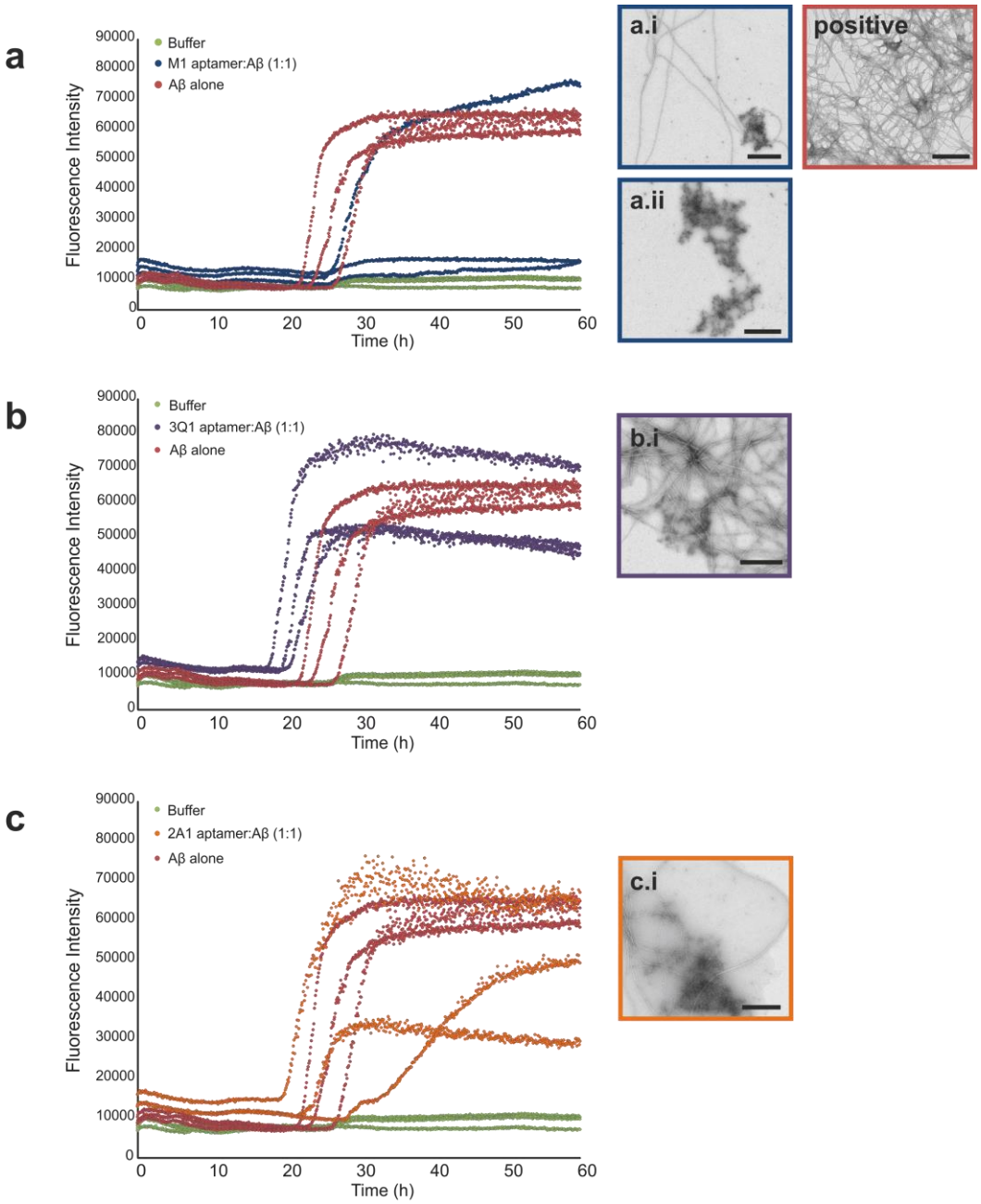

d

Aptamer	Average lag time (h)
M1	25.2
3Q1	18.42 ± 0.51
2A1	22.18 ± 2.22
No aptamer (positive)	23.77 ± 1.41

Figure 5.33 Assessment of the effects of aptamer incubation on Aβ40 fibril formation and morphology. Aβ40 fibril formation kinetics were monitored by Niad 4 fluorescence over 60 h, in 25 mM sodium phosphate, pH 7.5, at a final peptide concentration of 10 μM. 2'OH aptamer samples M1 **(a)**, 3Q1 **(b)** and 2A1 **(c)** were added at a final concentration of 10 μM and resultant Niad 4 fluorescence profiles are shown in blue, purple and orange, respectively. 10 μM Aβ40 alone (positive control) samples are shown in red and samples with 10 μM Niad 4 in fibril formation buffer are shown in green, in each case. Representative TEM images are given for each experimental condition assayed. In **(a)** a representative TEM is given for both the single replicate that showed enhanced Niad 4 fluorescence **(a. i)** and from a sample replicate that showed full inhibition of fibril formation **(a. ii)**. In **(b)** and **(c)**, representative TEM images from samples incubated in the presence of 3Q1 and 2A1, respectively, are given. Scale bars = 500 nm. **(d)** The average lag times for each condition were calculated by extrapolation of the slope of the elongation phase, of each replicate, to the time on the x-axis.

5.8 Discussion

Development of specific amyloid recognition molecules remains a major unmet need in diagnosis and therapeutic intervention for the many disorders related through this aberrant protein self-assembly reaction. Detailed knowledge of the structures and mechanisms underlying amyloid disorders also remains scarce, despite extensive research efforts, which hinders the rational design of such molecules. In this chapter, the specificity of RNA aptamers selected against two structurally distinct amyloid fibrils of Aβ40 was discussed, in an attempt to characterise ligands specific to single amyloid morphologies. It was found that, despite different RNA sequences being represented in the two selections, the resulting aptamers were able to recognise both assemblies with almost equal affinity. This cross-reactivity was extended to further amyloid fibril morphologies, assembled from both Aβ40 and the unrelated protein sequence α-synuclein. The reactivity was shown to be largely RNA sequence independent, but did depend on protein sequence to some extent, as shown by a lack of aptamer affinity for two simple, cross-β containing, fibrils formed from Aβ16-22 and ccβ-p.

A tendency towards generic amyloid fibril binding by RNA aptamers has been demonstrated by several other groups and in previous work in our laboratory. Bunka *et al.*[483] demonstrated that aptamer WL-2, raised against a worm-like β_2m fibril morphology, was able to react with three further forms of β_2m fibrils, as well as fibrils formed from unrelated protein sequence hen egg lysozyme. This aptamer was, however, not able to recognise fibrils from Aβ40, apomyoglobin or transthyretin, although the dot-blot assay used

provided only a qualitative assessment of binding. The results further the notion that amyloid assemblies share common epitopes, but protein sequence is influential in RNA binding. An RNA aptamer selected against scrapie-associated fibrils of the prion protein (PrP), isolated from hamster brain, was shown to bind both the target fibrils and a β-sheet rich oligomeric variant PrP-β, which also assembles into cross-β fibres[476]. In the case of anti-Aβ40 aptamers, Chapter 4 discussed the common theme of preferential fibril binding by aptamers raised against immobilised monomeric Aβ40 or its oligomeric assemblies, which was replicated in the data presented here (**Figure 5.22**). The anti-Aβ40 aptamer sequences generated by Rahimi and colleagues[494] which did not associate with their cognate oligomeric target, were shown to bind to fibrils from Aβ40, IAPP, lysozyme, prion 106-126 and, more weakly, calcitonin and insulin. Again this work further supports the data presented here, that aptamer recognition of fibrillar assemblies involves generic features of fibrils and/or RNA aptamers, and raising RNA aptamers against a specific fold is thus difficult to achieve.

In this work, the affinity of RNA aptamers for amyloid was assessed from a structural perspective. One obvious conserved feature of amyloid is the arrangement of β-strands in the cross-β architecture and this was perhaps the most likely candidate for providing a universal epitope for an RNA interaction. However, by use of model amyloid fibrils (from Aβ16-22 and ccβ-p) it was clear that the cross-β motif was not sufficient for binding. Comparison of these model amyloid structures, with the fibrils shown to have reactivity with the RNA (Aβ40 polymorphs and α-syn), is hindered in that there remains a lack of structural data for some of these assemblies, namely *de novo* Aβ40 and α-syn.

One commonality between the Aβ40 fibrils and those formed from α-syn, is the presence of disordered termini (residues 1-8 in 2A and 3Q fibrils and 1-30/109-140 in α-syn[611, 623]). In the seeded Aβ40 fibrils, the disordered N-terminus decorates the surface of the fibril (**Figure 5.34**) and, based on the proposed stacking of the core, rigid region of α-syn[611] (**Figure 5.11**), is likely to present in a similar manner on these fibrils. It is possible that a generic binding site could lie in these regions and evidence from binding of LMW heparin supports this hypothesis. A model for the LMW heparin-3Q fibril interaction determined using ssNMR by Madine *et al*. indicates that the flexible N-terminus is likely to be involved in the GAG binding epitope, although other binding sites were possible, based on their data[663]. Residues E3, R5 and H6 underwent significant chemical shift changes when incubated with excess LMW heparin, as well as residues E22, S26, N27 and K28, all of which are located in the turn of the β-strands, which lie in close proximity to the N-terminal region, due to the triangular geometry of this structure (**Figure 5.35 a** and **b**). As LMW heparin is

able to completely dissociate the RNA aptamers 2A1, 2A417, 3Q1 and 3Q319 from their bound state on this fibril, it suggests that RNA shares this heparin binding epitope. The fact that several of the amino acids involved in the flexible N-terminus of Aβ40 fibrils are positively charged, could be important, as the nature of the interaction is most likely electrostatic, based on the inability of the uncharged GAG, hyaluronic acid, to dissociate the same aptamers (**Figure 5.29**). As α-syn also possesses several positively charged residues in its flexible N-terminal region (5 lysines within the first 30 amino acids –**Figure 5.11**), it is feasible that the shared aptamer binding site accommodates these residues. On the other hand, the disordered C-terminal regions of α-syn fibrils are largely acidic and, therefore, are unlikely to be involved in the binding interface.

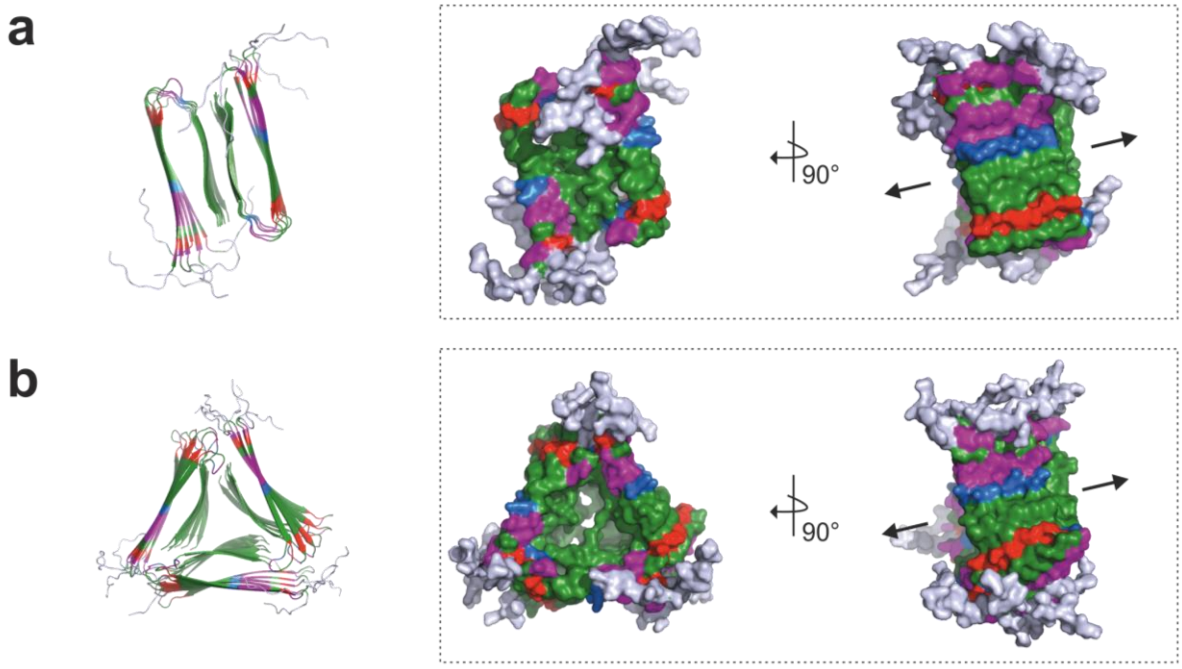

Figure 5.34 Structural models for **(a)** 2A[104] and **(b)** 3Q[105] Aβ40 fibrils. All structures are colour coded: polar (magenta), hydrophobic (green), positive (blue) and negatively charged (red) residues, except the N-terminal flexible regions (residues 1-8) which are not coloured, for clarity. Flexible N-terminal regions are modelled onto the fibrils without NMR restraints. Each model represents six layers of peptides arranged according to their 2- or 3-fold symmetries and viewed down the fibril axis, or turned 90° where indicated. 90° orientations display the cross-β architecture of the "flat-edge" of the fibril, with arrows representing the direction of the fibril axes. Images were made using pdb files 2LMN **(a)** and 2LMP **(b)** using PyMOL Molecular Graphics System (Schrödinger, LLC).

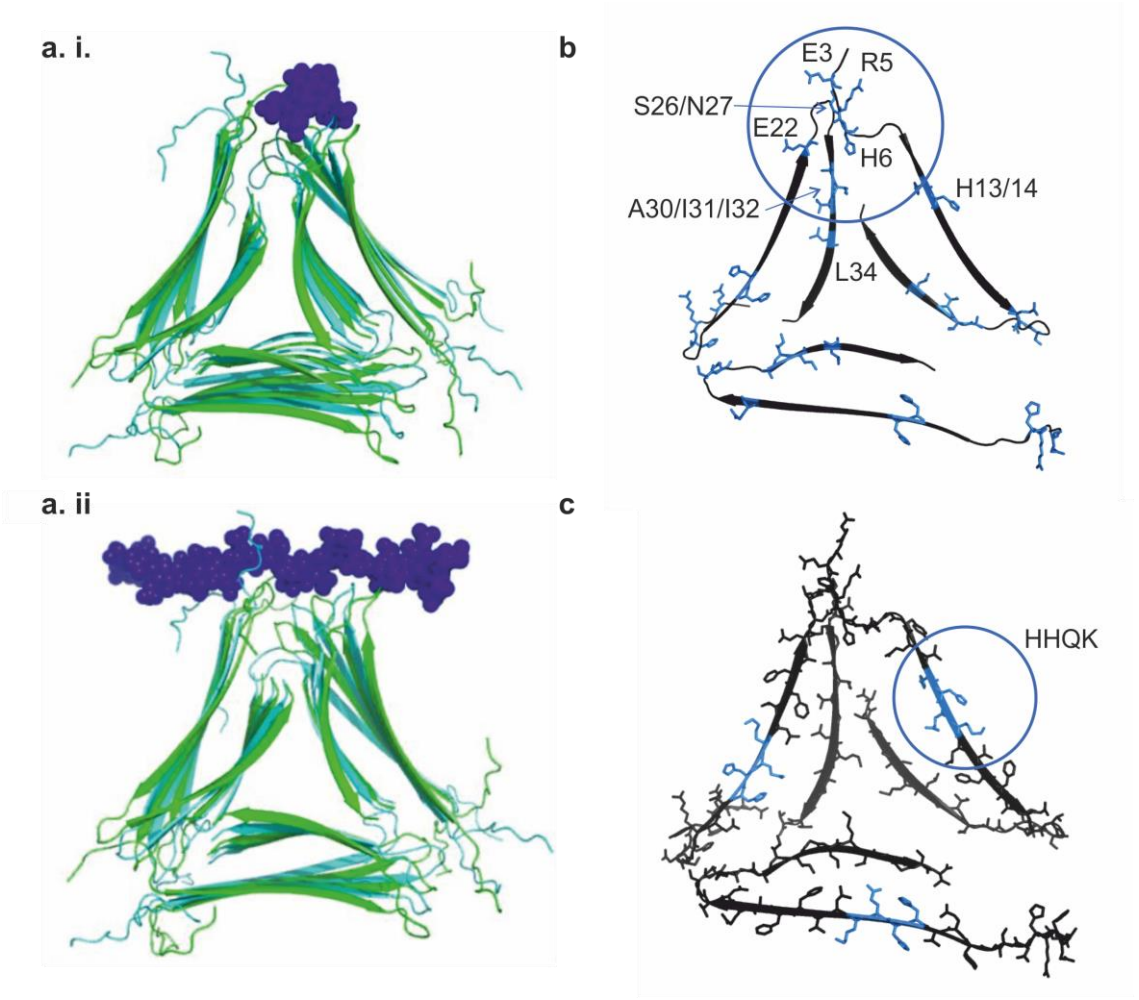

Figure 5.35 LMW heparin-3Q fibril binding models. **(a)** Two proposed binding models for LMW heparin to the "corner" epitope of 3Q fibrils. Models were generated using Autodock Vina and are taken, with permission, from Madine 2012[663]. Heparin can orientate along (i) or perpendicular (ii) to the fibril axis. **(b)** A single layer of three monomers in the 3Q fibril structure highlighting the residues subject to the largest chemical shift perturbations in ssNMR experiments (blue sticks). The proposed binding site is circled. **(c)** A second potential binding site at the position of residues HHQK is highlighted (blue sticks, circled). Images made from pdb file 2LMP using PyMOL Molecular Graphics System (Schrödinger, LLC).

An alternative potential binding site explored was the cluster of basic residues (HHQK) in the structured β-sheet regions of the fibrils. This was a second possible binding site for LMW heparin proposed by Madine *et al.*[663] (**Figure 5.35**), based on docking simulations and comparisons of simulated NMR data for theoretical binding sites to the experimentally derived spectra. This was ultimately not the preferred model due to fewer similarities in the data and fewer chemical shift perturbations in this area, although, of all the residues on

the external face of the β-sheet, only E22 and H14 are assigned[663]. Exploration of this line of enquiry was further motivated by the fact that the binding was likely to be mediated through the regular spacing of sulphate moieties in heparin (and possibly phosphates in RNA). It was thought that a periodic arrangement of positive charges on a fibril structure might complement the polyanionic pattern, in a scenario whereby the fibril acts as a polycation. This could be rationalised in entropic and enthalpic terms, as polyelectrolytes such as GAGs and polynucleotides possess charged groups linked by covalent bonds and, therefore, will bind tightly to counter ions, to decrease intramolecular electrostatic repulsions. They would therefore bind especially tightly to a polyelectrolyte carrying the opposite charge. This would also explain why much higher concentrations of salts were required to dissociate RNA structures from fibrils (**Figure 5.29**). In the cross-β architecture of amyloid, β-strands are spaced 4.7 Å apart. When β-strands are arranged parallel and in-register, as proposed for 2A and 3Q Aβ40 fibrils and α-syn, residues on the surface of the β-strands will align, forming a "stripe" of a single residue along the axis of the fibril (**Figure 5.34**). To test this hypothesis the model amyloid fibril ccβ-p (which is basic overall **Figure 5.18**) was used to probe the requirement for positive charges on a fibrillar surface but was shown not to associate with RNA. However, owing to the out-of-register arrangement of β-sheets, the positive charges are arranged in a staggered formation along the length of this fibril (**Figure 5.18**) and may not produce an optimal electrostatic surface for polyanions to bind.

In the case of 2A and 3Q fibrils, K16 presents on the surface, creating a well aligned positively charged "stripe". This residue, therefore, could be a potential polycationic site for RNA or GAGs to associate. Indeed, some preliminary data (**Figure 5.36**) with fibrils of variant K16A Aβ40 support this hypothesis. The ability of aptamers 2A1 and 3Q1 to bind to 2A and 3Q fibrils, elongated with K16A Aβ40 monomer, was reduced substantially compared with the WT Aβ40 fibrils. These mutant fibrils lack the stripes of positive charge on the fibril surface and the reduction in RNA association clearly indicates a role for this feature in the recognition. The in-register arrangement proposed for α-syn fibrils also produces a similar charge pattern and may explain the cross-reactivity for this fibril. Further work to examine the cross-reactivity between RNA and fibrils from other amyloidogenic peptides is required to evaluate the extent of this generic binding model. More structural information is also needed to allow a more detailed comparison of elements conserved between the fibrils that associate with RNA and those that do not. A more comprehensive mutagenesis study could also be employed to elucidate the likely binding

epitopes in Aβ40 fibrils, along with ssNMR characterisation, similar to that performed for LMW heparin[663].

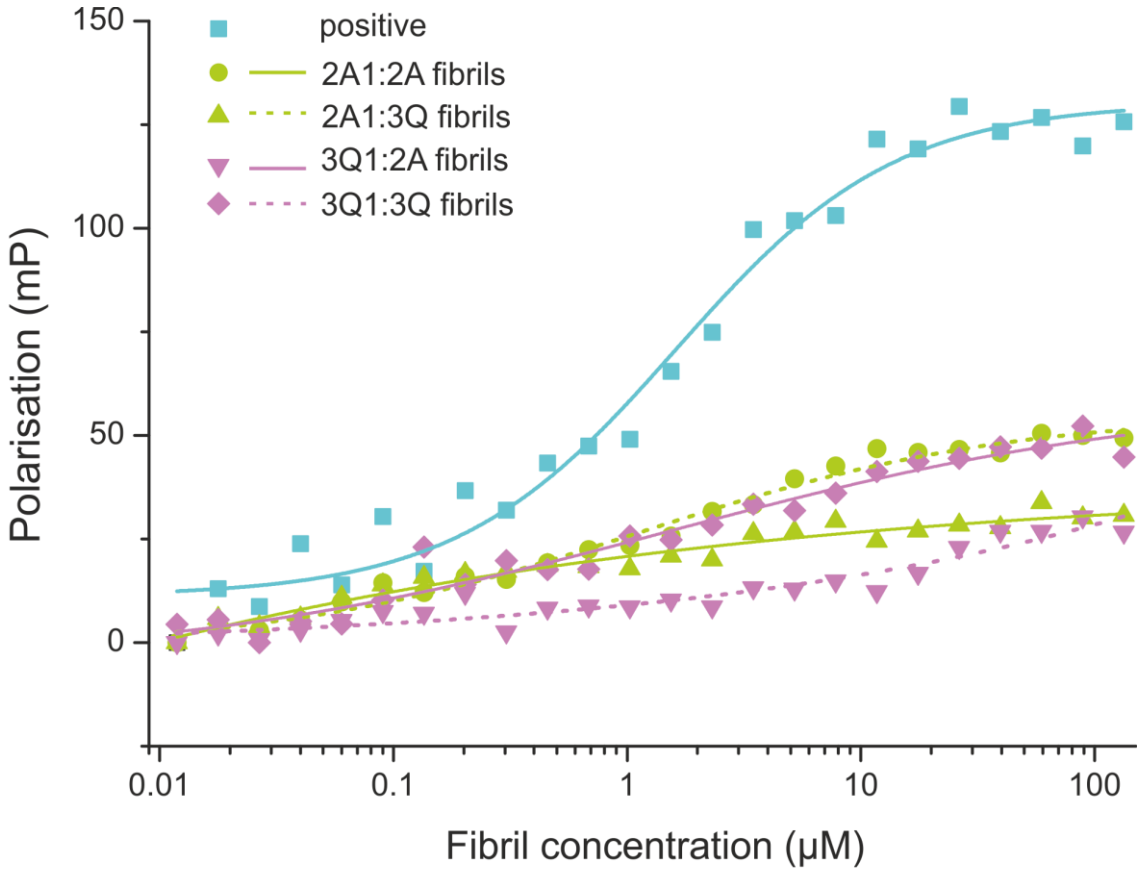

Figure 5.36 Aptamers display reduced affinity for K16A Aβ40 fibrils. FP analysis of aptamers 2A1 (green) and 3Q1 (pink) with increasing concentrations of 2A (solid lines) or 3Q (dotted lines) K16A fibrils. Data are compared to a single replicate of 3Q1 binding WT 3Q fibrils (pale blue squares) which is fitted to the Hill equation (**Equation 2.5**); K_d = 1.62 ± 0.25, n = 0.92 ± 0.14.

One issue with the comparison of the GAG and RNA binding mechanism presented here, is that LMW heparin was shown to dissociate the aptamer from both 3Q and 2A fibrils in a remarkably similar manner. This was surprising as the ssNMR data suggest that LMW heparin binds only weakly to 2A fibrils[663]. Binding of LMW heparin certainly does not induce the same chemical shift perturbations of the residues involved in binding, as observed in the 3Q interaction. This would suggest that if LMW heparin does bind 2A fibrils, even weakly, it would occur at a different site that is not detected by ssNMR. The competition data presented in this study, however, suggests a conserved binding

mechanism between LMW heparin and both fibrils, as the aptamer dissociation profiles are so similar (**Figure 5.27**). The preferred binding site proposed for the 3Q interaction encompasses the apices of the triangular 3Q fibril geometry, a feature that is not conserved in 2A fibrils. The possible secondary binding model, involving residues H13 and H14 (**Figure 5.35 c**), is close to K16 and consistent with the HHQK GAG binding epitope proposed by McLaurin *et al*.[652, 656] This site is located on the flat surface of the β-sheet and, therefore, is similarly arranged in both fibril types. Therefore, it may be possible that a second GAG binding site exists at this HHQK region, which is not detected through chemical shift perturbation, and could be the shared binding site for the RNA aptamers.

The idea of generic polyanion binding to amyloid fibrils has been studied by others, previous to this work. Indeed, GAGs are not the only polyanion found to be associated with fibrils *in vivo*[674, 675]. Nucleic acids have been found associated with both tau inclusions and Aβ40 plaques in *ex vivo* brain samples[674]. The effect of RNA and DNA on the promotion of tau[654, 676] and α-syn[677] aggregation, as well as the conversion of PrP^{c} to β-sheet rich PrP^{Sc}, has been documented and indicates an association by these molecules. DNA has also been shown to associate with the functional amyloid curli[675]. A study by Calamai and colleagues[660] went further in characterising the ubiquitous nature of polyanionic binding to amyloid, by comparing the associations of both ssDNA and dsDNA, ATP and two GAGs (heparin and heparan sulphate) to pre-formed aggregates of lysozyme and human muscle acylphosphatase (AcP), both of which form amyloid fibrils *in vitro*. They found all polyanions tested were able to bind to amyloid fibrils. These negatively charged species also increased the rate of aggregation of AcP. The data led to the conclusion that the interaction by polyanions is largely non-specific, as there was no obvious dependence on type of charged groups or structure of the polymers, or on the structure of the amyloid protein, in terms of either precursor monomer or aggregate morphology. The binding was also considered largely electrostatic, as high concentrations (> 100 mM) of magnesium salts were shown necessary to suppress the binding. From this it was concluded that polyanions are likely to contribute to the promotion of amyloid formation and the stabilisation of such species.

The initiation of tau amyloidosis is also known to be facilitated by negatively charged cofactors including heparin[654, 672], fatty acids[678, 679] and, crucially, RNA[676, 680]. In the absence of these accessory molecules, tau does not aggregate, except under extreme temperatures, pH or high salt concentrations[681]. Recently, Dinkel *et al*.[671] demonstrated that incubation of tau with RNA was able to produce the same fibril morphology as seen as a result of heparin-assisted nucleation. In addition, RNA was able to sustain tau propagation during successive

seeding rounds, indicating that the role of RNA is not limited to the initial nucleation step, but also drives the fibril elongation. The effect of RNA was confirmed to be due to a tight association of the polynuclotide and the fibril (rather than a transient interaction), by the addition of 500 mM NaCl, which reportedly caused only minor dissociation of the RNA molecules. Heparin was also used in their study to demonstrate the likelihood of a shared polycationic epitope and RNA displacement with a 2-fold excess concentration of heparin was seen.

The data presented here and that published by others, therefore, indicate that RNA associates with amyloid fibrils in a manner resembling several other negatively charged polymers. The interaction is likely to be electrostatically driven, but largely non-specific in terms of both the RNA sequence and that of the aggregated target structure.

The primary aim of this thesis was to determine whether specific aptamer sequences could be selected with a preference for individual amyloid morphologies, in the hope that novel research tools or diagnostic reagents could be developed to aid in the study and treatment of Alzheimer's disease. Owing to the generic, and probably backbone mediated, recognition of amyloid structures by RNA molecules, this was not achieved. The work, however, did reveal new insights into the nature of RNA-amyloid interactions, by changing both the amyloid and RNA structures and sequences. The study suggests a possible role of both nucleotide and amino acid sequences in modulating the associations, as seen by the differences (10-fold change in K_d) in dissociation constants observed for different aptamer sequences and/or amyloid precursors. This explains why certain sequences were amplified over others during selection. In addition, data indicates that RNA molecules could be influential on fibrillation pathways and the resultant morphology of aggregates. Furthermore, aptamers could be developed to serve as generic amyloid recognition reagents in amyloid imaging. Chapter 6 discusses possible future directions for this work and the wider implications of a universal amyloid binding model for RNA.

6 Concluding remarks and future directions

6.1 Implications

The isolation of specific detection reagents for amyloid assemblies is of paramount importance in advancing our knowledge of the structures involved in many of the most prevalent diseases in the developed world, including AD. The ability to discriminate between various distinct structures would enable identification of toxic assemblies, as well as aid in the development of more specific diagnostics and novel treatments. This thesis details work towards reaching this goal, through the development of nucleic acid aptamer based recognition molecules. RNA aptamers were selected against a few of the many assemblies of Aβ40 associated with AD, including the monomeric peptide and fibrils of distinct morphology. Chapter 3 outlines the selection process and the isolation of RNA pools enriched for sequences with clear conserved motifs and secondary structural elements, indicative of successful enrichment of specific aptamers. However, work in Chapter 4 determined that the aptamers selected against the monomeric Aβ amyloid precursor were unable to recognise this target assembly and instead displayed recognition of the aggregated form. During the characterisation of the anti-fibril RNA aptamer selections in Chapter 5, it became clear that RNA is able to recognise amyloid assemblies in a largely non-specific manner, analogous to other highly negatively charged polymers, such as GAGs. The binding mechanism is likely to be derived from phosphate backbone contacts with positively charged regions of the amyloid structures and, therefore, is not critically dependent on RNA sequence or secondary structure.

Collectively, the work indicates that RNA-based reagents may not be the most suitable technologies to employ in the development of specific recognition molecules towards different amyloid assemblies. Despite RNA aptamers previously demonstrating powerful discrimination between targets with only subtle structural differences[682, 683], this has yet to be replicated in the amyloid field. The data presented here suggest that selection of aptamers able to make specific contacts through unique secondary structural elements derived from their primary sequences, able to recognise different amyloid species, was not achieved, owing to the more energetically favourable interactions between the RNA backbone and the fibrillar targets dominating the selection process. Similarly, selections for aptamers with enhanced affinity for the monomeric peptide may not be possible due to the

inherent affinity of RNA for β-sheet rich aggregates, small amounts of which are inevitably present in the preparation of aggregation-prone peptides for selection. Even if the immobilisation strategy for the monomeric target could be improved to contain purely non-aggregated peptide, the propensity for backbone-mediated recognition of aggregates may outweigh any RNA sequence specific association with the monomer, which would render an aptamer insensitive in recognising monomers from a complex mix of amyloid assemblies.

Based on work conducted here and evidence described elsewhere[494, 671], the interaction of RNA and amyloid aggregates seems to be a general phenomenon. The nature of the interaction also extends to other biological polyanions such as GAGs, DNA and ATP[660]. This general polyanionic association could have significant biological implications. One likely outcome is that these negatively charged molecules contribute to the promotion of fibril formation, or stabilisation of resultant aggregates, *in vivo*. The fibrillation inducing effect of RNA, DNA and GAGs on several amyloidogenic proteins *in vitro*[649, 650, 654, 656, 657, 659, 660, 671] lends further credence to this conclusion. RNA[674, 684], predominantly neuronal mRNA[685], has been shown to be sequestered in amyloid plaques, which could result in compromised cellular proteostasis and represent a model for amyloid-induced toxicity, that has not been explored previously. Similarly, cellular functions mediated through other common cellular polyanions, such as GTP, ATP or even the protein-based polyanions tubulin and actin, could also be compromised upon abnormal association with aggregates. Native complexes formed by polyanionic molecules with ions or other biological electrolytes (ATP and Mg^{2+}, for example) could be disrupted by a more favourable association with polycationic amyloid structures, leading to cellular dysfunction.

Evidence for seemingly ubiquitous RNA-amyloid interactions also allows further speculation into the idea that amyloid structures could have had a role in the origin of life. It is generally agreed that RNA molecules, capable of both storing genetic information and catalysing the chemical reactions necessary to sustain life, preceded the current situation of DNA-based genetic material coding for proteins as the major biological catalysts[686]. However, the prebiotic formation of stable ribonucleotide polymers remains unclear, although catalysis on the surface of clay minerals is one possible route that is generally acknowledged[687-689]. Amyloid has also been proposed as an ancient protein conformation[690] and even postulated as a potential pre-RNA genetic molecule, through its ability to transfer information via templating and self-replication[691]. It has also been shown to function as a primordial enzyme[692]. It is possible that through a non-specific yet high affinity interaction, amyloid structures could have provided a surface template for early RNA polymerisation and stabilisation, more flexible and possibly more effective than clay. At the same time, RNA

interactions with amyloid could have stimulated further fibril growth. This suggests a possible mechanism where protein and nucleic acids co-evolved through the formation of amyloid structures[693]. The discovery of polyphosphate (polyP) as an ancient, universally-conserved and entirely inorganic molecular chaperone, with no clear substrate specificity[694], further indicates a role for polyanions in the very earliest stages of life.

6.2 Future directions

To enable a more thorough understanding of the amyloid-RNA interaction from a structural perspective, a more comprehensive cohort of fibrils would need to be tested and direct comparison of the structural elements involved in nucleic-acid binding probed. Mutagenesis studies or ssNMR mapping of the generic binding epitope could also shed some light on the residues involved in the interface, revealing any similarities between each fibril type. Further competition experiments could also be used to elucidate whether the generic binding is indeed shared by the many other biological polyanions mentioned above. To confirm whether the affinity for amyloid is mediated through the phosphate backbone as proposed, a comparison with an RNA molecule modified to contain a methylphosphonate backbone could be conducted. The methylphosphonate modification, where one of the non-bridging oxygen atoms of the inter-nucleotide linkage is replaced by a methyl group, renders the RNA backbone neutral and would therefore confirm the polyanionic binding mechanism proposed.

It would also be interesting to probe further the effect of RNA on amyloid formation and toxicity *in vitro* and *in vivo*. Investigation into the length-dependence of RNA binding and its effect on fibril formation *in vitro,* along with comparison to other polyanions known to affect fibril formation, would add further evidence to a general role for negatively charged polymers in amyloid formation. Sequencing the specific RNAs found associated with AD plaques might also help identify any possible toxic mechanisms involving alterations to proteostasis as a direct consequence of RNA sequestration. This would open up many interesting questions as to how the extracellular plaques collect the RNA molecules transcribed intracellularly; whether they associate with fibrillar assemblies in the cytosol and are subsequently trafficked out of the cell or whether the plaques simply sequester the RNA released from damaged neurons.

One practical outcome of these aptamer selections could be the development of generic amyloid detection reagents, based on the preliminary live-cell imaging demonstrated with fluorescently-labelled aptamer 3Q319 (**Figure 5.30** and **Figure 5.31**). Analysis of the ability of these RNA sequences to detect fibrillar structures seeded from *ex vivo* brain samples or to recognise plaques in post-mortem tissue, would further indicate a potential for these aptamers as imaging reagents in an *in vivo* setting. Whether aptamers are able to recognise pre-fibrillar, oligomeric structures is also yet to be assessed. If this proved to be the case, aptamers could provide invaluable insights into generic epitopes shared between oligomeric assemblies or provide novel, anti-oligomer detection reagents *in vivo*.

In order to use aptamer technologies to develop specific recognition molecules, able to distinguish between fibril morphologies or aggregation prone monomeric peptides, the inherent amyloid binding tendency would have to be addressed. If the generic aptamer binding epitope could be identified, selections against amyloid structures devoid of this structural element may prove effective. For example, selection against K16A Aβ40 fibrils, based on the suggestion that this single basic residue is important in the non-specific interaction (**Figure 5.36**), could promote recognition of other epitopes of the fibril structure, unique to that fibril morphology, and essentially overcome the bias posed by a more favourable backbone-mediated interaction.

Although the original aim of providing highly specific nucleic acid based recognition molecules for Aβ40 assemblies was not realised, work described herein demonstrates that RNA-amyloid interactions are dominated by backbone interactions, with bases adding only marginal specificity to different amyloid structures. The idea of using RNA aptamer selections to achieve this goal was motivated by the powerful discrimination demonstrated in other, non-amyloid selections, as well as the large number of possible conformations accessible to RNA-based ligands. The use of RNA aptamers also allowed access to great electrostatic potential in binding, and the known amyloid binding properties of GAGs serves as proof of polyanions as amyloid-binding reagents. This, coupled with the additional complexity in RNA structures, was hoped to lead to the generation of sequences with affinity and selectivity for the distinct assemblies. The finding that the RNA-amyloid interaction is generic and backbone-mediated has major implications, from novel toxicity mechanisms in amyloid disorders to the very fundamentals of biology.

7 Appendices

7.1 Appendix 1: Plasmid maps

7.1.1 PetSac MAβ40

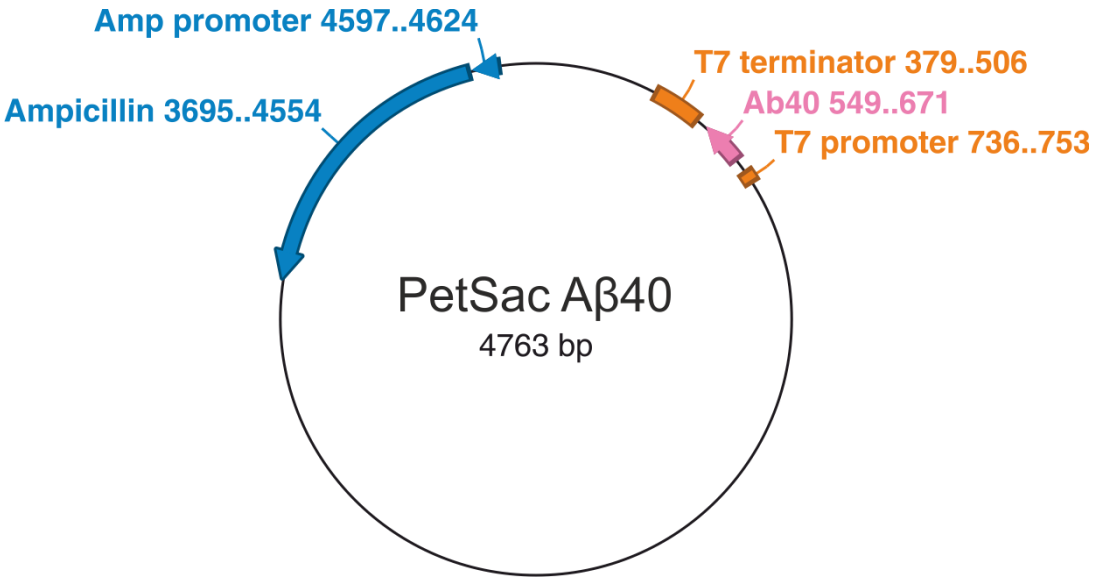

Appendix 7.1.1 Plasmid map of PetSac Aβ40 (a modified Pet3a plasmid with *Nde*I and *Sac*I cloning sites), kindly provided by Professor Dominic Walsh (Harvard Institute of Medicine, USA) and Dr. Sara Linse (Lund University, Sweden).

7.1.2 pET23a α-syn

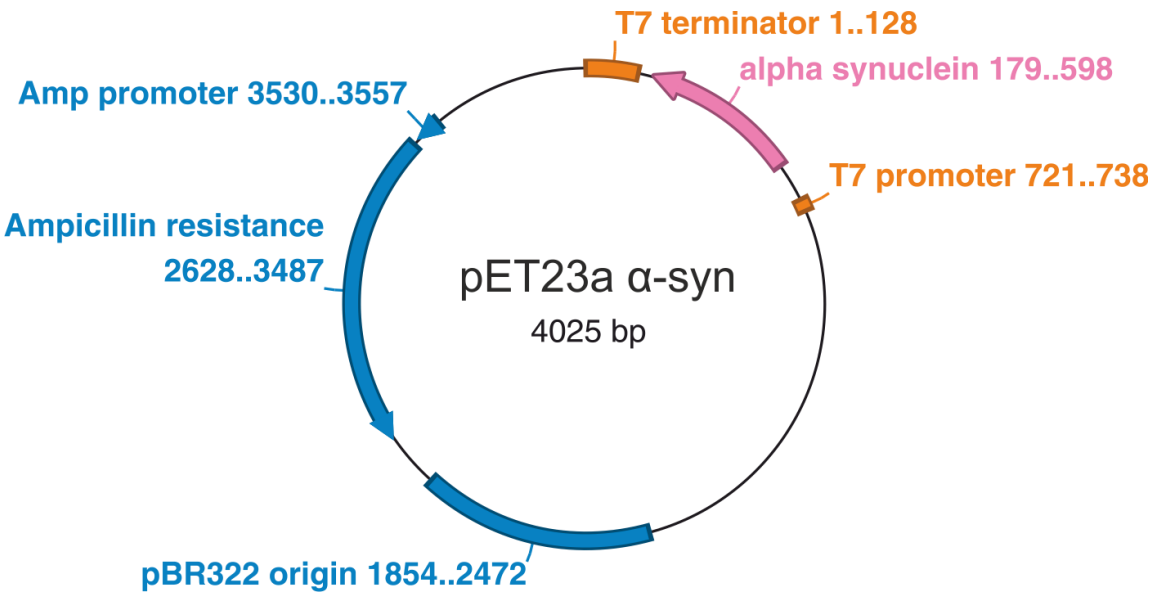

Appendix 7.3.2 Plasmid map of pET23a α-syn, kindly provided by Professor Jean Baum (Department of Chemistry and Chemical Biology, Rutgers University, NJ, USA).

7.2 Appendix 2: MS/MS ETD fragmentation spectra

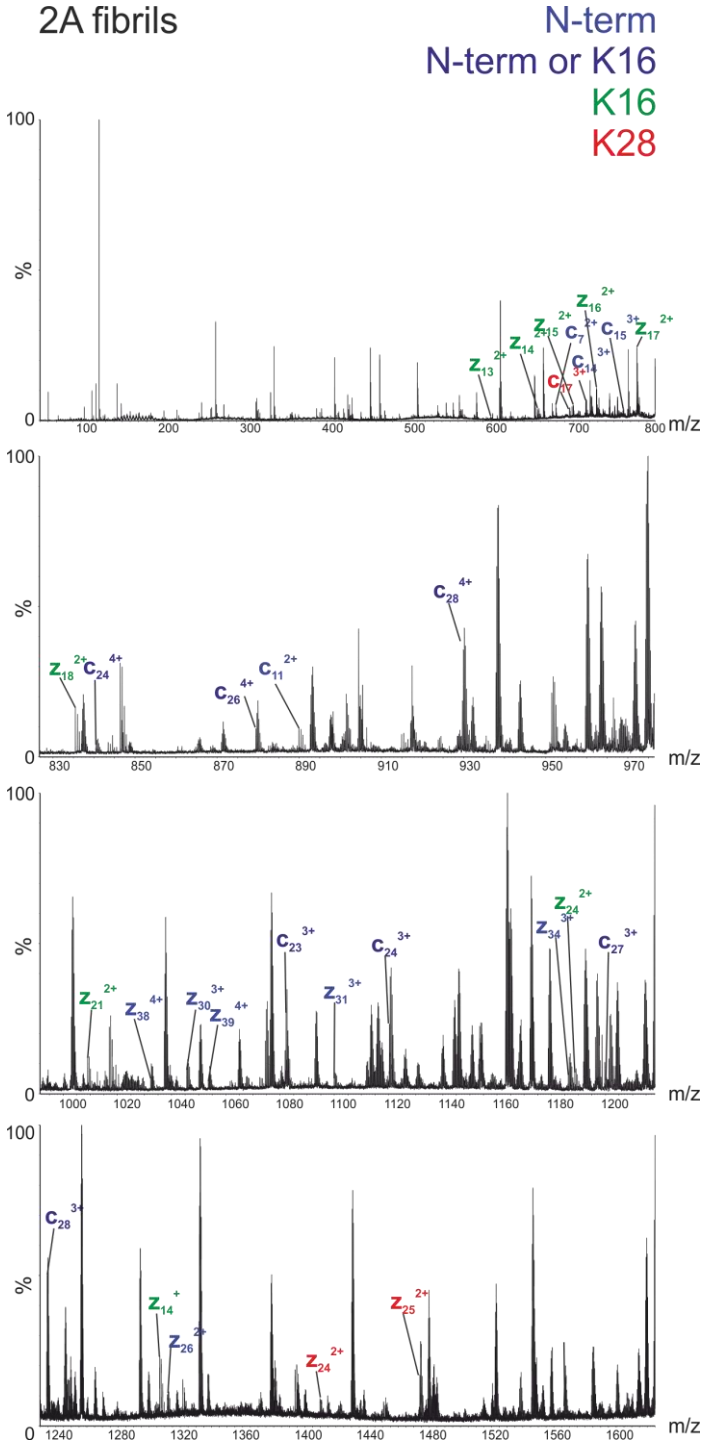

Appendix 7.2.1 Tandem MS (MS/MS) ETD data indicating the position of biotin modifications within the 2A fibril morphology. The spectrum has been split to focus on different m/z areas due to the high abundance of peaks. Peaks indicative of biotin location are labelled as follows: N-terminal modification (blue), K16 modification (green), K28 modification (red), either N-terminal or K16 modification (purple).

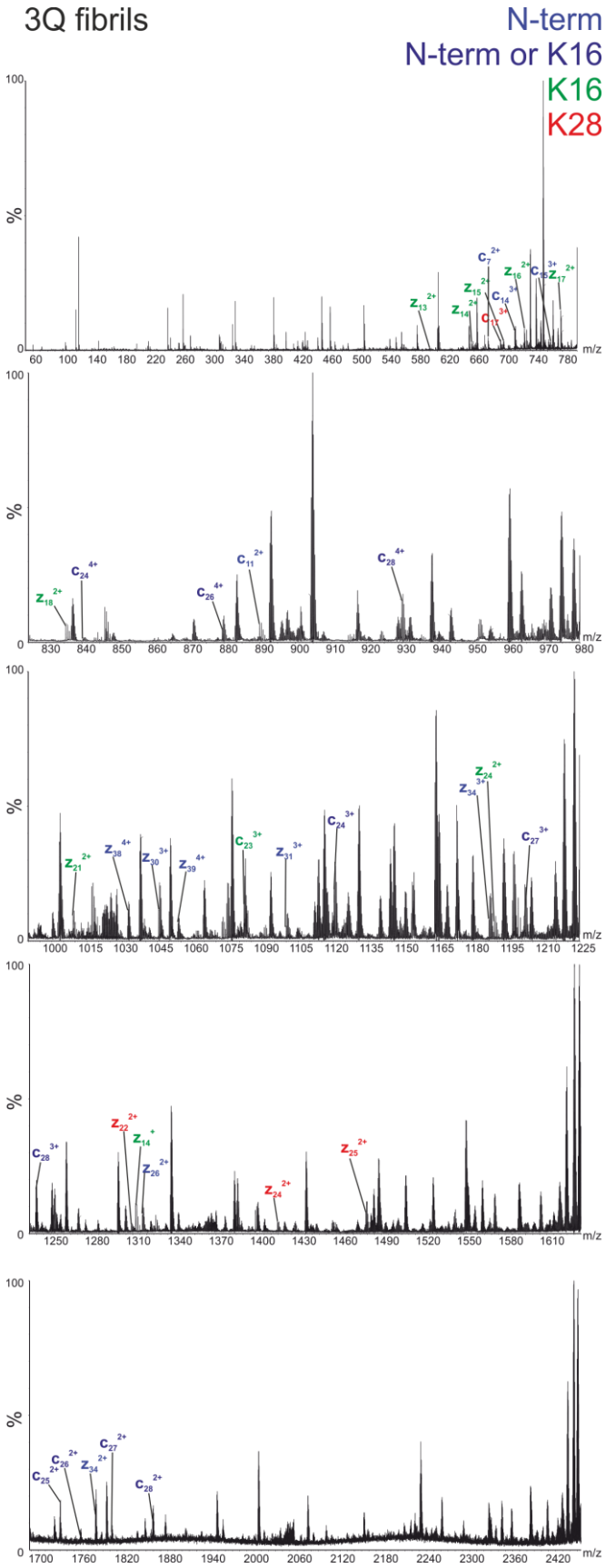

Appendix 7.2.2 MS/MS ETD data indicating the position of biotin modifications within the 3Q fibril morphology (as **Appendix 7.2.2**).

7.3 Appendix 3: Genebee multiple alignment analyses of NGS data

Consensus motifs are identified from the top 500 aptamer sequences from the filtered NGS data, for each of the selections: Aβ40 monomer (**Appendix 7.3.1**), 2A fibrils (**Appendix 7.3.2**) and 3Q fibrils (**Appendix 7.3.3**). In each case, the ten "supermotifs" with the highest power score (defined in reference [513]) are given. The corresponding power score is indicated in bold above each motif. Power scores higher than 7.00 are considered to significant. Aptamers within each motif are identified by their number (which corresponds to their frequency of occurrence) followed by the number of occurrences, e.g. 1-613 would indicate the most commonly occurring sequence (1) which occurs 613 times in the filtered data. The consensus of each motif is represented as a sequence logo (Weblogo[695]), with the height of each residue corresponding to the conservation at that position. Nucleotide bases at each position are colour coded as follows: A (green), T (red), G (yellow), C (blue). DNA sequences corresponding to RNA aptamers are given.

7.3.1 Anti-Aβ40 monomer aptamer selection

LOCAL SUPERMOTIF number 1, power **20.37**

```
          .+.++++++++++++++++++++.+++++++++++++++.++++++++
1-613     TAAGGGAAGTGTGCTGAGAGAGGGAAGTTGCGTAGCGAAGCACGATAACG
327-19    TATGGGAAGTGTGCTGAGAGAGGGAAGTTGCGTAGCGAAGCACGATAACG
372-18    TAAGGGAAGTGTGCTGAGAGAGGGAAGTTGCGTAGCGAAGCGCGATAACG
497-16    TAAGGGAAGTGTGCTGAGAGAGGGAGGTTGCGTAGCGAAGCACGATAACG
532-15    CAAGGGAAGTGTGCTGAGAGAGGGAAGTTGCGTAGCGAAGCACGATAACG
```

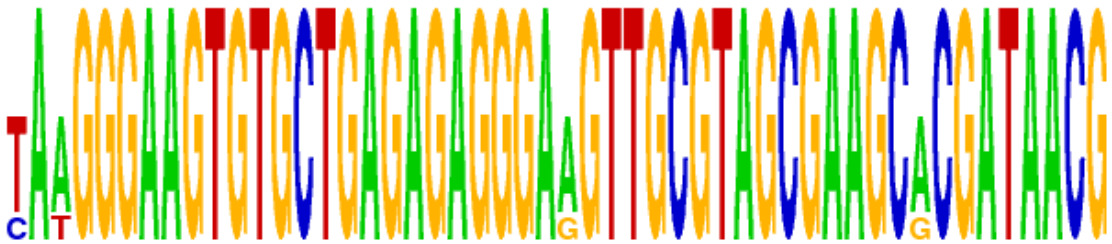

LOCAL SUPERMOTIF number 2, power **12.12**

```
          ++++++++++++++++++++++++++++++++++++++++++++++++++
230-22    ACAAGAGGGGAAGGCAGGGGATAGGGAGAGAAGGGCGCGGAGAAAGAGGA
238-22    gCAAGAGGGGAAGGCAGGGGATAGGGAGAGAAGGGCGCGGAGAAAGAGGA
```

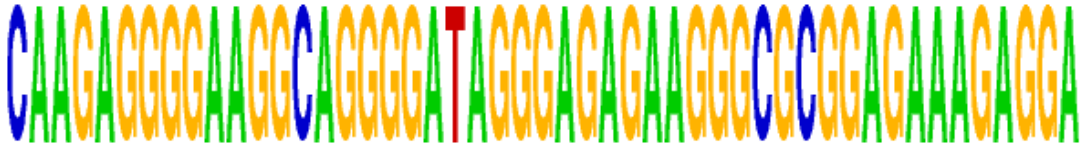

LOCAL SUPERMOTIF number 3, power **12.12**

```
          ++++++++++++++++++++++++++++++++++++++++++++++++++
50-41     AAGGGAAGGCAGATAAGTGAGAGTAAGAGTGGAAGGGAAGAAAGTACACA
454-16    gAGGGAAGGCAGATAAGTGAGAGTAAGAGTGGAAGGGAAGAAAGTACACA
```

LOCAL SUPERMOTIF number 4, power **12.03**

```
          ++++++++++++++++++++++++++++++++++++++++++++++++++++
214-23    AAGGGGAACAGAAAGAGGGAAAGGAGGGGAAAAAGGACAAAGCGAGAAAGG
540-15    AAGGGGAACAGAAAGAGGGAAAGGAGGGGAAAAAGGATAAAGCGAGAAAGG
```

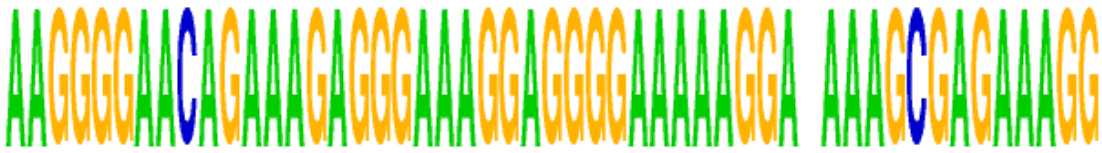

LOCAL SUPERMOTIF number 5, power **12.00**

```
          ++++++++++++++++++++++++++++++++++++++++++++++++++
233-22    GAGGATGGGAAGAGCCG-CGGAGGTAATGTTACAAAATGAGGTAGGAGGA
324-19    GAGGATGGGAAGAGCCGCCGGAGGTAATGTTACAAAATGAGGTAGGAGGA
```

LOCAL SUPERMOTIF number 6, power **11.92**

```
           ++++++++++++++++++++++++++++++++++++++++++++++++++
61-38      GAATGAGCGCGAAGGAGTATAAGAGGAGGAGGTAAAAGAGGGAACGAGGA
549-15     GAATGAGCGCGAAGGAGTATAAGAGAAGGAGGTAAAAGAGGGAACGAGGA
```

LOCAL SUPERMOTIF number 7, power **11.92**

```
          ++++++++++++++++++++++++++++++++++++++++++++++++++
4-114     GTAGAAAAGGACATGTAGGCATGATAGAAATTGAAGGGGGAAAGAACGCG
414-17    GTAGAAAAGGACATGTGGGCATGATAGAAATTGAAGGGGGAAAGAACGCG
```

LOCAL SUPERMOTIF number 8, power **11.92**

```
          ++++++++++++++++++++++++++++++++++++++++++++++++++
88-33     TAGGGAAAGGTAAAGAGAGTACCATGGATATGCTGGCGTAGCTAGACAAG
174-25    TAGGGAAAGGTAAAGAGAGTACCATGGACATGCTGGCGTAGCTAGACAAG
```

LOCAL SUPERMOTIF number 9, power **11.92**

```
          ++++++++++++++++++++++++++++++++++++++++++++++++++
53-41     ACACGAAGCGCGCGAATGGGTACGAAGGGAAGAGGAGGAGCGAGAAGGGA
80-34     ACACGAAGCGCGCGAAGGGGTACGAAGGGAAGAGGAGGAGCGAGAAGGGA
```

LOCAL SUPERMOTIF number 10, power **11.61**

```
          ++++++++++++++++++++++++++++++++++++++++++++++++
79-35     gAACAGGTAGGAGGTAAAAAGGGGATCGCGAGGAGAGGTGGAGAGG
588-14    TAACAGGTAGGAGGTAAAAAGGGGATCGCGAGGAGAGGTGGAGAGG
```

7.3.2 Anti-2A fibril aptamer selection

LOCAL SUPERMOTIF number 1, power **44.35**

```
                +++++++++++++++++++++++++++++++++++++++++++++++++++
2-16019         ACAAGAGGGAGGAGAGGGAGGAACGTTAGGGTAGCCGAGGAGCGGAGGGA
28-1303         gCAAGAGGGAGGAGAGGGAGGAACGTTAGGGTAGCCGAGGAGCGGAGGGA
117-239         tCAAGAGGGAGGAGAGGGAGGAACGTTAGGGTAGCCGAGGAGCGGAGGGA
148-192         ACAAGAGGGAGGAGAGGGAGGAACGTTAGGGTAGCCGAGGAGTGGAGGGA
153-187         ACAAGAGGGAGGAGAGGGAGGAGCGTTAGGGTAGCCGAGGAGCGGAGGGA
161-177         ACAAGAGGGAGGAGAGGGAGGAACGTTAGGGTGGCCGAGGAGCGGAGGGA
175-165         ACAAGAGGGAGGAGAGGGAGGAACGTTAGGGCAGCCGAGGAGCGGAGGGA
234-124         ACAAGAGGGAGGAGAGGGAGGAACGTTAGGGTAGCTGAGGAGCGGAGGGA
252-116         ACAAGAGGGAGGAGAGGGAGGAACGTTAGGGTAGCCGGGGAGCGGAGGGA
253-115         ACAAGAGGGGGGAGAGGGAGGAACGTTAGGGTAGCCGAGGAGCGGAGGGA
265-113         ACAAGAGGGAGGAGAGGGAGGAACGTTAGGGTAGTCGAGGAGCGGAGGGA
275-109         cCAAGAGGGAGGAGAGGGAGGAACGTTAGGGTAGCCGAGGAGCGGAGGGA
318-94          ACAAGAGGGAGGAGAGGGAGGAATGTTAGGGTAGCCGAGGAGCGGAGGGA
331-89          ACAAGAGGGAGGAGAGGGAGGAACGTTAGGGTAGCCGAGGAGCGGAGGaa
337-87          ACGAGAGGGAGGAGAGGGAGGAACGTTAGGGTAGCCGAGGAGCGGAGGGA
353-83          ACAAGAGGGAGGAGAGGGAGGAACGTTAGGGTAGCCGAGGAGCGGAGGGc
364-81          ACAAGAGGGAGGAGAGGGAGGAACGTTAGGGTAGCCAAGGAGCGGAGGGA
403-74          ACAAGAGGGAGGAGAGGGAGGAACGTTAGGGTAGCCGAGGAGCGGGGGGA
415-71          ACAAGAGGGAGGAGAGGGAGGAACGTTAGGGTAGCCGAGGAGCGGAGGGg
422-70          ACAAGAGGGAGGAGAGGGAGGAACGTTAGGGTAGCCGAGGGGCGGAGGGA
432-67          ACAAGAGGGAGGAGAGGGAGGAACGTTAGGGTAGCCGAGGAGCAGAGGGA
434-67          ACTAGAGGGAGGAGAGGGAGGAACGTTAGGGTAGCCGAGGAGCGGAGGGA
436-67          ACAAGAGGGAGGAGAGGGGGGAACGTTAGGGTAGCCGAGGAGCGGAGGGA
440-66          ACAGGAGGGAGGAGAGGGAGGAACGTTAGGGTAGCCGAGGAGCGGAGGGA
447-65          ACAAGGGGGAGGAGAGGGAGGAACGTTAGGGTAGCCGAGGAGCGGAGGGA
482-58          ACAAGAGGGAGGAGAGGGAGGAACGTTAGGATAGCCGAGGAGCGGAGGGA
495-57          ACAAGAGGGAGGAGAGGGAGGAACGTTGGGGTAGCCGAGGAGCGGAGGGA
500-57          ACAAGAGGGAGGAGAGGGAGGAACGTTAGGGTAGCCGAGAAGCGGAGGGA
```

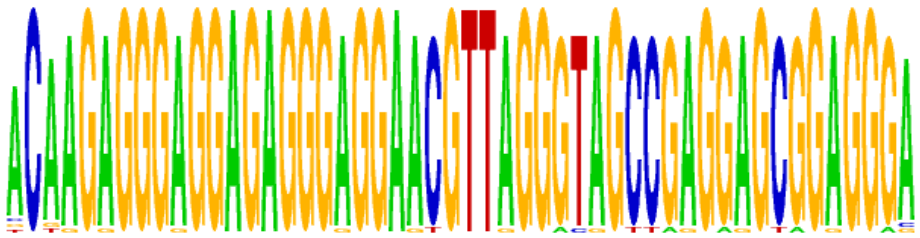

LOCAL SUPERMOTIF number 2, power **31.50**

```
                +++++++++++++++++++++++++++++++++++++++++++++++
3-13560         -GCGAAAGGGACGGACGAAAGGGAAGGGAAGGGCAGGGGATCTGACAGCG
134-210         -GCGAAAGGGACGGACGAAAGGGAAGGGAAGGGCAGGGGATCCGACAGCG
139-204         -tCGAAAGGGACGGACGAAAGGGAAGGGAAGGGCAGGGGATCTGACAGCG
192-150         -GCGAAAGGGACGGATGAAAGGGAAGGGAAGGGCAGGGGATCTGACAGCG
207-138         -GCGAAAGGGACGGACGAAAGGGAAGGGAAGGGCAGGGGATCTGACAGCc
216-134         -GCGAAAGGGGCGGACGAAAGGGAAGGGAAGGGCAGGGGATCTGACAGCG
282-107         -GCGAAAGGGACGGACGGAAGGGAAGGGAAGGGCAGGGGATCTGACAGCG
290-104         -GCGAAAGGGACGGACGAAAGGGAAGGGAAGGGCAGGGGATCTGGCAGCG
292-103         -GCGGAAGGGACGGACGAAAGGGAAGGGAAGGGCAGGGGATCTGACAGCG
297-101         -GCGAAAGGGACGGACGAAAGGGTAGGGAAGGGCAGGGGATCTGACAGCG
301-100         -GCGAGAGGGACGGACGAAAGGGAAGGGAAGGGCAGGGGATCTGACAGCG
354-83          -GCGAAGGGGACGGACGAAAGGGAAGGGAAGGGCAGGGGATCTGACAGCG
355-82          -GCGAAAGGGACGGACGAGAGGGAAGGGAAGGGCAGGGGATCTGACAGCG
387-75          -GCGAAAGGGTCGGACGAAAGGGAAGGGAAGGGCAGGGGATCTGACAGCG
396-75          -GCGAAAGGGACGGACGAAAGGGAAGGGAAGGGCAGGGGGTCTGACAGCG
397-74          gcgaAAAGGGACGGACGAAAGGGAAGGGAAGGGCAGGGGATCTGACAGCG
399-74          -GCGAAAGGGACGGACGAAAGGGAAGGGAAGGGCAGGGGATCTGACGGCG
427-68          -GCGAAAGGGACGGACGAAAGGGAAGGGAAGGGCAGGGGTTCTGACAGCG
429-67          -aCGAAAGGGACGGACGAAAGGGAAGGGAAGGGCAGGGGATCTGACAGCG
438-66          -GCGAAAGGGACAGACGAAAGGGAAGGGAAGGGCAGGGGATCTGACAGCG
444-65          -GCGAAAGGGACGGACGAAAGGGAAGGGAAGGGCAGGGGATCTGACTGCG
468-61          -gtGAAAGGGACGGACGAAAGGGAAGGGAAGGGCAGGGGATCTGACAGCG
480-58          -GCGAAAGGGACGGACGAAGGGGAAGGGAAGGGCAGGGGATCTGACAGCG
481-58          -GCGAAATGGACGGACGAAAGGGAAGGGAAGGGCAGGGGATCTGACAGCG
```

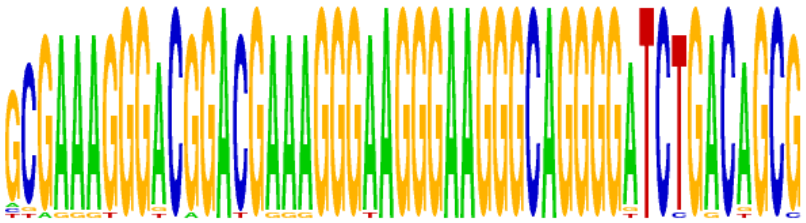

LOCAL SUPERMOTIF number 3, power **27.20**

```
                ...++++++++++++++++++++++++++++++++++++++++++++++++
1-51626         GGCAAACGGTAAGGCCAAAGGGACGAGGGTAGAGATTGATAGAAAGCCGC
16-2149         tGCAAACGGTAAGGCCAAAGGGACGAGGGTAGAGATTGATAGAAAGCCGC
75-397          gaCAAACGGTAAGGCCAAAGGGACGAGGGTAGAGATTGATAGAAAGCCGC
92-320          GGCAAACGGTAAGGCCAAAGGGACGAGGGTAGAGATTGATAGAAAGCCac
164-174         gtCAAACGGTAAGGCCAAAGGGACGAGGGTAGAGATTGATAGAAAGCCGC
199-144         cGCAAACGGTAAGGCCAAAGGGACGAGGGTAGAGATTGATAGAAAGCCGC
264-114         aGCAAACGGTAAGGCCAAAGGGACGAGGGTAGAGATTGATAGAAAGCCGC
381-78          GGAAAACGGTAAGGCCAAAGGGACGAGGGTAGAGATTGATAGAAAGCCGC
452-64          GGGAAACGGTAAGGCCAAAGGGACGAGGGTAGAGATTGATAGAAAGCCGC
```

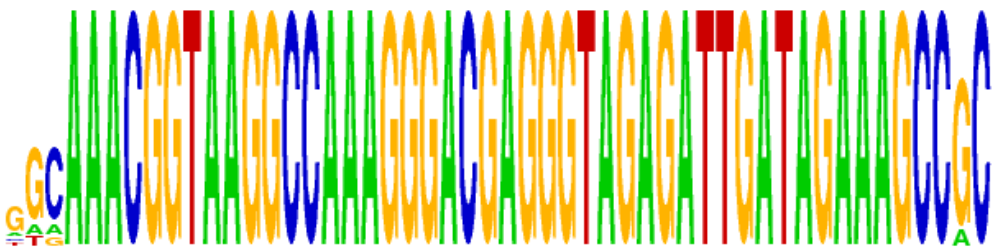

LOCAL SUPERMOTIF number 4, power **25.12**

```
          ++++++++++++++++++++++++++++++++++++++++++++++++.
4-12818   AAGCGAAGGGAGGGCAGGGAGAAGGGCGCTATGGATGGTACGATAAG
11-2655   AAGCGAAGGGAGGGCAGGGAGAAGGGCGCTATGGATGGTACGATAAC
23-1625   GAGCGAAGGGAGGGCAGGGAGAAGGGCGCTATGGATGGTACGATAAG
39-766    TAGCGAAGGGAGGGCAGGGAGAAGGGCGCTATGGATGGTACGATAAG
101-278   GAGCGAAGGGAGGGCAGGGAGAAGGGCGCTATGGATGGTACGATAAC
173-167   cAGCGAAGGGAGGGCAGGGAGAAGGGCGCTATGGATGGTACGATAAG
266-113   TAGCGAAGGGAGGGCAGGGAGAAGGGCGCTATGGATGGTACGATAAC
```

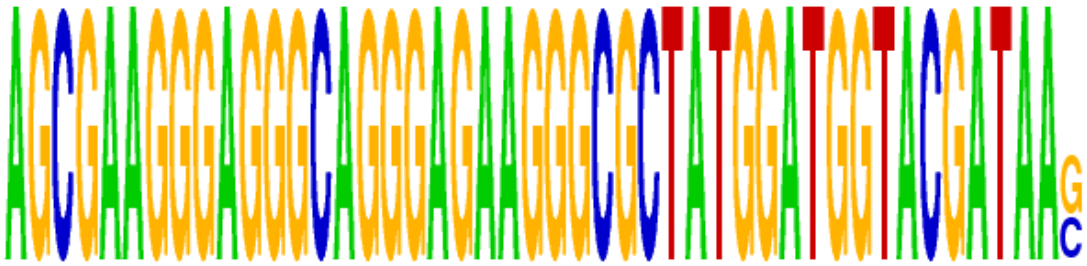

LOCAL SUPERMOTIF number 5, power **24.39**

```
          ++ ++++++++++++++++++++++++++++++++++++++++++++++++
1-51626   GG-CAAACGGTAAGGCCAAAGGGACGAGGGTAGAGATTGATAGAAAGCCGC-
16-2149   TG-CAAACGGTAAGGCCAAAGGGACGAGGGTAGAGATTGATAGAAAGCCGC-
27-1347   GG-CAAACGGTAAGGCCAAAGGGACGAGGGTAGAGATTGATAGAAGGCCGC-
37-932    GG-CAAACGGTAAGGCCGAAGGGACGAGGGTAGAGATTGATAGAAAGCCGC-
38-788    GG-CAGACGGTAAGGCCAAAGGGACGAGGGTAGAGATTGATAGAAAGCCGC-
48-647    GG-CAAACGGTAAGGCCAAAGGGACGAGGGTAGAGATTGATAGGAAGCCGC-
49-627    GG-CAAACGGTAAGGCCAAAGGGACGAGGGTAGAGATTGGTAGAAAGCCGC-
60-496    GG-CAAACGGTAAGGCCAAAGGGACGAGGGTAGAGATTGATGGAAAGCCGC-
75-397    -gaCAAACGGTAAGGCCAAAGGGACGAGGGTAGAGATTGATAGAAAGCCGC-
76-391    GG-CAAACGGTAAGGCCAAAGGGACGAGGGTAGAGATTGATAGAGAGCCGC-
82-358    GG-CAAACGGTAAGGCCAGAGGGACGAGGGTAGAGATTGATAGAAAGCCGC-
89-333    GG-CAAACGGTAAGGCCAAAGGGACGAGGGTAGAGATTGATAGAAAagccgc
90-330    GG-CGAACGGTAAGGCCAAAGGGACGAGGGTAGAGATTGATAGAAAGCCGC-
92-320    GG-CAAACGGTAAGGCCAAAGGGACGAGGGTAGAGATTGATAGAAAGCCac-
94-316    GGCAAAACGGTAAGGCCAAAGGGACGAGGGTAGAGATTGATAGAAAGCCGC-
95-315    GG-CAAACGGTAAGGCCAAAGGGATGAGGGTAGAGATTGATAGAAAGCCGC-
97-310    GG-CTAACGGTAAGGCCAAAGGGACGAGGGTAGAGATTGATAGAAAGCCGC-
125-227   GG-CAAACGGTAAGGCCAAAGGGACGAGGGCAGAGATTGATAGAAAGCCGC-
128-221   GG-CAAACGGTAAGGCCAAAGGGACAAGGGTAGAGATTGATAGAAAGCCGC-
131-217   GG-CAAACGGTAAGGCCAAAGGGACGAGGGTAGAGACTGATAGAAAGCCGC-
133-213   GG-CAAACGGTAAGGCCAAAGGGACGAGGGTAGAGGTTGATAGAAAGCCGC-
143-198   GG-CATACGGTAAGGCCAAAGGGACGAGGGTAGAGATTGATAGAAAGCCGC-
145-195   GG-CAAACGGTAAGGCCAAAGGGACGAGGGTAGAGATTGACAGAAAGCCGC-
146-194   GG-CAAACGGTAAGGCCAAAGGGGCGAGGGTAGAGATTGATAGAAAGCCGC-
164-174   -gtCAAACGGTAAGGCCAAAGGGACGAGGGTAGAGATTGATAGAAAGCCGC-
165-173   GG-CAAACGGTAAGGCCAAGGGGACGAGGGTAGAGATTGATAGAAAGCCGC-
181-161   GG-CAAACGGTAAGGCCAAAGGGACGAGGGTAGAGATTGATTGAAAGCCGC-
182-160   GG-CAAACGGTAAGGCCAAAGGGACGAGGGTTGAGATTGATAGAAAGCCGC-
186-156   GG-CAAGCGGTAAGGCCAAAGGGACGAGGGTAGAGATTGATAGAAAGCCGC-
199-144   cG-CAAACGGTAAGGCCAAAGGGACGAGGGTAGAGATTGATAGAAAGCCGC-
203-138   GG-CAAACGGTGAGGCCAAAGGGACGAGGGTAGAGATTGATAGAAAGCCGC-
206-138   GG-CAAACGGTAAGGCCAAAGGGACGAGGGTAGAGATTGATAGATAGCCGC-
```

```
214-136       GG-CAAACGGTAAGACCAAAGGGACGAGGGTAGAGATTGATAGAAAGCCGC-
219-133       GG-CAAACGGTAAGGCCAAAGGGACGAGGGTAGAGATCGATAGAAAGCCGC-
224-132       GG-CAAACGGTAAGGCCAAAGGGACGGGGGTAGAGATTGATAGAAAGCCGC-
240-122       GG-CAAACGGTAAGGCCAAAGGGACGAGGGTAGGGATTGATAGAAAGCCGC-
245-119       GG-CAAACGGTAAGGCCAAAGGGACGAGGGTGGAGATTGATAGAAAGCCGC-
248-117       GG-CAAACGGTAAGGCCAAAGGGACGAGGGTAGTGATTGATAGAAAGCCGC-
250-116       GGCTAAACGGTAAGGCCAAAGGGACGAGGGTAGAGATTGATAGAAAGCCGC-
259-115       GG-CAAACGGTAAGGCCATAGGGACGAGGGTAGAGATTGATAGAAAGCCGC-
264-114       aG-CAAACGGTAAGGCCAAAGGGACGAGGGTAGAGATTGATAGAAAGCCGC-
267-113       GG-CAAACGGTAAGGCCAAAGGGACGAGGGTAAAGATTGATAGAAAGCCGC-
269-112       GG-CAAACGGTAAGGCTAAAGGGACGAGGGTAGAGATTGATAGAAAGCCGC-
272-111       GG-CAAACGGTAAGGCCAAAGGGACGAGGGTAGAGATTGATAGAATGCCGC-
283-106       GG-CAAACGGTAAGGCCGAAGGGACGAGGGTAGAGATTGATAGAAGGCCGC-
296-101       GG-CAAACGGTAAGGCCAAAGGGACGAGGGTAGAGATTGATAGAAAGCTGC-
306-98        GG-TAAACGGTAAGGCCAAAGGGACGAGGGTAGAGATTGATAGAAAGCCGC-
307-98        GG-CAAACGGTAAGGCCAAAGGGACGAGGGTAGAGATTGATAGACAGCCGC-
309-98        GG-CAAACGGTAAGGTCAAAGGGACGAGGGTAGAGATTGATAGAAAGCCGC-
314-96        GG-CAAACGGTAAGGCCAAAGGGACGAGGGAAGAGATTGATAGAAAGCCGC-
329-90        GG-CAAACGGTAAGGCCAAAGGGACGAGGGTAGAGATTGATAGTAAGCCGC-
333-89        GG-CAAACGGTAAGGCCAAAGGGACGAGGGTAGAGATTGTTAGAAAGCCGC-
335-88        GG-CAAACGGTAAGGCCTAAGGGACGAGGGTAGAGATTGATAGAAAGCCGC-
343-87        GG-CAAACGGTAGGGCCAAAGGGACGAGGGTAGAGATTGATAGAAAGCCGC-
350-83        GG-CAAACGGTAAGGCCAAAGGGACGAGGGTAGAGATTGATAGAACGCCGC-
366-81        GG-CAAACGGTAAGGCCAATGGGACGAGGGTAGAGATTGATAGAAAGCCGC-
369-80        GG-CAAACAGTAAGGCCAAAGGGACGAGGGTAGAGATTGATAGAAAGCCGC-
372-79        GG-CAAACGGTAAGGCCAAAGGGACGAGGGTAGAAATTGATAGAAAGCCGC-
375-79        TG-CAAACGGTAAGGCCAAAGGGACGAGGGTAGAGATTGATAGAAGGCCGC-
376-78        GG-CAAACGGTAAGGCCAAAGGGACGAGGGTAGAGATAGATAGAAAGCCGC-
381-78        GG-AAAACGGTAAGGCCAAAGGGACGAGGGTAGAGATTGATAGAAAGCCGC-
391-75        GG-CAAACGGTAAGGCCAAAGAGACGAGGGTAGAGATTGATAGAAAGCCGC-
413-72        GG-CAAACGGTAAGGCCAAAGGGACGAGGGTAGAGATTGATAAAAAGCCGC-
414-71        GG-CAAACGATAAGGCCAAAGGGACGAGGGTAGAGATTGATAGAAAGCCGC-
416-71        GG-CAAACGGTAAGGCCAAAGGGACGAGGGTAGAGATTGGTAGAAGGCCGC-
420-71        GG-CAAACGGTAAGGCCAAAGGGACGAGGGTAGAGATTAATAGAAAGCCGC-
423-69        GG-CAAACGGTAAGGCCAAAGGGACGAGGGTAGAGATTGATATAAAGCCGC-
442-66        GG-CAAATGGTAAGGCCAAAGGGACGAGGGTAGAGATTGATAGAAAGCCGC-
452-64        GG-GAAACGGTAAGGCCAAAGGGACGAGGGTAGAGATTGATAGAAAGCCGC-
473-59        GG-CAAACGGTAAGGCCAAAGGGACGTGGGTAGAGATTGATAGAAAGCCGC-
485-58        GG-CAAACGGTAAGGCCAAAGGGACGAAGGTAGAGATTGATAGAAAGCCGC-
```

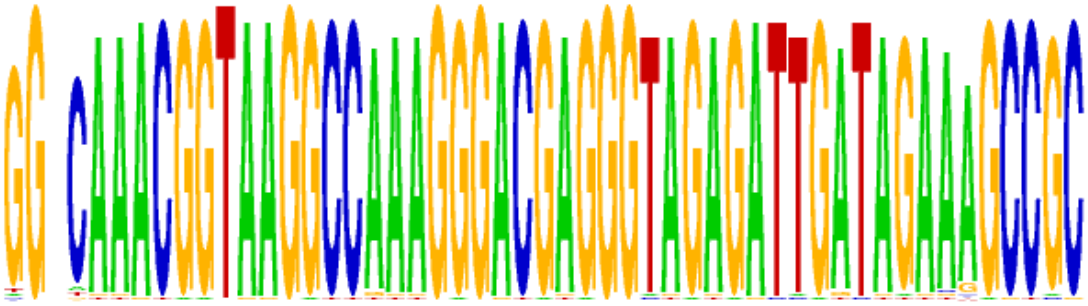

LOCAL SUPERMOTIF number 6, power **23.28**

```
           +++.+++++++++++++++++++++++++++++++++++++++++++++++.
10-3079    GGGTAGGGCAAGGGTAAGGGACCAGCGTACTGTCGTGTAAAGAGATGAGT
17-2147    GGGGAGGGCAAGGGTAAGGGACCAGCGTACTGTCGTGTAAAGAGATGAGT
20-1908    GGGTAGGGCAAGGGTAAGGGACCAGCGTACTGTCGTGTAAAGAGATGAGC
55-536     GGGGAGGGCAAGGGTAAGGGACCAGCGTACTGTCGTGTAAAGAGATGAGC
345-85     GGGTAGGGCAAGGGTAAGGGACCAGCGTACTGTCGTGTAAAGGGATGAGC
405-74     tGGGAGGGCAAGGGTAAGGGACCAGCGTACTGTCGTGTAAAGAGATGAGT
410-72     GGGGAGGGCAAGGGTAAGGGACCTGCGTACTGTCGTGTAAAGAGATGAGT
433-67     GGGGAGGGCAAGGGTAAGGGACCAGCGTACTGTCGTGTAAATAGATGAGT
476-59     GGGGAGGGCAAGGGTAAGGGACCAGCGTACTGTCGTGTAAAGAGATGGGT
```

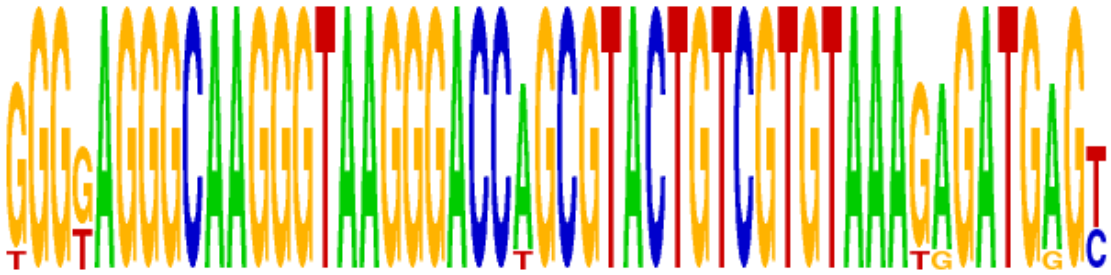

LOCAL SUPERMOTIF number 7, power **20.64**

```
           +++++++++++++++++++++++++++++++++++++++++++++++++.
14-2401    ATCACGAGTTCGGTCGATAGGGAAGGGAAGGGATGGAGGGACGACTGGAG
344-85     gTCACGAGTTCGGTCGATAGGGAAGGGAAGGGATGGAGGGACGACTGGAG
374-79     cTCACGAGTTCGGTCGATAGGGAAGGGAAGGGATGGAGGGACGACTGGAG
417-71     ATCACGAGTTCGGTCGATAGGGAAGGGAAGGGATGGAGGGACGACTGGAc
424-68     tTCACGAGTTCGGTCGATAGGGAAGGGAAGGGATGGAGGGACGACTGGAG
```

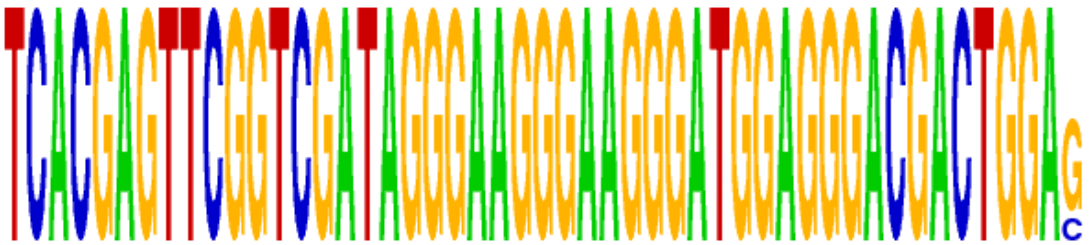

LOCAL SUPERMOTIF number 8, power **20.50**

```
          .++++++.++++++++++++++++++++++++++++++++++++++.
26-1409   AAGGGTGAAGGGAAGGGTGAAGGGAAGTTGACTTAGCGAGGTAATCAGTG
108-259   tAGGGTGAAGGGAAGGGTGAAGGGAAGTTGACTTAGCGAGGTAATCAGTG
158-181   gAGGGTGAAGGGAAGGGTGAAGGGAAGTTGACTTAGCGAGGTAATCAGTG
239-123   AAGGGTGAAGGGAAGGGTGAAGGGAAGTTGACTTAGCGAGGTAATCAGTc
294-102   AAGGGTGTAGGGAAGGGTGAAGGGAAGTTGACTTAGCGAGGTAATCAGTG
```

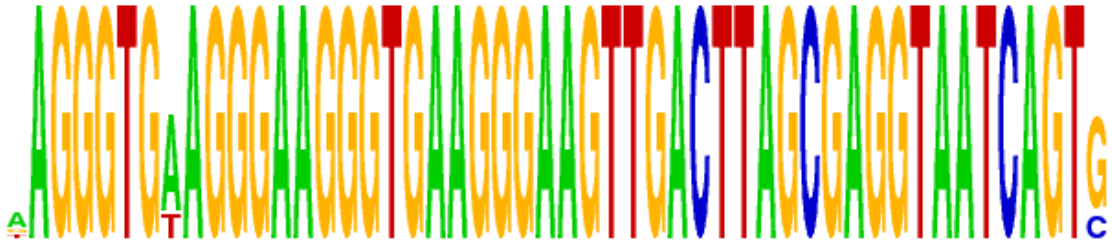

LOCAL SUPERMOTIF number 9, power **18.29**

```
          ..++++++++++++++++++++++++++++++++++++++++++++++
6-5043    -GAGAAAAGTCTGAGGGAGGAGAGAGGGAGGAAAAGACTACATCGCGGA
119-233   gagaAAAAGTCTGAGGGAGGAGAGAGGGAGGAAAAGACTACATCGCGGA
142-199   -tAGAAAAGTCTGAGGGAGGAGAGAGGGAGGAAAAGACTACATCGCGGA
183-159   -GAGGAAAGTCTGAGGGAGGAGAGAGGGAGGAAAAGACTACATCGCGGA
305-98    -ggGAAAAGTCTGAGGGAGGAGAGAGGGAGGAAAAGACTACATCGCGGA
358-82    -GAGAAAAGTCTGAGGGAGGAGAGAGGGAGGAAAAGACTACATCGCGGc
359-82    -GAGAAAAGTCTGAGGGAGGAGAGAGGGAGGAAGAGACTACATCGCGGA
421-70    -GAGAAAAGTCTGAGGGAGGAGAGAGGGAGGAAAGGACTACATCGCGGA
470-60    -GAGAAGAGTCTGAGGGAGGAGAGAGGGAGGAAAAGACTACATCGCGGA
486-58    -GAGAAAAGTCTGAGGGAGGAGAGAGGGAGGAAAAGGCTACATCGCGGA
497-57    -GAGAAAAGTCTGAGGGAGGAGAGAGGGAGGAAAAGACAACATCGCGGA
```

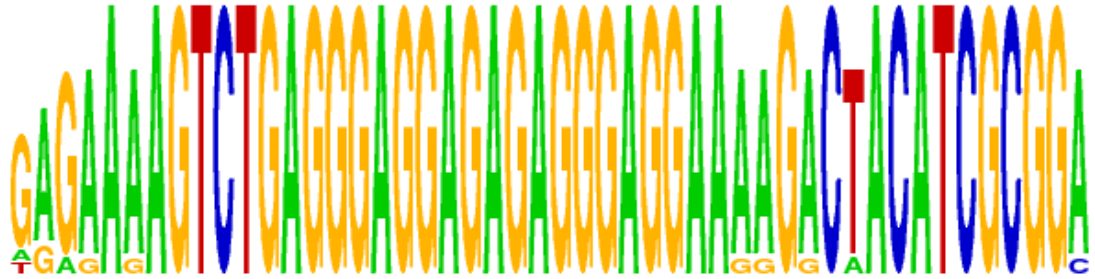

LOCAL SUPERMOTIF number 10, power **17.88**

```
          ++++++++++++++++++++++++++++++++++++++++++++++++++
40-761    aCCGGCAGGGATTAACAAAAGGGACGAGGGATGAGGGAAGAGGGGAATTG
225-131   tCCGGCAGGGATTAACAAAAGGGACGAGGGATGAGGGAAGAGGGGAATTG
271-112   gCCGGCAGGGATTAACAAAAGGGACGAGGGATGAGGGAAGAGGGGAATTG
431-67    cCCGGCAGGGATTAACAAAAGGGACGAGGGATGAGGGAAGAGGGGAATTG
```

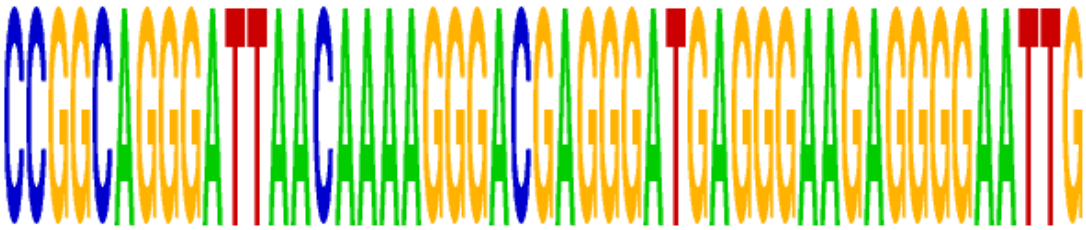

7.3.3 Anti-3Q fibril aptamer selection

LOCAL SUPERMOTIF number 1, power **19.50**

```
                . .  . ..  ..   . .  . .   .. ....++++++++++++ .. .  . . ..
7-88      ----------------------------------TTTGTTTTCTTTCTCTTCTCtaaggacgga--
16-68     -------------------acgT-----------TTTCTTTTCTTTCTCTTACATCcagg------
36-44     gtgtgGTATTTTCTTTCTCTTCTTCAGcac------
135-28    -------------------------------------CTTTTCTTTCTCTTTTTCttctaccttga
151-27    ------------------------------cgTATTTATTTTCTTTCTCTTGTCACggat------
158-26    ----------------------------caatgttaCATTTTCTTTCTCTTGTTACaa--------
168-26    ----------------------gttttcacgATGATTGTTTTCTTTCTCTTT---------------
174-26    ------------------------------------agaTTTTCTTTCTCTTAAGTctttagatg--
179-25    ------------------------------------cTATTTTCTTTCTCTTCCTGTtctacgtga-
183-25    --------------------------------gggTTTTCTTTCTTTCTCTTGATTGtcttg-----
251-22    ----aagtctcCG-----------------------ATTTTCTTTCTCTTTGTGcta--------
276-21    tttcatgatttCG-----------------------ATTTTCTTTCTCTTGga------------
279-21    ----------------------------cgaATAATTGTTTTCTTTCTCTCGTTCAct--------
286-20    --------------------------tttgtTGATCATTTTCTTTCTCTTTAGgcc----------
288-20    ----------------tcacgaT-----------TGTCTTTTCTTTCTCTTCAGTGc----------
301-20    ---------------------------------aggTCATTTACTTTCTCTTTTGACtatagt----
319-20    ------------------------atatcacgttaGTTTTTTCTTTCTCTTAAC------------
322-20    ----------------------------tcatttttcacaTTCTTTCTCTTGTactag--------
326-19    ----------------------------gttgcAATTATTTTCTTTCTCTTTGTGTCa--------
333-19     ---------------------------------tcTCGTTTCTTTCTCTTTCTTTCtctgtgg--
384-18    -------------acTG--------------------GTTTTCTTTCTATTCTTCctgtgtgt---
396-18    ----------------------------ttacATTTATTATCTTTCTCTTTCGTCtgt--------
411-18    --------------------------caacttcttcgTTTTATTTCTCTTAACgaa----------
416-18    ---------------cttttgtT-----------TGTTTTTTCTTTCTCTTCGTGaa----------
422-18    -----------attgTG--------------------GTTTTCTTTCTCTTCTTCAGtcg------
```

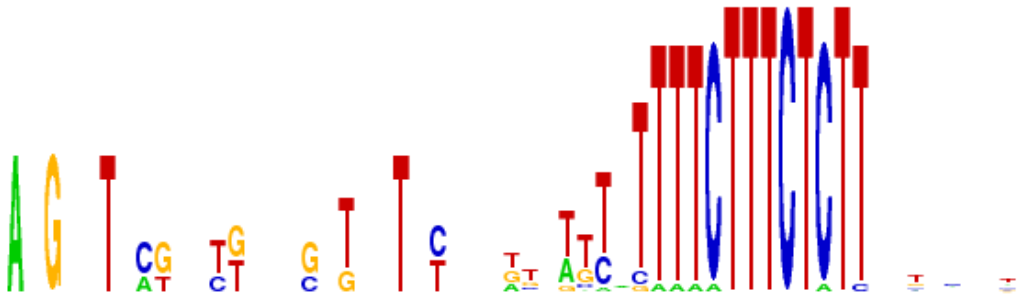

LOCAL SUPERMOTIF number 2, power **13.13**

```
                 ++++++++++.++.+++++++.++++++++
1-658            GGAGGGACATAGGAGTAGTGCATGGGTAGG
14-73            GGAGGGACATAGGAGTAGTGCGTGGGTAGG
308-20           GGAGGGACATGGGAGTAGTGCATGGGTAGG
442-17           GGAGGGACATAGGGGTAGTGCATGGGTAGG
```

LOCAL SUPERMOTIF number 3, power **13.08**

```
                .....   ......+.++++++++++.. .....   .
28-53         tgaatatgtTTATATCTTTCTTTCTCTTca-----------
174-26        -----------AGATTTTTCTTTCTCTTAAGTctttagatg
183-25        --------gggtTTTCTTTCTTTCTCTTgattgtcttg---
198-24        ---acacgaTTATTTGTTTCTTTCTCTTACGTt--------
229-23        ---acggataattgaCTTTCTTTCTCTTAACat--------
237-22        caaatcatgaTACATCTTTCTTTCTCTTtg-----------
319-20        -atatcacgTTAGTTTTTTCTTTCTCTTAAC----------
412-18        ----------ttcTTGTTTCTTTCTCTTAGtctgcggtaa-
418-18        ---------atcTTTCTTTCTTTCTCTTAGctgtctga---
```

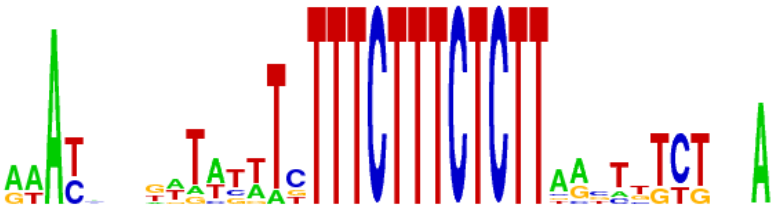

LOCAL SUPERMOTIF number 4, power **11.63**

```
                          ...     .  .... +.+.+.++..++++.....    .  .
19-65          ---------------------gTTTATTTCTCTTTCTTCtctaggaacgaa
42-41          cgataatTT-------------TCTCTTTTGCTTTCTTTTGAa--------
53-38          ---------------ctaATACTTTCTCTTTCTTTCTCTGTtgtg------
67-35          ------acT-------------TCTCTTTTCTTTCCTTCTATcacgcaa--
69-35          --------------caatttcATTTCTCATACTTTCTCTTGaa--------
73-34          ------tttttcacgattATTCTTTCTCTTGCTTTC---------------
79-33          -cgaattTT-------------TCTTTCTTACTTTCTCTTGcgt-------
97-31          -------aT-------------TCTCTTTTGTTTTCTTCTGAtctgcgaa-
136-28         ----------------------TTTGTTTTTCTTTCTCATCAaatacttgg
156-26         --------------------ttcTTGTTTATCTTTCTCTTCaTCGTCgta-
158-26         ----caATG-------------TTACATTTTCTTTCTCTTGTtacaa----
170-26         -actgtttT-------------TCTCTTTTCTTTCTTCCTgtg--------
183-25         --------------------gggTTTTCTTTCTTTCTCTTGaTTGTCTtg-
207-24         --------------cgaatatcaGT-tTTTTCTTTCTCATCtcta------
217-23         ----ttcTT-------------TCTCTTATACTTTCTCTTGTccatt----
219-23         --------------------ACTTTCTCTTATTTTCTCTGTat--------
232-22         --------------ttggtactaaTCTTTTTCTTTCTCTGgata-------
257-22         ---------------cgggTAATTTCTTTTTCTTTCTCTTGgagt------
275-21         ------------------cTTCTTTCTCTTTCTTTCTtcttttacgga---
288-20         --tcacgaT-------------TGTC-TTTTCTTTCTCTTCAgtgc-----
322-20         ----tcATT-------------TTTCACATTCTTTCTCTTGTactag----
333-19         -------------tctcgtTTCTTTCTCTTTCTTTCTCTGTgg--------
343-19         ttgacattT-------------TCTCTTTTCTCTCCGTCAATt--------
414-18         --------------agttaTAATTTATTTTTCTTTCTTCacggt-------
416-18         --------------cttttgtttGT-TTTTTCTTTCTCTTCgtgaa-----
418-18         ----------------------aTCTTTCTTTCTTTCTCTTAgCTGTCTga-
```

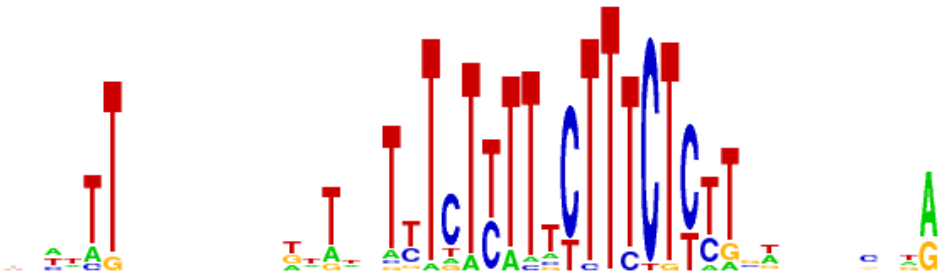

LOCAL SUPERMOTIF number 5, power **11.56**

```
                    ....  ...... .....+.++++++++++...  .   .
5-112          --------ttttTCATTAA---TGTCTTTTCTTTCTCGGGa---------
16-68          ----acgTTT--------------TCTTTTCTTTCTCTTacatccagg--
25-55          --------------------TTTGTTTTGTTTTTCTCTTCtcgataacgt
111-30         ------------------gaTTTGTTTTGTTTTTCTCTTAttcacgga--
123-29         -------ctgaaTCATTAA---TATCTTTTCTTTCTCTGG----------
256-22         ------atcT--------------TCTTTTCTTTCTCacagtgcgtagaa
257-22         cgggtaaTTT--------------CTTTTTCTTTCTCTTggagt------
269-21         --------atctgcgtatA---TATCTTTTCTTTCTCGGGg---------
288-20         ---------------TCACGATTGTCTTTTCTTTCTCTTCagtgc-----
319-20         ------------ataTCACGTTAGTTTTTTCTTTCTCTTAac--------
376-18         --------agtgttatttcatggGTATTTTCTTTCTCT------------
416-18|        --------------cttttGTTTGTTTTTTCTTTCTCTTCgtgaa-----
```

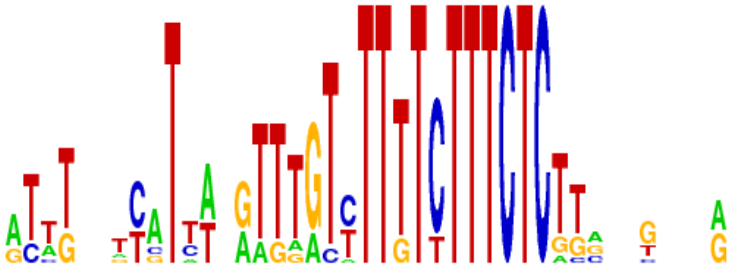

LOCAL SUPERMOTIF number 6, power **11.55**

```
                       . ..  ..  ...++++.++++++++    .
76-33          ------tacatgtaAGTTTTTTTCTCTTTTtacgga------
116-30         -------gatttctacTTTTCTTCTCTTTGAtaacgt-----
182-25         -------------CAGTTTTTTTCTCTTTTctctaaatcctc
199-24         ----aacctttcgaATTTTTCTTCTCTTTACGga--------
270-21         ------catttaaCATTTTTCTTCTCTTTTaaatcg------
310-20         ------aacattatcTTTTTCTTCTCTTTcgtcatt------
321-20         ---------attcttcTTTTCTTCTCTTTACGcgttaat---
379-18         gatccatgaacacatTTTTTCTTCTCTTTG------------
433-17         ---------actgCAGTATTTTTCTCTTTTgccccagga---
447-17         tcacgtttgtacaatTTTTTCTTCTCTTGGA-----------
```

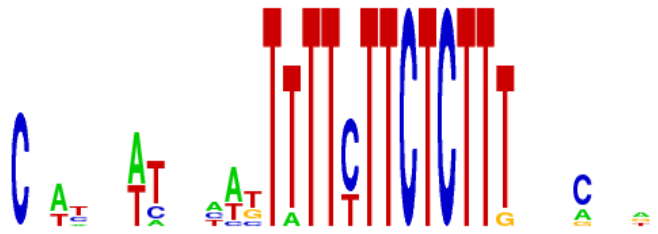

LOCAL SUPERMOTIF number 7, power **11.40**

```
                  ++++++++++++++++++. ++++++++++
46-39             AATTAGAAAACGTTTTTTTT-GGTCCGAGTA
122-29            AATTAGAAAACGTTTTTTTTtGGTCCGAGTA
359-19            AATTAGAAAACGTTTTTTT—GGTCCGAGTA
```

LOCAL SUPERMOTIF number 8, power **11.11**

```
                  ...+.+.++++++++++++++++++++++++
51-38             ---GTTGTTTTTTTCACGTCTTGTCTGTGCAA
238-22            GTTGTTTTTTTTTTCACGTCTTGTCTGTGCAA
252-22            GTTG-TTTTTTTTTCACGTCTTGTCTGTGCAA
```

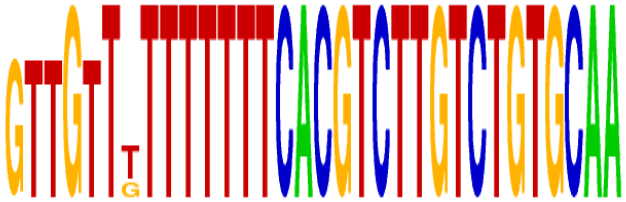

LOCAL SUPERMOTIF number 9, power **10.43**

```
              .  ..   . .. .  .      . .. ..           ... ... .    .
4-119     ----------------------------------------------------------act
16-68     ------------------------------------------------------acgT-------
40-43     ---------------------------------------------aggttttagT--------
62-36     ---------gCA-----------------------------------------------------
73-34     -------------tttttcacG-------------------------------------------
76-33     ------------------------tacaTG--------------------T--------------
110-30    ----------------------------------------------------aacgT--------
113-30    -----------------------------------------------------atT--------
116-30    ------------------------------------------------------------ga
119-29    ------------------------------------------------------------------
134-28    ----------------------acttctcgTG--------------------T--------------
174-26    --------------------AG--------------------------------------------
183-25    --------------------ggGT------------------------T--------------
198-24    ---------------------------------------------acacgattAT--------
207-24    ------------cgaatatcAG--------------------------------------------
211-23    -------------------agG---------------------------------------------
229-23    acggataaTTG-------------------------------------------------------
232-22    -------------------------------ttggtactA-----------AT--------------
237-22    ------------------------------------------------------caaatcatg
251-22    --aagtctccG-------------------------------------------------------
257-22    ---------------------------------------------cgggtaattT--------
285-20    ------------------------------------------------------------------
286-20    ------------------------------------------tttgttgAT--------
319-20    ----------atatcacgttAG--------------------------------------------
320-20    ------------------------------------------------------atagctgt
321-20    ------------------------------------------------------------------
322-20    --tcatttTTC-------------------------------------------------------
326-19    ---------------------------------gttgcA-----------AT--------------
333-19    ------------------------------------------------------------------
338-19    ----------------------------------------------------CAT--------
347-19    ----------------------GT----------------------------T--------------
348-19    ----------------------------------------------------aAT--------
382-18    -------------------------caacaTG--------------------T--------------
383-18    ------------------------------------------------------acggat
412-18    ------------------------------------------------------------------
416-18    ------------cttttgtttG--------------------------------------------
418-18    ----------------------------------------------------atcT--------
423-18    --------ctCA------------------------------------------------------
428-17    ------------------------------------gatttcacgaaCAT--------
```

```
                  .......+++.++++++++. .. .. . .
4-119 (4)         tcTCTTTGTTCTTTCTCTTAACgagta-----
16-68 (5)         --TTTCTTTTCTTTCTCTTACatccagg----
40-43 (11)        ----TTCATTCTTTCTCTTTCacg--------
62-36 (4)         ----ATTTTCCTTTATCTTTTCtctttgtcg-
73-34 (10)        ----ATTATTCTTTCTCTTGCTttc-------
76-33 (8)         ----AAGTTTTTTCTCTTtttacgga-----
110-30 (6)        ----TATTTTCTTTCTTCTTcgagttcac---
113-30 (4)        --TCTCTTTACTTTCTCTTAACgaactac---
116-30 (3)        tTtctacttttcttctcttTgataacgt----
119-29 (1)        ---cTTTTTTCTTTCTGTTttctctctcgttc
134-28 (12)       ----TTGTTTTTTTCTCTTGtgc---------
174-26 (3)        ----ATTTTTCTTTCTCTTAAgtctttagatg
183-25 (6)        ----TTCTTTCTTTCTCTTGattgtcttg---
198-24 (11)       ----TTGTTTCTTTCTCTTACgtt--------
207-24 (11)       ----TTTTTTCTTTCTCatctcta--------
211-23 (4)        ----TTTTTTCTTTCTtcaggattatcgcga-
229-23 (12)       -----ACTTTCTTTCTCTTAACat--------
232-22 (12)       ----CTTTTTCTTTCTCTggata---------
237-22 (10)       atacaTCTTTCTTTCTCTTTG-----------
251-22 (10)       -----ATTTTCTTTCTCTTTGTgcta------
257-22 (11)       ----CTTTTTCTTTCTCTTGgagt--------
285-20 (1)        agTCTTTGTTTTTTCTCTTGCTcctcatcg--
286-20 (10)       ----CATTTTCTTTTCTCTTtaggcc------
319-20 (13)       ----TTTTTTCTTTCTCTTAAC----------
320-20 (9)        tTTCTTTTTTACTTCTCTTAGg----------
321-20 (1)        aTtcttcttttcttctcttTacgcgttaat--
322-20 (10)       -----ACATTCTTTCTCTTgtactag------
326-19 (9)        ----TATTTTCTTTCTCTTTGTgtca------
333-19 (1)        --TCTCGTTTCTTTCTCTTTCTttctctgtgg
338-19 (4)        ----TATTTTCTTTTTCCTTGTtgtaaatgt-
```

```
347-19 (4)          ----CTCTTTGTTTCTCTTTCTatgcataga-
348-19 (4)          ----TTGTTTTTTTCACTTcttcattgtgt--
382-18 (9)          ----TTTTTCTTTTCTCTTacgggt-------
383-18 (7)          ccaaTCTTTACTTTCTCTTgtcca--------
412-18 (1)          -TTCTTGTTTCTTTCTCTTAGTctgcggtaa-
416-18 (11)         ----TTTTTTCTTTCTCTTcgtgaa-------
418-18 (5)          ----TTCTTTCTTTCTCTTAgctgtctga---
423-18 (5)          ----ATTATTCTTTCTCTTTTCgcgatttt--
428-17 (15)         ----TTTTTCCTTTTTCCTT------------
```

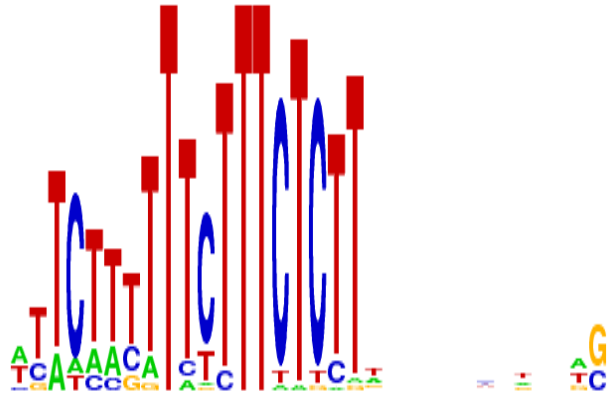

LOCAL SUPERMOTIF number 10, power **10.18**

```
                          . ...... .+++.++++..++++.. ....... .
6-90                ----------acgttttgaTTTCTCTTTACTTCTTCAGTc-------
32-47               ----------atTCT----TTTTCTCTTATCTTCTTCGGTgtcg----
56-38               ---------------gTTCTTTTCTATTTTCTTTCtCACTACGaa---
63-36               ------------aCT----TTTTTTCTTTCCTTCTtATCGACGaca--
67-35               --------------acttctcTTTTCTTTCCTTCTAtcacgcaa----
127-29              ------------------CTTTTTTCTTTTCTTCCtGTCTACGcggaa
170-26              ----------actgT----TTTTCTCTTTTCTTtcttcctgtg-----
261-22              acgtattctgcgaaT----TTTTCTCTTTCCTTC--------------
291-20              -----------actT----TTTTTTCTTTCCTTCTtATCGACGaca--
312-20              ---------------gatgTTGTTTATTTTCTTCTtCACTAacaa---
315-20              ----------------tttgTTTTTCTTTTCTTCTAgttcacgtta--
339-19              ------------acttTTCTTTTCTCTTATCTTCgaatgatg------
375-18              ------------TCT----TTTTCTCTTGTCTTCTtATgtccaatt--
384-18              ------------actggttTTCTTTCTATTCTTCCtGTgtgt------
432-17              ------------------acTTTCTCTTTTCTTCTggaatag------
```

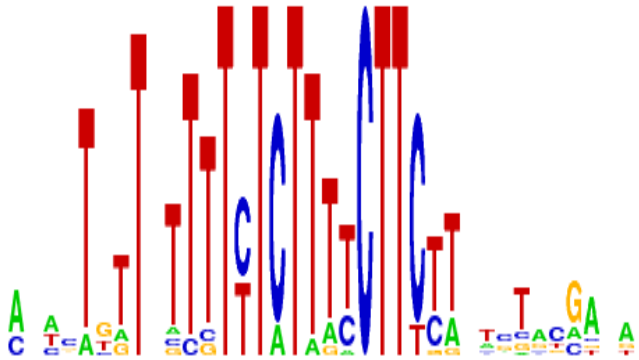

7.4 Appendix 4: Multiple alignment comparison with control aptamer sequences

The top ten consensus sequences comparing the lead aptamers from the three Aβ40 selections described in this thesis (**Figure 3.17**) to the control aptamer sequences used in Chapter 5, β55, DV1, RVGP1 and NGGA1 (Sections 5.5.1). Power scores are given as described in **Appendix 7.3.**

LOCAL SUPERMOTIF number 1, power **10.36**

```
       +++++++++++++++++++++++++++++++++++ +++++ +++++
2A1    GGCAAACGGUAAGGCCAAAGGGACGAGGGUAGAGAUUGAUAGAAAGCCGC
2A416  GGCAAACGGUAAGGCCAAAGGGACGAGGGUAGAGAUUGGUAGAAGGCCGC
```

LOCAL SUPERMOTIF number 2, power **8.60**

```
      .......... ......++..+...++++.....++..+..+..+.+....  .... .
2A1   ggcaaacgguAAGGCCAAAGGGACGAGGGUAGAGAUUGAUAGAAAGCCgc---------
2A359 -------------GAGAAAAGUCUGAGGGAGGAGAGAGGGAGGAAGAGAcuacaucgcg
2A416 ggcaaacgguAAGGCCAAAGGGACGAGGGUAGAGAUUGGUAGAAGGCCgc---------
M1    ----------------uAAGGGAAGUGUGCUGAGAGAGGGAAGUUGCGuagcgaagcac
M3    ---------gAGGUCGAAGGGGAUGAUGAAGUAGAAUUAGAGCA---------------
M214  ----------AAGGGGAACAGAAAGAGGGAAAGGAGGGGAAAAAGGACAaagcgagaaa
```

LOCAL SUPERMOTIF number 3, power **7.20**

```
       ... ..... .....+.+..+ ...++.++.....+.... .  .. .
2A1    -------ggcaAACGGUAAGGCCAAAGGGACGAGGGUAgagauugaua
2A359  -------------GAGAAAAGUCUGAGGGAGGAGAGAgggaggaagag
2A416  -------ggcaAACGGUAAGGCCAAAGGGACGAGGGUAgagauuggua
2A417  ggucgauaggGAAGGGAAGGGAUGGAGGGACGACUGGAc---------
M1     gugugcugagagAGGGAAGUUGCGUAGCGAAGcacgauaacg------
M50    gugagaguaaGAGUGGAAGGGAAGAAAGUACaca--------------
M53    gaauggguacGAAGGGAAGAGGAGGAGCGAGAAGGGA-----------
M214   agggaaaggaggggaaaAAGGACAAAGCGAgaaagg------------
```

LOCAL SUPERMOTIF number 4, power **6.9**

```
             .+...++..  +  ......+.+.....+ ..+.. ........ ....
2A359  ------gAGAAAAGUCUGAGGGAG--GAGAGAGGGAGGAAGAGA-----CUACAucgcgga
M1     -----uAAGGGAAGUGUGCUGAGAGAGGGAAGUUGCGUA-GCGAAGCACGAUAACg-----
M50    ------AAGGGAAGGCAGAUAAGUGAGAGUAAGAGUGGAAGGGAAGAAAGUACACa-----
M214   aaggggAACAGAAAGAGGGAAAGGAGGGGAAAAAGGACAAAGCGAGAAAGg----------
```

LOCAL SUPERMOTIF number 5, power **6.82**

```
                .         . ++.+++.+.+... +...++..  .  ....
2A39           -----------uAGCGAAGGGAGGGCAGGGAGAagggcgcuau
2A417          aguucggucgAUAGGGAAGGGAAGGGAUGGAGGgacgacugga
M50            -----------aAGGGAAGGCAGAUAAGUGAGAguaagagugg
M214           gggaacagaaAGAGGGAAAGGAGGGGAAAAAGGacaaagcgag
```

LOCAL SUPERMOTIF number 6, power **6.70**

```
           . ... . . ..       .  . ......++.+........ ++.+.......
2A39    ----------------------------uagCGAAGGGA-----GGGcAGGGAG-AAGG
2A417   cggucgauagGG----------------------AAGGGAAGGGAUGG-AGGGACGACUG
M5      ---gauaugcGG----------------------CAGGAAAGGAAACA-AGAGUACugcg
M50     ------aagggaaggcagauaagugagaguaagaguGGAAGGGAAGAA-AGUACACa---
M53     ----------acacgaagcgcgcgaauggguaCGAAGGGAAGAGGAGG-AGCGAG-AAGG
M174    --------------------------------uAGGGAAAGGUAAAG-AGAGUACCAUG
M214    --------------------------------aAGGGGAACAGAAAG-AGGGAA-AGGA


                ..   .  .. .
2A39 (26)       Gcgcuauggaugg
2A417 (48)      GAC----------
M5 (35)         acag---------
M50 (51)        -------------
M53 (49)        Ga-----------
M174 (27)       GACaugcuggcgu
M214 (26)       Ggggaaaaaggac
```

LOCAL SUPERMOTIF number 7, power **6.70**

```
                ...  . ......++..... ..............
2A39            ------uagcGAAGggagggCAGGGAGAAGGGcgcu
2A359           gagaaaagucugAGggaggaGAGAGGGAGGAAgaga
2A417           ggucgauagggAAGGGAAGGGAUGGAgggacgacug
M1              ---------uaAGGgaagugUGCUGAGAGAGGgaag
M5              -------gauaugcGGCAGGAAAGGAaacaagagua
M50             -----------AAGggaaggCAGAUAAGUGagagua
M53             gaagcgcgcgaAUGgguacgAAGGGAAGAGGaggag
M174            ----------uAGGgaaaggUAAAGAGAGuaccaug
M214            ggaacagaaaGAGGgaaaggAGGGGAAAAAGGacaa
M233            -------gaggauGggaagaGCCGCGGAGGUAaugu
```

LOCAL SUPERMOTIF number 8, power **6.69**

```
           ... . ........ .. ...... . .+............+..+ ....+...
B55     -----------uuuACC---------------GUAAGGCCugucuucguuugacagcggcu
2A1     ---------gGCAAACG---------------GUAAGGCCAaagggaCGAGGGUAGAGAUU
2A416   ---------gGCAAACG---------------GUAAGGCCAaagggaCGAGGGUAGAGAUU
M3      ----------------------gaggucgAAGGGGAUGAUgaaguaGAAUUAGAGCA---
M50     ----aagggaaggcagauaagugagaguaagaguggaagggAAGAAAGUACaca-------
M53     cacgaagcgcGCGAAUG---------------GGUACGAAGggaagaGGAGGAGCGAGAAG
M174    --------------uaG---------------GGAAAGGUAAAGAGAGUACcauggacaug
M214    ----------aaggggaacagaaagagggaAAGGAGGGGAAaaaggaCAAAGCGAGAAAGG
M233    ----------------gaggaugggaagagccgcgGAGGUAauguuaCAAAAUGAGGUAGG
```

LOCAL SUPERMOTIF number 9, power **6.60**

```
          ..... .....+.+...++.+.. .............++. . .. . .
2A1     ggcaaacgguaAGGCCAAA--GGGACG--AGGGUAGAGAUUGAUAGAAAgccgc------
2A417   -aucacgaguuCGGUCGAUAGGGAAGG-GAAGGGAUGGAGGGACGacuggac--------
M3      ----------GAGGUCGAAGGGGAUGA-UGAAGUAGAAUUAGAGCa--------------
M5      ---------gauaugC-----GGCAGGaAAGGAAACAAGAGUACUGCGAcag--------
M53     ---acacgaaGCGCGCGAAUGGGUACG-AAGGGAAGAGGAGGAGCGAGAAggga------
M214    -----------------AAGGGGAACA-GAAAGAGGGAAAGGAGGGGAAAaaggacaaag
```

LOCAL SUPERMOTIF number 10, power **6.58**

```
         .   .  .. .+..++.............++++.....  .
2A417   guucggucgauAGGGAAGGGAAGGGAUGGAGGGACGACUGGAC----------
M1      ---------uaAGGGAAGUGUGCUGAGAGAGGGAAGuugcguagcgaagcacg
M50     gaaggcagauAAGUGAGAGUAAGAGUGGAAGGGAAGAAAGUACaca-------
M214    ----aaggggAACAGAAAGAGGGAAAGGAGGGGAAAAAGG-ACaaagcgagaa
```

References

1. T.P.J. Knowles, M. Vendruscolo and C.M. Dobson. The amyloid state and its association with protein misfolding diseases. *Nat. Rev. Mol. Cell. Biol.*, 2014, **15**(6), pp.384-396.
2. C.M. Dobson. Protein folding and misfolding. *Nature*, 2003, **426**(6968), pp.884-890.
3. F. Chiti and C.M. Dobson. Protein misfolding, functional amyloid, and human disease. *Annu. Rev. Biochem.*, 2006, **75**(1), pp.333-366.
4. D. Eisenberg and M. Jucker. The amyloid state of proteins in human diseases. *Cell*, 2012, **148**(6), pp.1188-1203.
5. R. Virchow. Ueber eine im gehirn und rückenmark des menschen aufgefundene substanz mit der chemischen reaction der cellulose. *Archiv. F. Pathol. Anat.*, 1854, **6**(1), pp.135-138.
6. R. Virchow. Weitere mittheilungen über das vorkommen der pflanzlichen cellulose beim menschen. *Archiv. F. Pathol. Anat.*, 1854, **6**(2), pp.268-271.
7. A.S. Cohen. General introduction and a brief history of the amyloid fibril. *In:* Marrink. J and H. Van Rijswijk. M, eds. *Amyloidosis*. Dordrecht: Nijhoff, 1986, pp.3-19.
8. N. Friedreich and A. Kekulé. Zur Amyloidfrage. *Archiv. F. Pathol. Anat.*, 1859, **16**(1-2), pp.50-65.
9. H. Bennhold. Eine specifische amyloid-farbung mit kongorot. *Munch. Med. Wochenschr.*, 1922, (69), pp.1537-1538.
10. P. Divry and M. Florkin. Sur les propriétés optiques de l'amyloide. *C. R. Soc. Biol.*, 1927, (97), pp.1808-1810.
11. A.S. Cohen and E. Calkins. Electron microscopic observations on a fibrous component in amyloid of diverse origins. *Nature*, 1959, **183**(4669), pp.1202-1203.
12. L. Fruhling, J. Kempf and A. Porte. Structure et formation de la substance amyloid dans l'amylose expérimentale de la souris. Étude au microscope électronique *C. R. Acad. Sci.*, 1960, (250), pp.1385-1386.
13. R. Caesar. Die Feinstruktur von Milz und Leber bei experimenteller Amyloidose. *Zeitschrift für Zellforschung*, 1960, **52**(5), pp.653-673.
14. A.S. Cohen, A. Frensdorff, S. Lamprecht and E. Calkins. A study of the fine structure of the amyloid associated with familial mediterranean fever. *Am. J. Path.*, 1962, **41**(5), pp.567-578.
15. E.D. Eanes and G.G. Glenner. X-ray diffraction studies on amyloid filaments. *J. Histochem. Cytochem.*, 1968, **16**(11), pp.673-677.
16. L. Bonar, A.S. Cohen and M. Skinner. Characterisation of the amyloid fibril as a cross-β protein. *Proc. Soc. Exp. Biol. Med.*, 1969, (131), pp.1373-1375.
17. G.G. Glenner, W. Terry, M. Harada, C. Isersky and D. Page. Amyloid fibril proteins: Proof of homology with immunoglobulin light chains by sequence analyses. *Science*, 1971, **172**(3988), pp.1150-1151.
18. E.P. Benditt and N. Eriksen. Chemical classes of amyloid substance. *Am. J. Path.*, 1971, **65**(1), pp.231-252.

19. K. Sletten, P. Westermark and J.B. Natvig. Characterization of amyloid fibril proteins from medullary carcinoma of the thyroid. *J. Exp. Med.*, 1976, **143**(4), pp.993-998.
20. E.P. Benditt and N. Eriksen. Amyloid. A protein related to the subunit structure of human amyloid fibrils. *Proc. Natl. Acad. Sci.*, 1966, **55**(2), pp.308-316.
21. G.G. Glenner and C.W. Wong. Alzheimer's disease: Initial report of the purification and characterization of a novel cerebrovascular amyloid protein. *Biochem. Biophys. Res. Commun.*, 1984, **120**(3), pp.885-890.
22. J.D. Sipe, M.D. Benson, J.N. Buxbaum, S.-I. Ikeda, G. Merlini, M.J.M. Saraiva and P. Westermark. Amyloid fibril protein nomenclature: 2012 recommendations from the Nomenclature Committee of the International Society of Amyloidosis. *Amyloid*, 2012, **19**(4), pp.167-170.
23. Office for National Statistics Uk. *Mortality statistics: Deaths registered in England and Wales* [online]. 2012. [Accessed 28.08.2015]. [http://www.ons.gov.uk/ons/rel/vsob1/mortality-statistics--deaths-registered-in-england-and-wales--series-dr-/2012/sty-causes-of-death.html].
24. C. Dobson. Alzheimer's disease: addressing a twenty-first century plague. *Rend. Fis. Acc. Lincei*, 2015, **26**(3), pp.251-262.
25. Alzheimer's Disease International. *World Alzheimer's reports* [online]. 2015. [Accessed 28.08.2015]. [http://www.alz.co.uk/research/world-report-2015].
26. S.J. Olshansky, D.J. Passaro, R.C. Hershow, J. Layden, B.A. Carnes, J. Brody, L. Hayflick, R.N. Butler, D.B. Allison and D.S. Ludwig. A potential decline in life expectancy in the united states in the 21st century. *N. Engl. J. Med.*, 2005, **352**(11), pp.1138-1145.
27. Alzheimer's Society. *Financial cost of dementia* [online]. 2015. [Accessed 28.08.2015]. [http://www.alzheimers.org.uk/site/scripts/documents_info.php?documentID=418].
28. A.S.D. International. *Dementia statistics. Alzheimer's disease international* [online]. 2014. [Accessed 22/07/2014]. Available from: http://www.alz.co.uk/research/statistics [http://www.alz.co.uk/research/statistics].
29. C.B. Anfinsen, E. Haber, M. Sela and F.H. White. The kinetics of formation of native ribonuclease during oxidation of the reduced polypeptide chain. *Proc. Natl. Acad. Sci.*, 1961, **47**(9), pp.1309-1314.
30. C. Levinthal. Are there pathways of protein folding? *J. Chim. Phys.*, 1968, (65), pp.44-45.
31. R. Zwanzig, A. Szabo and B. Bagchi. Levinthal's paradox. *Proc. Natl. Acad. Sci.*, 1992, **89**(1), pp.20-22.
32. C. Levinthal. How to fold graciously. *In: Mossbauer Spectroscopy in Biological Systems: Proceedings of a meeting held at Allerton House*, Monticello, Illinois. University of Illinois, 1969, pp.22-24.
33. K.A. Dill and H.S. Chan. From Levinthal to pathways to funnels. *Nat. Struct. Mol.*, 1997, **4**(1), pp.10-19.
34. J. Schonbrun and K.A. Dill. Fast protein folding kinetics. *Proc. Natl. Acad. Sci.*, 2003, **100**(22), pp.12678-12682.

35. M. Vendruscolo, E. Paci, M. Karplus and C.M. Dobson. Structures and relative free energies of partially folded states of proteins. *Proc. Natl. Acad. Sci.*, 2003, **100**(25), pp.14817-14821.
36. D.J. Brockwell and S.E. Radford. Intermediates: ubiquitous species on folding energy landscapes? *Curr. Opin. Struct. Biol.*, 2007, **17**(1), pp.30-37.
37. T.R. Jahn and S.E. Radford. Folding versus aggregation: Polypeptide conformations on competing pathways. *Arch. Biochem. Biophys.*, 2008, **469**(1), pp.100-117.
38. A.J. Baldwin, T.P.J. Knowles, G.G. Tartaglia, A.W. Fitzpatrick, G.L. Devlin, S.L. Shammas, C.A. Waudby, M.F. Mossuto, S. Meehan, S.L. Gras, J. Christodoulou, S.J. Anthony-Cahill, P.D. Barker, M. Vendruscolo and C.M. Dobson. Metastability of native proteins and the phenomenon of amyloid formation. *J. Am. Chem. Soc.*, 2011, **133**(36), pp.14160-14163.
39. E. Gazit. The "correctly folded" state of proteins: Is it a metastable state? *Angew. Chem. Int. Edit.*, 2002, **41**(2), pp.257-259.
40. J.I. Guijarro, M. Sunde, J.A. Jones, I.D. Campbell and C.M. Dobson. Amyloid fibril formation by an SH3 domain. *Proc. Natl. Acad. Sci.*, 1998, **95**(8), pp.4224-4228.
41. F. Chiti, P. Webster, N. Taddei, A. Clark, M. Stefani, G. Ramponi and C.M. Dobson. Designing conditions for *in vitro* formation of amyloid protofilaments and fibrils. *Proc. Natl. Acad. Sci.*, 1999, **96**(7), pp.3590-3594.
42. B. Urbanc, L. Cruz, S. Yun, S.V. Buldyrev, G. Bitan, D.B. Teplow and H.E. Stanley. In silico study of amyloid β-protein folding and oligomerization. *Proc. Natl. Acad. Sci.*, 2004, **101**(50), pp.17345-17350.
43. S. Auer, F. Meersman, C.M. Dobson and M. Vendruscolo. A generic mechanism of emergence of amyloid protofilaments from disordered oligomeric aggregates. *PLoS. Comp. Biol.*, 2008, **4**(11), p.e1000222.
44. J.W. Kelly and W.E. Balch. Amyloid as a natural product. *J. Cell. Biol.*, 2003, **161**(3), pp.461-462.
45. D. Otzen. Functional amyloid: Turning swords into plowshares. *Prion*, 2010, **4**(4), pp.256-264.
46. E. Monsellier and F. Chiti. Prevention of amyloid-like aggregation as a driving force of protein evolution. *EMBO Rep.*, 2007, **8**(8), pp.737-742.
47. V.N. Uversky. Natively unfolded proteins: A point where biology waits for physics. *Prot. Sci.*, 2002, **11**(4), pp.739-756.
48. F.U. Hartl and M. Hayer-Hartl. Converging concepts of protein folding *in vitro* and *in vivo*. *Nat. Struct. Mol. Biol.*, 2009, **16**(6), pp.574-581.
49. A.L. Goldberg. Protein degradation and protection against misfolded or damaged proteins. *Nature*, 2003, **426**(6968), pp.895-899.
50. L. Ellgaard and A. Helenius. Quality control in the endoplasmic reticulum. *Nat. Rev. Mol. Cell. Biol.*, 2003, **4**(3), pp.181-191.
51. B. Meusser, C. Hirsch, E. Jarosch and T. Sommer. ERAD: the long road to destruction. *Nat. Cell. Biol.*, 2005, **7**(8), pp.766-772.
52. D. Pincus and P. Walter. A first line of defense against ER stress. *J. Cell. Biol.*, 2012, **198**(3), pp.277-279.
53. B. Bukau, J. Weissman and A. Horwich. Molecular chaperones and protein quality control. *Cell*, 2006, **125**(3), pp.443-451.

54. M. Stefani and C. Dobson. Protein aggregation and aggregate toxicity: new insights into protein folding, misfolding diseases and biological evolution. *J. Mol. Med.*, 2003, **81**(11), pp.678-699.
55. K. Richter, M. Haslbeck and J. Buchner. The heat shock response: Life on the verge of death. *Mol. Cell.*, 2010, **40**(2), pp.253-266.
56. J. Rothman and R. Schekman. Molecular mechanism of protein folding in the cell. *Cell*, 2011, **146**(6), pp.851-854.
57. T. Langer, C. Lu, H. Echols, J. Flanagan, M.K. Hayer and F.U. Hartl. Successive action of DnaK, DnaJ and GroEL along the pathway of chaperone-mediated protein folding. *Nature*, 1992, **356**(6371), pp.683-689.
58. J. Frydman, E. Nimmesgern, K. Ohtsuka and F.U. Hartl. Folding of nascent polypeptide chains in a high molecular mass assembly with molecular chaperones. *Nature*, 1994, **370**(6485), pp.111-117.
59. A.L. Horwich, G.W. Farr and W.A. Fenton. GroEL–GroES-mediated protein folding. *Chem. Rev.*, 2006, **106**(5), pp.1917-1930.
60. K. Braig, M. Simon, F. Furuya, J.F. Hainfeld and A.L. Horwich. A polypeptide bound by the chaperonin groEL is localized within a central cavity. *Proc. Natl. Acad. Sci.*, 1993, **90**(9), pp.3978-3982.
61. U. Woehlbier and C. Hetz. Modulating stress responses by the UPRosome: A matter of life and death. *Trends. Biochem. Sci.*, 2011, **36**(6), pp.329-337.
62. J.P. Taylor, F. Tanaka, J. Robitschek, C.M. Sandoval, A. Taye, S. Markovic-Plese and K.H. Fischbeck. Aggresomes protect cells by enhancing the degradation of toxic polyglutamine-containing protein. *Hum. Mol. Genet.*, 2003, **12**(7), pp.749-757.
63. D. Kaganovich, R. Kopito and J. Frydman. Misfolded proteins partition between two distinct quality control compartments. *Nature*, 2008, **454**(7208), pp.1088-1095.
64. H. Aguilaniu, L. Gustafsson, M. Rigoulet and T. Nyström. Asymmetric inheritance of oxidatively damaged proteins during cytokinesis. *Science*, 2003, **299**(5613), pp.1751-1753.
65. J. Winkler, A. Seybert, L. König, S. Pruggnaller, U. Haselmann, V. Sourjik, M. Weiss, A.S. Frangakis, A. Mogk and B. Bukau. Quantitative and spatio-temporal features of protein aggregation in Escherichia coli and consequences on protein quality control and cellular ageing. 2010, **29**(5), pp.910-923.
66. B. Liu, L. Larsson, V. Franssens, X. Hao, Sandra m. Hill, V. Andersson, D. Höglund, J. Song, X. Yang, D. Öling, J. Grantham, J. Winderickx and T. Nyström. Segregation of protein aggregates involves actin and the polarity machinery. *Cell*, 2011, **147**(5), pp.959-961.
67. A.B. Lindner, R. Madden, A. Demarez, E.J. Stewart and F. Taddei. Asymmetric segregation of protein aggregates is associated with cellular aging and rejuvenation. *Proc. Natl. Acad. Sci.*, 2008, **105**(8), pp.3076-3081.
68. R.R. Kopito and R. Sitia. Aggresomes and russell bodies: Symptoms of cellular indigestion? *EMBO Rep.*, 2000, **1**(3), pp.225-231.
69. R. García-Mata, Z. Bebök, E.J. Sorscher and E.S. Sztul. Characterization and dynamics of aggresome formation by a cytosolic GFP-chimera. *J. Cell. Biol.*, 1999, **146**(6), pp.1239-1254.

70. D.C. Rubinsztein. The roles of intracellular protein-degradation pathways in neurodegeneration. *Nature*, 2006, **443**(7113), pp.780-786.
71. B. Ravikumar, M. Futter, L. Jahreiss, V.I. Korolchuk, M. Lichtenberg, S. Luo, D.C.O. Massey, F.M. Menzies, U. Narayanan, M. Renna, M. Jimenez-Sanchez, S. Sarkar, B. Underwood, A. Winslow and D.C. Rubinsztein. Mammalian macroautophagy at a glance. *J. Cell. Sci.*, 2009, **122**(11), pp.1707-1711.
72. D. Voges, P. Zwickl and W. Baumeister. The 26S proteasome: A molecular machine designed for controlled proteolysis. *Annu. Rev. Biochem.*, 1999, **68**(1), pp.1015-1068.
73. K. Eden, R. Morris, J. Gillam, Cait e. Macphee and Rosalind j. Allen. Competition between primary nucleation and autocatalysis in amyloid fibril self-assembly. *Biophys. J.*, 2015, **108**(3), pp.632-643.
74. M. Jucker and L.C. Walker. Pathogenic protein seeding in Alzheimer disease and other neurodegenerative disorders. *Ann. Neurol.*, 2011, **70**(4), pp.532-540.
75. J.E. Gillam and C.E. Macphee. Modelling amyloid fibril formation kinetics: mechanisms of nucleation and growth. *J. Phys. Condens. Mat.*, 2013, **25**(37), p.373101.
76. T. Eichner and Sheena e. Radford. A diversity of assembly mechanisms of a generic amyloid fold. *Mol. Cell.*, 2011, **43**(1), pp.8-18.
77. S.I.A. Cohen, M. Vendruscolo, C.M. Dobson and T.P.J. Knowles. From macroscopic measurements to microscopic mechanisms of protein aggregation. *J. Mol. Biol.*, 2012, **421**(2–3), pp.160-171.
78. S.I.A. Cohen, S. Linse, L.M. Luheshi, E. Hellstrand, D.A. White, L. Rajah, D.E. Otzen, M. Vendruscolo, C.M. Dobson and T.P.J. Knowles. Proliferation of amyloid-β_{42} aggregates occurs through a secondary nucleation mechanism. *Proc. Natl. Acad. Sci.*, 2013, **110**(24), pp.9758-9763.
79. T.P.J. Knowles, C.A. Waudby, G.L. Devlin, S.I.A. Cohen, A. Aguzzi, M. Vendruscolo, E.M. Terentjev, M.E. Welland and C.M. Dobson. An analytical solution to the kinetics of breakable filament assembly. *Science*, 2009, **326**(5959), pp.1533-1537.
80. S.R. Collins, A. Douglass, R.D. Vale and J.S. Weissman. Mechanism of prion propagation: Amyloid growth occurs by monomer addition. *PLoS Biol.*, 2004, **2**(10), p.e321.
81. G. Meisl, X. Yang, E. Hellstrand, B. Frohm, J.B. Kirkegaard, S.I.A. Cohen, C.M. Dobson, S. Linse and T.P.J. Knowles. Differences in nucleation behavior underlie the contrasting aggregation kinetics of the Aβ40 and Aβ42 peptides. *Proc. Natl. Acad. Sci.*, 2014, **111**(26), pp.9384-9389.
82. M. Sunde, L.C. Serpell, M. Bartlam, P.E. Fraser, M.B. Pepys and C.C.F. Blake. Common core structure of amyloid fibrils by synchrotron X-ray diffraction. *J. Mol. Biol.*, 1997, **273**(3), pp.729-739.
83. O.S. Makin and L.C. Serpell. Structures for amyloid fibrils. *FEBS J.*, 2005, **272**(23), pp.5950-5961.
84. L.C. Serpell, M. Sunde, M.D. Benson, G.A. Tennent, M.B. Pepys and P.E. Fraser. The protofilament substructure of amyloid fibrils. *J. Mol. Biol.*, 2000, **300**(5), pp.1033-1039.
85. H.H. Bauer, U. Aebi, M. Häner, R. Hermann, M. Müller, T. Arvinte and H.P. Merkle. Architecture and polymorphism of fibrillar supramolecular assemblies

produced by *in vitro* aggregation of human calcitonin. *J. Struct. Biol.*, 1995, **115**(1), pp.1-15.

86. M. Saiki, S. Honda, K. Kawasaki, D. Zhou, A. Kaito, T. Konakahara and H. Morii. Higher-order molecular packing in Amyloid-like fibrils constructed with linear arrangements of hydrophobic and hydrogen-bonding side-chains. *J. Mol. Biol.*, 2005, **348**(4), pp.983-998.
87. J. Meinhardt, C. Sachse, P. Hortschansky, N. Grigorieff and M. Fändrich. Aβ(1-40) fibril polymorphism implies diverse interaction patterns in amyloid fibrils. *J. Mol. Biol.*, 2009, **386**(3), pp.869-877.
88. G.T. Westermark, K.H. Johnson and P. Westermark. Staining methods for identification of amyloid in tissue. *In: Methods in Enzymology*. Academic Press, 1999, pp.3-25.
89. H. Naiki, K. Higuchi, M. Hosokawa and T. Takeda. Fluorometric determination of amyloid fibrils *in vitro* using the fluorescent dye, thioflavine T. *Anal. Biochem.*, 1989, **177**(2), pp.244-249.
90. M.R. Nilsson. Techniques to study amyloid fibril formation *in vitro*. *Methods*, 2004, **34**(1), pp.151-160.
91. A.W.P. Fitzpatrick, G.T. Debelouchina, M.J. Bayro, D.K. Clare, M.A. Caporini, V.S. Bajaj, C.P. Jaroniec, L. Wang, V. Ladizhansky, S.A. Müller, C.E. Macphee, C.A. Waudby, H.R. Mott, A. De Simone, T.P.J. Knowles, H.R. Saibil, M. Vendruscolo, E.V. Orlova, R.G. Griffin and C.M. Dobson. Atomic structure and hierarchical assembly of a cross-β amyloid fibril. *Proc. Natl. Acad. Sci.*, 2013, **110**(14), pp.5468-5473.
92. C. Sachse, M. Fändrich and N. Grigorieff. Paired β-sheet structure of an Aβ(1-40) amyloid fibril revealed by electron microscopy. *Proc. Natl. Acad. Sci.*, 2008, **105**(21), pp.7462-7466.
93. A.T. Petkova, Y. Ishii, J.J. Balbach, O.N. Antzutkin, R.D. Leapman, F. Delaglio and R. Tycko. A structural model for Alzheimer's β-amyloid fibrils based on experimental constraints from solid state NMR. *Proc. Natl. Acad. Sci.*, 2002, **99**(26), pp.16742-16747.
94. C. Wasmer, A. Lange, H. Van Melckebeke, A.B. Siemer, R. Riek and B.H. Meier. Amyloid fibrils of the HET-s(218–289) prion form a β solenoid with a triangular hydrophobic core. *Science*, 2008, **319**(5869), pp.1523-1526.
95. T. Lührs, C. Ritter, M. Adrian, D. Riek-Loher, B. Bohrmann, H. Döbeli, D. Schubert and R. Riek. 3D structure of Alzheimer's amyloid-β(1–42) fibrils. *Proc. Natl. Acad. Sci.*, 2005, **102**(48), pp.17342-17347.
96. M. Fändrich and C.M. Dobson. The behaviour of polyamino acids reveals an inverse side chain effect in amyloid structure formation. *EMBO J.*, 2002, **21**(21), pp.5682-5690.
97. W. Qiang, W.-M. Yau, Y. Luo, M.P. Mattson and R. Tycko. Antiparallel β-sheet architecture in Iowa-mutant β-amyloid fibrils. *Proc. Natl. Acad. Sci.*, 2012, **109**(12), pp.4443-4448.
98. C. Liu, M. Zhao, L. Jiang, P.-N. Cheng, J. Park, M.R. Sawaya, A. Pensalfini, D. Gou, A.J. Berk, C.G. Glabe, J. Nowick and D. Eisenberg. Out-of-register β-sheets suggest a pathway to toxic amyloid aggregates. *Proc. Natl. Acad. Sci.*, 2012, **109**(51), pp.20913-20918.

99. G. Zandomeneghi, M.R.H. Krebs, M.G. Mccammon and M. Fändrich. FTIR reveals structural differences between native β-sheet proteins and amyloid fibrils. *Prot. Sci.*, 2004, **13**(12), pp.3314-3321.
100. M.R. Sawaya, S. Sambashivan, R. Nelson, M.I. Ivanova, S.A. Sievers, M.I. Apostol, M.J. Thompson, M. Balbirnie, J.J.W. Wiltzius, H.T. Mcfarlane, A.O. Madsen, C. Riekel and D. Eisenberg. Atomic structures of amyloid cross-β spines reveal varied steric zippers. *Nature*, 2007, **447**(7143), pp.453-457.
101. M.F. Mossuto, A. Dhulesia, G. Devlin, E. Frare, J.R. Kumita, P.P. De Laureto, M. Dumoulin, A. Fontana, C.M. Dobson and X. Salvatella. The non-core regions of human lysozyme amyloid fibrils influence cytotoxicity. *J. Mol. Biol.*, 2010, **402**(5), pp.783-796.
102. Y. Su, C.J. Sarell, M.T. Eddy, G.T. Debelouchina, L.B. Andreas, C.L. Pashley, S.E. Radford and R.G. Griffin. Secondary structure in the core of amyloid fibrils formed from human β2m and its truncated variant ΔN6. *J. Am. Chem. Soc.*, 2014, **136**(17), pp.6313-6325.
103. A.T. Petkova, R.D. Leapman, Z. Guo, W.M. Yau, M.P. Mattson and R. Tycko. Self-propagating, molecular-level polymorphism in Alzheimer's β-amyloid fibrils. *Science*, 2005, **307**(5707), pp.262-5.
104. A.T. Petkova, W.M. Yau and R. Tycko. Experimental constraints on quaternary structure in Alzheimer's β-amyloid fibrils. *Biochemistry*, 2006, **45**(2), pp.498-512.
105. A.K. Paravastu, R.D. Leapman, W.-M. Yau and R. Tycko. Molecular structural basis for polymorphism in Alzheimer's β-amyloid fibrils. *Proc. Natl. Acad. Sci.*, 2008, **105**(47), pp.18349-18354.
106. J.-X. Lu, W. Qiang, W.-M. Yau, C. Schwieters, S. Meredith and R. Tycko. Molecular structure of β-amyloid fibrils in Alzheimer's disease brain tissue. *Cell*, 2013, **154**(6), pp.1257-1268.
107. L. Bousset, L. Pieri, G. Ruiz-Arlandis, J. Gath, P.H. Jensen, B. Habenstein, K. Madiona, V. Olieric, A. Böckmann, B.H. Meier and R. Melki. Structural and functional characterization of two α-synuclein strains. *Nature Commun.*, 2013, **4**, p.2575.
108. B. Bolognesi, J.R. Kumita, T.P. Barros, E.K. Esbjorner, L.M. Luheshi, D.C. Crowther, M.R. Wilson, C.M. Dobson, G. Favrin and J.J. Yerbury. ANS binding reveals common features of cytotoxic amyloid species. *ACS Chem. Biol.*, 2010, **5**(8), pp.735-740.
109. M. Tuite, M. Howard and W.F. Xue. Dynamic prions revealed by magic. *Chem. Biol.*, 2014, **21**(2), pp.172-173.
110. B.H. Toyama, M.J.S. Kelly, J.D. Gross and J.S. Weissman. The structural basis of yeast prion strain variants. *Nature*, 2007, **449**(7159), pp.233-237.
111. M. Tanaka, S.R. Collins, B.H. Toyama and J.S. Weissman. The physical basis of how prion conformations determine strain phenotypes. *Nature*, 2006, **442**(7102), pp.585-589.
112. K. Frederick, G. Debelouchina, C. Kayatekin, T. Dorminy, A. Jacavone, Robert g. Griffin and S. Lindquist. Distinct prion strains are defined by amyloid core structure and chaperone binding site dynamics. *Chem. Biol.*, 2014, **21**(2), pp.295-305.

113. Jing l. Guo, Dustin j. Covell, Joshua p. Daniels, M. Iba, A. Stieber, B. Zhang, Dawn m. Riddle, Linda k. Kwong, Y. Xu, John q. Trojanowski and Virginia m.Y. Lee. Distinct α-synuclein strains differentially promote tau inclusions in neurons. *Cell*, 2013, **154**(1), pp.103-117.
114. G.T. Debelouchina, G.W. Platt, M.J. Bayro, S.E. Radford and R.G. Griffin. Magic angle spinning NMR analysis of β_2-microglobulin amyloid fibrils in two distinct morphologies. *J. Am. Chem. Soc.*, 2010, **132**(30), pp.10414-10423.
115. M. Jucker and L.C. Walker. Self-propagation of pathogenic protein aggregates in neurodegenerative diseases. *Nature*, 2013, **501**(7465), pp.45-51.
116. M. Goedert. Alzheimer's and Parkinson's diseases: The prion concept in relation to assembled Aβ, tau, and α-synuclein. *Science*, 2015, **349**(6248).
117. S. Baglioni, F. Casamenti, M. Bucciantini, L. Luheshi, N. Taddei, F. Chiti, C. Dobson and M. Stefani. Prefibrillar amyloid aggregates could be generic toxins in higher organisms. *J. Neurosci.*, 2006, **26**(31), pp.8160 - 8167.
118. K.A. Conway, S.-J. Lee, J.-C. Rochet, T.T. Ding, R.E. Williamson and P.T. Lansbury. Acceleration of oligomerization, not fibrillization, is a shared property of both α-synuclein mutations linked to early-onset Parkinson's disease: Implications for pathogenesis and therapy. *Proc. Natl. Acad. Sci.*, 2000, **97**(2), pp.571-576.
119. Y.J. Zhu, H. Lin and R. Lal. Fresh and nonfibrillar amyloid β protein(1–40) induces rapid cellular degeneration in aged human fibroblasts: evidence for AβP-channel-mediated cellular toxicity. *FASEB J.*, 2000, **14**(9), pp.1244-1254.
120. C. Nilsberth, A. Westlind-Danielsson, C.B. Eckman, M.M. Condron, K. Axelman, C. Forsell, C. Stenh, J. Luthman, D.B. Teplow, S.G. Younkin, J. Naslund and L. Lannfelt. The 'Arctic' APP mutation (E693G) causes Alzheimer's disease by enhanced Aβ protofibril formation. *Nat. Neurosci.*, 2001, **4**(9), pp.887-893.
121. M. Mendes Sousa, I. Cardoso, R. Fernandes, A. Guimarães and M.J. Saraiva. Deposition of transthyretin in early stages of familial amyloidotic polyneuropathy : Evidence for toxicity of nonfibrillar aggregates. *Am. J. Path.*, 2001, **159**(6), pp.1993-2000.
122. M. Bucciantini, E. Giannoni, F. Chiti, F. Baroni, L. Formigli, J. Zurdo, N. Taddei, G. Ramponi, C.M. Dobson and M. Stefani. Inherent toxicity of aggregates implies a common mechanism for protein misfolding diseases. *Nature*, 2002, **416**(6880), pp.507-511.
123. R. Kayed, E. Head, J. Thompson, T. Mcintire, S. Milton, C. Cotman and C. Glabe. Common structure of soluble amyloid oligomers implies common mechanism of pathogenesis. *Science*, 2003, **300**(5618), pp.486 - 489.
124. C.G. Glabe. Structural classification of toxic amyloid oligomers. *J. Biol. Chem.*, 2008, **283**(44), pp.29639-29643.
125. R. Kayed, E. Head, F. Sarsoza, T. Saing, C. Cotman, M. Necula, L. Margol, J. Wu, L. Breydo, J. Thompson, S. Rasool, T. Gurlo, P. Butler and C. Glabe. Fibril specific, conformation dependent antibodies recognize a generic epitope common to amyloid fibrils and fibrillar oligomers that is absent in prefibrillar oligomers. *Mol. Neurodegen.*, 2007, **2**(1), p.18.
126. I. Benilova, E. Karran and B. De Strooper. The toxic Aβ oligomer and Alzheimer's disease: an emperor in need of clothes. *Nat. Neurosci.*, 2012, **15**(3), pp.349-357.

127. L. Bertram and R.E. Tanzi. The genetic epidemiology of neurodegenerative disease. *J. Clin. Invest.*, 2005, **115**(6), pp.1449-1457.
128. M. Citron. Alzheimer's disease: strategies for disease modification. *Nat. Rev. Drug. Discov.*, 2010, **9**(5), pp.387-398.
129. S. Jain, N. Wood and D. Healy. Molecular genetic pathways in Parkinson's disease: A review. *Clin. Sci.*, 2005, **109**(4), pp.355-364.
130. I. Mckeith, J. Mintzer, D. Aarsland, D. Burn, H. Chiu, J. Cohen-Mansfield, D. Dickson, B. Dubois, J.E. Duda, H. Feldman, S. Gauthier, G. Halliday, B. Lawlor, C. Lippa, O.L. Lopez, J.C. Machado, J. O'brien and J. Playfer. Dementia with Lewy bodies. *Lancet Neurol.*, 2004, **3**(1), pp.19-28.
131. E. Norrby. Prions and protein-folding diseases. *Journal of Internal Medicine*, 2011, **270**(1), pp.1-14.
132. C.A. Ross and S.J. Tabrizi. Huntington's disease: from molecular pathogenesis to clinical treatment. *Lancet Neurol.*, 2011, **10**(1), pp.83-98.
133. M.C. Kiernan, S. Vucic, B.C. Cheah, M.R. Turner, A. Eisen, O. Hardiman, J.R. Burrell and M.C. Zoing. Amyotrophic lateral sclerosis. *The Lancet*, 2011, **377**(9769), pp.942-955.
134. G. Merlini, R.L. Comenzo, D.C. Seldin, A. Wechalekar and M.A. Gertz. Immunoglobulin light chain amyloidosis. *Expert. Rev. Hemat.*, 2013, **7**(1), pp.143-156.
135. J. Floege and M. Ketteler. β_2-microglobulin-derived amyloidosis: An update. *Kidney Int.*, 2001, **59**(S78), pp.S164-S171.
136. B.M.D. Granel, S.M.D.P. Valleix, J.M.D. Serratrice, P.M.D.P. Cherin, A.M.D. Texeira, P.M.D. Disdier, P.-J.M.D. Weiller and G.M.D. Grateau. Lysozyme amyloidosis: Report of 4 cases and a review of the literature. *Medicine*, 2006, **85**(1), pp.66-73.
137. Y. Ando, T. Coelho, J. Berk, M.W. Cruz, B.-G. Ericzon, S.-I. Ikeda, W.D. Lewis, L. Obici, V. Plante-Bordeneuve, C. Rapezzi, G. Said and F. Salvi. Guideline of transthyretin-related hereditary amyloidosis for clinicians. *Orphanet. J. Rare. Dis.*, 2013, **8**(1), p.31.
138. J.D. Gillmore, H.J. Lachmann, D. Rowczenio, J.A. Gilbertson, C.-H. Zeng, Z.-H. Liu, L.-S. Li, A. Wechalekar and P.N. Hawkins. Diagnosis, pathogenesis, treatment, and prognosis of hereditary fibrinogen Aα-chain amyloidosis. *J. Am. Soc. Nephrol.*, 2009, **20**(2), pp.444-451.
139. P. Westermark, A. Andersson and G.T. Westermark. Islet amyloid polypeptide, islet amyloid, and diabetes mellitus. *Physiol. Rev.*, 2011, **91**(3), pp.795-826.
140. S.D. Yan, X. Chen, J. Fu, M. Chen, H. Zhu, A. Roher, T. Slattery, L. Zhao, M. Nagashima, J. Morser, A. Migheli, P. Nawroth, D. Stern and A.M. Schmidt. RAGE and amyloid-β peptide neurotoxicity in Alzheimer's disease. *Nature*, 1996, **382**(6593), pp.685-691.
141. S.D. Yan, H. Zhu, A. Zhu, A. Golabek, H. Du, A. Roher, J. Yu, C. Soto, A.M. Schmidt, D. Stern and M. Kindy. Receptor-dependent cell stress and amyloid accumulation in systemic amyloidosis. *Nat. Med.*, 2000, **6**(6), pp.643-651.
142. M.N. Reed, J.J. Hofmeister, L. Jungbauer, A.T. Welzel, C. Yu, M.A. Sherman, S. Lesné, M.J. Ladu, D.M. Walsh, K.H. Ashe and J.P. Cleary. Cognitive effects of cell-derived and synthetically derived Aβ oligomers. *Neurobiol. Aging.*, 2011, **32**(10), pp.1784-1794.

143. A.J. Nicoll, S. Panico, D.B. Freir, D. Wright, C. Terry, E. Risse, C.E. Herron, T. O'malley, J.D.F. Wadsworth, M.A. Farrow, D.M. Walsh, H.R. Saibil and J. Collinge. Amyloid-β nanotubes are associated with prion protein-dependent synaptotoxicity. *Nature Commun.*, 2013, **4**, p.2416.
144. D.M. Walsh, A. Lomakin, G.B. Benedek, M.M. Condron and D.B. Teplow. Amyloid-β protein fibrillogenesis: Detection of a protofibrillar intermediate. *J. Biol. Chem.*, 1997, **272**(35), pp.22364-22372.
145. N.B. Last and A.D. Miranker. Common mechanism unites membrane poration by amyloid and antimicrobial peptides. *Proc. Natl. Acad. Sci.*, 2013, **110**(16), pp.6382-6387.
146. P. Cao, A. Abedini, H. Wang, L.-H. Tu, X. Zhang, A.M. Schmidt and D.P. Raleigh. Islet amyloid polypeptide toxicity and membrane interactions. *Proc. Natl. Acad. Sci.*, 2013, **110**(48), pp.19279-19284.
147. L. Pieri, K. Madiona, L. Bousset and R. Melki. Fibrillar α-synuclein and huntingtin Exon 1 assemblies are toxic to the cells. *Biophys. J.*, 2012, **102**(12), pp.2894-2905.
148. M. Bucciantini, D. Nosi, M. Forzan, E. Russo, M. Calamai, L. Pieri, L. Formigli, F. Quercioli, S. Soria, F. Pavone, J. Savistchenko, R. Melki and M. Stefani. Toxic effects of amyloid fibrils on cell membranes: the importance of ganglioside GM1. *FASEB J.*, 2012, **26**(2), pp.818-831.
149. A. Relini, N. Marano and A. Gliozzi. Misfolding of amyloidogenic proteins and their interactions with membranes. *Biomolecules*, 2013, **4**(1), p.20.
150. G.P. Gorbenko and P.K.J. Kinnunen. The role of lipid–protein interactions in amyloid-type protein fibril formation. *Chem. Phys. Lipids.*, 2006, **141**(1–2), pp.72-82.
151. M.F.M. Engel, L. Khemtémourian, C.C. Kleijer, H.J.D. Meeldijk, J. Jacobs, A.J. Verkleij, B. De Kruijff, J.A. Killian and J.W.M. Höppener. Membrane damage by human islet amyloid polypeptide through fibril growth at the membrane. *Proc. Natl. Acad. Sci.*, 2008, **105**(16), pp.6033-6038.
152. P. Narayan, K.A. Ganzinger, J. Mccoll, L. Weimann, S. Meehan, S. Qamar, J.A. Carver, M.R. Wilson, P. St. George-Hyslop, C.M. Dobson and D. Klenerman. Single molecule characterization of the interactions between Amyloid-β peptides and the membranes of hippocampal cells. *J. Am. Chem. Soc.*, 2013, **135**(4), pp.1491-1498.
153. D. Freeman, R. Cedillos, S. Choyke, Z. Lukic, K. Mcguire, S. Marvin, A.M. Burrage, S. Sudholt, A. Rana, C. O'connor, C.M. Wiethoff and E.M. Campbell. α-synuclein induces lysosomal rupture and cathepsin dependent reactive oxygen species following endocytosis. *PLoS One*, 2013, **8**(4), p.e62143.
154. J.-H. Lee, C.-S. Hong, S. Lee, J.-E. Yang, Y.I. Park, D. Lee, T. Hyeon, S. Jung and S.R. Paik. Radiating amyloid fibril formation on the surface of lipid membranes through unit-assembly of oligomeric species of α-synuclein. *PLoS One*, 2012, **7**(10), p.e47580.
155. H. Lin, R. Bhatia and R. Lal. Amyloid β protein forms ion channels: implications for Alzheimer's disease pathophysiology. *FASEB J.*, 2001, **15**(13), pp.2433-2444.
156. M.-C. Lin, T. Mirzabekov and B.L. Kagan. Channel formation by a neurotoxic prion protein fragment. *J. Biol. Chem.*, 1997, **272**(1), pp.44-47.

157. A. Quist, I. Doudevski, H. Lin, R. Azimova, D. Ng, B. Frangione, B. Kagan, J. Ghiso and R. Lal. Amyloid ion channels: A common structural link for protein-misfolding disease. *Proc. Natl. Acad. Sci.*, 2005, **102**(30), pp.10427-10432.
158. S. Campioni, B. Mannini, M. Zampagni, A. Pensalfini, C. Parrini, E. Evangelisti, A. Relini, M. Stefani, C.M. Dobson, C. Cecchi and F. Chiti. A causative link between the structure of aberrant protein oligomers and their toxicity. *Nat. Chem. Biol.*, 2010, **6**(2), pp.140-147.
159. A. Demuro, M. Smith and I. Parker. Single-channel Ca^{2+} imaging implicates Aβ1–42 amyloid pores in Alzheimer's disease pathology. *J. Cell. Biol.*, 2011, **195**(3), pp.515-524.
160. A. Laganowsky, C. Liu, M.R. Sawaya, J.P. Whitelegge, J. Park, M. Zhao, A. Pensalfini, A.B. Soriaga, M. Landau, P.K. Teng, D. Cascio, C. Glabe and D. Eisenberg. Atomic view of a toxic amyloid small oligomer. *Science*, 2012, **335**(6073), pp.1228-1231.
161. M.F.M. Engel. Membrane permeabilization by islet amyloid polypeptide. *Chem. Phys. Lipids.*, 2009, **160**(1), pp.1-10.
162. H. Zhao, E.K.J. Tuominen and P.K.J. Kinnunen. Formation of amyloid fibers triggered by phosphatidylserine-containing membranes. *Biochemistry*, 2004, **43**(32), pp.10302-10307.
163. P.M. Douglas and A. Dillin. Protein homeostasis and aging in neurodegeneration. *J. Cell. Biol.*, 2010, **190**(5), pp.719-729.
164. M.Y. Sherman and A.L. Goldberg. Cellular defenses against unfolded proteins: A cell biologist thinks about neurodegenerative diseases. *Neuron*, 2001, **29**(1), pp.15-32.
165. R.I. Morimoto. Proteotoxic stress and inducible chaperone networks in neurodegenerative disease and aging. *Gene Dev.*, 2008, **22**(11), pp.1427-1438.
166. H. Olzscha, S.M. Schermann, A.C. Woerner, S. Pinkert, M.H. Hecht, G.G. Tartaglia, M. Vendruscolo, M. Hayer-Hartl, F.U. Hartl and R.M. Vabulas. Amyloid-like aggregates sequester numerous metastable proteins with essential cellular functions. *Cell*, 2011, **144**(1), pp.67-78.
167. E. Cattaneo, D. Rigamonti, D. Goffredo, C. Zuccato, F. Squitieri and S. Sipione. Loss of normal huntingtin function: new developments in Huntington's disease research. *Trends Neurosci.*, 2001, **24**(3), pp.182-188.
168. C. Soto. Unfolding the role of protein misfolding in neurodegenerative diseases. *Nat. Rev. Neurosci.*, 2003, **4**(1), pp.49-60.
169. A.G. Reaume, J.L. Elliott, E.K. Hoffman, N.W. Kowall, R.J. Ferrante, D.R. Siwek, H.M. Wilcox, D.G. Flood, M.F. Beal, R.H. Brown, R.W. Scott and W.D. Snider. Motor neurons in Cu/Zn superoxide dismutase-deficient mice develop normally but exhibit enhanced cell death after axonal injury. *Nat. Genet.*, 1996, **13**(1), pp.43-47.
170. J.C. Sacchettini and J.W. Kelly. Therapeutic strategies for human amyloid diseases. *Nat. Rev. Drug. Discov.*, 2002, **1**(4), pp.267-275.
171. T.E. Golde, L.S. Schneider and E.H. Koo. Anti-Aβ therapeutics in Alzheimer's disease: The need for a paradigm shift. *Neuron*, 2011, **69**(2), pp.203-213.
172. Y. Huang and L. Mucke. Alzheimer mechanisms and therapeutic strategies. *Cell*, 2012, **148**(6), pp.1204-1222.

173. N.F. Schor. What the halted phase III γ-secretase inhibitor trial may (or may not) be telling us. *Ann. Neurol.*, 2011, **69**(2), pp.237-239.
174. G. Mallucci and J. Collinge. Rational targeting for prion therapeutics. *Nat. Rev. Neurosci.*, 2005, **6**(1), pp.23-34.
175. U. Blömer, L. Naldini, T. Kafri, D. Trono, I.M. Verma and F.H. Gage. Highly efficient and sustained gene transfer in adult neurons with a lentivirus vector. *J. Virol.*, 1997, **71**(9), pp.6641-6649.
176. D.A. Rubinson, C.P. Dillon, A.V. Kwiatkowski, C. Sievers, L. Yang, J. Kopinja, D.L. Rooney, M. Zhang, M.M. Ihrig, M.T. Mcmanus, F.B. Gertler, M.L. Scott and L. Van Parijs. A lentivirus-based system to functionally silence genes in primary mammalian cells, stem cells and transgenic mice by RNA interference. *Nat. Genet.*, 2003, **33**(3), pp.401-406.
177. B.L. Davidson and X.O. Breakefield. Viral vectors for gene delivery to the nervous system. *Nat. Rev. Neurosci.*, 2003, **4**(5), pp.353-364.
178. N. Daude, M. Marella and J. Chabry. Specific inhibition of pathological prion protein accumulation by small interfering RNAs. *J. Cell. Sci.*, 2003, **116**(13), pp.2775-2779.
179. H. Xia, Q. Mao, H.L. Paulson and B.L. Davidson. siRNA-mediated gene silencing *in vitro* and *in vivo*. *Nat. Biotech.*, 2002, **20**(10), pp.1006-1010.
180. B.L. Davidson and H.L. Paulson. Molecular medicine for the brain: silencing of disease genes with RNA interference. *Lancet Neurol.*, 2004, **3**(3), pp.145-149.
181. V.M. Miller, H. Xia, G.L. Marrs, C.M. Gouvion, G. Lee, B.L. Davidson and H.L. Paulson. Allele-specific silencing of dominant disease genes. *Proc. Natl. Acad. Sci.*, 2003, **100**(12), pp.7195-7200.
182. W. Colon and J.W. Kelly. Partial denaturation of transthyretin is sufficient for amyloid fibril formation *in vitro*. *Biochemistry*, 1992, **31**(36), pp.8654-8660.
183. Z. Lai, W. Colón and J.W. Kelly. The acid-mediated denaturation pathway of transthyretin yields a conformational intermediate that can self-assemble into amyloid. *Biochemistry*, 1996, **35**(20), pp.6470-6482.
184. P. Hammarström, R.L. Wiseman, E.T. Powers and J.W. Kelly. Prevention of transthyretin amyloid disease by changing protein misfolding energetics. *Science*, 2003, **299**(5607), pp.713-716.
185. J. Tatzelt, S.B. Prusiner and W.J. Welch. Chemical chaperones interfere with the formation of scrapie prion protein. *EMBO J.*, 1996, **15**(23), pp.6363-6373.
186. A.R. Salomon, K.J. Marcinowski, R.P. Friedland and M.G. Zagorski. Nicotine inhibits amyloid formation by the β-peptide. *Biochemistry*, 1996, **35**(42), pp.13568-13578.
187. M.A. Findeis, G.M. Musso, C.C. Arico-Muendel, H.W. Benjamin, A.M. Hundal, J.-J. Lee, J. Chin, M. Kelley, J. Wakefield, N.J. Hayward and S.M. Molineaux. Modified-peptide inhibitors of amyloid β-peptide polymerization. *Biochemistry*, 1999, **38**(21), pp.6791-6800.
188. C. Soto, M.S. Kindy, M. Baumann and B. Frangione. Inhibition of Alzheimer's amyloidosis by peptides that prevent β-sheet conformation. *Biochem. Biophys. Res. Commun.*, 1996, **226**(3), pp.672-680.
189. C.M. Dobson. Protein misfolding, evolution and disease. *Trends Biochem. Sci.*, 1999, **24**(9), pp.329-332.

190. E. Hughes, R.M. Burke and A.J. Doig. Inhibition of toxicity in the β-amyloid peptide fragment β-(25–35) using N-methylated derivatives: A general strategy to prevent amyloid formation. *J. Biol. Chem.*, 2000, **275**(33), pp.25109-25115.
191. J. Chabry, B. Caughey and B. Chesebro. Specific inhibition of *in vitro* formation of protease-resistant prion protein by synthetic peptides. *J. Biol. Chem.*, 1998, **273**(21), pp.13203-13207.
192. O.M.A. El-Agnaf, K.E. Paleologou, B. Greer, A.M. Abogrein, J.E. King, S.A. Salem, N.J. Fullwood, F.E. Benson, R. Hewitt, K.J. Ford, F.L. Martin, P. Harriott, M.R. Cookson and D. Allsop. A strategy for designing inhibitors of α-synuclein aggregation and toxicity as a novel treatment for Parkinson's disease and related disorders. *FASEB J.*, 2004.
193. L.A. Scrocchi, Y. Chen, S. Waschuk, F. Wang, S. Cheung, A.A. Darabie, J. Mclaurin and P.E. Fraser. Design of peptide-based inhibitors of human islet amyloid polypeptide fibrillogenesis. *J. Mol. Biol.*, 2002, **318**(3), pp.697-706.
194. Y. Nagai, T. Tucker, H. Ren, D.J. Kenan, B.S. Henderson, J.D. Keene, W.J. Strittmatter and J.R. Burke. Inhibition of polyglutamine protein aggregation and cell death by novel peptides identified by phage display screening. *J. Biol. Chem.*, 2000, **275**(14), pp.10437-10442.
195. S.A. Sievers, J. Karanicolas, H.W. Chang, A. Zhao, L. Jiang, O. Zirafi, J.T. Stevens, J. Munch, D. Baker and D. Eisenberg. Structure-based design of non-natural amino-acid inhibitors of amyloid fibril formation. *Nature*, 2011, **475**(7354), pp.96-100.
196. C.E. Bulawa, S. Connelly, M. Devit, L. Wang, C. Weigel, J.A. Fleming, J. Packman, E.T. Powers, R.L. Wiseman, T.R. Foss, I.A. Wilson, J.W. Kelly and R. Labaudinière. Tafamidis, a potent and selective transthyretin kinetic stabilizer that inhibits the amyloid cascade. *Proc. Natl. Acad. Sci.*, 2012, **109**(24), pp.9629-9634.
197. B. Cheng, H. Gong, H. Xiao, R.B. Petersen, L. Zheng and K. Huang. Inhibiting toxic aggregation of amyloidogenic proteins: A therapeutic strategy for protein misfolding diseases. *BBA Gen. Subjects.*, 2013, **1830**(10), pp.4860-4871.
198. J.M. Perchiacca, A.R.A. Ladiwala, M. Bhattacharya and P.M. Tessier. Structure-based design of conformation- and sequence-specific antibodies against amyloid β. *Proc. Natl. Acad. Sci.*, 2012, **109**(1), pp.84-89.
199. K. Sexton, K. Tichauer, K.S. Samkoe, J. Gunn, P.J. Hoopes and B.W. Pogue. Fluorescent affibody peptide penetration in glioma margin is superior to full antibody. *PLoS One*, 2013, **8**(4), p.e60390.
200. L.M. Luheshi, W. Hoyer, T.P. De Barros, I. Van Dijk Härd, A.-C. Brorsson, B. Macao, C. Persson, D.C. Crowther, D.A. Lomas, S. Ståhl, C.M. Dobson and T. Härd. Sequestration of the Aβ peptide prevents toxicity and promotes degradation *in vivo*. *PLoS Biol.*, 2010, **8**(3), p.e1000334.
201. R. Mishra, B. Bulic, D. Sellin, S. Jha, H. Waldmann and R. Winter. Small-Molecule Inhibitors of Islet Amyloid Polypeptide Fibril Formation. *Angew. Chem. Int. Edit.*, 2008, **47**(25), pp.4679-4682.
202. Y. Porat, A. Abramowitz and E. Gazit. Inhibition of amyloid fibril formation by polyphenols: structural similarity and aromatic interactions as a common inhibition mechanism. *Chem. Biol. Drug. Des.*, 2006, **67**(1), pp.27-37.
203. F. Meng, A. Abedini, A. Plesner, C.B. Verchere and D.P. Raleigh. The flavanol (−)-epigallocatechin 3-gallate inhibits amyloid formation by islet amyloid

polypeptide, disaggregates amyloid fibrils and protects cultured cells against IAPP induced toxicity. *Biochemistry*, 2010, **49**(37), pp.8127-8133.

204. P. Cao and D.P. Raleigh. Analysis of the inhibition and remodeling of islet amyloid polypeptide amyloid fibers by flavanols. *Biochemistry*, 2012, **51**(13), pp.2670-2683.
205. N. Ferreira, M.J. Saraiva and M.R. Almeida. Natural polyphenols inhibit different steps of the process of transthyretin (TTR) amyloid fibril formation. *FEBS Lett.*, 2011, **585**(15), pp.2424-2430.
206. D.E. Ehrnhoefer, J. Bieschke, A. Boeddrich, M. Herbst, L. Masino, R. Lurz, S. Engemann, A. Pastore and E.E. Wanker. EGCG redirects amyloidogenic polypeptides into unstructured, off-pathway oligomers. *Nat. Struct. Mol. Biol.*, 2008, **15**(6), pp.558-566.
207. N. Ferreira, M.J. Saraiva and M.R. Almeida. Epigallocatechin-3-gallate as a potential therapeutic drug for TTR-related amyloidosis: "*In Vivo*" evidence from FAP mice models. *PLoS One*, 2012, **7**(1), p.e29933.
208. L. Cegelski, J.S. Pinkner, N.D. Hammer, C.K. Cusumano, C.S. Hung, E. Chorell, V. Åberg, J.N. Walker, P.C. Seed, F. Almqvist, M.R. Chapman and S.J. Hultgren. Small-molecule inhibitors target *Escherichia coli* amyloid biogenesis and biofilm formation. *Nat. Chem. Biol.*, 2009, **5**(12), pp.913-919.
209. J. Mclaurin, M.E. Kierstead, M.E. Brown, C.A. Hawkes, M.H.L. Lambermon, A.L. Phinney, A.A. Darabie, J.E. Cousins, J.E. French, M.F. Lan, F. Chen, S.S.N. Wong, H.T.J. Mount, P.E. Fraser, D. Westaway and P.S. George-Hyslop. Cyclohexanehexol inhibitors of Aβ aggregation prevent and reverse Alzheimer phenotype in a mouse model. *Nat. Med.*, 2006, **12**(7), pp.801-808.
210. L. Jiang, C. Liu, D. Leibly, M. Landau, M. Zhao, M.P. Hughes and D.S. Eisenberg. Structure-based discovery of fiber-binding compounds that reduce the cytotoxicity of amyloid beta. *eLife*, 2013, **2**.
211. M. Landau, M.R. Sawaya, K.F. Faull, A. Laganowsky, L. Jiang, S.A. Sievers, J. Liu, J.R. Barrio and D. Eisenberg. Towards a pharmacophore for amyloid. *PLoS Biol.*, 2011, **9**(6), p.e1001080.
212. S.A. Frautschy and G.M. Cole. Why pleiotropic interventions are needed for Alzheimer's disease. *Molec. Neurobiol.*, 2010, **41**(2-3), pp.392-409.
213. L.L. Blazer and R.R. Neubig. Small molecule protein-protein interaction inhibitors as CNS therapeutic agents: Current progress and future hurdles. *Neuropsychopharmacol.*, 2008, **34**(1), pp.126-141.
214. M.M. Pallitto, J. Ghanta, P. Heinzelman, L.L. Kiessling and R.M. Murphy. Recognition sequence design for peptidyl modulators of β-amyloid aggregation and toxicity. *Biochemistry*, 1999, **38**(12), pp.3570-3578.
215. J.L. Tomic, A. Pensalfini, E. Head and C.G. Glabe. Soluble fibrillar oligomer levels are elevated in Alzheimer's disease brain and correlate with cognitive dysfunction. *Neurobiol. Dis.*, 2009, **35**(3), pp.352-358.
216. K.F. Winklhofer, A. Reintjes, M.C. Hoener, R. Voellmy and J. Tatzelt. Geldanamycin restores a defective heat shock response *in vivo*. *J. Biol. Chem.*, 2001, **276**(48), pp.45160-45167.
217. L.G.G.C. Verhoef, K. Lindsten, M.G. Masucci and N.P. Dantuma. Aggregate formation inhibits proteasomal degradation of polyglutamine proteins. *Hum. Mol. Genet.*, 2002, **11**(22), pp.2689-2700.

218. D. Jones. Modifying protein misfolding. *Nat. Rev. Drug. Discov.*, 2010, **9**(11), pp.825-827.
219. R. Kisilevsky, L.J. Lemieux, P.E. Fraser, X. Kong, P.G. Hultin and W.A. Szarek. Arresting amyloidosis *in vivo* using small-molecule anionic sulphonates or sulphates: implications for Alzheimer's disease. *Nat. Med.*, 1995, **1**(2), pp.143-148.
220. G. Miller. Stopping Alzheimer's before it starts. *Science*, 2012, **337**(6096), pp.790-792.
221. J.L. Price and J.C. Morris. Tangles and plaques in nondemented aging and "preclinical" Alzheimer's disease. *Ann. Neurol.*, 1999, **45**(3), pp.358-368.
222. M. Goedert and M.G. Spillantini. A century of Alzheimer's disease. *Science*, 2006, **314**(5800), pp.777-781.
223. M.J. Passmore, A. Ho and R. Gallagher. Behavioral and psychological symptoms in moderate to severe Alzheimer's disease: A palliative care approach emphasizing recognition of personhood and preservation of dignity. *J. Alzheimers. Dis.*, 2012, **29**(1), pp.1-13.
224. G. Blessed, B.E. Tomlinson and M. Roth. The association between quantitative measures of dementia and of senile change in the cerebral grey matter of elderly subjects. *Brit. J. Psychiat.*, 1968, **114**(512), pp.797-811.
225. V. Lee, B. Balin, L. Otvos and J. Trojanowski. A68: a major subunit of paired helical filaments and derivatized forms of normal Tau. *Science*, 1991, **251**(4994), pp.675-678.
226. J. Hardy and G. Higgins. Alzheimer's disease: the amyloid cascade hypothesis. *Science*, 1992, **256**(5054), pp.184-185.
227. M. Morris, S. Maeda, K. Vossel and L. Mucke. The many faces of tau. *Neuron*, 2011, **70**(3), pp.410-426.
228. R. Medeiros, D. Baglietto-Vargas and F.M. Laferla. The role of tau in Alzheimer's disease and related disorders. *CNS Neurosci. Ther.*, 2011, **17**(5), pp.514-524.
229. R. Dixit, J.L. Ross, Y.E. Goldman and E.L.F. Holzbaur. Differential regulation of dynein and kinesin motor proteins by tau. *Science*, 2008, **319**(5866), pp.1086-1089.
230. H.-L. Li, H.-H. Wang, S.-J. Liu, Y.-Q. Deng, Y.-J. Zhang, Q. Tian, X.-C. Wang, X.-Q. Chen, Y. Yang, J.-Y. Zhang, Q. Wang, H. Xu, F.-F. Liao and J.-Z. Wang. Phosphorylation of tau antagonizes apoptosis by stabilizing β-catenin, a mechanism involved in Alzheimer's neurodegeneration. *Proc. Natl. Acad. Sci.*, 2007, **104**(9), pp.3591-3596.
231. C. Reinhard, S.S. Hébert and B. De Strooper. The amyloid-β precursor protein: integrating structure with biological function. *EMBO J.*, 2005, **24**(23), pp.3996-4006.
232. C. Priller, T. Bauer, G. Mitteregger, B. Krebs, H.A. Kretzschmar and J. Herms. Synapse Formation and Function Is Modulated by the Amyloid Precursor Protein. *J. Neurosci.*, 2006, **26**(27), pp.7212-7221.
233. E.J. Coulson, K. Paliga, K. Beyreuther and C.L. Masters. What the evolution of the amyloid protein precursor supergene family tells us about its function. *Neurochem. Int.*, 2000, **36**(3), pp.175-184.

234. N.N. Nalivaeva and A.J. Turner. The amyloid precursor protein: A biochemical enigma in brain development, function and disease. *FEBS Lett.*, 2013, **587**(13), pp.2046-2054.
235. T.L. Young-Pearse, J. Bai, R. Chang, J.B. Zheng, J.J. Loturco and D.J. Selkoe. A critical function for β-amyloid precursor protein in neuronal migration revealed by *in utero* RNA interference. *J. Neurosci.*, 2007, **27**(52), pp.14459-14469.
236. V. Chow, M. Mattson, P. Wong and M. Gleichmann. An overview of APP processing enzymes and products. *Neuromol. Med.*, 2010, **12**(1), pp.1-12.
237. W.P. Esler, E.R. Stimson, J.R. Ghilardi, Y.-A. Lu, A.M. Felix, H.V. Vinters, P.W. Mantyh, J.P. Lee and J.E. Maggio. Point substitution in the central hydrophobic cluster of a human β-amyloid congener disrupts peptide folding and abolishes plaque competence. *Biochemistry*, 1996, **35**(44), pp.13914-13921.
238. L.O. Tjernberg, D.J.E. Callaway, A. Tjernberg, S. Hahne, C. Lilliehöök, L. Terenius, J. Thyberg and C. Nordstedt. A molecular model of Alzheimer amyloid β-peptide fibril formation. *J. Biol. Chem.*, 1999, **274**(18), pp.12619-12625.
239. C. Hilbich, B. Kisters-Woike, J. Reed, C.L. Masters and K. Beyreuther. Substitutions of hydrophobic amino acids reduce the amyloidogenicity of Alzheimer's disease βA4 peptides. *J. Mol. Biol.*, 1992, **228**(2), pp.460-473.
240. N.S. De Groot, F.X. Aviles, J. Vendrell and S. Ventura. Mutagenesis of the central hydrophobic cluster in Aβ42 Alzheimer's peptide. *FEBS J.*, 2006, **273**(3), pp.658-668.
241. F. Kamenetz, T. Tomita, H. Hsieh, G. Seabrook, D. Borchelt, T. Iwatsubo, S. Sisodia and R. Malinow. APP processing and synaptic function. *Neuron*, 2003, **37**(6), pp.925-937.
242. D. Yates and D.M. Mcloughlin. The molecular pathology of Alzheimer's disease. *Psychiatry*, 2008, **7**(1), pp.1-5.
243. M. Shoji, T. Golde, J. Ghiso, T. Cheung, S. Estus, L. Shaffer, X. Cai, D. Mckay, R. Tintner, B. Frangione and A. Et. Production of the Alzheimer amyloid beta protein by normal proteolytic processing. *Science*, 1992, **258**(5079), pp.126-129.
244. J.T. Jarrett, E.P. Berger and P.T. Lansbury. The C-Terminus of the β protein is critical in amyloidogenesis. *Ann. N. Y. Acad. Sci.*, 1993, **695**(1), pp.144-148.
245. F. Crawford, Z. Suo, C. Fang, A. Sawar, G. Su, G. Arendash and M. Mullan. The vasoactivity of Aβ peptides. *Ann. N. Y. Acad. Sci.*, 1997, **826**(1), pp.35-46.
246. A.M. Klein, N.W. Kowall and R.J. Ferrante. Neurotoxicity and oxidative damage of beta amyloid 1–42 versus beta amyloid 1–40 in the mouse cerebral cortex. *Ann. N. Y. Acad. Sci.*, 1999, **893**(1), pp.314-320.
247. Z. Suo, C. Fang, F. Crawford and M. Mullan. Superoxide free radical and intracellular calcium mediate Aβ1–42 induced endothelial toxicity. *Brain Res.*, 1997, **762**(1–2), pp.144-152.
248. H. Welander, J. Frånberg, C. Graff, E. Sundström, B. Winblad and L.O. Tjernberg. Aβ43 is more frequent than Aβ40 in amyloid plaque cores from Alzheimer disease brains. *J. Neurochem.*, 2009, **110**(2), pp.697-706.
249. T. Saito, T. Suemoto, N. Brouwers, K. Sleegers, S. Funamoto, N. Mihira, Y. Matsuba, K. Yamada, P. Nilsson, J. Takano, M. Nishimura, N. Iwata, C. Van Broeckhoven, Y. Ihara and T.C. Saido. Potent amyloidogenicity and pathogenicity of Aβ43. *Nat. Neurosci.*, 2011, **14**(8), pp.1023-1032.

250. E. Karran, M. Mercken and B.D. Strooper. The amyloid cascade hypothesis for Alzheimer's disease: an appraisal for the development of therapeutics. *Nat. Rev. Drug. Discov.*, 2011, **10**(9), pp.698-712.
251. B. Sommer. Alzheimer's disease and the amyloid cascade hypothesis: ten years on. *Curr. Opin. Pharmacol.*, 2002, **2**(1), pp.87-92.
252. A. Goate, M.-C. Chartier-Harlin, M. Mullan, J. Brown, F. Crawford, L. Fidani, L. Giuffra, A. Haynes, N. Irving, L. James, R. Mant, P. Newton, K. Rooke, P. Roques, C. Talbot, M. Pericak-Vance, A. Roses, R. Williamson, M. Rossor, M. Owen and J. Hardy. Segregation of a missense mutation in the amyloid precursor protein gene with familial Alzheimer's disease. *Nature*, 1991, **349**(6311), pp.704-706.
253. R. Sherrington, E.I. Rogaev, Y. Liang, E.A. Rogaeva, G. Levesque, M. Ikeda, H. Chi, C. Lin, G. Li, K. Holman, T. Tsuda, L. Mar, J.F. Foncin, A.C. Bruni, M.P. Montesi, S. Sorbi, I. Rainero, L. Pinessi, L. Nee, I. Chumakov, D. Pollen, A. Brookes, P. Sanseau, R.J. Polinsky, W. Wasco, H.a.R. Da Silva, J.L. Haines, M.A. Pericak-Vance, R.E. Tanzi, A.D. Roses, P.E. Fraser, J.M. Rommens and P.H. St George-Hyslop. Cloning of a gene bearing missense mutations in early-onset familial Alzheimer's disease. *Nature*, 1995, **375**(6534), pp.754-760.
254. E. Levy-Lahad, W. Wasco, P. Poorkaj, D. Romano, J. Oshima, W. Pettingell, C. Yu, P. Jondro, S. Schmidt, K. Wang and E. Al. Candidate gene for the chromosome 1 familial Alzheimer's disease locus. *Science*, 1995, **269**(5226), pp.973-977.
255. E.I. Rogaev, R. Sherrington, E.A. Rogaeva, G. Levesque, M. Ikeda, Y. Liang, H. Chi, C. Lin, K. Holman, T. Tsuda, L. Mar, S. Sorbi, B. Nacmias, S. Piacentini, L. Amaducci, I. Chumakov, D. Cohen, L. Lannfelt, P.E. Fraser, J.M. Rommens and P.H.S. George-Hyslop. Familial Alzheimer's disease in kindreds with missense mutations in a gene on chromosome 1 related to the Alzheimer's disease type 3 gene. *Nature*, 1995, **376**(6543), pp.775-778.
256. M.P. Murphy, S.N. Uljon, P.E. Fraser, A. Fauq, H.A. Lookingbill, K.A. Findlay, T.E. Smith, P.A. Lewis, D.C. Mclendon, R. Wang and T.E. Golde. Presenilin 1 regulates pharmacologically distinct γ-secretase activities. *J. Biol. Chem.*, 2000, **275**(34), pp.26277-26284.
257. E. Lana-Elola, S.D. Watson-Scales, E.M.C. Fisher and V.L.J. Tybulewicz. Down syndrome: searching for the genetic culprits. *Dis. Model. Mech.*, 2011, **4**(5), pp.586-595.
258. E. Corder, A. Saunders, W. Strittmatter, D. Schmechel, P. Gaskell, G. Small, A. Roses, J. Haines and M. Pericak-Vance. Gene dose of apolipoprotein E type 4 allele and the risk of Alzheimer's disease in late onset families. *Science*, 1993, **261**(5123), pp.921-923.
259. W.J. Strittmatter, A.M. Saunders, D. Schmechel, M. Pericak-Vance, J. Enghild, G.S. Salvesen and A.D. Roses. Apolipoprotein E: high-avidity binding to beta-amyloid and increased frequency of type 4 allele in late-onset familial Alzheimer disease. *Proc. Natl. Acad. Sci.*, 1993, **90**(5), pp.1977-1981.
260. D.M. Holtzman, K.R. Bales, T. Tenkova, A.M. Fagan, M. Parsadanian, L.J. Sartorius, B. Mackey, J. Olney, D. Mckeel, D. Wozniak and S.M. Paul. Apolipoprotein E isoform-dependent amyloid deposition and neuritic degeneration in a mouse model of Alzheimer's disease. *Proc. Natl. Acad. Sci.*, 2000, **97**(6), pp.2892-2897.

261. J. Kim, J.M. Basak and D.M. Holtzman. The role of apolipoprotein E in Alzheimer's disease. *Neuron*, 2009, **63**(3), pp.287-303.
262. N.G. Sgourakis, Y. Yan, S. Mccallum, C. Wang and A.E. Garcia. The Alzheimer's peptides Aβ40 and 42 adopt distinct conformations in water: A combined MD / NMR study. *J. Mol. Biol.*, 2007, **368**(5), pp.1448-1457.
263. H.N.M. Rushworth J. V. Lipid rafts: Linking Alzheimer's amyloid-β production, aggregation, and toxicity at neuronal membranes. *Int. J. Alzheimer. Dis.*, 2011, (603052), p.14.
264. G. Bitan, M.D. Kirkitadze, A. Lomakin, S.S. Vollers, G.B. Benedek and D.B. Teplow. Amyloid β-protein (Aβ) assembly: Aβ40 and Aβ42 oligomerize through distinct pathways. *Proc. Natl. Acad. Sci.*, 2003, **100**(1), pp.330-335.
265. S.L. Bernstein, N.F. Dupuis, N.D. Lazo, T. Wyttenbach, M.M. Condron, G. Bitan, D.B. Teplow, J.-E. Shea, B.T. Ruotolo, C.V. Robinson and M.T. Bowers. Amyloid-β protein oligomerization and the importance of tetramers and dodecamers in the aetiology of Alzheimer's disease. *Nat. Chem.*, 2009, **1**(4), pp.326-331.
266. D.M. Walsh and D.J. Selkoe. Aβ Oligomers – a decade of discovery. *J. Neurochem.*, 2007, **101**(5), pp.1172-1184.
267. R.D. Terry, E. Masliah, D.P. Salmon, N. Butters, R. Deteresa, R. Hill, L.A. Hansen and R. Katzman. Physical basis of cognitive alterations in Alzheimer's disease: Synapse loss is the major correlate of cognitive impairment. *Ann. Neurol.*, 1991, **30**(4), pp.572-580.
268. G.M. Shankar, S. Li, T.H. Mehta, A. Garcia-Munoz, N.E. Shepardson, I. Smith, F.M. Brett, M.A. Farrell, M.J. Rowan, C.A. Lemere, C.M. Regan, D.M. Walsh, B.L. Sabatini and D.J. Selkoe. Amyloid-β protein dimers isolated directly from Alzheimer's brains impair synaptic plasticity and memory. *Nat. Med.*, 2008, **14**(8), pp.837-842.
269. L.W. Hung, G.D. Ciccotosto, E. Giannakis, D.J. Tew, K. Perez, C.L. Masters, R. Cappai, J.D. Wade and K.J. Barnham. Amyloid-β Peptide (Aβ) neurotoxicity is modulated by the rate of peptide aggregation: Aβ dimers and trimers correlate with neurotoxicity. *J. Neurosci.*, 2008, **28**(46), pp.11950-11958.
270. S. Lesné, M.T. Koh, L. Kotilinek, R. Kayed, C.G. Glabe, A. Yang, M. Gallagher and K.H. Ashe. A specific amyloid-β protein assembly in the brain impairs memory. *Nature*, 2006, **440**(7082), pp.352-357.
271. Y. Gong, L. Chang, K.L. Viola, P.N. Lacor, M.P. Lambert, C.E. Finch, G.A. Krafft and W.L. Klein. Alzheimer's disease-affected brain: Presence of oligomeric Aβ ligands (ADDLs) suggests a molecular basis for reversible memory loss. *Proc. Natl. Acad. Sci.*, 2003, **100**(18), pp.10417-10422.
272. M.P. Lambert, A.K. Barlow, B.A. Chromy, C. Edwards, R. Freed, M. Liosatos, T.E. Morgan, I. Rozovsky, B. Trommer, K.L. Viola, P. Wals, C. Zhang, C.E. Finch, G.A. Krafft and W.L. Klein. Diffusible, nonfibrillar ligands derived from Aβ1-42 are potent central nervous system neurotoxins. *Proc. Natl. Acad. Sci.*, 1998, **95**(11), pp.6448-53.
273. G.M. Shankar, M.A. Leissring, A. Adame, X. Sun, E. Spooner, E. Masliah, D.J. Selkoe, C.A. Lemere and D.M. Walsh. Biochemical and immunohistochemical analysis of an Alzheimer's disease mouse model reveals the presence of multiple cerebral Aβ assembly forms throughout life. *Neurobiol. Dis.*, 2009, **36**(2), pp.293-302.

274. S. Matsumura, K. Shinoda, M. Yamada, S. Yokojima, M. Inoue, T. Ohnishi, T. Shimada, K. Kikuchi, D. Masui, S. Hashimoto, M. Sato, A. Ito, M. Akioka, S. Takagi, Y. Nakamura, K. Nemoto, Y. Hasegawa, H. Takamoto, H. Inoue, S. Nakamura, Y.-I. Nabeshima, D.B. Teplow, M. Kinjo and M. Hoshi. Two distinct amyloid β-protein (Aβ) assembly pathways leading to oligomers and fibrils identified by combined fluorescence correlation spectroscopy, morphology, and toxicity analyses. *J. Biol. Chem.*, 2011, **286**(13), pp.11555-11562.
275. J.P. Cleary, D.M. Walsh, J.J. Hofmeister, G.M. Shankar, M.A. Kuskowski, D.J. Selkoe and K.H. Ashe. Natural oligomers of the amyloid-β protein specifically disrupt cognitive function. *Nat. Neurosci.*, 2005, **8**(1), pp.79-84.
276. D.M. Hartley, C. Zhao, A.C. Speier, G.A. Woodard, S. Li, Z. Li and T. Walz. Transglutaminase induces protofibril-like amyloid β-protein assemblies that are protease-resistant and inhibit long-term potentiation. *J. Biol. Chem.*, 2008, **283**(24), pp.16790-16800.
277. R. Kayed, A. Pensalfini, L. Margol, Y. Sokolov, F. Sarsoza, E. Head, J. Hall and C. Glabe. Annular protofibrils are a structurally and functionally distinct type of amyloid oligomer. *J. Biol. Chem.*, 2009, **284**(7), pp.4230-4237.
278. J.M. Nussbaum, S. Schilling, H. Cynis, A. Silva, E. Swanson, T. Wangsanut, K. Tayler, B. Wiltgen, A. Hatami, R. Ronicke, K. Reymann, B. Hutter-Paier, A. Alexandru, W. Jagla, S. Graubner, C.G. Glabe, H.-U. Demuth and G.S. Bloom. Prion-like behaviour and tau-dependent cytotoxicity of pyroglutamylated amyloid-β. *Nature*, 2012, **485**(7400), pp.651-655.
279. T.V.P. Bliss and G.L. Collingridge. A synaptic model of memory: long-term potentiation in the hippocampus. *Nature*, 1993, **361**(6407), pp.31-39.
280. M. Necula, R. Kayed, S. Milton and C.G. Glabe. Small molecule inhibitors of aggregation indicate that Amyloid β oligomerization and fibrillization pathways are independent and distinct. *J. Biol. Chem.*, 2007, **282**(14), pp.10311-10324.
281. J. Lee, E.K. Culyba, E.T. Powers and J.W. Kelly. Amyloid-β forms fibrils by nucleated conformational conversion of oligomers. *Nat. Chem. Biol.*, 2011, **7**(9), pp.602-609.
282. C.A. Lasagna-Reeves, C.G. Glabe and R. Kayed. Amyloid-β annular protofibrils evade fibrillar fate in Alzheimer disease brain. *J. Biol. Chem.*, 2011, **286**(25), pp.22122-22130.
283. C.A. Lasagna-Reeves and R. Kayed. Astrocytes contain amyloid-β annular protofibrils in Alzheimer's disease brains. *FEBS Lett.*, 2011, **585**(19), pp.3052-3057.
284. P. Giannakopoulos, P.R. Hof, J.-P. Michel, J. Guimon and C. Bouras. Cerebral cortex pathology in aging and Alzheimer's disease: a quantitative survey of large hospital-based geriatric and psychiatric cohorts. *Brain Res. Rev.*, 1997, **25**(2), pp.217-245.
285. B.J. Cummings, C.J. Pike, R. Shankle and C.W. Cotman. β-amyloid deposition and other measures of neuropathology predict cognitive status in Alzheimer's disease. *Neurobiol. Aging.*, 1996, **17**(6), pp.921-933.
286. V.L. Villemagne, K.E. Pike, G. Chételat, K.A. Ellis, R.S. Mulligan, P. Bourgeat, U. Ackermann, G. Jones, C. Szoeke, O. Salvado, R. Martins, G. O'keefe, C.A. Mathis, W.E. Klunk, D. Ames, C.L. Masters and C.C. Rowe. Longitudinal assessment of

Aβ and cognition in aging and Alzheimer disease. *Ann. Neurol.*, 2011, **69**(1), pp.181-192.
287. H.J. Aizenstein, R.D. Nebes, J.A. Saxton, J.C. Price, C.A. Mathis, N.D. Tsopelas, S.K. Ziolko, J.A. James, B.E. Snitz, P.R. Houck, W. Bi, A.D. Cohen, B.J. Lopresti, S.T. Dekosky, E.M. Halligan and W.E. Klunk. Frequent amyloid deposition without significant cognitive impairment among the elderly. *Arch. Neurol.*, 2008, **65**(11), pp.1509-1517.
288. D.M. Walsh, D.M. Hartley, Y. Kusumoto, Y. Fezoui, M.M. Condron, A. Lomakin, G.B. Benedek, D.J. Selkoe and D.B. Teplow. Amyloid-β protein fibrillogenesis: Structure and biological activity of protofibrillar intermediates. *J. Biol. Chem.*, 1999, **274**(36), pp.25945-25952.
289. J.C. Stroud, C. Liu, P.K. Teng and D. Eisenberg. Toxic fibrillar oligomers of amyloid-β have cross-β structure. *Proc. Natl. Acad. Sci.*, 2012, **109**(20), pp.7717-7722.
290. R. Sultana, M. Perluigi and D.A. Butterfield. Oxidatively modified proteins in Alzheimer's disease (AD), mild cognitive impairment and animal models of AD: role of Aβ in pathogenesis. *Acta. Neuropathol.*, 2009, **118**(1), pp.131-150.
291. B. Cameron and G.E. Landreth. Inflammation, microglia, and Alzheimer's disease. *Neurobiol. Dis.*, 2010, **37**(3), pp.503-509.
292. C.K. Glass, K. Saijo, B. Winner, M.C. Marchetto and F.H. Gage. Mechanisms underlying inflammation in neurodegeneration. *Cell*, 2010, **140**(6), pp.918-934.
293. J.S. Jeong, A. Ansaloni, R. Mezzenga, H.A. Lashuel and G. Dietler. Novel mechanistic insight into the molecular basis of amyloid polymorphism and secondary nucleation during amyloid formation. *J. Mol. Biol.*, 2013, **425**(10), pp.1765-1781.
294. P. Arosio, R. Cukalevski, B. Frohm, T.P.J. Knowles and S. Linse. Quantification of the concentration of Aβ42 propagons during the lag phase by an amyloid chain reaction assay. *J. Am. Chem. Soc.*, 2014, **136**(1), pp.219-225.
295. A.R. George and D.R. Howlett. Computationally derived structural models of the β-amyloid found in Alzheimer's disease plaques and the interaction with possible aggregation inhibitors. *Biopolymers*, 1999, **50**(7), pp.733-741.
296. L. Li, T.A. Darden, L. Bartolotti, D. Kominos and L.G. Pedersen. An atomic model for the pleated β-sheet structure of Aβ amyloid protofilaments. *Biophys. J.*, 1999, **76**(6), pp.2871-2878.
297. N.D. Lazo and D.T. Downing. Amyloid fibrils may be assembled from β-helical protofibrils. *Biochemistry*, 1998, **37**(7), pp.1731-1735.
298. I. Bertini, L. Gonnelli, C. Luchinat, J. Mao and A. Nesi. A new structural model of Aβ40 fibrils. *J. Am. Chem. Soc.*, 2011, **133**(40), pp.16013-16022.
299. Y. Xiao, B. Ma, D. Mcelheny, S. Parthasarathy, F. Long, M. Hoshi, R. Nussinov and Y. Ishii. Aβ(1-42) fibril structure illuminates self-recognition and replication of amyloid in Alzheimer's disease. *Nat. Struct. Mol. Biol.*, 2015, **22**(6), pp.499-505.
300. I. Kheterpal, A. Williams, C. Murphy, B. Bledsoe and R. Wetzel. Structural features of the Aβ amyloid fibril elucidated by limited proteolysis. *Biochemistry*, 2001, **40**(39), pp.11757-11767.
301. T.L.S. Benzinger, D.M. Gregory, T.S. Burkoth, H. Miller-Auer, D.G. Lynn, R.E. Botto and S.C. Meredith. Propagating structure of Alzheimer's β-amyloid((10–

35)) is parallel β-sheet with residues in exact register. *Proc. Natl. Acad. Sci.*, 1998, **95**(23), pp.13407-13412.
302. M. Török, S. Milton, R. Kayed, P. Wu, T. Mcintire, C.G. Glabe and R. Langen. Structural and dynamic features of Alzheimer's Aβ peptide in amyloid fibrils studied by site-directed spin labeling. *J. Biol. Chem.*, 2002, **277**(43), pp.40810-40815.
303. A. Olofsson, A.E. Sauer-Eriksson and A. Öhman. The solvent protection of Alzheimer amyloid-β-(1–42) fibrils as determined by solution NMR spectroscopy. *J. Biol. Chem.*, 2006, **281**(1), pp.477-483.
304. Y. Masuda, S. Uemura, R. Ohashi, A. Nakanishi, K. Takegoshi, T. Shimizu, T. Shirasawa and K. Irie. Identification of physiological and toxic conformations in Aβ42 aggregates. *ChemBioChem*, 2009, **10**(2), pp.287-295.
305. M. Schmidt, C. Sachse, W. Richter, C. Xu, M. Fändrich and N. Grigorieff. Comparison of Alzheimer Aβ(1–40) and Aβ(1–42) amyloid fibrils reveals similar protofilament structures. *Proc. Natl. Acad. Sci.*, 2009, **106**(47), pp.19813-19818.
306. M. Ahmed, J. Davis, D. Aucoin, T. Sato, S. Ahuja, S. Aimoto, J.I. Elliott, W.E. Van Nostrand and S.O. Smith. Structural conversion of neurotoxic amyloid-β1-42 oligomers to fibrils. *Nat. Struct. Mol. Biol.*, 2010, **17**(5), pp.561-567.
307. B. Ma and R. Nussinov. Polymorphic triple β-Sheet structures contribute to amide hydrogen/deuterium (H/D) exchange protection in the Alzheimer amyloid β42 peptide. *J. Biol. Chem.*, 2011, **286**(39), pp.34244-34253.
308. K. Pauwels, T.L. Williams, K.L. Morris, W. Jonckheere, A. Vandersteen, G. Kelly, J. Schymkowitz, F. Rousseau, A. Pastore, L.C. Serpell and K. Broersen. Structural basis for increased toxicity of pathological Aβ42:Aβ40 ratios in Alzheimer disease. *J. Biol. Chem.*, 2012, **287**(8), pp.5650-5660.
309. B. O'nuallain, A.D. Williams, P. Westermark and R. Wetzel. Seeding specificity in amyloid growth induced by heterologous fibrils. *J. Biol. Chem.*, 2004, **279**(17), pp.17490-17499.
310. J. Stöhr, C. Condello, J.C. Watts, L. Bloch, A. Oehler, M. Nick, S.J. Dearmond, K. Giles, W.F. Degrado and S.B. Prusiner. Distinct synthetic Aβ prion strains producing different amyloid deposits in bigenic mice. *Proc. Natl. Acad. Sci.*, 2014, **111**(28), pp.10329-10334.
311. Z.J. Wynn and J.L. Cummings. Cholinesterase inhibitor therapies and neuropsychiatric manifestations of Alzheimer's disease. *Dement. Geriatr. Cogn. Dis.*, 2004, **17**(1-2), pp.100-108.
312. W. Danysz and C.G. Parsons. Alzheimer's disease, β-amyloid, glutamate, NMDA receptors and memantine – searching for the connections. *Br. J. Pharmacol.*, 2012, **167**(2), pp.324-352.
313. R.C. Green, L.S. Schneider, D.A. Amato, A.P. Beelen, G. Wilcock, E.A. Swabb and K.H. Zavitz. Effect of tarenflurbil on cognitive decline and activities of daily living in patients with mild Alzheimer disease: A randomized controlled trial. *J. Amm. Med. Ass.*, 2009, **302**(23), pp.2557-2564.
314. K.G. Yiannopoulou and S.G. Papageorgiou. Current and future treatments for Alzheimer's disease. *Ther. Adv. Neurol. Dis.*, 2013, **6**(1), pp.19-33.
315. X. Luo and R. Yan. Inhibition of BACE1 for therapeutic use in Alzheimer's disease. *Int. J. Clin. Exp. Path.*, 2010, **3**(6), pp.618-628.

316. L. Désiré, E. Blondiaux, J. Carrière, R. Haddad, O. Sol, P. Fehlbaum-Beurdeley, R. Einstein, W. Zhou and M.P. Pando. Blood transcriptomic biomarkers of Alzheimer's disease patients treated with EHT 0202. *J. Alzheimer. Dis.*, 2013, **34**(2), pp.469-483.
317. Y.-J. Wang, H.-D. Zhou and X.-F. Zhou. Clearance of amyloid-beta in Alzheimer's disease: progress, problems and perspectives. *Drug. Discov. Today.*, 2006, **11**(19–20), pp.931-938.
318. T. Wisniewski and U. Konietzko. Amyloid-β immunisation for Alzheimer's disease. *Lancet Neurol.*, 2008, **7**(9), pp.805-811.
319. C. Janus, J. Pearson, J. Mclaurin, P.M. Mathews, Y. Jiang, S.D. Schmidt, M.A. Chishti, P. Horne, D. Heslin, J. French, H.T.J. Mount, R.A. Nixon, M. Mercken, C. Bergeron, P.E. Fraser, P. St George-Hyslop and D. Westaway. Aβ peptide immunization reduces behavioural impairment and plaques in a model of Alzheimer's disease. *Nature*, 2000, **408**(6815), pp.979-982.
320. D. Morgan, D.M. Diamond, P.E. Gottschall, K.E. Ugen, C. Dickey, J. Hardy, K. Duff, P. Jantzen, G. Dicarlo, D. Wilcock, K. Connor, J. Hatcher, C. Hope, M. Gordon and G.W. Arendash. Aβ peptide vaccination prevents memory loss in an animal model of Alzheimer's disease. *Nature*, 2000, **408**(6815), pp.982-985.
321. D. Schenk, R. Barbour, W. Dunn, G. Gordon, H. Grajeda, T. Guido, K. Hu, J. Huang, K. Johnson-Wood, K. Khan, D. Kholodenko, M. Lee, Z. Liao, I. Lieberburg, R. Motter, L. Mutter, F. Soriano, G. Shopp, N. Vasquez, C. Vandevert, S. Walker, M. Wogulis, T. Yednock, D. Games and P. Seubert. Immunization with amyloid-β attenuates Alzheimer-disease-like pathology in the PDAPP mouse. *Nature*, 1999, **400**(6740), pp.173-177.
322. E. Check. Nerve inflammation halts trial for Alzheimer's drug. *Nature*, 2002, **415**(6871), pp.462-462.
323. W.F. Goure, G.A. Krafft, J. Jerecic and F. Hefti. Targeting the proper amyloid-β neuronal toxins: a path forward for Alzheimer's disease immunotherapeutics. *Alzheimer. Res. Ther.*, 2014, **6**(4), pp.42-42.
324. H. Hampel, L.S. Schneider, E. Giacobini, M. Kivipelto, S. Sindi, B. Dubois, K. Broich, R. Nisticò, P.S. Aisen and S. Lista. Advances in the therapy of Alzheimer's disease: targeting amyloid beta and tau and perspectives for the future. *Exp. Rev. Neurother.*, 2014, **15**(1), pp.83-105.
325. M. Hölttä, O. Hansson, U. Andreasson, J. Hertze, L. Minthon, K. Nägga, N. Andreasen, H. Zetterberg and K. Blennow. Evaluating amyloid-β oligomers in cerebrospinal fluid as a biomarker for Alzheimer's disease. *PLoS One*, 2013, **8**(6), p.e66381.
326. L.-F. Lue, Y.-M. Kuo, A.E. Roher, L. Brachova, Y. Shen, L. Sue, T. Beach, J.H. Kurth, R.E. Rydel and J. Rogers. Soluble amyloid β peptide concentration as a predictor of synaptic change in Alzheimer's disease. *Am. J. Path.*, 1999, **155**(3), pp.853-862.
327. Y.J. Yu and R.J. Watts. Developing therapeutic antibodies for neurodegenerative disease. *Neurotherapeutics*, 2013, **10**(3), pp.459-472.
328. F. Gervais, J. Paquette, C. Morissette, P. Krzywkowski, M. Yu, M. Azzi, D. Lacombe, X. Kong, A. Aman, J. Laurin, W.A. Szarek and P. Tremblay. Targeting soluble Aβ peptide with tramiprosate for the treatment of brain amyloidosis. *Neurobiol. Aging.*, 2007, **28**(4), pp.537-547.

329. J. DíAz-Nido, F. Wandosell and J. Avila. Glycosaminoglycans and β-amyloid, prion and tau peptides in neurodegenerative diseases. *Peptides*, 2002, **23**(7), pp.1323-1332.
330. I. Santa-Maria, F. Hernández, J. Del Rio, F.J. Moreno and J. Avila. Tramiprosate, a drug of potential interest for the treatment of Alzheimer's disease, promotes an abnormal aggregation of tau. *Mol. Neurodegen.*, 2007, **2**, pp.17-17.
331. A. Bilikiewicz and W. Gaus. Colostrinin (a naturally occurring, proline-rich, polypeptide mixture) in the treatment of Alzheimer's disease. *J. Alzheimer. Dis.*, 2004, **6**(1), pp.17-26.
332. J. Mclaurin, R. Golomb, A. Jurewicz, J.P. Antel and P.E. Fraser. Inositol stereoisomers stabilize an oligomeric aggregate of Alzheimer amyloid- β peptide and inhibit Aβ-induced toxicity. *J. Biol. Chem.*, 2000, **275**(24), pp.18495-18502.
333. A. Bush, W. Pettingell, G. Multhaup, M. D Paradis, J. Vonsattel, J. Gusella, K. Beyreuther, C. Masters and R. Tanzi. Rapid induction of Alzheimer Aβ amyloid formation by zinc. *Science*, 1994, **265**(5177), pp.1464-1467.
334. C.S. Atwood, R.D. Moir, X. Huang, R.C. Scarpa, N.M.E. Bacarra, D.M. Romano, M.A. Hartshorn, R.E. Tanzi and A.I. Bush. Dramatic aggregation of Alzheimer Aβ by Cu(II) is induced by conditions representing physiological acidosis. *J. Biol. Chem.*, 1998, **273**(21), pp.12817-12826.
335. A.K. Sharma, S.T. Pavlova, J. Kim, D. Finkelstein, N.J. Hawco, N.P. Rath, J. Kim and L.M. Mirica. Bifunctional compounds for controlling metal-mediated aggregation of the Aβ(42) peptide. *J. Am. Chem. Soc.*, 2012, **134**(15), pp.6625-6636.
336. E.L. Sampson, L. Jenagaratnam and R. Mcshane. Metal protein attenuating compounds for the treatment of Alzheimer's dementia. *Cochrane. Database. Syst. Rev.*, 2012, **5**, pp.CD005380-CD005380.
337. N.G. Faux, C.W. Ritchie, A. Gunn, A. Rembach, A. Tsatsanis, J. Bedo, J. Harrison, L. Lannfelt, K. Blennow, H. Zetterberg, M. Ingelsson, C.L. Masters, R.E. Tanzi, J.L. Cummings, C.M. Herd and A.I. Bush. PBT2 rapidly improves cognition in Alzheimer's disease: Additional phase II analyses. *J. Alzheimer. Dis.*, 2010, **20**(2), pp.509-516.
338. S. Weggen, M. Rogers and J. Eriksen. NSAIDs: small molecules for prevention of Alzheimer's disease or precursors for future drug development? *Trends. Pharmacol. Sci.*, 2007, **28**(10), pp.536-543.
339. H.P. Lee, X. Zhu, G. Casadesus, R.J. Castellani, A. Nunomura, M.A. Smith, H.-G. Lee and G. Perry. Antioxidant approaches for the treatment of Alzheimer's disease. *Exp. Rev. Neurother.*, 2010, **10**(7), pp.1201-1208.
340. S.A. Shumaker, C. Legault, S.R. Rapp and Et Al. Estrogen plus progestin and the incidence of dementia and mild cognitive impairment in postmenopausal women: The women's health initiative memory study: a randomized controlled trial. *J. Amm. Med. Ass.*, 2003, **289**(20), pp.2651-2662.
341. M.T. Koh, R.P. Haberman, S. Foti, T.J. Mccown and M. Gallagher. Treatment strategies targeting excess hippocampal activity benefit aged rats with cognitive impairment. *Neuropsychopharmacol.*, 2009, **35**(4), pp.1016-1025.

342. J.J. Palop and L. Mucke. Amyloid-β-induced neuronal dysfunction in Alzheimer's disease: from synapses toward neural networks. *Nat. Neurosci.*, 2010, **13**(7), pp.812-818.
343. L. Verret, Edward o. Mann, Giao b. Hang, Albert m.I. Barth, I. Cobos, K. Ho, N. Devidze, E. Masliah, Anatol c. Kreitzer, I. Mody, L. Mucke and Jorge j. Palop. Inhibitory interneuron deficit links altered network activity and cognitive dysfunction in Alzheimer model. *Cell*, 2012, **149**(3), pp.708-721.
344. H. Harris and D.C. Rubinsztein. Control of autophagy as a therapy for neurodegenerative disease. *Nat. Rev. Neurol.*, 2012, **8**(2), pp.108-117.
345. M. Chintamaneni and M. Bhaskar. Biomarkers in Alzheimer's disease: A review. *ISRN Pharma.*, 2012, **2012**, p.6.
346. C. Humpel and T. Hochstrasser. Cerebrospinal fluid and blood biomarkers in Alzheimer's disease. *World J. Psychiatry.*, 2011, **1**(1), pp.8-18.
347. C. Humpel. Identifying and validating biomarkers for Alzheimer's disease. *Trends. Biotechnol.*, 2011, **29**(1), pp.26-32.
348. A. Lockhart, J.R. Lamb, T. Osredkar, L.I. Sue, J.N. Joyce, L. Ye, V. Libri, D. Leppert and T.G. Beach. PIB is a non-specific imaging marker of amyloid-beta (Aβ) peptide-related cerebral amyloidosis. *Brain*, 2007, **130**(10), pp.2607-2615.
349. M.D. Ikonomovic, W.E. Klunk, E.E. Abrahamson, C.A. Mathis, J.C. Price, N.D. Tsopelas, B.J. Lopresti, S. Ziolko, W. Bi, W.R. Paljug, M.L. Debnath, C.E. Hope, B.A. Isanski, R.L. Hamilton and S.T. Dekosky. Post-mortem correlates of *in vivo* PiB-PET amyloid imaging in a typical case of Alzheimer's disease. 2008, **131**(6), pp.1630-1645.
350. B.J. Bacskai, M.P. Frosch, S.H. Freeman and Et Al. Molecular imaging with pittsburgh compound b confirmed at autopsy: A case report. *Arch. Neurol.*, 2007, **64**(3), pp.431-434.
351. D.F. Wong, P.B. Rosenberg, Y. Zhou, A. Kumar, V. Raymont, H.T. Ravert, R.F. Dannals, A. Nandi, J.R. Bražić, W. Ye, J. Hilton, C. Lyketsos, H.F. Kung, A.D. Joshi, D.M. Skovronsky and M.J. Pontecorvo. *In vivo* imaging of amyloid deposition in Alzheimer disease using the radioligand 18F-AV-45 (flobetapir F 18). *J. Nucl. Med.*, 2010, **51**(6), pp.913-920.
352. N. Nelissen, K. Van Laere, L. Thurfjell, R. Owenius, M. Vandenbulcke, M. Koole, G. Bormans, D.J. Brooks and R. Vandenberghe. Phase 1 study of the pittsburgh compound B derivative 18F-flutemetamol in healthy volunteers and patients with probable Alzheimer disease. *J. Nucl. Med.*, 2009, **50**(8), pp.1251-1259.
353. C.C. Rowe, U. Ackerman, W. Browne, R. Mulligan, K.L. Pike, G. O'keefe, H. Tochon-Danguy, G. Chan, S.U. Berlangieri, G. Jones, K.L. Dickinson-Rowe, H.P. Kung, W. Zhang, M.P. Kung, D. Skovronsky, T. Dyrks, G. Holl, S. Krause, M. Friebe, L. Lehman, S. Lindemann, L.M. Dinkelborg, C.L. Masters and V.L. Villemagne. Imaging of amyloid β in Alzheimer's disease with 18F-BAY94-9172, a novel PET tracer: proof of mechanism. *Lancet Neurol.*, 2008, **7**(2), pp.129-135.
354. C.C. Rowe, S. Pejoska, R.S. Mulligan, G. Jones, J.G. Chan, S. Svensson, Z. Cselényi, C.L. Masters and V.L. Villemagne. Head-to-head comparison of 11C-PiB and 18F-AZD4694 (NAV4694) for β-amyloid imaging in aging and dementia. *J. Nucl. Med.*, 2013, **54**(6), pp.880-886.

355. K. Blennow and E. Vanmechelen. CSF markers for pathogenic processes in Alzheimer's disease: Diagnostic implications and use in clinical neurochemistry. *Brain Research Bulletin*, 2003, **61**(3), pp.235-242.
356. D. Strozyk, K. Blennow, L.R. White and L.J. Launer. CSF Aβ 42 levels correlate with amyloid-neuropathology in a population-based autopsy study. *Neurology*, 2003, **60**(4), pp.652-656.
357. G.B. Frisoni, M. Bocchetta, G. Chételat, G.D. Rabinovici, M.J. De Leon, J. Kaye, E.M. Reiman, P. Scheltens, F. Barkhof, S.E. Black, D.J. Brooks, M.C. Carrillo, N.C. Fox, K. Herholz, A. Nordberg, C.R. Jack, W.J. Jagust, K.A. Johnson, C.C. Rowe, R.A. Sperling, W. Thies, L.-O. Wahlund, M.W. Weiner, P. Pasqualetti, C. Decarli and I.S.N.P.I.A. For. Imaging markers for Alzheimer disease: Which vs how. *Neurology*, 2013, **81**(5), pp.487-500.
358. O. Hansson, H. Zetterberg, P. Buchhave, U. Andreasson, E. Londos, L. Minthon and K. Blennow. Prediction of Alzheimer's disease using the CSF Aβ42/Aβ40 ratio in patients with mild cognitive impairment. *Dement. Geriatr. Cogn. Dis.*, 2007, **23**(5), pp.316-320.
359. B. Dubois, H.H. Feldman, C. Jacova, H. Hampel, J.L. Molinuevo, K. Blennow, S.T. Dekosky, S. Gauthier, D. Selkoe, R. Bateman, S. Cappa, S. Crutch, S. Engelborghs, G.B. Frisoni, N.C. Fox, D. Galasko, M.-O. Habert, G.A. Jicha, A. Nordberg, F. Pasquier, G. Rabinovici, P. Robert, C. Rowe, S. Salloway, M. Sarazin, S. Epelbaum, L.C. De Souza, B. Vellas, P.J. Visser, L. Schneider, Y. Stern, P. Scheltens and J.L. Cummings. Advancing research diagnostic criteria for Alzheimer's disease: the IWG-2 criteria. *Lancet Neurol.*, 2014, **13**(6), pp.614-629.
360. D.H.J. Bunka and P.G. Stockley. Aptamers come of age – at last. *Nat. Rev. Microbio.*, 2006, **4**(8), pp.588-596.
361. A.D. Keefe, S. Pai and A. Ellington. Aptamers as therapeutics. *Nat. Rev. Drug. Discov.*, 2010, **9**(7), pp.537-550.
362. C.L. Esposito, S. Catuogno, V. De Franciscis and L. Cerchia. New insight into clinical development of nucleic acid aptamers. *Discov. Med.*, 2011, **11**(61), pp.487-96.
363. M. Famulok, G. Mayer and M. Blind. Nucleic acid aptamers from selection *in vitro* to applications *in vivo*. *Acc. Chem. Res.*, 2000, **33**(9), pp.591-599.
364. J.F. Lee, G.M. Stovall and A.D. Ellington. Aptamer therapeutics advance. *Curr. Opin. Chem. Biol.*, 2006, **10**(3), pp.282-289.
365. A. Serganov and D.J. Patel. Ribozymes, riboswitches and beyond: regulation of gene expression without proteins. *Nat. Rev. Genet.*, 2007, **8**(10), pp.776-790.
366. E.A. Doherty and J.A. Doudna. Ribozyme structures and mechanisms. *Annu. Rev. Biochem.*, 2000, **69**(1), pp.597-615.
367. M. Mandal and R.R. Breaker. Gene regulation by riboswitches. *Nat. Rev. Mol. Cell. Biol.*, 2004, **5**(6), pp.451-463.
368. B.J. Tucker and R.R. Breaker. Riboswitches as versatile gene control elements. *Curr. Opin. Struct. Biol.*, 2005, **15**(3), pp.342-348.
369. A.D. Ellington and J.W. Szostak. *In vitro* selection of RNA molecules that bind specific ligands. *Nature*, 1990, **346**(6287), pp.818-822.
370. G.S. Baird. Where are all the aptamers? *Am. J. Clin. Path.*, 2010, **134**(4), pp.529-531.

371. S. Missailidis and A. Hardy. Aptamers as inhibitors of target proteins. *Exp. Opin. Ther. Pat.*, 2009.
372. D.L. Robertson and G.F. Joyce. Selection *in vitro* of an RNA enzyme that specifically cleaves single-stranded DNA. *Nature*, 1990, **344**(6265), pp.467-468.
373. C. Tuerk and L. Gold. Systematic evolution of ligands by exponential enrichment: RNA ligands to bacteriophage T4 DNA polymerase. *Science*, 1990, **249**(4968), pp.505-510.
374. V.B. Pinheiro, A.I. Taylor, C. Cozens, M. Abramov, M. Renders, S. Zhang, J.C. Chaput, J. Wengel, S.-Y. Peak-Chew, S.H. Mclaughlin, P. Herdewijn and P. Holliger. Synthetic genetic polymers capable of heredity and evolution. *Science*, 2012, **336**(6079), pp.341-344.
375. J.C. Cox and A.D. Ellington. Automated selection of anti-protein aptamers. *Bioorg. Med. Chem.*, 2001, **9**(10), pp.2525-2531.
376. J.C. Cox, A. Hayhurst, J. Hesselberth, T.S. Bayer, G. Georgiou and A.D. Ellington. Automated selection of aptamers against protein targets translated *in vitro*: from gene to aptamer. *Nucleic Acids Res.*, 2002, **30**(20), p.e108.
377. S. Klug and M. Famulok. All you wanted to know about SELEX. *Mol. Biol. Rep.*, 1994, **20**(2), pp.97-107.
378. T.S. Misono and P.K.R. Kumar. Selection of RNA aptamers against human influenza virus hemagglutinin using surface plasmon resonance. *Anal. Biochem.*, 2005, **342**(2), pp.312-317.
379. M. Khati, M. Schüman, J. Ibrahim, Q. Sattentau, S. Gordon and W. James. Neutralization of infectivity of diverse R5 clinical isolates of human immunodeficiency virus type 1 by gp120-binding 2'F-RNA aptamers. *J. Virol.*, 2003, **77**(23), pp.12692-12698.
380. M. Berezovski, A. Drabovich, S.M. Krylova, M. Musheev, V. Okhonin, A. Petrov and S.N. Krylov. Nonequilibrium capillary electrophoresis of equilibrium mixtures: A universal tool for development of aptamers. *J. Am. Chem. Soc.*, 2005, **127**(9), pp.3165-3171.
381. S. Arnold, G. Pampalakis, K. Kantiotou, D. Silva, C. Cortez, S. Missailidis and G. Sotiropoulou. One round of SELEX for the generation of DNA aptamers directed against KLK6. *Biol. Chem.*, 2012, **393**(5), p.343.
382. R. Wilson, C. Bourne, R.R. Chaudhuri, R. Gregory, J. Kenny and A. Cossins. Single-step selection of bivalent aptamers validated by comparison with SELEX using high-throughput sequencing. *PLoS One*, 2014.
383. J.C. Cox, P. Rudolph and A.D. Ellington. Automated RNA selection. *Biotechnol. Progr.*, 1998, **14**(6), pp.845-850.
384. A.D. Keefe and S.T. Cload. SELEX with modified nucleotides. *Curr. Opin. Chem. Biol.*, 2008, **12**(4), pp.448-456.
385. E. Uhlmann, A. Peyman, A. Ryte, A. Schmidt and E. Buddecke. Use of minimally modified antisense oligonucleotides for specific inhibition of gene expression. *In: Methods in Enzymology*. Academic Press, 2000, pp.268-284.
386. L. Beigelman, J.A. Mcswiggen, K.G. Draper, C. Gonzalez, K. Jensen, A.M. Karpeisky, A.S. Modak, J. Matulic-Adamic, A.B. Direnzo, P. Haeberli, D. Sweedler, D. Tracz, S. Grimm, F.E. Wincott, V.G. Thackray and N. Usman. Chemical modification of hammerhead ribozymes: Catalytic activity and nuclease resistance. *J. Biol. Chem.*, 1995, **270**(43), pp.25702-25708.

387. P.E. Burmeister, S.D. Lewis, R.F. Silva, J.R. Preiss, L.R. Horwitz, P.S. Pendergrast, T.G. Mccauley, J.C. Kurz, D.M. Epstein, C. Wilson and A.D. Keefe. Direct *in vitro* selection of a 2'-O-Methyl aptamer to VEGF. *Chem. Biol.*, 2005, **12**(1), pp.25-33.
388. Y. Lin, Q. Qiu, S.C. Gill and S.D. Jayasena. Modified RNA sequence pools for *in vitro* selection. *Nucleic Acids Res.*, 1994, **22**(24), pp.5229-5234.
389. D. Jellinek, L.S. Green, C. Bell, C.K. Lynott, N. Gill, C. Vargeese, G. Kirschenheuter, D.P.C. Mcgee and P. Abesinghe. Potent 2'-Amino-2'-deoxypyrimidine RNA inhibitors of basic fibroblast growth factor. *Biochemistry*, 1995, **34**(36), pp.11363-11372.
390. Y. Lin, D. Nieuwlandt, A. Magallanez, B. Feistner and S.D. Jayasena. High-affinity and specific recognition of human thyroid stimulating hormone (hTSH) by *in vitro*-selected 2'-amino-modified RNA. *Nucleic Acids Res.*, 1996, **24**(17), pp.3407-3414.
391. D. Proske, S. Gilch, F. Wopfner, H.M. Schätzl, E.-L. Winnacker and M. Famulok. Prion-protein-specific aptamer reduces PrP^{Sc} formation. *ChemBioChem*, 2002, **3**(8), pp.717-725.
392. C.P. Rusconi, E. Scardino, J. Layzer, G.A. Pitoc, T.L. Ortel, D. Monroe and B.A. Sullenger. RNA aptamers as reversible antagonists of coagulation factor IXa. *Nature*, 2002, **419**(6902), pp.90-94.
393. E.W.M. Ng, D.T. Shima, P. Calias, E.T. Cunningham, D.R. Guyer and A.P. Adamis. Pegaptanib, a targeted anti-VEGF aptamer for ocular vascular disease. *Nat. Rev. Drug. Discov.*, 2006, **5**(2), pp.123-132.
394. G. Biesecker, L. Dihel, K. Enney and R.A. Bendele. Derivation of RNA aptamer inhibitors of human complement C5. *Immunopharmacology*, 1999, **42**(1–3), pp.219-230.
395. P.E. Burmeister, C. Wang, J.R. Killough, S.D. Lewis, L.R. Horwitz, A. Ferguson, K.M. Thompson, P.S. Pendergrast, T.G. Mccauley, M. Kurz, J. Diener, S.T. Cload, C. Wilson and A.D. Keefe. 2´-deoxy purine, 2´-O-methyl pyrimidine (dRmY) aptamers as candidate therapeutics. *Oligonucleotides*, 2006, **16**(4), pp.337-351.
396. Y. Kato, N. Minakawa, Y. Komatsu, H. Kamiya, N. Ogawa, H. Harashima and A. Matsuda. New NTP analogs: the synthesis of 4'-thioUTP and 4'-thioCTP and their utility for SELEX. *Nucleic Acids Res.*, 2005, **33**(9), pp.2942-2951.
397. L.C. Bock, L.C. Griffin, J.A. Latham, E.H. Vermaas and J.J. Toole. Selection of single-stranded DNA molecules that bind and inhibit human thrombin. *Nature*, 1992, **355**(6360), pp.564-566.
398. M. Kuwahara, K. Hanawa, K. Ohsawa, R. Kitagata, H. Ozaki and H. Sawai. Direct PCR amplification of various modified DNAs having amino acids: Convenient preparation of DNA libraries with high-potential activities for *in vitro* selection. *Bioorgan. Med. Chem.*, 2006, **14**(8), pp.2518-2526.
399. M. Mehedi Masud, M. Kuwahara, H. Ozaki and H. Sawai. Sialyllactose-binding modified DNA aptamer bearing additional functionality by SELEX. *Bioorgan. Med. Chem.*, 2004, **12**(5), pp.1111-1120.
400. A. Shoji, M. Kuwahara, H. Ozaki and H. Sawai. Modified DNA aptamer that binds the (R)-isomer of a thalidomide derivative with high enantioselectivity. *J. Am. Chem. Soc.*, 2007, **129**(5), pp.1456-1464.
401. N.K. Vaish, R. Larralde, A.W. Fraley, J.W. Szostak and L.W. Mclaughlin. A novel, modification-dependent ATP-binding aptamer selected from an RNA library

incorporating a cationic functionality. *Biochemistry*, 2003, **42**(29), pp.8842-8851.
402. T. Schoetzau, J. Langner, E. Moyroud, I. Roehl, S. Vonhoff and S. Klussmann. Aminomodified nucleobases: Functionalized nucleoside triphosphates applicable for SELEX. *Bioconj. Chem.*, 2003, **14**(5), pp.919-926.
403. J. Kang, M.S. Lee, J.A. Copland, B.A. Luxon and D.G. Gorenstein. Combinatorial selection of a single stranded DNA thioaptamer targeting TGF-beta1 protein. *Bioorg. Med. Chem. Lett.*, 2008, **18**(6), pp.1835-1839.
404. J. Kang, M.S. Lee, S.J. Watowich and D.G. Gorenstein. Combinatorial selection of a RNA thioaptamer that binds to Venezuelan equine encephalitis virus capsid protein. *FEBS Lett.*, 2007, **581**(13), pp.2497-2502.
405. D.J. King, J.G. Safar, G. Legname and S.B. Prusiner. Thioaptamer interactions with prion proteins: Sequence-specific and non-specific binding sites. *J. Mol. Biol.*, 2007, **369**(4), pp.1001-1014.
406. R. Padilla and R. Sousa. A Y639F/H784A T7 RNA polymerase double mutant displays superior properties for synthesizing RNAs with non-canonical NTPs. *Nucleic Acids Res.*, 2002, **30**(24), p.e138.
407. J. Chelliserrykattil and A.D. Ellington. Evolution of a T7 RNA polymerase variant that transcribes 2'-O-methyl RNA. *Nat. Biotech.*, 2004, **22**(9), pp.1155-1160.
408. S. Kluszmann, A. Nolte, R. Bald, V.A. Erdmann and J.P. Furste. Mirror-image RNA that binds D-adenosine. *Nat. Biotech.*, 1996, **14**(9), pp.1112-1115.
409. G.W. Ashley. Modeling, synthesis, and hybridization properties of (L)-ribonucleic acid. *J. Am. Chem. Soc.*, 1992, **114**(25), pp.9731-9736.
410. J. Ruckman, L.S. Green, J. Beeson, S. Waugh, W.L. Gillette, D.D. Henninger, L. Claesson-Welsh and N. Janjic. 2'-Fluoropyrimidine RNA-based aptamers to the 165-amino acid form of vascular endothelial growth factor (VEGF165): Inhibition of receptor binding and VEGF-induced vascular permeability through interactions requiring the exon 7-encoded domain. *J. Biol. Chem.*, 1998, **273**(32), pp.20556-20567.
411. R.M. Boomer, S.D. Lewis, J.M. Healy, M. Kurz, C. Wilson and T.G. Mccauley. Conjugation to polyethylene glycol polymer promotes aptamer biodistribution to healthy and inflamed tissues. *Oligonucleotides*, 2005, **15**(3), pp.183-195.
412. J.M. Healy, S.D. Lewis, M. Kurz, R.M. Boomer, K.M. Thompson, C. Wilson and T.G. Mccauley. Pharmacokinetics and biodistribution of novel aptamer compositions. *Pharm. Res.*, 2004, **21**(12), pp.2234-2246.
413. S.R. Watson, Y.-F. Chang, D.a.N. O'connell, L. Weigand, S. Ringquist and D.H. Parma. Anti-L-selectin aptamers: Binding characteristics, pharmacokinetic parameters, and activity against an intravascular target *in vivo*. *Antisense Nucleic Acid Drug Dev.*, 2000, **10**(2), pp.63-75.
414. P.C. De Smidt, T.L. Doan, S.D. Falco and T.J.C.V. Berkel. Association of antisense oligonucleotides with lipoproteins prolongs the plasma half-life and modifies the tissue distribution. *Nucleic Acids Res.*, 1991, **19**(17), pp.4695-4700.
415. H. Dougan, D.M. Lyster, C.V. Vo, A. Stafford, J.I. Weitz and J.B. Hobbs. Extending the lifetime of anticoagulant oligodeoxynucleotide aptamers in blood. *Nucl. Med. Biol.*, 2000, **27**(3), pp.289-297.
416. M.C. Willis, B. Collins, T. Zhang, L.S. Green, D.P. Sebesta, C. Bell, E. Kellogg, S.C. Gill, A. Magallanez, S. Knauer, R.A. Bendele, P.S. Gill and N. Janjić. Liposome-

anchored vascular endothelial growth factor aptamers. *Bioconj. Chem.*, 1998, **9**(5), pp.573-582.

417. R. White, C. Rusconi, E. Scardino, A. Wolberg, J. Lawson, M. Hoffman and B. Sullenger. Generation of species cross-reactive aptamers using toggle-SELEX. *Mol. Ther.*, 2001, **4**(6), pp.567-573.
418. N. Derbyshire, S.J. White, D.H.J. Bunka, L. Song, S. Stead, J. Tarbin, M. Sharman, D. Zhou and P.G. Stockley. Toggled RNA aptamers against aminoglycosides allowing facile detection of antibiotics using gold nanoparticle assays. *Anal. Chem.*, 2012, **84**(15), pp.6595-6602.
419. M.C. Golden, B.D. Collins, M.C. Willis and T.H. Koch. Diagnostic potential of PhotoSELEX-evolved ssDNA aptamers. *J. Biotech.*, 2000, **81**(2–3), pp.167-178.
420. A. Vater, F. Jarosch, K. Buchner and S. Klussmann. Short bioactive Spiegelmers to migraine-associated calcitonin gene-related peptide rapidly identified by a novel approach: Tailored-SELEX. *Nucleic Acids Res.*, 2003, **31**(21), p.e130.
421. K.-T. Guo, A. Paul, C. Schichor, G. Ziemer and H.P. Wendel. CELL-SELEX: Novel perspectives of aptamer-based therapeutics. *Int. J. Mol. Sci.*, 2008, **9**(4), pp.668-678.
422. M. Famulok and G. Mayer. Aptamers as tools in molecular biology and immunology. *In: Combinatorial Chemistry in Biology*. Berlin: Springer-Verlag Berlin, 1999, pp.123-136.
423. T.L. Symensma, L. Giver, M. Zapp, G.B. Takle and A.D. Ellington. RNA aptamers selected to bind human immunodeficiency virus type 1 Rev *in vitro* are Rev responsive *in vivo*. *J. Virol.*, 1996, **70**(1), pp.179-187.
424. M. Thomas, S. Chédin, C. Carles, M. Riva, M. Famulok and A. Sentenac. Selective targeting and inhibition of yeast RNA polymerase II by RNA aptamers. *J. Biol. Chem.*, 1997, **272**(44), pp.27980-27986.
425. M. Blind, W. Kolanus and M. Famulok. Cytoplasmic RNA modulators of an inside-out signal-transduction cascade. *Proc. Natl. Acad. Sci.*, 1999, **96**(7), pp.3606-3610.
426. H. Shi, B.E. Hoffman and J.T. Lis. RNA aptamers as effective protein antagonists in a multicellular organism. *Proc. Natl. Acad. Sci.*, 1999, **96**(18), pp.10033-10038.
427. G. Mayer, M. Blind, W. Nagel, T. Böhm, T. Knorr, C.L. Jackson, W. Kolanus and M. Famulok. Controlling small guanine–nucleotide-exchange factor function through cytoplasmic RNA intramers. *Proc. Natl. Acad. Sci.*, 2001, **98**(9), pp.4961-4965.
428. C.-H.B. Chen, G.A. Chernis, V.Q. Hoang and R. Landgraf. Inhibition of heregulin signaling by an aptamer that preferentially binds to the oligomeric form of human epidermal growth factor receptor-3. *Proc. Natl. Acad. Sci.*, 2003, **100**(16), pp.9226-9231.
429. J.A. Sandberg, V.P. Parker, K.S. Blanchard, D. Sweedler, J.A. Powell, A. Kachensky, L. Bellon, N. Usman, T. Rossing, E. Borden and L.M. Blatt. Pharmacokinetics and tolerability of an antiangiogenic ribozyme (Angiozyme™) in healthy volunteers. *J. Clin. Pharma.*, 2000, **40**(12), pp.1462-1469.
430. M.K. Bijsterbosch and T.J.C. Van Berkel. Native and modified lipoproteins as drug delivery systems. *Adv. Drug Deliv. Rev.*, 1990, **5**(3), pp.231-251.

431. D. Castanotto and J.J. Rossi. The promises and pitfalls of RNA-interference-based therapeutics. *Nature*, 2009, **457**(7228), pp.426-433.
432. M. Famulok, M. Blind and G. Mayer. Intramers as promising new tools in functional proteomics. *Chem. Biol.*, 2001, **8**(10), pp.931-939.
433. H. Xing, L. Tang, X. Yang, K. Hwang, W. Wang, Q. Yin, N.Y. Wong, L.W. Dobrucki, N. Yasui, J.A. Katzenellenbogen, W.G. Helferich, J. Cheng and Y. Lu. Selective delivery of an anticancer drug with aptamer-functionalized liposomes to breast cancer cells *in vitro* and *in vivo*. *J. Mater. Chem. B.*, 2013, **1**(39), pp.5288-5297.
434. J.O. Mcnamara, E.R. Andrechek, Y. Wang, K.D. Viles, R.E. Rempel, E. Gilboa, B.A. Sullenger and P.H. Giangrande. Cell type-specific delivery of siRNAs with aptamer-siRNA chimeras. *Nat. Biotech.*, 2006, **24**(8), pp.1005-1015.
435. T.C. Chu, K.Y. Twu, A.D. Ellington and M. Levy. Aptamer mediated siRNA delivery. *Nucleic Acids Res.*, 2006, **34**(10), pp.e73-e73.
436. S. Aggarwal. What's fueling the biotech engine - 2012 to 2013. *Nat. Biotech.*, 2014, **32**(1), pp.32-39.
437. S.R. Robinson, G.M. Bishop, H.-G. Lee and G. Münch. Lessons from the AN 1792 Alzheimer vaccine: lest we forget. *Neurobiol. Aging.*, 2004, **25**(5), pp.609-615.
438. K. Takahasi, M. Yoneyama, T. Nishihori, R. Hirai, H. Kumeta, R. Narita, M. Gale Jr, F. Inagaki and T. Fujita. Nonself RNA-sensing mechanism of RIG-I helicase and activation of antiviral immune responses. *Mol. Cell.*, 2008, **29**(4), pp.428-440.
439. S.S. Diebold, T. Kaisho, H. Hemmi, S. Akira and C. Reis E Sousa. Innate antiviral responses by means of TLR7-mediated recognition of single-stranded RNA. *Science*, 2004, **303**(5663), pp.1529-1531.
440. D. Yu, D. Wang, F.-G. Zhu, L. Bhagat, M. Dai, E.R. Kandimalla and S. Agrawal. Modifications incorporated in CpG motifs of oligodeoxynucleotides lead to antagonist activity of toll-like receptors 7 and 9. *J. Med. Chem.*, 2009, **52**(16), pp.5108-5114.
441. A.F. Labrijn, P. Poignard, A. Raja, M.B. Zwick, K. Delgado, M. Franti, J. Binley, V. Vivona, C. Grundner, C.-C. Huang, M. Venturi, C.J. Petropoulos, T. Wrin, D.S. Dimitrov, J. Robinson, P.D. Kwong, R.T. Wyatt, J. Sodroski and D.R. Burton. Access of antibody molecules to the conserved coreceptor binding site on glycoprotein gp120 is sterically restricted on primary human immunodeficiency virus type 1. *J. Virol.*, 2003, **77**(19), pp.10557-10565.
442. C. Cohen, M. Forzan, B. Sproat, R. Pantophlet, I. Mcgowan, D. Burton and W. James. An aptamer that neutralizes R5 strains of HIV-1 binds to core residues of gp120 in the CCR5 binding site. *Virology*, 2008, **381**(1), pp.46-54.
443. A.K. Dey, C. Griffiths, S.M. Lea and W. James. Structural characterization of an anti-gp120 RNA aptamer that neutralizes R5 strains of HIV-1. *RNA*, 2005, **11**(6), pp.873-884.
444. R. Ratnapriya and E.Y. Chew. Age-related macular degeneration – clinical review and genetics update. *Clin. Genet.*, 2013, **84**(2), pp.160-166.
445. U. Chakravarthy. Year 2 efficacy results of two randomized controlled clinical trials of Pegaptanib for neovascular age-related macular degeneration. *Ophthalmology*, 2006, **113**(9), pp.1508.e1-1508.e25.

446. X. Ni, M. Castanares, A. Mukherjee and S.E. Lupold. Nucleic acid aptamers: clinical applications and promising new horizons. *Cur. Med. Chem.*, 2011, **18**(27), pp.4206-4214.
447. P. Sundaram, H. Kurniawan, M.E. Byrne and J. Wower. Therapeutic RNA aptamers in clinical trials. *Euro. J. Pharma. Sci.*, 2013, **48**(1–2), pp.259-271.
448. J.M. Binning, D.W. Leung and G.K. Amarasinghe. Aptamers in virology: Recent advances and challenges. *Front. Microbiol.*, 2012, **3**, p.29.
449. J. Wang, H. Jiang and F. Liu. *In vitro* selection of novel RNA ligands that bind human cytomegalovirus and block viral infection. *RNA*, 2000, **6**(4), pp.571-583.
450. A. Biroccio, J. Hamm, I. Incitti, R. De Francesco and L. Tomei. Selection of RNA aptamers that are specific and high-affinity ligands of the Hepatitis C virus RNA-dependent RNA polymerase. *J. Virol.*, 2002, **76**(8), pp.3688-3696.
451. P. Bellecave, C. Cazenave, J. Rumi, C. Staedel, O. Cosnefroy, M.-L. Andreola, M. Ventura, L. Tarrago-Litvak and T. Astier-Gin. Inhibition of hepatitis C Virus (HCV) RNA polymerase by DNA aptamers: Mechanism of inhibition of *in vitro* RNA synthesis and effect on HCV-infected cells. *Antimicrob. Agents. Chemother.*, 2008, **52**(6), pp.2097-2110.
452. K. Germer, M. Leonard and X. Zhang. RNA aptamers and their therapeutic and diagnostic applications. *Int. J. Biochem. Mol. Biol.*, 2013, **4**(1), pp.27-40.
453. S.D. Jayasena. Aptamers: An emerging class of molecules that rival antibodies in diagnostics. *Clin. Chem.*, 1999, **45**(9), pp.1628-1650.
454. B. Soontornworajit and Y. Wang. Nucleic acid aptamers for clinical diagnosis: cell detection and molecular imaging. *Anal. Bioanal. Chem.*, 2011, **399**(4), pp.1591-1599.
455. S. Tombelli, M. Minunni and M. Mascini. Aptamers-based assays for diagnostics, environmental and food analysis. *Biomol. Eng.*, 2007, **24**(2), pp.191-200.
456. C.D. Pieve, A.C. Perkins and S. Missailidis. Anti-MUC1 aptamers: radiolabelling with 99mTc and biodistribution in MCF-7 tumour-bearing mice. *Nucl. Med. Biol.*, 2009, **36**(6), pp.703-710.
457. P. Dua, S. Kim and D.-K. Lee. Nucleic acid aptamers targeting cell-surface proteins. *Methods*, 2011, **54**(2), pp.215-225.
458. E. Levy-Nissenbaum, A.F. Radovic-Moreno, A.Z. Wang, R. Langer and O.C. Farokhzad. Nanotechnology and aptamers: applications in drug delivery. *Trends. Biotechnol.*, 2008, **26**(8), pp.442-449.
459. M.K. Yu, Y.Y. Jeong, J. Park, S. Park, J.W. Kim, J.J. Min, K. Kim and S. Jon. Drug-loaded superparamagnetic iron oxide nanoparticles for combined cancer imaging and therapy *in vivo*. *Angew. Chem. Int. Edit.*, 2008, **47**(29), pp.5362-5365.
460. V. Bagalkot, L. Zhang, E. Levy-Nissenbaum, S. Jon, P.W. Kantoff, R. Langer and O.C. Farokhzad. Quantum dot−aptamer conjugates for synchronous cancer imaging, therapy, and sensing of drug delivery based on bi-fluorescence resonance energy transfer. *Nano. Lett.*, 2007, **7**(10), pp.3065-3070.
461. J. Charlton, J. Sennello and D. Smith. *In vivo* imaging of inflammation using an aptamer inhibitor of human neutrophil elastase. *Chem. Biol.*, 1997, **4**(11), pp.809-816.

462. Z.-Q. Cui, Q. Ren, H.-P. Wei, Z. Chen, J.-Y. Deng, Z.-P. Zhang and X.-E. Zhang. Quantum dot-aptamer nanoprobes for recognizing and labeling influenza A virus particles. *Nanoscale*, 2011, **3**(6), pp.2454-2457.
463. M.V. Yigit, D. Mazumdar and Y. Lu. MRI detection of thrombin with aptamer functionalized superparamagnetic iron oxide nanoparticles. *Bioconj. Chem.*, 2008, **19**(2), pp.412-417.
464. B.J. Hicke, A.W. Stephens, T. Gould, Y.-F. Chang, C.K. Lynott, J. Heil, S. Borkowski, C.-S. Hilger, G. Cook, S. Warren and P.G. Schmidt. Tumor targeting by an aptamer. *J. Nucl. Med.*, 2006, **47**(4), pp.668-678.
465. H. Shi, X. He, K. Wang, X. Wu, X. Ye, Q. Guo, W. Tan, Z. Qing, X. Yang and B. Zhou. Activatable aptamer probe for contrast-enhanced in vivo cancer imaging based on cell membrane protein-triggered conformation alteration. *Proc. Natl. Acad. Sci.*, 2011, **108**(10), pp.3900-3905.
466. E.N. Brody, M.C. Willis, J.D. Smith, S. Jayasena, D. Zichi and L. Gold. The use of aptamers in large arrays for molecular diagnostics. *Molec. Diagnos.*, 1999, **4**(4), pp.381-388.
467. C. Yewale, D. Baradia, I. Vhora, S. Patil and A. Misra. Epidermal growth factor receptor targeting in cancer: A review of trends and strategies. *Biomaterials*, 2013, **34**(34), pp.8690-8707.
468. Y. Wan, Y.-T. Kim, N. Li, S.K. Cho, R. Bachoo, A.D. Ellington and S.M. Iqbal. Surface-immobilized aptamers for cancer cell isolation and microscopic cytology. *Cancer. Res.*, 2010, **70**(22), pp.9371-9380.
469. S. Shigdar, J. Lin, Y. Yu, M. Pastuovic, M. Wei and W. Duan. RNA aptamer against a cancer stem cell marker epithelial cell adhesion molecule. *Cancer. Sci.*, 2011, **102**(5), pp.991-998.
470. Y. Song, Z. Zhu, Y. An, W. Zhang, H. Zhang, D. Liu, C. Yu, W. Duan and C.J. Yang. Selection of DNA aptamers against epithelial cell adhesion molecule for cancer cell imaging and circulating tumor cell capture. *Anal. Chem.*, 2013, **85**(8), pp.4141-4149.
471. T.S. Romig, C. Bell and D.W. Drolet. Aptamer affinity chromatography:: combinatorial chemistry applied to protein purification. *J. Chromatogr. B.*, 1999, **731**(2), pp.275-284.
472. M. Michaud, E. Jourdan, A. Villet, A. Ravel, C. Grosset and E. Peyrin. A DNA aptamer as a new target-specific chiral selector for HPLC. *J. Am. Chem. Soc.*, 2003, **125**(28), pp.8672-8679.
473. R.B. Kotia, L. Li and L.B. Mcgown. Separation of nontarget compounds by DNA aptamers. *Anal. Chem.*, 2000, **72**(4), pp.827-831.
474. K. Hartmuth, H.-P. Vornlocher and R. Lührmann. Tobramycin affinity tag purification of spliceosomes. *In:* D. Schoenberg, ed. *mRNA Processing and Metabolism*. Humana Press, 2004, pp.47-64.
475. S.B. Prusiner, M.R. Scott, S.J. Dearmond and F.E. Cohen. Prion protein biology. *Cell*, 1998, **93**(3), pp.337-348.
476. A. Rhie, L. Kirby, N. Sayer, R. Wellesley, P. Disterer, I. Sylvester, A. Gill, J. Hope, W. James and A. Tahiri-Alaoui. Characterization of 2'-Fluoro-RNA aptamers that bind preferentially to disease-associated conformations of prion protein and inhibit conversion. *J. Biol. Chem.*, 2003, **278**(41), pp.39697-39705.

477. N.M. Sayer, M. Cubin, A. Rhie, M. Bullock, A. Tahiri-Alaoui and W. James. Structural determinants of conformationally selective, prion-binding aptamers. *J. Biol. Chem.*, 2004, **279**(13), pp.13102-9.
478. S. Weiss, D. Proske, M. Neumann, M.H. Groschup, H.A. Kretzschmar, M. Famulok and E.L. Winnacker. RNA aptamers specifically interact with the prion protein PrP. *J. Virol.*, 1997, **71**(11), pp.8790-8797.
479. S. Sekiya, F. Nishikawa, K. Noda, P.K.R. Kumar, T. Yokoyama and S. Nishikawa. *In vitro* selection of RNA aptamers against cellular and abnormal isoform of mouse prion protein. *Nucleic Acids Symp. Ser.*, 2005, **49**(1), pp.361-362.
480. D. Peretz, R.A. Williamson, Y. Matsunaga, H. Serban, C. Pinilla, R.B. Bastidas, R. Rozenshteyn, T.L. James, R.A. Houghten, F.E. Cohen, S.B. Prusiner and D.R. Burton. A conformational transition at the N terminus of the prion protein features in formation of the scrapie isoform 1. *J. Mol. Biol.*, 1997, **273**(3), pp.614-622.
481. S. Supattapone, P. Bosque, T. Muramoto, H. Wille, C. Aagaard, D. Peretz, H.-O.B. Nguyen, C. Heinrich, M. Torchia, J. Safar, F.E. Cohen, S.J. Dearmond, S.B. Prusiner and M. Scott. Prion protein of 106 residues creates an artificial transmission barrier for prion replication in transgenic mice. *Cell*, 1999, **96**(6), pp.869-878.
482. T. Eichner and S.E. Radford. Understanding the complex mechanisms of β_2-microglobulin amyloid assembly. *FEBS J.*, 2011, **278**(20), pp.3868-3883.
483. D.H.J. Bunka, B.J. Mantle, I.J. Morten, G.A. Tennent, S.E. Radford and P.G. Stockley. Production and characterization of RNA aptamers specific for amyloid fibril epitopes. *J. Biol. Chem.*, 2007, **282**(47), pp.34500-34509.
484. C.J. Sarell, T.K. Karamanos, S.J. White, D.H.J. Bunka, A.P. Kalverda, G.S. Thompson, A.M. Barker, P.G. Stockley and S.E. Radford. Distinguishing closely-related amyloid precursors using an RNA aptamer. *J. Biol. Chem.*, 2014.
485. K. Pauwels, T.L. Williams, K.L. Morris, W. Jonckheere, A. Vandersteen, G. Kelly, J. Schymkowitz, F. Rousseau, A. Pastore, L.C. Serpell and K. Broersen. Structural basis for increased toxicity of pathological Aβ(42):Aβ(40) ratios in Alzheimer disease. *J. Biol. Chem.*, 2012, **287**(8), pp.5650-5660.
486. J. Seeliger, F. Evers, C. Jeworrek, S. Kapoor, K. Weise, E. Andreetto, M. Tolan, A. Kapurniotu and R. Winter. Cross-amyloid interaction of Aβ and IAPP at lipid membranes. *Angew. Chem. Int. Edit.*, 2012, **51**(3), pp.679-683.
487. B.I. Giasson, M.S. Forman, M. Higuchi, L.I. Golbe, C.L. Graves, P.T. Kotzbauer, J.Q. Trojanowski and V.M.Y. Lee. Initiation and synergistic fibrillization of tau and alpha-synuclein. *Science*, 2003, **300**(5619), pp.636-640.
488. C.E. Macphee and C.M. Dobson. Formation of mixed fibrils demonstrates the generic nature and potential utility of amyloid nanostructures. *J. Am. Chem. Soc.*, 2000, **122**(51), pp.12707-12713.
489. C.J. Sarell, L.A. Woods, Y. Su, G.T. Debelouchina, A.E. Ashcroft, R.G. Griffin, P.G. Stockley and S.E. Radford. Expanding the repertoire of amyloid polymorphs by co-polymerization of related protein precursors. *J. Biol. Chem.*, 2013, **288**(10), pp.7327-7337.
490. C.J. Sarell, T.K. Karamanos, S.J. White, D.H.J. Bunka, A.P. Kalverda, G.S. Thompson, A.M. Barker, P.G. Stockley and S.E. Radford. Distinguishing closely

related amyloid precursors using an RNA aptamer. *J. Biol. Chem.*, 2014, **289**(39), pp.26859-26871.

491. F. Ylera, R. Lurz, V.A. Erdmann and J.P. Fürste. Selection of RNA aptamers to the Alzheimer's disease amyloid peptide. *Biochem. Biophys. Res. Commun.*, 2002, **290**(5), pp.1583-1588.
492. C.T. Farrar, C.M. William, E. Hudry, T. Hashimoto and B.T. Hyman. RNA aptamer probes as optical imaging agents for the detection of amyloid plaques. *PLoS One*, 2014, **9**(2), p.e89901.
493. T. Takahashi, K. Tada and H. Mihara. RNA aptamers selected against amyloid β-peptide (Aβ) inhibit the aggregation of Aβ. *Mol. Biosystems*, 2009, **5**(9), pp.986-991.
494. F. Rahimi, K. Murakami, J.L. Summers, C.-H.B. Chen and G. Bitan. RNA aptamers generated against oligomeric Aβ40 recognize common amyloid aptatopes with low specificity but high sensitivity. *PLoS One*, 2009, **4**(11), p.e7694.
495. K. Tsukakoshi, R. Harada, K. Sode and K. Ikebukuro. Screening of DNA aptamer which binds to α-synuclein. *Biotechnol. Lett.*, 2010, **32**(5), pp.643-648.
496. K. Tsukakoshi, K. Abe, K. Sode and K. Ikebukuro. Selection of DNA aptamers that recognize α-synuclein oligomers using a competitive screening method. *Anal. Chem.*, 2012, **84**(13), pp.5542-5547.
497. O.V. Mitkevich, N.V. Kochneva-Pervukhova, E.R. Surina, S.V. Benevolensky, V.V. Kushnirov and M.D. Ter-Avanesyan. DNA aptamers detecting generic amyloid epitopes. *Prion*, 2012, **6**(4), pp.400-406.
498. C.F. Barbas, D.R. Burton, J.K. Scott and G.J. Silverman. Quantitation of DNA and RNA. *Cold. Spring. Harb. Protoc.*, 2007, (11).
499. D.M. Walsh, E. Thulin, A.M. Minogue, N. Gustavsson, E. Pang, D.B. Teplow and S. Linse. A facile method for expression and purification of the Alzheimer's disease-associated amyloid β-peptide. *FEBS J.*, 2009, **276**(5), pp.1266-1281.
500. E. Gasteiger, C. Hoogland, A. Gattiker, S.E. Duvaud, M.R. Wilkins, R.D. Appel and A. Bairoch. Protein identification and analysis tools on the ExPASy server. *In:* J.M. Walker, ed. *The proteomics Protocols Handbook*. Humana Press, 2005, pp.571-607.
501. M. Lambert, A. Barlow, B. Chromy, C. Edwards, R. Freed, M. Liosatos, T. Morgan, I. Rozovsky, B. Trommer, K. Viola, P. Wals, C. Zhang, C. Finch, G. Krafft and W. Klein. Diffusible, nonfibrillar ligands derived from Aβ1-42 are potent central nervous system neurotoxins. *Proc. Natl. Acad. Sci.*, 1998, **95**(11), pp.6448 - 6453.
502. M. Meyer-Luehmann, T.L. Spires-Jones, C. Prada, M. Garcia-Alloza, A. De Calignon, A. Rozkalne, J. Koenigsknecht-Talboo, D.M. Holtzman, B.J. Bacskai and B.T. Hyman. Rapid appearance and local toxicity of amyloid-β plaques in a mouse model of Alzheimer's disease. *Nature*, 2008, **451**(7179), pp.720-724.
503. P. Lewczuk, H. Esselmann, M. Otto, J.M. Maler, A.W. Henkel, M.K. Henkel, O. Eikenberg, C. Antz, W.-R. Krause, U. Reulbach, J. Kornhuber and J. Wiltfang. Neurochemical diagnosis of Alzheimer's dementia by CSF Aβ42, Aβ42/Aβ40 ratio and total tau. *Neurobiol. Aging.*, 2004, **25**(3), pp.273-281.
504. Y. Nekooki-Machida, M. Kurosawa, N. Nukina, K. Ito, T. Oda and M. Tanaka. Distinct conformations of *in vitro* and *in vivo* amyloids of huntingtin-exon1 show different cytotoxicity. *Proc. Natl. Acad. Sci.*, 2009, **106**(24), pp.9679-9684.

505. K.W. Tipping, T.K. Karamanos, T. Jakhria, M.G. Iadanza, S.C. Goodchild, R. Tuma, N.A. Ranson, E.W. Hewitt and S.E. Radford. pH-induced molecular shedding drives the formation of amyloid fibril-derived oligomers. *Proc. Natl. Acad. Sci.*, 2015, **112**(18), pp.5691-5696.
506. G.L. Rosano and E.A. Ceccarelli. Recombinant protein expression in *Escherichia coli*: advances and challenges. *Front. Microbiol.*, 2014, **5**, p.172.
507. I.A. Kaltashov and S.J. Eyles. *Mass Spectrometry in Structural Biology and Biophysics: Architecture, Dynamics, and Interaction of Biomolecules.* Second ed. New Jersey: John Wiley & Sons, Inc., 2012.
508. Y. Huang, F. Eckstein, R. Padilla and R. Sousa. Mechanism of ribose 2'-group discrimination by an RNA polymerase. *Biochemistry*, 1997, **36**(27), pp.8231-8242.
509. L.G. Brieba and R. Sousa. Roles of histidine 784 and tyrosine 639 in ribose discrimination by T7 RNA polymerase. *Biochemistry*, 2000, **39**(5), pp.919-923.
510. L.T.C. Franca, E. Carrilho and T.B. Kist. A review of DNA sequencing techniques. *Quarterly Reviews of Biophysics*, 2002, **35**(02), pp.169-200.
511. Illumina. *Illumina Miseq sequencing* [online]. 2014. [Accessed 24/07/2014]. Available from: http://www.illumina.com/systems/miseq/performance_specifications.ilmn.
512. M. Zuker. Mfold web server for nucleic acid folding and hybridization prediction. *Nucleic Acids Res.*, 2003, **31**(13), pp.3406-3415.
513. L.I. Brodskiĭ, V.V. Ivanov, I.L. Kalaĭdzidis, A.M. Leontovich, V.K. Nikolaev, S.I. Feranchuk and D.V. A. GeneBee-NET: An Internet based server for biopolymer structure analysis. *Biokhimiia*, 1995, **60**(8), pp.1221-30.
514. M.A. Quail, M. Smith, P. Coupland, T.D. Otto, S.R. Harris, T.R. Connor, A. Bertoni, H.P. Swerdlow and Y. Gu. A tale of three next generation sequencing platforms: comparison of Ion Torrent, Pacific Biosciences and Illumina MiSeq sequencers. *BMC. Genomics.*, 2012, **13**, pp.341-341.
515. M.L. Bochman, K. Paeschke and V.A. Zakian. DNA secondary structures: stability and function of G-quadruplex structures. *Nat. Rev. Genet.*, 2012, **13**(11), pp.770-780.
516. O. Kikin, L. D'antonio and P.S. Bagga. QGRS Mapper: a web-based server for predicting G-quadruplexes in nucleotide sequences. *Nucleic Acids Res.*, 2006, **34**, pp.W676-W682.
517. L.O. Tjernberg, J. Näslund, F. Lindqvist, J. Johansson, A.R. Karlström, J. Thyberg, L. Terenius and C. Nordstedt. Arrest of β-amyloid fibril formation by a pentapeptide ligand. *J. Biol. Chem.*, 1996, **271**(15), pp.8545-8548.
518. L.O. Tjernberg, C. Lilliehöök, D.J.E. Callaway, J. Näslund, S. Hahne, J. Thyberg, L. Terenius and C. Nordstedt. Controlling amyloid β-peptide fibril formation with protease-stable ligands. *J. Biol. Chem.*, 1997, **272**(19), pp.12601-12605.
519. C. Grönwall, A. Jonsson, S. Lindström, E. Gunneriusson, S. Ståhl and N. Herne. Selection and characterization of affibody ligands binding to Alzheimer amyloid β peptides. *J. Biotech.*, 2007, **128**(1), pp.162-183.
520. V.M.Y. Lee. Amyloid binding ligands as Alzheimer's disease therapies. *Neurobiol. Aging.*, 2002, **23**(6), pp.1039-1042.

521. F.L. Palhano, J. Lee, N.P. Grimster and J.W. Kelly. Toward the molecular mechanism(s) by which EGCG treatment remodels mature amyloid fibrils. *J. Am. Chem. Soc.*, 2013, **135**(20), pp.7503-7510.
522. L.M. Young, J.C. Saunders, R.A. Mahood, C.H. Revill, R.J. Foster, L.-H. Tu, D.P. Raleigh, S.E. Radford and A.E. Ashcroft. Screening and classifying small-molecule inhibitors of amyloid formation using ion mobility spectrometry–mass spectrometry. *Nat. Chem.*, 2015, **7**(1), pp.73-81.
523. D.E. Ehrnhoefer, J. Bieschke, A. Boeddrich, M. Herbst, L. Masino, R. Lurz, S. Engemann, A. Pastore and E.E. Wanker. EGCG redirects amyloidogenic polypeptides into unstructured, off-pathway oligomers. *Nat. Struct. Mol.*, 2008, **15**(6), pp.558-566.
524. D. Howlett, P. Cutler, S. Heales and P. Camilleri. Hemin and related porphyrins inhibit β-amyloid aggregation. *FEBS Lett.*, 1997, **417**(2), pp.249-251.
525. K. Ono, K. Hasegawa, H. Naiki and M. Yamada. Curcumin has potent anti-amyloidogenic effects for Alzheimer's β-amyloid fibrils *in vitro*. *J. Neurosci. Res.*, 2004, **75**(6), pp.742-750.
526. J.R. Harris. *In vitro* fibrillogenesis of the amyloid β1–42 peptide: cholesterol potentiation and aspirin inhibition. *Micron*, 2002, **33**(7–8), pp.609-626.
527. J. Mclaurin, R. Cecal, M.E. Kierstead, X. Tian, A.L. Phinney, M. Manea, J.E. French, M.H.L. Lambermon, A.A. Darabie, M.E. Brown, C. Janus, M.A. Chishti, P. Horne, D. Westaway, P.E. Fraser, H.T.J. Mount, M. Przybylski and P. St George-Hyslop. Therapeutically effective antibodies against amyloid–β peptide target amyloid-β residues 4-10 and inhibit cytotoxicity and fibrillogenesis. *Nat. Med.*, 2002, **8**(11), pp.1263-1269.
528. B. Solomon, R. Koppel, E. Hanan and T. Katzav. Monoclonal antibodies inhibit *in vitro* fibrillar aggregation of the Alzheimer β-amyloid peptide. *Proc. Natl. Acad. Sci.*, 1996, **93**(1), pp.452-455.
529. J. Legleiter, D.L. Czilli, B. Gitter, R.B. Demattos, D.M. Holtzman and T. Kowalewski. Effect of different anti-Aβ antibodies on Aβ fibrillogenesis as assessed by atomic force microscopy. *J. Mol. Biol.*, 2004, **335**(4), pp.997-1006.
530. H.J. Fu, B. Liu, J.L. Frost and C.A. Lemere. Amyloid-β immunotherapy for Alzheimer's disease. *CNS Neurol. Disord. Drug Targets*, 2010, **9**(2), pp.197-206.
531. B. O'nuallain and R. Wetzel. Conformational Abs recognizing a generic amyloid fibril epitope. *Proc. Natl. Acad. Sci.*, 2002, **99**(3), pp.1485-1490.
532. K.P.R. Nilsson. Small organic probes as amyloid specific ligands – past and recent molecular scaffolds. *FEBS Lett.*, 2009, **583**(16), pp.2593-2599.
533. C. Wu, J. Scott and J.-E. Shea. Binding of congo red to amyloid protofibrils of the Alzheimer Aβ(9–40) peptide probed by molecular dynamics simulations. *Biophys. J.*, 2012, **103**(3), pp.550-557.
534. D.H.J. Bunka, O. Platonova and P.G. Stockley. Development of aptamer therapeutics. *Curr. Opin. Pharmacol.*, 2010, **10**(5), pp.557-562.
535. J. Lauren, D.A. Gimbel, H.B. Nygaard, J.W. Gilbert and S.M. Strittmatter. Cellular prion protein mediates impairment of synaptic plasticity by amyloid-β oligomers. *Nature*, 2009, **457**(7233), pp.1128-1132.
536. M. Blind and M. Blank. Aptamer selection technology and recent advances. *Mol. Ther. Nucleic Acids*, 2015, **4**, p.e223.

537. E.L. Van Dijk, Y. Jaszczyszyn and C. Thermes. Library preparation methods for next-generation sequencing: Tone down the bias. *Exp. Cell. Res.*, 2014, **322**(1), pp.12-20.
538. M.L. Doyle. Characterization of binding interactions by isothermal titration calorimetry. *Curr. Opin. Biotech.*, 1997, **8**(1), pp.31-35.
539. M. Pellecchia, I. Bertini, D. Cowburn, C. Dalvit, E. Giralt, W. Jahnke, T.L. James, S.W. Homans, H. Kessler, C. Luchinat, B. Meyer, H. Oschkinat, J. Peng, H. Schwalbe and G. Siegal. Perspectives on NMR in drug discovery: a technique comes of age. *Nat. Rev. Drug. Discov.*, 2008, **7**(9), pp.738-745.
540. M. Jerabek-Willemsen, T. André, R. Wanner, H.M. Roth, S. Duhr, P. Baaske and D. Breitsprecher. Microscale thermophoresis: Interaction analysis and beyond. *J. Mol. Struct.*, 2014, **1077**, pp.101-113.
541. M. Jerabek-Willemsen, C.J. Wienken, D. Braun, P. Baaske and S. Duhr. Molecular interaction studies using microscale thermophoresis. *Assay Drug Dev. Techn.*, 2011, **9**(4), pp.342-353.
542. S.a.I. Seidel, P.M. Dijkman, W.A. Lea, G. Van Den Bogaart, M. Jerabek-Willemsen, A. Lazic, J.S. Joseph, P. Srinivasan, P. Baaske, A. Simeonov, I. Katritch, F.A. Melo, J.E. Ladbury, G. Schreiber, A. Watts, D. Braun and S. Duhr. Microscale thermophoresis quantifies biomolecular interactions under previously challenging conditions. *Methods*, 2013, **59**(3), pp.301-315.
543. K. Zillner, M. Jerabek-Willemsen, S. Duhr, D. Braun, G. Längst and P. Baaske. Microscale thermophoresis as a sensitive method to quantify protein:nucleic acid interactions in solution. *Methods in Molecular Biology*, 2012, **815**, pp.241-252.
544. Jeroen r.P.M. Strating, L. Van der linden, L. Albulescu, J. Bigay, M. Arita, L. Delang, P. Leyssen, Hilde m. Van der schaar, Kjerstin h.W. Lanke, Hendrik j. Thibaut, R. Ulferts, G. Drin, N. Schlinck, Richard w. Wubbolts, N. Sever, Sarah a. Head, Jun o. Liu, Philip a. Beachy, Maria a. De matteis, Matthew d. Shair, Vesa m. Olkkonen, J. Neyts and Frank j.M. Van kuppeveld. Itraconazole inhibits enterovirus replication by targeting the oxysterol-binding protein. *Cell. Rep.*, 2015, **10**(4), pp.600-615.
545. L.R.F. De Sousa, H. Wu, L. Nebo, J.B. Fernandes, M.F.D.G.F. Da Silva, W. Kiefer, M. Kanitz, J. Bodem, W.E. Diederich, T. Schirmeister and P.C. Vieira. Flavonoids as noncompetitive inhibitors of Dengue virus NS2B-NS3 protease: Inhibition kinetics and docking studies. *Bioorgan. Med. Chem.*, 2015, **23**(3), pp.466-470.
546. M.H. Savolainen, X. Yan, T.T. Myöhänen and H.J. Huttunen. Prolyl oligopeptidase enhances α-synuclein dimerization via direct protein-protein Interaction. *J. Biol. Chem.*, 2015, **290**(8), pp.5117-5126.
547. M. Mukherjea, M.Y. Ali, C. Kikuti, D. Safer, Z. Yang, H. Sirkia, V. Ropars, A. Houdusse, David m. Warshaw and H.L. Sweeney. Myosin VI must dimerize and deploy its unusual lever arm in order to perform its cellular roles. *Cell. Rep.*, 2014, **8**(5), pp.1522-1532.
548. Euripedes de a. Ribeiro, Jr., N. Pinotsis, A. Ghisleni, A. Salmazo, Petr v. Konarev, J. Kostan, B. Sjöblom, C. Schreiner, Anton a. Polyansky, Eirini a. Gkougkoulia, Mark r. Holt, Finn l. Aachmann, B. Žagrović, E. Bordignon, Katharina f. Pirker, Dmitri i. Svergun, M. Gautel and K. Djinović-Carugo. The structure and regulation of human muscle α-actinin. *Cell*, 2014, **159**(6), pp.1447-1460.

549. S.H.A. Gandham, D.E. Volk, G.L.R. Lokesh, M. Neerathilingam and D.G. Gorenstein. Thioaptamers targeting dengue virus type-2 envelope protein domain III. *Biochem. Biophys. Res. Commun.*, 2014, **453**(3), pp.309-315.
550. H.L. Marks, M.V. Pishko, G.W. Jackson and G.L. Coté. Rational design of a bisphenol A aptamer selective surface-enhanced raman scattering nanoprobe. *Anal. Chem.*, 2014, **86**(23), pp.11614-11619.
551. E. Eliahoo, A. Marx, H. Manor and A. Alian. A novel open-barrel structure of octameric translin reveals a potential RNA entryway. *J. Mol. Biol.*, 2015, **427**(4), pp.756-762.
552. Y. Guo, T.H. Scheuermann, C.L. Partch, D.R. Tomchick and K.H. Gardner. Coiled-coil coactivators play a structural role mediating interactions in hypoxia inducible factor heterodimerization. *J. Biol. Chem.*, 2015, **290**(12), pp.7707-7721.
553. J. Witosch, E. Wolf and N. Mizuno. Architecture and ssDNA interaction of the timeless-tipin-RPA complex. *Nucleic Acids Res.*, 2014, **42**(20), pp.12912-12927.
554. J. Sambrook, Russell, D. W. *Molecular cloning: A laboratory manual.* 3rd ed. New York: Cold Spring Harbor Laboratory Press, 2001.
555. J.R. Lakowicz. *Principles of fluorescence spectroscopy.* Third ed. New York, USA: Springer, 2006.
556. C.J. Sarell, C.D. Syme, S.E.J. Rigby and J.H. Viles. Copper(II) binding to amyloid-β fibrils of Alzheimer's disease reveals a picomolar affinity: Stoichiometry and coordination geometry are independent of Aβ oligomeric form. *Biochemistry*, 2009, **48**(20), pp.4388-4402.
557. N.C. Maiti, D. Jiang, A.J. Wain, S. Patel, K.L. Dinh and F. Zhou. Mechanistic studies of Cu(II) binding to amyloid-β peptides and the fluorescence and redox behaviors of the resulting complexes. *J. Phys. Chem. B*, 2008, **112**(28), pp.8406-8411.
558. N.J. Moerke. Fluorescence polarization (FP) assays for monitoring peptide-protein or nucleic acid-protein binding. *In: Current Protocols in Chemical Biology*. John Wiley & Sons, Inc., 2009.
559. H.H. Nguyen, J. Park, S. Kang and M. Kim. Surface plasmon resonance: A versatile technique for biosensor applications. *Sensors (Basel, Switzerland)*, 2015, **15**(5), pp.10481-10510.
560. I.D. Parsons, B. Persson, A. Mekhalfia, G.M. Blackburn and P.G. Stockley. Probing the molecular mechanism of action of co-repressor in the *E. coli* methionine repressor-operator complex using surface plasmon resonance (SPR). *Nucleic Acids Res.*, 1995, **23**(2), pp.211-216.
561. P. Schuck and H. Zhao. The role of mass transport limitation and surface heterogeneity in the biophysical characterization of macromolecular binding processes by SPR biosensing. *Method. Mol. Biol.*, 2010, **627**, pp.15-54.
562. R. James, C. Kleanthous and G.R. Moore. The biology of E colicins: paradigms and paradoxes. *Microbiology*, 1996, **142**(7), pp.1569-1580.
563. J.E. Ladbury and B.Z. Chowdhry. Sensing the heat: the application of isothermal titration calorimetry to thermodynamic studies of biomolecular interactions. *Chem. Biol.*, 1996, **3**(10), pp.791-801.
564. M.a.A. O'neill and S. Gaisford. Application and use of isothermal calorimetry in pharmaceutical development. *Int. J. Pharm.*, 2011, **417**(1–2), pp.83-93.

565. M.D. Sam and R.T. Clubb. Preparation and optimization of protein–DNA complexes suitable for detailed NMR studies. *Method. Mol. Biol.*, 2012, **831**, pp.219-232.
566. F. Frank, N. Sonenberg and B. Nagar. Structural basis for 5′-nucleotide base-specific recognition of guide RNA by human AGO2. *Nature*, 2010, **465**(7299), pp.818-822.
567. C.G. Kalodimos, N. Biris, A.M.J.J. Bonvin, M.M. Levandoski, M. Guennuegues, R. Boelens and R. Kaptein. Structure and flexibility adaptation in nonspecific and specific protein-DNA complexes. *Science*, 2004, **305**(5682), pp.386-389.
568. M. Bardelli, E. Livoti, L. Simonelli, M. Pedotti, A. Moraes, A.P. Valente and L. Varani. Epitope mapping by solution NMR spectroscopy. *J. Mol. Recognit.*, 2015, **28**(6), pp.393-400.
569. Rule G.S and H. T.K. *Fundamentals of protein NMR spectroscopy.* Focus on Structural Biology. Springer Netherlands, 2006.
570. E.B. Erba and R. Zenobi. Mass spectrometric studies of dissociation constants of noncovalent complexes. *Annu. Rep. Prog. Chem. Sect. C. Phys. Chem.*, 2011, **107**(0), pp.199-228.
571. C.V. Robinson, E.W. Chung, B.B. Kragelund, J. Knudsen, R.T. Aplin, F.M. Poulsen and C.M. Dobson. Probing the nature of noncovalent interactions by mass spectrometry. A study of protein−CoA ligand binding and assembly. *J. Am. Chem. Soc.*, 1996, **118**(36), pp.8646-8653.
572. M.J. Greig, H. Gaus, L.L. Cummins, H. Sasmor and R.H. Griffey. Measurement of macromolecular binding using electrospray mass spectrometry. Determination of dissociation constants for oligonucleotide: serum albumin complexes. *J. Am. Chem. Soc.*, 1995, **117**(43), pp.10765-10766.
573. K.A. Sannes-Lowery, R.H. Griffey and S.A. Hofstadler. Measuring dissociation constants of RNA and aminoglycoside antibiotics by electrospray ionization mass spectrometry. *Anal. Biochem.*, 2000, **280**(2), pp.264-271.
574. J.A. Loo. Studying noncovalent protein complexes by electrospray ionization mass spectrometry. *Mass Spectrom. Rev.*, 1997, **16**(1), pp.1-23.
575. C.T. Veros and N.J. Oldham. Quantitative determination of lysozyme-ligand binding in the solution and gas phases by electrospray ionisation mass spectrometry. *Rapid Commun. Mass. Spectrom.*, 2007, **21**(21), pp.3505-3510.
576. Y.-Q. Chu, X.-H. Dai, D. Jiang, G.-Y. Jiang, X. Fang and C.-F. Ding. Studies on the non-covalent interactions between cyclodextrins and aryl alkanol piperazine derivatives by mass spectrometry and fluorescence spectroscopy. *Rapid Commun. Mass. Spectrom.*, 2010, **24**(15), pp.2255-2261.
577. C.J. Wienken, P. Baaske, U. Rothbauer, D. Braun and S. Duhr. Protein-binding assays in biological liquids using microscale thermophoresis. *Nature Commun.*, 2010, **1**, p.100.
578. S. Duhr and D. Braun. Why molecules move along a temperature gradient. *Proc. Natl. Acad. Sci.*, 2006, **103**(52), pp.19678-19682.
579. S. Luzi, Y. Kondo, E. Bernard, L.K.J. Stadler, M. Vaysburd, G. Winter and P. Holliger. Subunit disassembly and inhibition of TNFα by a semi-synthetic bicyclic peptide. *Protein Eng. Des. Sel.*, 2015, **28**(2), pp.45-52.
580. W.B. Stine, L. Jungbauer, C. Yu and M.J. Ladu. Preparing synthetic Aβ in different aggregation states. *Method. Mol. Biol.*, 2011, **670**, pp.13-32.

581. D. Burdick, B. Soreghan, M. Kwon, J. Kosmoski, M. Knauer, A. Henschen, J. Yates, C. Cotman and C. Glabe. Assembly and aggregation properties of synthetic Alzheimer's A4/β amyloid peptide analogs. *J. Biol. Chem.*, 1992, **267**(1), pp.546-554.
582. G. Habicht, C. Haupt, R.P. Friedrich, P. Hortschansky, C. Sachse, J. Meinhardt, K. Wieligmann, G.P. Gellermann, M. Brodhun, J. Götz, K.-J. Halbhuber, C. Röcken, U. Horn and M. Fändrich. Directed selection of a conformational antibody domain that prevents mature amyloid fibril formation by stabilizing Aβ protofibrils. *Proc. Natl. Acad. Sci.*, 2007, **104**(49), pp.19232-19237.
583. D. Nieuwlandt, M. Wecker and L. Gold. *In vitro* selection of RNA ligands to Substance P. *Biochemistry*, 1995, **34**(16), pp.5651-5659.
584. G. Bitan, A. Lomakin and D.B. Teplow. Amyloid β-protein oligomerization: Prenucleation interactions revealed by photo-induced crosslinking of unmodified proteins. *J. Biol. Chem.*, 2001, **276**(37), pp.35176-35184.
585. F. Rahimi, P. Maiti and G. Bitan. Photo-induced cross-linking of unmodified proteins (PICUP) applied to amyloidogenic peptides. *J Vis. Exp.*, 2009, (23), p.1071.
586. R. Kayed, E. Head, J.L. Thompson, T.M. Mcintire, S.C. Milton, C.W. Cotman and C.G. Glabe. Common structure of soluble amyloid oligomers implies common mechanism of pathogenesis. *Science*, 2003, **300**(5618), pp.486-489.
587. R. Kayed and C.G. Glabe. Conformation-dependent anti β-amyloid oligomer antibodies. *In:* K. Indu and W. Ronald, eds. *Methods in Enzymology*. Academic Press, 2006, pp.326-344.
588. T.L. Mann and U.J. Krull. Fluorescence polarization spectroscopy in protein analysis. *Analyst*, 2003, **128**(4), pp.313-317.
589. M. Fändrich, J. Meinhardt and N. Grigorieff. Structural polymorphism of Alzheimer Aβ and other amyloid fibrils. *Prion*, 2009, **3**(2), pp.89-93.
590. H. Prinz. Hill coefficients, dose–response curves and allosteric mechanisms. *J. Chem. Biol.*, 2010, **3**(1), pp.37-44.
591. M. Goedert. Alpha-synuclein and neurodegenerative diseases. *Nat. Rev. Neurosci.*, 2001, **2**(7), pp.492-501.
592. W.S. Davidson, A. Jonas, D.F. Clayton and J.M. George. Stabilization of α-synuclein secondary structure upon binding to synthetic membranes. *J. Biol. Chem.*, 1998, **273**(16), pp.9443-9449.
593. T.S. Ulmer, A. Bax, N.B. Cole and R.L. Nussbaum. Structure and dynamics of micelle-bound human α-synuclein. *J. Biol. Chem.*, 2005, **280**(10), pp.9595-9603.
594. P.H. Jensen, M.S. Nielsen, R. Jakes, C.G. Dotti and M. Goedert. Binding of α-synuclein to brain vesicles is abolished by familial Parkinson's disease mutation. *J. Biol. Chem.*, 1998, **273**(41), pp.26292-26294.
595. K. Uéda, H. Fukushima, E. Masliah, Y. Xia, A. Iwai, M. Yoshimoto, D.A. Otero, J. Kondo, Y. Ihara and T. Saitoh. Molecular cloning of cDNA encoding an unrecognized component of amyloid in Alzheimer disease. *Proc. Natl. Acad. Sci.*, 1993, **90**(23), pp.11282-11286.
596. B.I. Giasson, I.V.J. Murray, J.Q. Trojanowski and V.M.-Y. Lee. A hydrophobic stretch of 12 amino acid residues in the middle of α-synuclein is essential for filament assembly. *J. Biol. Chem.*, 2001, **276**(4), pp.2380-2386.

597. D.F. Clayton and J.M. George. Synucleins in synaptic plasticity and neurodegenerative disorders. *J. Neurosci. Res.*, 1999, **58**(1), pp.120-129.
598. A. Iwai, E. Masliah, M. Yoshimoto, N. Ge, L. Flanagan, H.A. Rohan De Silva, A. Kittel and T. Saitoh. The precursor protein of non-Aβ component of Alzheimer's disease amyloid is a presynaptic protein of the central nervous system. *Neuron*, 1995, **14**(2), pp.467-475.
599. R. Jakes, M.G. Spillantini and M. Goedert. Identification of two distinct synucleins from human brain. *FEBS Lett.*, 1994, **345**(1), pp.27-32.
600. D.E. Cabin, K. Shimazu, D. Murphy, N.B. Cole, W. Gottschalk, K.L. Mcilwain, B. Orrison, A. Chen, C.E. Ellis, R. Paylor, B. Lu and R.L. Nussbaum. Synaptic vesicle depletion correlates with attenuated synaptic responses to prolonged repetitive stimulation in mice lacking α-synuclein. *J. Neurosci.*, 2002, **22**(20), pp.8797-8807.
601. A. Abeliovich, Y. Schmitz, I. Fariñas, D. Choi-Lundberg, W.-H. Ho, P.E. Castillo, N. Shinsky, J.M.G. Verdugo, M. Armanini, A. Ryan, M. Hynes, H. Phillips, D. Sulzer and A. Rosenthal. Mice lacking α-synuclein display functional deficits in the nigrostriatal dopamine system. *Neuron*, 2000, **25**(1), pp.239-252.
602. D.D. Murphy, S.M. Rueter, J.Q. Trojanowski and V.M.-Y. Lee. Synucleins are developmentally expressed, and α-synuclein regulates the size of the presynaptic vesicular pool in primary hippocampal neurons. *J. Neurosci.*, 2000, **20**(9), pp.3214-3220.
603. L. Yavich, H. Tanila, S. Vepsäläinen and P. Jäkälä. Role of α-synuclein in presynaptic dopamine recruitment. *J. Neurosci.*, 2004, **24**(49), pp.11165-11170.
604. D.A. Scott, I. Tabarean, Y. Tang, A. Cartier, E. Masliah and S. Roy. A pathologic cascade leading to synaptic dysfunction in α-synuclein-induced neurodegeneration. *J. Neurosci.*, 2010, **30**(24), pp.8083-8095.
605. V.M. Nemani, W. Lu, V. Berge, K. Nakamura, B. Onoa, M.K. Lee, F.A. Chaudhry, R.A. Nicoll and R.H. Edwards. Increased expression of alpha-synuclein reduces neurotransmitter release by inhibiting synaptic vesicle reclustering after endocytosis. *Neuron*, 2010, **65**(1), pp.66-79.
606. L.C. Serpell, J. Berriman, R. Jakes, M. Goedert and R.A. Crowther. Fiber diffraction of synthetic α-synuclein filaments shows amyloid-like cross-β conformation. *Proc. Natl. Acad. Sci.*, 2000, **97**(9), pp.4897-4902.
607. M.G. Spillantini, R.A. Crowther, R. Jakes, M. Hasegawa and M. Goedert. α-Synuclein in filamentous inclusions of Lewy bodies from Parkinson's disease and dementia with Lewy bodies. *Proc. Natl. Acad. Sci.*, 1998, **95**(11), pp.6469-6473.
608. M.G. Spillantini, M.L. Schmidt, V.M.Y. Lee, J.Q. Trojanowski, R. Jakes and M. Goedert. α-synuclein in Lewy bodies. *Nature*, 1997, **388**(6645), pp.839-840.
609. S. Engelender. Ubiquitination of α-synuclein and autophagy in Parkinson's disease. *Autophagy*, 2008, **4**(3), pp.372-374.
610. J. Lowe, H. Mcdermott, I. Pike, I. Spendlove, M. Landon and R.J. Mayer. αB crystallin expression in nonlenticular tissues and selective presence in ubiquitinated inclusion bodies in human disease. *J. Pathol.*, 1992, **166**(1), pp.61-68.
611. G. Comellas, L.R. Lemkau, A.J. Nieuwkoop, K.D. Kloepper, D.T. Ladror, R. Ebisu, W.S. Woods, A.S. Lipton, J.M. George and C.M. Rienstra. Structured regions of

α-synuclein fibrils include the early-onset Parkinson's disease mutation sites. *J. Mol. Biol.*, 2011, **411**(4), pp.881-895.

612. D. Eliezer, E. Kutluay, R. Bussell Jr and G. Browne. Conformational properties of α-synuclein in its free and lipid-associated states. *J. Mol. Biol.*, 2001, **307**(4), pp.1061-1073.
613. P.H. Weinreb, W. Zhen, A.W. Poon, K.A. Conway and P.T. Lansbury. NACP, A protein implicated in Alzheimer's disease and learning is natively unfolded. *Biochemistry*, 1996, **35**(43), pp.13709-13715.
614. H.A. Lashuel, C.R. Overk, A. Oueslati and E. Masliah. The many faces of α-synuclein: from structure and toxicity to therapeutic target. *Nat. Rev. Neurosci.*, 2013, **14**(1), pp.38-48.
615. K.M. Danzer, D. Haasen, A.R. Karow, S. Moussaud, M. Habeck, A. Giese, H. Kretzschmar, B. Hengerer and M. Kostka. Different species of α-synuclein oligomers induce calcium influx and seeding. *J. Neurosci.*, 2007, **27**(34), pp.9220-9232.
616. N. Cremades, S. Cohen, E. Deas, A. Abramov, A. Chen, A. Orte, M. Sandal, R. Clarke, P. Dunne, F. Aprile, C. Bertoncini, N. Wood, T. Knowles, C. Dobson and D. Klenerman. Direct observation of the interconversion of normal and toxic forms of α-synuclein. *Cell*, 2012, **149**(5), pp.1048-1059.
617. T.T. Ding, S.-J. Lee, J.-C. Rochet and P.T. Lansbury. Annular α-synuclein protofibrils are produced when spherical protofibrils are incubated in solution or bound to brain-derived membranes. *Biochemistry*, 2002, **41**(32), pp.10209-10217.
618. H.A. Lashuel, B.M. Petre, J. Wall, M. Simon, R.J. Nowak, T. Walz and P.T. Lansbury Jr. α-Synuclein, especially the Parkinson's disease-associated mutants, forms pore-like annular and tubular protofibrils. *J. Mol. Biol.*, 2002, **322**(5), pp.1089-1102.
619. K.A. Conway, S.-J. Lee, J.-C. Rochet, T.T. Ding, R.E. Williamson and P.T. Lansbury. Acceleration of oligomerization, not fibrillization, is a shared property of both α-synuclein mutations linked to early-onset Parkinson's disease: Implications for pathogenesis and therapy. *Proc. Natl. Acad. Sci.*, 2000, **97**(2), pp.571-576.
620. A. Der-Sarkissian, C.C. Jao, J. Chen and R. Langen. Structural organization of α-synuclein fibrils studied by site-directed spin labeling. *J. Biol. Chem.*, 2003, **278**(39), pp.37530-37535.
621. M. Chen, M. Margittai, J. Chen and R. Langen. Investigation of α-synuclein fibril structure by site-directed spin labeling. *J. Biol. Chem.*, 2007, **282**(34), pp.24970-24979.
622. H. Miake, H. Mizusawa, T. Iwatsubo and M. Hasegawa. Biochemical characterization of the core structure of α-synuclein filaments. *J. Biol. Chem.*, 2002, **277**(21), pp.19213-19219.
623. M. Vilar, H.-T. Chou, T. Lührs, S.K. Maji, D. Riek-Loher, R. Verel, G. Manning, H. Stahlberg and R. Riek. The fold of α-synuclein fibrils. *Proc. Natl. Acad. Sci.*, 2008, **105**(25), pp.8637-8642.
624. H. Heise, W. Hoyer, S. Becker, O.C. Andronesi, D. Riedel and M. Baldus. Molecular-level secondary structure, polymorphism, and dynamics of full-length α-synuclein fibrils studied by solid-state NMR. *Proc. Natl. Acad. Sci.*, 2005, **102**(44), pp.15871-15876.

625. L.R. Lemkau, G. Comellas, K.D. Kloepper, W.S. Woods, J.M. George and C.M. Rienstra. Mutant protein A30P α-synuclein adopts wild-type fibril structure, despite slower fibrillation kinetics. *J. Biol. Chem.*, 2012, **287**(14), pp.11526-11532.
626. L.R. Lemkau, G. Comellas, S.W. Lee, L.K. Rikardsen, W.S. Woods, J.M. George and C.M. Rienstra. Site-specific perturbations of alpha-synuclein fibril structure by the Parkinson's disease associated mutations A53T and E46K. *PLoS One*, 2013, **8**(3), p.e49750.
627. C. Vlad, K. Lindner, C. Karreman, S. Schildknecht, M. Leist, N. Tomczyk, J. Rontree, J. Langridge, K. Danzer, T. Ciossek, A. Petre, M.L. Gross, B. Hengerer and M. Przybylski. Autoproteolytic fragments are intermediates in the oligomerization- aggregation of Parkinson's disease protein alpha-synuclein as revealed by ion mobility mass spectrometry. *ChemBioChem*, 2011, **12**(18), pp.2740-2744.
628. J.-P. Colletier, A. Laganowsky, M. Landau, M. Zhao, A.B. Soriaga, L. Goldschmidt, D. Flot, D. Cascio, M.R. Sawaya and D. Eisenberg. Molecular basis for amyloid-β polymorphism. *Proc. Natl. Acad. Sci.*, 2011, **108**(41), pp.16938-16943.
629. C. Hilbich, B. Kisters-Woike, J. Reed, C.L. Masters and K. Beyreuther. Aggregation and secondary structure of synthetic amyloid βA4 peptides of Alzheimer's disease. *J. Mol. Biol.*, 1991, **218**(1), pp.149-163.
630. H. Inouye, P.E. Fraser and D.A. Kirschner. Structure of β-crystallite assemblies formed by Alzheimer β-amyloid protein analogues: analysis by x-ray diffraction. *Biophys. J.*, 1993, **64**(2), pp.502-519.
631. P.E. Fraser, J.T. Nguyen, W.K. Surewicz and D.A. Kirschner. pH-dependent structural transitions of Alzheimer amyloid peptides. *Biophys. J.*, 1991, **60**(5), pp.1190-1201.
632. K. Halverson, P.E. Fraser, D.A. Kirschner and P.T. Lansbury. Molecular determinants of amyloid deposition in Alzheimer's disease: conformational studies of synthetic Aβ-protein fragments. *Biochemistry*, 1990, **29**(11), pp.2639-2644.
633. J.J. Balbach, Y. Ishii, O.N. Antzutkin, R.D. Leapman, N.W. Rizzo, F. Dyda, J. Reed and R. Tycko. Amyloid fibril formation by Aβ16-22, a seven-residue fragment of the Alzheimer's β-amyloid peptide, and structural characterization by solid state NMR. *Biochemistry*, 2000, **39**(45), pp.13748-13759.
634. A.K. Mehta, K. Lu, W.S. Childers, Y. Liang, S.N. Dublin, J. Dong, J.P. Snyder, S.V. Pingali, P. Thiyagarajan and D.G. Lynn. Facial symmetry in protein self-assembly. *J. Am. Chem. Soc.*, 2008, **130**(30), pp.9829-9835.
635. Y. Liang, S.V. Pingali, A.S. Jogalekar, J.P. Snyder, P. Thiyagarajan and D.G. Lynn. Cross-strand pairing and amyloid assembly. *Biochemistry*, 2008, **47**(38), pp.10018-10026.
636. J. Madine, H.A. Davies, C. Shaw, I.W. Hamley and D.A. Middleton. Fibrils and nanotubes assembled from a modified amyloid-β peptide fragment differ in the packing of the same β-sheet building blocks. *Chem. Commun.*, 2012, **48**(24), pp.2976-2978.
637. M. Cheon, I. Chang and Carol k. Hall. Spontaneous formation of twisted Aβ(16-22) fibrils in large-scale molecular-dynamics simulations. *Biophys. J.*, 2011, **101**(10), pp.2493-2501.

638. G.W. Preston, S.E. Radford, A.E. Ashcroft and A.J. Wilson. Analysis of amyloid nanostructures using photo-cross-linking: *In situ* comparison of three widely used photo-cross-linkers. *ACS Chem. Biol.*, 2014, **9**(3), pp.761-768.
639. R.A. Kammerer, D. Kostrewa, J. Zurdo, A. Detken, C. García-Echeverría, J.D. Green, S.A. Müller, B.H. Meier, F.K. Winkler, C.M. Dobson and M.O. Steinmetz. Exploring amyloid formation by a *de novo* design. *Proc. Natl. Acad. Sci.*, 2004, **101**(13), pp.4435-4440.
640. M.O. Steinmetz, Z. Gattin, R. Verel, B. Ciani, T. Stromer, J.M. Green, P. Tittmann, C. Schulze-Briese, H. Gross, W.F. Van Gunsteren, B.H. Meier, L.C. Serpell, S.A. Müller and R.A. Kammerer. Atomic models of *de novo* designed ccβ-Met amyloid-like fibrils. *J. Mol. Biol.*, 2008, **376**(3), pp.898-912.
641. J.D. Esko, K. Kimata and U. Lindahl. *Essentials of glycobiology.* 2nd ed. New York: Cold Spring Harbour Laboratory Press, 2009.
642. J.D.S. Antonio and R.V. Iozzo. Glycosaminoglycans: Structure and biological functions. *In: eLS*. John Wiley & Sons, Ltd, 2001.
643. J.H. Su, B.J. Cummings and C.W. Cotman. Localization of heparan sulfate glycosaminoglycan and proteoglycan core protein in aged brain and Alzheimer's disease. *Neuroscience*, 1992, **51**(4), pp.801-813.
644. J. Van Horssen, P. Wesseling, L.P.W.J. Van Den Heuvel, R.M.W. De Waal and M.M. Verbeek. Heparan sulphate proteoglycans in Alzheimer's disease and amyloid-related disorders. *Lancet Neurol.*, 2003, **2**(8), pp.482-492.
645. A.D. Snow, H. Mar, D. Nochlin, K. Kimata, M. Kato, S. Suzuki, J. Hassell and T.N. Wight. The presence of heparan sulfate proteoglycans in the neuritic plaques and congophilic angiopathy in Alzheimer's disease. *Am. J. Path.*, 1988, **133**(3), pp.456-463.
646. T. Ariga, T. Miyatake and R.K. Yu. Role of proteoglycans and glycosaminoglycans in the pathogenesis of Alzheimer's disease and related disorders: Amyloidogenesis and therapeutic strategies—A review. *J. Neurosci. Res.*, 2010, **88**(11), pp.2303-2315.
647. C.E. Reilly. Crucial role of heparan sulfate proteoglycan (agrin) in β-amyloid formation in Alzheimer's disease. *J. Neurol.*, 2000, **247**(8), pp.663-664.
648. J. Mclaurin, T. Franklin, X. Zhang, J. Deng and P.E. Fraser. Interactions of Alzheimer amyloid-β peptides with glycosaminoglycans. *Euro. J. Biochem.*, 1999, **266**(3), pp.1101-1110.
649. G.M. Castillo, W. Lukito, T.N. Wight and A.D. Snow. The sulfate moieties of glycosaminoglycans are critical for the enhancement of β-amyloid protein fibril formation. *J. Neurochem.*, 1999, **72**(4), pp.1681-1687.
650. G.M. Castillo, C. Ngo, J. Cummings, T.N. Wight and A.D. Snow. Perlecan binds to the β-amyloid proteins (Aβ) of Alzheimer's disease, accelerates Aβ fibril formation, and maintains Aβ fibril stability. *J. Neurochem.*, 1997, **69**(6), pp.2452-2465.
651. P.E. Fraser, J.T. Nguyen, D.T. Chin and D.A. Kirschner. Effects of sulfate ions on Alzheimer β/A4 peptide assemblies: Implications for amyloid fibril-proteoglycan interactions. *J. Neurochem.*, 1992, **59**(4), pp.1531-1540.
652. J. Mclaurin and P.E. Fraser. Effect of amino-acid substitutions on Alzheimer's amyloid-β peptide–glycosaminoglycan interactions. *Euro. J. Biochem.*, 2000, **267**(21), pp.6353-6361.

653. J. Madine, J.C. Clayton, E.A. Yates and D.A. Middleton. Exploiting a 13C-labelled heparin analogue for *in situ* solid-state NMR investigations of peptide-glycan interactions within amyloid fibrils. *Org. Biomol. Chem.*, 2009, **7**(11), pp.2414-2420.
654. M. Goedert, R. Jakes, M.G. Spillantini, M. Hasegawa, M.J. Smith and R.A. Crowther. Assembly of microtubule-associated protein tau into Alzheimer-like filaments induced by sulphated glycosaminoglycans. *Nature*, 1996, **383**(6600), pp.550-553.
655. H.K. Paudel and W. Li. Heparin-induced conformational change in microtubule-associated protein tau as detected by chemical cross-linking and phosphopeptide mapping. *J. Biol. Chem.*, 1999, **274**(12), pp.8029-8038.
656. J.A. Cohlberg, J. Li, V.N. Uversky and A.L. Fink. Heparin and other glycosaminoglycans stimulate the formation of amyloid fibrils from α-synuclein *in vitro*. *Biochemistry*, 2002, **41**(5), pp.1502-1511.
657. F. Meng, A. Abedini, B. Song and D.P. Raleigh. Amyloid formation by pro-islet amyloid polypeptide processing intermediates: Examination of the role of protein heparan sulfate interactions and implications for islet amyloid formation in type 2 diabetes. *Biochemistry*, 2007, **46**(43), pp.12091-12099.
658. I. Yamaguchi, H. Suda, N. Tsuzuike, K. Seto, M. Seki, Y. Yamaguchi, K. Hasegawa, N. Takahashi, S. Yamamoto, F. Gejyo and H. Naiki. Glycosaminoglycan and proteoglycan inhibit the depolymerization of β_2-microglobulin amyloid fibrils *in vitro*. *Kidney Int.*, 2003, **64**(3), pp.1080-1088.
659. A. Relini, S. De Stefano, S. Torrassa, O. Cavalleri, R. Rolandi, A. Gliozzi, S. Giorgetti, S. Raimondi, L. Marchese, L. Verga, A. Rossi, M. Stoppini and V. Bellotti. Heparin strongly enhances the formation of β2-microglobulin amyloid fibrils in the presence of type I collagen. *J. Biol. Chem.*, 2008, **283**(8), pp.4912-4920.
660. M. Calamai, J.R. Kumita, J. Mifsud, C. Parrini, M. Ramazzotti, G. Ramponi, N. Taddei, F. Chiti and C.M. Dobson. Nature and significance of the interactions between amyloid fibrils and biological polyelectrolytes. *Biochemistry*, 2006, **45**(42), pp.12806-12815.
661. J.J. Valle-Delgado, M. Alfonso-Prieto, N.S. De Groot, S. Ventura, J. Samitier, C. Rovira and X. Fernàndez-Busquets. Modulation of Aβ42 fibrillogenesis by glycosaminoglycan structure. *FASEB J.*, 2010, **24**(11), pp.4250-4261.
662. A.D. Cardin and H.J. Weintraub. Molecular modeling of protein-glycosaminoglycan interactions. *Arterioscler. Thromb. Vasc. Biol.*, 1989, **9**(1), pp.21-32.
663. J. Madine, M.J. Pandya, M.R. Hicks, A. Rodger, E.A. Yates, S.E. Radford and D.A. Middleton. Site-specific identification of an Aβ fibril–heparin interaction site by using solid-state NMR spectroscopy. *Angew. Chem.*, 2012, **124**(52), pp.13317-13320.
664. W.-F. Xue, A.L. Hellewell, W.S. Gosal, S.W. Homans, E.W. Hewitt and S.E. Radford. Fibril fragmentation enhances amyloid cytotoxicity. *J. Biol. Chem.*, 2009, **284**(49), pp.34272-34282.
665. S.C. Goodchild, T. Sheynis, R. Thompson, K.W. Tipping, W.-F. Xue, N.A. Ranson, P.A. Beales, E.W. Hewitt and S.E. Radford. β_2-microglobulin amyloid fibril-

induced membrane disruption is enhanced by endosomal lipids and acidic pH. *PLoS One*, 2014, **9**(8), p.e104492.

666. T. Jakhria, A.L. Hellewell, M.Y. Porter, M.P. Jackson, K.W. Tipping, W.-F. Xue, S.E. Radford and E.W. Hewitt. β_2-microglobulin amyloid fibrils are nanoparticles that disrupt lysosomal membrane protein trafficking and inhibit protein degradation by lysosomes. *J. Biol. Chem.*, 2014, **289**(52), pp.35781-35794.
667. M.Y. Porter, K.E. Routledge, S.E. Radford and E.W. Hewitt. Characterization of the response of primary cells relevant to dialysis-related amyloidosis to β_2-microglobulin monomer and fibrils. *PLoS One*, 2011, **6**(11), p.e27353.
668. I.J. Morten, W.S. Gosal, S.E. Radford and E.W. Hewitt. Investigation into the role of macrophages in the formation and degradation of β_2-microglobulin amyloid fibrils. *J. Biol. Chem.*, 2007, **282**(40), pp.29691-29700.
669. M.V. Berridge, P.M. Herst and A.S. Tan. Tetrazolium dyes as tools in cell biology: New insights into their cellular reduction. *In: Biotechnology Annual Review*. Elsevier, 2005, pp.127-152.
670. L. Agholme, T. Lindström, K. Kågedal, J. Marcusson and M. Hallbeck. An *in vitro* model for neuroscience: Differentiation of SH-SY5Y cells into cells with morphological and biochemical characteristics of mature neurons. *J. Alzheimer. Dis.*, 2010, **20**(4), pp.1069-1082.
671. P.D. Dinkel, M.R. Holden, N. Matin and M. Margittai. RNA Binds to tau fibrils and sustains template-assisted growth. *Biochemistry*, 2015, **54**(30), pp.4731-4740.
672. M. Pérez, J.M. Valpuesta, M. Medina, E. Montejo De Garcini and J. Avila. Polymerization of τ into filaments in the presence of heparin: The minimal sequence required for τ - τ interaction. *J. Neurochem.*, 1996, **67**(3), pp.1183-1190.
673. E.E. Nesterov, J. Skoch, B.T. Hyman, W.E. Klunk, B.J. Bacskai and T.M. Swager. *In vivo* optical imaging of amyloid aggregates in brain: Design of fluorescent markers. *Angew. Chem. Int. Edit.*, 2005, **44**(34), pp.5452-5456.
674. S.D. Ginsberg, P.B. Crino, V.M.Y. Lee, J.H. Eberwine and J.Q. Trojanowski. Sequestration of RNA in Alzheimer's disease neurofibrillary tangles and senile plaques. *Ann. Neurol.*, 1997, **41**(2), pp.200-209.
675. I. Cherny, L. Rockah, O. Levy-Nissenbaum, U. Gophna, E.Z. Ron and E. Gazit. The formation of *Escherichia coli* curli amyloid fibrils is mediated by prion-like peptide repeats. *J. Mol. Biol.*, 2005, **352**(2), pp.245-252.
676. T. Kampers, P. Friedhoff, J. Biernat, E.M. Mandelkow and E. Mandelkow. RNA stimulates aggregation of microtubule-associated protein tau into Alzheimer-like paired helical filaments. *FEBS Lett.*, 1996, **399**(3), pp.344-349.
677. D. Cherny, W. Hoyer, V. Subramaniam and T.M. Jovin. Double-stranded DNA stimulates the fibrillation of α-synuclein *in vitro* and is associated with the mature fibrils: An electron microscopy study. *J. Mol. Biol.*, 2004, **344**(4), pp.929-938.
678. M.E. King, V. Ahuja, L.I. Binder and J. Kuret. Ligand-dependent tau filament formation: Implications for Alzheimer's disease progression. *Biochemistry*, 1999, **38**(45), pp.14851-14859.

679. D.M. Wilson and L.I. Binder. Free fatty acids stimulate the polymerization of tau and amyloid beta peptides. *In vitro* evidence for a common effector of pathogenesis in Alzheimer's disease. *Am. J. Path.*, 1997, **150**(6), pp.2181-2195.
680. M. Hasegawa, R.A. Crowther, R. Jakes and M. Goedert. Alzheimer-like changes in microtubule-associated protein tau induced by sulfated glycosaminoglycans: Inhibition of microtubule binding, stimulation of phosphorylation, and filament assembly depend on the degree of sulfation. *J. Biol. Chem.*, 1997, **272**(52), pp.33118-33124.
681. R.A. Crowther, O.F. Olesen, M.J. Smith, R. Jakes and M. Goedert. Assembly of Alzheimer-like filaments from full-length tau protein. *FEBS Lett.*, 1994, **337**(2), pp.135-138.
682. R.D. Jenison, S.C. Gill, A. Pardi and B. Polisky. High-resolution molecular discrimination by RNA. *Science*, 1994, **263**(5152), pp.1425-9.
683. C. Mannironi, A. Di Nardo, P. Fruscoloni and G.P. Tocchini-Valentini. *In vitro* selection of dopamine RNA ligands. *Biochemistry*, 1997, **36**(32), pp.9726-9734.
684. S.D. Ginsberg, J.E. Galvin, T.S. Chiu, V.M.Y. Lee, E. Masliah and J.Q. Trojanowski. RNA sequestration to pathological lesions of neurodegenerative diseases. *Acta. Neuropathol.*, 1998, **96**(5), pp.487-494.
685. S.D. Ginsberg, P.B. Crino, S.E. Hemby, J.A. Weingarten, V.M.Y. Lee, J.H. Eberwine and J.Q. Trojanowski. Predominance of neuronal mRNAs in individual Alzheimer's disease senile plaques. *Ann. Neurol.*, 1999, **45**(2), pp.174-181.
686. Alberts. B, Johnson. A and Lewis. J. *Molecular biology of the cell.* 4th ed. New York: Garland Science, 2002.
687. J. Ferris and G. Ertem. Oligomerization of ribonucleotides on montmorillonite: reaction of the 5'-phosphorimidazolide of adenosine. *Science*, 1992, **257**(5075), pp.1387-1389.
688. J.P. Ferris and G. Ertem. Montmorillonite catalysis of RNA oligomer formation in aqueous solution. A model for the prebiotic formation of RNA. *J. Am. Chem. Soc.*, 1993, **115**(26), pp.12270-12275.
689. G. Ertem and J.P. Ferris. Template-directed synthesis using the heterogeneous templates produced by montmorillonite catalysis. A possible bridge between the prebiotic and RNA worlds. *J. Am. Chem. Soc.*, 1997, **119**(31), pp.7197-7201.
690. Y.O. Chernoff. Amyloidogenic domains, prions and structural inheritance: rudiments of early life or recent acquisition? *Curr. Opin. Chem. Biol.*, 2004, **8**(6), pp.665-671.
691. C.P.J. Maury. Origin of life. Primordial genetics: Information transfer in a pre-RNA world based on self-replicating β-sheet amyloid conformers. *J. Theor. Biol.*, 2015, **382**, pp.292-297.
692. C.M. Rufo, Y.S. Moroz, O.V. Moroz, J. Stöhr, T.A. Smith, X. Hu, W.F. Degrado and I.V. Korendovych. Short peptides self-assemble to produce catalytic amyloids. *Nat. Chem.*, 2014, **6**(4), pp.303-309.
693. T. Dale. Protein and nucleic acid together: A mechanism for the emergence of biological selection. *J. Theor. Biol.*, 2006, **240**(3), pp.337-342.
694. M. Gray, W.-Y. Wholey, N. Wagner, C. Cremers, A. Mueller-Schickert, N. Hock, A. Krieger, E. Smith, R. Bender, J. Bardwell and U. Jakob. Polyphosphate is a primordial chaperone. *Mol. Cell.*, 2014, **53**(5), pp.689-699.

695. G.E. Crooks, G. Hon, J.-M. Chandonia and S.E. Brenner. WebLogo: A Sequence Logo Generator. *Genome Research*, 2004, **14**(6), pp.1188-1190.